UNIVERSITE DE BRETAGNE OCCIDENTALE

UBO
CNRS
IFREMER
ORSTOM
BRGM

GIS OCEANOLOGIE ET GEODYNAMIQUE

# THESE DE DOCTORAT D'ETAT
ès Sciences
Mention : GEOPHYSIQUE

Sujet :

# Contribution à l'étude des mécanismes de formation des marges continentales passives

Présentée par Jean-Claude SIBUET

Soutenue le 15 mai 1987 devant le Jury composé de :

Président : Mr. René BLANCHET
Rapporteur : Mr. Xavier LE PICHON, de l'Académie des Sciences
Examinateurs : Mr. Lucien MONTADERT
Mr. Georges PASCAL
Mr. Robert B. WHITMARSH

IFREMER

BREST 1987

Les exemples qu'on prend pour prouver d'autres choses, si on voulait prouver les exemples, on prendrait les autres choses pour en être les exemples ; car, comme on croit toujours que la difficulté est à ce qu'on veut prouver, on trouve les exemples plus clairs et aidant à le montrer. Ainsi, quand on veut montrer une chose générale, il faut en donner la règle particulière d'un cas...

Pascal

(Les Pensées)

à mes parents,

à Myriam, Nicolas, Olivier et Laurent

# A V A N T - P R O P O S

**********

Mes remerciements s'adressent tout d'abord à Xavier Le Pichon, aujourd'hui membre de l'Académie et Professeur au Collège de France, qui m'a associé dès 1969 à la formidable aventure que fut la création du Département Scientifique du Centre Océanologique de Bretagne. Je dois dire bien humblement qu'ignorant tout de la mer, il a été non seulement un maître mais aussi un exemple par sa façon de percevoir les problèmes, de communiquer son sens critique et son esprit de synthèse servis par un enthousiasme permanent. S'il n'est resté que quelques années à Brest, après avoir créé un département pluridisciplinaire, il demeure un guide que je respecte tant pour ses qualités scientifiques que morales. J'espère que la collaboration fructueuse maintenue ces quinze dernières années à travers des projets nationaux et internationaux se poursuivra dans l'avenir.

Dès 1977, la formation du GIS "Océanologie et Géodynamique" regroupait le Département des Géosciences Marines de l'IFREMER et le Département des Sciences de la Terre de l'U.B.O. C'est sous la direction et l'impulsion de René Blanchet, Professeur de géodynamique à l'U.B.O., que les liens entre chercheurs ont été renforcés et qu'une réelle dynamique est née, grâce à une participation à l'enseignement et à

l'encadrement des étudiants. Comme tous mes collègues, je l'assure de toute ma reconnaissance d'avoir mené à bien cette entreprise et d'avoir mis sa compétence scientifique au service de la communauté géologique et géophysique brestoise.

Le monde de la géologie et de la géophysique marines est un microcosme où les idées scientifiques s'affrontent. J'ai pu avoir avec Lucien Montadert, responsable du Département "Géologie-Géophysique" de l'IFP, des discussions presque passionnelles mais toujours courtoises qui ont contribué à renforcer l'estime et l'amitié que je lui porte. Il m'honore aujourd'hui en acceptant de juger ce travail.

Georges Pascal, Professeur de géophysique à l'U.B.O., et Bob Whitmarsh, géophysicien à l'Institute of Oceanographic Sciences de Wormley et spécialiste de renom en sismique réfraction marine, ont tous deux accepté de participer à ce jury. Qu'ils soient assurés de toute ma gratitude. A la suite de cette étude des processus de formation des marges continentales de l'Atlantique nord-est, je ne peux que souhaiter qu'une collaboration fructueuse s'établisse entre nous pour acquérir et interpréter les futures données de sismique réfraction sur les marges de l'éperon de Goban et ouest-ibérique.

Le travail à la mer peut parfois être ingrat et éprouvant. Cependant, il a été accompagné pour moi de nombreuses joies, grâce à de réels liens d'amitié avec des marins de GENAVIR et des collègues de

mission. Il a également été l'occasion d'échanges scientifiques constructifs, sans cesse renouvelés au cours des dizaines de campagnes effectuées sur les navires français de l'IFREMER et étrangers, notamment le Glomar Challenger. L'organisation des opérations en mer m'a tout particulièrement fait ressentir que la recherche océanographique résulte d'un travail d'équipe qui se prolonge naturellement à terre. Ceci se traduit par le grand nombre de co-auteurs des publications jointes à ce mémoire. Ils ont tous contribué à la réussite des programmes entrepris et si aujourd'hui je soumets cette thèse, c'est grâce à eux. Je ne peux ici que les remercier collectivement.

Ce travail est le fruit de nombreuses collaborations scientifiques et techniques au sein du Département des Géosciences Marines et de GENAVIR. Sans pouvoir nommer ici tous mes collègues et amis, je redis à chacun ma profonde et durable reconnaissance. Enfin, l'élaboration et la réalisation de ce mémoire ont pu bénéficier de la compétence et du dévouement de Daniel Carré, Jean-Pierre Mazé et Serge Monti qui ont contribué à la réalisation de l'illustration, et de Nicole Uchard et Jacqueline Quentel qui ont assuré la frappe du manuscrit.

# S O M M A I R E

**********

Geol. Soc., 143, p. 45-52. 187

(8) Sibuet J.-C., et Ryan W.B.F., 1979. Site 398 : Evolution of the West Iberian continental margin in the framework of the early evolution of the North Atlantic Ocean. In Sibuet J.-C., Ryan W.B.F. et al., Initial Reports of the Deep Sea Drilling Project, 47, part 2, Washington, U.S. Government Printing Office, p. 761-775. 195

(9) Sibuet J.-C., Mazé J.-P., Amortila P., et Le Pichon X., 1987. Physiography and structure of the western Iberian continental margin off Galicia from Sea-Beam and seismic data. In Boillot G., Winterer E.L., et al., Proc., Init. Repts (Pt A), ODP 103, p. 77-97. 210

III - <u>Interprétation des données géologiques et géophysiques régionales concernant les marges de l'Atlantique Nord-Est</u> 231

(10) Montadert L., de Charpal O., Roberts D., Guennoc P., et Sibuet J.-C., 1979. Northeast Atlantic passive margins : rifting and subsidence processes. In Deep Drilling results in the Atlantic Ocean : continental margins and paleoenvironment, M. Talwani, W.W. Hay, et W.B.F. Ryan (eds), M. Ewing Series 3, American Geophysical Union,

Washington, p. 164-186. 232

(11) Lallemand S., et Sibuet J.-C., 1986. Tectonic implications of canyon directions over the northeast Atlantic continental margins. Tectonics, 5, p. 1125-1143. 265

(12) Diament M., Sibuet J.-C., et Hadaoui A., 1986. Isostasy of the northern bay of Biscay continental margin. Geophys. J. R.A.S., 86, p. 893-907. 284

IV - Modèles de formation des marges continentales passives en extension 299

(13) Foucher J.-P., et Sibuet J.-C., 1980. Thermal regime of the northern bay of Biscay continental margin in the vicinity of the D.S.D.P. sites 400 -402. In the evolution of passive continental margins in the light of recent Deep Drilling Results, by P. Kent, A.S. Laughton, D.G. Roberts, et E.W.J. Jones (eds), The Royal Society, London, p. 157-167. 300

(14) Le Pichon X., et Sibuet J.-C., 1981. Passive margins : a model of formation. J. Geophys. Res., 86, p. 3708-3720. 311

(15) Foucher J.-P., Le Pichon X., et Sibuet J.-C., 1982. The ocean-continent transition in the uniform lithospheric stretching model : role of partial melting in the mantle.

Phil. Trans. R. Soc. Lond., A 305, p. 27-43. 324

(16) Le Pichon X., Angelier J., et Sibuet J.-C., 1983. Subsidence and stretching. In Studies in continental margin geology, Watkins J.S., et Drake C.L. (eds), AAPG Memoir 34, Tulsa, p. 731-741. 341

# P R E M I E R E  P A R T I E

## CONTRIBUTION A L'ETUDE DES MECANISMES DE

## FORMATION DES MARGES CONTINENTALES PASSIVES

# I - INTRODUCTION

Les hypothèses de formation et d'évolution des marges passives en extension font appel à un ou plusieurs mécanismes. Elles peuvent être divisées en quatre groupes :

- le fluage de la croûte continentale inférieure en direction de l'océan sous l'effet d'une surcharge différentielle (Bott, 1973) ;
- le métamorphisme crustal qui, par augmentation de la densité des roches de la croûte inférieure, entraîne une subsidence (Falvey, 1974 ; Artemjev et Artyushkov, 1971) ;
- l'amincissement crustal par soulèvement et érosion (Sleep, 1971), par étirement uniforme (McKenzie, 1978 ; Le Pichon et Sibuet, 1981), ou par intrusions volcaniques (Royden et al., 1980).
- l'amincissement par failles plates (Wernicke, 1985).

Sur les marges très sédimentées, comme la marge nord-américaine, l'effet de la surcharge sédimentaire peut être retiré par "backstripping" (e.g. Watts et Steckler, 1979 ; Beaumont et al., 1982) pour accéder à la subsidence tectonique. Cependant, la rigidité flexurale de la lithosphère, la compaction des sédiments, la paléobathymétrie et les mouvements eustatiques sont des facteurs dont

l'indétermination ou les erreurs affectent la détermination de la subsidence tectonique. Cette subsidence tectonique se décompose en une subsidence initiale, produite lors de la formation de la marge, suivie d'une subsidence thermique. L'amplitude de la subsidence initiale dépend des mécanismes de formation de la marge ; la subsidence thermique est due au refroidissement de la lithosphère et dépend également des mécanismes de formation de la marge.

En revanche, sur les marges passives peu sédimentées, comme dans l'Atlantique Nord-Est, il n'est pas possible de déterminer la subsidence tectonique avec une précision suffisante, parce que la paléobathymétrie est trop imprécise en domaine bathyal inférieur. Cependant, comme les épaisseurs sédimentaires sont très faibles, nous pouvons accéder aux styles de déformations des séries antérifts et de la croûte continentale supérieure. En particulier, la géométrie des systèmes de failles normales ou listriques permet de contraindre les modèles de formation des marges (e.g. Montadert et al., 1979 ; Le Pichon et Sibuet, 1981).

Partant de l'ensemble des données géologiques et géophysiques obtenues sur les marges de l'Atlantique Nord-Est, le but de ce travail est de définir les directions de l'extension pour les différents segments de marges, puis de contraindre les modèles de formation des

marges, afin d'essayer de quantifier l'extension. Le schéma proposé est un essai d'intégration des contraintes géologiques et géophysiques actuellement à notre disposition, sachant que les futures données sur la structure profonde des marges pourront le remettre en cause très rapidement. Les premières conséquences cinématiques de ce schéma sont examinées.

## II - ESTIMATION DE LA DIRECTION DES PALEOCONTRAINTES LORS DE LA PHASE DE RIFTING DES MARGES DE L'ATLANTIQUE NORD-EST

Les marges continentales de l'Atlantique Nord-Est se sont formées par distension du Jurassique supérieur au Crétacé moyen, au cours d'un ou de plusieurs épisodes de rifting (e.g. Mauffret et Montadert, 1987). De l'éperon de Goban au banc de Galice, elles présentent généralement des structures en blocs basculés (e.g. Montadert et al., 1979 ; Le Pichon et Sibuet, 1981) caractéristiques de la déformation cassante de la partie supérieure de la croûte continentale. Si la direction de la contrainte principale est parallèle aux directions des zones de fractures en domaine océanique, en revanche il est difficile d'estimer les directions des contraintes horizontales principales lors de l'épisode de rifting. En effet, nous ne disposons sur les marges passives que d'éléments structuraux permettant de déduire des cartes de fracturation ou des rosaces de directions d'accidents, "pondérées" ou "non pondérées", suivant que l'on tient compte ou non de la taille de chaque accident (Lallemand et Sibuet, 1986).

Les accidents structuraux sont d'ailleurs souvent restreints aux failles normales limitant les blocs basculés, sans qu'il soit possible de mettre en évidence une composante de cisaillement éventuelle le long de ces failles. Sur certaines marges, comme la marge de l'éperon de

Goban, des failles plus ou moins perpendiculaires aux précédentes délimitent des panneaux de blocs basculés. Le Pichon et Sibuet (1981) ont montré que de telles failles pouvaient présenter des rejets verticaux et horizontaux variables le long de leur tracé. Finalement, une dernière famille de failles correspond au rejeu d'éléments structuraux antérieurs repris au cours de l'épisode de rifting (e.g. Lallemand et Sibuet, 1986).

Excepté pour la mer Rouge ou le golfe de Suez, on ne dispose que rarement d'observations de terrain par submersible permettant des mesures de terrain sur les objets géologiques appropriés. Nous sommes donc limités à l'utilisation de résultats de modèles expérimentaux et analytiques appliqués aux seules données structurales.

Dans les rifts continentaux ou sur les marges passives, la direction du déplacement relatif des plaques est perpendiculaire ou oblique à la direction du rift (ou à la limite océan-continent). Dans le cas d'un rifting oblique, les deux composantes d'extension et de cisaillement, respectivement perpendiculaire et parallèle au rift, contribuent à la formation de celui-là. Le rapport des amplitudes des composantes d'extension et de cisaillement dépend de l'angle aigu $\alpha$ entre les directions du rift et du mouvement relatif entre les côtés opposés du rift. Withjack et Jamison (1986) ont décrit l'état des contraintes et le réseau de failles normales et de cisaillement produit

par un rifting oblique, en utilisant indépendamment des techniques analytiques et expérimentales. Nous nous proposons d'appliquer ces techniques aux marges de l'Atlantique Nord-Est et en particulier à différents segments des marges du golfe de Gascogne. En effet, de nombreux auteurs (e.g. Bacon et Gray, 1970 ; Montadert et Winnock, 1971 ; Boillot, 1984) ont suggéré que le mouvement relatif de la péninsule ibérique par rapport à l'Europe stable, au cours du rifting Crétacé inférieur, se faisait en direction du sud-ouest. En revanche, sur la base d'arguments cinématiques (e.g. Choukroune et al., 1973 ; Olivet et al., 1984 ; Savostin et al., 1986) relatifs à la direction du mouvement de l'Afrique par rapport à l'Europe au cours du Crétacé inférieur, ce mouvement se ferait plutôt en direction du sud-est et se prolongerait par le même type de mouvement au cours de la formation du domaine océanique du golfe de Gascogne. En dépit des restrictions propres à la méthode de Withjack et Jamison (1986), il est possible de l'utiliser pour choisir entre ces deux hypothèses dans lesquelles la direction du mouvement de l'Ibérie par rapport à l'Europe diffère de 90° au cours du rifting.

1) Méthode de Withjack et Jamison (1986)

Le dispositif expérimental est constitué par deux plaques verticales de 30 cm de longueur, distantes de 23 cm et dont l'une est fixe. La base du dispositif est un ruban de caoutchouc simulant le comportement ductile de la partie inférieure de la croûte. Une couche d'argile molle de 2,5 cm d'épaisseur simule le comportement fragile de la croûte supérieure. L'axe du rift est parallèle aux plaques verticales. La plaque mobile est déplacée parallèlement à la plaque fixe suivant un angle $\alpha$ pouvant varier de 0° (cisaillement pur) à 90° (extension pure) par rapport à la direction du rift. Des marques circulaires à la surface de l'argile donnent l'état des contraintes avant expérimentation. Au cours de l'expérience, les cercles se déforment en ellipses dont les grands axes sont dans la direction de la plus grande extension horizontale ($\epsilon_{H1}$) et les petits axes dans la direction de la plus grande contraction horizontale ($\epsilon_{H2}$). Les rapports des longueurs des axes au diamètre initial des cercles donnent les valeurs des déformations principales horizontales. La valeur de la déformation principale verticale $\epsilon_v$ est calculée en supposant qu'il n'y a pas de changement de volume au cours de l'expérience. Ce modèle d'argile très simple ne rend compte ni de la nature hétérogène de la croûte, ni évidemment du facteur temps, sachant que l'apparition d'un

rift océanique ne se fait qu'après plusieurs dizaines de M.a.. Néanmoins, il semble que si la vitesse de déformation affecte l'espacement et le décalage des failles, elle n'affecte pas leur direction (Bain and Beebe, 1954 ; Oertel, 1965).

Withjack et Jamison (1986) ont calculé analytiquement les contraintes et l'orientation des failles après un déplacement infinitésimal, ainsi que la déformation après des mouvements finis. Il existe une très bonne correspondance entre les résultats expérimentaux et analytiques. La figure 1 montre la rosace des directions de fractures par rapport à la direction R du rift, ainsi que la direction de la plus grande déformation horizontale $\epsilon_{H1}$ pour différentes valeurs de l'angle $\alpha$.

Withjack et Jamison (1986) ont appliqué les résultats de leurs modèles aux golfes de Californie et d'Aden, deux rifts continentaux miocènes produits par un rifting oblique. Ils expliquent ainsi la présence et l'orientation des failles normales à composante de cisaillement et de failles de cisaillement le long des marges du golfe de Californie, mais aussi la direction oblique par rapport au rift de nombreuses failles normales observées le long des marges des golfes de Californie et d'Aden.

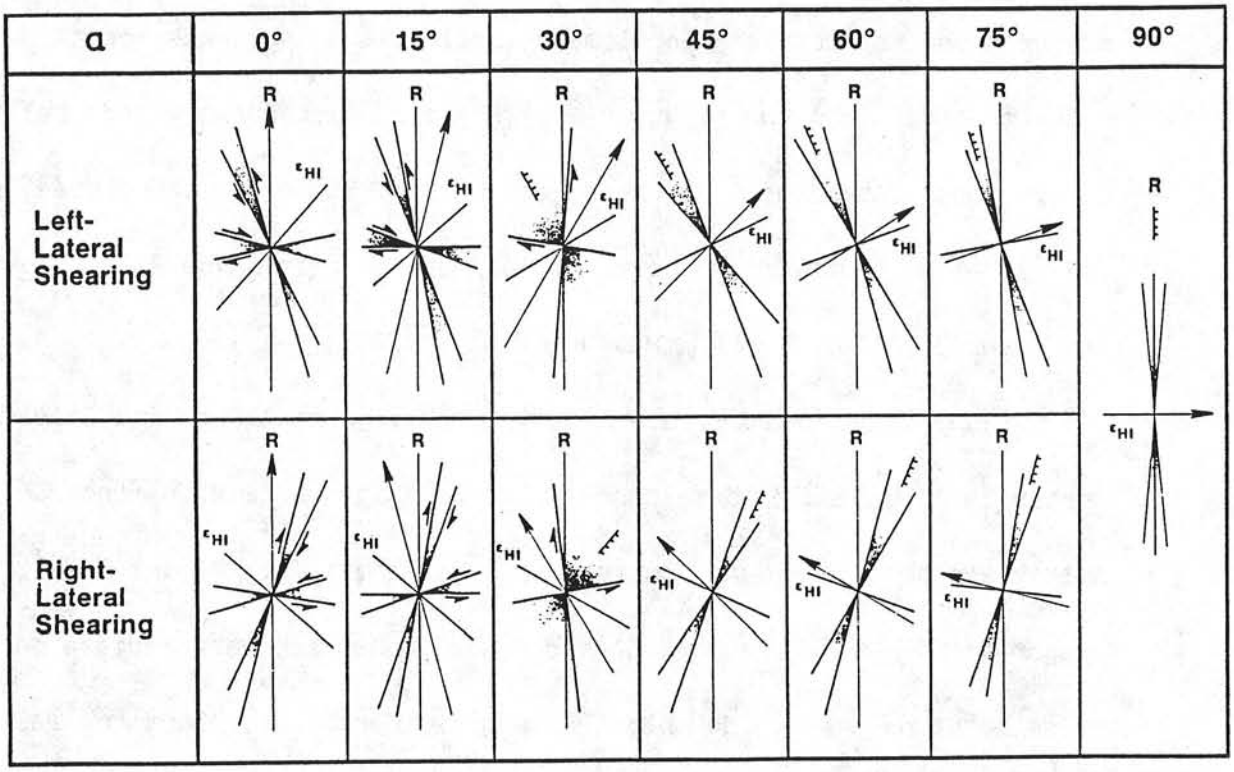


Figure 1 : Diagramme de directions des failles prédites par le modèle de rifting oblique développé par Withjack et Jamison (1986). R est la direction du rift. L'axe fléché indique la direction du déplacement entre les côtés opposés du rift. $\epsilon_{H1}$ est la direction de la plus grande déformation horizontale. Les lignes avec les petites flèches indiquent la direction des failles à composante décrochante. Les lignes avec hachures correspondent aux failles normales.

### a) La marge de l'éperon de Goban

La marge de l'éperon de Goban est limitée par la baie de Porcupine au nord-ouest et l'escarpement Jean-Charcot au sud-est. Elle présente une structure globalement cylindrique sur une centaine de kilomètres de longueur (figures 2 et 3) et résulte du mouvement relatif des plaques Amérique du Nord et Europe. Elle a été créée par amincissement crustal au cours de la phase de rifting datée du Crétacé inférieur à l'Albien moyen (Masson et al., 1985).

Une carte structurale détaillée (figure 4) a été établie à partir de l'ensemble des données de sismique réflexion monotrace et multitrace obtenues dans cette région (figure 5, Sibuet et al., en préparation). La marge de l'éperon de Goban est caractérisée par la présence d'une série de blocs basculés dont les plans de failles normales sont orientés N161° (table 1), de horsts et grabens (figure 6) parfois limités latéralement par des failles orientées N68° (table 1) de même orientation que les zones de fractures identifiées dans le domaine océanique adjacent. Il faut cependant noter la présence d'un accident majeur orienté N132° (table 1), recoupant l'ensemble du domaine. C'est probablement un accident ancien ayant rejoué au cours de l'épisode de rifting en faille normale avec composante de cisaillement dextre.

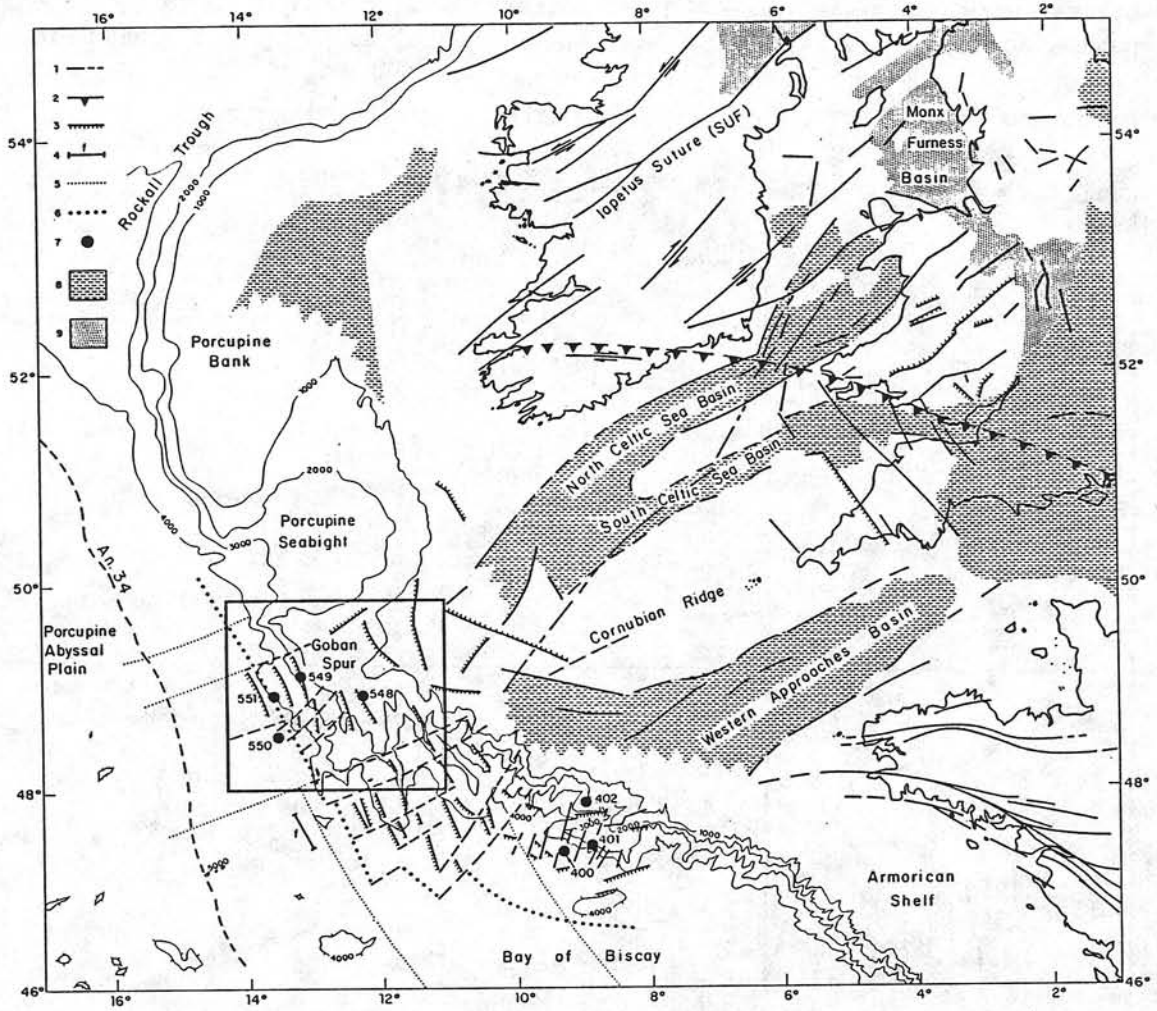


Figure 2 : Carte générale de l'Europe du Sud-Ouest et des marges adjacentes. La bathymétrie est en mètres (Lallemand et al., 1985a et b). Signification des symboles : 1) failles d'après Sibuet et al. (1984) ; 2) front varisque ; 3) failles normales ou listriques ; 5) directions d'ouverture de l'Atlantique Nord et du Golfe de Gascogne (Olivet et al., 1984) ; 6) limite continent-océan ; 7) sites de forages des legs DSDP 48 et 80 ; 8) limite des bassins jurassiques ; 9) bassins triasiques.

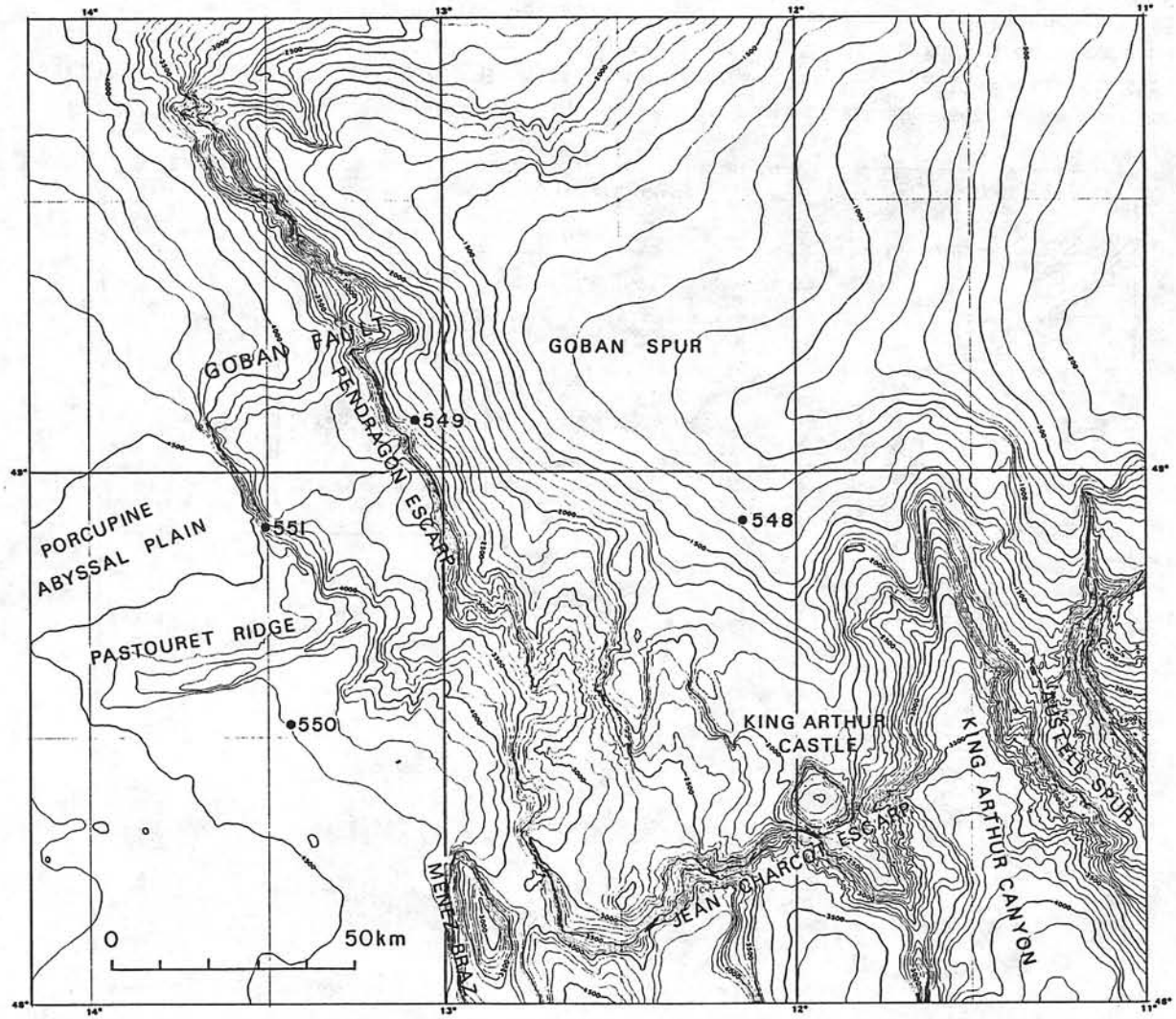


Figure 3 : Carte bathymétrique de la marge de l'éperon de Goban (Sibuet et al., 1984) correspondant au cadre de la figure 2. Elle a été établie à partir de l'ensemble des données bathymétriques Sea-beam et conventionnelles disponibles ainsi que des données GLORIA. Les profondeurs sont en mètres (1500 m/s). L'intervalle de contourage est de 100 m. Les sites de forages du leg DSDP 80 sont indiqués.

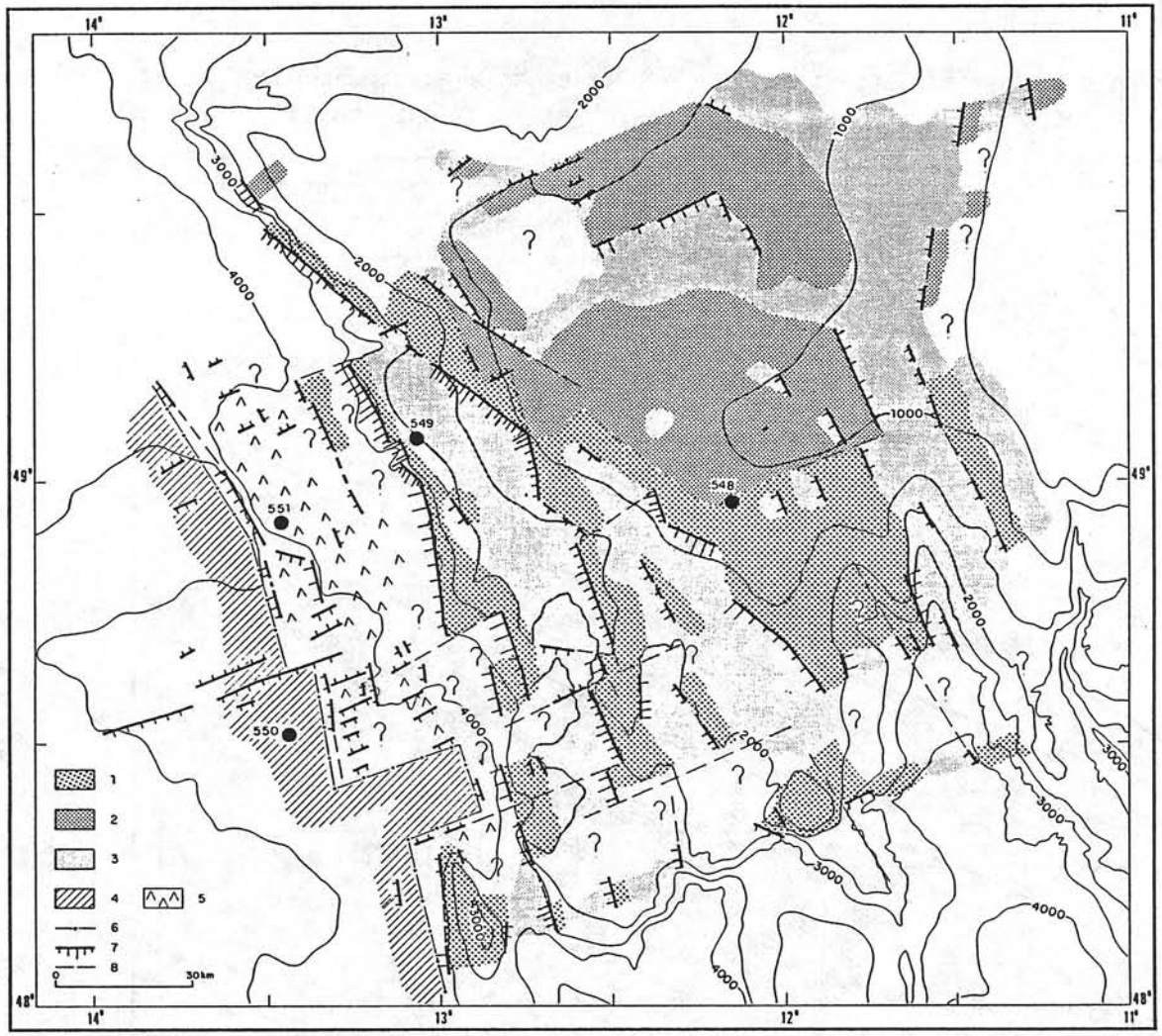


Figure 4 : Schéma structural de la marge de l'éperon de Goban (Sibuet et al., en préparation) établi en utilisant toutes les données sismiques disponibles (figure 5). Bathymétrie simplifiée de la figure 3. Signification des symboles : 1) socle paléozoïque ; 2) socle antérift indifférencié ; 3) bassins synrifts ; 4) Domaine océanique ; 5) épanchements volcaniques en domaine continental aminci ; 6) limite continent-océan ; 7) failles normales avec indications de l'amplitude du rejet vertical ; 8) failles transverses.

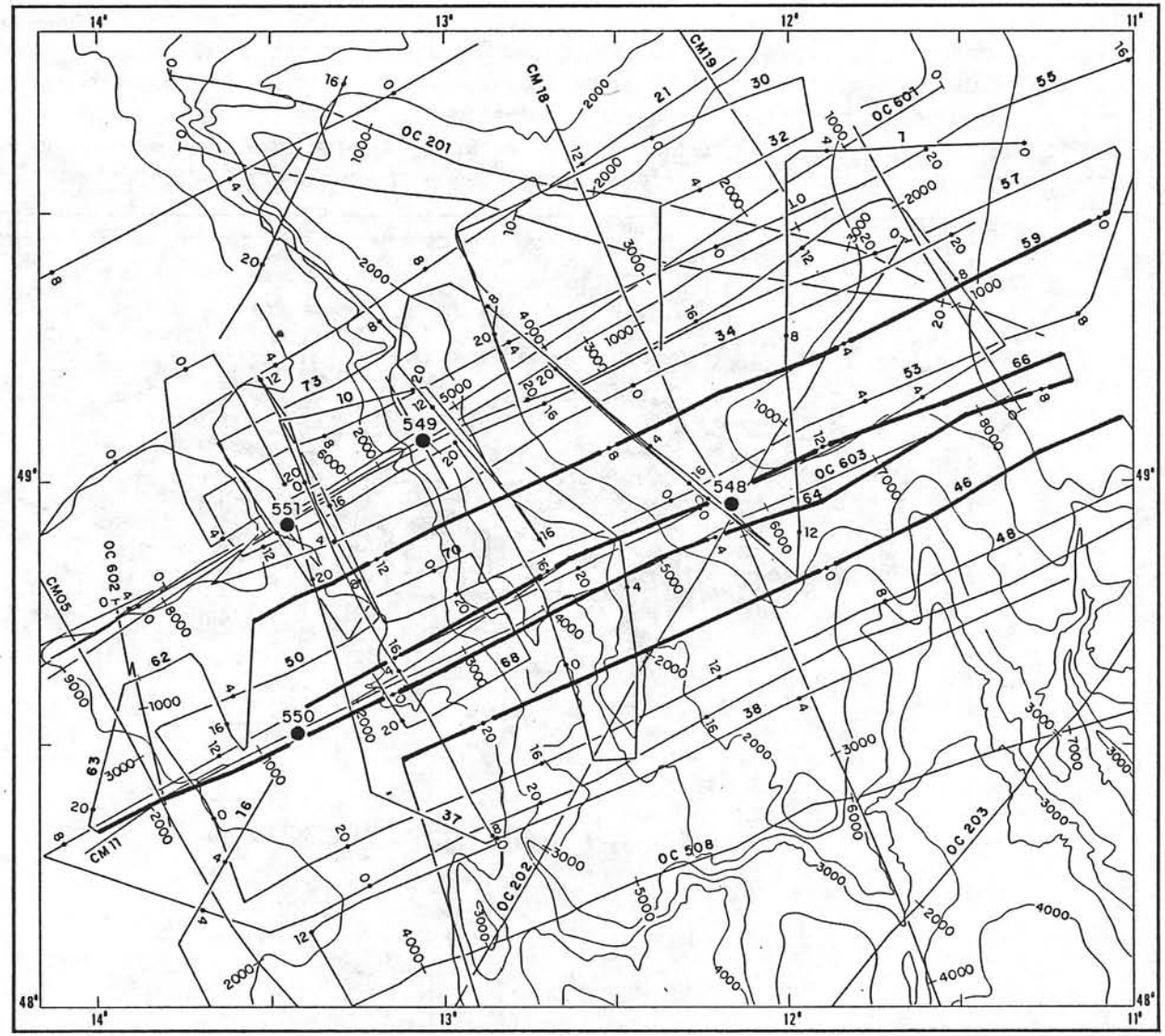


Figure 5 : Plan de position des profils sismique monotrace et multitrace (profils OC et CM) utilisés pour établir la carte structurale de la figure 4. Localisation des profils de la figure 6 en traits gras.

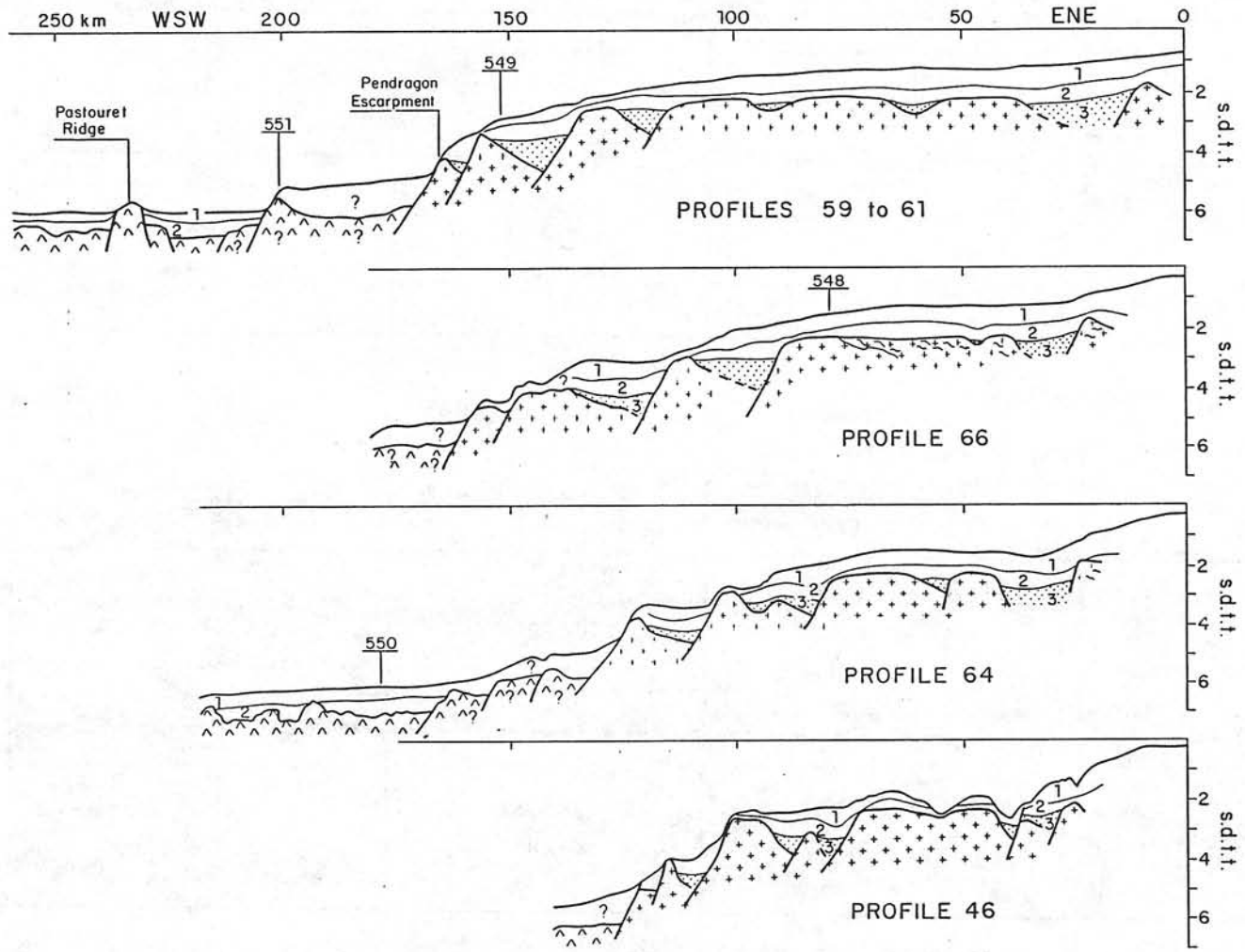


Figure 6 : Interprétation de 4 profils sismiques obtenus perpendiculairement à la marge de l'éperon de Goban. Exagération verticale : 10. Localisation des profils sur la figure 5. Signification des symboles : unité acoustique 1, Actuel à Oligocène supérieur ; unité acoustique 2, Oligocène inférieur à Albien moyen ; unité acoustique 3, Albien moyen à Crétacé inférieur (séries synrifts) ; +, socle continental ; ^, croûte océanique ou volcanisme en domaine continental aminci.

| | Failles normales | Failles de cisaillement | Autres failles avec composante de cisaillement | Rift (limite continent-océan) |
|---|---|---|---|---|
| Marge de l'éperon de Goban | 161±7° (16 val.) | 68°±2° (9 val.) | 132°±7° (4 val.) | 162°±9° (5 val.) |
| Marge celtique | 115°±12° (20 val.) | 24°±7° (13 val.) | 83°±4° (9 val.) | entre 100° et 138° |
| Marge armoricaine | / | / | 20-30° 40° 60° (Lallemand et Sibuet, 1986) | 135° |
| Marge nord_espagnole | 62°±6° (12 val.) | 133°±2° (6 val.) | / | 95° |
| Marge ouest_ibérique | 3°±6° | / | 69°±3° 58°±3° | 0° |

Table 1 : directions des failles et du rift sur les marges de l'Atlantique Nord-Est, avec nombre de mesures correspondant à chaque famille d'accidents et écart-type.

La limite continent-océan suit probablement le pied de la ride topographique en bas de pente qui avait été interprétée comme un bloc basculé érodé dans sa partie sommitale avant les forages du leg 80 (de Graciansky, Poag et al., 1985a). Les résultats du site 551 (de Graciansky, Poag et al., 1985b) ont montré l'existence sur la ride d'une coulée basaltique plane sous la craie du Cénomanien supérieur. Une anomalie magnétique dipolaire allongée de forte amplitude, associée à cette coulée basaltique, définit son extension latérale (figure 7). Cette coulée s'est mise en place à la fin de l'épisode de rifting dans le demi-graben limité par les deux rides topographiques en bas de pente (figure 4). Une vitesse de 5,5 km/s est attribuée à ce corps volcanique à partir des données de sismique réfraction obtenues à l'aide de sonobouées mises en oeuvre au cours de la campagne Norestlante II (Sibuet et al., en préparation).

Le profil WAM, réalisé en 1985 dans le cadre des programmes BIRPS et ECORS, passe par le site 551 et est orienté perpendiculairement à la direction de la marge. Il montre que cette coulée volcanique s'est probablement propagée vers le Nord-Est à partir de centres d'émission localisés au niveau de la dernière ride topographique (figure 8). Aucun réflecteur n'est observé au sein de cette ride. En revanche, une croûte inférieure litée, ayant les mêmes caractéristiques lithologiques qu'en mer Celtique (Cheadle et al., 1986), existe sous la ride mais disparaît

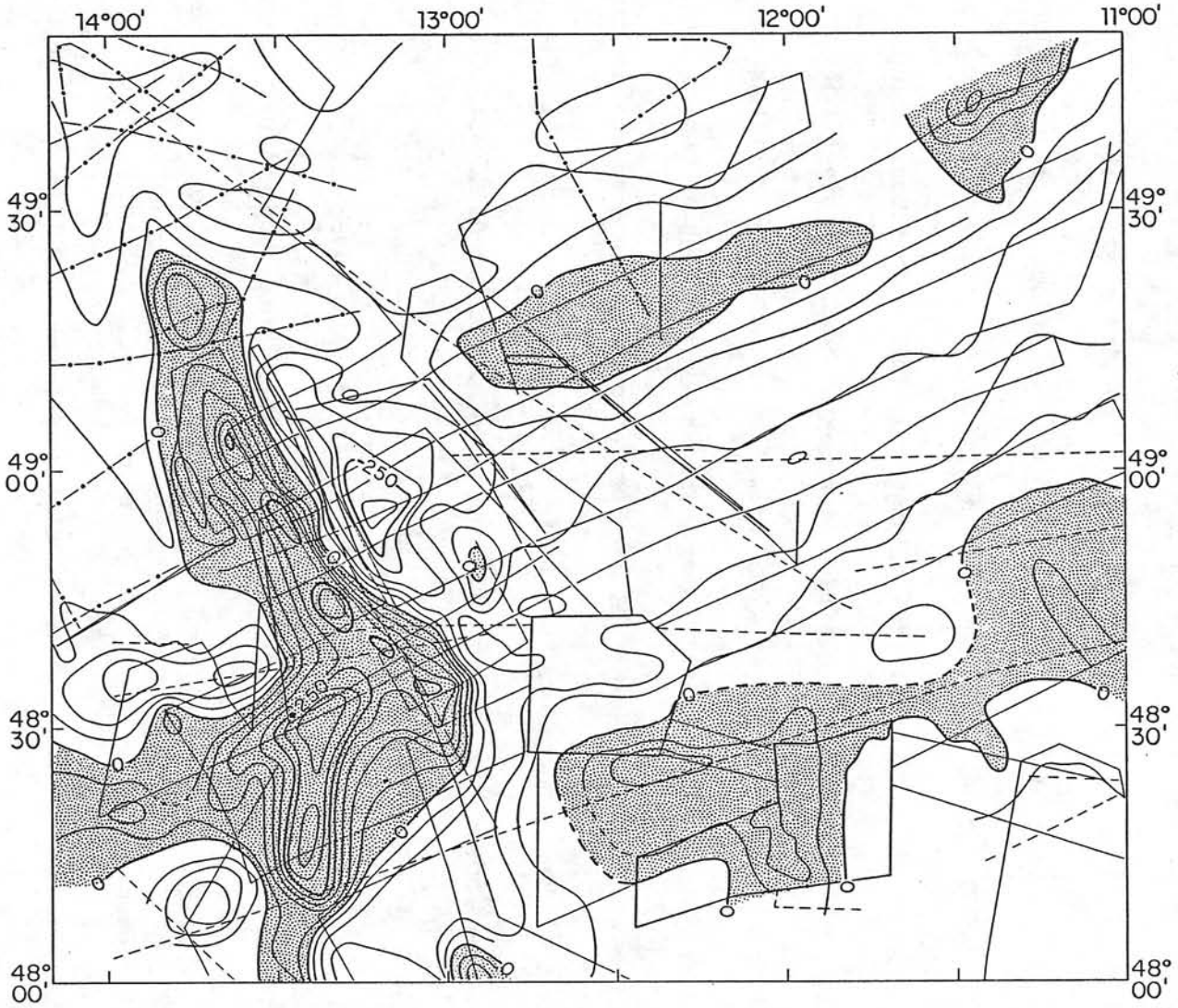


Figure 7 : Carte des anomalies du champ magnétique terrestre réduites par l'IGRF 1980 et localisation des profils utilisés. L'intervalle de contourgae est de 50 nT. Les anomalies positives sont en gris. L'extension horizontale du volcanisme entre les deux derniers blocs basculés de bas de marge (représentée sur la figure 4) est marquée par une anomalie dipolaire allongée.

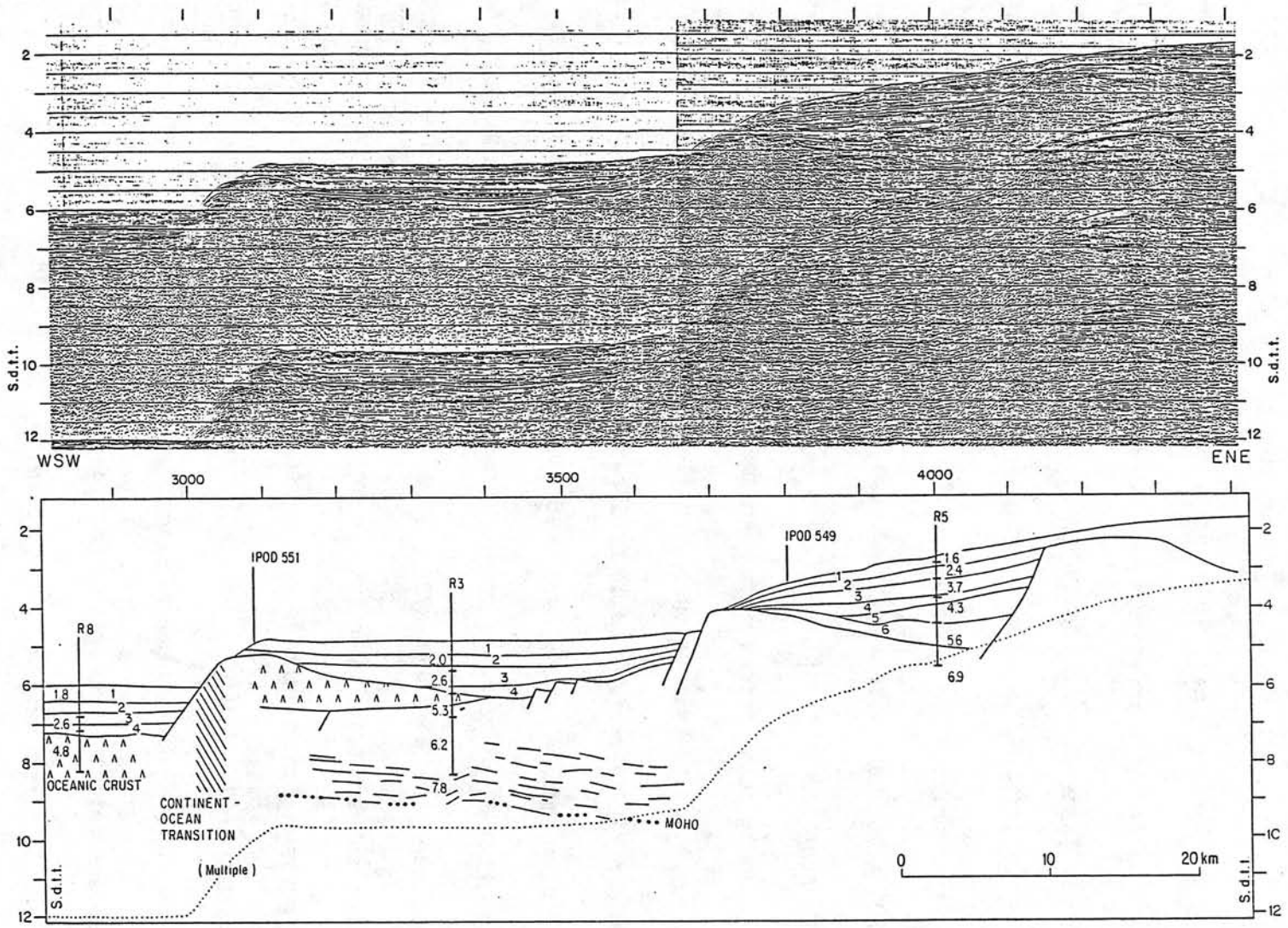


Figure 8 : Profil sismique WAM (Western Approaches Margin) réalisé par les groupes BIRPS et ECORS et passant par les sites de forages 549 et 551. Seule la section correspondant aux trois blocs basculés les plus profonds est montrée. Noter la géométrie du corps volcanique dont les centres d'émission sont au niveau du dernier bloc basculé et la présence d'une croûte inférieure litée entre les deux derniers blocs basculés.

à la limite continent-océan proposée (figure 4). Cette ride ferait donc encore partie du domaine continental aminci et serait un bloc basculé largement affecté par un volcanisme de type "haut marginal", souvent décrit dans la littérature, et mis en place dans la partie profonde du bassin, juste avant la séparation des continents.

La limite continent-océan (figure 4) correspond à une série de segments orientés N162° (table 1), décalés par des zones de fractures marginales. Les directions de l'axe du rift (R) et des failles normales (NF) sont donc voisines ; les failles de cisaillement (F), peu nombreuses, sont approximativement perpendiculaires aux failles normales (figure 9). L'application, triviale ici, de la méthode de Withjack et Jamison (1986) montre que le déplacement entre les côtés opposés du rift (ici les marges de l'éperon de Goban et Nord-Américaine), et la direction $\epsilon_{H1}$ de la plus grande déformation horizontale en tension, sont confondues et orientées N72°. La marge de l'éperon de Goban est donc une marge en extension pure ($\alpha$ = 90°). Les zones de fractures en domaine océanique étant orientées N70° entre la limite continent-océan et l'anomalie 34 (Sibuet et al., 1984), la direction du mouvement de l'Amérique du Nord par rapport à l'Europe est donc constante (N70°) du Crétacé inférieur au Crétacé supérieur, c'est-à-dire au cours du rifting et de la formation du domaine océanique le plus ancien.

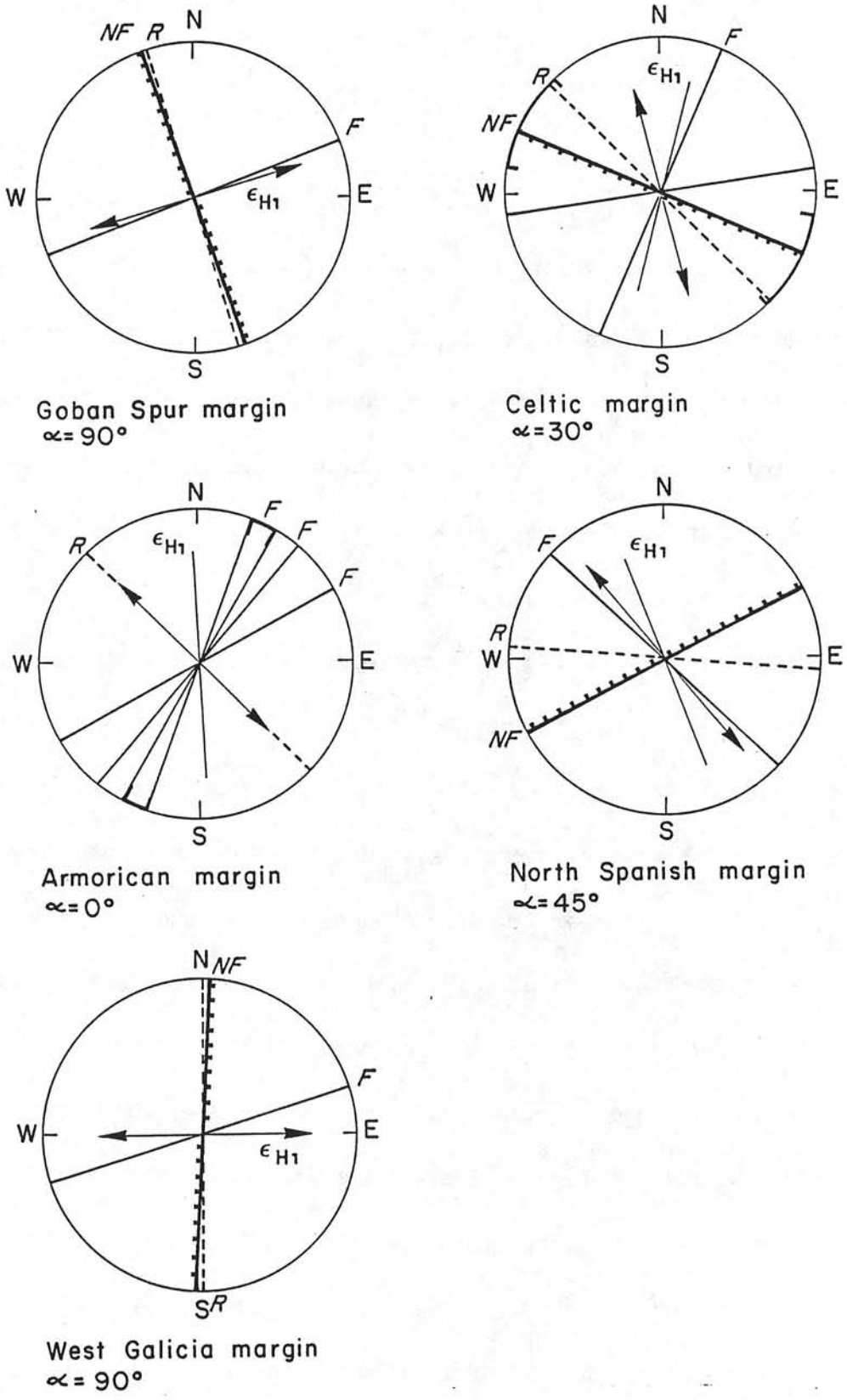


Figure 9 : Diagrammes de Withjack et Jamison (1986) correspondant aux différentes marges de l'Atlantique Nord-Est (table 1). Même légende des symboles que dans la figure 1.

**b) la marge celtique**

La marge celtique a été particulièrement étudiée au cours des phases de préparation puis d'exploitation du leg DSDP 48 (e.g. Montadert, Roberts et al., 1979 ; Montadert et al., 1979). Elle résulte du mouvement relatif des plaques Europe et Ibérie mais présente une structure générale moins cylindrique que celle de la marge de l'éperon de Goban (Lallemand et al., 1985a et b). Elle a été créée par amincissement crustal au cours de la phase de rifting qui aurait commencé au Jurassique supérieur - Crétacé inférieur et se serait terminée au Barrémien, du fait de l'absence de l'anomalie J dans le golfe de Gascogne, ou à l'Albien d'après Montadert et al. (1979).

La carte structurale détaillée de la figure 10 a été établie à partir de l'ensemble des données de sismique réflexion disponibles en 1978 (Montadert et al., 1979). La marge celtique est caractérisée par la présence d'une série de blocs basculés limités par des failles normales orientées N115° entre les longitudes 9° et 10°W (table 1). Entre les longitudes 8 et 9°W, les failles orientées N83° (table 1) limitent les bordures des escarpements de Meriadzek et de Trevelyan. Elles ont été réactivées au cours de la phase de compression pyrénéenne, les rejeux verticaux pouvant atteindre 1500 m dans le canyon de Shamrock (Pastouret et al., 1981). Des failles normales appartenant à la famille de

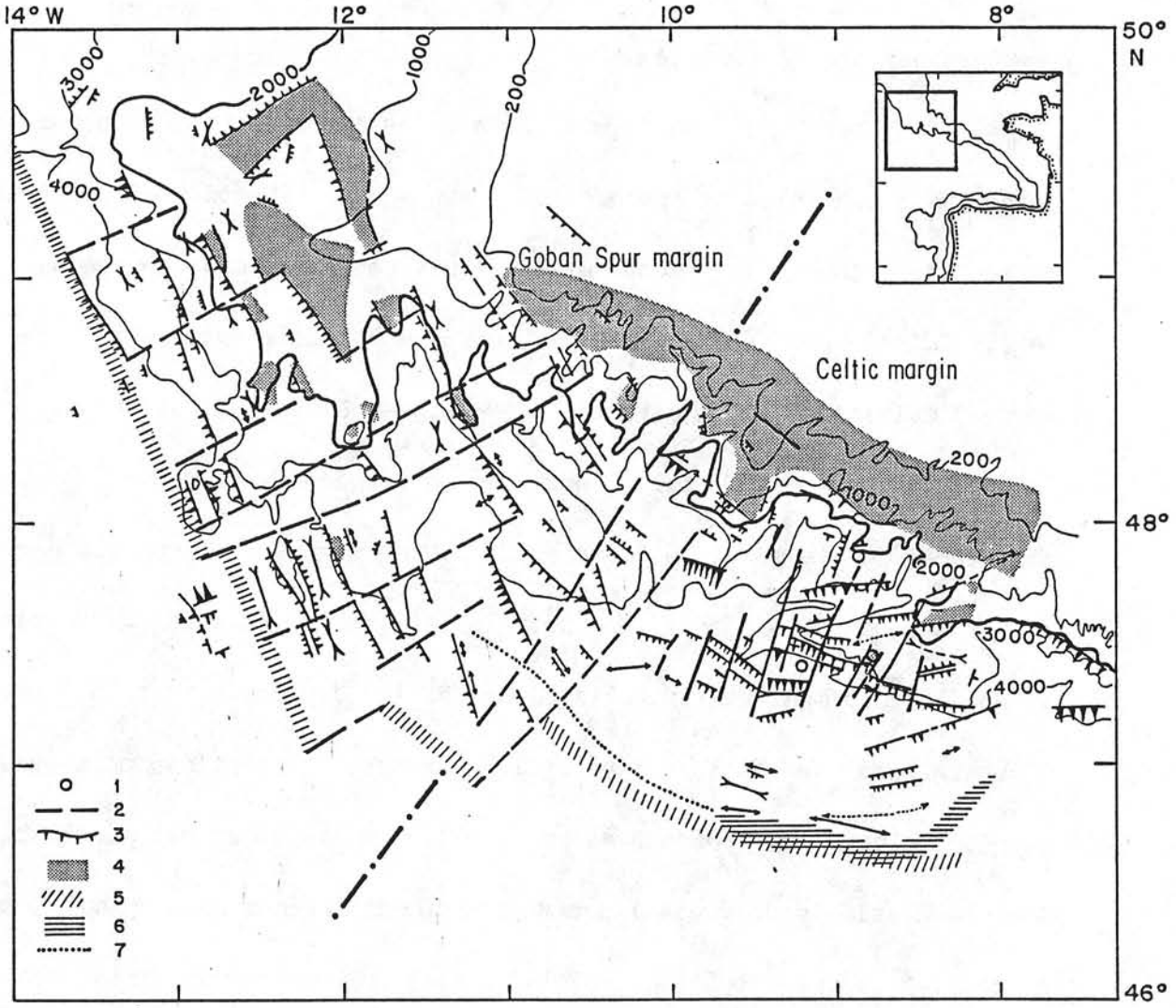


Figure 10 : Schéma structural des marges de l'éperon de Goban et celtique (d'après Montadert et al., 1979) montrant la distribution géographique des surfaces d'érosion. Légende des symboles : 1) sites des forages DSDP ; 2) failles transverses ; 3) failles normales ; 4) surfaces d'érosion Crétacé inférieur ; 5) limite continent-océan ; 6) compression Tertiaire inférieur ; 7) plis ou failles Tertiaire inférieur.

directions N115° existent également dans ce secteur. Nous supposons donc que les failles normales de la marge celtique sont essentiellement représentées par la famille N115°.

Le schéma de la figure 10 fait ressortir un réseau de failles transverses sensiblement perpendiculaires à la direction générale des marges de l'éperon de Goban et celtique. La plus grande partie de ces failles n'ont pas été observées sur les profils sismiques obtenus perpendiculairement à la direction des marges. Elles ont été déduites de la répartition des failles normales observées. Le nouveau schéma structural de la marge de l'éperon de Goban (figure 4), établi à partir de l'ensemble très dense de profils sismiques (figure 5) obtenus perpendiculairement et parallèlement à la direction de la marge, illustre bien le fait que les failles transverses sont peu nombreuses. De plus, lorsqu'un réseau serré de lignes sismiques est disponible, Chenet et al. (sous presse) ont montré que très souvent il n'existe pas de failles perpendiculaires à la direction des rifts continentaux décalant les extrémités des failles normales en-échelon. Il en est probablement de même pour la marge celtique où le réseau de failles transverses orientées N24° (table 1) est certainement moins développé qu'il n'apparaît sur la figure 10.

La limite continent-océan, identifiée à partir de quelques profils de sismique réflexion et de magnétisme, est assez mal définie

(entre N100° et N138°, table 1).

Les diagrammes de Withjack et Jamison (1986) suggèrent que l'angle $\alpha$ est voisin de 30° (figure 9). La direction adoptée pour le rift (N135°) est alors proche d'une des bornes extrêmes (table 1). Au cours du rifting, le mouvement de la marge nord-espagnole par rapport à la marge celtique aurait suivi la direction N165° et la direction $\varepsilon_{H1}$ de la plus grande déformation horizontale en tension serait N15°.

**c) la marge armoricaine**

Contrastant avec les marges celtique et de l'éperon de Goban, la marge armoricaine présente une pente continentale abrupte. Linéaire sur 300 km de longueur, elle est orientée N135°. Elle a été interprétée par Le Pichon et al. (1971) comme une marge en cisaillement, du fait de son parallèlisme avec les directions d'ouverture du domaine océanique adjacent. La pente continentale étant abrupte, les blocs basculés ne sont réellement observés que dans la partie inférieure de la marge où ils sont enfouis sous les sédiments postrifts, (Barbier et al., 1986 ; Le Pichon et Barbier, 1987). L'orientation des blocs basculés n'est donc pas directement accessible. Cependant, une étude statistique de la direction des canyons (Lallemand et Sibuet, 1986) montre que la plupart des canyons suivent les directions N20°-30°, N40° et N60° (figure 11,

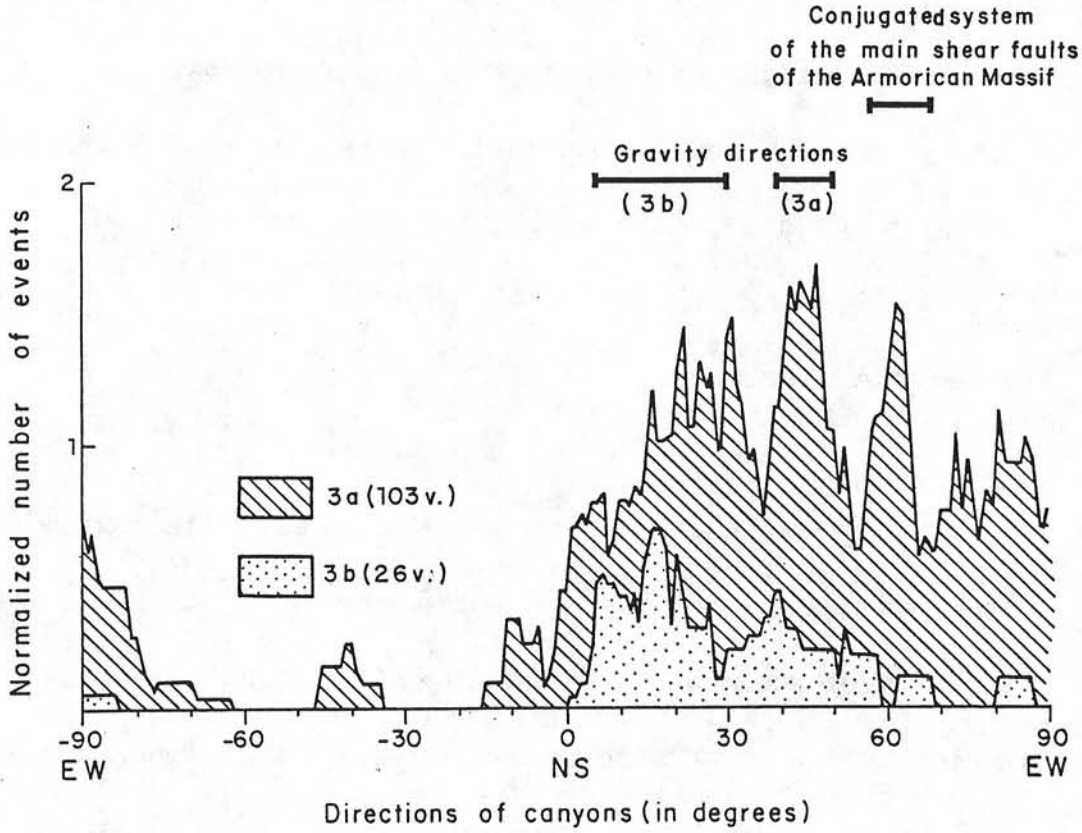


Figure 11 : Directions des canyons sur la marge armoricaine. Les zones 3a et 3b correspondent aux portions de marges orientées respectivement N135° (la plus grande partie de la marge armoricaine) et N110° (au nord du plateau des Landes). Les directions gravitaires correspondent aux lignes de plus grande pente. Le nombre normalisé d'événements est la fréquence des longueurs cumulées de segments de canyons exprimée en fonction de la direction des canyons (Lallemand et Sibuet, 1986).

table 1). Les directions N20°-30° et N40° sont des directions de plus grande pente et pourraient être d'origine gravitaire. La direction N60° pourrait correspondre à des failles avec composante de cisaillement. La limite continent-océan est orientée N135° (Derégnaucourt et Boillot, 1982) parallèlement à la direction générale de la marge armoricaine.

Les diagrammes de Withjack et Jamison (1986) suggèrent que $\alpha$ = 0° (cisaillement pur, figure 9). Les directions observées N40° et N60° correspondent au secteur des failles de cisaillement dextre des modèles expérimentaux et analytiques de Withjack et Jamison (1986, figure 1). La direction de plus grande pente N40° serait donc également une direction structurale. Au cours du rifting le mouvement de la plaque Ibérie par rapport à la plaque Europe aurait suivi la direction N135° et la direction $\epsilon_{H1}$ de la plus grande déformation horizontale en tension serait N178°.

**d) la marge nord-espagnole**

La marge nord-espagnole, globalement orientée E-W, était l'homologue de la marge celtique avant l'ouverture du golfe de Gascogne. Elle a été reprise au cours du Tertiaire inférieur par la tectonique compressive liée à la phase pyrénéenne avec formation du fossé marginal nord-espagnol (e.g. Sibuet et Le Pichon, 1971 ; Boillot et al., 1979).

Elle présente une pente continentale abrupte qui contraste avec la morphologie de la marge celtique. Les directions principales de fractures, généralement attribuées à la tectonique hercynienne ou tardi-hercynienne, ont été reprises au cours du rifting puis lors des phases de compression tertiaire, comme l'ont montré les plongées du submersible Cyana (groupe Cybère, 1984). C'est ainsi que les failles normales qui se sont développées lors de l'épisode de rifting ont rejoué en failles inverses au cours de la compression Eocène (figure 12 ; Témine, 1984). Leur direction est N62° (table 1) dans la région de la figure 12. La même direction caractérise ce type d'accidents tout le long de la marge nord-espagnole et guide le cheminement des canyons (figure 13, Lallemand et Sibuet, 1986). Les failles transverses sont orientées N133° (table 1). La limite continent-océan actuelle, située au pied de la pente continentale, ne correspond plus à la limite continent-océan initiale. En l'absence d'indication précise, nous prenons donc comme direction du rift la direction générale N95° de la portion occidentale de la marge nord-espagnole.

Les diagrammes de Withjack et Jamison (1986) suggèrent que $\alpha$ = 45° (figure 9). Au cours du rifting, le mouvement de la plaque Europe par rapport à la plaque Ibérie aurait donc suivi la direction N140° et la direction $\epsilon_{H1}$ de la plus grande déformation horizontale en tension

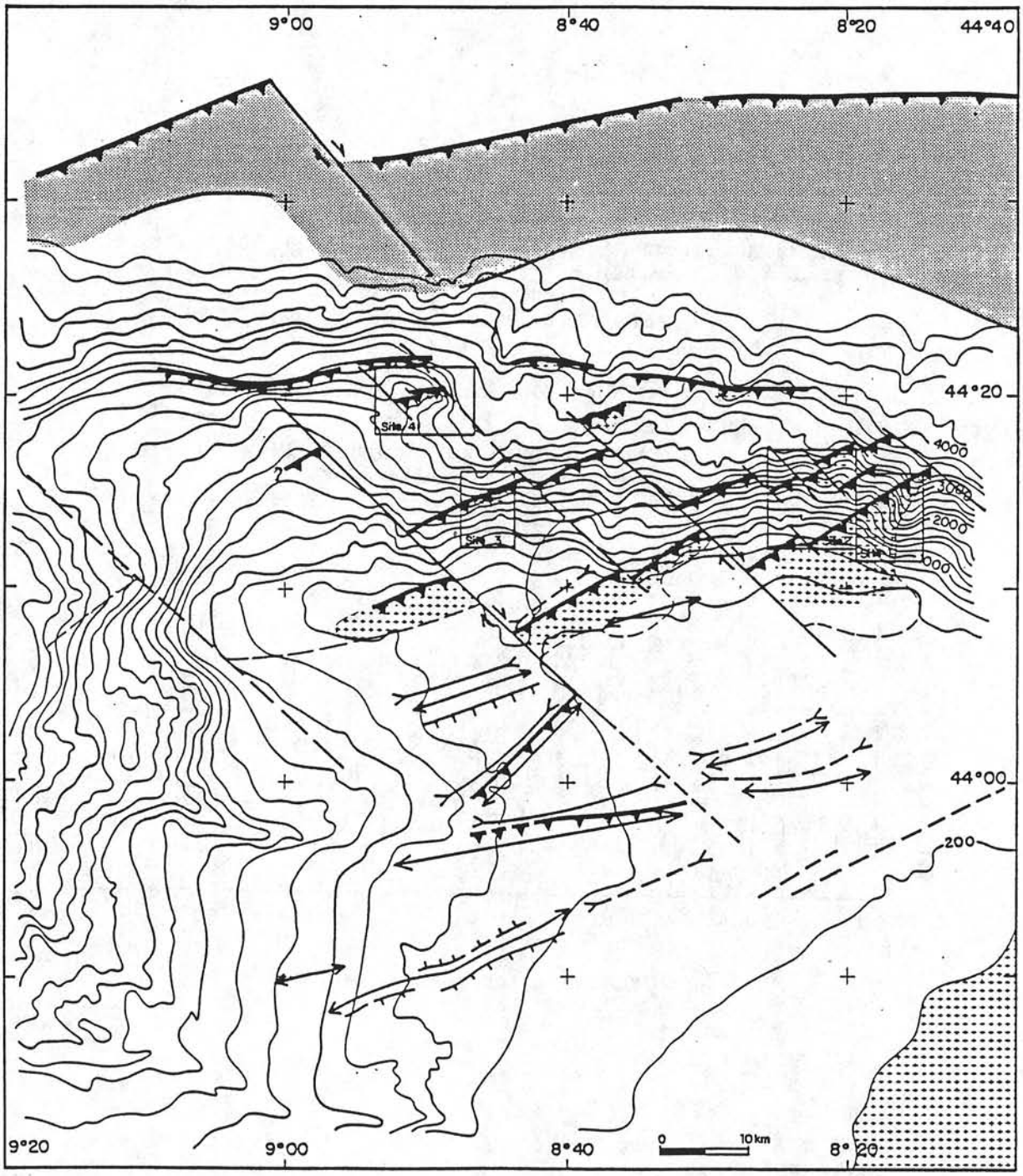


Prisme d'accrétion tectonique

Zone de socle

Faille normale

Faille inverse

Décrochement

Axe synclinal

Axe anticlinal

Figure 12 : Schéma structural interprétatif du plateau et de la pente continentale du promontoire d'Ortégal (marge nord-espagnole) d'après Témine (1984).

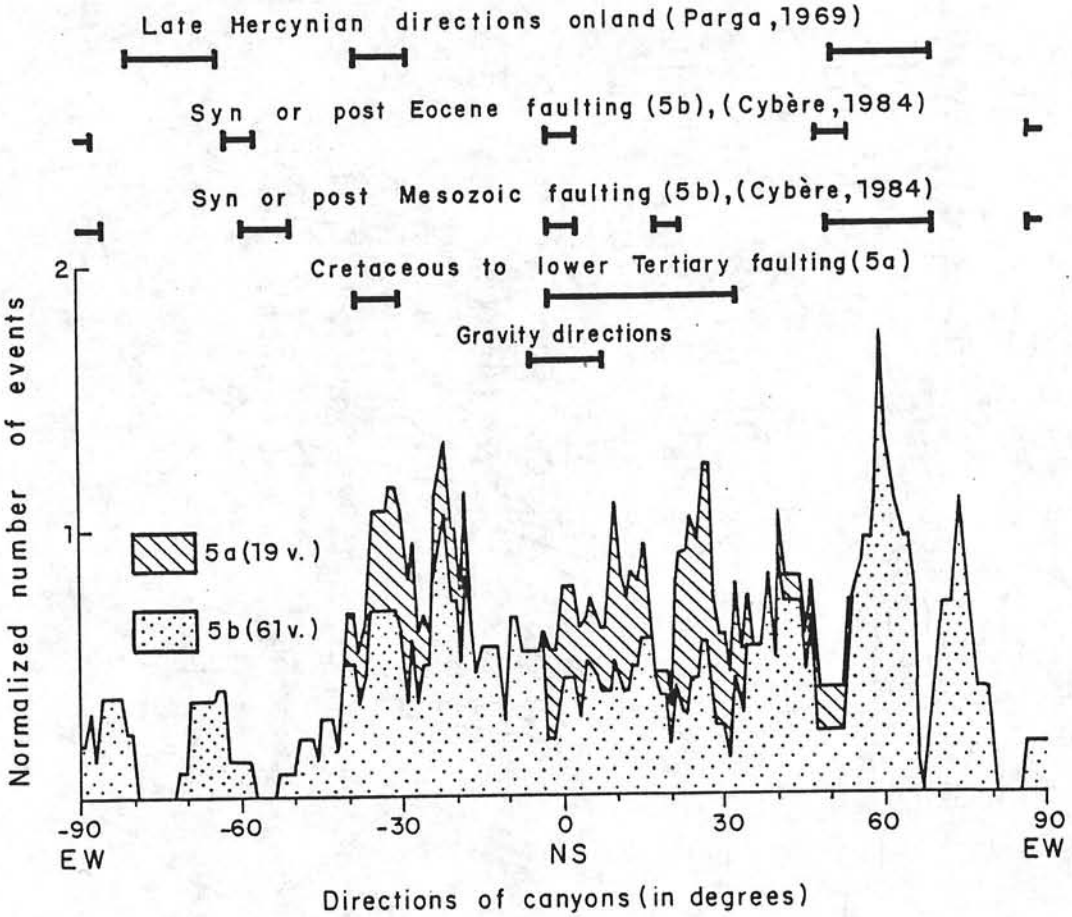


Figure 13 : Directions des canyons sur la marge nord-espagnole. Les zones 5a et 5b correspondent aux portions de marges respectivement au Sud et à l'Ouest du plateau des Landes. Les directions gravitaires correspondent aux lignes de plus grande pente. Le nombre normalisé d'événements est la fréquence des longueurs cumulées de segments de canyons exprimée en fonction de la direction des canyons (Lallemand et Sibuet, 1986).

serait N 160°.

**e) la marge ouest-ibérique**

La marge ouest-ibérique (figure 14a), située au sud-ouest du banc de Galice sensu stricto, a fait l'objet de nombreuses campagnes océanographiques, notamment dans le cadre de la préparation et de la valorisation des forages IPOD (leg 47B, Sibuet, Ryan et al., 1979) et ODP (leg 103, Boillot et al., 1985, 1986a). L'épisode de rifting est daté Jurassique supérieur à Barrémien-Aptien inférieur. Il se décomposerait en deux phases de rifting distinctes (Mauffret et Montadert, 1987). Cette marge est caractérisée par une série de blocs basculés orientés nord-sud, à forte extension latérale (50 km). Les failles normales limitant les blocs basculés sont orientées N3° (figure 14b, table 1). Dans le voisinage de la transition continent-océan, des péridotites ont été draguées (Boillot et al., 1980) et forées (Boillot et al., 1985, 1986a) sur une structure topographique orientée nord-sud et se prolongeant vers le nord jusqu'à la pente continentale du banc de Galice, où les mêmes péridotites ont été draguées (figure 14a, Sibuet et al., 1987) et prélevées par submersible (Boillot et al., 1986b). Quelques rares failles transverses, orientées N58° à N69° (figure 14b, table 1) décalent très faiblement les blocs basculés de la marge

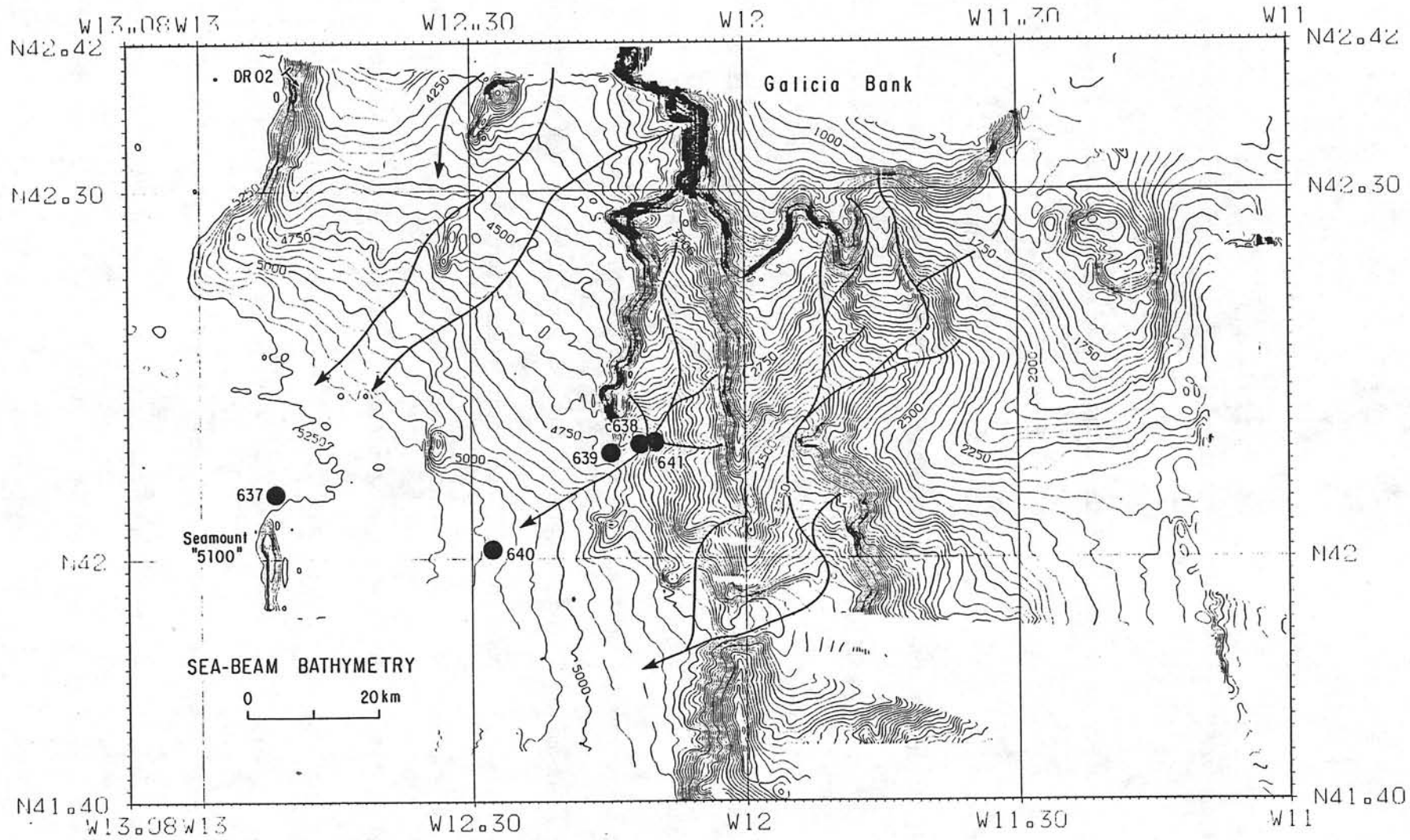


Figure 14a : Carte bathymétrique Sea-beam de la marge ouest-ibérique. Les profondeurs sont en mètres (1500 m/s). L'intervalle de contourage est de 50 m. Les sites de forages ODP sont indiqués. Le tracé des principaux canyons est figuré.

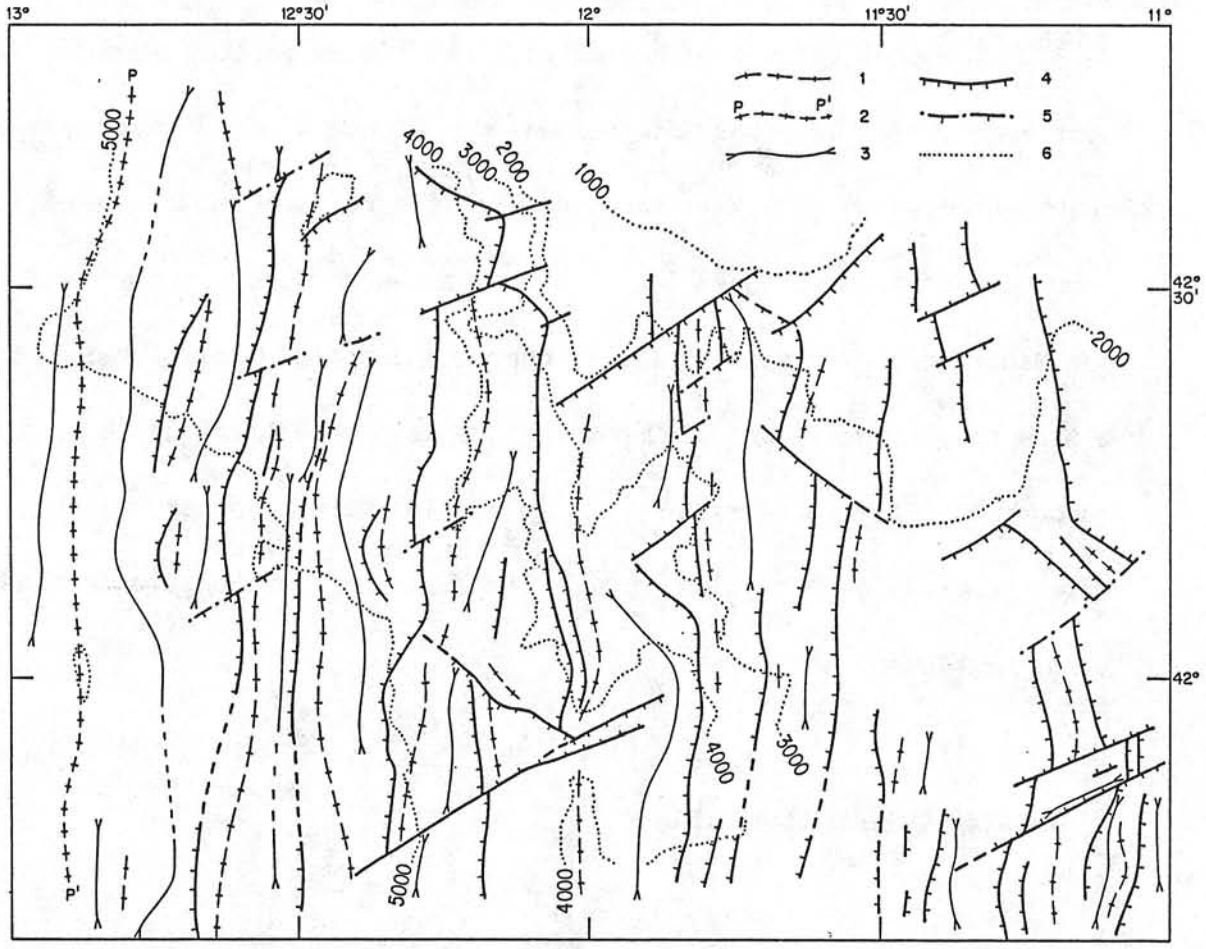


Figure 14b : Schéma structural de la marge ouest-ibérique (Thommeret, communication personnelle, 1987) établi en utilisant toutes les données sismiques disponibles. Signification des symboles : 1) sommet des blocs basculés ou rides ; 2) sommet de la ride de péridotite ; 3) axe des bassins ; 4) failles normales ; 5) failles transverses ; 6) bathymétrie simplifiée.

(Thommeret, communication personnelle, 1987). Si nous supposons, en première approximation, que la ride de péridotites correspond à la limite continent-océan, l'orientation du rift est nord-sud (table 1).

Les directions de l'axe du rift (R) et des failles normales (NF) sont donc voisines. Les diagrammes de Withjack et Jamison (1986) suggèrent que $\alpha = 90°$ (extension pure, figure 9). Au cours du rifting (nous supposons ici que les deux phases tectoniques mises en évidence par Mauffret et Montadert (1987) correspondent aux mêmes directions de contraintes principales), le mouvement de la plaque Amérique du Nord par rapport à l'Ibérie aurait donc suivi la direction est-ouest, et la direction $\epsilon_{H1}$ de la plus grande déformation horizontale en tension serait également est-ouest.

2) Discussion des résultats

Les résultats concernant les marges de l'Atlantique Nord-Est sont récapitulés dans la table 2 et sur la figure 15. Tous les types de marges sont représentés, depuis les marges en extension pure ($\alpha = 90°$, marges de l'éperon de Goban et ouest-ibérique) jusqu'aux marges en cisaillement pur ($\alpha = 0°$, marge armoricaine), en passant par les marges à rifting oblique ($\alpha = 30°$, marge celtique ; $\alpha = 45°$, marge nord-espagnole). Les directions d'ouverture des domaines océaniques du golfe

| | $\alpha$ | $\epsilon_{H1}$ | A |
|---|---|---|---|
| Marge de l'éperon de Goban | 90° | N73° | N73° |
| Marge celtique | 30° | N16° | N166° |
| Marge armoricaine | 0° | N178° | N135° |
| Marge nord-espagnole | 45° | N160° | N140° |
| Marge ouest-ibérique | 90° | N90° | N90° |

Table 2 : valeurs de $\alpha$ (angle aigu entre la direction R du rift et la direction de déplacement de la marge homologue par rapport à la marge considérée), $\epsilon_{H1}$ (direction de la plus grande déformation horizontale en tension) et A (direction du déplacement relatif des plaques au cours de l'épisode de rifting par rapport à la marge considérée).

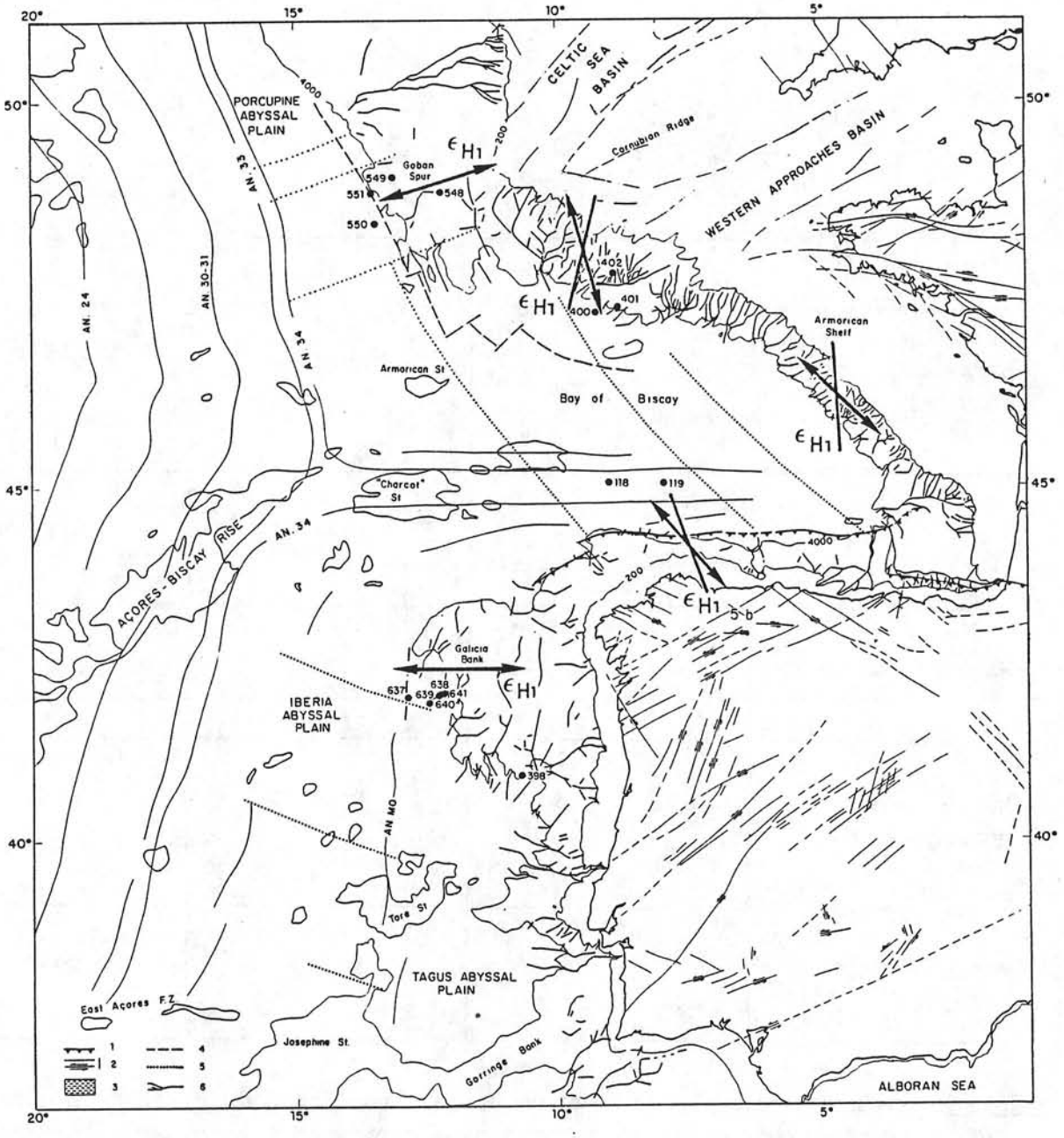


Figure 15 : Schéma structural général de l'Atlantique Nord-Est et linéations magnétiques en domaine océanique (Sibuet et al., 1987). Signification des symboles : 1) front de chevauchement nord-ibérique ; 2) failles tardi-hercyniennes ; 4) limite continent-océan ; 5) directions d'ouverture de l'Atlantique Nord-Est et du golfe de Gascogne ; 6) tracé des canyons sur les marges continentales. Les flèches et les segments en trait gras représentent respectivement la direction du déplacement relatif des plaques au cours de l'épisode de rifting par rapport à la marge considérée et la direction de la plus grande déformation horizontale en tension (table 2).

de Gascogne et de l'Atlantique Nord-Est sont reportées sur la figure 15 (Lallemand et Sibuet, 1986). On constate que les directions du déplacement relatif des plaques, au cours du rifting, par rapport à la plaque où se situe la marge considérée, sont sensiblement parallèles aux directions d'ouverture du domaine océanique adjacent, à l'exception de la marge ouest-ibérique où l'angle entre ces deux directions est d'une vingtaine de degrés.

Cette correspondance est remarquable pour la marge de l'éperon de Goban (N73°, comparable à la direction N70° des zones de fractures océaniques) et pour les marges du golfe de Gascogne. Lallemand et Sibuet (1986) ont montré, à partir des directions des accidents antérieurs à la phase de rifting, que la rotation de l'Ibérie par rapport à l'Europe (depuis le Jurassique terminal) était voisine de 23°. Les marges celtique et nord-espagnole étant homologues, la direction du mouvement le long de la marge nord-espagnole avant la phase de rifting serait de 140° + 23° = 163°, à comparer avec la direction N166° correspondant à la marge celtique.

De même, comme l'avaient montré Le Pichon et al. (1971), la direction du mouvement le long de la marge armoricaine est parallèle à la direction de la marge et à la direction d'ouverture du domaine océanique adjacent. Si les mouvements de l'Amérique du Nord et de l'Ibérie par rapport à l'Europe se font dans la même direction, au cours

de la phase de rifting et au cours de la première phase d'accrétion océanique, il doit en être de même pour le mouvement de l'Amérique du Nord par rapport à l'Ibérie. Or, il existe un angle d'environ 20° (figure 15) entre les directions d'ouverture correspondant à la phase de rifting et à l'accrétion océanique (paramètres de Olivet et al., 1984). Cette différence n'est peut-être pas significative, eu égard aux limites de la méthode utilisée. Elle pourrait toutefois résulter d'un mouvement anti-horaire du banc de Galice par rapport à l'Ibérie, au cours de la phase de rifting, entraînant la formation du bassin intérieur situé entre le banc de Galice et le plateau continental espagnol. Cette hypothèse pourrait expliquer l'existence de deux épisodes distincts de rifting (Oxfordien-Kimméridgien inférieur à Valanginien et Valanginien à Hauterivien) bien qu'il ne soit pas possible d'affirmer qu'il y ait eu changement de direction de l'extension d'une phase à l'autre (Mauffret et Montadert, 1987).

La direction de la plus grande déformation horizontale en tension $\epsilon_{H1}$ rapportée à la plaque Europe est de N16° pour la marge celtique, N178° pour la marge armoricaine et de N3° (N160° + 23°) pour la marge nord-espagnole. La valeur moyenne de $\epsilon_{H1}$ est N6°, c'est-à-dire approximativement nord-sud pour les marges du golfe de Gascogne, au cours de l'épisode de rifting. En ce qui concerne les marges en extension pure de l'éperon de Goban et ouest-ibérique, $\epsilon_{H1}$ est

perpendiculaire à la direction générale des marges et de leurs blocs basculés.

Une limitation importante de la méthode est qu'elle ignore l'hétérogénéité de la croûte continentale. Lallemand et Sibuet (1986) ont montré que les directions structurales anciennes étaient reprises au cours de la phase de rifting. La déformation de la croûte continentale fragile peut donc être différente de celle du matériau homogène des modèles. De plus, la direction du rift n'est pas forcément identique à la direction de la limite continent-océan. Malgré ces limitations, la cohérence des résultats obtenus sur les marges des golfes de Californie et d'Aden (Withjack et Jamison, 1986) et de l'Atlantique Nord-Est est satisfaisante.

Les directions du mouvement des plaques Amérique du Nord et Ibérie par rapport à l'Europe sont donc les mêmes au cours du rifting crétacé inférieur et au cours de la phase initiale de formation du domaine océanique ancien. Ceci conforte l'approche de Olivet et al. (1984) qui, sur la base d'arguments de cohérence des mouvements cinématiques à l'échelle de l'océan Atlantique, ont montré qu'il est impossible que le mouvement de l'Ibérie par rapport à l'Europe suive, au cours de la phase de rifting, une direction très différente de celle de l'ouverture océanique. Le mouvement de l'Ibérie vers le sud-ouest au cours de la phase de rifting, proposé par Bacon et Gray (1970) et repris

par Boillot (1984), n'existe pas. Si l'extension des marges au cours de la phase de rifting peut être estimée, il est alors possible de reconstruire la position des continents autour de l'Atlantique Nord au Jurassique terminal. L'objet du chapitre suivant sera de mieux cerner les mécanismes de formation des marges pour accéder à une estimation de l'extension des marges au cours de la phase de rifting.

## III - MECANISMES DE FORMATION DES MARGES CONTINENTALES EN EXTENSION : EXEMPLE DE LA MARGE OUEST-IBERIQUE

A partir du modèle d'étirement homogène de la lithosphère (Mc Kenzie, 1978), Le Pichon et Sibuet (1981) et Le Pichon et al. (1982) ont proposé le modèle du paquet de cartes basculant avec un angle de plus en fort en direction du domaine océanique. Ils se sont appuyés sur des mesures de l'extension superficielle réalisées à partir de la géométrie des blocs basculés observés sur les marges nord-Gascogne et ouest-ibérique. Comme l'extension superficielle est compatible avec l'amincissement de la croûte continentale (figure 16), ils ont suggéré que le mécanisme d'étirement uniforme s'appliquait à l'ensemble de la lithosphère. Les mesures de flux de chaleur réalisées sur la marge celtique sont compatibles avec un tel modèle (Foucher et Sibuet, 1980).

Cependant, Chenet et al. (1983) ont mis en cause la validité de la méthode de détermination de l'extension superficielle en reprenant l'interprétation de la géométrie du bloc basculé utilisé, à titre d'exemple, par Le Pichon et Sibuet (1981, figure 17). Ce bloc basculé, situé au pied de la terrasse de Mériadzek, était le seul exemple de sismique multitrace migrée, publié à cette époque. La queue du bloc, en contact avec la faille normale limitant le bloc amont, présente en effet des failles antithétiques dont l'interprétation en termes d'extension a

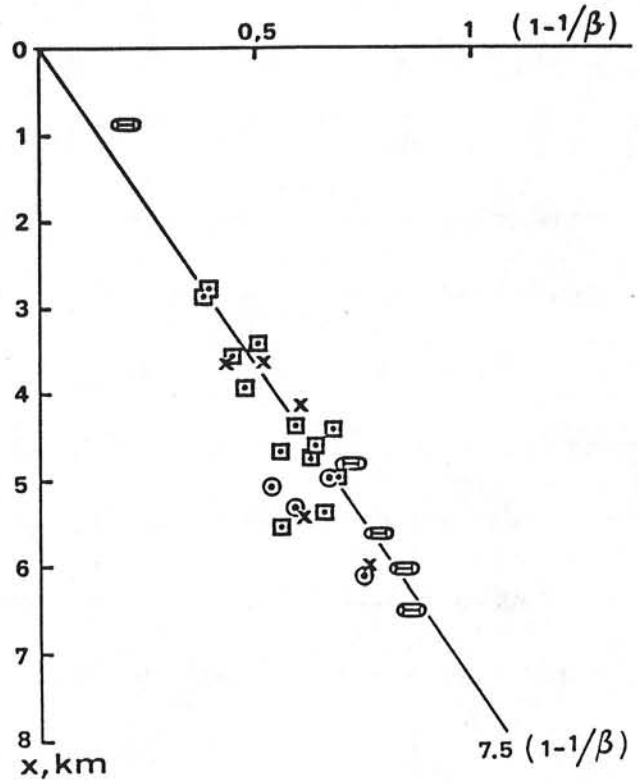


Figure 16 : Relation entre l'amincissement crustal et la profondeur (Le Pichon et Sibuet, 1981). Les ovales correspondent aux données de réfraction, les autres symboles aux mesures d'extension superficielle.

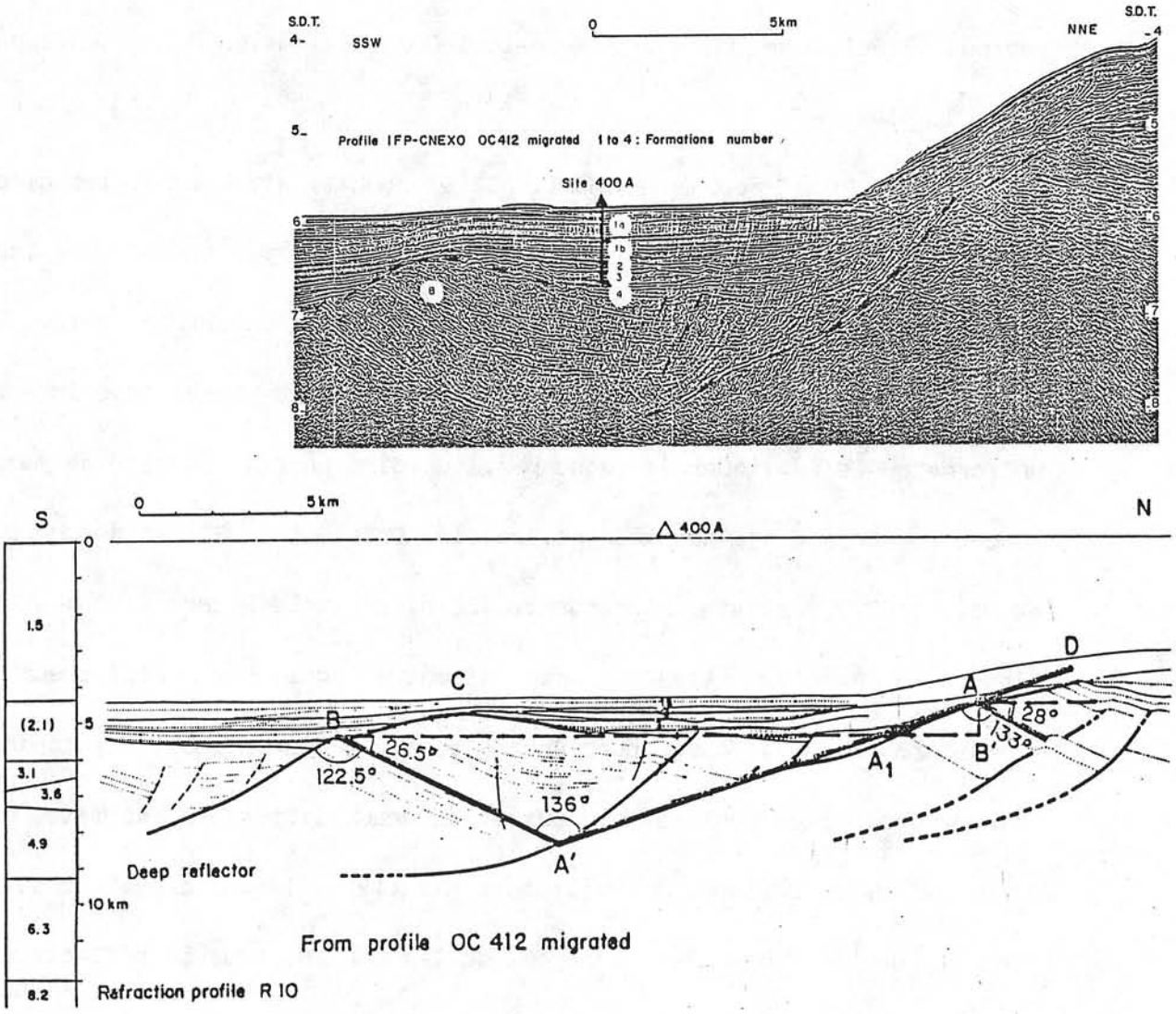


Figure 17 : Bloc basculé au pied de la marge celtique (escarpement de Trévelyan) et interprétation (Montadert et al., 1979 ; Le Pichon et Sibuet, 1981).

été sujette à discussion (Le Pichon et al., 1983 ; Chenet et al., 1983). Pour pallier cette difficulté, la plus grande partie des blocs basculés retenus ultérieurement pour le calcul de l'extension ne présente pas cette complexité.

Pour Brun et Choukroune (1983) et Brun et al. (1985), les blocs basculés de la marge nord-Gascogne auraient glissé par gravité, le long d'une surface de décollement correspondant à l'interface entre la couverture mésozoïque et le substratum hercynien. Le modèle d'étirement uniforme ne s'appliquerait donc pas, au moins pour la portion de marge où cette surface de décollement, appelée "réflecteur S" par de Charpal et al. (1978), existe. Cependant, Barbier et Le Pichon (1986) et Le Pichon et Barbier (1987) ont démontré que le réflecteur S correspond, sous la marge nord-Gascogne, à une discontinuité tectonique intracrustale recoupant des niveaux structuraux différents. De même, sur la marge ouest-ibérique, si Boillot et al. (1985, 1986a) croyaient avoir montré, sur la base des forages du leg ODP 103, que le réflecteur S pouvait correspondre à l'interface entre la couverture sédimentaire mésozoïque et le substratum hercynien, en revanche les plongées de la campagne Galinaute (Boillot et al., 1986b) ont établi que les blocs basculés contiennent des éléments de socle (granodiorites). Le réflecteur S est donc bien un réflecteur intracrustal, contrairement à l'affirmation de Brun et Choukroune (1983).

1) Géométrie et nature de l'horizon S sous la marge celtique

L'horizon S correspond à la limite inférieure des blocs basculés. Il a été mis en évidence sur les marges nord-Gascogne et ouest-ibérique (figures 17 et 18, e.g. Montadert et al., 1979) mais est absent sur la marge de l'éperon de Goban (figure 8). Les failles limitant les blocs basculés sont généralement limitées au réflecteur S. Parfois, elles se prolongent sous le réflecteur S. Sous la marge nord-Gascogne, le réflecteur S plonge en direction du continent mais il n'est plus identifié sous la pente continentale.

A partir d'une méthode d'inversion des vitesses sismiques (initialement proposée par Le Pichon et al., 1968), Barbier et al. (1986) et Le Pichon et Barbier (1987) ont calculé les vitesses de tranche, depuis le sommet des blocs jusqu'à l'horizon S, à partir d'un réseau régulier de 6 500 km de données de sismique réflexion multitrace. Près de la limite continent-océan de la marge celtique, dans le secteur de la terrasse de Mériadzek, une vitesse de 4,6 km/s a été calculée pour les sédiments antérifts (figure 19). En bas de pente continentale, les blocs basculés sont plus épais. Ils sont constitués d'une partie supérieure litée, identique à celle observée en bas de marge, et d'une partie inférieure non litée. La vitesse moyenne est de

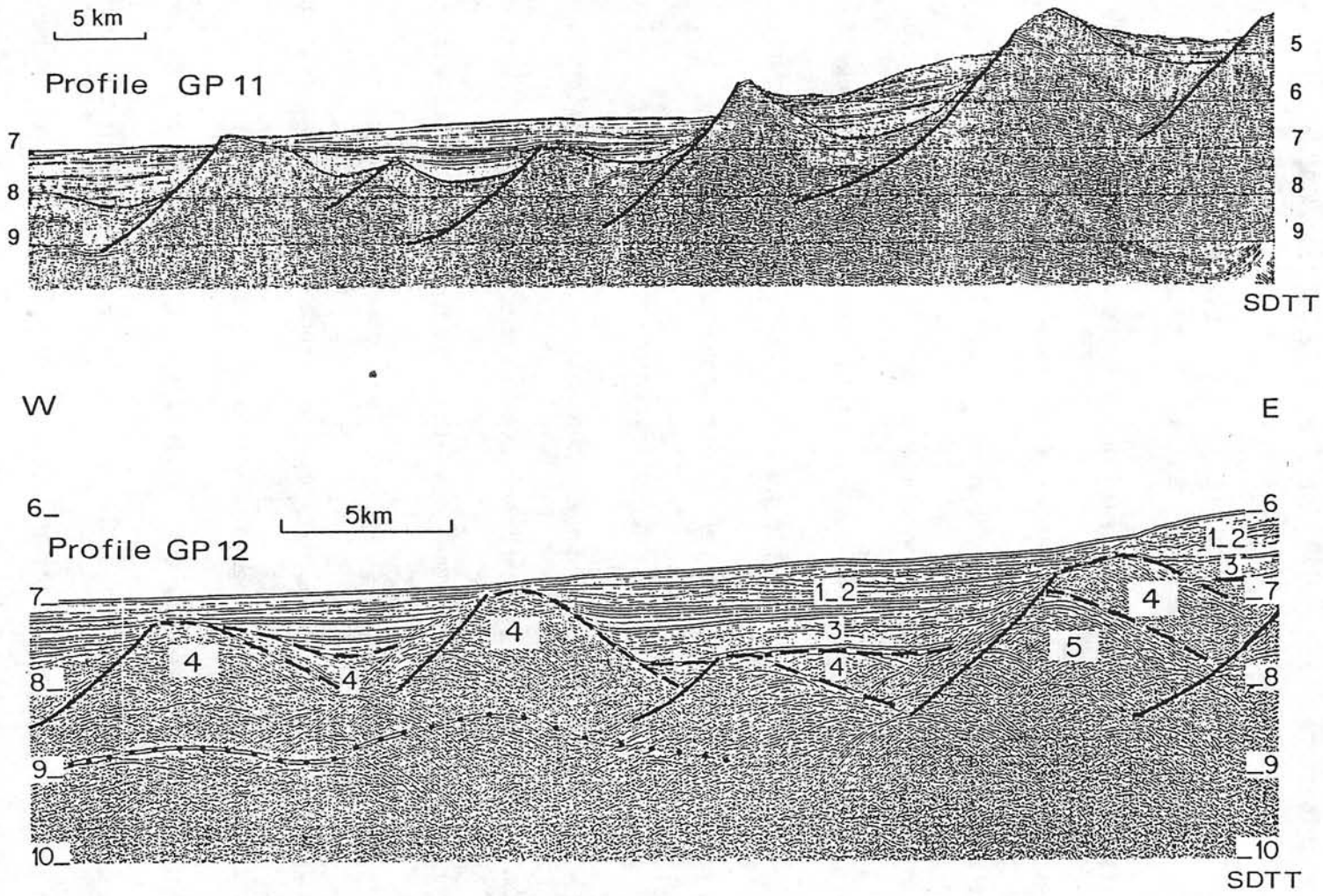


Figure 18 : Exemple de profil sismique obtenu sur la marge ouest -ibérique montrant la structuration de la marge en blocs basculés et la présence du réflecteur S en bas de marge (Sibuet et al., 1987).

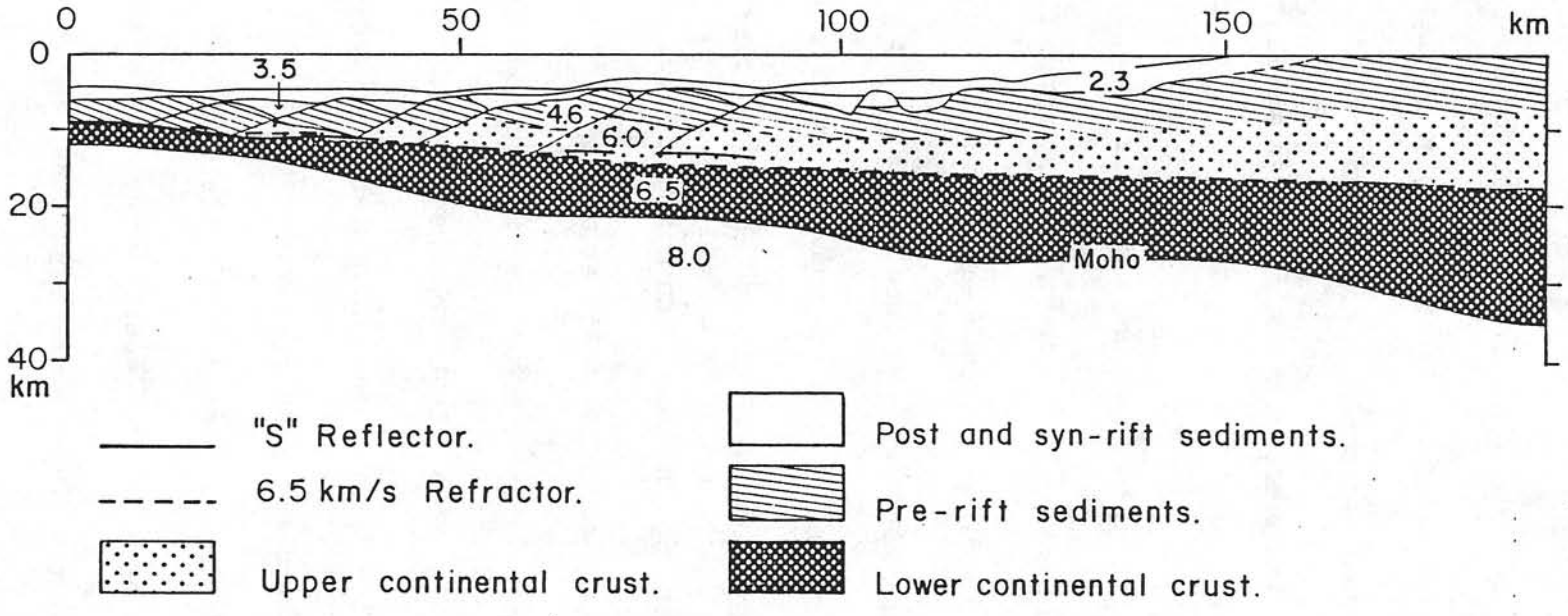


Figure 19 : Coupe profondeur d'un profil perpendiculaire à la marge celtique (Barbier et al., 1986).

5,2 km/s. En supposant une vitesse de tranche moyenne de 4,6 km/s pour la partie litée, la partie non litée aurait une vitesse moyenne de 6,0 km/s, caractéristique de la croûte continentale supérieure. La comparaison avec les données de réfraction de Ginzburg et al. (1985) montre que l'horizon réfracteur, correspondant à l'interface 6,0-6,5 km/s, est à la même profondeur que le réflecteur S et représenterait donc la même discontinuité.

Le réflecteur S met donc en contact la base des blocs basculés avec la croûte inférieure à 6,5 km/s. Il s'approfondit de 8 km en bas de marge à 13,5 km en bas de pente continentale. Il ne peut donc être considéré comme une surface de décollement le long de laquelle les blocs basculés auraient glissé par gravité, en direction du bas de la marge, comme l'ont proposé Brun et Choukroune (1983) et Brun et al. (1985). La profondeur du Moho, calculée d'après les données de réfraction (Ginzburg et al., 1985) et de gravimétrie (Lalaut, 1981), permet de connaître l'épaisseur de la tranche située entre le réflecteur S et le Moho. Cette tranche s'épaissit de 2 km en bas de marge à 9 km au pied de la pente continentale. Barbier et al. (1986) et Le Pichon et Barbier (1987) concluent donc que les blocs basculés du pied de la pente continentale celtique comprennent une partie supérieure de 4 à 5 km d'épaisseur de sédiments jurassiques (4,6 km/s), et une partie inférieure constituée de croûte continentale

supérieure (6,0 km/s) pouvant atteindre 5 km d'épaisseur. En bas de marge, les blocs basculés sont trop peu épais pour contenir de la croûte continentale supérieure. Ils reposent directement sur la croûte inférieure à 6,5 km/s. L'horizon S recoupe donc des niveaux crustaux de plus en plus profonds en direction de la pente continentale.

Sous la marge armoricaine, la profondeur de l'horizon S varie de 9 à 10 km en bas de marge à 11 km au pied de la pente continentale. Dans la région où le réflecteur S est observé, le Moho est situé à environ 1 à 2 km en dessous de ce réflecteur. Notons que cette marge a fonctionné en cisaillement.

2) Géométrie et nature du réflecteur S sous la marge ouest-ibérique

Sous la marge ouest-ibérique, le réflecteur S disparaît à une dizaine de kilomètres à l'est de l'axe de la ride de péridotite, structure située à la transition continent-océan (figures 14 et 20) ou proche de celle-ci. Son extension latérale, de l'ordre de 35 km en direction de la pente continentale, est beaucoup plus faible que sous la marge nord-Gascogne (90 km). Le profil sismique de la figure 18 montre que le réflecteur S s'arrête brutalement avant d'atteindre le pied de la pente continentale, sans qu'une variation notable de l'épaisseur des blocs basculés et des séries syn et postrifts soit

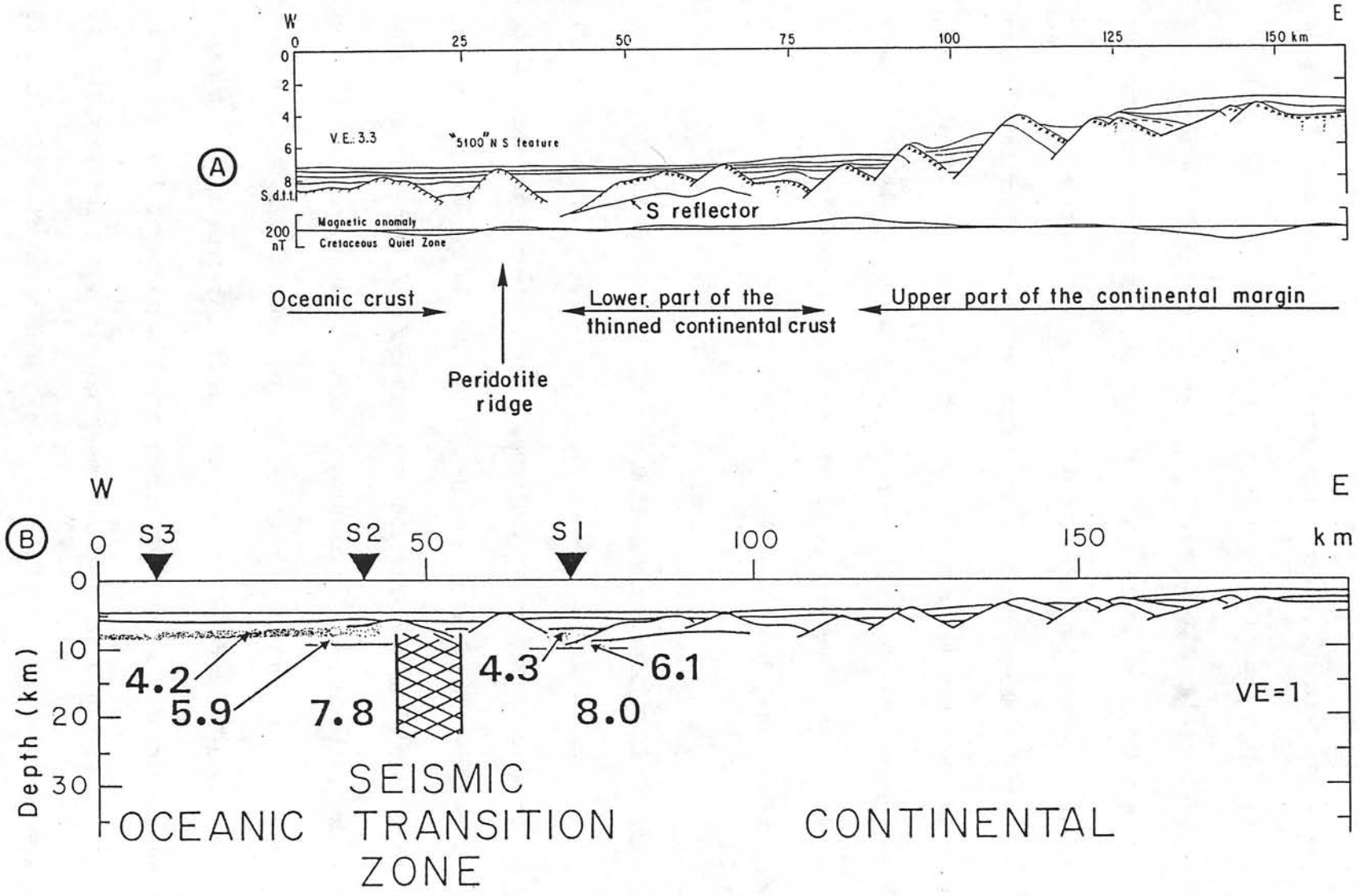


Figure 20 : A : Interprétation du profil sismique composite (GP 11 et GP 12, figure 18) obtenu perpendiculairement à la marge ouest-ibérique.
B : Coupe profondeur du même profil avec indications de vitesses (km/s) obtenues à partir des profils de sismique réfraction S1, S2 et S3 (Sibuet et al., 1987).

observée. Le même phénomène est observé sur l'ensemble des 5 profils multitraces obtenus perpendiculairement à la marge (Mauffret et Montadert, 1987). La disparition du réflecteur S ne semble donc pas liée à une atténuation du signal réfléchi avec la profondeur. Je propose que ce réflecteur correspond à une surface de décollement apparaissant à l'interface des milieux ductiles et cassants, lorsque le facteur d'extension devient trop élevé, ce qui expliquerait sa disparition sous la pente. Au contraire, Le Pichon et Barbier (1987) et Barbier et al. (1986) ont attribué la disparition du réflecteur S à une pénétration insuffisante de la sismique réflexion utilisée.

Sur les coupes temps, le réflecteur S présente un effet de remontée sous les blocs basculés dû au contraste latéral de vitesses. La mauvaise connaissance de la vitesse de tranche des blocs basculés ne permet pas de restituer correctement la morphologie du réflecteur S. Cependant, en supposant une vitesse de 2,9 km/s pour les sédiments synrifts et de 4,3 km/s pour les blocs basculés (résultats peu contraints des profils réfraction non inversés, Sibuet et al., 1987), le réflecteur S serait sensiblement plan. Il peut parfois présenter une forte dénivelée à regard vers l'océan, au droit des plans de failles limitant les blocs basculés (figure 21). Cette dénivelée est interprétée comme un effet de rampe par Mauffret et Montadert (1987).

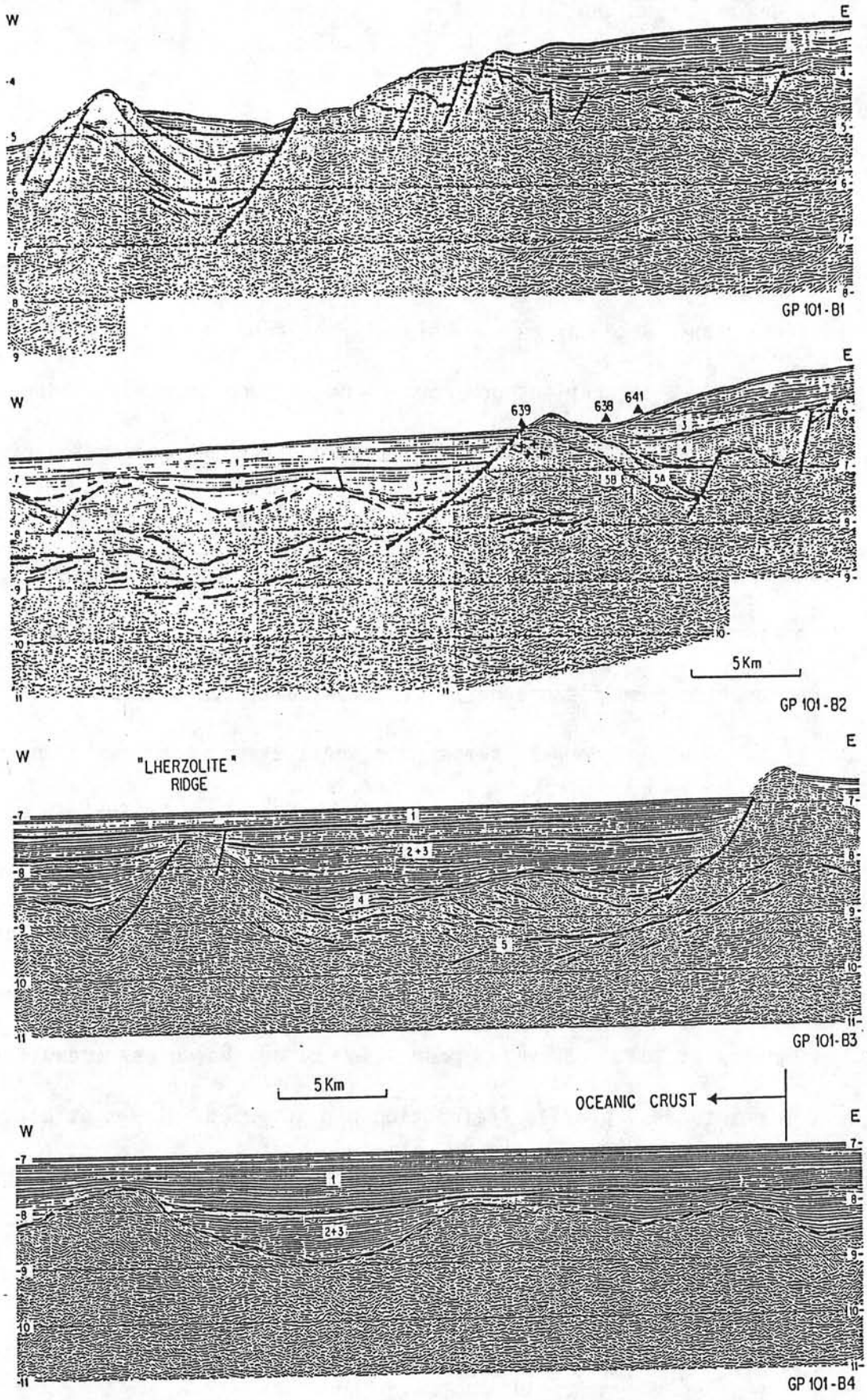


Figure 21 : Profils sismiques multitraces GP101 et GP102 obtenus sur la marge ouest-ibérique. Le réflecteur S correspond à une zone de réflecteurs atteignant 0,6 s.t.d. d'épaisseur. Légende des symboles : 1) Actuel à Oligocène ; 2) Eocène à Campanien ; 3) Cénomanien moyen à Aptien terminal ; 4) Aptien terminal à Hauterivien ; 5A) Hauterivien à Valanginien ; 5B) Jurassique terminal (Mauffret et Montadert, 1987).

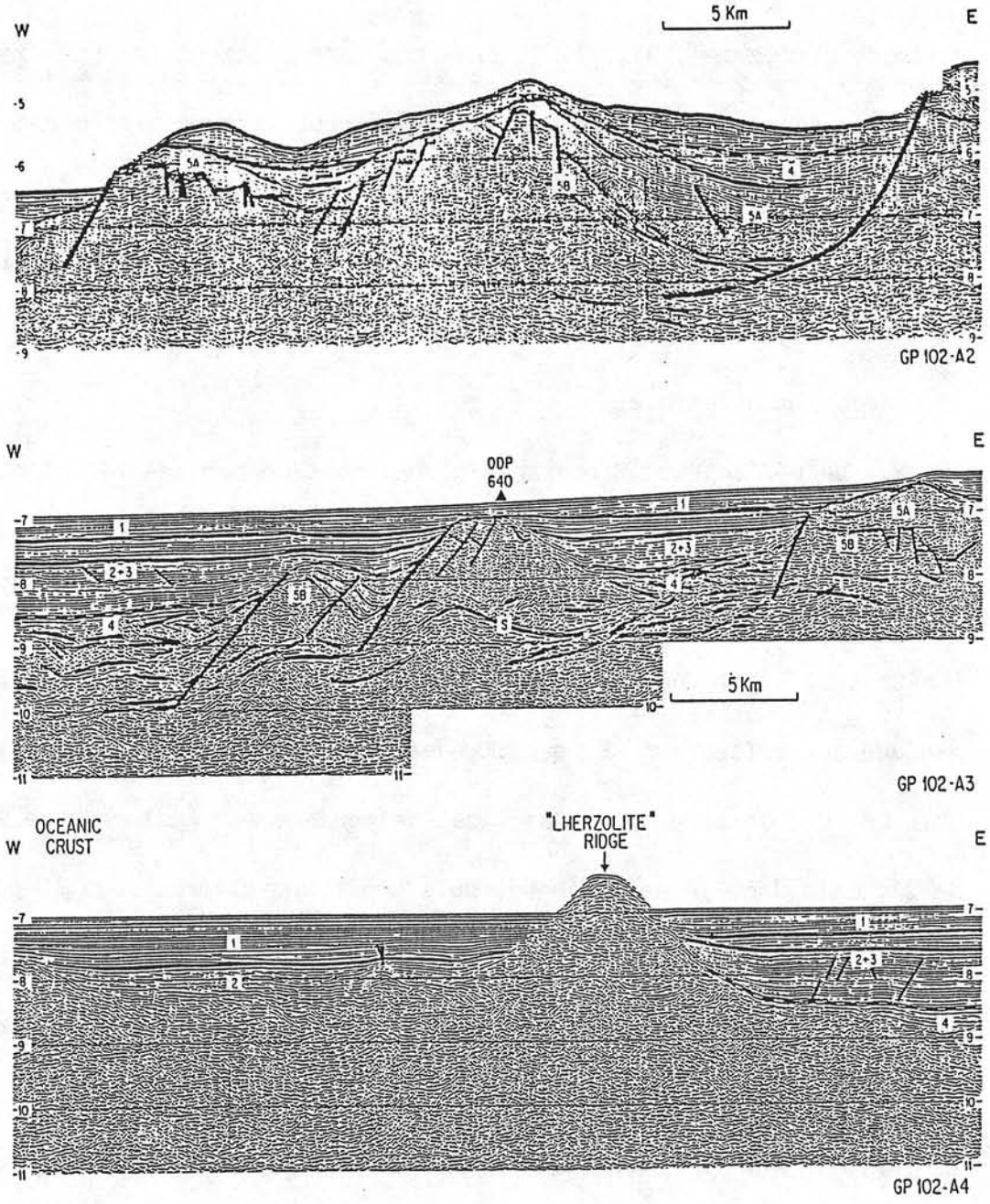


Figure 21 : ( suite )

Si le réflecteur S se présente parfois sous la forme d'un seul réflecteur (figure 18), il correspond généralement à une zone de réflecteurs de 0,4 à 0,6 s.t.d. d'épaisseur (figure 21), c'est-à-dire environ 1,5 km d'épaisseur, en supposant que cette zone soit intracrustale (6,0 ou 6,5 km/s). Le Pichon et Barbier (1987) arrivent à la même conclusion. Il s'agirait donc d'une zone de cisaillement et non d'un décollement simple.

Le réflecteur S présente globalement un pendage vers l'océan de 1,6 s.t.d. sur 35 km, pour le profil GP101, et de 1,9 s.t.d. sur 32 km, pour le profil GP102 (figure 21). En tenant compte d'un réajustement isostatique local dû à la surcharge des sédiments syn et postrifts, le pendage du réflecteur S serait de 2° en direction de l'océan (figure 22). En bas de marge nord-Gascogne, ce pendage est également de l'ordre de 2°, mais dans le sens opposé, puis croît brutalement sous la pente.

Deux phases de rifting ont été identifiées sur la marge ouest - ibérique (Mauffret et Montadert, 1987). La première est d'âge Oxfordien-Kimméridgien inférieur à Valanginien, la deuxième d'âge Valanginien à Hauterivien. Cette dernière phase est la phase majeure de rifting au cours de laquelle les sédiments synrifts de la première phase de rifting ont été repris (Boillot et al., 1985, 1986a, 1986b). L'épaisseur des blocs basculés incluant les sédiments synrifts de la première phase

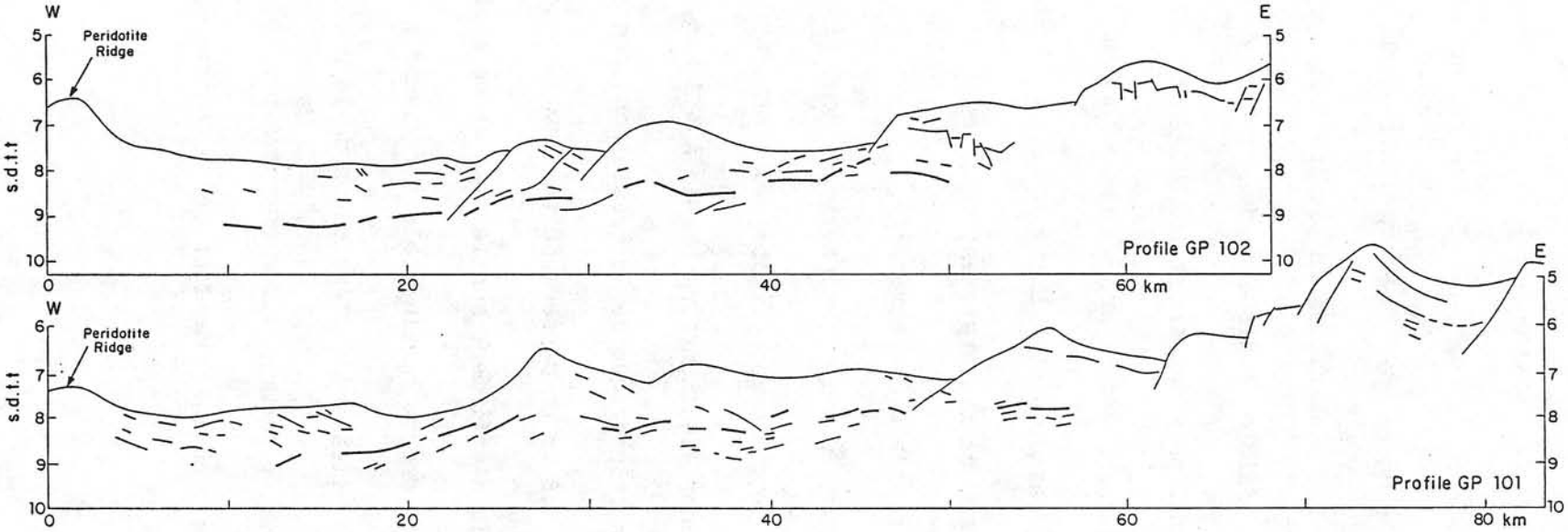


Figure 22 : Interprétation des profils sismiques multitraces GP 101 et GP 102 où la surcharge sédimentaire correspondant aux unités acoustiques 1 à 4 de la figure 21 (sédiments syn et postrifts) a été retirée, en supposant un réajustement isostatique local et une densité moyenne des sédiments de 2,2 g/cm³. Le réflecteur S (ou le toit de la zone de réflecteurs) est en trait gras. Noter la pente du réflecteur S en direction de l'océan.

varie de 0,9 à 1,4 s.d.t. (figures 18 et 21). Cette fourchette est la même que pour les blocs du bas de la marge nord-Gascogne. Par comparaison avec les données de la marge nord-Gascogne, la partie inférieure des blocs basculés situés en pied de marge pourrait donc ne contenir qu'une très faible épaisseur de croûte continentale. En revanche, plus à l'Est, près des sites de forages 638, 639 et 641, des granodiorites ont été observées et prélevées le long du plan de failles limitant deux blocs basculés (Boillot et al., 1986b). Une forte épaisseur de la croûte continentale est donc impliquée dans les blocs basculés de la partie centrale de la marge.

Les données du profil réfraction non inversé S, tiré perpendiculairement à la marge (figure 20, Sibuet et al., 1987) suggèrent que la couche sédimentaire basale à 4,3 km/s repose sur une couche à 6,1 km/s caractéristique de la croûte continentale supérieure. Le Moho est à environ 1,5 km en-dessous du toit de la couche à 6,1 km/s. Il n'est pas possible d'affirmer, sur la base de ce profil réfraction, qu'il n'existe pas de croûte continentale inférieure à 6,5 km/s, parce que le contraste de vitesse et l'épaisseur de la croûte continentale amincie sont faibles. De même, il n'est pas possible de dire si le réflecteur S est au toit ou à l'intérieur de la couche à 6,1 km/s.

3) Mesure de l'extension dans la croûte cassante

Sur l'exemple du bloc basculé de la marge nord-Gascogne (figure 17), Le Pichon et al. (1983) ont montré d'une part qu'il faut tenir compte des parties érodées des blocs basculés dans le calcul de l'extension, et d'autre part que l'extension calculée en surface était inférieure à l'extension calculée à partir des couches inférieures des blocs d'un facteur pouvant atteindre 20 %. Sur la marge ouest-ibérique, la partie sommitale des blocs basculés est souvent érodée. Il faut donc en tenir compte dans le calcul de l'extension. En revanche, les queues de blocs sont bien moins déformées que dans l'exemple de la figure 17, au moins pour les blocs de la pente continentale et l'extension calculée en surface ne diffère que de quelques % de l'extension calculée dans la partie inférieure du bloc.

Le calcul de l'extension est fait à partir d'un réflecteur peu déformé situé à l'intérieur du bloc considéré (figure 23). Il est rapporté au point P, milieu de la partie sommitale du bloc, dont la profondeur est corrigée de la surcharge des sédiments syn et postrifts (ajustement isostatique local). La figure 24 donne la profondeur des blocs basculés en fonction de $(1-1/\beta)$, pour les différents blocs basculés de la marge ouest-ibérique. Ces blocs, numérotés depuis le haut de la marge, ont été recoupés plusieurs fois par les profils sismiques

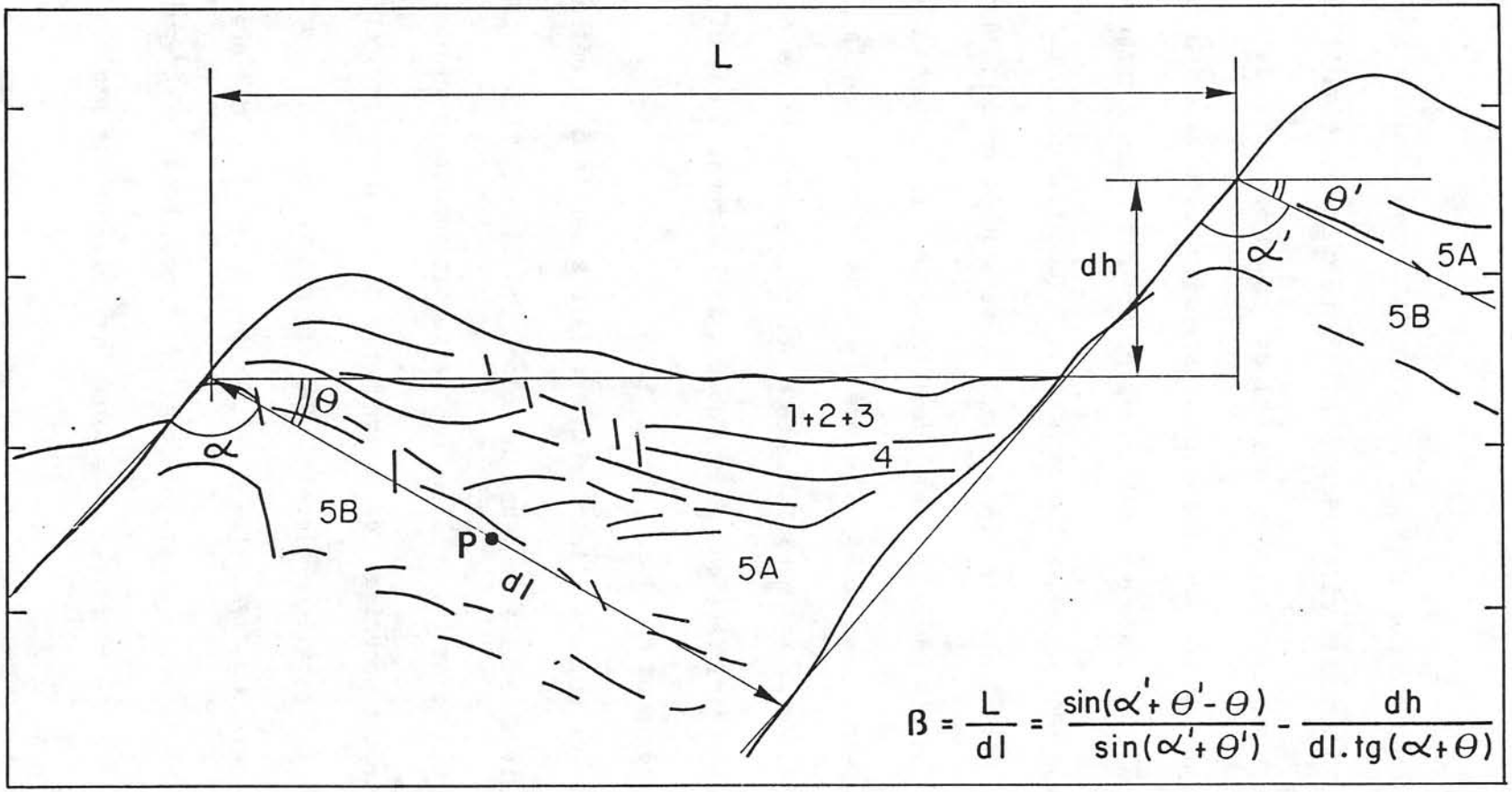


Figure 23 : Calcul de l'extension superficielle sur un exemple de bloc basculé de la marge ouest-ibérique.

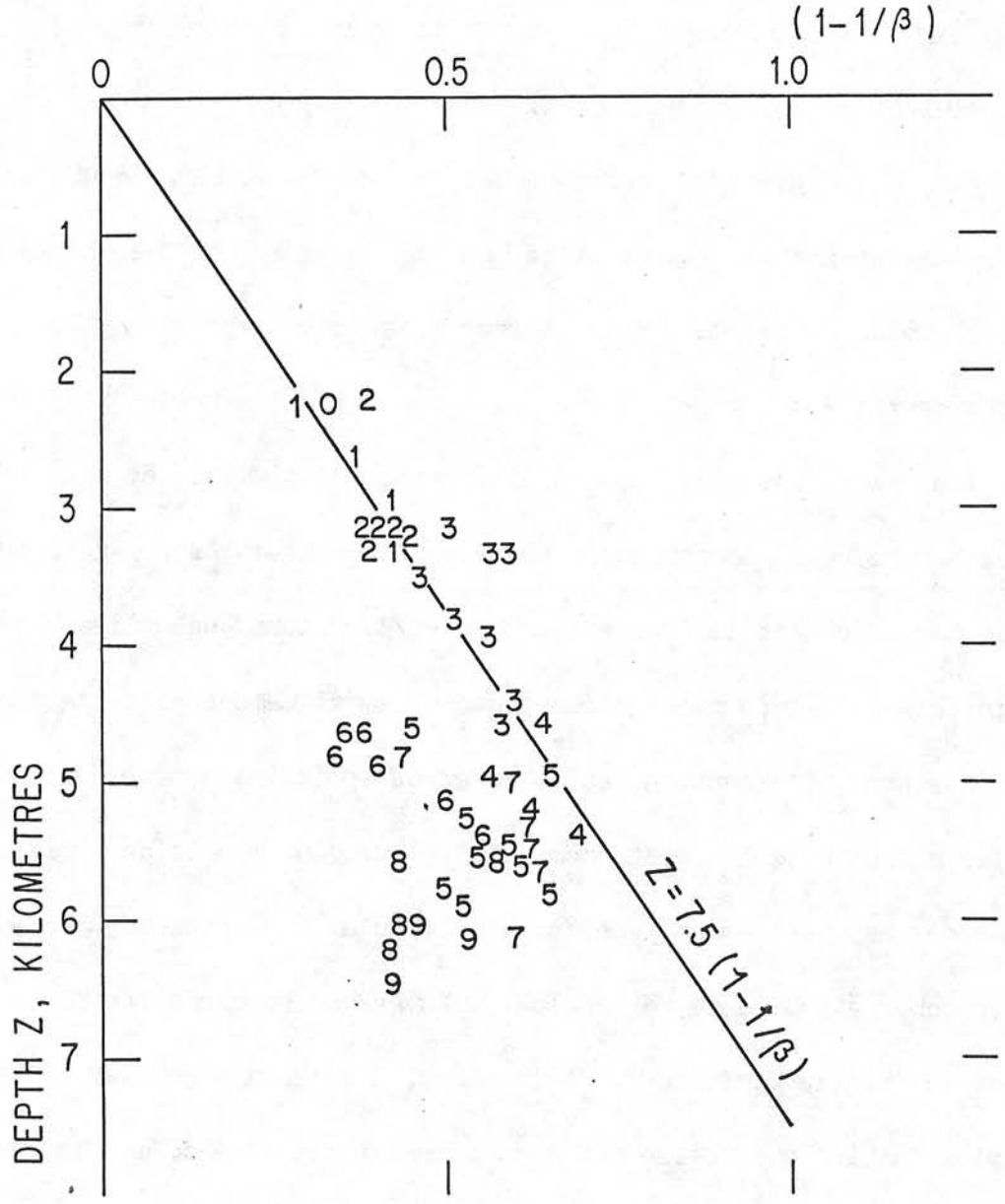


Figure 24 : Valeurs de l'extension superficielle en fonction de la profondeur. Les nombres de 0 à 9 correspondent aux blocs basculés numérotés de la partie supérieure de la marge ouest-ibérique en direction de l'océan.

de la campagne Seagal (Sibuet et al., 1987). Le bloc 9 correspond à la ride de péridotite. Il a été conservé parce qu'il pourrait correspondre, au nord de la montagne 5100, à une structure dissymétrique de type bloc basculé (Mauffret et Montadert, 1987).

La figure 25 reprend les mêmes données, avec une indication supplémentaire sur la qualité de la mesure et une barre d'erreur correspondant à un réajustement isostatique dû à la surcharge sédimentaire de type plaque, pour des valeurs extrêmes raisonnables de l'épaisseur élastique de la lithosphère (Diament et al., 1986). Les valeurs correspondant aux 5 premiers blocs basculés à partir du haut de la marge suivent la droite $Z = 7,5(1-1/\beta)$, alors que celles de la partie inférieure de la marge s'écartent systématiquement de cette droite. Par conséquent, l'extension en surface déterminée à partir des mesures sur les blocs basculés est compatible avec un modèle de formation de la marge par étirement uniforme, jusqu'à une profondeur de 5,5 km (surcharge sédimentaire exclue). En ce qui concerne les blocs basculés de la partie inférieure de la marge, l'extension mesurée est nettement plus faible que celle que l'on pourrait attendre du modèle d'étirement uniforme, même si certains blocs sont à une profondeur inférieure à celle du bloc 4. Ce phénomène apparaît également sur le graphique de Le Pichon et Sibuet (1981), bien que le nombre de mesures soit plus faible et que la dispersion des mesures soit plus forte.

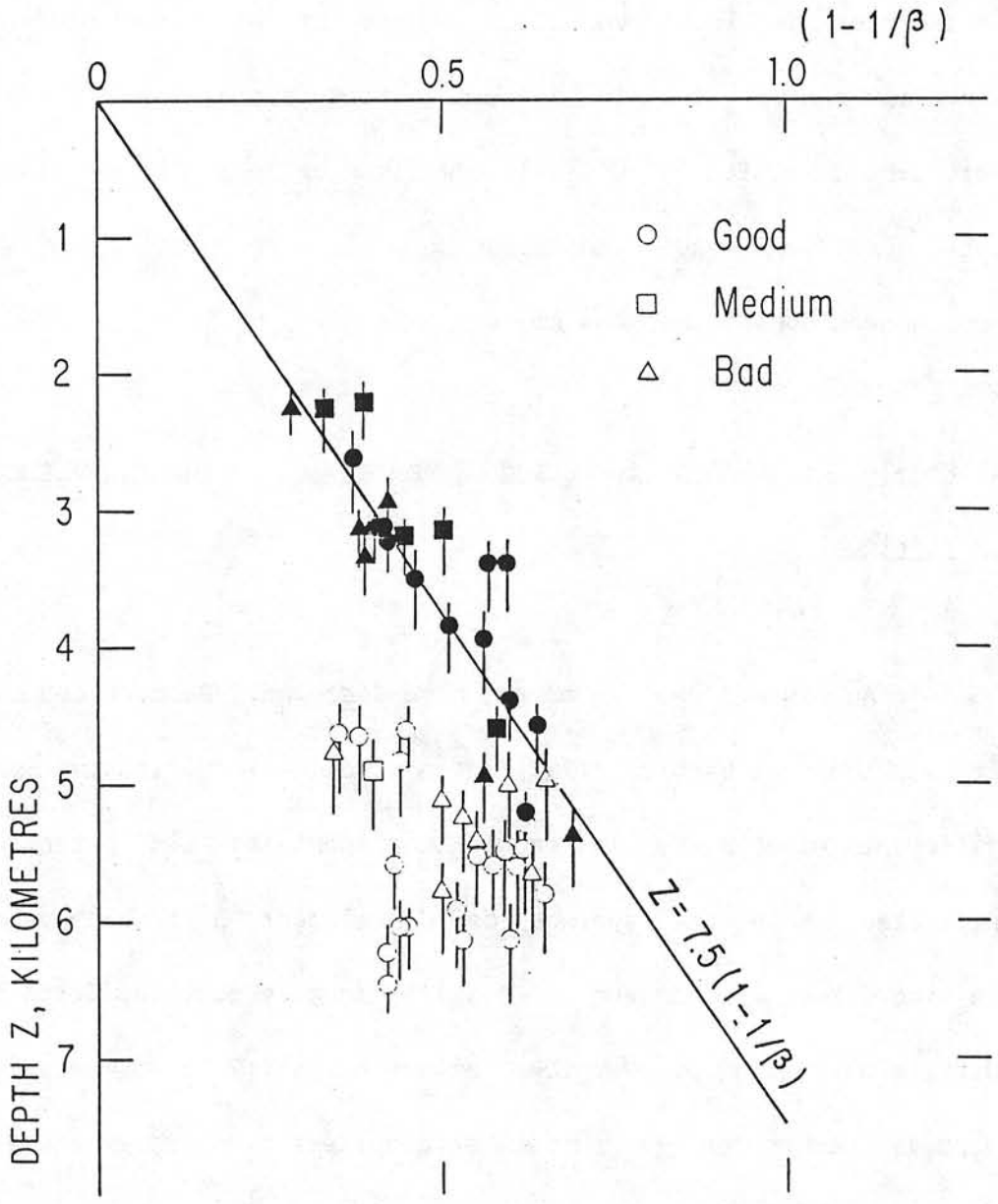


Figure 25 : Mêmes valeurs de l'extension superficielle en fonction de la profondeur que dans la figure 24. Les symboles en noir correspondent aux blocs basculés (0 à 4) de la partie supérieure de la marge. Les symboles évidés correspondent aux blocs basculés situés en dessus du réflecteur S. Les barres d'erreurs correspondent à un réajustement isostatique du poids des sédiments syn et postrifts de type local ou régional.

Les figures 26 et 27 donnent l'angle de basculement θ des blocs en fonction de leur profondeur. Comme Le Pichon et Sibuet (1981) l'avaient montré, l'angle de basculement augmente avec la profondeur mais semble limité à une valeur maximum de 20 à 30°. Les données sont aussi dispersées que dans leur exemple, en particulier pour les profondeurs supérieures à 4 km.

4) Modèle proposé de formation des marges en extension du type ouest - ibérique

Au niveau de la marge nord-Gascogne, Barbier et al. (1986) et Le Pichon et Barbier (1987) ont montré que le réflecteur S recoupait différents niveaux de la croûte continentale. Ils interprétent ce réflecteur comme une surface de décollement à faible pendage qui rejoindrait en profondeur la limite fragile-ductile. Cette hypothèse diffère de celle de Wernicke et Burchfiel (1982) et Wernicke (1985), dans la mesure où la surface de décollement ne traverse pas toute la croûte continentale. Le Pichon et Barbier (1987) suggèrent que cette surface de décollement prendrait naissance à une quinzaine de kilomètres de profondeur, à la limite fragile-ductile et se propagerait vers le haut à travers la croûte continentale supérieure (figure 28). Au fur et à mesure que l'extension augmente, des failles antithétiques se

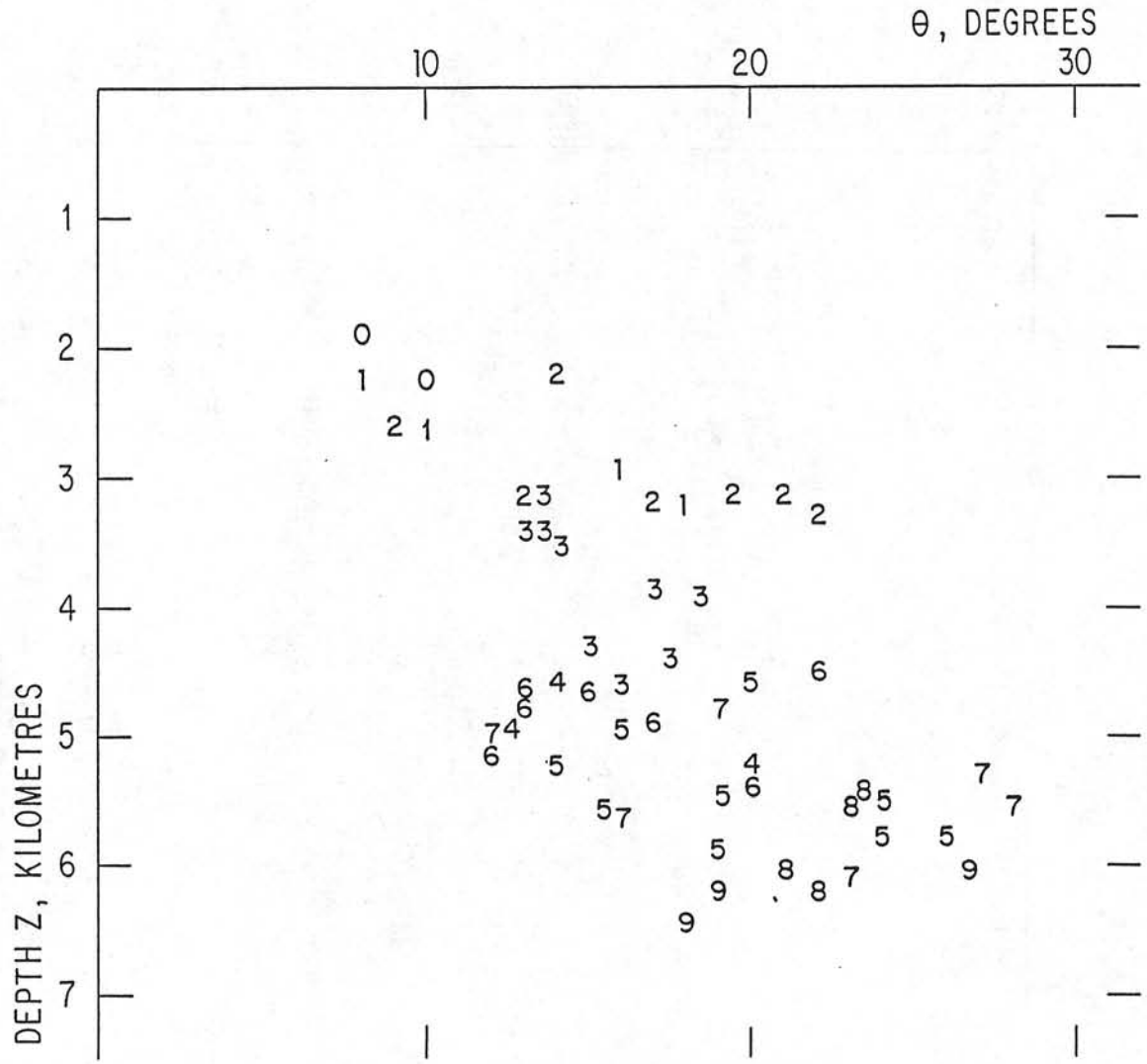


Figure 26 : Angle de basculement θ des blocs en fonction de la profondeur. Les nombres de 0 à 9 correspondent aux blocs basculés numérotés de la partie supérieure de la marge ouest-ibérique en direction de l'océan.

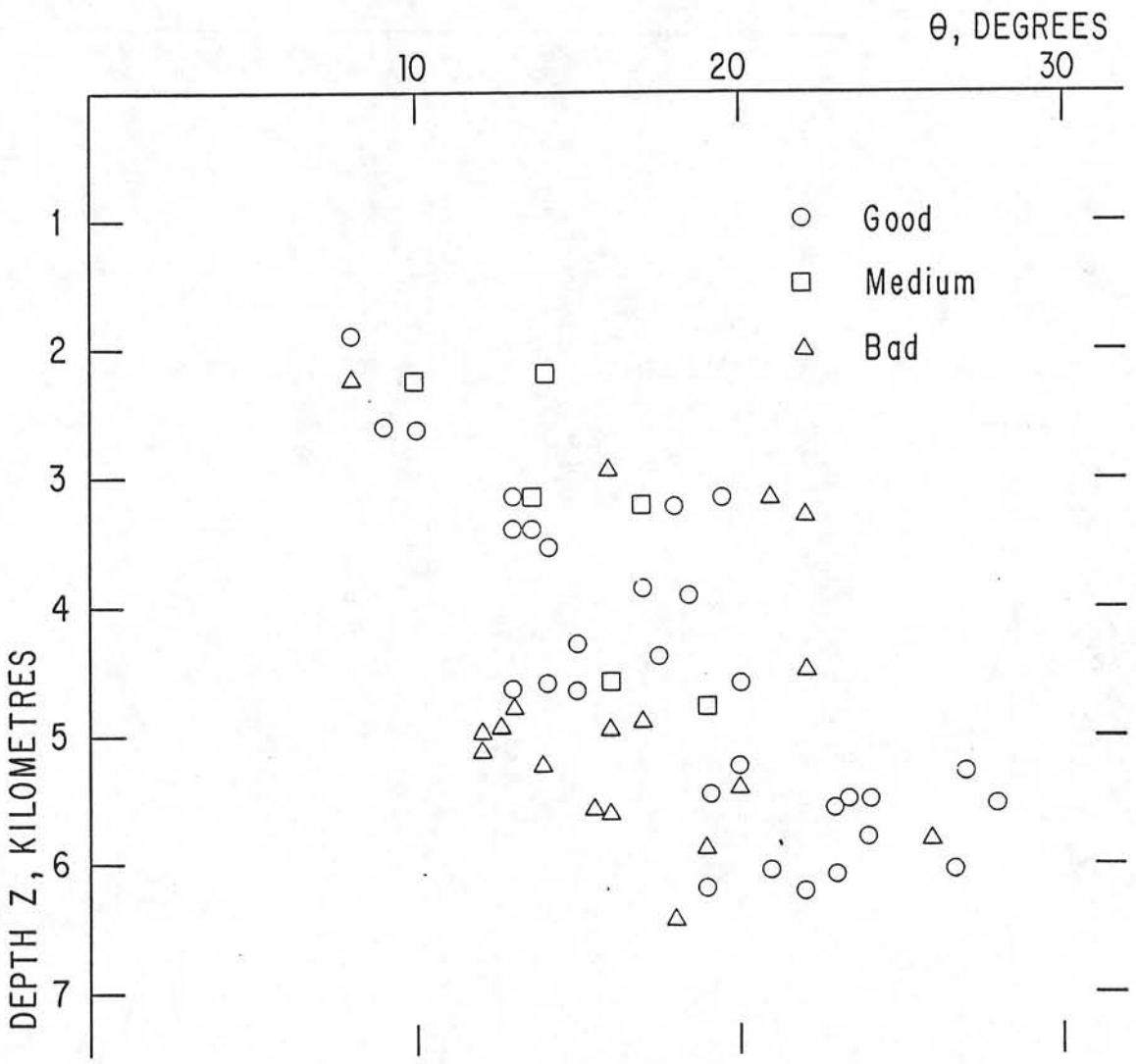


Figure 27 : Angle de basculement θ des blocs en fonction de la profondeur avec une information sur la qualité des mesures.

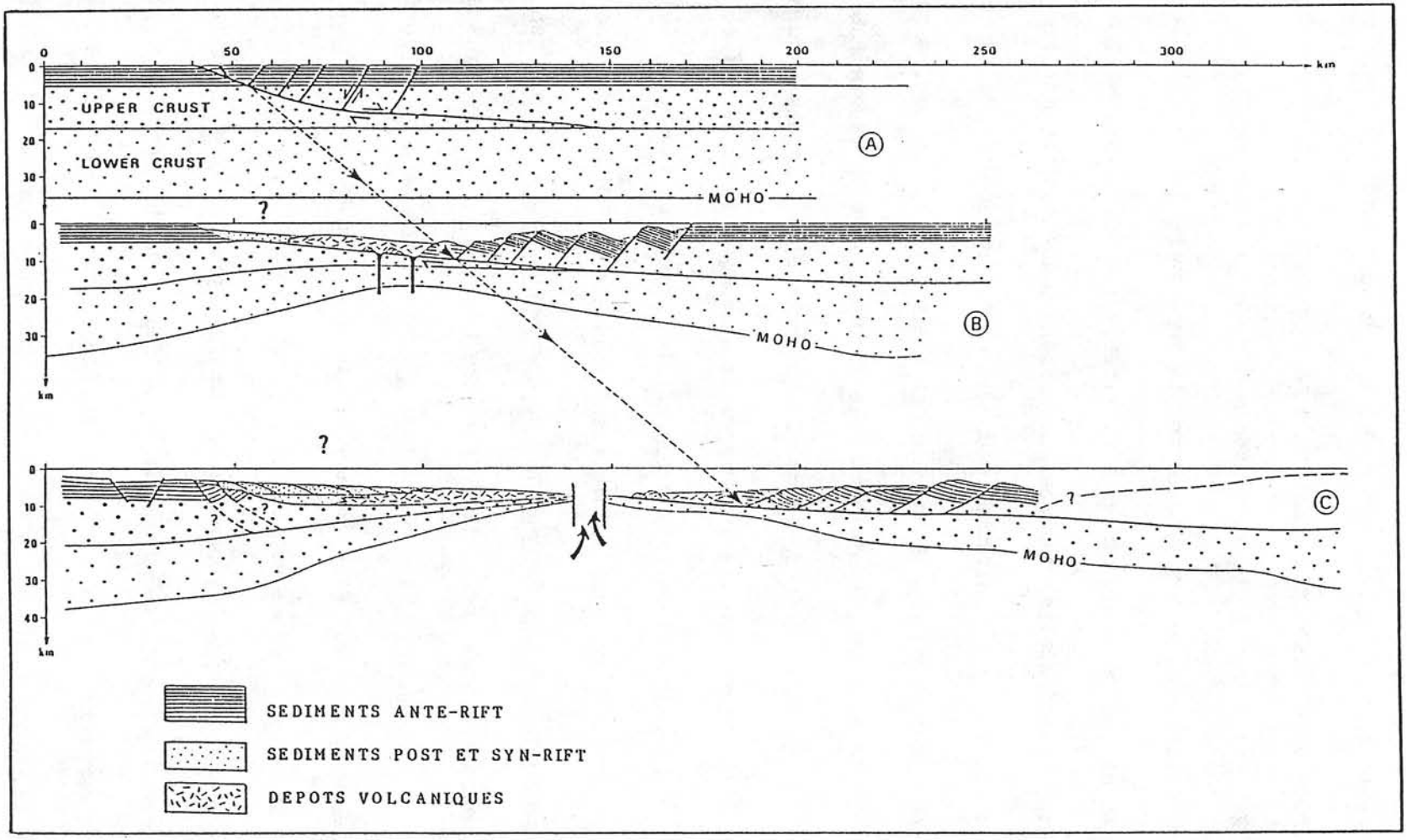


A = stade initial
B = stade de rifting
C = stade de début d'accrétion océanique

Figure 28 : Différents stades d'évolution de la marge nord-Gascogne et de sa marge conjuguée (modèle de Le Pichon et Barbier, 1987).

développeraient, donnant naissance à des blocs dont le basculement augmenterait avec l'extension. Sur la marge opposée, il n'y aurait pas ou peu de blocs basculés et les sédiments syn et postrifts pourraient être directement en contact avec la croûte supérieure.

Au niveau de la marge ouest-ibérique, nous avons montré que l'extension superficielle mesurée correspond à l'extension prédite par le modèle d'étirement uniforme pour la partie supérieure de la marge jusqu'à une profondeur de 5,5 km (blocs basculés 0 à 4 de la figure 24 figurés par des symboles pleins sur la figure 25). Le réflecteur S est absent sous cette portion de marge. Il apparaît plus à l'ouest, du bloc 5 au bloc 8. Pour la partie inférieure de la marge, là où le réflecteur S a été cartographié, l'extension superficielle mesurée (symboles évidés sur la figure 25) est plus faible que l'extension prédite par le modèle d'étirement uniforme. On peut donc penser que l'horizon S correspondrait, comme pour la marge nord-Gascogne, à une surface de décollement. Cependant, le mécanisme donnant naissance à cette surface de décollement pourrait être différent pour les deux marges.

En ce qui concerne la marge nord-Gascogne, une discontinuité traversant la croûte supérieure aurait joué comme surface de cisaillement le long de laquelle les deux compartiments de croûte cassante auraient coulissé. Cette surface disparaîtrait lorsqu'elle rejoint la croûte inférieure ductile (Le Pichon et Barbier, 1987). Dans

cette hypothèse, l'amincissement crustal est d'autant plus important que le pendage de la surface de cisaillement est plus fort. Lorsque cette surface devient presque horizontale et a quasiment rejoint le niveau ductile, il n'y a plus d'amincissement significatif.

En ce qui concerne la marge ouest-ibérique, l'horizon S apparaîtrait au cours de l'étirement uniforme, lorsque les taux d'extension seraient supérieurs à 2,8-3,2, c'est-à-dire à partir du moment où le basculement des blocs atteint une valeur limite de l'ordre de 20 à 30° (figure 26). En effet, si le bloc reste rigide et ne peut basculer davantage, une discontinuité mécanique doit apparaître à la limite fragile-ductile. Il n'en demeure pas moins que l'extension superficielle mesurée est inférieure à celle prédite par le modèle d'étirement uniforme. Or, Boillot et al. (1985 et 1986a) ont montré que la partie supérieure des blocs basculés de bas de marge (site ODP 640) est constituée de sédiments d'âge valanginien. Ces blocs seraient donc constitués en grande partie de sédiments synrifts déposés dans la partie profonde du bassin au cours de la première phase de rifting du Jurassique terminal au Valanginien, puis repris au cours de la seconde phase de rifting. L'extension mesurée en bas de marge ne serait donc qu'une partie de l'extension totale. Les données de la marge ouest-ibérique sont donc compatibles avec le modèle d'étirement uniforme bien que l'on ne puisse pas exclure, à la fin du rifting, le fonctionnement

d'une faille de décollement, comme celle proposée par Le Pichon et Barbier (1987) pour la marge nord-Gascogne. Bien que l'émergence d'une telle faille de décollement ne soit mise en évidence ni sur la marge ouest-ibérique, ni sur la marge symétrique (Tankard et Welsink, sous presse), si une telle faille fonctionnait en cisaillement à la fin du rifting, il n'est pas évident qu'elle puisse être repérée du fait de la forte épaisseur sédimentaire.

Nous proposons un modèle de formation des marges passives en extension par étirement uniforme dans lequel l'interface fragile-ductile se comporterait comme une surface cohérente jusqu'à une valeur maximum de ß pouvant atteindre localement 2,8 à 3,2 (figure 29, schémas 1 et 2), dans le voisinage de l'axe du bassin. A la fin du rifting, une surface incohérente se développerait au niveau de l'interface fragile-ductile précédente (figure 29, schéma 3). Cette interface incohérente progresserait le long de la surface cohérente précédente et se développerait symétriquement des deux côtés du bassin (exemple possible de la marge ouest-ibérique, figure 29, schéma 3). Remarquons que les deux stades d'évolution du rifting (pré et post fonctionnement de la surface incohérente) ne sont pas nécessairement liés à l'existence des deux phases de rifting crétacé inférieur identifiées par Mauffret et Montadert (1987).

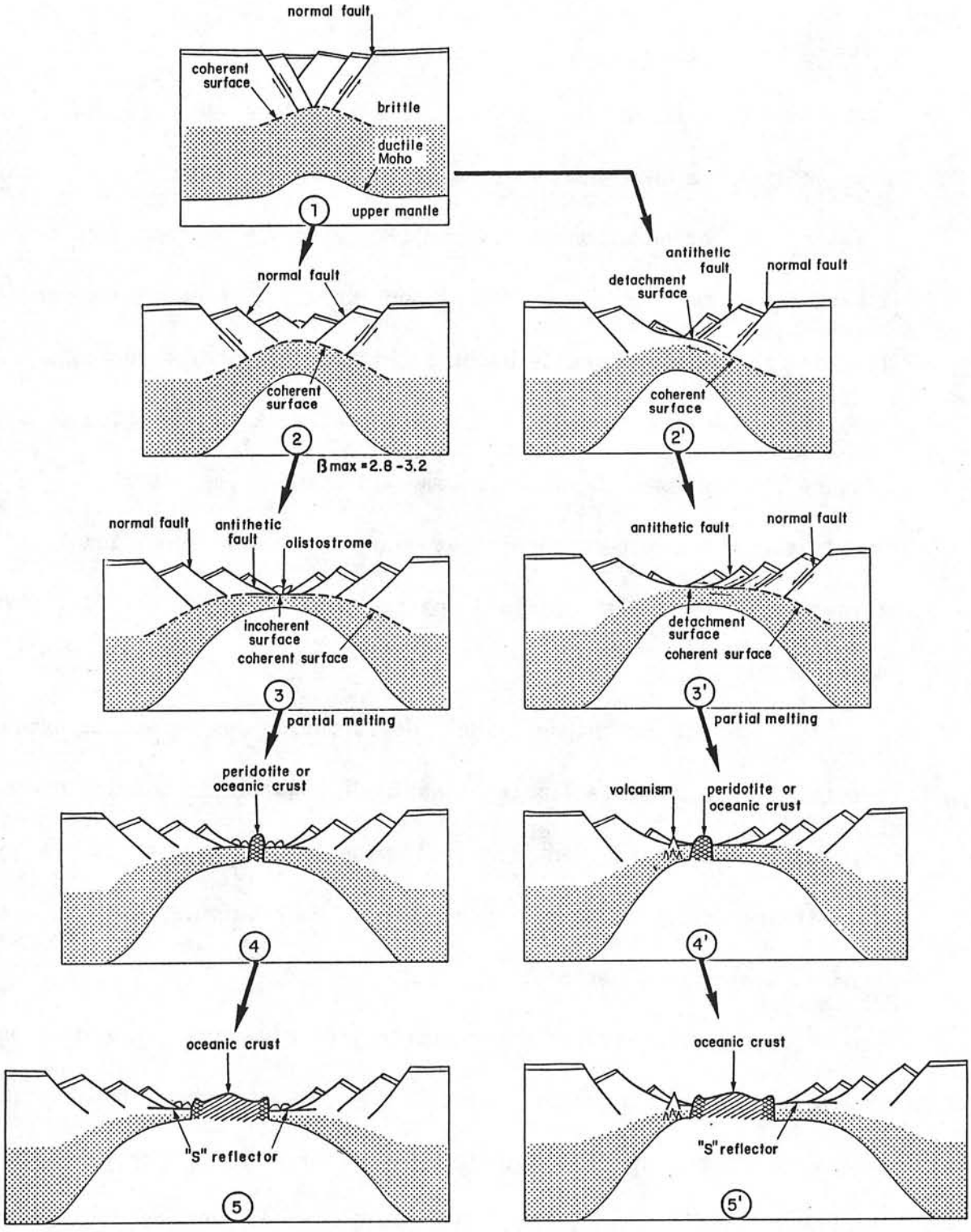


Figure 29 : Schéma du modèle proposé de formation des marges continentales en extension (exagération verticale de l'ordre de 2).

Des discontinuités intra-crustales (zones de suture, de cisaillement, failles normales,...) antérieures au rifting peuvent exister dans la croûte supérieure. Dans la mesure où un accident majeur présente une orientation telle qu'il puisse être repris au cours de l'extension, une surface de décollement privilégiée se développerait le long de cet accident dès le début du rifting (hypothèse de Le Pichon et Barbier) ou à partir d'un stade intermédiaire de la formation du bassin (figure 29, schémas 2' et 3'). Comme la lithosphère s'amincit, le toit de l'asthénosphère remonterait et du magmatisme superficiel, lié à l'augmentation de la fusion partielle (Foucher et al., 1982), apparaîtrait.

Au cours du stade final de formation des marges, l'extension crustale atteindrait la limite à partir de laquelle le domaine océanique apparaît, avec mise en place éventuelle, au cours de la phase transitoire, de péridotites provenant du manteau supérieur (figure 29, schémas 4 et 5 ou 4' et 5').

Lorsqu'une surface incohérente se développe, le modèle prédit une augmentation du cisaillement soit des continents en direction de l'axe du rift dans l'hypothèse de l'étirement uniforme, soit d'un continent vers l'autre, dans l'hypothèse de la surface de décollement (figure 29).

De nombreux bassins intra-continentaux se forment suivant les deux processus envisagés. Une faille pré-existante majeure joue le rôle de surface de décollement et son fonctionnement induit la formation de failles normales antithétiques limitant les blocs basculés. De nombreux exemples existent dans la province des "Basin and Range" (e.g. Allmendiger et al., 1983 ; Wernicke et Burchfiel, 1982 ; Anderson et al., 1983 ; bassin d'Albuquerque, Snelson, communication personnelle, 1980).

C'est à partir de tels exemples que Wernicke (1985) a proposé un modèle (figure 30) où le fonctionnement d'une zone de cisaillement affectant toute la lithosphère entraîne un amincissement important de celle-ci. Boillot et al. (1985, 1986a et 1987) ont repris cette hypothèse en la poussant à l'extrême. Ils expliquent ainsi la présence de péridotites serpentinisées près de la transition continent-océan (montagne 5100), par dénudation tectonique du manteau (figure 31). A partir d'une comparaison des données structurales et stratigraphiques des Grands Bancs de Terre-Neuve et de la marge ouest-ibérique, Tankard et Welsink (sous presse) expliquent également le fonctionnement des deux marges homologues à partir du modèle de Wernicke (1985). Mais, dans ce dernier cas, la surface de décollement plongerait du banc de Galice en direction de la marge américaine !

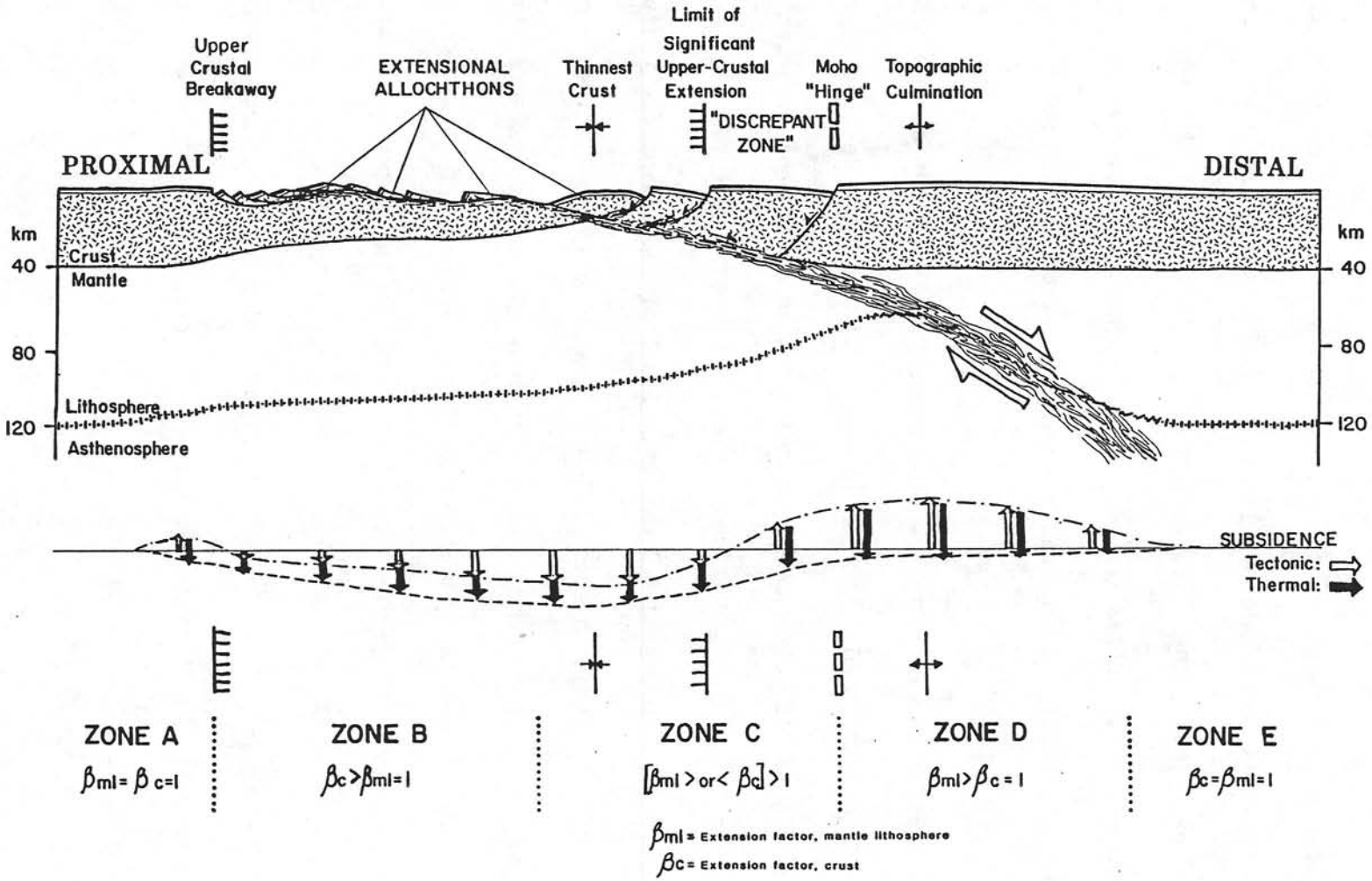


Figure 30 : Modèle de formation des marges en extension par glissement le long d'une zone de décollement intra-lithosphérique (Wernicke, 1985).

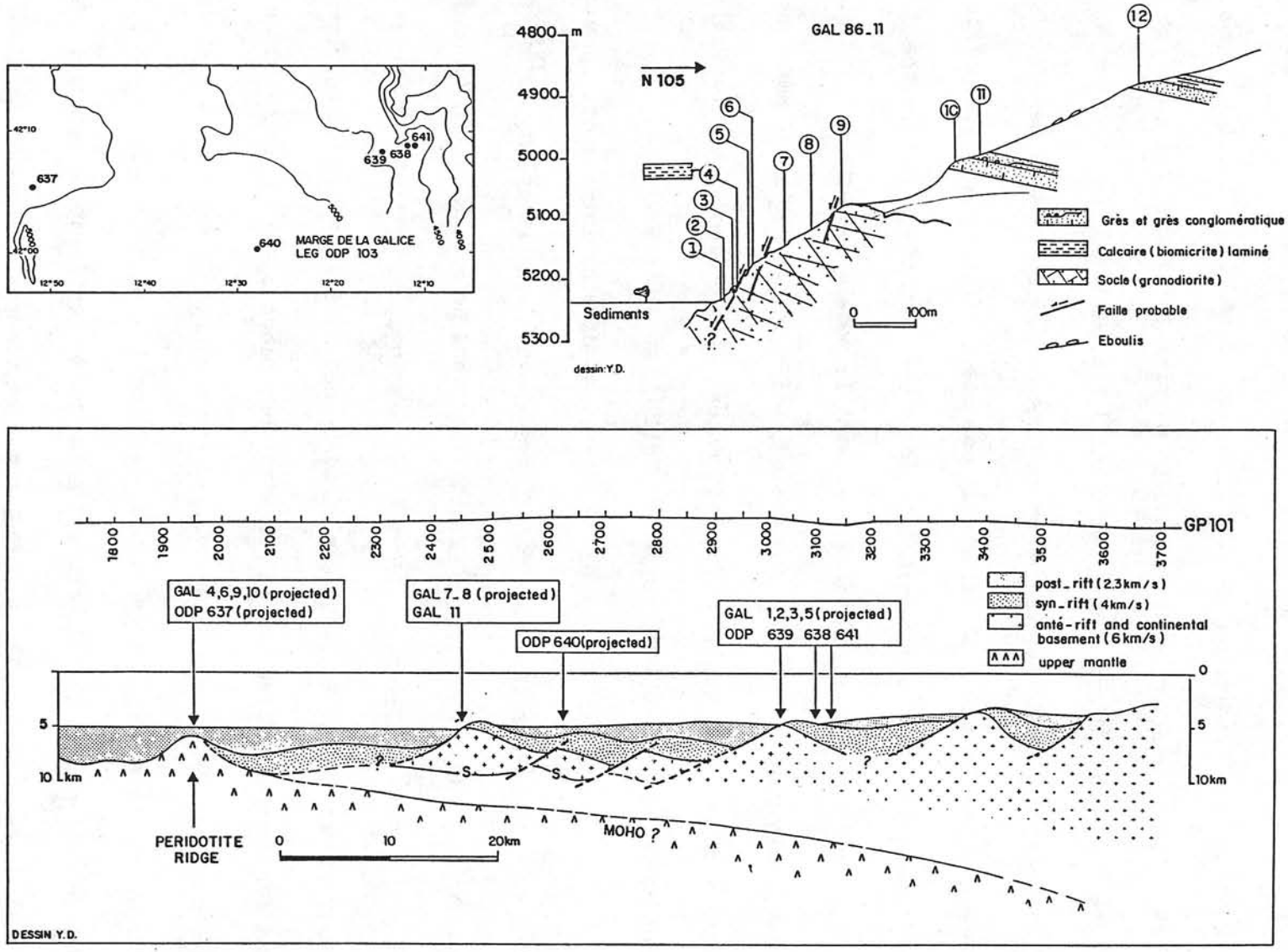


Figure 31 : Modèle de dénudation tectonique du manteau (Boillot et al., 1987).

Les nouvelles données géophysiques de la marge ouest-ibérique semblent en contradiction aussi bien avec le modèle de Boillot et al. (1985, 1986a) que celui de Tankard et Welsink (sous presse). En effet, il n'y a pas d'arguments montrant l'existence d'une surface de décollement majeure remontant sous le banc de Galice ou sous les Grands Bancs de Terre-Neuve. De plus, il semble difficile d'associer le réflecteur S, dont l'extension latérale est limitée à une surface de décollement intra-lithosphèrique, suivant le modèle de Wernicke (1985). Actuellement, nous n'avons aucune indication permettant d'affirmer que cette surface de décollement serait encore plus profonde, au niveau du Moho par exemple, comme le suggèrent Boillot et al. (1987).

Il existe de nombreux exemples de bassins intra-continentaux plus ou moins symétriques, mais rares sont les exemples de rifts symétriques (Bally, 1981). Certaines sections du graben Viking (Thomas et al., 1985 ; Ziegler, 1982) et du bassin de More (Hamar et Hjelle, 1984) montrent une telle symétrie. L'absence de fluage et de diapirisme salifère permet de suivre la géométrie des blocs basculés jusqu'à l'axe des grabens. Des surfaces de décollement majeures ne semblent pas avoir été à l'origine de la formation de ces bassins. Bien que l'on n'ait pas d'information sur la structure de la croûte continentale amincie, ces bassins pourraient avoir été formés par étirement uniforme, sans que le stade où le réflecteur S apparaît ne soit atteint. A l'appui de cette

hypothèse, Barton et Wood (1984) montrent que les données de subsidence obtenues à partir des forages du graben central de la mer du Nord, ainsi que les contraintes de la modèlisation des données de réfraction concernant la structure de la croûte continentale amincie sont expliquées par le modèle d'étirement uniforme.

Nous avons donc les deux termes extrêmes de l'évolution des bassins intra-continentaux : le bassin symétrique, où le modèle d'étirement uniforme semble s'appliquer, et le bassin dissymétrique, où une surface de décollement semble fonctionner dès le début de l'extension. La marge ouest-ibérique serait l'aboutissement, par le mécanisme d'étirement uniforme, de l'évolution d'un bassin symétrique, l'horizon S ne représentant qu'une surface de décollement mécanique à l'interface fragile-ductile. En revanche, la marge nord-Gascogne pourrait correspondre à l'évolution finale d'un bassin dissymétrique, ou à l'évolution intermédiaire d'un bassin symétrique évoluant en bassin dissymétrique à partir d'une certaine valeur de l'extension.

Le mécanisme proposé est obscurci ou ne s'applique pas pour certaines marges passives en extension. En effet, les résultats préliminaires de sismique réfraction (bouées perdables) obtenus parallèlement à la marge de l'éperon de Goban montrent l'existence d'une croûte inférieure à 7,7 km/s d'au moins 5 km d'épaisseur, sous une croûte supérieure à 5,6-6,3 km/s (figure 32). L'erreur sur la

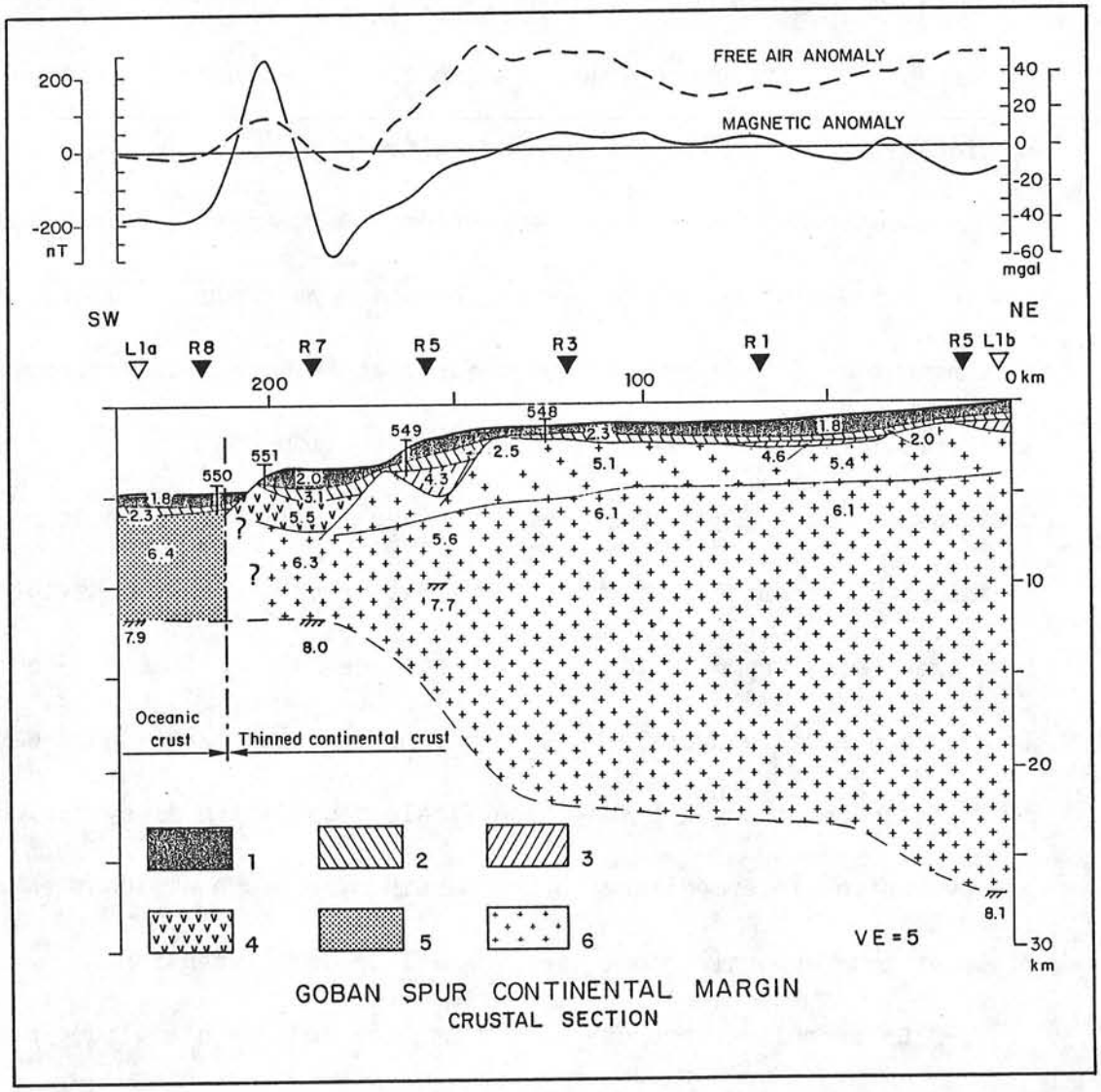


Figure 32 : Structure en vitesse de la marge de l'éperon de Goban. Légende des symboles : 1) et 2) sédiments postrifts ; 3) sédiments synrifts ; 4) volcanisme en domaine continental aminci ; 5) croûte océanique ; 6) croûte continentale.

détermination de la vitesse 7,7 km/s peut être importante. Or, l'un des principaux résultats du projet LASE est la mise en évidence, sous la marge américaine, d'une croûte inférieure à 7,2 km/s de 6 à 9 km d'épaisseur ne présentant pas de discontinuité de vitesse de part et d'autre de la transition continent-océan (Lase study group, 1986). Des vitesses de l'ordre de 7,0 à 7,5 km/s ont également été observées sur de nombreuses marges passives en extension (Nouvelle Ecosse, Keen et al., 1975 ; Australie, Falvey et Middleton, 1981 ; Nord-Ouest Afrique, Weigel et al., 1982). Le groupe Lase (1986) suggère que cette couche à 7,2 km/s aurait une origine plutonique (gabbros) et aurait été mise en place au cours du rifting ou juste après. La fusion partielle du manteau supérieur, conséquence de la remontée des isothermes lors de l'épisode de rifting, puis le refroidissement des produits de fusion dans la partie inférieure de la croûte, entraîneraient la formation d'une couche plutonique similaire à celle de la partie inférieure de la croûte océanique (Foucher et al., 1982).

Le seul bloc basculé permettant de quantifier l'extension superficielle sur la marge de l'éperon de Goban (figures 8 et 32, au niveau du site DSDP 549) est à une profondeur corrigée de 3,45 km pour $\beta$ = 1,20. L'absence du réflecteur S pourrait être due aux faibles valeurs de cette extension superficielle. Dans l'hypothèse de l'étirement uniforme, la profondeur du bloc est de 2 km trop forte pour $\beta$=1,20. La

présence de matériel dense dans la partie inférieure de la croûte amincie pourrait expliquer une partie de la trop forte subsidence de la marge au niveau du site 549. Mais, si l'extension est faible ($\beta < 2$), le taux de fusion partielle et les produits de refroidissement sont donc peu importants (quelques %, Foucher et al., 1982). Comment expliquer alors l'absence d'une telle couche plutonique à 7,2 km/s sous les marges nord-Gascogne et ouest-ibérique ? L'acquisition de données de réfraction précises sur les deux marges de l'éperon de Goban et ouest-ibérique devient donc une priorité pour mieux comprendre les différents mécanismes de formation des marges.

## IV - QUELQUES CONSEQUENCES DU MODELE PROPOSE

Les mesures de flux de chaleur et de sismique réfraction déjà obtenues sur certaines marges ou qui seront obtenues sur les marges de l'éperon de Goban et ouest-ibérique devraient permettre de tester ce modèle ou de le préciser. En particulier, l'existence d'anomalies de flux de chaleur dissymétriques sur les marges correspondantes du nord de la mer Rouge (Martinez et Cochran, sous presse) ou du nord de la Méditerranée occidentale (Burrus et Foucher, 1986) pourrait être expliquée par le fonctionnement d'une surface de décollement. Les conséquences qui découlent du modèle proposé sont multiples. Nous ne développerons ici que les contraintes apportées par ce modèle sur les reconstructions cinématiques prenant en compte la direction et l'amplitude de l'extension au cours du rifting et les conséquences du modèle sur l'érosion des blocs basculés lors de leur glissement et de leur basculement les uns par rapport aux autres.

### 1 - Conséquences cinématiques

Pour reconstituer la position des continents autour de l'océan Atlantique Nord et Central au cours du Jurassique, il est nécessaire de quantifier l'extension Jurassique supérieur - Crétacé inférieur des

marges et bassins intracontinentaux de l'Atlantique Nord et des continents adjacents. Une première tentative a été réalisée par Savostin et al. (1986) en supposant que l'extension était perpendiculaire aux structures distensives et que les marges et bassins intra-continentaux avaient été formés par étirement uniforme. Bien que ces hypothèses soient grossières, Savostin et al. (1986) ont montré que les mouvements obtenus pour les plaques autour de l'Atlantique Nord durant la phase de rifting étaient cohérents et plus ou moins dans la même direction que les mouvements postérieurs. L'application de la méthode de Withjack et Jamison (1986) aux marges de l'Atlantique Nord-Est a permis d'obtenir la direction probable de l'extension pendant le rifting entre l'Amérique du Nord, l'Europe et l'Ibérie.

Moyennant des hypothèses plausibles sur les directions d'ouverture des bassins intra-continentaux, nous pouvons supposer que le système des directions de déplacement des différentes plaques est à peu près contraint. Il n'en est pas de même en ce qui concerne la quantification de l'extension suivant ces directions. Quel que soit le mécanisme de formation des marges, si l'extension est mesurée parallèlement à $\epsilon_{H1}$, il faut introduire une correction due à l'obliquité du rifting. Les diagrammes de prédiction de la direction des failles produites par un rifting oblique (Withjack et Jamison, 1986) montrent que l'angle $\gamma$ entre la direction des failles normales limitant les

blocs basculés et la direction de l'extension varie en fonction de l'angle $\alpha$ entre les directions du rift et de l'extension (table 3, figures 33 et 34) suivant la loi empirique suivante $\gamma = 28,8 + \sin \alpha / 0,0163$ pour $30° < \alpha < 90°$.

$\alpha$ et $\gamma$ étant exprimés en degrés.

L'extension superficielle ou crustale étant mesurée parallèlement à $\epsilon_{H1}$ (perpendiculairement à la direction des blocs basculés), il faut donc diviser cette valeur par sin $\gamma$ pour tenir compte du rifting oblique. La figure 35 donne le facteur multiplicatif à appliquer à la valeur de l'extension mesurée en fonction de $\alpha$. Il augmente exponentiellement avec l'obliquité du rifting. Pour la marge celtique ($\alpha \approx 30°$), le facteur correctif serait de 1,17.

L'extension totale entre deux continents peut être calculée dans l'hypothèse de l'étirement uniforme, à partir de l'extension superficielle ou à partir de la géométrie de la croûte continentale amincie (Le Pichon et Sibuet, 1981). En revanche, lorsque l'extension se traduit par le fonctionnement d'une surface incohérente se développant le long d'un accident crustal antérieur (modèle Le Pichon et Barbier, 1987), le point crucial est de savoir si le volume de croûte continentale est conservé. S'il l'est, les mesures de réfraction permettent de donner la quantité d'extension totale entre deux continents.

| $\alpha$ | $\gamma$ | $1/\sin\gamma$ |
|---|---|---|
| 90° | 90° | 1 |
| 75° | 88° | 1 |
| 60° | 81° | 1,01 |
| 45° | 75° | 1,04 |
| 30° | 59° | 1,17 |

Table 3 : Variation de l'angle $\gamma$ en fonction de l'obliquité du rifting d'après le modèle de Withjack et Jamison (1986). $\alpha$, angle entre les directions du rift et de l'extension ; $\gamma$ angle entre les directions des failles normales et de l'extension. $1/\sin\gamma$ est le facteur correctif à appliquer à l'extension mesurée parallèlement à la plus grande déformation horizontale $\epsilon_{H1}$.

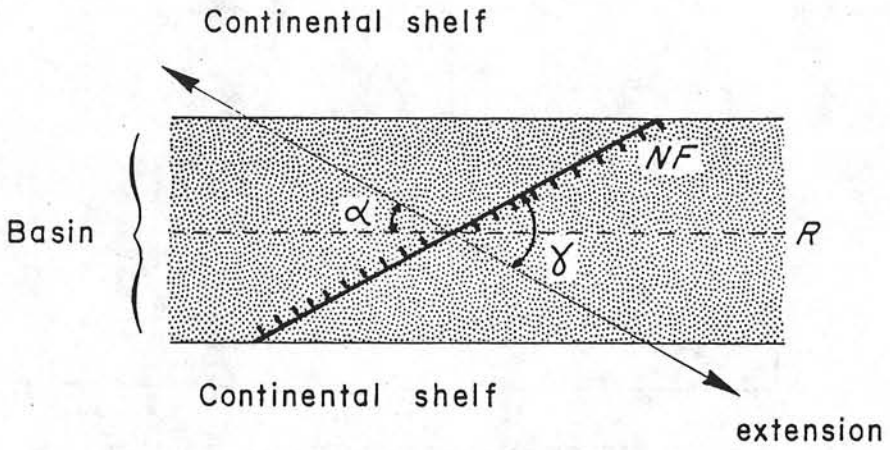


Figure 33 : Schéma d'un bassin avec rifting oblique. N, faille normale ; α, angle aigu entre la direction R du rift et la direction de déplacement entre les côtés opposés du rift (axe fléché) ; $\gamma$ angle entre les directions des failles normales et de l'extension.

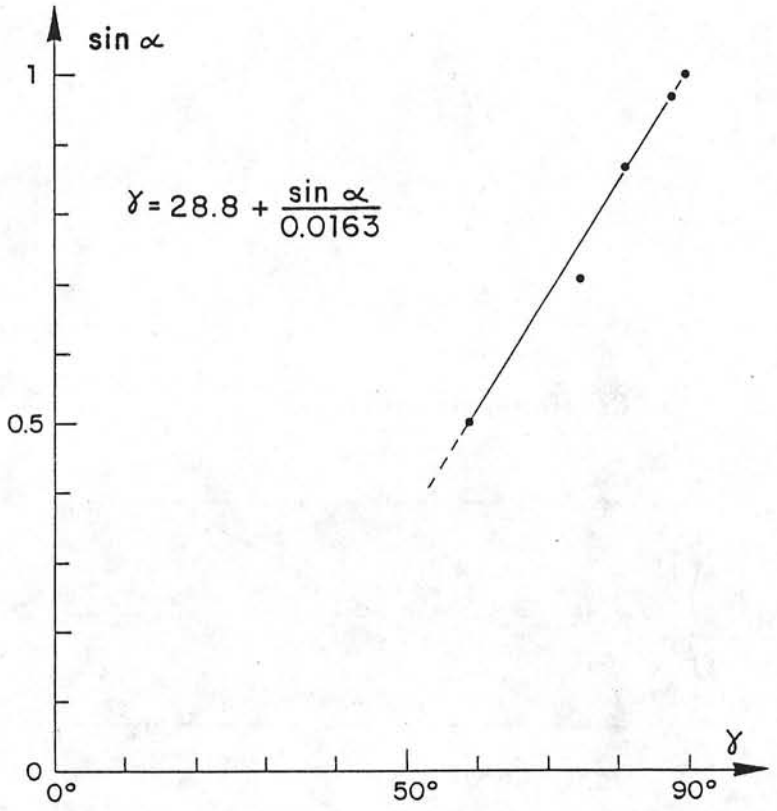


Figure 34 : Loi empirique de correspondance entre l'angle $\gamma$ entre les directions des failles normales et de l'extension et sin α, α étant l'obliquité du rifting.

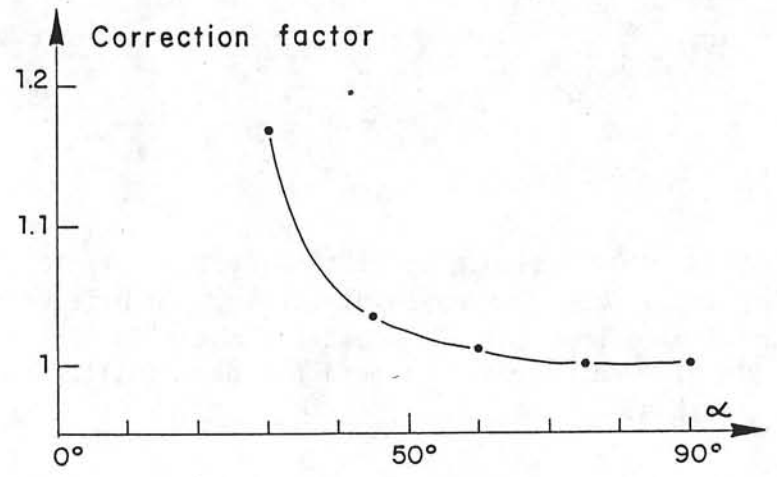


Figure 35 : Facteur correctif à appliquer à la valeur de l'extension en fonction de l'obliquité α du rifting.

2 - Conséquences sur l'érosion des blocs basculés

Les crêtes des blocs basculés situés en haut de marge sont souvent tronquées par des surfaces généralement planes, horizontales ou à faible pendage vers l'océan, formant un angle pouvant atteindre plus de 10° avec la stratification des séries antérifts (figures 36 et 37). Ces surfaces ont été interprétées comme des reliques de surfaces d'érosion sub-aérienne créées à la fin ou juste après la phase de rifting (Montadert et al., 1979 ; Groupe Galice, 1979 ; Sibuet et Ryan, 1979). L'amplitude de l'érosion peut atteindre 1 km (figure 37). La distribution géographique des surfaces d'érosion sur les marges celtique et de l'éperon de Goban (figure 10) montre qu'elles se situent essentiellement à des profondeurs inférieures à 2 km. Sur la marge ouest-ibérique, les surfaces d'érosion se trouvent également dans le même contexte (Sibuet et Ryan, 1979). Nous proposons de montrer que l'érosion sub-aérienne des blocs basculés est à la fois la conséquence du basculement des blocs amenant leur partie sommitale à l'air libre et de l'effet de la conduction latérale entraînant un soulèvement des bords du rift.

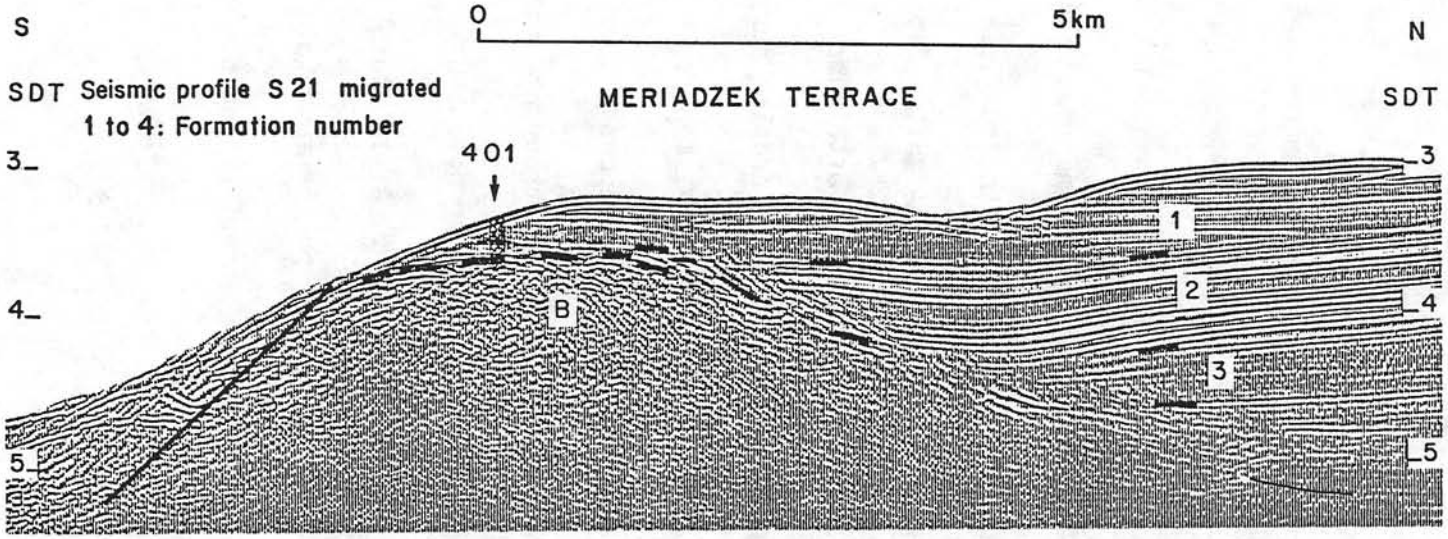


Figure 36 : Profil sismique migré obtenu sur la terrasse de Mériadzek (Montadert, Roberts et al., 1979). La crête du bloc a été érodée au cours de la phase du rifting. Des carbonates de plateforme du Jurassique supérieur -Crétacé basal ont été forés au site DSDP 401.

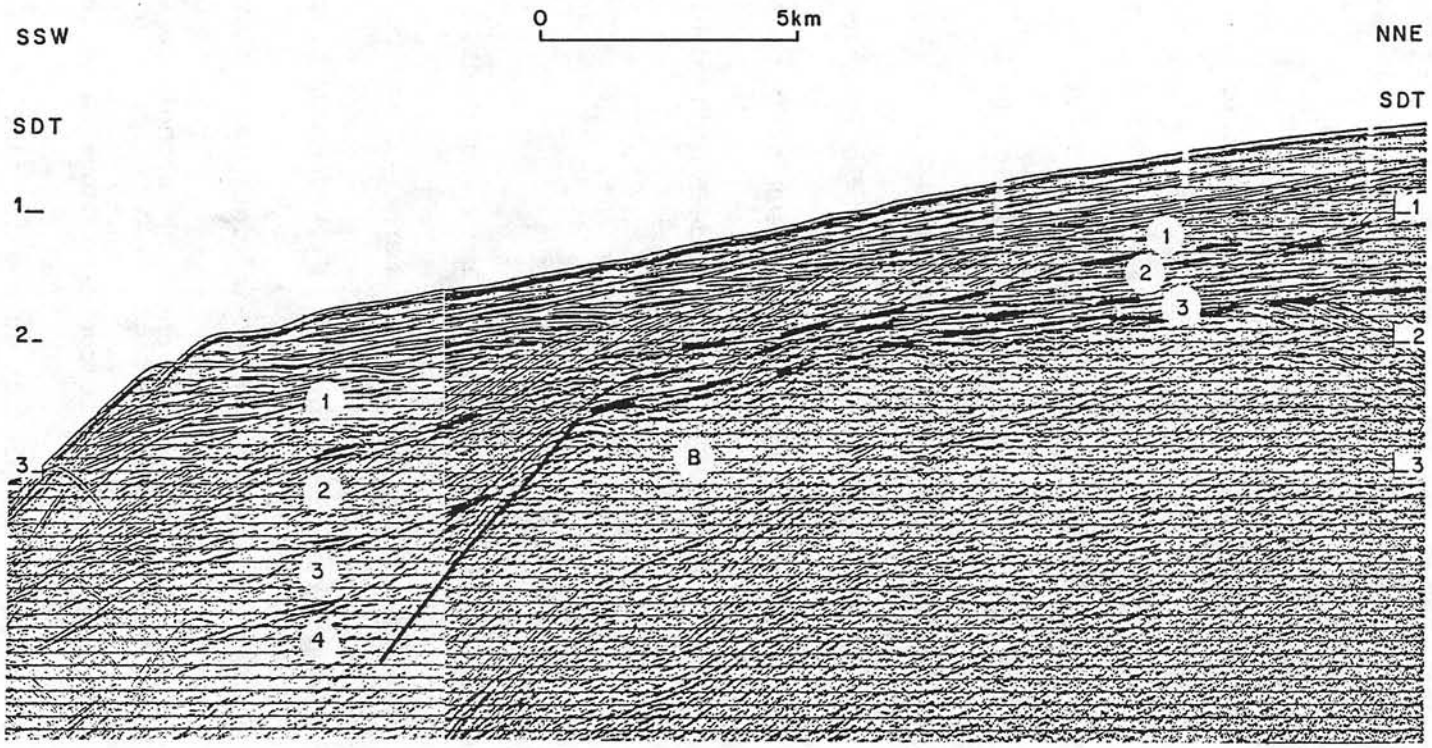


Figure 37 : Profil sismique multitrace CM14 obtenu sur la marge nord-Gascogne (Montadert et al., 1979). La surface d'érosion est constituée de deux surfaces planes distinctes.

Nous avons vu que le modèle d'étirement uniforme s'appliquait à la marge ouest-ibérique au moins jusqu'à une valeur $\beta_{max}$ de 2,8 à 3,2 et que la phase de rifting affectait une lithosphère continentale dont le toit était proche du niveau de la mer (carbonates de plateforme du Jurassique terminal). Le facteur d'étirement $\beta$ est fonction des paramètres qui définissent la géométrie des blocs basculés (figure 23, Le Pichon et Sibuet, 1981).

$$\beta = \sin(\alpha'+\theta'-\theta)/\sin(\alpha'+\theta') - dh/dltg(\alpha'+\theta')$$

où $\alpha$ est le supplément de l'angle du plan de faille par rapport au pendage des couches, $\theta$ est l'angle de basculement des blocs, $\alpha'$ et $\theta'$ étant relatifs au bloc amont précédent, dl est la largeur initiale du bloc et dh est la différence de hauteur entre deux blocs consécutifs.

$\beta$ est également fonction de la profondeur h+dh du bloc à la fin du rifting :

$$h+dh = 3,6(1-1/\beta)$$

En éliminant $\beta$ de ce système de deux équations, nous pouvons donc modéliser la morphologie d'une marge. A titre d'exemple, connaissant les paramètres dl, dh, $\alpha$ et $\theta$ pour chaque bloc basculé du profil perpendiculaire à la marge ouest-ibérique de la figure 20, nous constatons une bonne correspondance entre la morphologie et le modèle (figure 38). En particulier, la bonne correspondance entre les positions des blocs basculés de l'exemple et du modèle démontre la validité du

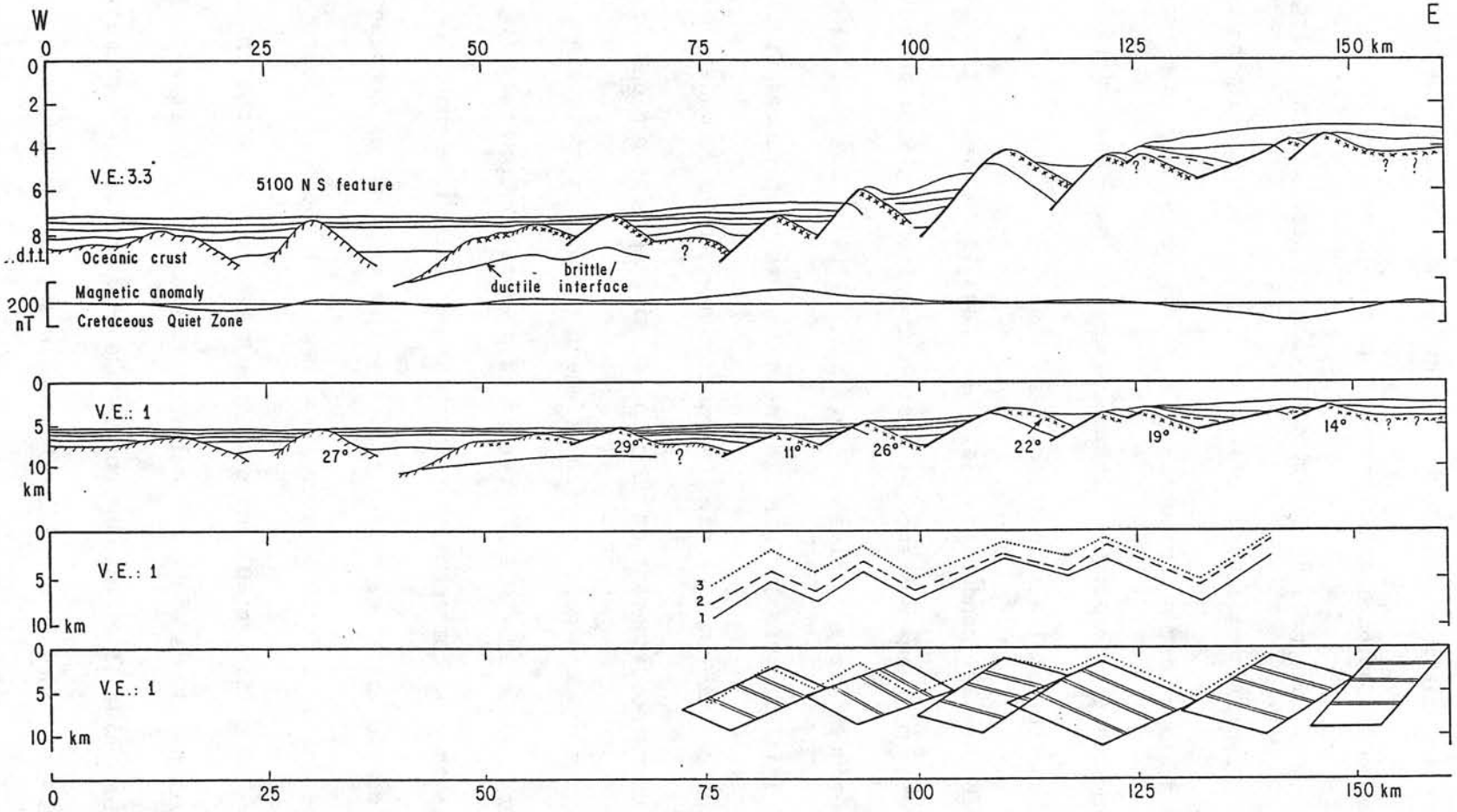


Figure 38 : Essai de modélisation de la formation de la partie supérieure de la marge ouest-ibérique dans l'hypothèse de l'étirement uniforme. Les lignes brisées 1, 2 et 3 représentent la morphologie simplifiée du toit des blocs basculés respectivement à la profondeur actuelle, réajustée de la surcharge des sédiments post et synrifts, et après le rifting dans le cadre du modèle d'étirement uniforme. Le graphique du bas montre la bonne correspondance globale entre la morphologie de la marge après le rifting et la distribution des blocs basculés supposés rigides connaissant dh, dl, $\alpha$ et $\theta$ pour chaque bloc.

modèle d'étirement uniforme pour toute la partie supérieure de la marge. Des essais de modélisation complémentaires ont permis de montrer que les blocs situés près du rebord du plateau continental peuvent émerger quelles que soient les valeurs de $\alpha$ et $\theta$ si dl > 10 km. A condition que la largeur des blocs soit supérieure à 10 km, nous avons donc un premier mécanisme permettant d'expliquer la présence de surfaces d'érosion affectant la partie sommitale des blocs basculés.

L'effet de la conduction latérale dans le modèle d'étirement uniforme a été mis en évidence et testé par Watremez (1980) puis par différents auteurs (e.g. Alvarez et al., 1984). Le modèle bi-dimensionnel initial, résolu par la méthode des différences finies, suppose un étirement instantané. Les deux conséquences du modèle sont d'une part un refroidissement et donc une subsidence plus rapides de la zone étirée, et d'autre part un réchauffement et donc un soulèvement de la lithosphère non étirée près du rebord du plateau continental (figure 39). La croissance du bombement et sa hauteur maximale h dépendent de la largeur $\Delta x$ de la zone de transition. Avec les valeurs des constantes choisies par Watremez (1980), pour $\Delta x$ = 50 km, h = 400 m, et pour $\Delta x$ = 100 km, h = 150 m (figure 40), mais la valeur maximale du bombement est atteinte environ 10 Ma après l'étirement instantané (Alvarez et al., 1984). De plus, Alvarez et al. ont montré que l'amplitude du bombement B augmentait avec la durée t du rifting selon la loi empirique :

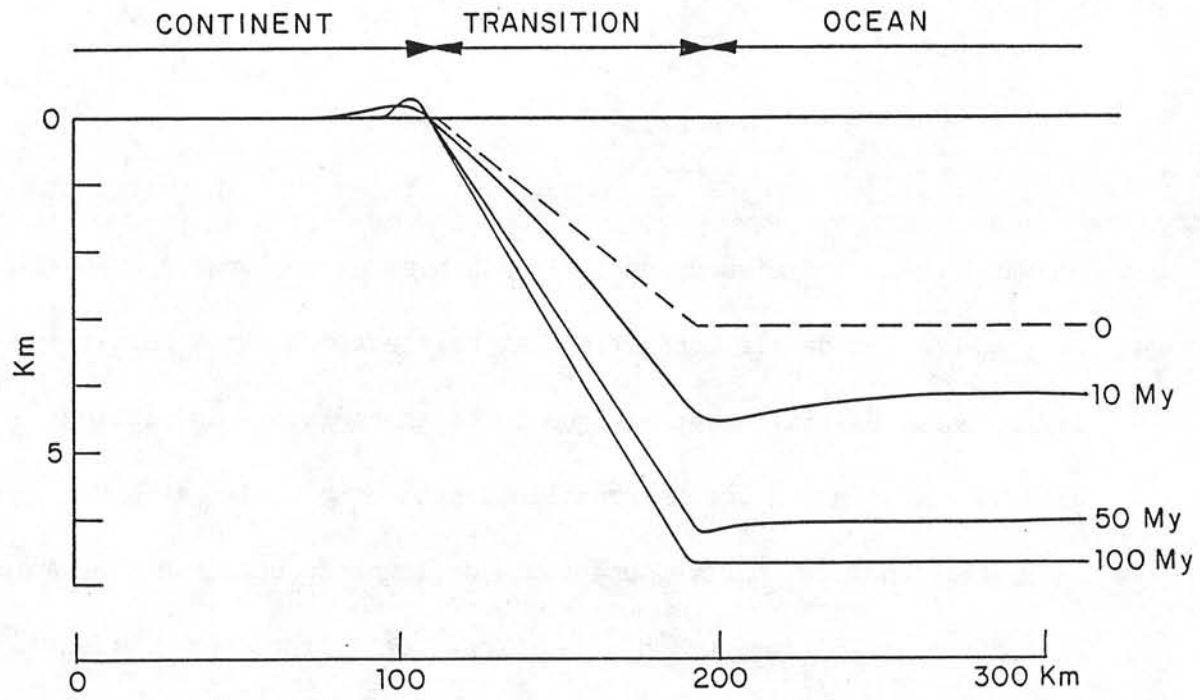


Figure 39 : Modèle bi-dimensionnel de subsidence d'une marge formé par étirement uniforme instantané. La largeur de la marge est de 80 km, $\beta_{max}$ = 7 (Watremez, 1980).

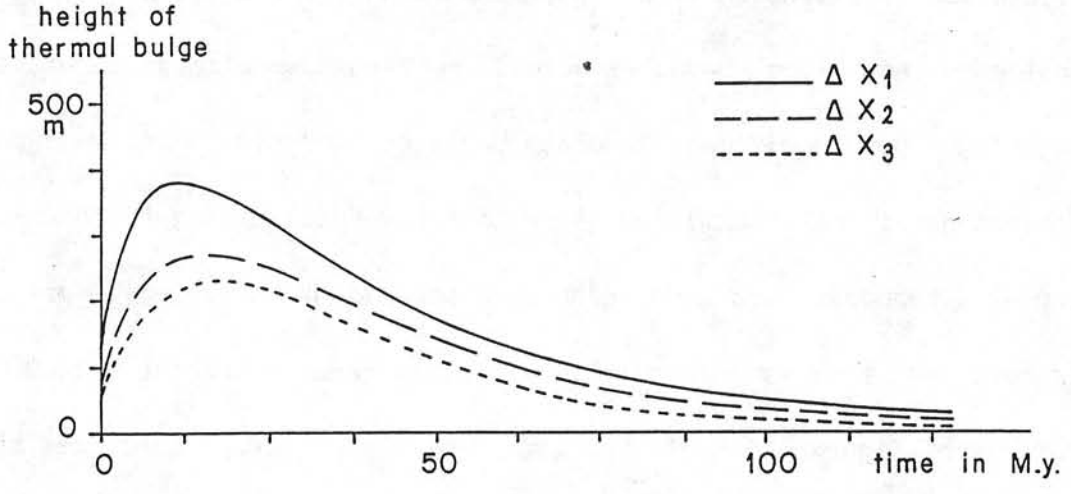


Figure 40 : Variations de hauteur maximale du bombement thermique en fonction du temps pour des largeurs de marges Δx1 = 50 km, Δx2 = 80 km et Δx3 = 100 km (Watremez, 1980).

$B = 21,5t^{0.213}\ \beta h_L/L$

pour $5<t<50$

B étant exprimé en mètres et t en Ma, $h_L$ et $L=2\Delta x$ étant respectivement l'épaisseur de la lithosphère et la largeur du bassin.

L'effet de la conduction latérale est donc très faible au début de la phase de rifting et maximum juste après la fin du rifting, ce qui va dans le sens d'une surrection des blocs basculés et d'une érosion maximales dans la partie supérieure de la pente continentale. Au cours du rifting, la largeur de la bande de lithosphère affectée par l'extension pourrait augmenter, les failles limitant les blocs basculés commençant à jouer de plus en plus tardivement en direction du continent. Autrement dit, à contrainte constante, la déformation initiale et la subsidence seraient très importantes au début du rifting et diminueraient avec le temps, au fur et à mesure que le domaine affecté par l'extension serait plus important. Dans cette hypothèse, la subsidence des blocs basculés actuellement en bas de marge serait très rapide au début du rifting, la crête des blocs basculés n'arrivant pas à l'émersion (si dl<10 km) ou ne restant pas suffisamment à l'air libre pour être érodée. Ces deux mécanismes pourraient expliquer la présence des surfaces érodées essentiellement limitées à la tranche 0-2000 m de profondeur (figure 10). Toutefois, dans le golfe de Suez, les blocs basculés de la partie supérieure de la marge ont émergé et ont été

érodés après une première phase de subsidence. Cette surrection pourrait être liée à un bombement asthénosphérique (X. Le Pichon, communication personnelle, 1987).

Les surfaces d'érosion sont planes ou très légèrement concaves vers le bas. Cette concavité pourrait être le résultat d'une érosion sub-aérienne contemporaine de l'émersion et de la rotation des blocs basculés suivant le mécanisme suggéré dans la figure 41. L'angle de surfaces d'érosion planes avec l'horizontale a été mesuré pour 14 blocs basculés de la marge celtique dont la longueur initiale dl est comprise entre 9 et 24 km. Le pendage moyen est de 1,0°±1,3° en direction de l'océan. Dans le modèle d'étirement uniforme, la subsidence thermique d'une marge formée il y a 120 M.a. (Le Pichon et Sibuet, 1981) est

$$Z_{th} = 3,9\ (1-1/\beta)$$

c'est-à-dire de 2,7 km pour $\beta_{max} = 3,2$. En supposant que la largeur de la marge celtique soit $\Delta x = 150$ km, le basculement de la marge dû à la subsidence thermique serait de 1°. Le pendage moyen des surfaces d'érosion de 1° vers l'océan correspond donc à la subsidence thermique de la marge celtique. Il est probable que la subsidence thermique calculée à partir d'autres modèles (e.g. surface de décollement) donnerait une valeur du basculement de la marge peu différente.

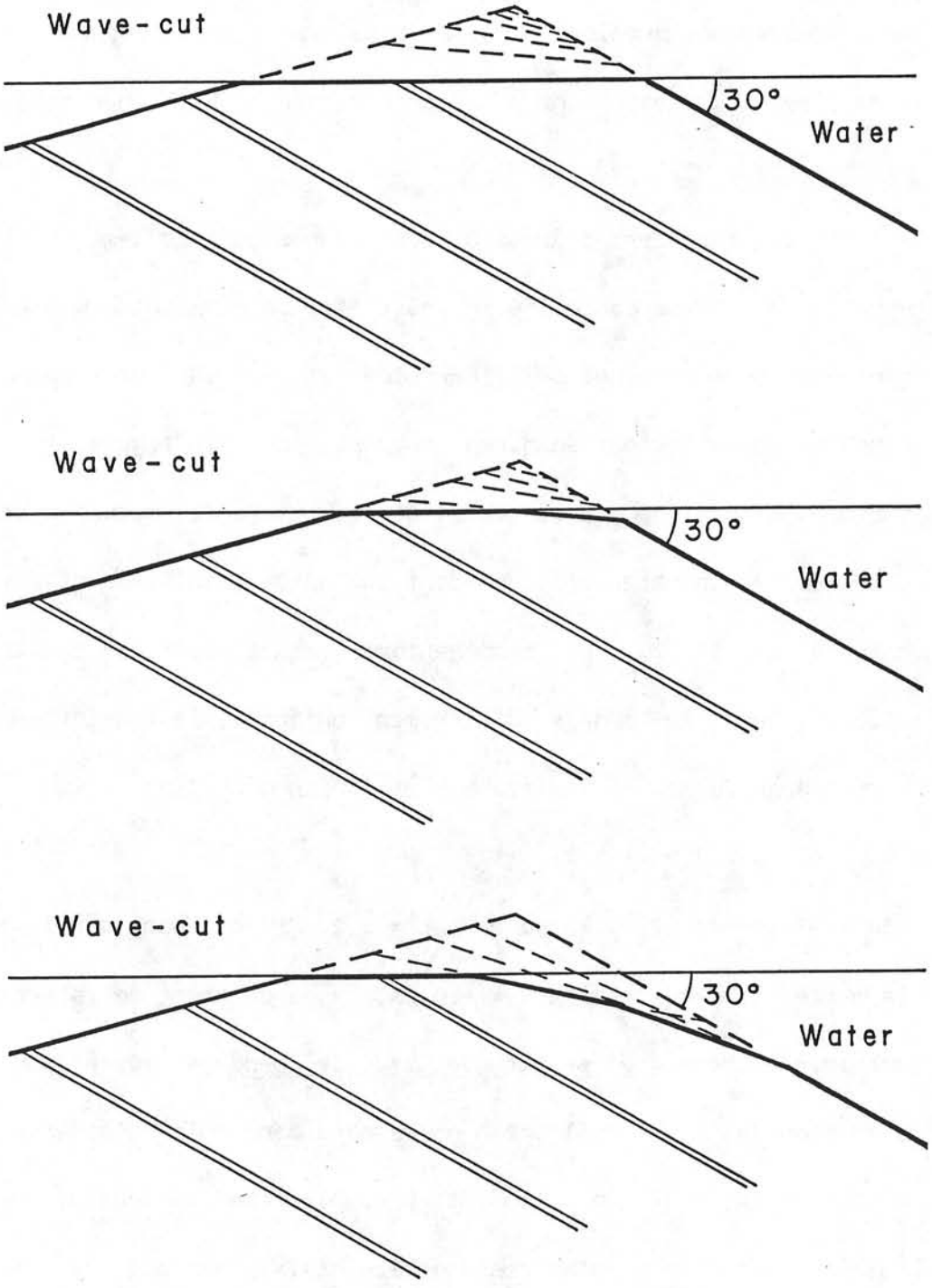


Figure 41 : Mécanismes possibles d'érosion sub-aérienne de la crête des blocs basculés au cours de leur rotation. En haut, surface plane (exemple de la figure 36) ; au milieu, deux surfaces planes (exemple de la figure 37) ; en bas, surface à facettes multiples.

## V - CONCLUSIONS

Les modèles de formation et d'évolution des marges continentales passives n'ont pu être élaborés, modifiés et testés seulement parce que de nombreux levés géologiques et géophysiques de détail on été acquis, notamment par les institutions françaises et anglaises, sur les marges peu sédimentées de l'Atlantique Nord-Est. L'intégration de l'ensemble de ces données nous amène aux conclusions suivantes :

- Au cours de l'épisode de rifting, les directions des mouvements des plaques Amérique du Nord, Europe et Ibérie sont identiques aux directions d'ouverture du domaine océanique adjacent.

- Quantifier l'extension totale résultant du rifting nécessite de mieux appréhender les processus de formation des marges. Les valeurs de l'extension superficielle, mesurées à partir de la géométrie des blocs basculés de la marge ouest-ibérique, sont compatibles avec le modèle d'étirement uniforme pour la partie supérieure de la marge, jusqu'à une profondeur de 5,5 km. En bas de marge, le réflecteur S est observé. Il est interprété comme une discontinuité mécanique qui apparaîtrait pour des valeurs de l'extension supérieures à 2,8-3,2, lorsque le basculement des blocs atteint la valeur limite de 20 à 30°. L'extension mesurée est inférieure à celle prédite par le modèle d'étirement uniforme car elle ne rend compte que d'une partie de

l'extension, celle qui affecte les sédiments synrifts déposés au début du rifting. Les données de la marge ouest-ibérique sont cependant compatibles avec le modèle d'étirement uniforme. Ce type de marge pourrait être considéré comme l'évolution finale d'un bassin intra-continental symétrique créé par étirement uniforme.

Au contraire, en ce qui concerne la marge nord-Gascogne, Le Pichon et Barbier (1987) supposent qu'une surface de décollement, traversant toute la croûte supérieure jusqu'à l'interface fragile-ductile, aurait fonctionné dès le début de la phase de rifting. Les failles limitant les blocs basculés seraient alors des failles antithétiques. Ce type de marge pourrait être considéré comme l'évolution finale d'un bassin intra-continental asymétrique où une surface de décollement reprendrait un accident ancien et fonctionnerait dès le début de l'extension.

A titre d'hypothèse, nous proposons un modèle de formation des marges continentales par étirement uniforme dans lequel, après une phase d'extension, où localement l'extension peut atteindre 2,8 à 3,2, la surface cohérente située à la transition fragile-ductile évoluerait en surface incohérente. Lorsque des accidents structuraux majeurs existent dans la croûte continentale, un accident particulier pourrait être utilisé comme surface de décollement privilégiée. Cette surface de décollement pourrait fonctionner dès le début du rifting (modèle Le

Pichon et Barbier) ou à partir d'un stade intermédiaire de formation du bassin.

BIBLIOGRAPHIE

Allmendiger R.W., Sharp J.W., Von Tish D., Serpa L., Brown L., Kaufman S., Oliver J., et Smith R.B., 1983. Cenozoic and mesozoic structure of the eastern Basin and Range from COCORP seismic reflection data. Geology, 11, p. 532-536.

Alvarez F., Virieux J., et Le Pichon X., 1984. Thermal consequences of lithosphere extension over continental margins : the initial stretching phase. Geophys. J.R. Astr. Soc., 78, p. 389-411.

Anderson R.E., Zoback M.L., et Thompson G.A., 1983. Implications of selected subsurface data on the structural form and evolution of some basins in the northern Basin and range province, Nevada and Utah. Geol. Soc. Am. Bull., 94, p. 1055-1072.

Artemjev M.E., et Arthyshkov E.V., 1971. Structure and isostasy of the Baikal rift and the mechanism of rifting. J. Geophys. Res., 76, p. 1197-1211.

Bacon M., et Gray F., 1970. A gravity survey in the eastern part of the Bay of Biscay. Earth Planet. Sci. Letters, 10, p. 101-105.

Bain G.W., et Beebe J.H., 1954. Scale model reproduction of tension faults. Am. J. Sci., 252, p. 745-754.

Bally A.W., 1981. Atlantic-type margins. In Geology of passive continental margins : history, structure and sedimentologic record (with special emphasis on the Atlantic margin), Bally A.W., Watts A.B., Grow J.A., Manspeizer W., Bernoulli D., Schreiber C., et Hunt J.M. (eds.), Am. Assoc. Petrol. Geol., Education course note series 19, 1, p. 1-48.

Barbier F., Le Pichon X., et Duvergé J., 1986. Structure profonde de la marge Nord-Gascogne. Implications sur le mécanisme de rifting et de formation de la marge continentale. Bull. Centres Rech. Explor. - Prod. Elf Aquitaine, 10, 1, p. 105-121.

Barton P., et Wood R., 1984. Tectonic evolution of the North Sea Basin : crustal stretching and subsidence. Geophys. J. R. Ast. Soc., 79, p. 987 - 1022.

Beaumont C., Keen C.E., et Boutilier R., 1982. On the evolution of rifted continental margins : Comparison of models and observations for the Nova Scotian margin. Geophys. J.R. Astron. Soc., 70, p. 667-715.

Boillot G., Auxiêtre J., Dunand J., Dupeuble P., et Mauffret A., 1979. The northwestern iberian margin : a Cretaceous passive margin deformed during Eocene. In Deep Drilling Results in the Atlantic Ocean : continental margins and Paleoenvironment, Talwani M., Hay W., et Ryan W.B.F. (eds.), M. Ewing series 3, American Geophysical Union, Washington D.C., p. 138-153.

Boillot G., Grimaud S., Mauffret A., Mougenot D., Kornprobst J., Mergoil-Daniel J., et Torrent G., 1980. Ocean-continent transition off the Iberian margin : a serpentinite diapir west of Galicia Bank. Earth Planet. Sci. Letters, 48, p. 23-34.

Boillot G., 1984. Some remarks on the continental margins in the Aquitaine and French Pyrenees. Geol. mag., 121, p. 407-412.

Boillot G., Winterer E., et al., 1985. Résultats préliminaires de la campagne 103 du Joides Resolution (Ocean Drilling Program) au large de la Galice (Espagne) : sédimentation et distension pendant le "rifting" d'une marge stable ; hypothèse d'une dénudation tectonique. C.R. Acad. Sc., Paris, 301, p. 627-632.

Boillot G., Winterer E., et al., 1986a. Rifting processes and possible tectonic denudation of the upper mantle on the Galicia margin (Spain) : preliminary results of ODP Leg 103. Geotimes, 31, p. 15-17.

Boillot G., Comas M., Girardeau J., Kornprobst J., Loreau J.-P., Malod J., Mougenot D., et Moullade M., 1986 b. Fonds sous-marins basaltiques et ultramafiques au pied d'une marge stable. Résultats préliminaires de la campagne Galinaute (plongées du submersible Nautile à l'Ouest de l'Espagne). C.R. Acad. Sc., Paris, 303, p. 1719-1724.

Boillot G., Recq M., Winterer E.L., Meyer A.W., Applegate J., Baltuck M., Bergen J.A., Comas M.C., Davies T.A., Dunham K., Evans C.A., Girardeau J., Goldberg G., Haggerty J., Jansa L.F., Johnson J.a., Kasahara J., Loreau J.-P., Luna-Sierra E., Moullade M., Ogg J., Sarti M., Thurow J., et Williamson M., 1987. Tectonic denudation of the upper mantle along passive margins : a model based on drilling results (ODP leg 103, western Galicia margin, Spain). Tectonophysics, 132, p. 335-342.

Bott M.H.P., 1973. Shelf subsidence in relation to the evolution of young continental margins. In Implications of continental drift to the Earth Sciences, Tarling D.H., et Runcorn S.K. (eds.), Academic Press,

London, 2, p. 675.

Brun J.-P., et Choukroune P., 1983. Normal faulting, block tilting and "décollement" in a stretched crust. Tectonics, 2, p. 345-356.

Brun J.-P., Choukroune P., et Faugère E., 1985. Les discontinuités significatives de l'amincissement crustal : application aux marges passives, Bull. Soc. Géol. France, 8, p. 139-144.

Burrus J., et Foucher J.-P., 1986. Contribution to the thermal regime of the Provençal basin based on flumed heat flow surveys and previous investigations, Tectonophysics, 128, p. 303-334.

Cheadle M., Matthews D., Warner M., Mascle A., Gariel O., Montadert M., Lefort J.-P., Le Gall B., Sibuet J.-C., Cazes M., et Schroeder M., 1986. Deep seismic reflection profiling between England, France and Ireland. Journal of the Geological Society, London, 143, p. 45-52.

Chenet P.-Y., Montadert L., Gairaud H., et Roberts D., 1983. Extension ratio measurements on the Galicia, Portugal and Northern Biscay continental margins : Implications for evolutionary models of passive continental margins. In Studies in continental margin geology, Watkins

J.S., et Drake C.L. (eds.), Am. Assoc. Petrol. Geol. memoir 34, p. 703-715.

Chenet P.-Y., Coletta B., Letouzey J., Desforges G., Ousset E., et Zaghloul E., sous presse. Structures associated with extensional tectonics in the Suez rift, J. Geol. Soc., Proceedings of the Continental extensional tectonics meeting, Durham, Avril 1985.

Choukroune P., Le Pichon X., Seguret M., et Sibuet J.-C., 1973. Bay of Biscay and Pyrénées. Earth Planet Sci. Letters, 18, p. 109-118.

de Charpal O., Guennoc P., Montadert L., et Roberts D.G., 1978. Rifting, crustal attenuation and subsidence in the Bay of Biscay. Nature, 275, p. 706-711.

de Graciansky P.-C., Poag C.W., et al., 1985a. Initial Reports of the Deep Sea Drilling Project, 80, Washington, U.S. Government Printing Office.

de Graciansky P.-C., Poag C.W., et al., 1985b. Site 551. In de Graciansky P.-C., Poag C.W., et al., Initial Reports of the Deep Sea Drilling Project, 80, Washington, U.S. Government Printing Office, p.

357-385.

Derégnaucourt D., et Boillot G., 1982. Structure géologique du Golfe de Gascogne, Bull. Bur. Rech. Géol. Min. 2, 1, 3, Géol. Gîtes Miner. Fr., p. 149-178.

Diament M., Sibuet J.-C., et Hadaoui A., 1986. Isostasy of the northern bay of Biscay continental margin. Geophys. J. R.A.S., 86, p. 893-907.

Falvey D.A., 1974. The development of continental margins in plate tectonic theory. Aust. Pet. Explor. Assoc. J., 14, p. 95-106.

Falvey D.A., et Middleton M.F., 1981. Passive continental margins : evidence for a pre-breakup deep crustal metamorphic subsidence mechanism. In colloquium on Geology of continental margins (C3), Oceanologica Acta, 4, p. 103-114.

Foucher J.-P., et Sibuet J.-C., 1980. Thermal regime of the northern bay of Biscay continental margin in the vicinity of the D.S.D.P. sites 400 - 402. Phil. Trans. R. Soc. Lond., A294, p. 157-167.

Foucher J.-P., Le Pichon X., et Sibuet J.-C., 1982. The ocean-continent transition in the uniform lithospheric stretching model : role of partial melting in the mantle. Phil. Trans. R. Soc. Lond., A 305, p. 27-43.

Ginzburg A., Whitmarsh R.B., Roberts D.G., Montadert L., Camus A.L., et Avedik F., 1985. The deep seismic structure of the northern continental margin of the Bay of Biscay, Annales Geophysicae, 3, p. 499-510.

Groupe Cybère, 1984. La marge déformée du Nord-Ouest de l'Espagne. Publications du CNEXO, Paris, Résultats des campagnes à la mer, 29, 135 p.

Groupe Galice, 1979. The continental margin off Galicia and Portugal : acoustical stratigraphy, dredge stratigraphy, and structural evolution. In Sibuet J.-C., Ryan W.B.F. et al., Initial Reports of the Deep Sea Drilling Project, 47, part 2, Washington (U.S. Government Printing Office), p. 633-662.

Hamar G.P., et Hjelle K., 1984. Tectonic framework of the More Basin and the northern North Sea. In Petroleum Geology of the North European margin, Spencer A.M., et al., (eds.), Graham and Trotman Ltd, London, p.

349-358.

Keen C.E., Keen M.J., Barrett D.L., et Heffler D.E., 1975. Some aspects of the ocean-continent transition at the continental margin of eastern North-America. In offshore geology of eastern Canada, 2, Regional geology, Van den Linden, W.J.M. et Wade, J.A. (eds.), Geol. Surv., Can. Pap., 74-30, p. 189-197.

Lalaut P., 1981. Contribution à l'étude de la structure profonde du Golfe de Gascogne par méthodes gravimétriques. Thèse 3ème Cycle, Université Pierre et Marie Curie, Paris 6, 131 p.

Lallemand S., Mazé J.-P., Monti S., et Sibuet J.-C., 1985a. Présentation d'une carte bathymétrique de l'Atlantique nord-est. C.R. Acad. Sc. Paris, t. 300, 4, p. 145-149.

Lallemand S., Mazé J.-P., Monti S., et Sibuet J.-C., 1985b. Carte bathymétrique de l'Atlantique Nord-Est, échelle 1/2400000, CNEXO, Paris, diffusée par le BRGM, Service Promotion et Vente, BP 6009, 45018 Orléans Cédex.

Lallemand S., et Sibuet J.-C., 1986. Tectonic implications of canyon directions over the northeast Atlantic continental margins. Tectonics, 5, p. 1125-1143.

Lase Study group, 1986. Deep structure of the US East Coast passive margin from large aperture seismic experiments (LASE). Marine and Petroleum Geology, 3, p. 234-242.

Le Pichon X., Ewing J., et Houtz R.E., 1968. Deep-sea sediments velocity determination while reflection profiling. J. Geophys. Res., 73, p. 2597-2615.

Le Pichon X., Bonnin J., Francheteau J., et Sibuet J.-C., 1971. Une hypothèse d'évolution tectonique du golfe de Gascogne. In Histoire structurale du golfe de Gascogne, Debyser J., Le Pichon X., et Montadert L. (eds.). Technip. Paris, VI-11, p. 1-44.

Le Pichon X., et Sibuet J.-C., 1981. Passive margins : a model of formation. J. Geophys. Res., 86, p. 3708-3720.

Le Pichon X., Angelier J., et Sibuet J.-C., 1982. Plate boundaries and extensional tectonics. Tectonophysics, 81, p. 239-256.

Le Pichon X., Angelier J., et Sibuet J.-C., 1983. Subsidence and stretching. Studies in continental margin geology, Watkins J.S., and Clarke C.L. (eds), AAPG Memoir n° 29, Tulsa, p. 731-741.

Le Pichon X., et Barbier F., 1987. Passive margin formation by low-angle faulting within the upper crust : the northern Bay of Biscay margin. Tectonics, 6, p. 133-150.

Martinez F., et Cochran J.R., sous presse. Structure and tectonics of the northern Red Sea : Catching a continental margin between rifting and drifting.

Masson D.G., Montadert L., Scrutton R.A., et Gruvel J.P., 1985. Evolution of the Goban Spur : History of a starved passive margin. In Graciansky P.-C. de, Poag C.W., et al., Initial Reports of the Deep Sea Drilling Project, 80, Washington, U.S. Government Printing Office, p. 115-1140.

Mauffret A., et Montadert L., 1987. Rift tectonics on the passive continental margin off Galicia (Spain). Marine and Petroleum Geology, 4, p. 49-70.

McKenzie D., 1978. Some remarks on the development of sedimentary basins. Earth Planet. Sci. Lett., 40, p. 25-32.

Montadert L., et Winnock E., 1971. L'histoire structurale du Golfe de Gascogne. In Histoire structurale du golfe de Gascogne, J. Debyser, X. Le Pichon et L. Montadert (eds.). Technip, Paris, VI-16, p. 1-18.

Montadert L., Roberts D.G., et al., 1979. Initial Reports of the Deep-sea Drilling Project, v. 48, Washington, U.S. Government Printing Office.

Montadert L., de Charpal O., Roberts D., Guennoc P., et Sibuet J.-C., 1979. Northeast Atlantic passive margins : rifting and subsidence processes. In Deep Drilling results in the Atlantic Ocean : continental margins and paleoenvironment, edited by M. Talwani, W.W.Hay, et W.B.F. Ryan, M. Ewing Series 3, American Geophysical Union, Washington, p. 164-186.

Oertel G., 1965. The mechanism of faulting in clay experiments. Tectonophysics, 2, p. 343-393.

Olivet J.-L., Bonnin J., Beuzart P., et Auzende J.-M., 1984. Cinématique de l'Atlantique Nord et Central. In Publications du Centre National pour l'Exploitation des Océans, Paris, 108 p.

Pastouret L., Auffret G.A., Auzende J.-M., Beuzart P., Dubois P., Séguret M., Sigal J., et Vanney J.-R., 1981. La marge continentale armoricaine, résultats d'observations en submersible et de dragages dans le canyon Shamrock. C.R. Acad., t. 292, p. 741-748.

Royden L., Sclater J.G., et von Herzen R.P., 1980. Continental margin subsidence and heat flow : important parameters in formation of petroleum hydrocarbons. Am. Assoc. Pet. Geol. Bull., 64, p. 173-187.

Savostin, L.A., Sibuet, J.-C., Zonenshain L.-P., Le Pichon X., et Roulet M.-J., 1986. Kinematic evolution of Tethys belt from the Atlantic Ocean to Pamir since the Triassic. Tectonophysics, 123, p. 1-35.

Sibuet J.-C., et Le Pichon X., 1971. Structure gravimétrique du golfe de Gascogne et le fossé marginal nord espagnol. In Histoire Structurale du golfe de Gascogne, J. Debyser, X. Le Pichon et L. Montadert (eds.), Technip. Paris, VI-9, p. 1-18.

Sibuet J.-C., et Ryan W.B.F., 1979. Site 398 : Evolution of the West Iberian continental margin in the framework of the early evolution of the North Atlantic Ocean. In Sibuet J.-C., Ryan W.B.F. et al., Initial Reports of the Deep Sea Drilling Project, 47, part 2, Washington (U.S. Government Printing Office), p. 761-775.

Sibuet J.-C., Ryan W.B.F., et al., 1979. Initial Reports of the Deep Sea Drilling Project, 47, part 2, Washington, U.S. Government Printing Office.

Sibuet J.-C., Mathis B., Pastouret L., Auzende J.-M., Foucher J.-P., Hunter P.M., Guennoc P., de Graciansky P.-C., Montadert L., et Masson D.G., 1984. Morphology and basement structures of the Goban Spur continental margin (NE Atlantic) and the role of the Pyrenean orogeny. Initial Reports of the Deep-Sea Drilling Project, 80, Washington, U.S. Government Printing Office, p. 1153-1165.

Sibuet J.-C., Mazé J.-P., Amortila P., et Le Pichon X., 1987. Physiography and structure of the western Iberian continental margin off Galicia from Sea-Beam and seismic data. In Boillot, G., Winterer, E.L., et al., Proc., Init. Repts (Pt A), ODP, 103, p. 77-97.

Sleep N.H., 1971. Thermal effects of the formation of Atlantic continental margins by continental breakup. Geophys. J.R. Astron. Soc., 24, p. 325-350.

Tankard A.J., et Welsink H.J., sous presse. Extensional tectonics and stratigraphy of the Hibernia oil field, Grand Bands of Newfoundland. Am. Assoc. Pet. Geol. Bull.

Témine D., 1984. Contribution à l'étude géologique de la marge Nord-Ouest de l'Espagne. Thèse 3ème Cycle, Université Pierre et Marie Curie, Paris, 213 p.

Thomas B.M., Moller-Pedersen P., Whitaker M.F., et Shaw N.D., 1985. Organic facies and hydrocarbon distributions in the Norwegian North Sea. In Petroleum geochemistry in exploration of the Norwegian shelf, Thomas B.M. et al. (eds.), Graham and Trotman Ltd, London, p. 3-26.

Watremez P., 1980. Flux de chaleur sur le massif armoricain et sur la marge continentale : essai de modèlisation de l'évolution thermique de la marge armoricaine. Thèse 3ème cycle, Université de Bretagne Occidentale, Brest, 108 p.

Watts A.B., et Steckler M.S., 1979. Subsidence and eustasy at the continental margin of eastern North America. In Deep Drilling results in the Atlantic ocean : continental margins and Paleoenvironment, Talwani M., Hay W.W., et Ryan W.B.F. (eds.), M. Ewing Series 3, American Geophysical Union, Washington D.C., p. 218-234.

Weigel W., Wissmann G., et Goldflam P., 1982. Deep seismic structure (Mauritania and Central Morocco). In Geology of the Northwest African continental margin, von Rad U., Hinz K., Sarnthein M., et Seibold E. (eds.), Springer-Verlag, Berlin, p. 132-159.

Wernicke B., et Burchfiel B.C., 1982. Modes of extensional tectonics. Journal of Structural Geology, 4, p. 105-115.

Wernicke B., 1985. Uniform-sense normal simple shear of the continental lithosphere. Can. J. Earth Sci., 22, p. 108-125.

Withjack M.O., et Jamison W.R., 1986. Deformation produced by oblique rifting. Tectonophysics, 126, p. 99-124.

Ziegler P.A., 1982. Faulting and graben formation in western and central Europe. In the evolution of sedimentary basins, Kent P., Bott M.H.P., McKenzie D.P., et Williams C.A. (eds.), Phil. Trans. R. Soc. Lond., A305, p. 113-143.

# D E U X I E M E  P A R T I E

## PUBLICATIONS RELATIVES AU SUJET

## I - CARTES DE SYNTHESE DES DONNEES GEOPHYSIQUES DE L'ATLANTIQUE NORD-EST

(1) Lallemand S., Mazé J.-P., Monti S., et Sibuet J.-C., 1985. Présentation d'une carte bathymétrique de l'Atlantique Nord-Est. C.R. Acad. Sc. Paris, 300, p. 145-149.

(2) Lalaut P., Sibuet J.-C., et Williams C.A., 1981. Présentation d'une carte gravimétrique de l'Atlantique Nord-Est. C.R. Acad. Sc. Paris, 292, p. 597-599.

(3) Guennoc P., Jonquet H., et Sibuet J.-C., 1979. Présentation d'une carte magnétique de l'Atlantique Nord-Est. C.R. Acad. Sc. Paris, 288, p. 1011-1013.

(4) Verhoef J., Collette B.J., Miles P.R., Searle R.C., Sibuet J.-C., et Williams C.A., 1986. Magnetic anomalies in the Northeast Atlantic ocean (35-50°N). Mar. Geophys. Res., 8, p. 1-25.

GÉOLOGIE MARINE. — *Présentation d'une carte bathymétrique de l'Atlantique Nord-Est.* Note de **Serge Lallemand, Jean-Pierre Mazé, Serge Monti** et **Jean-Claude Sibuet,** présentée par Georges Millot.

On présente une carte bathymétrique de l'Atlantique Nord-Est intégrant l'ensemble des données conventionnelles disponibles et des données du sondeur multifaisceaux « Sea-beam » acquises jusqu'à ce jour.

*MARINE GEOLOGY.* — New Bathymetric Map of the Northeast Atlantic Ocean.

*A bathymetric compilation in the North-East Atlantic based on available conventional data and all Sea-beam data acquired by the R. V.* Jean Charcot *is presented.*

Des cartes magnétique [1] et gravimétrique [2] de l'Atlantique Nord-Est ont été présentées à l'Académie des Sciences le 2 avril 1979 [3] et le 16 février 1981 [4]. Nous sommes en mesure de présenter aujourd'hui, pour la même partie de l'Océan Atlantique, une carte bathymétrique [5], complétant ainsi une série de documents relatifs à la façade maritime ouest de la France. Ce document a été réalisé en utilisant deux sources de données : les cartes bathymétriques conventionnelles, établies à partir de données obtenues à l'aide des sondeurs à faisceau large (30°), dont tous les navires océanographiques sont équipés; les informations du sondeur multifaisceaux « Sea-beam » en fonctionnement sur le N. O. *Jean Charcot* depuis 1977 [6]. Le « Sea-beam » est un système émettant puis recevant 16 faisceaux étroits et adjacents dans le plan perpendiculaire à l'axe longitudinal du navire. La largeur de la bande de terrain levée est approximativement égale aux deux tiers de la profondeur d'eau.

Le document (*pl. I*) a été réalisé en projection Mercator en utilisant l'ellipsoïde W.G.S. 72, à l'échelle du 1/2 400 000 à 41°N, de 1°W à 20°W en longitude et de 36°N à 51°N en latitude. Les courbes bathymétriques sont exprimées en mètres corrigés par les tables de Matthews [7]. Les courbes topographiques ont été généralisées à partir des cartes espagnoles et anglaises ([8] à [10]). L'équidistance des courbes est de 200 m à terre comme en mer, l'isobathe 100 m étant reportée en pointillés. Au verso du document (*pl. II*), lisible par transparence, figurent la toponymie ainsi que les références des documents récents et transits « Sea-beam » qui ont été utilisés pour modifier les cartes de Laughton et coll. [9], interpolées des brasses en mètres, et de Roberts et coll. [10]. Les données conventionnelles nouvelles utilisées sont les cartes bathymétriques publiées depuis 1974 correspondant aux orles 1 à 13 sur la planche II ([11] à [20]), les cartes GEBCO (General Bathymetric Chart of the Oceans of the International Hydrographic Organization) du Golfe de Gascogne [21] et de l'Ouest de la Mer Celtique (orle n° 14 sur la planche II [22]). Dans un premier temps, elles ont été incorporées au document de base, établi à partir des cartes de Laughton et coll. [9] et de Roberts et coll. [10]. Dans un deuxième temps, les cartes bathymétriques « Sea-beam » de détail, correspondant aux orles 15 à 39 sur la planche II ([6], [23] à [34]) ainsi que les transits « Sea-beam » T 1 à T 20 [35] (*pl. II*) ont été incorporés.

La carte des transits et zones levés par le N. O. *Jean Charcot* (*pl. II*) montre que de nombreux travaux ont été réalisés ces dernières années sur les marges continentales de l'Atlantique Nord-Est. Ces travaux l'ont été dans le cadre de la préparation et de l'exploitation des forages profonds des phases IPOD puis AODP (parcours 47 *b*, 48 et 80 du *Glomar Challenger* et parcours 103 de la plate-forme SEDCO 471), mais aussi dans le cadre des programmes des différentes institutions françaises. Les grands traits

0249-6305/85/30000145 $ 2.00 

EXPLICATION DES PLANCHES

*Planche I*

Carte bathymétrique de l'Atlantique Nord-Est.
*Bathymetric map of the North-East Atlantic.*

*Planche II*

Toponymie et références des cartes bathymétriques récentes et transits « Sea-beam », correspondant au verso de la planche I.
*Legend and references of recent bathymetric maps and Sea-Beam profiles, corresponding to the verso of Plate I.*

bathymétriques de l'Atlantique Nord-Est étaient bien sûr connus depuis les travaux de Berthois ([11], [36] et [37]), mais nous disposons maintenant d'un document plus précis pour les marges continentales, qui devrait cependant être amélioré en ce qui concerne le domaine océanique.

Ce travail a été réalisé au Centre de Brest de l'IFREMER. Les chefs de mission des campagnes et transits du N. O. *Jean Charcot* nous ont permis d'utiliser les données bathymétriques. P. M. Hunter, D. Mougenot et J.-R. Vanney nous ont apporté leur collaboration. Nous présentons cette carte bathymétrique de l'Atlantique Nord-Est à l'Académie des Sciences. Le B.R.G.M. en assurera la diffusion et la vente [5]. Nous déposerons à l'Académie pour ses archives, un exemplaire au 1/2 400 000 en couleurs, pour en permettre la consultation.

Contribution IFREMER n° 22, Département Géosciences marines.

Remise le 19 novembre 1984.

RÉFÉRENCES BIBLIOGRAPHIQUES

[1] P. GUENNOC, H. JONQUET et J.-C. SIBUET, *Carte magnétique de l'Atlantique Nord-Est, anomalies du champ total*, échelle 1/2 400 000, Centre National pour l'Exploitation des Océans (CNEXO), Paris, diffusée par le B.R.G.M., Service Promotion et Vente, B. P. n° 6009, 45018 Orléans Cedex, 1978.

[2] P. LALAUT, J.-C. SIBUET et C. A. WILLIAMS, *Carte gravimétrique de l'Atlantique Nord-Est, anomalies à l'air libre en mer, anomalies de Bougueur à terre*, échelle 1/2 400 000, CNEXO, diffusée par le B.R.G.M., 1981.

[3] P. GUENNOC, H. JONQUET et J.-C. SIBUET, *Comptes rendus*, 288, série D, 1979, p. 1011-1013.

[4] P. LALAUT, J.-C. SIBUET et C. A. WILLIAMS, *Comptes rendus*, 292, série II, 1981, p. 597-600.

[5] S. LALLEMAND, J.-P. MAZE, S. MONTI et J.-C. SIBUET, *Carte bathymétrique de l'Atlantique Nord-Est*, échelle 1/2 400 000, CNEXO, diffusée par le B.R.G.M., 1983.

[6] V. RENARD et J.-P. ALLENOU, *Revue hydrographique internationale*, Monaco, 56, 1979, p. 35-71.

[7] D. H. MATTHEWS, *Tables of the Velocity of Sound in Pure Water and Seawater*, Hydrographic Department, Admiralty, H. D. 282, 1939.

[8] *Atlas Geografico de España*, Instituto Geografico y Catastral, Madrid, feuilles 1, 2, 3, 5, 6, 7, 9, 10, 11, 12, 13, 14, 1961.

[9] A. S. LAUGHTON, D. G. ROBERTS et R. GRAVES, *Mid-Atlantic Ridge to Southwest Europe, Bathymetry of the North-East Atlantic*, sheet 3, Institute of Oceanographic Sciences, Wormley, England, 1975.

[10] D. G. ROBERTS, P. M. HUNTER et A. S. LAUGHTON, *Continental Margin Around the British Isles, Bathymetry of the North-East Atlantic*, sheet 2, Institute of Oceanographic Sciences, Wormley, England, 1977.

[11] L. BERTHOIS, *Golfe de Gascogne*, échelle 1/500 000, CNEXO, diffusée par le B.R.G.M., 1974.

[12] G. COPPIER et D. MOUGENOT, *Bull. Soc. géol. Fr.*, (7), 24, 1982, p. 421-431.

[13] D. DEREGNAUCOURT et G. BOILLOT, *Bull. B.R.G.M.*, 2, 1982, p. 149-178.

[14] S. MONTI, *Carte bathymétrique de la Méditerranée Occidentale*, échelle 1/1 500 000, CNEXO, diffusée par le B.R.G.M., 1979.

[15] D. MOUGENOT, Géologie de la marge portugaise, *Thèse Sc.*, Université Paris-VI, en préparation.

[16] D. MOUGENOT et J.-R. VANNEY, *Bull. Inst. Géol. Bassin d'Aquitaine*, Bordeaux, 31, 1981, p. 131-139.

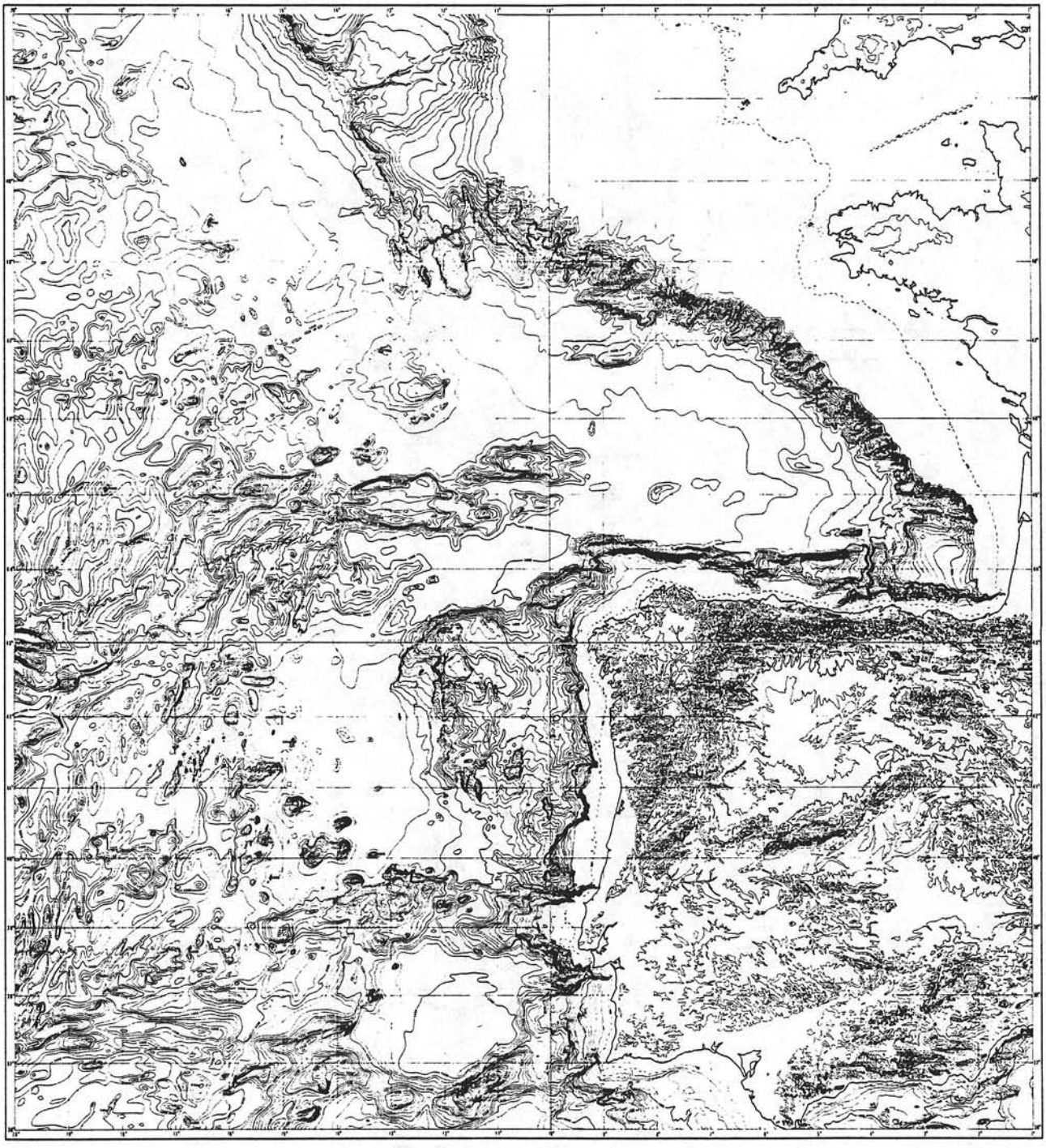

PLANCHE II/*PLATE II*

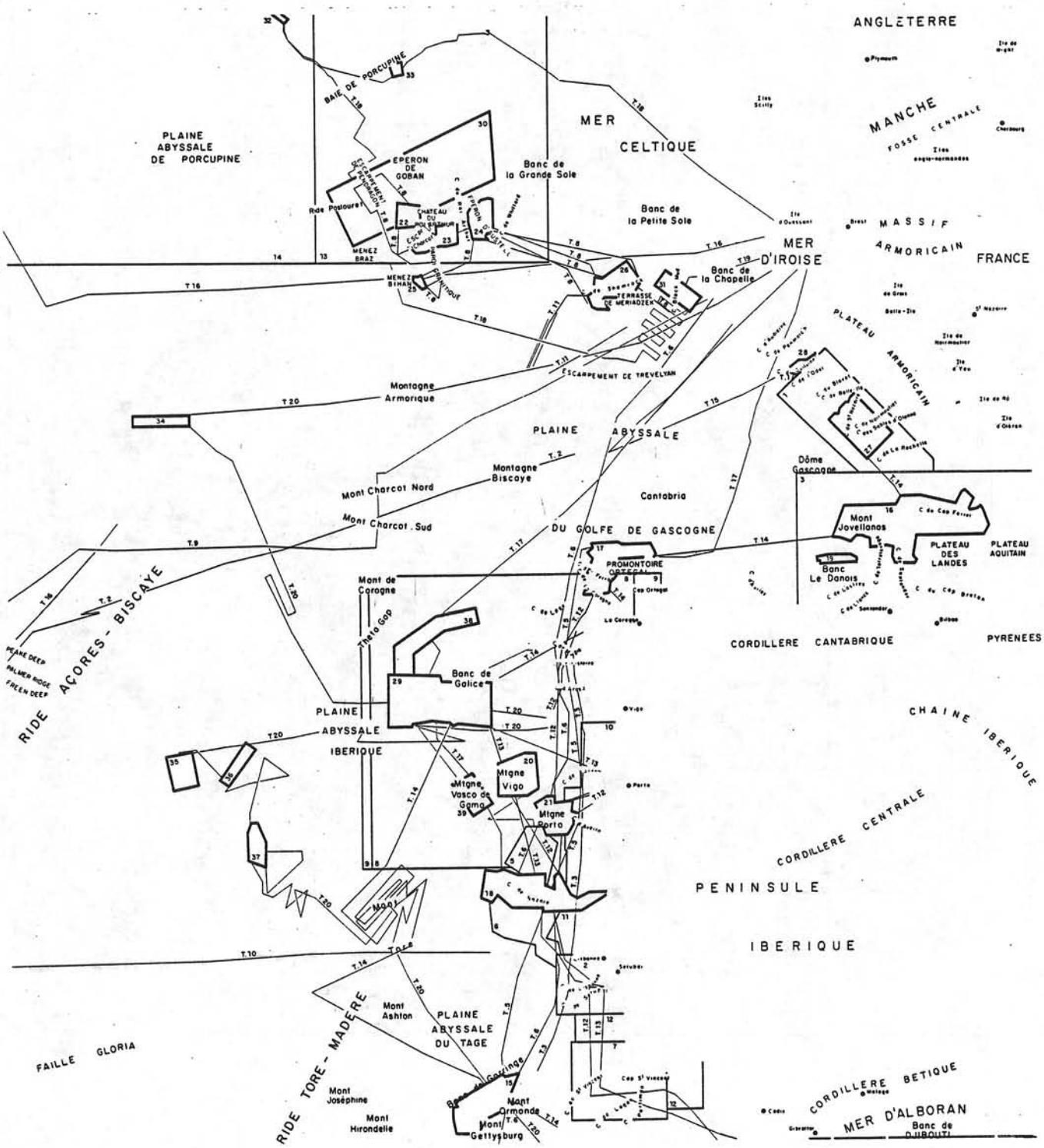

[17] J.-C. SIBUET et L. BERTHOIS, Initial Reports of the Deep-Sea Drilling Project leg 47 *b*, 1979, p. 753-760.

[18] J.-R. VANNEY, J.-L. AUXIETRE et J.-P. DUNAND, *Ann. Inst. Océanogr. Paris*, 55, 1979, p. 5-20.

[19] J.-R. VANNEY et D. MOUGENOT, *Memorias dos servicos geologicos de Portugal*, Lisboa, 28, 1981, 150 p.

[20] P. M. HUNTER et N. H. KENYON, *Bathymetry of Porcupine Seabight and Porcupine Bank*, Institute of Oceanographic Sciences, Wormley, England (sous presse).

[21] *GEBCO Plotting* sheet 43, Service hydrographique et océanographique de la Marine, Brest, 1983.

[22] *GEBCO Plotting* sheet CO29, Hydrographic Department, Ministry of Defense, Taunton, Somerset, Great-Britain, 1982.

[23] P. BEUZART, A. LE LANN, S. MONTI, J.-M. AUZENDE et J.-L. OLIVET, *Bull. Soc. géol. Fr.*, (7), 21, 1979, p. 557-562.

[24] F. COUMES, J.-M. FROIDEFOND, J.-J. NAUDIN et R. PRUD'HOMME, *Bull. Soc. géol. Fr.*, (7), 21, 1979, p. 563-568.

[25] GROUPE TRANSMARGE, *Comptes rendus*, 294, série II, 1982, p. 1099-1102.

[26] GROUPE TRANSMARGE, *Levé au large du Cap Ortégal* (en préparation).

[27] J. A. MALOD et J.-R. VANNEY, *Ann. Inst. Océanogr.*, Paris, 56, 1980, p. 73-83.

[28] D. MOUGENOT et coll., *Porto and Vigo Seamounts on the Portuguese Continental Margin : Comparison Between Sea-Beam, Gloria an Seismic Reflexion* (en préparation).

[29] L. PASTOURET, P. BEUZART et S. MONTI, *Bull. Soc. géol. Fr.*, (7), 24, 1982, p. 407-411.

[30] L. PASTOURET, *Carte bathymétrique des canyons sud-armoricains de Saint-Nazaire, de Noirmoutier, des Sables d'Olonne et d'Oléron*, CNEXO, diffusée par le B.R.G.M., 1984.

[31] J.-C. SIBUET, *Levé Seagal sur la marge portugaise* (en préparation).

[32] J.-C. SIBUET, B. MATHIS, L. PASTOURET, J.-M. AUZENDE, J.-P. FOUCHER, P. M. HUNTER, P. GUENNOC, P.-C. DE GRACIANSKY, L. MONTADERT et D. G. MASSON, *Morphology and Basement Structures of the Goban Spur Continental Margin (NE Atlantic) and the Role of the Pyrenean Orogeny*, Initial Reports of Deep-Sea Drilling Project Leg 80, (sous presse).

[33] J.-C. SIBUET, B. MATHIS et P. M. HUNTER, La ride Pastouret (plaine abyssale de Porcupine) : une structure éocène, *Comptes rendus*, 299, série II, 1984, p. 1391-1396.

[34] J.-L. OLIVET, *Levés Norestlante* II (en préparation).

[35] *Transits « Sea-beam » des campagnes du N. O.* Jean Charcot. T. 1 : V. RENARD, *Essais Sea-Beam*, 1977; T. 2 : H. D. NEEDHAM, *Vema*, 1977; T. 3 : L. BERTHOIS, *Romancha*, 1977; T. 4 : J. LEMAIRE, *Seafer I*, 1978; T. 5 : S. MONTI, *Transeagor*, 1978; T. 6 : J.-C. SIBUET, *Transwal*, 1979; T. 7 : J. LEMAIRE, *Seafer II*, 1979; T. 8 : L. PASTOURET, *Marmor*, 1979; T. 9 : H. BOUGAULT, *Mapco*, 1979; T. 10 : H. D. NEEDHAM, *Barlis*, 1981; T. 11 : D. DESBRUYERES, *Biogas*, 1981; T. 12 : G. BOILLOT, D. MOUGENOT et J.-R. VANNEY, *Transmarge*, 1981-1982; T. 13 : J.-C. SIBUET, *Seagal*, 1982; T. 14 : L. PASTOURET et P. BEUZART, *Stratigas*, 1982; T. 15 : J.-P. ALLENOU, *Essais Charcot*, 1983; T. 16 : A. COLIN DE VERDIERE, *Topogulf*, 1982; T. 17 : J.-R. VANNEY, *Transmarge* 83, 1983; T. 18 : J.-C. SIBUET, *Norestlante I*, 1983; T. 19 : L. D'OZOUVILLE, *Essais Sonar*, 1983; T. 20 : J.-L. OLIVET, *Norestlante* II, 1983.

[36] L. BERTHOIS, R. BRENOT et P. AILLOUD, *Rev. Trav. Inst. Pêches Marit.*, 29, 1965, p. 321-342.

[37] L. BERTHOIS, R. BRENOT et J. DEBYSER, *Rev. Inst. Franç. Petr. Ann. Comb. Liquides*, 23, 1968, p. 1046-1049.

S. L. : *Laboratoire de Géologie dynamique, Département des Sciences de la Terre, Université d'Orléans*, 45046 *Orléans Cedex;*

J.-P. M., S. M. et J.-C. S. : *IFREMER, Centre de Brest*, B. P. n° 337, 29273 *Brest Cedex.*

GÉOPHYSIQUE. — *Présentation d'une carte gravimétrique de l'Atlantique Nord-Est* [1]. Note (*) de **Philippe Lalaut, Jean-Claude Sibuet** et **Carol Williams,** présentée par Georges Millot.

On présente une carte des anomalies à l'air libre de l'Atlantique Nord-Est intégrant l'ensemble des données gravimétriques marines disponibles.

*A compilation of free-air anomalies in the North-East Atlantic based on available gravity data is presented.*

Le 2 avril 1979 a été présentée à l'Académie des Sciences une carte magnétique de l'Atlantique Nord-Est [2]. Nous sommes en mesure de présenter aujourd'hui, pour la même partie de l'Océan Atlantique, une carte gravimétrique. Dans le cadre du programme

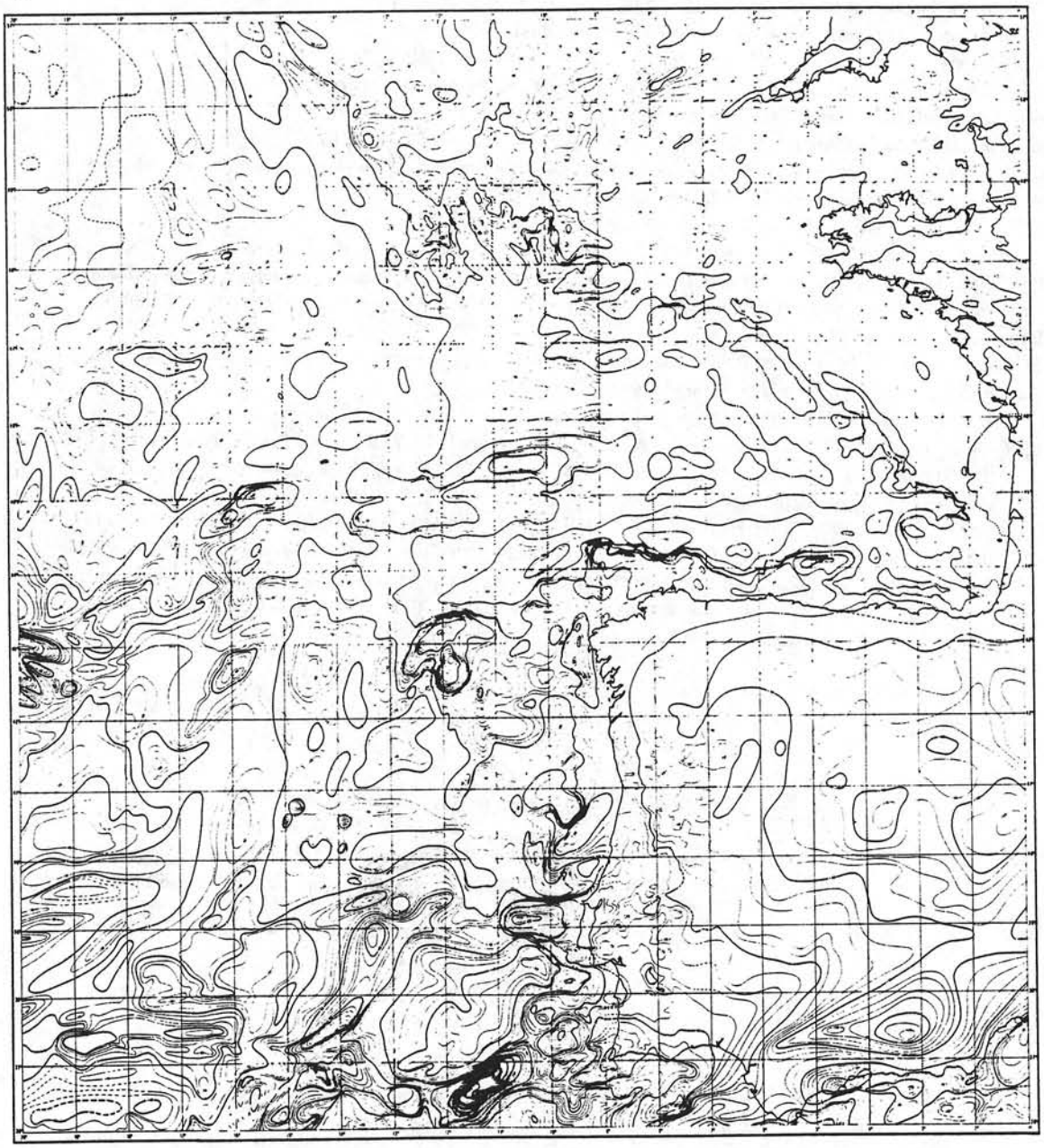

Fig. 1. — Carte gravimétrique de l'Atlantique Nord-Est : anomalies à l'air libre en mer, anomalies de Bouguer à terre.

I.P.O.D. (International Phase of Ocean Drilling), deux parcours du navire foreur *Glomar Challenger* ont été effectués en 1976, sur les marges de l'Atlantique Nord-Est. Des forages ont été réalisés au sud du Banc de Galice (site 398, Ouest Portugal [3]) et sur la marge celtique (site 399 à 402 [4]). D'autres forages sont programmés en 1981, sur la marge celtique. marge

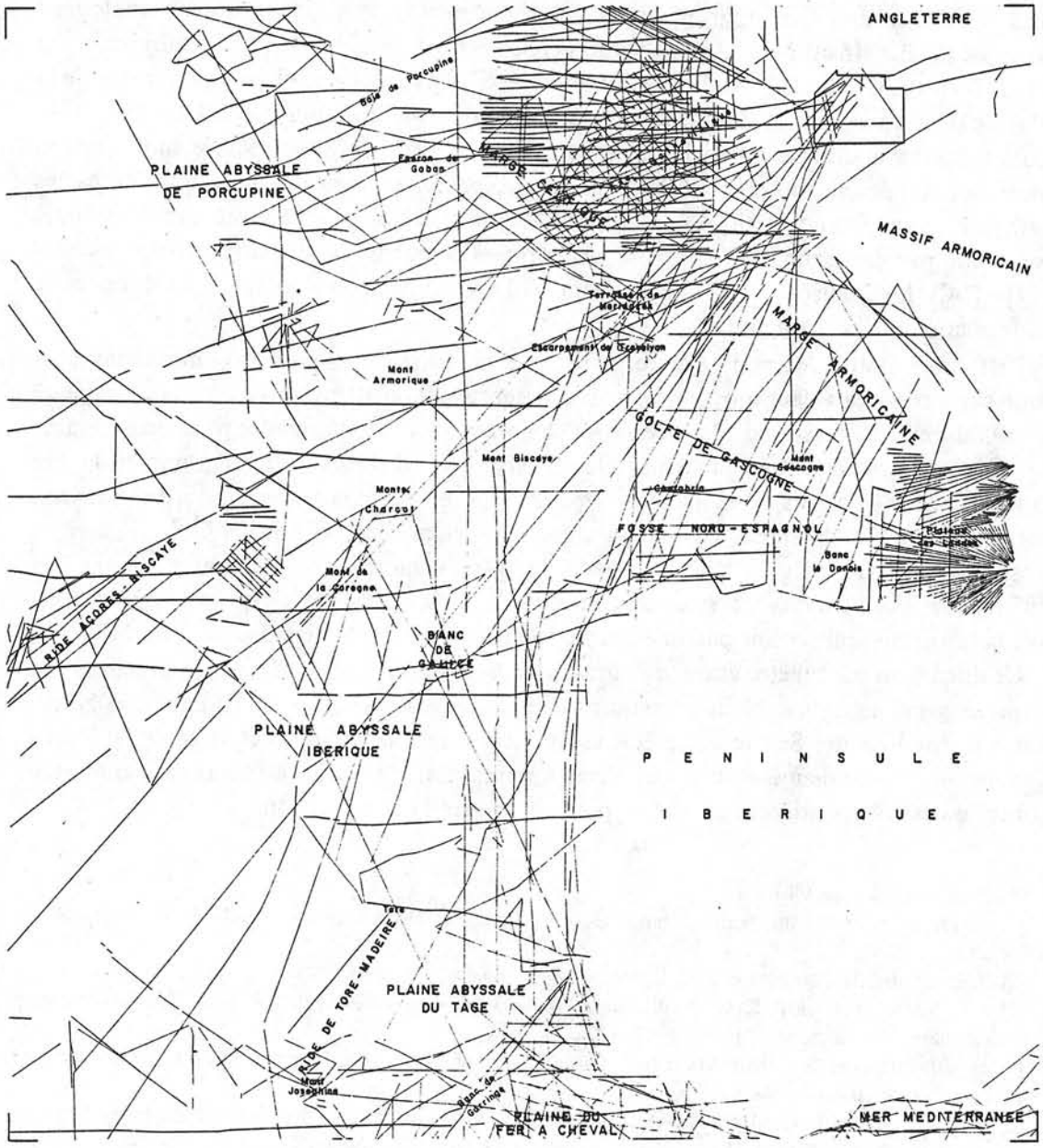


Fig. 2. – Contrôle des routes gravimétriques marines et toponymie. Les deux figures sont superposables et représentent la réduction photographique au 1/11 700 000 des documents originaux au 1/2 400 000.

peu sédimentée, où il est possible d'atteindre les séries antérieures à sa formation (séries « ante-rifting ») [5]. L'interprétation des données gravimétriques permet notamment de préciser les densités et natures de structures créées lors de l'épisode de formation de la marge continentale (blocs basculés) ou postérieurement (constructions récifales, diapirs) [6]. Cette carte s'étend en latitude de la ligne Açores-Gibraltar, au sud des îles Britanniques, et en

longitude, du continent européen à 20° W (*fig.* 1). Une interprétation complète de cette carte est en cours ([6], [7]).

Plus de 100 000 valeurs gravimétriques ont été compilées et réduites en utilisant l'ellipsoïde international de 1930. Elles proviennent des organismes suivants : Bureau gravimétrique international (F.), Centre océanologique de Bretagne (F.), Defense Mapping Agency (U.S.A.), Deutsches Ozeanographisches Datenzentrum (R.F.A.), Institute of Geological Sciences (G.B.), Institute of Oceanographic Sciences (G.B.), National Geophysical and Solar-Terrestrial Data Center (U.S.A.), Service Hydrographique et Océanographique de la Marine (F.), University of Cambridge (G.B.), University of Edinburgh (G.B.).

La carte des anomalies à l'air libre de l'Atlantique Nord-Est [8] est rédigée en projection Mercator à l'échelle du 1/2 400 000 (même projection et même échelle que les cartes bathymétrique [9] et magnétique ([2], [10]) de l'Atlantique Nord-Est. Elle est complétée sur le continent par les anomalies de Bouguer reprises à partir de documents déjà publiés ([11] à [14]). L'équidistance des courbes est de 10 mGal (*fig.* 1). Le contrôle des données de surface apparaît sur la figure 2.

Une étude statistique a été effectuée sur les différences de valeurs aux intersections de routes utilisées. La valeur moyenne de ces différences est de 10 mGal avec un écart-type de 10 mGal, ce qui correspond à la précision que l'on est en droit d'attendre pour un ensemble de mesures gravimétriques marines de provenances diverses. L'histogramme de ces différences fait ressortir deux pics anormaux à 14 et 30 mGal, le premier pic pouvant correspondre à la différence de niveau entre les systèmes de référence I.G.S.N. 71 et de Postdam. Si l'on corrige le niveau moyen des profils anormaux, la valeur moyenne des différences observées aux intersections est alors de 4 mGal et l'écart-type de 4 mGal. Ceci justifie un choix qui ne soit pas inférieur à 10 mGal pour l'équidistance des courbes.

Ce document n'a pu être établi que grâce aux institutions qui nous ont communiqué des données gravimétriques. Nous présentons cette carte gravimétrique de l'Atlantique Nord-Est à l'Académie des Sciences. Le B.R.G.M. en assurera la diffusion et la vente [8]. Nous déposerons à l'Académie pour ses archives un exemplaire au 1/2 400 000 en couleurs avec contrôle des routes utilisées au verso, pour permettre la consultation.

(*) Remise le 9 février 1981.

[1] Contribution n° 715 du Centre océanologique de Bretagne (Département de Géologie, Géophysique et Géochimie marines).

[2] P. GUENNOC, H. JONQUET et J.-C. SIBUET, *Comptes rendus*, 288, série D, 1979, p. 1011.

[3] J.-C. SIBUET et W. B. F. RYAN et coll., *Initial Reports of the Deep Sea Drilling Project*, U.S. Government Printing Office, Washington, 47, part 2, 1979, 787 p.

[4] L. MONTADERT et D. G. ROBERTS et coll., *Initial Reports of the Deep Sea Drilling Project*, U.S. Government Printing Office, Washington, 48, 1183 p.

[5] L. MONTADERT et D. G. ROBERTS et coll., *Site* 401, *in* L. MONTADERT, D. G. ROBERTS et coll., *Initial Reports of the Deep Sea Drilling Project*, U.S. Government Printing Office, Washington, 48, 1979, p. 73-124.

[6] P. LALAUT, J.-C. SIBUET et C. A. WILLIAMS, *Interprétation de la carte gravimétrique de l'Atlantique Nord-Est* (en préparation).

[7] J.-C. SIBUET et coll., *Evolution de l'Atlantique Nord-Est* (en préparation).

[8] P. LALAUT, J.-C. SIBUET et C. A. WILLIAMS, *Carte gravimétrique de l'Atlantique Nord-Est, échelle* 1/2 400 000, 1981, publiée par le Centre national pour l'Exploitation des Océans (C.N.E.X.O.), Paris, diffusée par le B.R.G.M., Service Promotion et Vente, B.P. n° 6009, 45018 Orléans Cedex (à l'impression).

[9] A. S. LAUGHTON, D. G. ROBERTS et R. GRAVES, *Deep-Sea Research*, 22, 1975, p. 791-810.

[10] P. GUENNOC, H. JONQUET et J.-C. SIBUET, *Carte magnétique de l'Atlantique Nord-Est, anomalies du champ total, échelle* 1/2 400 000, 1978, publiée par le Centre national pour l'Exploitation des Océans (C.N.E.X.O.), Paris, diffusée par le B.R.G.M., Service Promotion et Vente, B.P. n° 6009, 45018 Orléans Cedex.

[11] *Avance del Mapa Gravimetrico, Peninsula Iberica, Anomalias Bouguer*, 1972, Servicio de Cartographia y Talleres del Instituto Geografico y Catastral, Madrid.

[12] *Carta Gravimetrica de Portugal*, 1958, Instituto Geografico e Cadastral, Lisboa.

[13] Comité national français de Géodésie et Géophysique, cartes gravimétriques de France, 1951-1956, complétées en 1960 et 1969 par S. Coron.

[14] S. I. MAROOF, *J. Geol. Soc. Lond.*, 130, 1974, p. 471-474.

P. L. et J.-C. S. : *Centre océanologique de Bretagne*, B.P. n° 337, 29273 *Brest Cedex;*

C.A.W. : *University of Cambridge, Madingley Rise, Madingley Road, Cambridge, CB3 OEZ, England.*

GÉOPHYSIQUE. — *Présentation d'une carte magnétique de l'Atlantique Nord-Est* [1]. Note (*) de **Pol Guennoc, Hélène Jonquet** et **Jean-Claude Sibuet,** présentée par Georges Millot.

On présente une carte des anomalies du champ magnétique terrestre de l'Atlantique Nord-Est intégrant les données aéromagnétiques et les données de surface disponibles.

*A compilation of magnetic anomalies in the North-East Atlantic based on available aeromagnetic and surface data is presented.*

Dans le cadre du programme I.P.O.D. (International Phase of Ocean Drilling), deux parcours du navire foreur « Glomar Challenger » ont été effectués en 1976, sur les marges de l'Atlantique Nord-Est. Des forages ont été réalisés au sud des Bancs de Galice (site 398, Ouest Portugal [2]) et sur la marge armoricaine (sites 399 à 402 [3]). Aussi bien pour documenter les propositions de sites de forages, que pour interpréter les données de forages, il était nécessaire de réaliser une compilation des données magnétiques débordant largement le cadre du levé aéromagnétique du golfe de Gascogne [4]. La zone retenue s'étend en latitude de la ligne Açores-Gibraltar au sud des îles Britanniques, et en longitude, du continent européen à l'ouest de l'anomalie 34 (limite Santonien-Campanien datée 79 M. A. d'après van Hinte [5]). Cette carte magnétique du domaine océanique anté-Crétacé terminal (*fig.*) est donc l'un des documents de base permettant de définir les mouvements initiaux entre Amérique du Nord, Europe et Espagne ([6], [7], [8]).

Environ 50 000 km de profils magnétiques obtenus depuis 1959 ont été compilés. Les données ont été réduites en utilisant l'I.G.R.F. (International Geomagnetic Reference Field) 1965.0 [9] pour les données antérieures à 1975.0, et l'I.G.R.F. 1975.0 [10] pour les données postérieures à 1975.0. Elles proviennent des organismes suivants : Cambridge University (G.B.), Centre océanologique de Bretagne (F), Bedford Institute (Canada), Durham University (G.B.), Institut français du Pétrole (F), Institute of Oceanographic Sciences (G.B.), Lamont-Doherty Geological Observatory (U.S.A.), Netherlands Hydrographic Department (H), Service hydrographique de la Marine (F), Université Pierre-et-Marie-Curie (F).

La précision des mesures de surface (de l'ordre de 50 nT) est difficile à évaluer, puisqu'elle dépend à la fois de la précision de la navigation (de l'ordre de la dizaine de kilomètres pour certains profils anciens obtenus de 1959 à 1969) et de la méthode de réduction des données (champ magnétique de référence extrapolé dans le temps). Le contrôle des données de surface apparaît sur la carte magnétique de l'Atlantique Nord-Est [11] rédigée en projection Mercator à l'échelle du 1/2 400 000 (même projection et même échelle que la carte bathymétrique de l'Atlantique Nord-Est [12]). L'équidistance des courbes est de 50 nT (*fig.*).

Des levés aéromagnétiques d'excellente qualité ont été réalisés en Manche et au-dessus du golfe de Gascogne. Les altitudes de vol et l'époque de réduction de ces levés étant différentes, les courbes ne sont pas continues d'un levé aéromagnétique à l'autre (*fig.*). Néanmoins, nous avons choisi d'intégrer ces données aéromagnétiques à la carte présentée plutôt que d'utiliser les données de surface existantes, moins nombreuses, moins précises et moins homogènes que ces dernières. Les documents aéromagnétiques utilisés sont au nombre de trois :

— carte magnétique du golfe de Gascogne (C.N.R.S., I.N.A.G., I.P.G. Paris) : altitude de vol 500 m, données réduites à 1968.5;

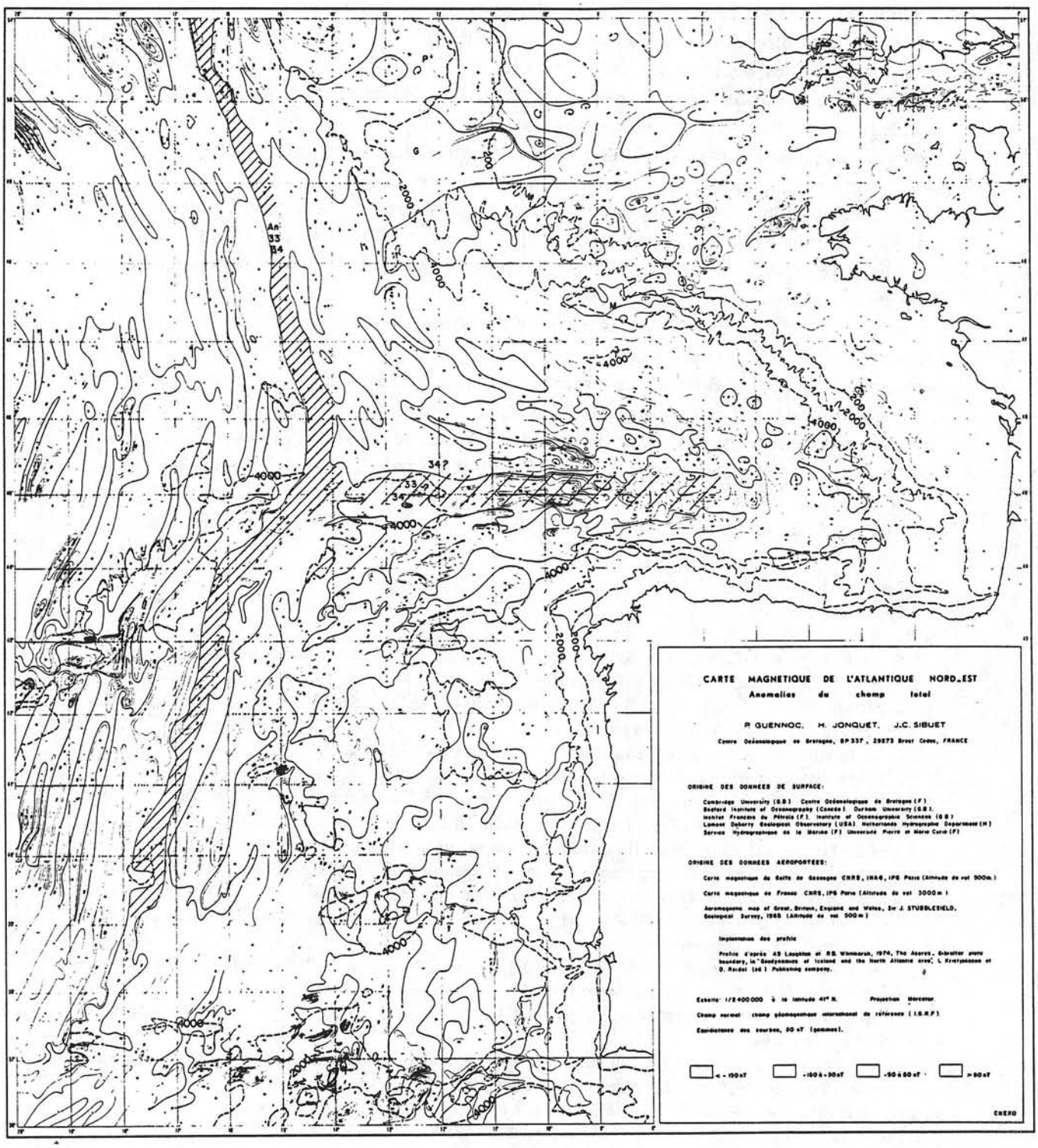


Carte magnétique de l'Atlantique Nord-Est : anomalies du champ total.
Bathymétrie simplifiée d'après Laughton et coll. [12]. Identification des anomalies magnétiques 33-34.

– carte magnétique de France (C.N.R.S., I.P.G. Paris) : altitude de vol 3 000 m;

– carte aéromagnétique de Grande-Bretagne, Angleterre et Pays de Galles (T. Stubblesield, Geological Survey, 1965) : altitude de vol 500 m.

A la frontière entre les données aéromagnétiques du golfe de Gascogne et les données de surface utilisées, les courbes ont été raccordées car, globalement, l'erreur commise est inférieure à la précision des mesures de surface. Le document présenté se prête donc davantage à une interprétation semi-quantitative, s'appuyant sur la forme et l'amplitude moyenne des anomalies magnétiques, qu'à une interprétation quantitative, nécessitant une prolongation du champ magnétique terrestre à une même altitude.

Une identification préliminaire des anomalies magnétiques a déjà permis de replacer les données du forage I.P.O.D. 398 effectué sur la marge ouest de la péninsule ibérique dans le contexte de l'évolution cinématique de l'Atlantique Nord ([6], [7]). Une interprétation plus complète de cette carte est en cours [8].

Ce document n'a pu être établi que grâce aux institutions qui nous ont communiqué des données magnétiques. Nous tenons à les remercier. De plus, cette carte est dédiée à la mémoire d'Eugène Le Borgne, inspirateur et maître d'œuvre du programme de levés aéromagnétiques de la France, du golfe de Gascogne et de la Méditerranée occidentale, qui a suivi avec dévouement et compétence les premiers travaux de l'un d'entre nous (J. C. Sibuet). Nous présentons cette carte magnétique de l'Atlantique Nord-Est à l'Académie des Sciences. Le B.R.G.M. en assure la diffusion et la vente [11]. Nous déposons à l'Académie pour ses archives, un exemplaire au 1/240 000 en couleurs, pour en permettre la consultation.

(*) Remise le 26 mars 1979.

[1] Contribution n° 638 du Centre océanologique de Bretagne (Département de Géologie, Géophysique, Géochimie marines).

[2] W. B. F. Ryan et J.-C. Sibuet et coll., Initial Reports of the Deep Sea Drilling Project (leg 47 B), U.S. Government Printing Office, Washington (sous presse).

[3] L. Montadert et D. G. Roberts et coll., Initial Reports of the Deep Sea Drilling Project (leg 48), U.S. Government Printing Office, Washington (sous presse).

[4] E. Le Borgne et J. Le Mouel, *Comptes rendus*, 271, série D, 1970, p. 1167.

[5] J. E. van Hinte, *Amer. Assoc. Petrol. Geol. Bull.*, 60, 1976, p. 498-516.

[6] J.-C. Sibuet et W. B. F. Ryan, *Site* 398 : *Evolution of the West Iberian Passive Continental Margin in the Framework of the Early Evolution of the North Atlantic Ocean* in W. B. F. Ryan et J.-C. Sibuet et coll., Initial Reports of the Deep Sea Drilling Project (Leg 47 B), U.S. Government Printing Office, Washington (sous presse).

[7] J.-C. Sibuet et coll, Deep Drilling results of Leg 47 B (Galicia Bank area) in the framework of the early evolution of the North Atlantic ocean, in *Phil. Trans. Roy. Soc. London* (sous presse).

[8] J.-C. Sibuet, P. Guennoc, H. Jonquet et C. A. Williams, *Interprétation de la carte magnétique de l'Atlantique Nord-Est* (en préparation).

[9] International Geomagnetic Reference Field 1965.0. I.A.G.A., Commission 2, Working Group 4, *Analysis of the Geomagnetic Field*, (*J. Geophys. Res.*, 74, n° 17, 1969, p. 4407-4408).

[10] International Geomagnetic Reference Field, 1975. I.A.G.A., Division 1, Study, *Group. J. Geophys. Res.*, 81, n° 28, 1976, p. 5163-5164.

[11] P. Guennoc, H. Jonquet et J.-C. Sibuet, *Carte magnétique de l'Atlantique Nord-Est, anomalies du champ total*, échelle 1/2 400 000, 1978, publiée par le Centre national pour l'Exploitation des Océans (C.N.E.X.O.), Paris, diffusée par le B.R.G.M., Service Promotion et Vente, B.P. n° 6009, 45018 Orléans Cedex.

[12] A. S. Laughton, D. G. Roberts et R. Graves, *Deep-Sea Research*, 22, 1975, p. 791-810.

H. J. et J.-C. S. : *Centre océanologique de Bretagne*,
B.P. n° 337, 29273 *Brest Cedex;*

P. G. : *Département de Géologie marine du B.R.G.M.*,
B.P. n° 6009, 45018 *Orléand Cedex.*

# MAGNETIC ANOMALIES IN THE NORTHEAST ATLANTIC OCEAN (35°–50° N)

J. VERHOEF[1], B. J. COLLETTE[1], P. R. MILES[2], R. C. SEARLE[2], J.-C. SIBUET[3], and C. A. WILLIAMS[4]

(Received 14 October, 1985)

**Abstract.** A magnetic anomaly chart is presented of the Northeast Atlantic Ocean between 35° and 50° N. This chart is based upon measurements obtained during the period 1956–1984. In this paper a description is given of the data set, of the computer program which was used to obtain grid values from the data points and of the subsequent contouring. As a check on the accuracy and internal consistency of the data set, a cross-over analysis was performed for different parts of the area.

A general description of the magnetic anomalies is given against the background of the known structure of the area. A detailed interpretation of the anomalies falls outside the scope of this paper.

## 1. Introduction

This paper presents a magnetic anomaly chart from the compilation of total magnetic intensity measurements obtained in the Northeast Atlantic Ocean during the period 1956–1984. The magnetic data were collected during detailed surveys (e.g. Black *et al.*, 1964; Matthews *et al.*, 1969; Krause and Watkins, 1970; Aumento *et al.*, 1971; Searle and Whitmarsh, 1978; Twigt *et al.*, 1979; Searle, 1980; Whitmarsh *et al.*, 1982), and from numerous measurements made during passage through the area (unpublished data of the contributing institutes). This chart follows those previously published by Guennoc *et al.* (1979) and Roberts *et al.* (1985), formerly referred to as Roberts and Jones (unpublished).

The total compilation, the gridding process and the subsequent contouring were done by computer. As a check on the accuracy and internal consistency of the total data set, a cross-over analysis was performed for different parts of the area.

The boundaries of the area of the chart are 35°–50° N and 2°–32° W. The greater part of the area is occupied by the Eurasian plate. West of the Mid-Atlantic Ridge is the American plate and south of the Azores–Gibraltar plate boundary the African plate. At the junction of these plate boundaries is the Azores triple junction. For reasons of comparison with existing charts in this area (e.g. Laughton *et al.*, 1975), the scale used for the enclosed chart is 1: 2 400 000 at 41° N.

This paper will describe the total data set, the procedure followed in the preparation of the contours and the major magnetic features of the area. The detailed interpretation of their origin falls outside the scope of this paper.

[1] Vening Meinesz Laboratorium, University of Utrecht, Utrecht, The Netherlands.
[2] Institute of Oceanographic Sciences, Wormley, United Kingdom.
[3] Ifremer, Centre de Brest, Brest, France.
[4] Bullard Laboratories, University of Cambridge, Cambridge, United Kingdom.

*Marine Geophysical Researches* **8** (1986) 1–25.

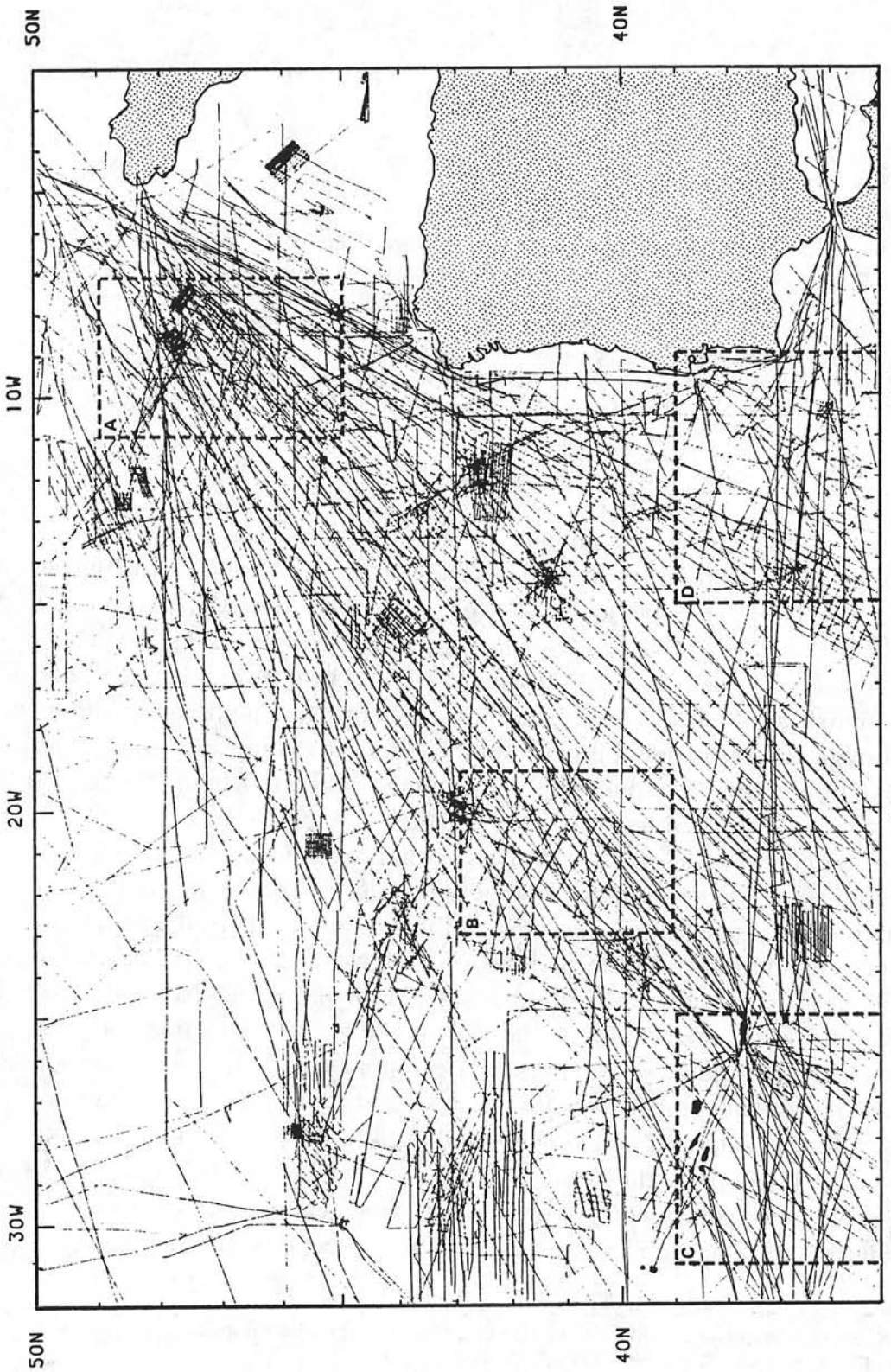


Fig. 1. Trackchart of the data coverage used in the compilation. Subareas A–D indicate where a cross-over analysis was performed.

## 2. Description of Data Set

The data set used in the compilation of the magnetic chart of the European plate consists of the tracks obtained by the Bullard Laboratories of the University of Cambridge (U.K.); the Institute of Oceanographic Sciences at Wormley (U.K.); the Institut Français de Recherche pour l'Exploration de la Mer (Ifremer) at Brest (France) and the Vening Meinesz Laboratorium, University of Utrecht (The Netherlands). Additional data were obtained from the NOAA- National Geophysical and Solar-Terrestrial Data Center. The trackchart of the magnetic data is shown in Figure 1, while Table I specifies the different sources.

The measurements were performed over the period 1956–1984. Figure 2

TABLE I
Total data set

| Origin | Total of km |
|---|---|
| United Kingdom | 171 900 |
| France | 57 250 |
| The Netherlands | 147 330[a] |
| NOAA data center | 85 750 |
| | 462 230[b] |

[a] About 15% of the data are from the Hydrographic Service of the Royal Netherlands Navy.
[b] The coverage of magnetic data along tracks shown is about 96%.

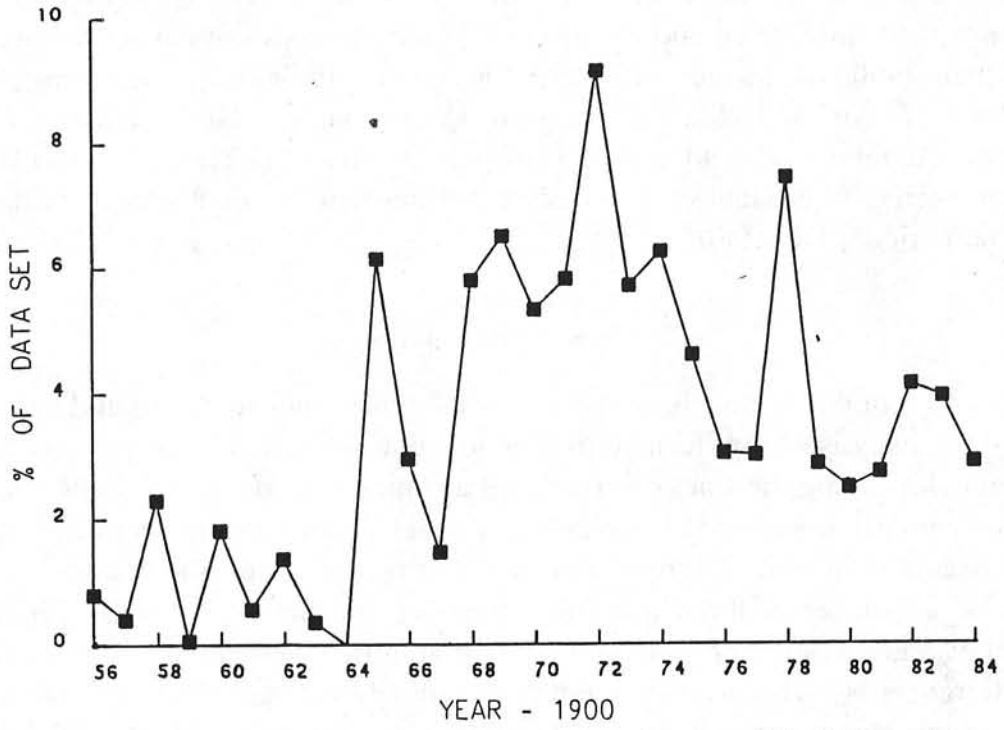


Fig. 2. Data distribution over the period 1965–1984. Note that about 8% of the total data set was obtained before 1965.

shows the distribution of the data as a function of the year. From this Figure it follows that about 8% of the measurements were performed before 1965 and that, with the exception of 1964, there are magnetic data for every year during the period 1956–1984.

## 3. Reduction to Anomalies

The reduction of the total intensity magnetic values to a common datum level is usually done by removing the long wavelength component with a time dependent reference field. In this compilation the anomalies were calculated relative to the IAGA reference fields (IAGA Division I working group 1, 1981): DGRF 1965, DGRF 1970, DGRF 1975 and IGRF 1980.

These reference fields consist of a model of the main field at 1965.0 (DGRF 1965), 1970.0 (DGRF 1970) and 1975.0 (DGRF 1975) with linear interpolation of the model coefficients for intervening dates. A provisional reference field is defined for the interval 1975.0 to 1980.0 (PGRF 1975) and in the IGRF 1980 field a secular variation forecast model is included.

The above mentioned reference fields are defined from 1965 on. Since about 8% of the measurements were performed before 1965 and since we wanted to include these data also in our compilation, it was decided, as a first approximation, to extrapolate the reference field DGRF 1965 backwards in time to 1956.

Figures 3a and 3b show examples of the reference fields in the area, together with their secular variation, i.e. the increase in one year. The values for the reference field varies from about 42000 nT in the southeastern part of the area to more than 49000 nT in the northwest. The secular variation varies from about 10 nT/a to about −40 nT/a for the year 1975. The secular variation for the extrapolated reference field IGRF 1960 varies from 20 nT/a to −10 nT/a. In general, there is a gradual eastward shift for the lines of equal secular variation over the period 1960–1980.

## 4. Cross-over Analysis

In order to estimate the accuracy and internal consistency of the total data set, a cross-over analysis was performed in four subareas labeled A–D in Figure 1. The magnetic data along the tracks were stored as time-series on magnetic tape and a computer program was used to calculate the coordinates and times of the points of intersection of the different ship-tracks together with the values of the magnetic anomalies at these locations (Verhoef and Scholten, 1983). Figure 4 gives a histogram of the cross-over errors for area B. The definition of the sign of the differences is such that they denote the anomaly value of the track compared to the older one at a crossing. The observed mean value of −14 nT of the 1293 crossings, with a standard deviation of 52 nT, denotes that the secular variation

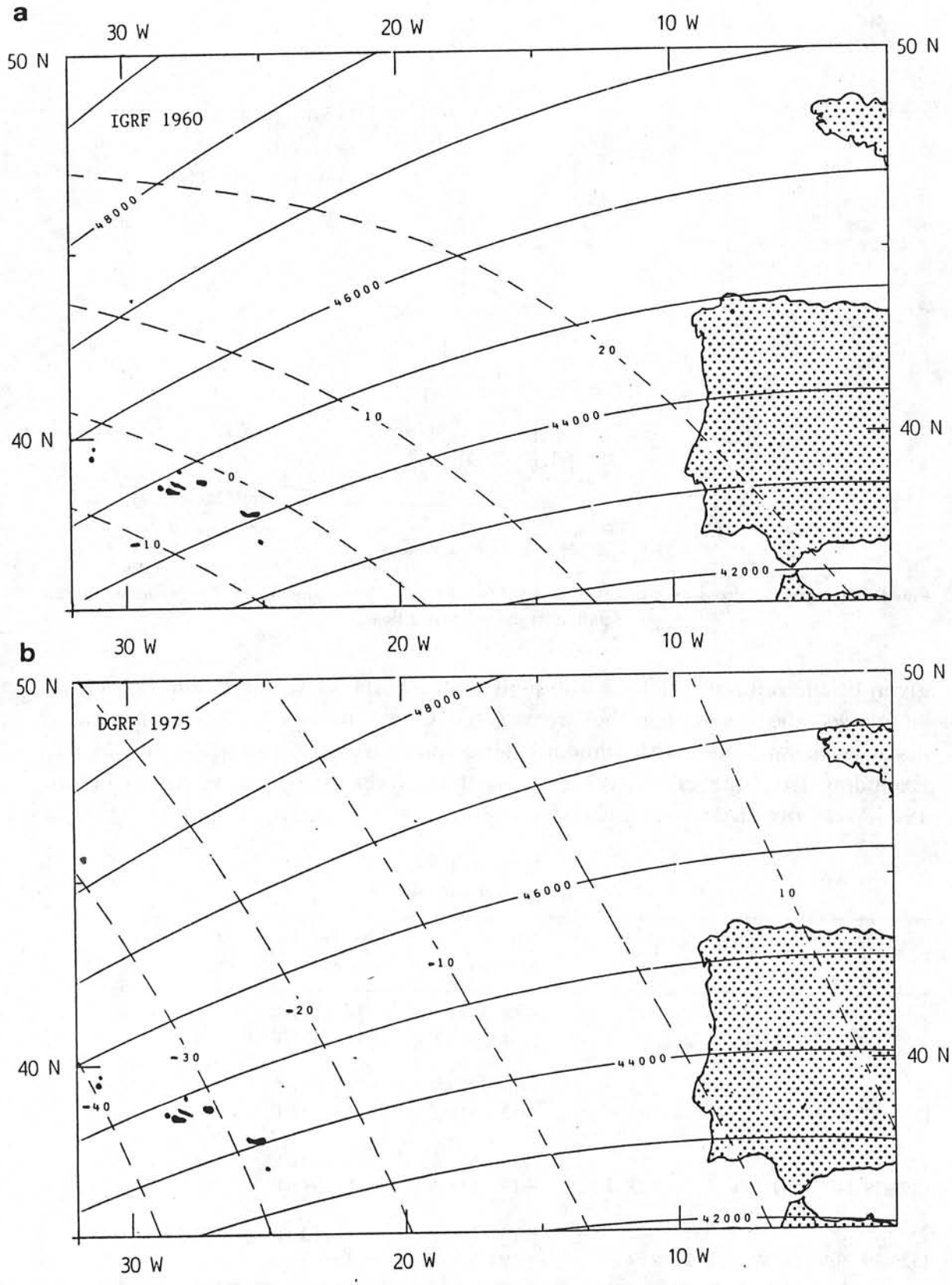


Fig. 3a–b. Total magnetic intensity values of the references fields (continuous lines) with a contour interval of 1000 nT. The dashes denote the secular variation, contour interval 10 nT/a. The field IGRF 1960 (in a) denotes an extrapolation of the DGRF 1965 field.

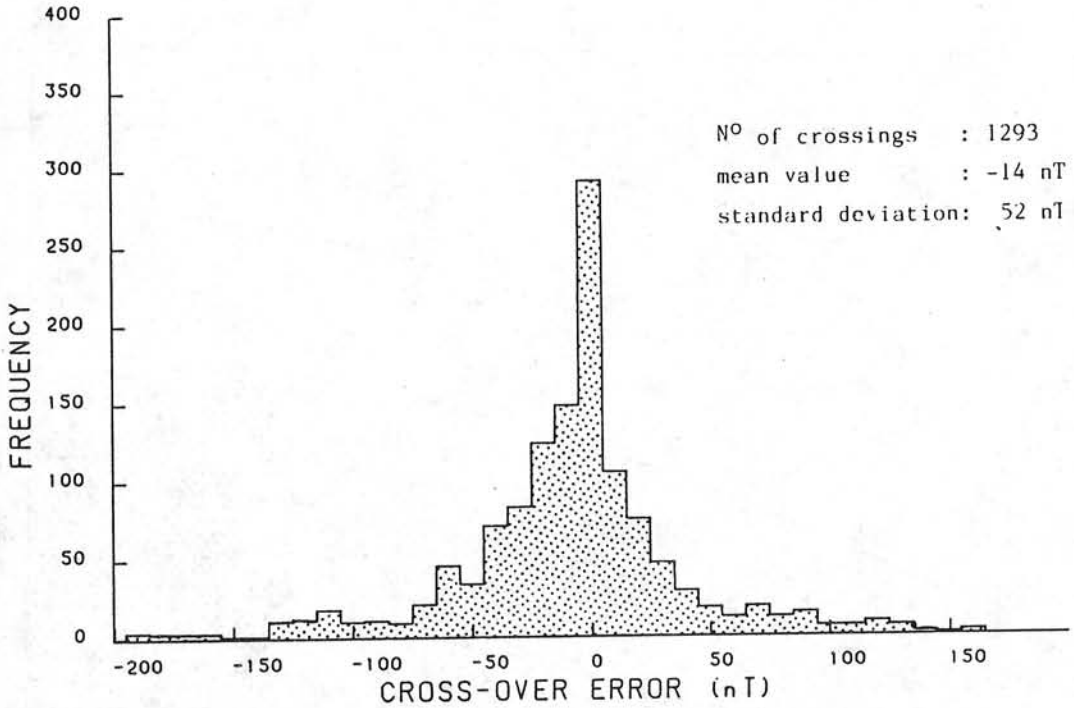


Fig. 4. Histogram of cross-over errors for area B (see Figure 1 for the location). Anomalies are given relative to the reference fields.

given by the reference fields is too high. Table II shows, in the column observed anomalies, the results for the areas A–D. One observes for all four areas a negative mean value, with standard deviations varying between 48 and 62 nT. Excluding from the cross-over analysis those tracks which were sailed before 1965, one obtains a mean value closer to zero in areas A and D where a

TABLE II
Cross-over analysis

| Area | Number of crossings | Observed anomalies | Corrected anomalies | Corrected anomalies[a] |
|---|---|---|---|---|
| *A* | 1) 3095 | −14 ± 48 nT | 14 ± 46 nT | 1.3 ± 4.9 nm |
| (45°–49° N/7°–11° W) | 2) 2520 | − 4 ± 39 nT | 15 ± 43 nT | |
| *B* | 1) 1293 | −14 ± 52 nT | 3 ± 51 nT | 0.1 ± 2.0 nm |
| (39°–43° N/19°–23° W) | 2) 1203 | −13 ± 51 nT | 3 ± 50 nT | |
| *C* | 1) 803 | −20 ± 62 nT | − 5 ± 60 nT | −0.2 ± 1.7 nm |
| (35°–39° N/25°–31° W) | 2) 729 | −19 ± 61 nT | − 6 ± 59 nT | |
| *D* | 1) 1394 | −25 ± 57 nT | − 4 ± 50 nT | 0.0 ± 3.1 nm |
| (35°–39° N/9°–14° W) | 2) 1259 | −19 ± 52 nT | − 1 ± 48 nT | |

[a]Mean value and standard deviation calculated with respect to local gradient at crossing.
1) Total data set used for cross-over analysis.
2) Only tracks sailed after 1964 used in cross-over analysis.

significant number of the crossings have one track sailed before 1965. In addition, the standard deviations decrease slightly for all areas when the tracks before 1965 are excluded.

The results of the cross-over analysis thus indicate that, after applying the reference fields, the magnetic anomalies are still time dependent. In order to eliminate this time-dependency, especially for the tracks sailed before 1965, it was decided to define an extra correction. This was done by grouping the data into periods of five years, except for the data before 1965 which were all put into one group. From the data for the different groups, grid values were calculated using a large low-pass wavelength of the applied digital filter (see next section for a description of the computer program used for the calculation of the grid values). In doing so, only the long wavelengths of the anomalies remain. In order to reduce possible edge effects, the data used in the calculation of the grid values were, wherever possible, extended beyond the standard area. The resulting grid values were next smoothed by applying a two-dimensional running mean procedure with a Gaussian weight function (halfwidth 1000 km).

The resulting long wavelength anomalies are given in Table III as a $4° \times 4°$ grid, together with a code indicating the number of data points in the $4° \times 4°$ subarea. The values for the period 1956–1964 are significantly larger than those for the other periods. This indicates that the first approximation for the reference field for this period (the backward extrapolation of the DGRF 1965) gives rise to higher secular variation residues than the later, better defined reference fields.

The long wavelength anomalies given in Table III can be used to define additional terms of the correction for the secular variation defined by the reference fields, as required by the present data set. These terms were computed as follows. The values for the different periods were assumed to hold for the year halfway through the respective period (i.e. 1960, 1967, 1972, 1977, and 1982). For the years in between linear interpolation was used to obtain the correction. As a reference year the year 1977 was taken, since the period 1975–1979 is the most recent one for which the reference fields are defined in a definitive way. The actual correction is then obtained by correcting the magnetic anomalies for the differences of the grid values of that year with the values of the period 1975–1979.

Figure 5a shows the histogram of the cross-over errors for area B after the above correction was applied. The mean value is close to zero and the standard deviation is somewhat reduced. Table II shows the results for the four areas in the column corrected anomalies. Although in general the mean values are now close to zero, an exception is formed by area A where the correction was too large, resulting in a positive mean value of 14 nT. The results when the tracks sailed before 1965 are excluded are no longer significantly different.

Although Table II indicates that there is no systematic error left, the standard deviations still amount to 60 nT. The short period variations of the magnetic field, i.e. the daily variations, are not taken into account by the reference fields.

TABLE III

Long wavelength anomalies after reduction for reference fields (in nT)

| | Longitude | | | | | | |
|---|---|---|---|---|---|---|---|
| Latitude | 30° W | 26° W | 22° W | 18° W | 14° W | 10° W | 6° W |
| Period 1956–1964 | | | | | | | |
| 49° N | 100 (a) | 98 (b) | 95 (a) | 84 (a) | 71 (b) | 58 (c) | 34 (c) |
| 45° N | 98 (a) | 100 (c) | 98 (a) | 97 (c) | 102 (c) | 102 (c) | 88 (b) |
| 41° N | – | 106 (b) | 98 (b) | 103 (b) | 120 (c) | 129 (c) | – |
| 37° N | – | 97 (b) | 85 (b) | – | 120 (b) | 127 (c) | 121 (b) |
| Period 1965–1969 | | | | | | | |
| 49° N | −1 (a) | −7 (a) | – | −5 (b) | 4 (c) | 10 (b) | 8 (c) |
| 45° N | 26 (c) | 27 (b) | 28 (c) | 27 (c) | 34 (c) | 45 (c) | 46 (c) |
| 41° N | 40 (c) | 52 (c) | 57 (b) | 55 (c) | 58 (c) | 66 (c) | – |
| 37° N | 33 (b) | 53 (c) | 68 (c) | 76 (b) | 67 (c) | 51 (c) | 45 (b) |
| Period 1970–1974 | | | | | | | |
| 49° N | −1 (b) | −4 (b) | −4 (c) | 5 (c) | 16 (c) | 18 (c) | 22 (c) |
| 45° N | 40 (b) | 36 (c) | 29 (c) | 27 (c) | 29 (c) | 28 (c) | 27 (b) |
| 41° N | 64 (a) | 56 (c) | 47 (c) | 42 (c) | 41 (c) | 35 (c) | – |
| 37° N | 60 (c) | 52 (c) | 43 (c) | 45 (c) | 45 (c) | 28 (c) | 17 (b) |
| Period 1975–1979 | | | | | | | |
| 49° N | −18 (a) | −1 (a) | 16 (a) | 21 (a) | 23 (c) | 21 (c) | 19 (c) |
| 45° N | 26 (c) | 29 (c) | 29 (c) | 28 (c) | 31 (c) | 29 (c) | 27 (b) |
| 41° N | 47 (c) | 45 (c) | 40 (c) | 40 (c) | 42 (c) | 35 (c) | – |
| 37° N | 47 (c) | 45 (c) | 40 (c) | 48 (c) | 52 (b) | 33 (c) | 13 (b) |
| Period 1980–1984 | | | | | | | |
| 49° N | −14 (b) | – | −10 (a) | 13 (a) | 23 (c) | −2 (c) | −31 (b) |
| 45° N | 1 (b) | 1 (b) | 1 (b) | 8 (b) | 9 (c) | −15 (c) | −52 (c) |
| 41° N | 8 (b) | 12 (c) | 11 (c) | 12 (c) | 10 (c) | −5 (c) | – |
| 37° N | 6 (c) | 8 (c) | 10 (b) | 16 (b) | 16 (c) | 17 (c) | 30 (b) |

Explanation:
– No data in subarea.
(a) Less than 1000 data points in subarea.
(b) Between 1000 and 5000 data points in subarea.
(c) More than 5000 data points in subarea.

In local landbased surveys the daily variations are corrected by using the recordings of the geomagnetic field intensity as a function of time from the various magnetic observatories. On open sea this cannot be done reliably when the land base stations are far away. Reagan and Rodriguez (1981) give world wide averages of the amplitudes of the daily variations at different latitudes. Between latitudes 35° and 50° N the amplitudes of the total field daily variations

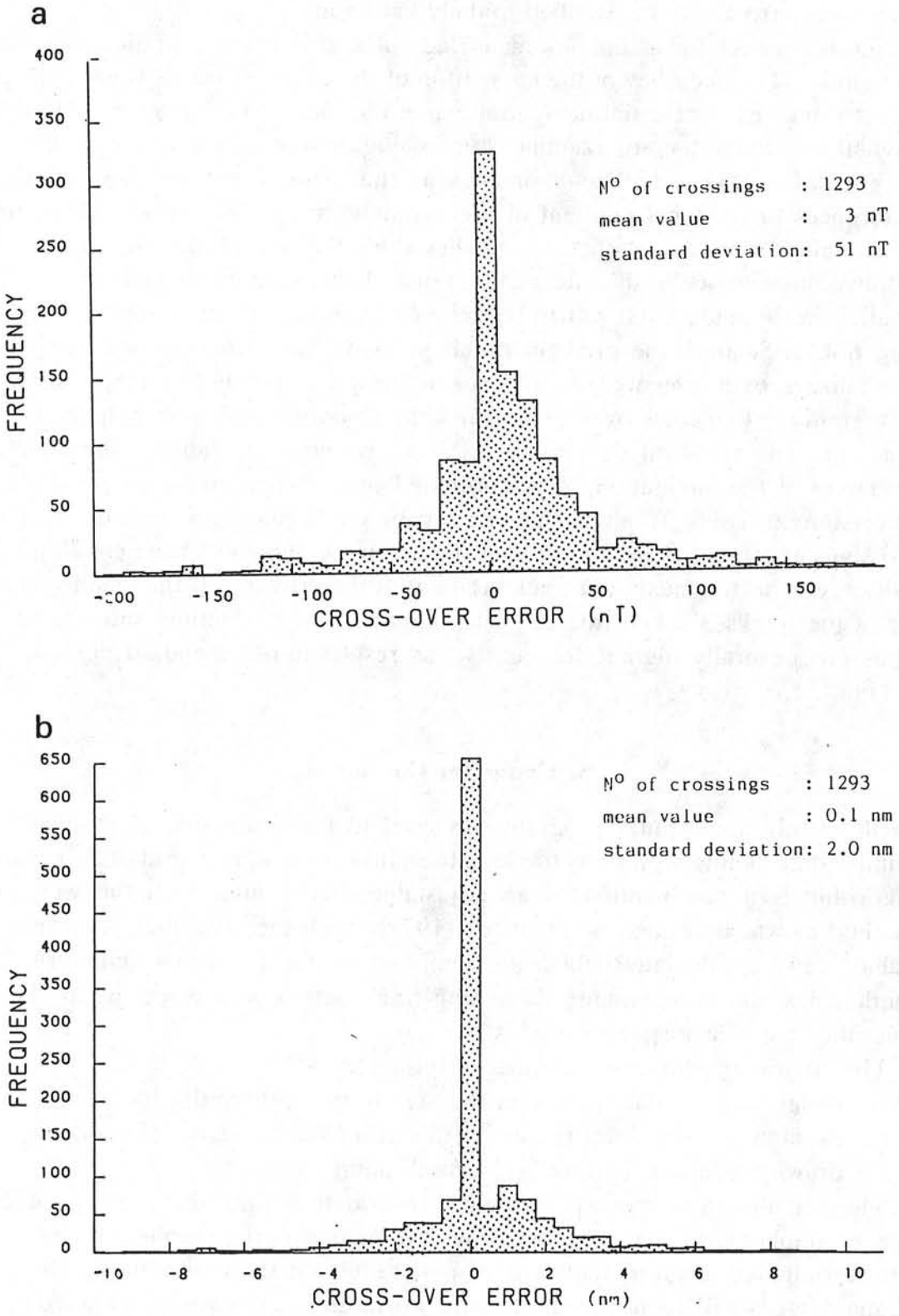


Fig. 5. Histogram of cross-over errors for area B, using the corrected anomalies (a). In (b) the cross-over errors are related to the local gradient at the crossing.

are about 50 nT. This indicates that at least part of the standard deviation of the cross-over errors may be ascribed to daily variations.

Another source for errors of a measured value at intersection points lies in the navigation. The accuracy of the navigation of the different tracks is variable; the oldest tracks have celestial navigation while the more recent ones have satellite navigation. In order to examine how navigation errors may influence the differences in the magnetic anomalies at the cross-overs, we referred these differences to the local gradient of the magnetic anomalies. This local gradient was obtained from the magnetic anomalies along the two intersecting tracks lying within 3 nm distance of the intersection point. Two alternative calculations of the gradient were made. First was to take the maximum gradient along the intersecting tracks. Second, the gradient obtained along both tracks was averaged by normalizing over the area around the intersection point. Figure 5b shows a histogram of the cross-over errors in area B normalized with respect to the gradient. The standard deviation of 2.0 nm would then indicate the standard deviation of the navigation errors, provided that navigation errors are the only error-source. Table II gives the mean values and standard deviations at the crossings expressed in the gradient of the magnetic anomaly at the crossing. The values refer to the maximum track gradient at the crossing. If the mean gradient along the tracks is taken (the second calculation), the resulting standard deviations are generally higher. In area B this results into a standard deviation of 2.4 nm.

## 5. Computer Contouring

In this study a computer program was used to transform the approximate 1.2 million data points along the tracks into values on a square grid. The gridding algorithm is a combination of an adjustable digital filter with the weighting method as was described by Slootweg (1978). With the computer program grid values can be calculated which are unbiased by the track-line geometry. The method has the disadvantage that along-track details with wavelengths shorter than the mean track spacing are lost.

The computer contouring consists of three steps:

(1) generating a square grid over the area to be contoured;

(2) estimating mesh point values for this grid from the data point values;

(3) drawing contour lines using the mesh point values.

The calculation of mesh point values from data points which are not evenly spaced implies a kind of filtering. The computer program applied in this study uses a weighted mean method with a spatial filter for the weighting function. As spatial filter, a 6 dB/octave roll off Butterworth filter is chosen. The choice of the cut-off wavelength of the filter depends on the data point distribution and expected spectral content of the variable to be contoured. In general, data points along a ship-track are more closely spaced than in directions perpendicular to it.

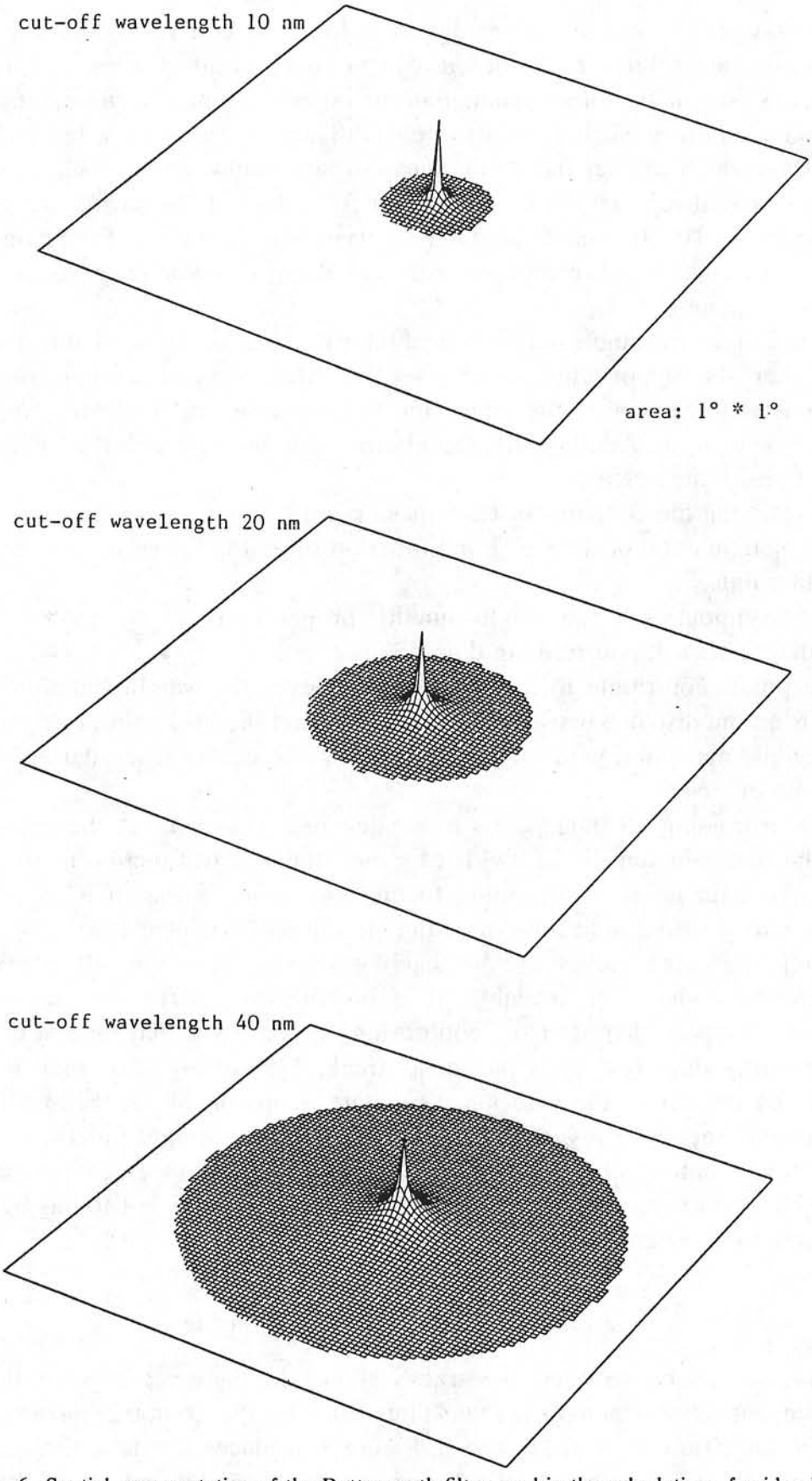


Fig. 6. Spatial representation of the Butterworth filter used in the calculation of grid values.

If one chooses the cut-off wavelength too low, the coherent structure of the resulting contour lines is disturbed by the data point distribution, i.e. the ship-tracks. If, on the other hand, the cut-off wavelength is chosen too high, short wavelength detail is lost in the chart. Thus an optimum value has to be established which will depend on the mean distance between the tracks. Figure 6 gives the spatial representation of the filter for values of the cut-off wavelength of respectively 10, 20, and 40 nm. One observes how the radius of the data points which contribute to the calculated value at the grid point depends upon this cut-off wavelength.

The use of an adjustable mathematical filter in the gridding algorithm gives the chartmaker the opportunity to choose the filter constants, minimizing data distribution effects, and at the same time to know how much filtering will occur for any wavelength. Additionally, the filtering will also diminish the influence of residual positioning errors.

The resulting file contains for each mesh point:

(a) the summation of the weighting function times the values of the contributing data points,

(b) the summation of the weight function proper, and

(c) the number of contributing data points.

Data points contribute to a grid value whenever the weight function, which depends on the distance between the data point and the grid point, is higher than 0.3% of the maximum value. This maximum value occurs when data point and grid point coincide.

After processing all data points one calculates the values at the grid points from the obtained sum in (a) divided by the total weight function of (b). If the number of data points contributing to one grid point is less than an arbitrary limit, a zero is stored indicating 'no value' in areas of low density.

Storing the three values a–c for each grid points has the advantage that, whenever new data are available, it is possible to update the contour file. Moreover, suppose that after the contouring one observes that several contours are obviously disturbed by a particular track. Eliminating this track is easily possible by correcting the values a–c for data points of this track, by adding a hypothetical track with reverse values and resetting the weight function.

The final contour chart is produced by drawing line segments within the elementary grid squares. The end points of these segments are found by linear interpolation between the mesh points.

## 6. Filtering Effect of the Contouring

The mean distance between the tracks shown in Figure 1 is such that the optimum cut-off wavelength for the filter used by the computer program was found to be 20 nm. As can be seen in Figure 1 at places the data distribution is not dense enough to obtain reliable grid-values with this cut-off wavelength.

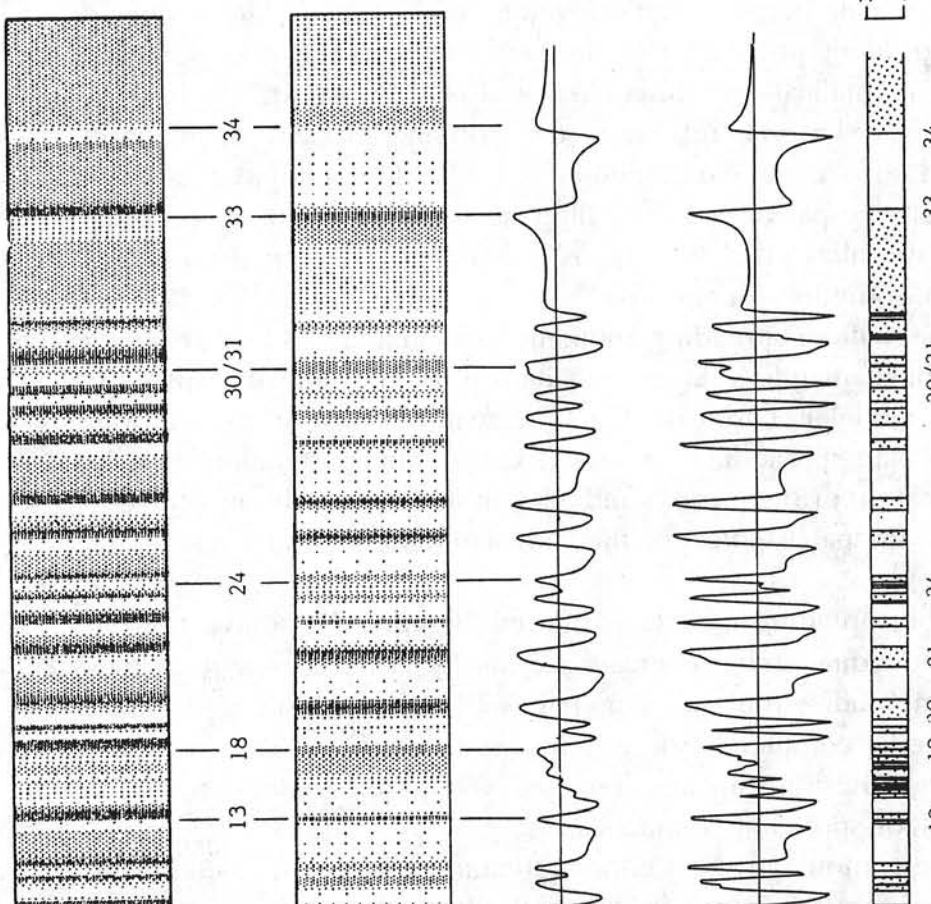


Fig. 7a-d. Calculated seafloor spreading anomalies (a) using the time scale of Lowrie and Alvarez (1981). The magnetic parameters were obtained from the paleo-poles of Irving and Irving (1982). In (b) the influence of the contouring on the shape of the anomalies is shown. The calculated anomalies from (a) are contoured on a grid of 0.05 degrees using a Butterworth filter with a cut-off wavelength of 20 nm (see (c), where the darkest shading corresponds with the strongest positive anomalies). In (d) the effect of a directional derivative is taken in a direction of 270° and slopes in this direction show as the lighter shadings.

Here the grid values were calculated using a two dimensional running mean procedure with a Gaussian weight function, rather than using a larger cut-off wavelength in the gridding process. The distance between the grid points at which the magnetic anomalies were calculated was chosen at 0.05 degree, i.e. N–S at a distance of 5.5 km. Therefore, in the gridding process wavelengths shorter than about 11 km are eliminated and an anti-alias filter should be applied before the gridding can be performed. The filter used by the computer program can function as the anti-alias filter. The filtering effect of a 20 nm Butterworth filter is demonstrated in Figures 7a and 7b.

Figure 7a shows the seafloor spreading anomalies, calculated at 41° N assuming a plan-parallel horizontal magnetic layer with its top at 3 km and its bottom at 4 km. The magnetic model is based on the time scale of Lowrie and Alvarez (1981) using a fixed half-spreading rate of 1.2 cm/a. The parameters for the inclination and declination of the present and ancient magnetic field, indicated in Figure 7, follow from the paleo-poles for the Eurasian plate given by Irving and Irving (1982).

Figure 7b shows the spreading anomalies filtered 20 nm, 6 dB/octave roll-off. One observes that individual short reversals are hardly visible, sometimes they only show as small amplitude variations. Anomalies 30 and 31, showing in Figure 7a as two peaks, become completely merged into one anomaly 30/31 in Figure 7b. The effect of the filtering can also be observed in the reduction of the amplitude of the seafloor spreading anomalies.

Figure 7c shows the contours of the seafloor spreading anomalies, calculated at a grid of 0.05 degree, using the 20 nm Butterworth filter for the contouring. The anomalies were calculated for the area around 41° N.

The presentation of the grid values by way of a contour chart has the disadvantage that small amplitude lineations with amplitudes smaller than the contour interval may get lost. A possible solution lies in the presentation of a three dimensional view of the grid values, as was done for the spatial representation of the filter used in the gridding process (see Figure 6). Another possible solution can be found in the presentation of slopes instead of the values itself. For this the directional derivative of the grid values can be used. The direction depends on the slopes one wants to enhance. For instance if the direction chosen is the seafloor spreading direction the slopes of the seafloor spreading anomalies will line up and enhance the position of the anomalies. Figure 7d shows the result for the calculated seafloor spreading anomalies.

## 7. Final Editing

The cross-over analysis was only performed for parts of the total area. This leaves open the possibility that there remain parts of tracks whose magnetic anomalies are not consistent with those of other adjacent tracks. In order to find these tracks, or parts of them, the following procedure was adopted. First the grid

values were calculated using all data. From these grid values, synthetic anomalies were calculated along all tracks. The residuals, i.e. the difference between the anomalies used in the calculation of the grid values and the anomalies obtained from them, should then be short wavelength anomalies with no bias. However, if a track (or part) has anomalies which are not consistent with those of other adjacent tracks then the residuals will be biased and have the same sign over a longer distance. Therefore, the residuals were averaged from the time-series of the tracks over four hour blocks, about 65 km, and these averages were printed. All those parts of tracks where these averages have the same sign over a 24 h period (with an average ship's speed of 9 knots over a distance of about 480 km) were eliminated from the data set. However, if the part of the track runs along a continuous anomaly of one sign, then that part was not eliminated. Also parts where the averages have high values and no adjacent seamounts or islands occur were eliminated. In total, using the above described procedure about 2% of the data set was discarded.

## 8. The Contour Charts of the Magnetic Anomalies

Following the above described procedure, contour lines were drawn from the grid values as shown in Figure 8 and in the accompanying map at a scale of 1 : 2 400 000 at 41° N. Areas where the data distribution was not dense enough to obtain reliable contours were filled in using a two dimensional running mean procedure with a Gaussian weight function. These areas are shown at the back of the map with boxes. Also shown are the track lines from Figure 1. Discontinuous track lines denote places where data gaps of more than 30 min occur (approx. 8 km at 9 knots).

The directional derivative of the magnetic anomalies is given in Figure 9. The direction was chosen to be 285°, thus enhancing the seafloor spreading anomalies.

## 9. Magnetic Anomalies Reduced to the Pole

In general, magnetic anomalies are phase-shifted when observed away from the magnetic pole. The shift in position, or skewness, of the magnetic anomalies is caused by the nonverticality of the involved magnetic vectors. These vectors are the remanent magnetization vector and the present field vector (e.g., Verhoef, 1984). This phase-shift of the magnetic anomalies can, in principle, be eliminated if the orientation of these two magnetic vectors is known. This is termed reduction to the pole.

Assuming that the bodies causing the magnetic anomalies are two-dimensional structures, the reduction to the pole can be made by correcting for the phase-shift parameter theta (Schouten, 1971). For three dimensional structures the correction for the skewness of magnetic anomalies can be described by the


Fig. 8. Magnetic anomalies of the main chart shaded as in Figure 7c.

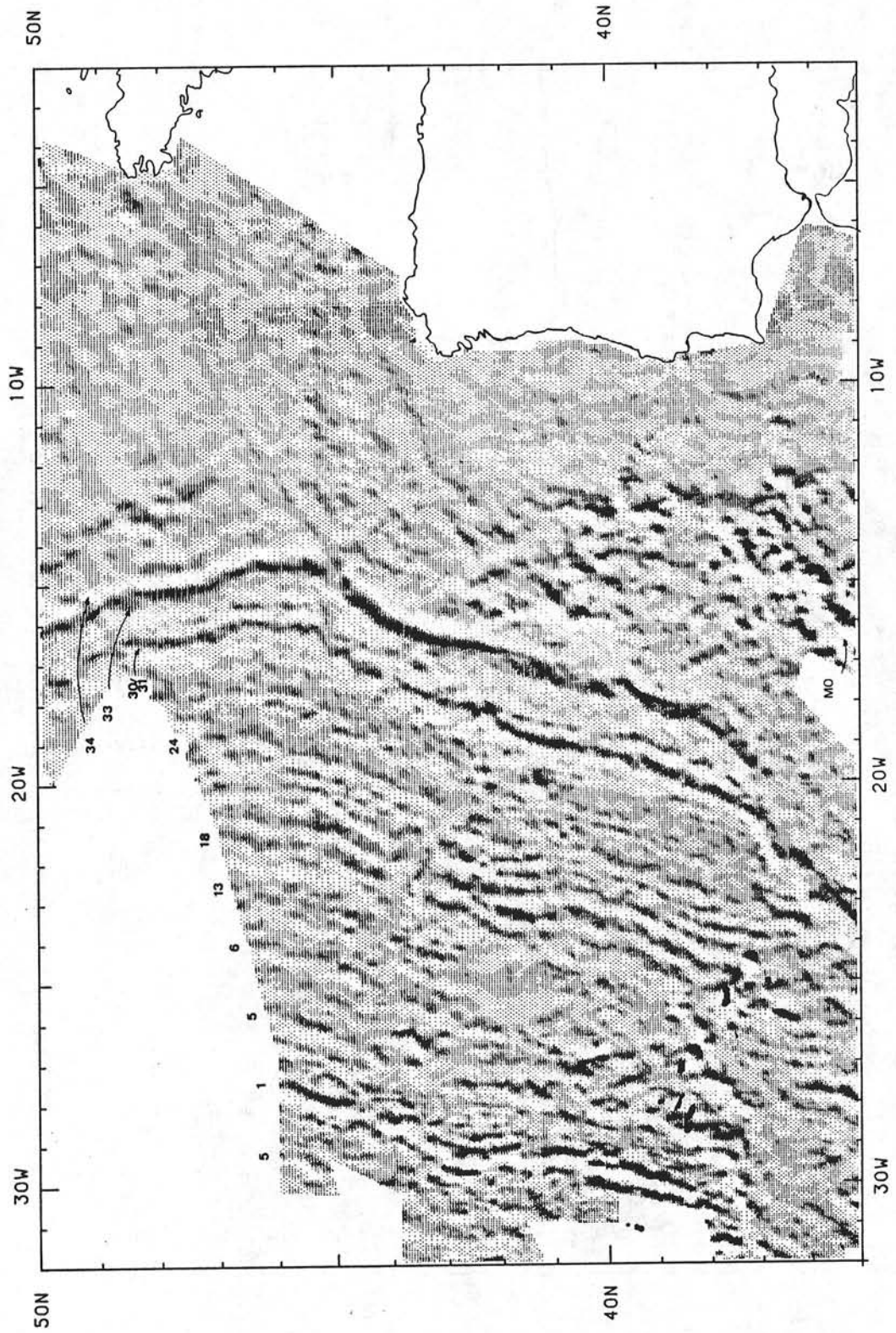


Fig. 9. Directional derivative of Figure 8 (285°) shaded as in Figure 7d.

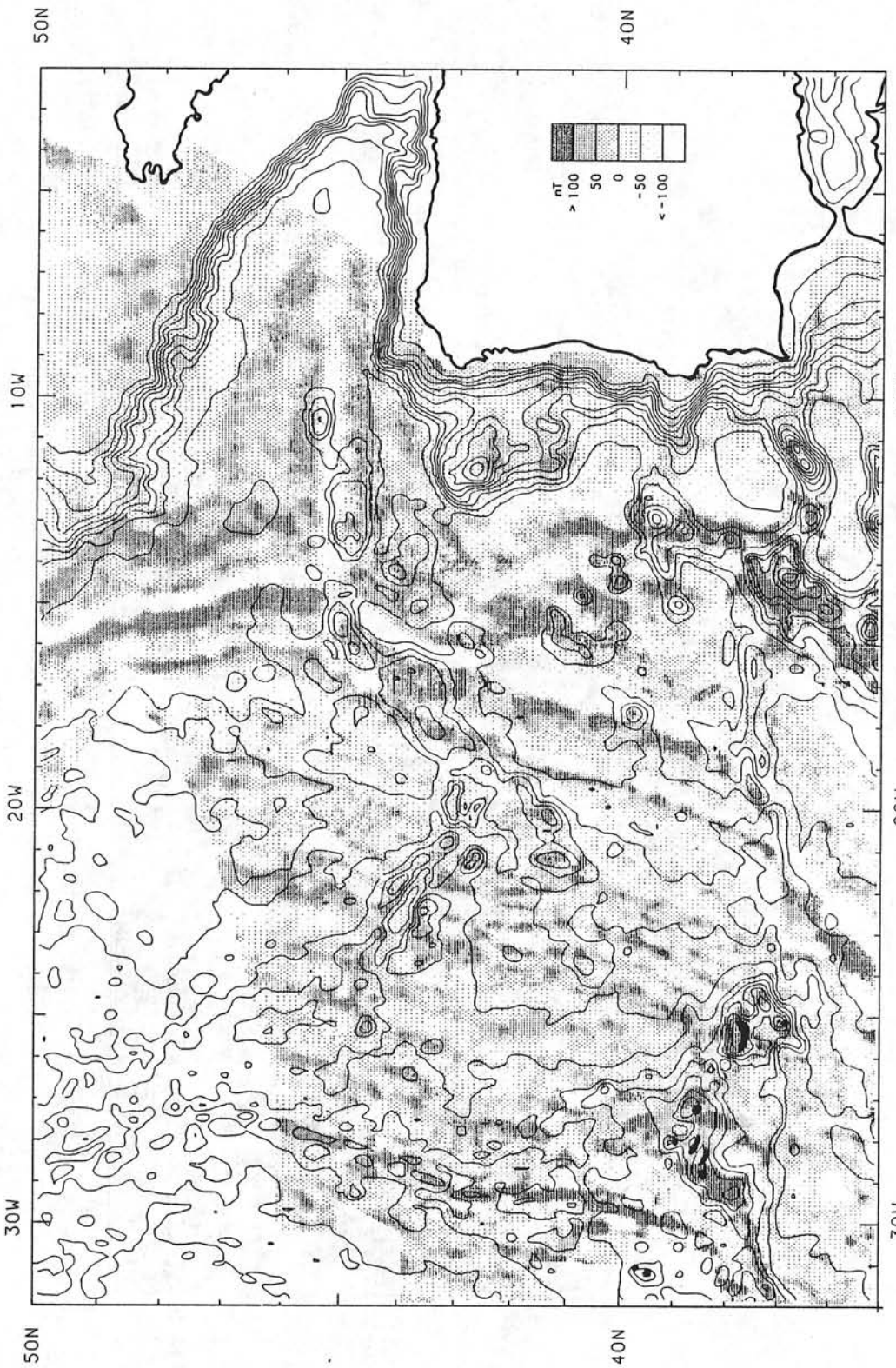


Fig. 10. Magnetic anomalies of Figure 8 reduced to the pole and merged with the bathymetry (Figure 11).

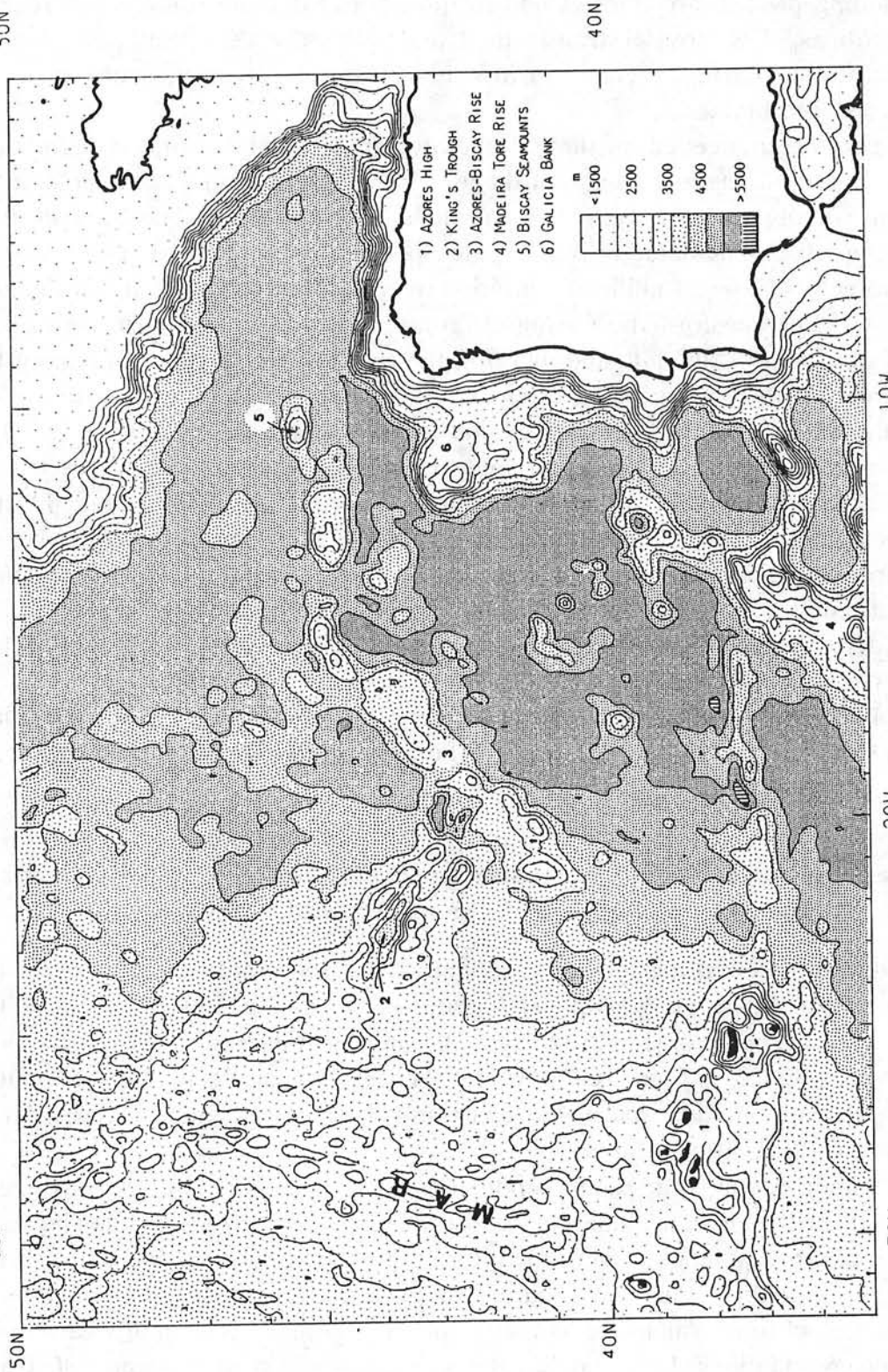


Fig. 11. Bathymetry of the area with a contour interval of 500 m. The chart is based on the Navoceano digital bathymetric data base on a 5' grid (DBDB5, 1984)

operator 'reduction to the pole' (RP) defined in the Fourier domain (Le Mouël *et al.*, 1972). The magnetic anomalies as defined from the grid values obtained after the gridding process are transformed to the Fourier domain using standard 2-D FFT routines. The Fourier transformed anomalies are then multiplied by the RP-operator and after inverse transformation the reduced to the pole magnetic anomalies are obtained.

The parameters needed for the RP-operator are the inclination and declination of the present magnetic field and of the ancient magnetic field, i.e. the field at the time the involved structures obtained their magnetization. The ancient field parameters were calculated using the paleo-poles of Irving and Irving (1982). As the parameters show a significant variation over the area involved, it was decided to perform the transformation using different sets of parameters for the eastern and western half of the data and merging the results. For the western part of the area (west of 19° W) the parameters are as follows: remanent inclination: 54°, remanent declination: −2°, present inclination: 59° and present declination: −17°. For the eastern part of the area (east of 20° W) the parameters used are: remanent inclination: 46°, remanent declination: 1°, present inclination: 59° and present declination: −12°. The variation in range of parameters for each area compared to those actually used were: remanent inclination: ±8°, remanent declination: ±1°, present inclination: ±5° and present declination: ±2°. The reduced to the pole anomalies in the area between 19° and 20° W were then merged. The results are shown in Fig. 10, together with the bathymetric contours. These bathymetric contours are taken from the digital bathymetric data base (DBDB5, 1984). Figure 11 shows the same bathymetric contours with the addition of shading.

## 10. Identification of Seafloor Spreading Anomalies, Kinematic Implications and the Relation of Magnetic Anomalies with Bathymetry

The data presented in this magnetic anomaly chart represent three aspects in the development of marine geology and geophysics off SW Europe. First is the fidelity in resolving geomagnetic reversal signatures in the oceanic crust. Second, concerns the space and time relationships between the various tectonic provinces existing throughout the area of the chart and third, the magnetic expression of important bathymetric features.

The major seafloor spreading anomalies identified in Figure 8 have been defined from the reversal timescale of Lowrie and Alvarez (1981) as shown in Figure 7 and the enhanced resolution afforded by the directional derivative of the magnetic anomalies shown in Figure 9. Figure 9 enables the identification of magnetic isochrons which are not evident in Figure 8, the main chart or in previous compilations. In particular, the weak anomaly seen between 30/31 and 33 can be traced almost continuously from the European-African plate boundary up to 50° N. This anomaly is identified as anomaly 32. Anomaly 24 is seen clearly

to the north and south of King's Trough with the anomaly lineations on the south flank of this feature substantiating the interpretation of Miles and Kidd (in press). Anomaly 13 follows the interpretation of previous authors (e.g., Srivastava and Tapscott, in press) as the most prominent anomaly lineation of this age in an area of subdued anomaly amplitudes and low data coverage.

Anomaly identification and tracing of isochrons is difficult between anomalies 6 to 18 although a number of identifications have been made (Archambault, 1984; Srivastava and Tapscott, in press). Anomaly 6 is readily identifiable as well as anomaly 5. It is possible that anomaly 5 is traceable through the Azores complex.

The ridge-anomaly (anomaly 1) stands out by its large amplitude. It is dissected by a number of offsets in our area of coverage (Searle and Laughton, 1977; Bhattacharyya *et al.*, 1975).

Anomaly 34 marks the end of the Cretaceous Magnetic Quiet Period. A problem of the oldest identifiable anomalies in this part of the Atlantic (Mesozoic anomaly MO or anomaly J) concerns their location or extent. In Figure 9 the easternmost magnetic lineation extends due north along 30° W to 41° N, the latter position being the ocean-continent boundary west of Galicia Bank (Groupe Galice, 1979).

The early comprehensive analysis of magnetic anomalies given by Pitman and Talwani (1972) for the North Atlantic, and the kinematic studies which subsequently used the results, were significantly modified by the re-identification of anomalies 31 and 32 as 33 and 34 by Cande and Kristoffersen (1977). A consequent reconstruction (Kristoffersen, 1978) illustrated the significance of an anomaly 33 reconstruction overlap as quantifying a NW Tertiary motion of the Iberian plate. More recently, Iberia is proposed to have moved with Africa until anomaly 10 time (Srivastava and Tapscott, in press). The later publications on North Atlantic reconstructions affecting the area of the chart have used magnetic anomaly lineations as major constraints back to the Campanian (anomaly 33). The Cretaceous Magnetic Quiet Period and the Mesozoic anomalies adjacent to the Portuguese margin provide poor constraints on closure reconstructions (Sullivan, 1983; Olivet *et al.*, 1984; Masson and Miles, 1984; Srivastava and Tapscott, in press).

In Figure 10 the magnetic anomalies reduced to the pole show several outstanding correlations with the regional bathymetry and structure. Additionally there is a relationship between large bathymetric features and the occurrence of very large magnetic anomalies. These relations are most evident over the Mid-Atlantic Ridge (MAR in Figure 11), the Azores (1), King's Trough (2), the seamounts on the southern Azores-Biscay Rise (3) and the Madeira-Tore Rise (4). Interesting exceptions are the Biscay seamounts (5) and the seamount which flanks anomaly 33 at 40° N/18° W. Galicia Bank (6) shows clearly as the seaward continuation of the continent-ocean crustal boundary N of the Iberian Peninsula. The Azores-Gibraltar plate boundary shows from lineations both in the bathymetry and reduced to the pole anomalies.

## 11. General Discussion

The early formation of oceanic crust in the area of the North Atlantic covered by the chart remains controversial in its palaeo-tectonics if not in time. Emplacement of oceanic crust around the continental margins of SW Europe began in Late Aptian west of Galicia Bank (Sibuet and Ryan, 1979) and in the northern Bay of Biscay (Montadert *et al.*, 1979) and in Lower Albian west of the Goban Spur continental margin (Masson *et al.*, 1984). To the east of Goban Spur the ocean-continent boundary of the North Biscay margin, which lies well off the continental slope, is marked by the magnetic anomalies. The same seems true for the compressed southern margin which extends westward of the Iberian Peninsula and passes north of Galicia Bank. A number of initial spreading geometries have been proposed for the otherwise ill constrained areas of oldest oceanic crust adjacent to the margins (Olivet *et al.*, 1984; Masson and Miles, 1984; Sullivan, 1983; Srivastava and Tapscott, in press). The existence of Iberia as a separate micro-plate, its relative motion and the degree of continental overlap in alternative reconstructions (particularly Galicia Bank) has featured in much of the literature on this area.

A spreading triple junction existed to the west of Biscay from the mid Albian following the initiation of spreading between Eurasia and North America (Williams, 1975). Spreading in Biscay probably stopped after anomaly 34 times. This extinct triple junction is evident on the chart at 45° N/14.5° W. West of Iberia confused anomalies result partially from Late Cretaceous and Miocene compressive phases in the area of the Madeira-Tore Rise.

As said before, the identification of Mesozoic anomaly MO (or anomaly J) north of the Azores-Gibraltar plate boundary in this area is difficult. The DSDP and ODP programs have sites drilled south and west of Galicia Bank which are located on rotated fault blocks of a rifted margin. If this type of structure is continuous to the south in the deep waters off Portugal, this is one way of explaining the low amplitude anomalies in this area.

The Tertiary deformation of the north Spanish margin is well documented (Le Pichon and Sibuet, 1971; Boillot *et al.*, 1979; Grimaud *et al.*, 1982; Olivet *et al.*, 1984 and Groupe Cybere, 1984). The proposed interpretations have implications for the area west of the Iberian Peninsula. West of the prominent magnetic anomaly 33 a number of interesting features exist which have not been fully explained. Two major features, King's Trough and the Azores-Biscay Rise, have appeared in much of the literature on this area (e.g., Searle and Whitmarsh, 1978; Whitmarsh *et al.*, 1982). An important aspect of these features concerns the significance of the Pyrenean orogeny to their origin and development. Whitmarsh *et al.* (1982) found no evidence of subduction or transform motion being related to the Azores-Biscay Rise. The data in this paper suggests a continuity of magnetic lineations over the Rise as can be seen on the chart and in Figures 8 and 10. These results directly affect proposals requiring part of the

Azores-Biscay Rise to be a plate boundary (Grimaud *et al.*, 1982; Olivet *et al.*, 1983; Grimaud *et al.*, 1983; Srivastava and Tapscott, in press; cf., also Schouten *et al.*, in prep.) Apart from the topographic effect of the seamounts on the southern part of the Rise, this feature shows no significant magnetic characteristic. King's Trough trends across the magnetic isochrons and produces some disturbance in the linearity of the anomalies, particularly on its southern flank. This flank has been discussed extensively (Le Pichon and Sibuet, 1971; Searle and Whitmarsh, 1978; Grimaud *et al.*, 1982; Olivet *et al.*, 1983; Olivet *et al.*, 1984). Small offset fracture zones (Schouten and White, 1980) flanking King's Trough, near 42° N/22° W, have been postulated from the magnetic anomalies 18–24 (Miles and Kidd, in press).

In the SW corner of the chart, the Azores triple junction has a large effect on the anomalies (Searle, 1980). The Tydeman Fracture Zone (Twigt *et al.*, 1979; Collette *et al.*, 1984) can be seen along the southern margin of the chart at 36° N south of the extensive lineation of the East Azores Fracture Zone noted above from the reduced to the pole anomalies. To the north of the Azores, at 41° N on the ridge, the magnetic anomaly contours may suggest that the Kurchatov fracture zone (Searle and Laughton, 1977) can be traced east as far as the Azores-Biscay Rise, its trend correlating with the southern limit of the seamounts on this part of the Azores-Biscay Rise.

## Acknowledgements

Particular thanks are extended to J. H. M. Hoofd for the data preparation and his perseverance in the data presentation and copy proofing of the chart. Dr. M. T. Jones of MIAS is thanked for making a large amount of 'inaccessable' data accessible which significantly influenced the results of this work.

The first author (J. V.) acknowledges the funding obtained for the project from the Netherlands Organization for the Advancement of Pure Science (ZWO) through the Stichting AWON.

## References

Archambault, M. F.: 1984, 'Evolution cinématique post-Eocène de l'Atlantique Nord et Central. Implications sur le fonctionnement des Açores et l'évolution due domaine méditerranéen occidental', Ph.D. Thesis, Université de Bretagne Occidentale, 211 pp.

Aumento, F. D., Loncarevic, B. D., and Ross, D. I.: 1971, 'Hudson Geotraverse: Geology of the Mid-Atlantic Ridge at 45° N', *Phil. Trans. Roy. Astr. Soc. London*, A **268**, 623–650.

Bhattacharyya, P. J., Hyndman, R. D., and Keen, M. J.: 1975, 'The Mid-Atlantic Ridge near 45° N, XXIII, Analysis of Bathymetric and Magnetic Data', *Can. J. Earth Sci.*, **12**, 337–346.

Black, M., Hill, A. S., Laughton, A. S., and Matthews, D. H.: 1964, 'Three Non Magnetic Seamounts off the Iberian Coast', *Quat. J. Geol. Soc. Lond.* **121**, 477–517.

Boillot, G., Dupeuble, P.-A., and Malod, J.: 1979, 'Subduction and Tectonics on the Continental Margin of Northern Spain', *Mar. Geol.* **32**, 53–70.

Cande, S. C. and Kristofferson, Y.: 1977, 'Late Cretaceous Magnetic Anomalies in the North Atlantic', *Earth Planet. Sci. Lett.* **35**, 215–224.

Collette, B.J., Slootweg, A. P., Verhoef, J., and Roest, W. R.: 1984, 'Geophysical Investigations of the Floor of the Atlantic Ocean between 10° and 38° N (Kroonvlag-project)', *Proc. Kon. Ned. Ak. Wet.*, series B, **87**, 1–76.

DBDB5: 1984, 'Navoceano Digital Bathymetric Data Base, Unclassified'.

Grimaud, S., Boillot, G., Collette, B. J., Maufret, A., Miles, P. R., and Roberts, D. G.: 1982, 'Western Extension of the Iberian-European Plate Boundary During the Early Cenozoic (Pyrenean) Convergence: A New Model', *Mar. Geol.* **45**, 63–77.

Grimaud, S., Boillot, G., Collette, B. J., Maufret, A., Miles, P. R., and Roberts, D. G.: 1983, 'Western Extension of the Iberian-European Plate Boundary During the Early Cenozoic (Pyrenean) Convergence: A New Model-Reply', *Mar. Geol.* **53**, 238–239.

Groupe Cybère: 1984, 'La marge déformée du Nord-Ouest de l'Espagne', *Cnexo publications, Résultats des campagnes à la mer* **29**, 135 pp.

Groupe Galice: 1979, 'The Continental Margin off Galicia and Portugal: Acoustical Stratigraphy, Dredge Stratigraphy and Structural Evolution', in Sibuet, J.-C., Ryan, W. B. F. *et al.*, *Init. Repts. DSDP*, **47**, part 2, Washington (U.S. Govt. Printing Office), pp. 633–662.

Guennoc, P., Jonquet, H., and Sibuet, J.-C.: 1979, 'Présentation d'une carte magnetique de l'Atlantique Nord-Est', *C. R. Acad. Sci. Paris*, Ser. D, **288**, pp. 1011–1013.

IAGA Division I Working Group: 1981, 'International Geomagnetic Reference Fields: DGRF 1965, DGRF 1970, DGRF 1975, and IGRF 1980', *EOS Trans. Am. Geophys. Un.* **62**, 1169.

Irving, E. and Irving, G. A.: 1982, 'Apparent Polar Wander Paths Carboniferous through Cenozoic and the Assembly of Gondwana', *Geophys. Surf.* **5**, 141–189.

Krause, D. C. and Watkins, N. D.: 1970, 'North Atlantic Crustal Genesis in the Vicinity of the Azores', *Geophys. J. Roy. Astr. Soc.* **19**, 261–283.

Kristofferson, Y.: 1978, 'Seafloor Spreading and the Early Opening of the North Atlantic', *Earth. Planet. Sci. Lett.* **38**, 273–290.

Laughton, A. S., Roberts, D. G., and Graves, R.: 1975, 'Bathymetry of the Northeast Atlantic: Mid-Atlantic Ridge to Southwest Europe', *Deep Sea Res.*, **22**, 791–810.

Le Mouël, J. L., Galdeano, A., and Le Pichon, X.: 1972, 'Remanent Magnetization Vector Direction and the Statistical Properties of Magnetic Anomalies', *Geophys. J. Roy. Astr. Soc.* **30**, 353–371.

Le Pichon, X., and Sibuet, J.-C.: 1971, 'Western Extension of the Boundary between European and Iberian Plates During the Pyrenean Opening', *Earth Planet. Sci. Lett.* **12**, 83–88.

Lowrie, W. and Alvarez, W.: 1981, 'One Hundred Million Years of Geomagnetic Polarity History', *Geology* **9**, 392–397.

Masson, D. G., and Miles, P. R.: 1984, 'Mesozoic Seafloor Spreading between Iberia, Europe and North America', *Mar. Geol.* **56**, 279–288.

Masson, D. G., Montadert, L., Scrutton, R. A., and Gruvel, J.-P.: 1984, 'Evolution of the Goban Spur: History of a Starved Passive Margin', in Graciansky, P.-C., Poag, C. W. *et al.*, *Init. Repts. DSDP*, **80**, Washington (U.S. Govt. Printing Office), pp. 1115–1140.

Matthews, D. H., Laughton, A. S., Pugh, D. T., Jones, E. J. W., Sunderland, J., Takin, M., and Bacon, M.: 1969, 'Crustal Structure and Origin of Peake and Freen Deeps, N.E. Atlantic', *Geophys. J. Roy. Astr. Soc.* **18**, 517–542.

Miles, P. R. and Kidd, R. B.: in press, 'Correlation of Seafloor Spreading Magnetic Anomalies across King's Trough, N.E. Atlantic Ocean', in *Init. Repts. DSDP*, **94**, Washington (U.S. Govt. Printing Office).

Montadert, L., Roberts, D. G., de Charpal, O., and Guennoc, P.: 1979, 'Rifting and Subsidence of the Northern Continental Margin of the Bay of Biscay', in Montadert, L., Roberts, D. G. *et al.*, *Init. Repts. DSDP* **48**, Washington (U.S. Govt. Printing Office), pp. 1025–1060.

Olivet, J.-L., Auzende, J. M., and Beuzart, P.: 1983, 'Western Extension of the Iberian-European Plate Boundary During the Early Cenozoic (Pyrenean) Convergence: A New Model-Comment', *Mar. Geol.* 53, 237–238.

Olivet, J.-L., Bonnin, J., Beuzart, P., and Auzende, J. M.: 1984, 'Cinématique de l'Atlantique Nord et Central', *CNEXO Rep. Sci. Tech.* **54**, 108 pp.

Pitman, III, W. C., and Talwani, M.: 1972, 'Sea-Floor Spreading in the North Atlantic', *Geol. Soc. Am. Bull.* **83**, 619–646.

Reagan, R. D., and Rodriguez, P.: 1981, 'An Overview of the External Magnetic Field with Regard to Magnetic Surveys', *Geophys. Surv.* **4**, 255–297.

Roberts, D. G., Jones, M. T., and Hunter, P. M.: 1985, 'Magnetic Anomalies in the Northeast Atlantic', Inst. Ocean. Sci. Rep., **207**, 9 pp +2 charts.

Schouten, J. A.: 1971, 'A Fundamental Analysis of Magnetic Anomalies over Ocean Ridges', *Mar. Geophys. Res.* **1**, 111–144.

Schouten, H., and White, R. S.: 1980, 'Zero Offset Fracture Zones', *Geology* **8**, 175–179.

Schouten, H., Srivastava, S. P., and Klitgord, K. D.: in prep., 'Iberian Plate Kinematics: The African Connection'.

Searle, R. C.: 1980, 'Tectonic Pattern of the Azores Spreading Centre and Triple Junction', *Earth Planet. Sci. Lett.* **51**, 415–434.

Searle, R. C., and Laughton, A. S.: 1977, 'Sonar Studies of the Mid-Atlantic Ridge and the Kurchatov Fracture Zone', *J. Geophys. Res.* **82**, 5313–5328.

Searle, R. C., and Whitmarsh, R. B.: 1978, 'The Structure of King's Trough, Northeast Atlantic, from Bathymetric, Seismic and Gravity Studies', *Geophys. J. R. Astr. Soc.* **53**, 259–287.

Sibuet, J.-C., and Ryan, W. B. F.: 1979, 'Site 398: Evolution of the West-Iberian Passive Continental Margin in the Framework of the Early Evolution of the North Atlantic Ocean', in Sibuet J.-C., Ryan W. B. F. *et al.*, *Init. Repts. DSDP* **47**, part 2, Washington (U.S. Govt. Printing Office), pp. 461–475.

Slootweg, A. P.: 1978, 'Computer Contouring with a Digital Filter', *Mar. Geophys. Res.* **3**, 401–405.

Srivastava, S. P., and Tapscott, C. R.: in press, 'Plate Kinematics of the North Atlantic', in Tucholke, B. E., and Vogt, P. R. (eds.), *The Geology of North America*: *The Western Atlantic Region*, Geol. Soc. Am. DNAG series **1**..

Sullivan, K. D.: 1983, 'The Newfoundland Basin: Ocean-Continent Boundary and Mesozoic Seafloor Spreading History', *Earth Planet. Sci. Lett.* **62**, 321–329.

Twigt, W., Slootweg, A. P., and Collette, B. J.: 1979, 'Topography and Magnetic Analysis of an Area Southeast of the Azores (36° N, 23° W)', *Mar. Geoph. Res.* **4**, 91–104.

Verhoef, J.: 1984, 'Geophysical Study of the Atlantis-Meteor Seamount Complex', Ph.D. thesis, *Geologica Ultraiectina* **38**, 153 pp.

Verhoef, J., and Scholten, R. D.; 1983, 'Cross-Over Analysis of Marine Magnetic Anomalies', *Mar. Geophys. Res.* **5**, 421–435.

Whitmarsh, R. B., Ginzburg, A., and Searle, R. C.: 1982, 'The Structure and Origin of the Azores-Biscay Rise, North-east Atlantic Ocean', *Geophys. J. Roy. Astr. Soc.* **70**, 79–107.

Williams, C. A.: 1975, 'Seafloor Spreading of the Bay of Biscay and its Relationship to the North Atlantic', *Earth Planet. Sci. Lett.* **24**, 440–456.

(5) Sibuet J.-C., Mathis B., Pastouret L., Auzende J.-M., Foucher J.-P., Hunter P.M., Guennoc P., de Graciansky P.-C., Montadert L., et Masson D.G., 1984. Morphology and basement structures of the Goban Spur continental margin (NE Atlantic) and the role of the Pyrenean orogeny. Initial Reports of the Deep-Sea Drilling Project, 80, Washington, U.S. Government Printing Office, p. 1153-1165.

(6) Sibuet J.-C., Mathis B., et Hunter P.M., 1984. La ride Pastouret (plaine abyssale de Porcupine) : une structure éocène. C.R. Acad. Sc. Paris, 299, p. 1391-1396.

(7) Cheadle M., Matthews D., McGeary S., Warner M., Mascle A., Gariel O., Montadert L., Lefort J.-P., Le Gall B., Sibuet J.-C., Cazes M., et Schroeder I.J., 1986. Deep seismic reflection profiling between England, France and Ireland. J. Geol. Soc., 143, p. 45-52.

(8) Sibuet J.-C., et Ryan W.B.F., 1979. Site 398 : Evolution of the West Iberian continental margin in the framework of the early evolution of the North Atlantic Ocean. In Sibuet J.-C., Ryan W.B.F. et al., Initial Reports of the Deep Sea Drilling Project, 47, part 2, Washington, U.S. Government Printing Office, p. 761-775.

(9) Sibuet J.-C., Mazé J.-P., Amortila P., et Le Pichon X.,1987. Physiography and structure of the western Iberian continental margin off Galicia from Sea-Beam and seismic data. In Boillot G., Winterer E.L., et al., Proc., Init. Repts (Pt A), ODP, 103, p. 77-97.

Reprinted from Graciansky, P. C. de, Poag, C. W., et. al., 1984
*Initial Reports of the Deep Sea Drilling Project*, Volume LXXX, Washington (U.S. Government Printing Office)

# 56. MORPHOLOGY AND BASEMENT STRUCTURES OF THE GOBAN SPUR CONTINENTAL MARGIN (NORTHEASTERN ATLANTIC) AND THE ROLE OF THE PYRENEAN OROGENY[1]

Jean-Claude Sibuet, Benoît Mathis,
Léo Pastouret,[2] Jean-Marie Auzende, Jean-Paul Foucher, Peter M. Hunter, Pol Guennoc,
Pierre-Charles de Graciansky, Lucien Montadert, and Douglas G. Masson[3]

## ABSTRACT

A new bathymetric map, based mainly on Seabeam data, has been established for the Goban Spur area during a postcruise survey of DSDP Leg 80. Using both Seabeam data and a new series of eight seismic profiles obtained perpendicular to the continental margin, we have constructed a new detailed structural map of the Goban Spur continental margin which clearly reveals Caledonian and Variscan trends. Both the thinning of the Goban Spur continental crust, from Early Cretaceous (late Cimmerian phase) to middle Albian time, and subsequent widening of the adjacent oceanic domain, from middle Albian to Campanian time, resulted from tensional movements in a N70° direction which followed Caledonian trends. During the rifting phase, the tops of the tilted fault blocks remained close to sea level. The rapid subsidence of the margin seems to have occurred in the early Albian during the last stage of rifting.

Eocene intraplate deformation affected the whole Goban Spur continental margin, but is particularly evident at the Pastouret Ridge, a reactivated oceanic fracture zone. The oceanic domain underwent a slight intraplate compression, which fractured the old oceanic crust through its entire thickness, probably along previous zones of weakness, such as fracture zones.

## INTRODUCTION

During DSDP Leg 80, four sites (548–551) were drilled on the starved continental margin of Goban Spur and on the adjacent Porcupine Abyssal Plain (Figs. 1 and 2). The main objectives of this cruise were to investigate the structural evolution and depositional history of a series of tilted fault-blocks and half-grabens and their thin Cretaceous and Tertiary cover.

During October 1983, a CNEXO (Centre National pour l'Exploitation des Océans) postcruise survey was conducted in this area on the R/V *Jean Charcot* (Fig. 3), equipped with a bathymetric mapping system and a single-channel high-speed seismic-reflection survey system. Sound sources were two 1.5-l water guns or four 9-l air guns. Altogether, 2300 km of profiles were acquired. As Seabeam gives the bathymetry in a band about two-thirds as wide as water depth, the survey was designed to avoid any ambiguity about the lateral extension and correlation of morphologic features from profile to profile over the entire surveyed area (Fig. 3). The postrift sedimentary cover is thin, so most of the basement features are recorded in the morphology, and their trends have been clearly established.

In this chapter, we present a new bathymetric map (Fig. 2) based on all available conventional, Seabeam, and GLORIA data, and a map of basement features (Fig. 3) showing the main structural trends. These data are examined in the light of drilling results from Leg 80 and data from observations and sampling during recent dives of the *Cyana* submersible on the Pendragon Escarpment and on King Arthur's Castle (Fig. 2). We also discuss these data within the regional geological framework, showing that the Goban Spur continental margin was formed in an area previously affected by the Caledonian and Variscan orogenies. And we examine the intraplate consequences of the Pyrenean orogeny, especially as regards the oceanic domain, where a new bathymetric feature, named the Pastouret Ridge, has been discovered, and where the entire thickness of ocean crust has clearly been faulted.

## REGIONAL TECTONIC SETTING

The Goban Spur continental margin, about 200 km long, is located south of the Porcupine Sea Bight (Fig. 1), and it results from the relative motion of North America and Europe. It was created by crustal thinning during a rifting phase dated Early Cretaceous (late Cimmerian phase) to middle Albian (Masson et al., this vol.). The end of this rifting phase corresponds to the first creation of ocean crust. Southeastward of the Goban Spur continental margin, the Celtic margin is a result of the separation of Iberia and Europe. Although the rifting phase also started there during the late Cimmerian phase (Late Jurassic–Early Cretaceous), the onset of spreading has been dated as Aptian to middle Albian (Montadert, Roberts, de Charpal, et al., 1979).

The Goban Spur continental margin seems to have been affected, before its formation, by both the Caledonian and Variscan orogenies, and by their related tensional phases and wrench-faulting.

---

[1] Graciansky, P. C. de, Poag, C. W., et al., *Init. Repts. DSDP*, 80: Washington (U.S. Govt. Printing Office).

[2] Deceased September 14, 1983.

[3] Addresses: (Sibuet, Pastouret, Auzende, Foucher) Centre Océanologique de Bretagne, B. P. 337, 29273 Brest Cedex, France; (Mathis) GIS Océanologie et Géodynamique, Faculté des Sciences, Avenue Le Gorgeu, Brest, France; (Hunter, Masson) Inst. of Oceanographic Sciences, Brook Road, Wormley, Surrey, U. K.; (Guennoc) Bureau de Recherches Géologiques et Minières, Centre Océanologique de Bretagne, B. P. 337, 29273 Brest Cedex, France; (de Graciansky) École Nationale Supérieure des Mines, 60 Boulevard Saint-Michel, 75272 Paris Cedex 06, France; (Montadert) Institut Français du Pétrole, 1–4 Avenue de Bois-Préau, 92506 Rueil Cedex, France.

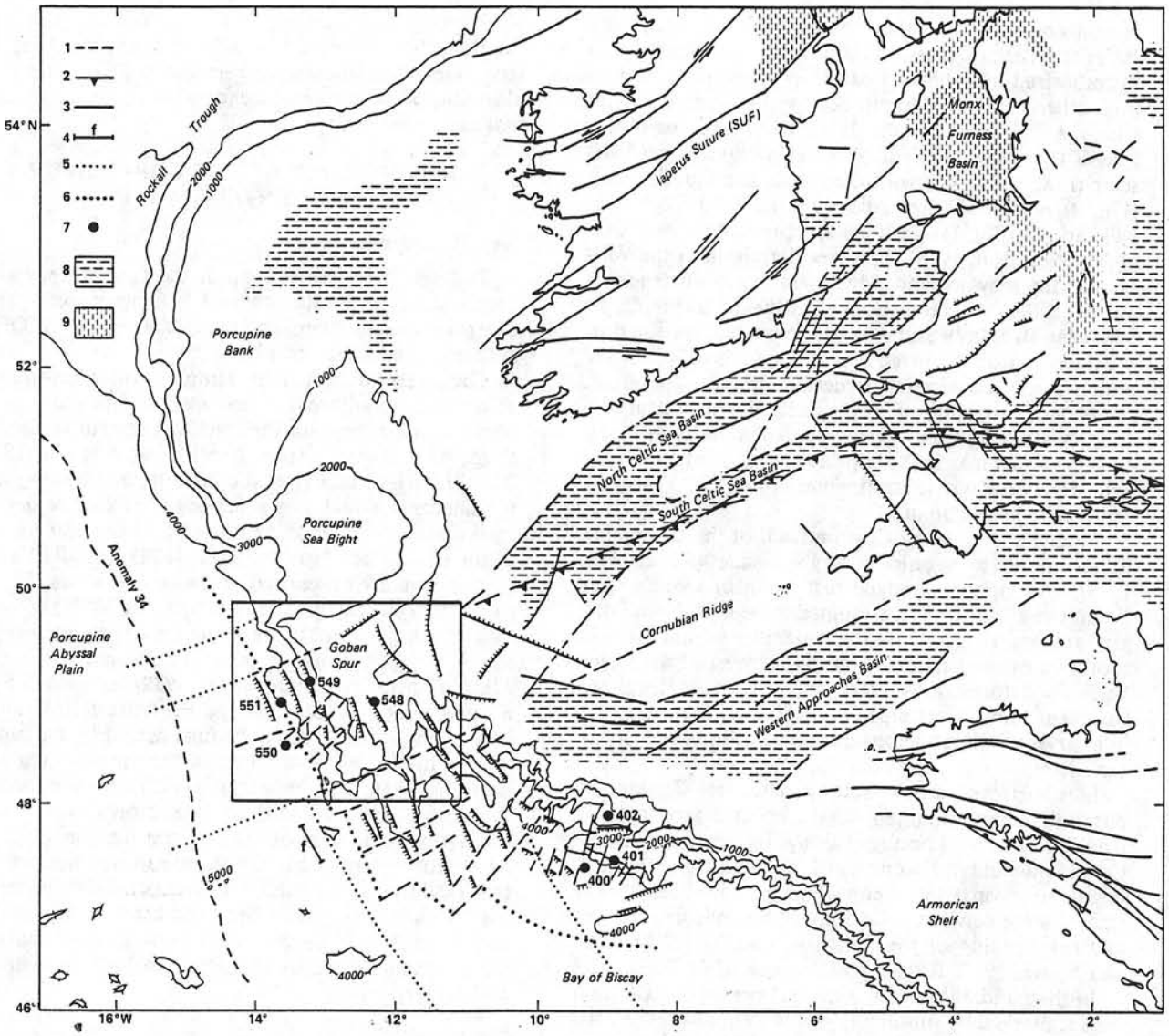


Figure 1. Generalized sketch of southwestern Europe, indicating the location of the Goban Spur survey done with the *Jean Charcot* during the Norestlante I cruise. (Bathymetry in meters.) Key to symbols (upper left corner): 1 = Faults in Ireland (from Max et al. [1983]; in Great Britain and in the Celtic Sea, Pegrum and Mounteney [1978]; on the continental margins, Montadert, Roberts, de Charpal, et al. [1979] and this study). 2 = Variscan front from Gardiner and Sheridan (1981). 3 = Normal or listric faults. 4 = Location of the seismic profile shown in Figure 9. 5 = Theoretical directions of the initial opening of the North Atlantic Ocean (Olivet et al., in press). 6 = Continent–ocean boundary (Montadert, Roberts, de Charpal, et al., 1979, and Masson et al., this vol.). 7 = DSDP sites drilled during Legs 48 and 80. 8 = Approximate present limit of Jurassic sediments (Pegrum and Mounteney, 1978). 9 = Triassic basins.

## Chronology and Nature of Paleozoic Deformations

The Caledonides resulted from the collision of continents that closed the Iapetus Ocean between the middle Silurian (420 m.y. ago; Paleozoic ages from Van Eysinga [1975] geological timetable; Mesozoic and Cenozoic ages from Odin [1982]) and the early Devonian (380 m.y. ago). The Iapetus Suture, located along the Southern Uplands Fault (Fig. 1), follows the general NE–SW orientation of the Caledonides fold belt (Leggett et al., 1983), and lies in the direct prolongation of the northwestern border of the Porcupine Sea Bight.

Between mid-Devonian and early Carboniferous time (365–335 m.y. ago), a large sediment basin, the Cornish–Rhenish Basin (Ziegler, 1978, 1981) developed under a tensional setting in an area stretching from Germany to the Celtic shelf. The position of the northern boundary of the Cornish–Rhenish basin is at present poorly documented. Between the late early Carboniferous (late Visean, 325 m.y. ago) and the middle late Carboniferous (late Westphalian, 295 m.y. ago), the Cornish-Rhenish Basin was incorporated into the Variscan deformation belt. Because the Variscan facies patterns and deformation trends were controlled primarily by the

morphology of the southern margins of the Celtic Sea-Wales and Brabant massifs, Gardiner and Sheridan (1981) hypothesized that the Variscan front, previously located in southern Ireland, should follow the arcuate Bristol Channel lineament, which flanks the Celtic Sea-Wales Massif (Fig. 1). If their hypothesis is correct, the Variscan front could be coincident with the Goban Fault (Fig. 2), which lies immediately north of DSDP Sites 549 and 551 (Fig. 1) (Gardiner and Sheridan, 1981; Dingle and Scrutton, 1979). This new definition of the Variscan front may explain why there is no evidence of WNW–ESE Variscan structural influence in the Celtic Sea (as in Brittany), and why basement reactivation during the Mesozoic occurred mainly along the ENE–WSW and NE–SW Caledonian structural trends. Therefore, the previous location of the Variscan front in southern Ireland is not rejected, because this feature is associated there with clear strike-slip faulting (Lefort, this vol.) and affects the whole continental crust (SWAT profile, Matthews, pers. comm.).

Granite intrusions of Cornwall and of the Cornubian Ridge, marked by negative gravity anomalies (Sibuet 1972, 1973), and granites dredged just south of Goban Spur (Pautot et al., 1976) are presumed to be of Variscan origin, and are aligned on a trend parallel to and 100 km southeast of the Variscan front. Northwest of the front, Variscan deformations seem only to reflect localized basement movements allied with lithological variations in a series of disconnected basins (Gardiner and Sheridan, 1981).

Late Variscan wrench-faulting, dated late Carboniferous to early Permian (Stephanian, 285 m.y. ago, to Autunian, 270 m.y. ago) occurred along the previous NE–SW Caledonian and Variscan trends, but also along the conjugate directions, and is considered to have been a transitional stage between the closing of the Paleozoic oceans and the opening of the Mesozoic ones (e.g., Arthaud and Matte, 1977; Russell and Smythe, 1983).

In the middle Permian, a general period of extension began, marked by subsidence in the Celtic Sea, the Bristol Channel, the Western Approaches Basin, and the areas of the future plate margins. These features continued to subside during the Triassic (204–245 m.y. ago), when clear graben features appeared (Kent, 1978). The overall Triassic extension heralded the breakup of Pangaea. By late Triassic time, the Variscan fold belt expressed only disjointed low relief within the monotonous flat plain of northwestern Europe (Ziegler, 1978). But until the Early Cretaceous crustal separation was achieved in the Bay of Biscay and the North Atlantic, most of northwestern Europe was subjected to regional extension, especially in the Porcupine Sea Bight, Celtic Sea, Bristol Channel, and Western Approaches Basin, where thick sedimentary strata accumulated (Fig. 1).

In conclusion, the geological development of the Goban Spur area seems to have been largely controlled by structural and physiographic features created during the Caledonian orogeny. The Variscan orogeny also affected this area, since the Variscan front seems to be located southeast of the Porcupine Sea Bight. Older NE–SW Caledonian features were probably reactivated during the Variscan orogeny. During the late Variscan strike-slip faulting, the conjugate NW–SE trends appeared for the first time. Then, during the Permian to Triassic tensional phase, both conjugate trends were occupied by normal and shear faults.

## MORPHOLOGY OF THE GOBAN SPUR CONTINENTAL MARGIN

### New Bathymetric Map

The new bathymetric map of the Goban Spur area, constructed from data acquired by conventional large-aperture echo-sounders and the Seabeam and GLORIA systems, is presented in Figure 2.

The Seabeam system is a multibeam echo-sounder comprising 16 adjacent narrow beams. The width of the contour swath beneath the track is approximately two-thirds of the water depth (Renard and Allenou, 1979). The GLORIA Mark II of the Institute of Oceanographic Sciences is a dual-scan sonar towed at shallow depths, with a maximum scanning range of 30 km on each side of the ship's track (Somers et al., 1978). GLORIA sonographs have been produced at the same scale as the Seabeam data (working scale, 1:250,000 at 38°N).

The track control of Seabeam data is shown on Figure 3. Detailed Seabeam maps established during the Marmor cruise (Pastouret et al., 1982) for Austell Spur, King Arthur's Castle, and the Pendragon Escarpment have been incorporated in the final map (Fig. 2), and are located in Figure 3. Conventional bathymetric data (e.g., Berthois, 1966; Laughton et al., 1975) have been used to fill the gaps in the Seabeam data. North of 49°20′N, the bathymetric map of Hunter and Kenyon (in press) has been incorporated. Depths are in uncorrected meters (1500 m/s). In addition, GLORIA data available for the vicinity of Austell Spur and King Arthur's Castle and King Arthur Canyon have been used to constrain the direction of trends identified on both bathymetric and GLORIA data.

### Morphology

The Goban Spur continental margin is limited to the northwest by the Porcupine Sea Bight and to the southeast by the Jean Charcot Escarpment (Fig. 2). The general orientation of this escarpment is N70°, corresponding to the Caledonian or late Hercynian directions, although this N70° direction seems to be slightly offset by ESE–WNW trends, which are also the fault trends observed on the Celtic margin (Fig. 1).

The Jean Charcot Escarpment was called "South Boundary Fault" by Dingle and Scrutton (1979) and the Jean Charcot Escarpment by Pastouret et al. (1982). We proposed to retain the latter designation, mainly because the Dingle and Scrutton name was defined only with respect to the Goban Spur continental margin.

The NW–SE-trending Pendragon Escarpment and another NW–SE escarpment—located 35 km southeastward, close to DSDP Site 551, and named "Outer Boundary Fault" by Dingle and Scrutton (1979)—are offset or stopped by NE–SW faults such as the Goban Fault (Fig. 2).

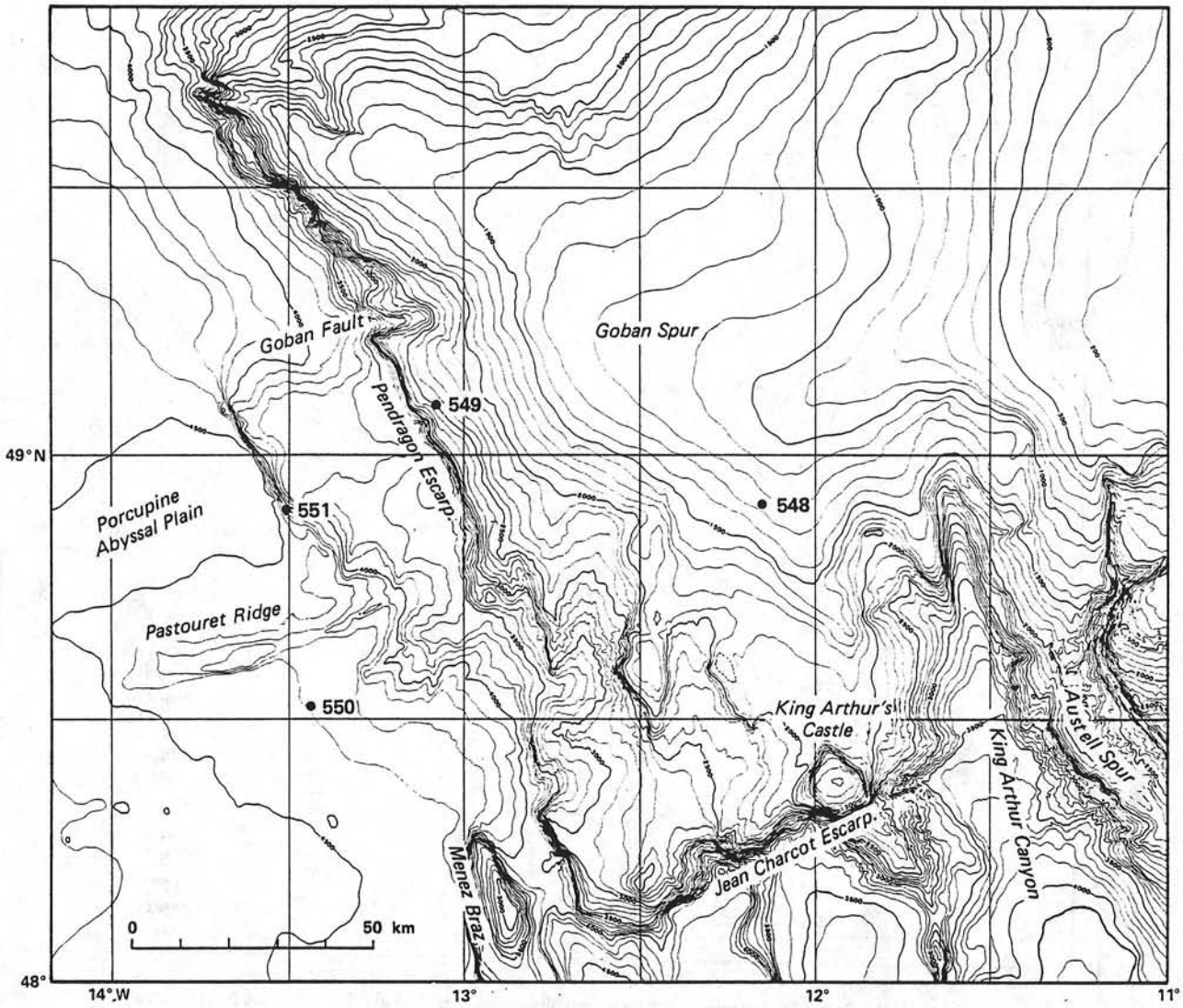


Figure 2. Bathymetric map, in Mercator projection, of the Goban Spur continental margin, established from Seabeam data (locations of tracks and local surveys [Pastouret et al., 1982] in Figure 3), conventional data (Berthois, 1966; Laughton et al., 1975; Hunter and Kenyon, in press), and unpublished GLORIA data from IOS. Depths are in uncorrected meters (1500 m/s). Contour spacing every 100 meters. Locations of DSDP sites drilled during Leg 80 are shown. The Pastouret Ridge is a newly named bathymetric feature.

On the Porcupine Abyssal Plain, 4500 m deep, a new bathymetric feature, oriented roughly N70°, about 50 km long and 300 m high, was discovered during the Norestlante cruise. We propose to name this feature "Pastouret Ridge," in memory of Léo Pastouret, who was particularly involved in the geological investigations of the Celtic and Goban Spur continental margins.

North of the Jean Charcot Escarpment, the bathymetry of the Goban Spur continental margin is complicated by the presence of several NNW–SSE-trending canyons, such as King Arthur Canyon. South of the Jean Charcot Escarpment, the average water depth over the continental margin is more than 1000 m greater than north of the escarpment. This portion of the continental margin, at the intersection of the Goban Spur and Celtic continental margins, has probably been affected by the interaction of tectonic movements linked to the formation of both margins during the Early Cretaceous. Nevertheless, the main structural trends of this area, such as Granite Cliff, Menez Bihan (Pautot et al., 1976), Menez Braz, and the Pendragon Escarpment, are oriented N330°.

We infer from the directions of morphologic trends that the formation and evolution of this portion of the North Atlantic continental margin have been controlled mainly by the previous Caledonian and late Variscan orogenic trends, as previously indicated by continental geological evidence.

## STRUCTURE AND GEOLOGICAL EVOLUTION OF THE GOBAN SPUR CONTINENTAL MARGIN

During the Norestlante cruise, 2300 km of single-channel seismic reflection profiles were collected in the area

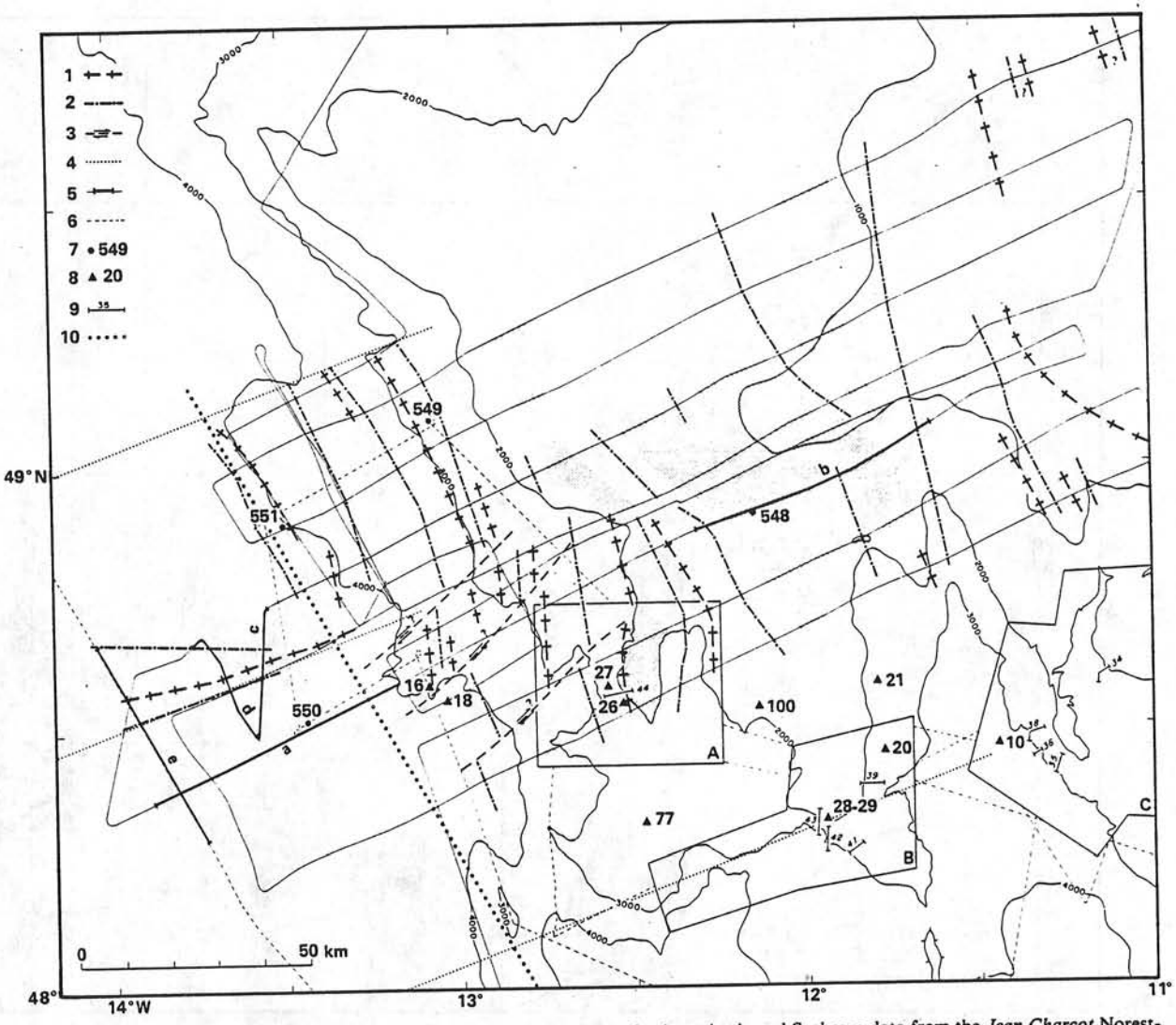


Figure 3. Structural map of the Goban Spur continental margin, established using seismic and Seabeam data from the *Jean Charcot* Norestlante I cruise. Simplified bathymetry from Figure 2. Boxes A, B, and C are previous Seabeam detailed surveys done in 1979 during the *Jean Charcot* Marmor cruise (Pastouret, et al., 1982). Shaded areas correspond to the eroded surfaces of tilted blocks. Key to symbols (upper left corner): 1 = Axis of highs. 2 = Axis of depressions. 3 = Possible faults. 4 = Theoretical directions of the initial opening of the North Atlantic Ocean (Olivet et al., in press). 5, thin lines = Locations of seismic and Seabeam profiles used in this study; thick lines = Location of seismic profiles a to e shown in Figs. 4 to 6 and 8. 6 = Complementary Seabeam tracks used to establish the bathymetric map of Figure 2. 7 = DSDP sites drilled during Leg 80. 8 = Dredgings (Auffret et al., 1979; Dingle and Scrutton, 1979). 9 = Locations of *Cyana* dives. 10 = Continent–ocean boundary.

of Goban Spur (Fig. 3). Two types of seismic sources were used: two 1.5-l water guns towed at 10 knots with a shot spacing of 10 s; and four 9-l air guns towed at 6 knots with a shot spacing of 30 s (in order to have better penetration and to deploy sonobuoy refraction experiments).

Eight parallel profiles with 8-mile spacing were collected in the region of Leg 80 sites, from the continental shelf to the typical oceanic domain (Fig. 3). Their ENE–WSW orientation is perpendicular to the direction of the continental margin. Because Seabeam data are available in real time, it was possible to identify the geometry of all features marked by topographic expression and to follow their lateral extension and orientation, and consequently to correlate them from profile to profile. A few complementary short profiles were implemented to follow structures or to specify the termination of structures.

## Basement Structures of the Goban Spur Continental Margin

The starved Goban Spur continental margin is characterized by a series of tilted fault-blocks, horsts, and grabens trending roughly parallel to the NW–SE direction of the continental slope (Montadert, Roberts, de Charpal, et al., 1979; Dingle and Scrutton, 1979; Masson et al., this vol.). The position of the continent–ocean boundary (Figs. 1 and 3) has been located on the basis of magnetic, seismic, and drilling data (Montadert, de Charpal, et al., 1979; Masson et al., this vol.).

Using both Seabeam and seismic data, the positions of depressions and highs within the rift system have been inferred over the whole area (Fig. 3). These structures trend N–S or NNW–SSE. North of the surveyed area, the NNW–SSE features are interrupted by the Goban Fault, oriented N70°, as shown on the bathymetric map (Fig. 2) and known from the previous work of Dingle and Scrutton (1979). Near 48.5°N, 13°W, three tectonic lines of discontinuity, oriented N45°, are visible. Also in this area, N–S trends are recognized. On the basis of this detailed survey, we infer an abrupt change in the trends of structures or a juxtaposition of different structural provinces, rather than a progressive bending of structures from N335° to N360°, as suggested by Masson et al. (this vol.). The three tectonic lines of discontinuity just mentioned follow the previous Caledonian and Variscan trends, and delimit different structural provinces. Horizontal movements of unknown limited extent could have taken place along these lines during the rifting phase.

In the oceanic domain, the sediments of the Porcupine Abyssal Plain bury the basement features, except for the topographically high Pastouret Ridge (Figs. 2–5). The southern flank of the Pastouret Ridge is a fault trending N71°, which is almost exactly the direction of the Goban Fault, of the Jean Charcot Escarpment, and of the theoretical directions of the early opening of the North Atlantic Ocean in this region (Le Pichon et al., 1977; Olivet et al., in press; Figs. 1 and 3). This suggests that the Pastouret Ridge is an oceanic fracture zone which has been subsequently reactivated.

Consequently, the formation both of the Goban Spur continental margin, from the Early Cretaceous (130 m.y. ago) to the middle Albian (100 m.y. ago), and then of the adjacent oceanic domain, from the middle Albian (100 m.y. ago) to the Campanian (Anomaly 33, 80 m.y. ago), resulted from N70° tensional movements which were parallel to the Caledonian trends. This is because initial plate motions are severely constrained by previous structural features of the continents, which become lines of weakness that guide early motions of plates (e.g., Sibuet and Mascle, 1978; Olivet et al., in press). In the case of the North America–Eurasian continent (Pangaea), the ENE–WSW Caledonian and Hercynian directions preferentially controlled the initial motion of continents along the oldest direction of the Charlie-Gibbs Fracture Zone (e.g., Olivet et al., 1974), which also corresponds to the orientation of the northern border of Porcupine Bank and of the southern Rockall Bank.

### Nature and Significance of Pre-Rift Basement Structures

The seismic profile of Figure 6 shows that the pre-rift basement is not homogeneous but consists of alternate opaque and layered sequences. The inclined layered sequences (e.g., between 4.30 and 5.00 on Fig. 6) are pre-rift sedimentary sequences, older than Late Jurassic, which tilted during rifting. The progressive tilting and the contemporaneous sedimentation are evidenced here by the convergence of syn-rift reflectors toward the ocean (Fig. 6 between 5.00 and 5.20). The continental basement was sampled by drilling at Sites 548 and 549 and by dredging (Auffret et al., 1979; Dingle and Scrutton, 1979) on the southern part of Goban Spur (Fig. 3). In 1982, during the Cymor II cruise, several sampling dives (Fig. 3) with the *Cyana* submersible were made on the Pendragon Escarpment, King Arthur's Castle, and Austell Spur. Preliminary results of these dives are compared with the drilling and dredging results.

At DSDP Sites 548 and 549, the basement consists of middle (365 m.y. old) to upper (350 m.y. old) Devonian graphitic quartzites and black shales (Lefort et al., this vol.) belonging to the Hercynian basement. Nearly vertical bedding, a slight metamorphic cleavage, and micaceous lineations indicate Hercynian tectonism (de Graciansky et al., in press).

Sampling during the *Cyana* dives on King Arthur's Castle and the Pendragon Escarpment (Figs. 3 and 7) recovered numerous sedimentary and metamorphic Paleozoic rocks. *Cyana* dive 44 (Fig. 3), on the Pendragon Escarpment, sampled a structural situation similar to that of DSDP Site 549. The Paleozoic basement, sampled at water depths between 2200 and 2500 m, is composed of schists and gneisses (Fig. 7) of higher metamorphic grade than the rocks recovered at DSDP Sites 548 and 549. Five dives (39–43) were made around King Arthur's Castle (Fig. 3). The lithologic description (Fig. 7) shows that the basement there also consists of Paleozoic schists and gneisses, as for the basement sampled on dive 44. Abundant fragments of chloritic schists affected by a low-grade metamorphism (Auffret et al., 1979; Dingle and Scrutton, 1979) have also been dredged in this area.

Granitic rocks, mainly granodiorites, have been dredged on the Granite Cliff and Menez Bihan, two features just south of the Jean Charcot Escarpment (Fig. 3). Rb–Sr and K–Ar dating give a 275 m.y. (total-rock) or 290 m.y. (biotite) age for these rocks attributed to the Hercynian basement (Auffret et al., 1979). In the Goban Spur area, Upper Jurassic shallow-water limestones characteristic of intertidal environments were reported only on the Granite Cliff (Auffret et al., 1979), although these samples may not have been in place. It is only at the level of DSDP Site 401, 200 km southeastward, that white shallow-water limestones of perireefal environment have been reported (Site 401 chapter, Montadert, Roberts, et al., 1979).

Thus, in the Goban Spur area, basement rocks are mainly middle Devonian (365-m.y.-old) and lower Carboniferous (335-m.y.-old) schists, gneisses, and limestones emplaced in shallow-water conditions, with some granitic intrusions. These Paleozoic rocks were affected by metamorphism during the Variscan phase, and show an increasing metamorphic grade from Sites 548 and 549 toward the south. These observations are compatible with a location of the Variscan front in the northern part of the Goban Spur area, as hypothesized by Gardiner and Sheridan (1981) (Fig. 1), and with a southward bending of the main Variscan deformation-trend from Brittany in the direction of the Iberian Peninsula replaced in its initial position (Sibuet, 1973). The Celtic Sea basins were intruded during the Variscan orogeny by

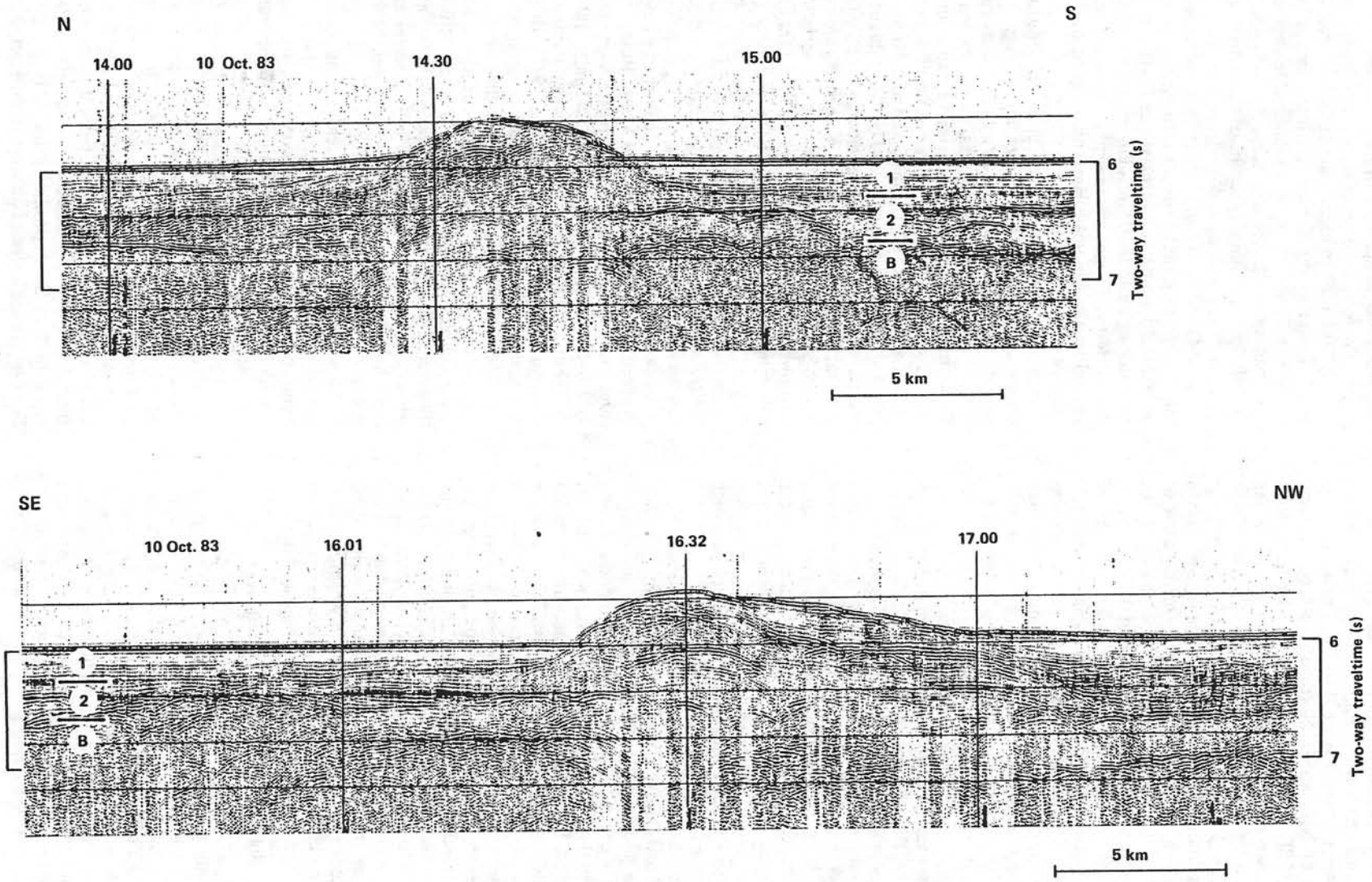


Figure 4. CNEXO high-speed single-channel seismic profiles across the Pastouret Ridge and located as profile c (N–S) and d (SE–NW) in Figure 3. The main acoustic units are: Unit 1, upper Oligocene to Present; Unit 2, upper Albian to lower Eocene; B, oceanic basement.

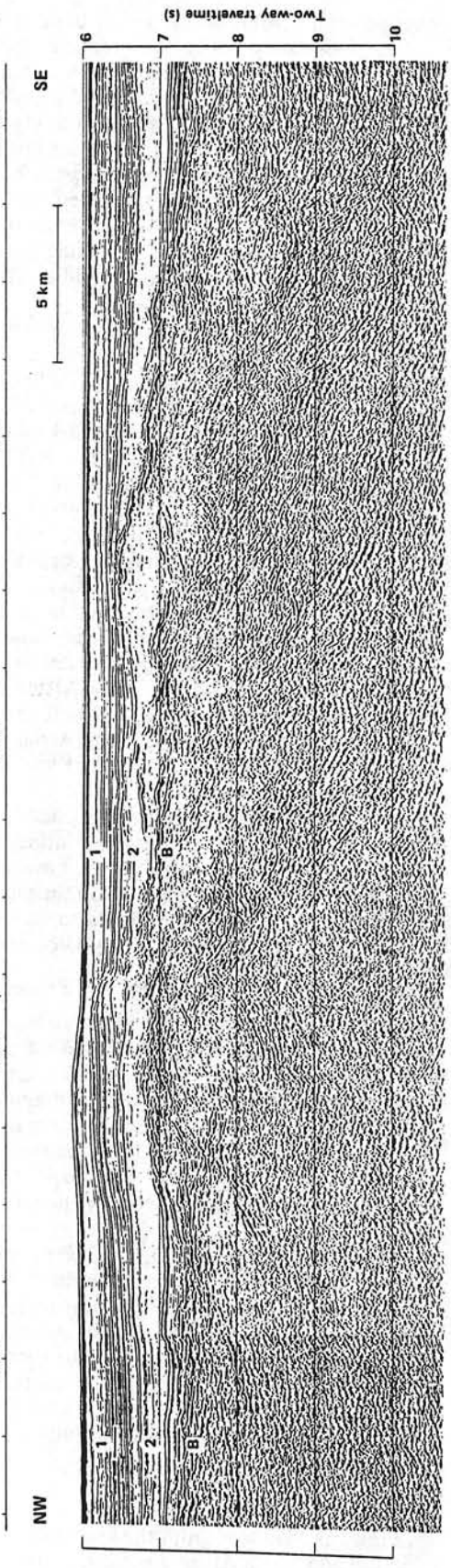


Figure 5. IOS multichannel seismic profile CM 05, migrated by IFP across the western part of the Pastouret Ridge and located as profile e in Figure 3. The main acoustic units are: Unit 1, upper Oligocene to Present; Unit 2, upper Albian to Lower Eocene; B, oceanic basement.

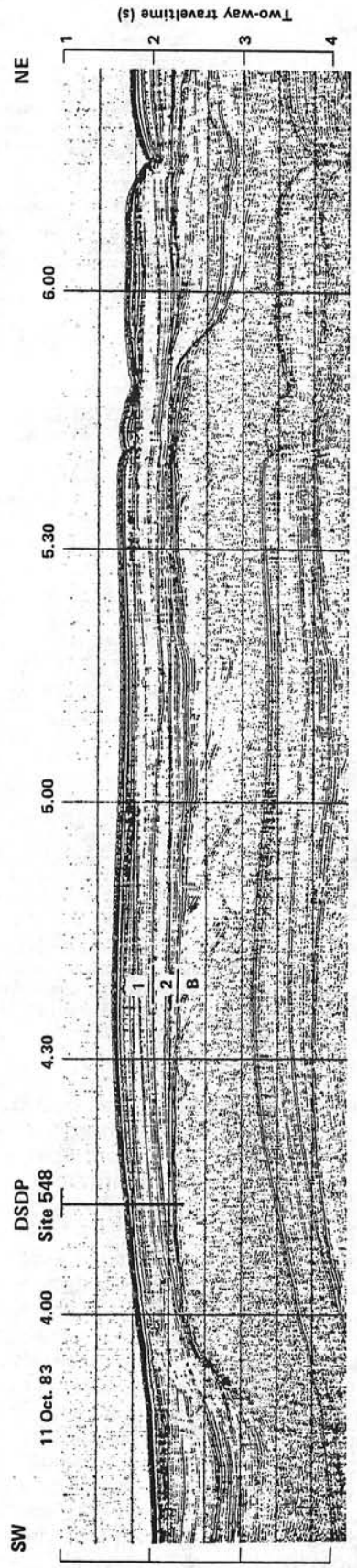


Figure 6. CNEXO high-speed (11 knots) single-channel seismic profile using two waterguns and shown as profile b in Figure 3. Drilling at Site 548 penetrated through the eroded surface of a tilted block. The main acoustic units are: Unit 1, upper Oligocene to Present; Unit 2, upper Albian to lower Oligocene; B, pre-rift.

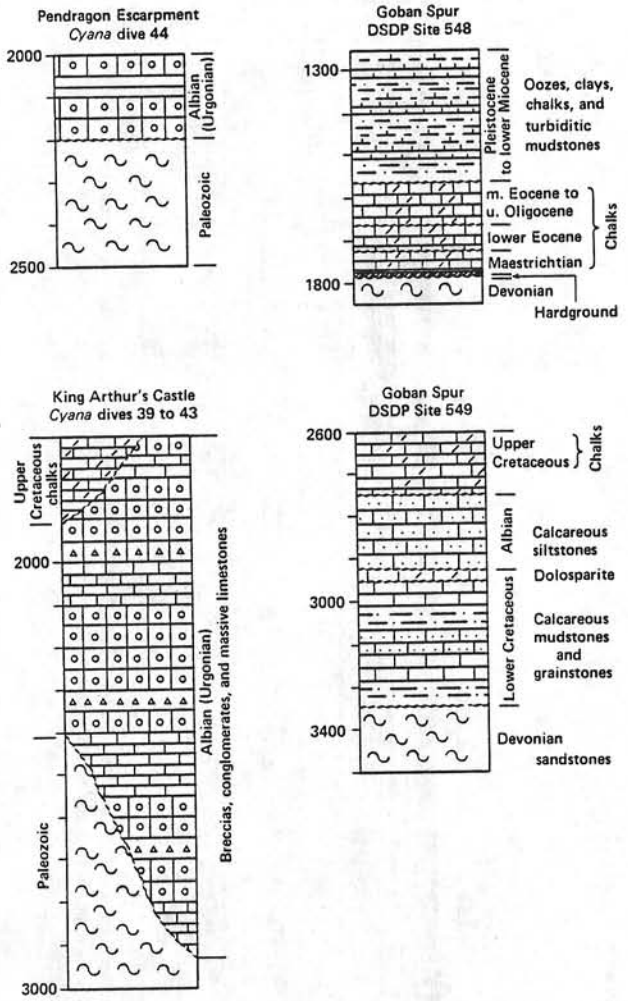


Figure 7. Lithostratigraphic comparisons between Sites 548 and 549, drilled on the tilted fault blocks, and *Cyana* dives on the Pendragon Escarpment and the flanks of King Arthur's Castle. Locations of DSDP sites and *Cyana* dives in Figure 3. Depths are in meters below sea level.

granites belonging to the batholithic axis (Sibuet, 1972, 1973), which can be followed straight from Cornwall to the foot of the continental margin on Granite Cliff, south of the Jean Charcot Escarpment (Fig. 1).

### Nature and Significance of Syn-Rift Deposits

In the Goban Spur area, a rifting phase began in the Early Cretaceous and ended in the latest early Albian (Masson et al., this vol.). At Site 549, the oldest syn-rift sediments are shallow-water interbedded calcareous and noncalcareous sandy mudstones and mudstones (Barremian, 113 m.y. old) (Site 549 chapter, this vol.). These sediments are overlain by a thin dolosparitic bed (Fig. 7), possibly an Aptian remnant, which in turn is overlain by a series of uppermost lower and middle Albian (98–102-m.y.-old) calcareous siltstones deposited in a bathyal environment. If the presence of this unconformity was associated with a major sea-level drop in the middle Aptian (110 m.y. ago; Vail et al., 1977), the change from a shallow-water to a bathyal environment corresponds to a post-Aptian deepening of the margin.

At Site 550, situated about 15 km west of the continent–ocean boundary, the oldest sediments on the ocean crust are early late Albian (98 m.y. old; Müller, this vol.; Sigal and Magniez, this vol.). Coupling the dating of the oldest syn-rift and the youngest post-rift sediments at Site 549 and the dating of the oldest sediments above the ocean crust at Site 550, Masson et al. (this vol.) propose to date the transition from rifting to spreading between latest early Albian and middle Albian (98–102 m.y. ago).

On the Pendragon Escarpment, at 2200 m water depth, *Cyana* dive 44 (Figs. 3 and 7) showed that an erosional unconformity exists between the Paleozoic basement and the overlying sedimentary sequence, composed of alternating conglomerates and massive limestones of the Urgonian facies. Similarly, *Cyana* dives 39 to 43, on the flanks of King Arthur's Castle, (Figs. 3 and 7) showed that above the erosional unconformity there exists an alternation of conglomerates, breccias, and massive limestone layers of the Urgonian facies, deposited in the early Albian and more than 1000 m thick. These detritics contain reworked fragments from both the Paleozoic basement and the interbedded Urgonian limestones. This shows that, simultaneously with the building of a carbonate platform during early Albian times, major faults were active on the continental margin. In contrast, on the eastern flank of King Arthur's Castle, Upper Cretaceous chalk (200 m thick) was deposited in a deeper environment.

Along the Meriadzek Escarpment and Shamrock Canyon, located on the Armorican continental margin in the vicinity of DSDP Leg 48 sites, observations from a submersible also suggest an important phase of faulting dated early Albian or just after, also linked to the onset of spreading in the Bay of Biscay (Groupe Cymor, 1981).

### Interpretation in Terms of Rifting Processes

During the rifting phase, in which tilted fault-blocks developed and rotated, it seems that the tops of the tilted blocks remained close to sea level, as shown by the observations at Site 549, on the Pendragon Escarpment, and on King Arthur's Castle. This could have resulted from the relative uplift of the oceanward parts of the blocks during rotation along their longitudinal axes, which would have compensated for the regional subsidence due to stretching.

During the early Albian, there was a distinct increase of subsidence, probably because most of the tilting of the deeper blocks had occurred during the beginning of the rifting phase, so the degree of subsidence should be directly linked to the increase of the stretching factor in the upper part of the continental margin.

Finally, in the middle Albian, the post-rift phase began, and the whole margin thermally subsided.

### Eocene Deformations

The relative northward motion of Africa with respect to Eurasia, deduced from the kinematic evolution of the central and North Atlantic oceans, started in the Late Cre-

taceous. The convergence rate was maximum from the Late Cretaceous to the late Eocene (34 m.y.), and then decreased slightly (e.g., Olivet et al., in press; Savostin et al., in press). The consequence on the Iberian Plate was a northwestward motion with respect to Europe, around a pole located southwest of Iberia. The Pyrenees and the North Spanish marginal trough resulted from this compressional phase. The plate motion lasted from the Late Cretaceous to the late Eocene, with maximum activity during the Eocene.

Linked to the relative convergent motion of Iberia and Eurasia, intraplate tectonics developed on both the Iberian Plate (e.g., Groupe Galice, 1979) and the Eurasian Plate (e.g., Montadert, de Charpal, et al., 1979; Masson and Parson, 1983). On land, numerous studies show that the deformation occurred in France, Great Britain, and Germany, and was created by compression along a 10–20°N direction (de Charpal et al., 1974; Bergerat and Geyssant, 1980; Letouzey and Trémolières, 1980). Following the orientations of pre-existing structures, this compression phase created strike-slip faults, reverse faults, folds, and uplifts.

On the north Biscay margin, the faulting caused the uplift and creation of the Trevelyan Escarpment; but this tectonized E–W-trending belt disappears toward the northwest. There it merges into a single strike-slip fault system, oriented NW–SE, which can be followed as far as the southern edge of Goban Spur (Montadert, de Charpal, et al., 1979). Other effects of the late Eocene deformation include elongated folds oriented broadly E–W on the Meriadzek and Trevelyan escarpments, rejuvenated rift-faults, reverse faults, and even some thrusts along pre-existing E–W discontinuities in the basement. When the basement discontinuities are oriented roughly NW–SE, as on the Armorican margin and the Gascony ridge, the N–S Eocene compression is marked essentially by faults with a strike-slip component (Montadert, de Charpal, et al., 1979).

On the Goban Spur continental margin, all the Norestlante seismic profiles (Fig. 3) show evidence of this late Eocene tectonic phase. As an example, the two seismic profiles of Figures 6 and 8, which include DSDP Sites 548 and 550, show a slight but very clear unconformity at the limit between acoustic Units 1 and 2. This seismic unconformity, characterized by onlapping reflectors in the overlying sediments, is a consequence of a tectonic deformation. It can be traced over the whole area.

Using velocities measured on samples from Sites 548 and 550 (site chapters, Sites 548 and 550, this vol.), identification of the main stratigraphic gaps leads us to a correlation between the acoustic stratigraphy and the lithostratigraphy slightly different from the one proposed in the site chapters. The discontinuity between acoustic Units 1 and 2 is correlated with the lower Oligocene–upper Oligocene hiatus identified at 348 m sub-bottom at Site 548, and with the lower Eocene–upper Oligocene hiatus identified at 312 m sub-bottom at Site 550.

The Pastouret Ridge is the most striking Eocene structural feature of the Goban Spur area. Illustrated by the three seismic profiles of Figures 4 and 5, the deformation there affects both the ocean crust and the overlying sediments. On the migrated section of Figure 5 (between shot-points 3100 and 3400, in the western part of the Pastouret Ridge (Fig. 3), the deformed sediments correspond to a faulted monocline and consequently to a motion with a compressional component. Faint evidence of fracturing within the ocean crust is provided by the presence of features dipping on the outside of the Pastouret Ridge near shot-point 3200. In the central part of the Pastouret Ridge, where its topographic relief is about 300 m, the deformation always seems to occur along a fault oriented N70° and situated on the southern flank of the ridge. The direct correlation of the seismic units with the Site 550 lithostratigraphy allows us to establish that the end of the deformation occurred at the boundary of acoustic Units 1 and 2 and belongs to the Eocene deformation pattern. Since the orientation of the ridge coincides with the directions of the oceanic flow-lines, we conclude that the Pastouret Ridge is an Eocene rejuvenated oceanic fracture zone.

Another example of Eocene deformation is shown in Figure 9 (shot-point 1000). Reverse faulting affects both the ocean crust and the sediment layers older than Oligocene. During the Norestlante II cruise (*Le Suroit*, March 1984), we have demonstrated that this Eocene feature is oriented N70°, as is the Pastouret Ridge.

The Eocene deformation observed in the Porcupine Abyssal Plain affected preferentially the previous oceanic fracture zones. Consequently, under a slight intraplate compressional component, the old ocean crust of the Porcupine Abyssal Plain has been fractured along preexisting fracture zones. This example could represent the early stage of overthrusting within the ocean crust.

Another very important point is that the features within the ocean crust can be followed down to 8.5 s (two-way traveltime), which is 1.5 to 2.0 s (two-way traveltime) below the top of the ocean crust, with a dipping angle about 25 to 35° and a spacing between faults about 10 to 15 km (Fig. 9). If the velocity within the ocean crust is about 6 km/s, these features affect 4.5 to 6 km of ocean crust, which corresponds roughly to the 5 km expected thickness of a 100-m.y.-old normal ocean crust. The Moho discontinuity is not visible on the profile, but it seems that the faulting affects the whole thickness of the ocean crust. Because the seismic line is oriented very near to the strike direction of the ocean crust, Masson et al. (this vol.) interpret these features as oblique crossings of normal faults of the type formed at mid-ocean ridges. We have established that parts of these features were reactivated during the Eocene compression and belong to the fracture-zone pattern.

On the northern Bay of Biscay and Goban Spur continental margins and in the adjacent oceanic domain of the Bay of Biscay and Porcupine Abyssal Plain, the Eocene intraplate deformation affects both the crust and the overlying sediments. Typical compressive structures (folds and reverse faults) seem to be more frequent along E–W trends (e.g., Cantabria, Trevelyan, Porcupine Abyssal Plain), and strike-slip faulting (with a compressive component) more frequently trends NW–SE or NE–SW (e.g., Gascony Ridge, NW–SE trend along the Armorican margin, southern part of Porcupine Sea Bight, Pas-

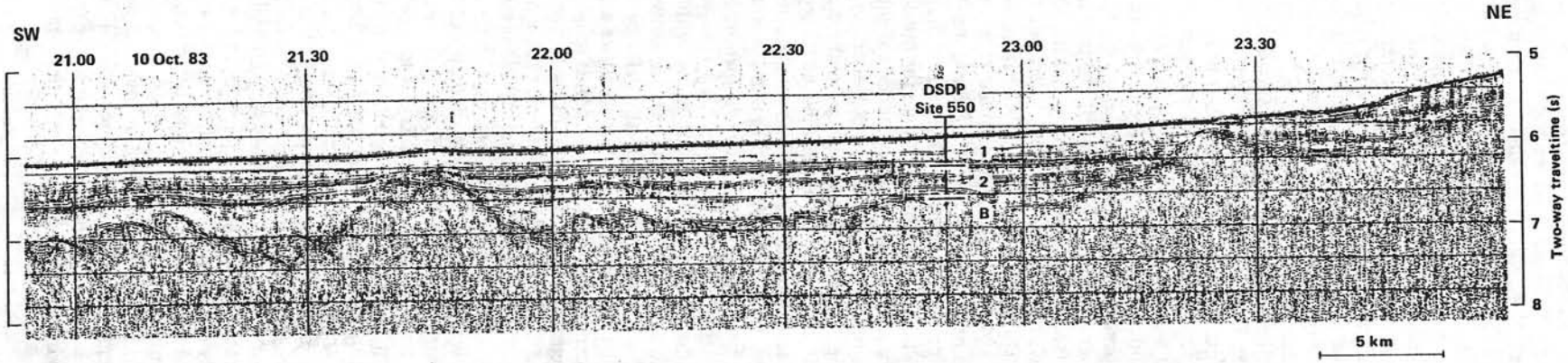


Figure 8. CNEXO high-speed single-channel seismic profile shown as profile a in Figure 3. Drilling at Site 550 penetrated the oceanic basement. The main acoustic units are: Unit 1, upper Oligocene to Present; Unit 2, upper Albian to lower Eocene; B, oceanic basement.

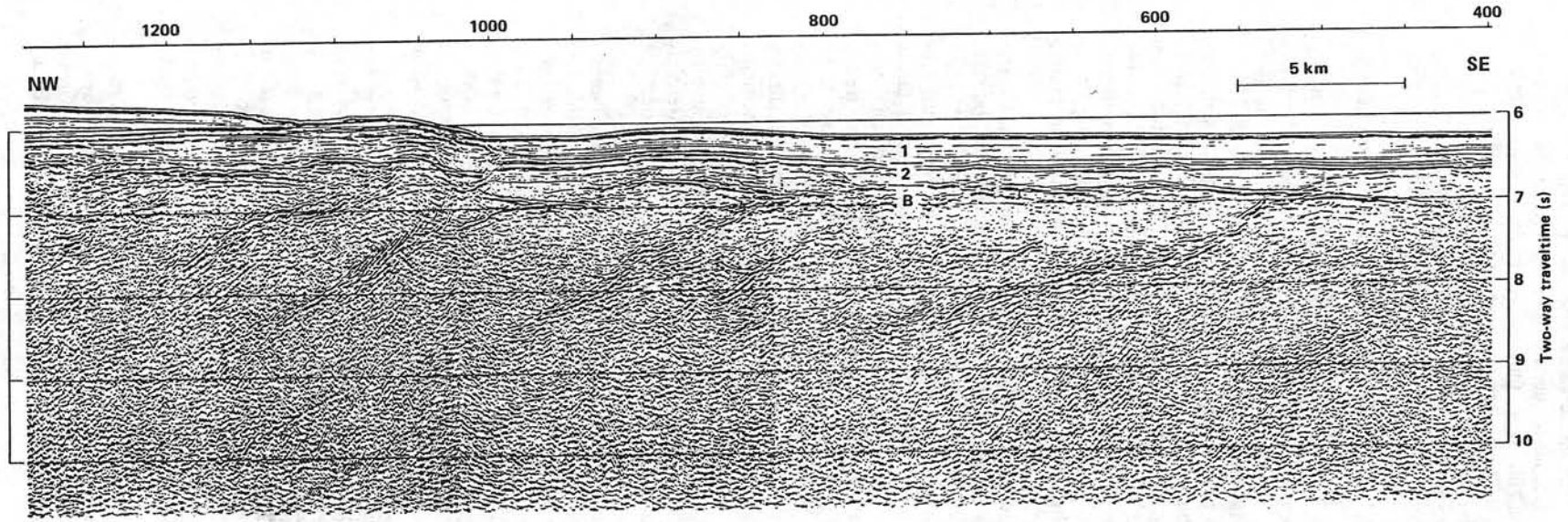


Figure 9. IOS multichannel seismic profile CM 05, migrated by IFP and located in the Porcupine Abyssal Plain as profile f in Figure 1. The main acoustic units are: Unit 1, upper Oligocene to Present; Unit 2, upper Albian to lower Eocene; B, oceanic basement.

touret Ridge). These observations are compatible with a submeridian compression, as proposed on the basis of land data (Letouzey and Trémolières, 1980).

## CONCLUSIONS

1. A new bathymetric map based on Seabeam, conventional, and GLORIA data has been established, and a structural map has been proposed based on Seabeam data and seismic profiles oriented perpendicular to the continental margin. This structural map reveals Caledonian and Variscan trends.

2. Trends in a N70° direction, corresponding to Caledonian trends, have been identified both on the thinned continental crust (Goban Fault, Jean Charcot Escarpment) and on the oceanic domain (Pastouret Ridge).

3. The continental margin and the adjacent oceanic domain resulted from continuous tensional movement along the N70° Caledonian direction from the Early Cretaceous to the Campanian.

4. Subsidence of the tops of tilted blocks in the upper part of the continental margin seems to have occurred preferentially at the end of the rifting episode during the early Albian.

5. Eocene intraplate deformation affected the whole Goban Spur continental margin.

6. Under a slight intraplate compression, the old ocean crust of the Porcupine Abyssal Plain was fractured again over its entire thickness along previous fracture zones, which are considered as zones of weakness. In particular, the Pastouret Ridge corresponds to a reactivated fracture zone.

## ACKNOWLEDGMENTS

This chapter is dedicated to Léo Pastouret, who died September 14, 1983 after a short illness. Léo was particularly involved in the geology of the Celtic and Goban Spur continental margins, and had initiated a large program on the evolution of these margins, using seismic profiling, Seabeam morphology, dredging, and diving. He conducted several cruises, the last one being the Cymor II cruise (summer 1982), during which the *Cyana* submersible was operated on the southern part of the Goban Spur continental margin. Preliminary results of the Cymor II cruise have been incorporated in this chapter.

The authors are especially indebted to the crews of the *Jean Charcot* and *Le Suroit*, and for financial support from the Centre National pour l'Exploitation des Océans. Jean-Pierre Mazé made the illustrations. René Blanchet, Guy Pautot, and Wylie Poag critically reviewed the manuscript and offered helpful suggestions. This is contribution 861 of the Centre Océanologique de Bretagne.

## REFERENCES

Arthaud, F., and Matte, P., 1977. Late Paleozoic strike slip faulting in southern Europe and northern Africa: result of a right lateral shear zone between the Appalachians and the Urals. *Geol. Soc. Am. Bull.*, 88:1305–1320.

Auffret, G. A., Pastouret, L., Cassat, G., de Charpal, O., Cravatte, J., et al., 1979. Dredged rocks from the Armorican and Celtic margins. *In* Montadert, L., Roberts, D. G., et al., *Init. Repts. DSDP*, 48: Washington (U.S. Govt. Printing Office), 995–1014.

Bergerat, F., and Geyssant, J., 1980. La fracturation tertiaire de l'Europe du Nord; résultat de la collision Afrique–Europe. *C. R. Seances Acad. Sci.*, 290:1521–1524.

Berthois, L. (Ed.), 1966. *Bathymetric Maps of the Continental Slope and Shelf*: Paris (Centre Nat. Rech. Scientif.).

de Charpal, O., Trémolières, P., Jean, F., and Masse, P., 1974. Un exemple de tectonique de plate-forme. Les Causses majeures. *Rev. Inst. Fr. Pet.*, 29:715–732.

de Graciansky, P. C., Poag, C. W., Cunningham, R., Loubere, P., Masson, D. G., et al., in press. The Goban Spur transect. Geologic evolution of a sediment-starved passive continental margin. *Geol. Soc. Am. Bull.*

Dingle, R. V., and Scrutton, R. A., 1979. Sedimentary succession and tectonic history of a marginal plateau (Goban Spur, southwest of Ireland). *Mar. Geol.*, 33:45–69.

Gardiner, P. R. R., and Sheridan, D. J. R., 1981. Tectonic framework of the Celtic Sea and adjacent areas with special reference to the location of the Variscan front. *J. Structural Geol.*, 3:317–331.

Groupe Cymor (Pastouret, L., Auffret, G. A., Auzende, J.-M., Beuzart, P., Dubois, P., et al.), 1981. La marge continentale armoricaine, résultats d'observation en submersible et de dragages dans le canyon Shamrock. *C. R. Seances Acad. Sci.*, 292:741–748.

Groupe Galice (Auzende, J.-M., Jonquet H., Olivet, J.-L., Sibuet, J.-C., Auxiétre, J.-L., et al.), 1979. The continental margin of Galicia and Portugal: acoustical stratigraphy, dredge stratigraphy and structural evolution. *In* Sibuet, J.-C., Ryan, W. B. F., et al., *Init. Repts. DSDP*, 47, Pt. 2: Washington (U.S. Govt. Printing Office), 633–662.

Hunter, P. M., and Kenyon, N. H., in press. *Bathymetry of Porcupine Seabight and Porcupine Bank*. Institute of Oceanographic Sciences, Wormley, England.

Kent, P. E., 1978. Mesozoic vertical movements in Britain and the surrounding continental shelf. *In* Bowes, D. R., and Leake, B. E. (Eds.), *Crustal Evolution in North-western Britain and Adjacent Regions*. Geol. J. Spec. Issue, 10:309–324.

Laughton, A. S., Roberts, D. G., and Graves, R., 1975. Bathymetry of the northeast Atlantic: Mid-Atlantic Ridge to southwest Europe. *Deep Sea Res.*, 22:791–810.

Leggett, J. L., McKerrow, W. S., and Soper, N. J., 1983. A model for the crustal evolution of southern Scotland. *Tectonics*, 2:187–210.

Le Pichon, X., Sibuet J.-C., and Francheteau, J., 1977. The fit of continents around the North Atlantic Ocean. *Tectonophysics*, 38: 169–209.

Letouzey, J., and Trémolières, D., 1980. Paleostress field around the Mediterranean since the Mesozoic from microtectonics: comparisons with plate tectonic data. *Proc. 26th Int. Geol. Congr.*, Mem. Bur. Rech. Geol. Min., 115:261–273.

Masson, D. G., and Parson, L. M., 1983. Eocene deformation on the continental margin SW of the British Isles. *J. Geol. Soc. London*, 140:913–920.

Max, M. D., Ryan, P. D., and Inamdar, D. D., 1983. A magnetic deep structural geology interpretation of Ireland. *Tectonics*, 2:431–452.

Montadert, L., Roberts, D. G., de Charpal, O., and Guennoc, P., 1979. Rifting and subsidence of the northern continental margin of the Bay of Biscay. *In* Montadert, L., Roberts, D. G., et al., *Init. Repts. DSDP*, 48: Washington (U.S. Govt. Printing Office), 1025–1060.

Montadert, L., de Charpal, O., Roberts, D., Guennoc, P., and Sibuet, J.-C., 1979. Northeast Atlantic passive continental margins; rifting and subsidence processes. *In* Talwani, M., Hay, W., and Ryan, W. B. F. (Eds.), *Deep Drilling Results in the Atlantic Ocean: Continental Margins and Paleoenvironment*: Washington (Am. Geophys. Union), Maurice Ewing Series, 3:154–186.

Montadert, L., Roberts, D. G., et al., 1979. Site 401. *In* Montadert, L., Roberts, D. G., et al., *Init. Repts. DSDP*, 48: Washington (U.S. Govt. Printing Office), 73–124.

Odin, G. S., 1982. *Numerical Dating in Stratigraphy*: Chichester, England (Wiley).

Olivet, J.-L., Bonnin, J., Beuzart, P., and Auzende, J.-M., in press. *Cinématique de l'Atlantique Nord et Central.* Publications du Centre National pour l'Exploitation des Océans, Paris.

Olivet, J.-L., Le Pichon, X., Monti, S., and Sichler, B., 1974. Charlie-Gibbs fracture zone. *J. Geophys. Res.*, 79:2059–2072.

Pastouret, L., Beuzart, P., and Monti, S., 1982. Présentation de cartes bathymétriques de la marge continentale armoricaine et celte, golfe de Gascogne. *Bull. Soc. Geol. France*, 24:407–411.

Pautot, G., Renard, V., Auffret, G. A., Pastouret, L., and de Charpal, O., 1976. A granite cliff deep in the North Atlantic. *Nature*, 263: 669–672.

Pegrum, R. M., and Mounteney, N., 1978. Rift basins flanking North Atlantic Ocean and their relation to North Sea area. *Am. Assoc. Petrol. Geol. Bull.*, 62:419–441.

Renard, V., and Allenou, J.-P., 1979. Le Sea-Beam, sondeur à multifaisceaux du N/O Jean Charcot. Description, évaluation et premiers résultats. *Rev. Hydrogr. Int.* (Monaco), 56:35–71.

Russell, M. J., and Smythe, D. K., 1983. Origin of the Oslo graben in relation to the Hercynian–Alleghenian orogeny and lithospheric rifting in the North Atlantic. *Tectonophysics*, 94:457–472.

Savostin, L. A., Sibuet, J.-C., Zonenshain, L. P., and LePichon, X., in press. Kinematic evolution of Tethys. *Tectonophysics*.

Sibuet, J.-C., 1972. Contribution de la gravimétrie à l'étude de la Bretagne et du plateau continental adjacent. *Compt. Rend. Soc. Geol. France*, 3:124–128.

_____, 1973. South Armorican shear zone and continental fit before the opening of the Bay of Biscay. *Earth. Planet. Sci. Lett.*, 18: 153–157.

Sibuet, J. C., and Mascle, J., 1978. Plate kinematic implications of Atlantic equatorial fracture zone trends. *J. Geophys. Res.*, 44: 601–624.

Somers, M. L., Carson, R. M., Revie, J. A., Edge, R. H., Barrow, B. J., et al., 1978. GLORIA II: an improved long-range sidescan sonar. *Oceanology International*: London (B. P. S., Exhibitions, Ltd.), pp. 16–24.

Vail, P. R., Mitchum, R. M., and Thompson, S., III. 1977. Seismic stratigraphy and global changes of sea level, part 3: relative changes of sea level coastal onlaps. Mem. Am. Assoc. Petrol. Geol., 26: 63–81.

Van Eysinga, F. W. B., 1975. *Geological Time Table* (3rd ed.): Amsterdam (Elsevier).

Ziegler, P. A., 1978. Northwestern Europe: tectonics and basin development. *Geol. Mijnbouw*, 57:589–626.

_____, 1981. Evolution of sedimentary basins in north-west Europe. *In* Illing, L. V., and Hobson, G. D. (Eds.), *Petroleum Geology of the Continental Shelf of North-West Europe*: London (Institute of Petroleum), pp. 9–36.

**Date of Initial Receipt: February 15, 1984**
**Date of Acceptance: April 5, 1984**

GÉOPHYSIQUE. — La ride Pastouret (plaine abyssale de Porcupine) : une structure éocène [1].

Note de **Jean-Claude Sibuet, Benoit Mathis** et **Peter Hunter,** présentée par Xavier Le Pichon.

Reçue le 10 septembre 1984.

Une carte bathymétrique détaillée de la marge continentale de l'Éperon de Goban (S.W. Irlande) a été établie à partir des données Sea-Beam. Une nouvelle structure bathymétrique d'une soixantaine de kilomètres de longueur et de 300 m de hauteur a été découverte en bas de pente continentale. Elle a été baptisée ride Pastouret. Cette structure a été formée lors de la phase de compression pyrénéenne par déformation intraplaque le long d'une ancienne zone de fracture océanique.

*GEOPHYSICS.* — The Pastouret Ridge (Porcupine Abyssal Plain): an Eocene Structure.

*A new bathymetric map, mainly based on Sea-Beam data has been established for the Goban Spur continental margin (S.W. Ireland). Eocene intraplate deformation has affected the whole area but is particularly evident at the Pastouret ridge, a new bathymetric feature which is a reactivated oceanic fracture zone.*

Au cours de la campagne Norestlante I (octobre 1983) du N.O. *Jean-Charcot*, 2 300 km de profils Sea-Beam et de sismique réflexion ont été réalisés sur la marge continentale de l'Éperon de Goban (S. W. Irlande). Les profils étaient implantés perpendiculairement à la marge avec un espacement de l'ordre de 8 miles, de façon à éviter toute ambiguïté sur la validité des corrélations morphologiques de profil à profil.

La carte bathymétrique (*fig.*) a été élaborée en utilisant simultanément les données obtenues à l'aide des sondeurs conventionnels, du sondeur multifaisceaux « Sea-Beam » du N.O. *Jean-Charcot* et du sonar latéral « Gloria ». Le Sea-Beam est un sondeur comportant 16 faisceaux étroits juxtaposés permettant de couvrir en continu une bande bathymétrique dont la largeur est égale aux deux tiers de la profondeur d'eau [2]. Le « Gloria Mark II » de l'Institute of Oceanographic Sciences est un sonar latéral dont la portée latérale maximale est de 30 km de part et d'autre de la route du navire [3].

Les cartes bathymétriques Sea-Beam de détail établies par Pastouret et coll. [4] pour l'Éperon d'Austell, le château du Roi Arthur et l'escarpement de Pendragon ont été incorporées dans la compilation des données Sea-Beam. Pour compléter l'information, les données bathymétriques conventionnelles ([5], [6]) ont été utilisées. Au Nord de 42°20′N la carte bathymétrique de Hunter et Kenyon [7] a également été incorporée. Finalement dans la zone de l'Eperon d'Austell et du château du Roi Arthur, les données Gloria ont permis de contraindre les directions morphologiques.

La marge continentale de l'Éperon de Goban est limitée au Sud-Est par l'escarpement Jean-Charcot et au Nord-Ouest par la baie de Porcupine (*fig.* ). La faille de Goban, située dans la partie septentrionale de cette marge, et l'escarpement Jean-Charcot sont des accidents orientés N 70° qui correspondent aux directions calédoniennes et/ou tardi-hercyniennes mises en évidence à terre et sur le plateau continental adjacent [8]. L'escarpement de Pendragon et celui situé au niveau du site D.S.D.P. 551, orientés N 150°, sont des plans de failles limitant les deux derniers blocs basculés du domaine continental aminci en bordure du domaine océanique ([8], [9]). Ces escarpements, individualisés au Crétacé inférieur lors de la phase de structuration de la marge, pourraient également correspondre au rejeu d'accidents conjugués calédoniens et/ou tardi-hercyniens [8]. Comme la direction initiale d'ouverture du domaine océanique adjacent (plaine abyssale de Porcupine) est N 70° [10], il est probable que la formation de la marge continentale

0249-6305/84/02991391 $2.00 

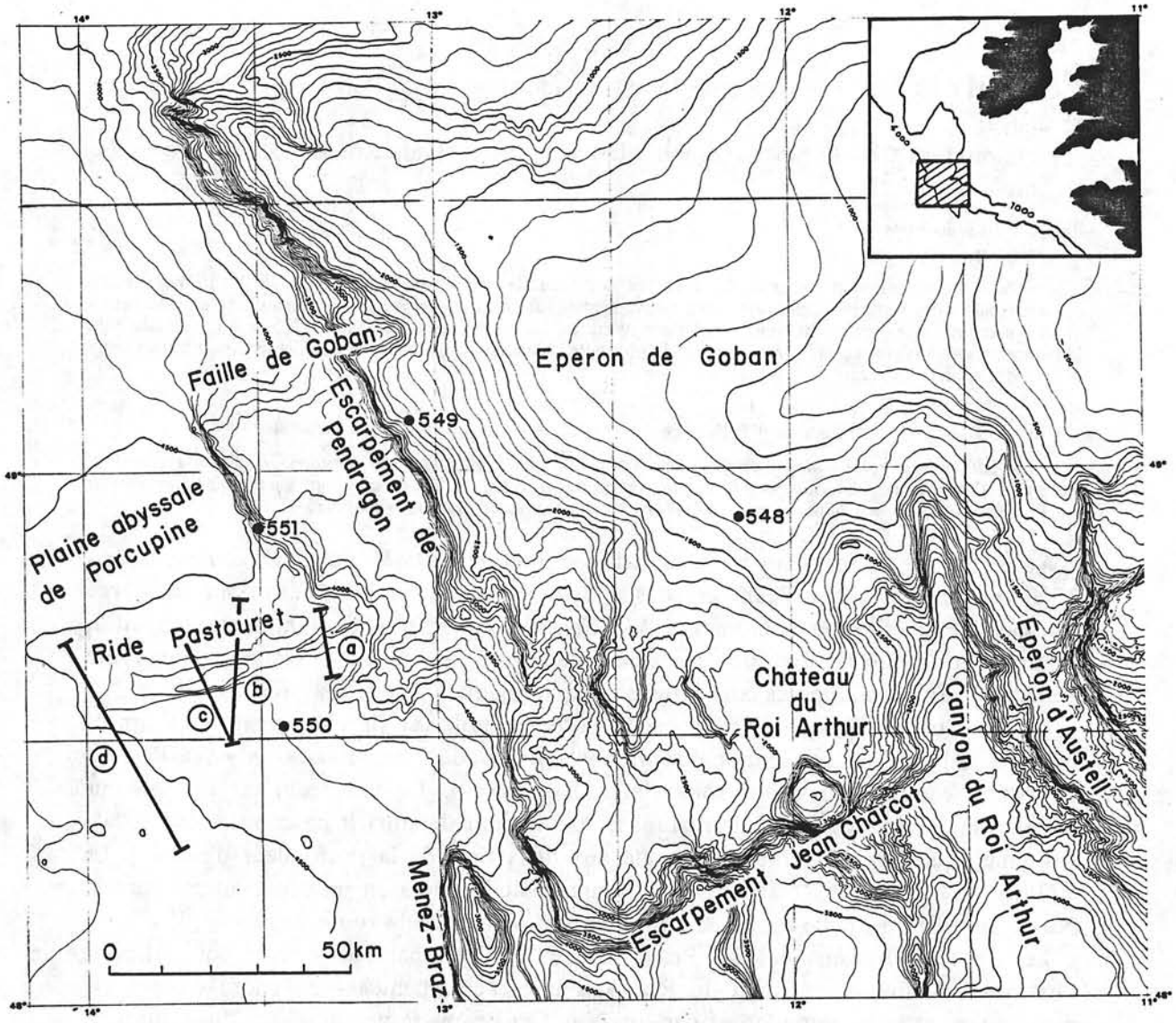


Carte bathymétrique en projection Mercator de la marge continentale de l'Éperon de Goban établie à partir des données Sea-Beam (Campagne Norestlante I et 4], conventionnelles 5, 6, 7) et Gloria. Les profondeurs sont en mètres non corrigés (1 500 m/s). L'espacement des isobathes est de 100 m. Les sites de forages du Leg D.S.D.P. 80 sont localisés. Les quatre profils sismiques (*planches* I et II) recoupant la ride Pastouret sont positionnés.

*The bathymetric map of the Goban Spur continental margin has been established using conventional* (5, 6, 7), *Sea-Beam* (*Norestlante I cruise and* 4) *and Gloria data. Mercator projection. Depths in uncorrected metres* (1,500 *m/s*). *Isobath spacing:* 100 *m. Locations of Leg* 80 *D.S.D.P. sites and of the four seismic profiles* (plates *I and II*) *are shown.*

## Explications des Planches

### *Planche I*

Profils sismiques CNEXO monotrace haute vitesse (10 nœuds) obtenus à travers la ride Pastouret. Exagération verticale : 4. Localisation des profils *a* (Norestlante II, mars 1984) et *b* (Norestlante I, octobre 1983) sur la figure. Les principales unités acoustiques sont identifiées par corrélations avec les données lithostratigraphiques du site 550 (12) : unité 1, Oligocène supérieur à actuel; Unité 2 : Albien supérieur à Éocène inférieur; B, croûte océanique.

*CNEXO high speed single channel seismic profiles* (10 *knots*) *obtained across the Pastouret Ridge. Vertical exaggeration:* 4. *Locations of seismic profiles a* (*Norestlante II cruise, March* 1984) *and b* (*Norestlante I cruise, October* 1983) *are shown in the figure. The main acoustic units are identified by correlation with D.S.D.P. site* 550 *lithostratigraphic units* (12) *: Unit* 1, *Upper Oligocene to Recent; Unit* 2, *Upper Albian to Lower Eocene; B, oceanic crust.*

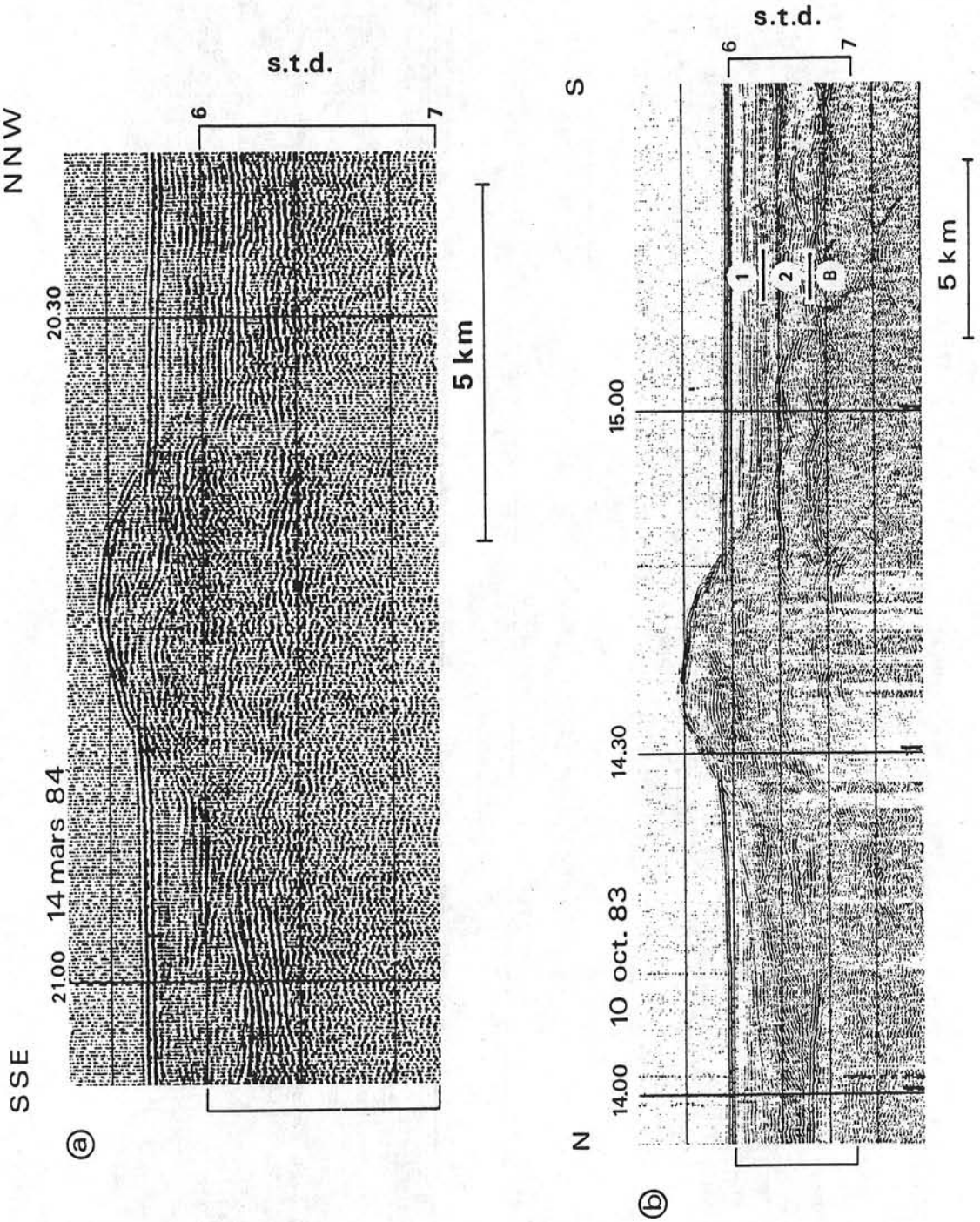
NNW
SSE
20.30
14 mars 84
21.00
s.t.d.
6
7
5 km
ⓐ
S
N
15.00
14.30
10 oct. 83
14.00
s.t.d.
6
7
1
2
B
5 km
ⓑ

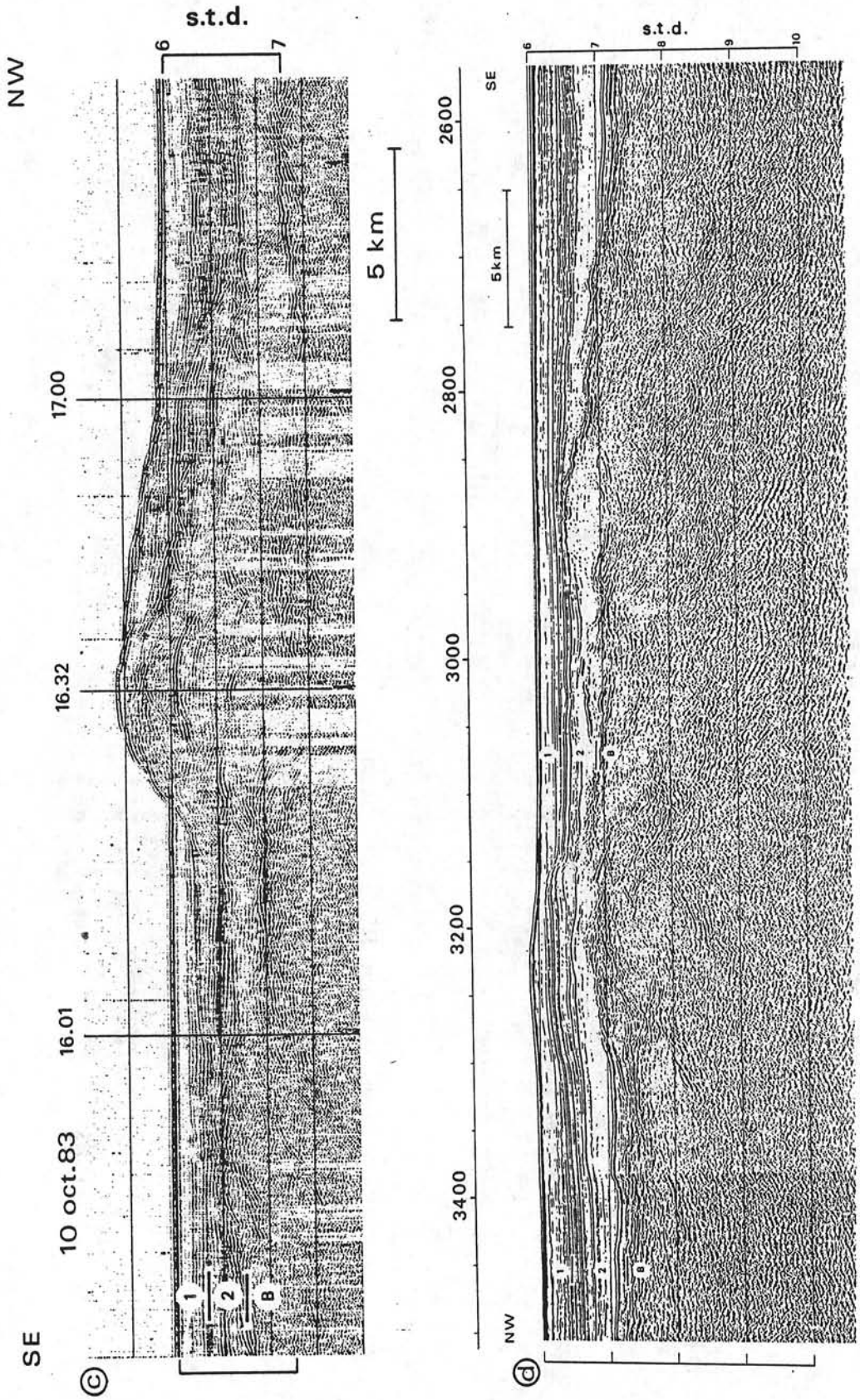
NW
s.t.d.
6
7
17.00
16.32
16.01
10 oct.83
SE
5 km
1
2
B
c
2600
2800
3000
3200
3400
SE
s.t.d.
6
7
8
9
10
5km
1
2
B
NW
d

*Planche II*

Profils sismiques obtenus à travers la ride Pastouret et localisés sur la figure. Exagération verticale :4. *c*, profil sismique CNEXO monotrace haute vitesse (10 nœuds); *d*, profil multitrace IOS CMO 5 migré par l'I.F.P. Les principales unités acoustiques sont identifiées par corrélations avec les données lithostratigraphiques du site 550 (12) : unité 1, Oligocène supérieur à actuel; Unité 2 : Albien supérieur à Eocène inférieur; B. croûte océanique.

*Seismic profiles obtained across the Pastouret Ridge and located in the figure. Vertical exaggeration:* 4. *c, CNEXO high speed single channel seismic profile* (10 *knots); d, multichannel seismic profile CMO 5 obtained by IOS and processed by I.F.P.* (8). *The main acoustic units are identified by correlation with D.S.D.P. site* 550 *lithostratigraphic units* (12)*: Unit* 1, *Upper Oligocene to Recent; Unit* 2, *Upper Albian to Lower Eocene; B, oceanic crust.*

de l'Éperon de Goban puis du domaine océanique adjacent du Crétacé inférieur au Campanien résulte d'une extension suivant la même direction N 70°. Dans cette hypothèse, le mouvement initial des plaques Amérique et Europe aurait donc été guidé par les directions calédoniennes et/ou tardi-hercyniennes [8].

A 4 500 m de profondeur, dans la plaine abyssale de Porcupine, une nouvelle structure bathymétrique orientée N 70°, d'une soixantaine de kilomètres de longueur et de 300 m de hauteur a été découverte au cours de la campagne Norestlante I (*fig.*). Cette structure a été baptisée « ride Pastouret » en hommage à Léo Pastouret [11] qui était particulièrement impliqué dans les études de stratigraphie et d'évolution verticale des marges celtique et de l'Éperon de Goban.

Les profils sismiques recoupant la ride Pastouret, montrent qu'elle a été mise en place à la fin du dépôt de l'unité acoustique 2 (*planches* 1 et 2). Par corrélation avec les données lithostratigraphiques du site D.S.D.P. 550 proche [12], la mise en place de cette ride est datée Eocène supérieur. La ride Pastouret serait donc une manifestation intraplaque de la phase pyrénéenne. De plus, la faille délimitant le flanc sud de la ride Pastouret est orientée suivant une direction N 70° correspondant à la direction d'ouverture initiale de l'Atlantique Nord au niveau de la plaine abyssale de Porcupine [10]. La ride Pastouret est donc une ancienne zone de fracture océanique remobilisée à l'Éocène. A une centaine de kilomètres au Sud de la ride Pastouret, une faille inverse orientée N 70° décale à la fois la croûte océanique et les couches sédimentaires ante-Oligocène [8]. Cette observation suggère qu'une composante compressive a affecté de façon privilégiée d'anciennes zones de fractures océaniques de la plaine abyssale de Porcupine, donnant ainsi naissance à des structures topographiques comme la ride Pastouret.

RÉFÉRENCES BIBLIOGRAPHIQUES

[1] Contribution n° 864 du Centre Océanologique de Bretagne (Département de Géologie, Géophysique et Géochimie marines).

[2] V. RENARD et J.-P. ALLENOU, *Rev. Hydrographique internationale*, Monaco, 56, 1979, p. 35-71.

[3] M. L. SOMERS, R. M. CARSON, J. A. REVIE, R. H. EDGE, B. J. BARROW et A. G. ANDREWS, In : *Oceanology International*, 78, Technical Session J, London, B.P.S. exhibitions Ltd., 1978, p. 16-24.

[4] L. PASTOURET, P. BEUZART et S. MONTI, *Bull. Soc. géol. Fr.*, 24, 1982, p. 407-411.

[5] L. BERTHOIS, *Cartes bathymétriques du plateau et de la pente continentale*, 11 feuilles, L. BERTHOIS éd., imprimées par le Centre Nat. Rech. Scientifique, Paris, 1966.

[6] A. S. LAUGHTON, D. G. ROBERTS et R. GRAVES, *Deep-Ses Res.*, 22, 1975, p. 791-810.

[7] P. M. HUNTER et N. H. KENYON, *Bathymetry of Porcupine Seabight and Porcupine Bank*, 3 sheets, Institute of Oceanographic Sciences, Wormley, Angleterre, (sous presse).

[8] J.-C. SIBUET, B. MATHIS, L. PASTOURET, J.-M. AUZENDE, J.-P. FOUCHER, P. HUNTER, P. GUENNOC, P.-C. DE GRACIANSKY, L. MONTADERT et D. MASSON, *Morphology and Basement Structures of the Goban Spur*

*Continental Margin (N.E. Atlantic) and the Role of the Pyrenean Orogeny*, Initial Reports of the Deep Sea Drilling Project, U.S. Government Printing Office, Washington, 80 (sous presse).

[9] D. G. MASSON, L. MONTADERT et R. SCRUTTON, *Regional Geology of the Goban Spur Continental Margin*, Initial Reports of the Deep Sea Drilling Project, U.S. Government Printing Office, Washington, 80 (sous presse).

[10] J.-L. OLIVET, J. BONNIN, P. BEUZART et J.-M. AUZENDE, *Cinématique de l'Atlantique Nord et Central*, Publications du Centre National pour l'Exploitation des Océans, Paris (sous presse).

[11] Décédé le 14 septembre 1983.

[12] P.-C. DE GRACIANSKY, W. POAG et coll., Site chapter 550, Initial Reports of the Deep Sea Drilling Project, U.S. Government Printing Office, Washington, 80 (sous presse).

J.-C. S. : *Centre Océanologique de Bretagne*, B.P. n° 337, 29273 *Brest Cedex;*

B. M. : *G.I.S., Océanologie et Géodynamique, Faculté des Sciences, avenue Le-Gorgeu, Brest;*

P. H. : *Institute of Oceanographic Sciences, Brook Road, Wormley, Surrey, U.K.*

*Journal of the Geological Society, London,* Vol. **143,** 1986, pp. 45–52, 7 figs. Printed in Northern Ireland.

# Deep seismic reflection profiling between England, France and Ireland

BRITISH INSTITUTIONS REFLECTION PROFILING SYNDICATE (BIRPS)[1,3] & ETUDE DE LA CROÛTE CONTINENTALE ET OCÉANIQUE PAR RÉFLEXION ET RÉFRACTION SISMIQUE (ECORS)[2,4]

**Abstract:** The South West Approaches Traverse comprises 1600 km of profiling to 15 seconds two-way time . The profiles were planned to investigate Variscan structures in the crust and upper mantle. In Ireland, SW England and NW France, Variscan deformation and granite intrusion extend from Middle Devonian to Early Permian time, about 370 to 270 Ma ago. We have imaged a normal fault dipping gently south under the Celtic Sea that corresponds at surface, in position and trend, with the Variscan 'front' and can be traced down to at least 20 km depth. As under Caledonian Britain to the north, the lower crust is everywhere strongly reflective from about 6 seconds two-way time down to the Moho at about 10 seconds. The Haig Fras granite and Cornubian batholith, crossed west of the Isles of Scilly, appear only as unusually shallow portions of the lower crustal reflectors.

Data for the South West Approaches Traverse (SWAT) were acquired by Seismic Profilers Ltd in September and November 1983. Their ship towed a wide airgun array with four subarrays totalling 5800 cu. in. fired at 2000 p.s.i. every 50 m. The signal was detected by a hydrophone streamer 3 km long towed at 15 m depth and having 60 sections, giving 30-fold cover. Processing was carried out by Seismograph Services (England) Limited, working closely with BIRPS.

In order to reduce the risk of side echoes through the water or the rocks, the profiles were arranged to be perpendicular to the coastline and to the trend of sedimentary basins known to the oil industry (Naylor & Shannon 1982) (Fig. 1). They cross the Cornubian granite batholith and other Variscan structures (Hutton & Sanderson 1984), as well as WSW-trending monoclines, faults and geophysical anomalies in the English Channel (Smith & Curry 1975). The interpretations presented here are based on unmigrated time-sections (Figs 2 and 4) supplemented by some preliminary 2-D depth migrations of the line drawings. The lines on Figs 2 and 4 were traced through prominent correlations observed on the 1:50,000-scale processed records. The original tracings have been digitized and reduced for publication. The SWAT results add to those already obtained north of Scotland along Moine and Outer Isles deep seismic reflection traverse (MOIST) (Brewer & Smythe 1984) and off NW Britain along WINCH (Brewer *et al.* 1983).

We assume that the reflections we observe from crystalline rocks originate from areally extensive contrasts in their physical properties. It follows that reflections from ancient structures will have been overprinted by the effects of more recent tectonic events. The most recent event that we recognize is Tertiary compression, responsible for the inversion of some Mesozoic sedimentary basins, for example, the folding of the North Celtic Sea Basin (profile 4, Figs 2 and 3) and the monoclines in the Eastern Channel Basin (profile 11, Fig. 4), one of which is exposed on the Isle of Wight. But the dominant event is the post-Carboniferous subsidence responsible for the formation of the sedimentary basins (Ziegler 1982). We believe that its effects overprint Variscan and Caledonian structures on the reflection profiles.

The two deepest basins are the North Celtic Sea Basin and the Plymouth Bay Basin (Fig. 1) which respectively attain depths of about 9 km (on profile 5, Fig. 2) and about 10 km (on profile 9, Fig. 4), converting to depth using appropriate interval velocities.

SWAT lines 2, 4 and 5 (Fig. 2) cross the North Celtic Sea Basin; a fourth crossing of its eastward extension is provided by the southernmost profile of WINCH. The sediments infilling the basin are Triassic to late Cretaceous in age (Naylor & Shannon 1982, and British, French, and Irish published offshore geological maps). The four deep profiles show that the basin varies in structure along its length. Profile 5, the westernmost, shows a symmetrical basin without an underlying fault. Interpretation of profile 4 (Fig. 3) shows the basin in the hanging wall of a low angle fault, which has a ramp-and-flat geometry and a mean apparent southerly dip of 17°. This fault can be traced down until it merges with the uppermost reflectors of the lower crust at a depth of about 20 km. Steep listric normal faults interpreted within the basin sediments do not displace the fault plane reflection and could merge with it. This décollement may have acted as a normal fault during the formation of the basin. Inspection of commercial non-exclusive seismic survey lines close to our profile 4, to which we have been given access by Western Geophysical and Merlin Profilers, showed that the strike of the upper ramp of the fault is 100°, which is the local strike of the Variscan front on land. The reflection on profile 4, interpreted here as a low-angle fault,

[1] *Bullard Laboratories, Department of Earth Sciences, University of Cambridge, Madingley Rise, Madingley Road, Cambridge, UK CB3 0EZ.*

[2] *Institut Francais du Pétrole, 1 Avenue de Bois-Préau, 92506 Rueil-Malmaison, Hauts-de-Seine, France.*

[3] M. Cheadle, D. Matthews, S. McGeary, M. Warner, and Associates E. J. Armstrong, D. Blundell, A. Chadwick, G. Day and J. W. F. Edwards.

[4] A. Mascle, O. Gariel, L. Montadert, J. P. Lefort, B. Le Gall, J-C. Sibuet, M. Cazes and I. J. Schroeder.

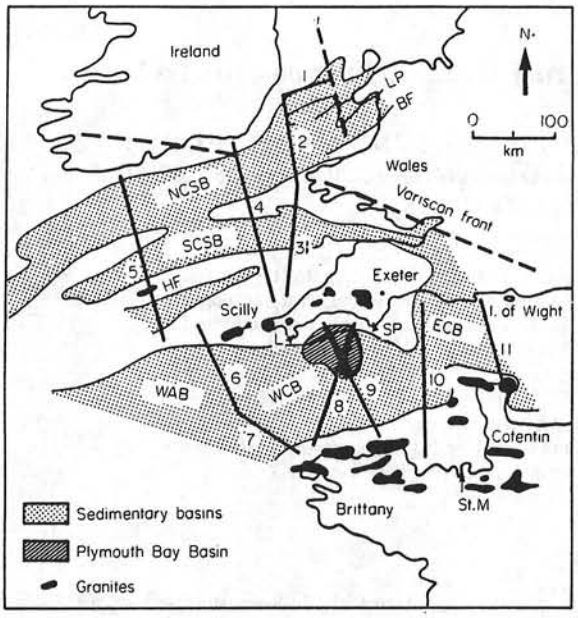


**Fig. 1.** Map showing parts of England, Ireland, Wales and NW France, with SWAT profiles (solid lines), and the southern end of the WINCH profile (broken line). Cornubian (SW England) and Brittany granites are shown in solid black. Shading indicates principal post-Carboniferous sedimentary basins; ECB, Eastern Channel Basin; NCSB, North Celtic Sea Basin; SCSB, South Celtic Sea Basin; WAB, Western Approaches Basin; WCB, Western Channel Basin. Diagonal ruling marks the Plymouth Bay Basin which underlies part of the Western Channel Basin. BF, Bala Fault; HF, Haig Fras; L, Lizard; LP, Lleyn Peninsula; SP, Start Point; St. M., Saint Malo.

does not persist quite up to the seabed, but extrapolation suggests that it would be exposed precisely where profile 4 intersects the traditional Variscan front (Dunning 1977). We therefore suggest that the low-angle fault seen on profile 4 is related to the Variscan front which is generally thought to be a sole thrust on land, but which has been reactivated here as a Mesozoic normal fault, locally controlling both the trend and structure of the North Celtic Sea Basin. Elsewhere the basin has a Caledonian trend. Reactivation of pre-existing Palaeozoic thrusts as low angle normal faults has been proposed to account for basins seen on MOIST (Brewer & Smythe 1984) and on WINCH (Brewer *et al.* 1983). Profile 2 also crosses the traditional position of the Variscan front but here the reflection is much less continuous. This profile supports the suggestion of Barr *et al.* (1981) that the offshore continuation of the Caledonian Bala Fault system controls the southern margin of the North Celtic Sea Basin. Farther to the east, the basin bifurcates around the Lleyn Peninsula of north-west Wales (Naylor & Shannon 1982) and was crossed by WINCH (Fig. 1). Here too we believe its form is controlled by reactivated Caledonian faults (Brewer *et al.* 1983).

It is clear from profile 4 that the normal fault that in its upper part follows the Variscan front, penetrates to a depth of about 20 km near the midpoint of the profile, much as Shackleton *et al.* (1982) sketched it at the north end of their figure 7c. It has a ramp- and flat geometry. Both statements are consistent with results from other profiles (Brewer 1984) that cross the Variscan Front farther east in England, the Strait of Dover, Belgium and Germany, and in the Paris Basin (Bois *et al.* in press), but in Europe there is little or no evidence of reactivation. Comparing profiles 4 and 2 we might conclude that reactivation improves the continuity of reflections from faults. However, unreactivated faults have been seen on reflection profiles in the U.S.A. and elsewhere (Brewer *et al.* 1980).

Other reflections that we relate tentatively to Variscan faulting include one with a southerly dip north of Cornwall, as seen at the south ends of profiles 3 and 4. The northerly dipping events off the Cotentin and Brittany peninsulas, that cut continental crust, might conceivably be of pre-Variscan age (profiles 7–11) (Autran *et al.* 1980).

Industrial drilling shows that the deep Plymouth Bay basin (Fig. 1) contains a thick sequence of Permo-Triassic red beds. Unusually strong reflectors within this sequence seen on profiles 8 and 9 (Fig. 4) are tentatively identified as lavas because 3-D modelling indicates that their presence could account for the isolated magnetic anomaly over the basin. Profiles 8 and 9 (Fig. 4) show that the basin overlies southerly dipping reflection events (F) that Day & Edwards (1983) correlate with the Carrick, Lizard and Start thrusts, of Variscan age, on land in SW England (Leveridge *et al.* 1984). These reflections are not continuous on the SWAT profiles and we are not sure whether they are primary reflections or not. Farther west, on profiles 6 and 7 (Fig. 5), there definitely are continuous southerly dipping reflections, named here the Scilly Isles Fault System, that can be followed into the reflective lower crust to depths of at least 20 km. These reflections have been traced to the continental margin on shallow commercial profiles (Day & Edwards 1983). We see the Plymouth Bay Basin as a deep unfaulted basin. However neither the top of the reflective lower crust nor the Moho is depressed (in time) beneath it. Beneath the Basin we see a strong reflection at c. 6 seconds two-way time (twt) which we cannot explain but, which we suspect may be related to the origin of the basin. This reflection comes in earlier than the usual top of the reflective lower crust.

A seafloor exposure of the Haig Fras granite is crossed on profile 5 (Fig. 6), and profile 6 (Fig. 4) crosses the gravity anomaly of the Cornubian grainte batholith just west of the Scilly Isles. The Cornubian batholith is a major Variscan feature of late Carboniferous age which can be traced from the continental margin by a negative Bouguer anomaly (Lalaut *et al.* 1981; Day & Williams 1970) and surface exposures as far as Dartmoor, a distance of 600 km. Granitic rocks dredged from the foot of the continental slope have yielded radiometric ages similar to those from the Dartmoor granite (Auffret *et al.* 1979). Gravity modelling by Bott suggested that the Dartmoor granite extends down to at least 10 km (Brooks *et al.* 1983), and Edwards (1984) has modelled the shape of the offshore Haig Fras and Scilly Isles granites. We see no reflections that would serve to outline the granites, but under the granites the reflections characteristic of the lower crust come in about 3 seconds earlier than elsewhere, at about 3.5 seconds twt off Scilly, i.e. at a depth of about 10.25 km calculated at 5.85 km/s, the velocity measured by Holder & Bott (1971). Similar observations have been made over granites off the coast of France (Fig. 1) crossed at the south end of profiles 10 and 11, although it is not certain whether these granites are

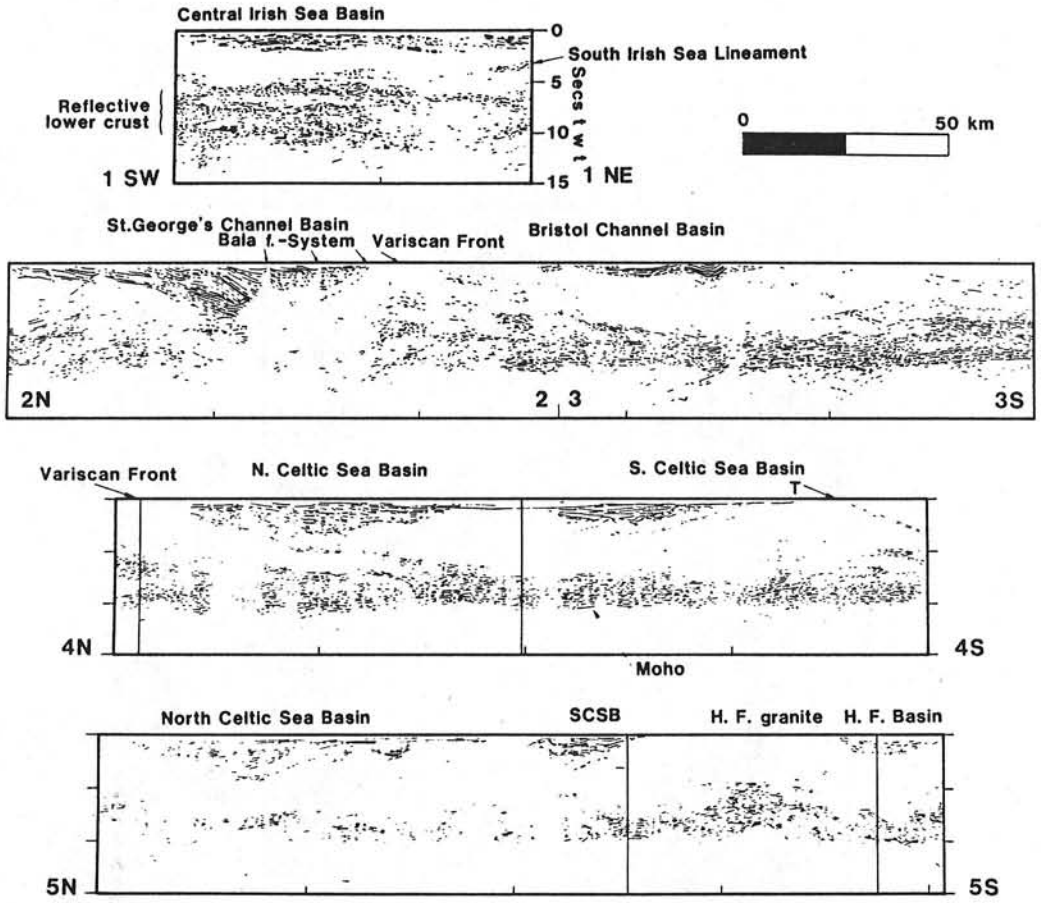


**Fig. 2.** Line drawings of unmigrated time sections of SWAT profiles 1–5. Approximately true scale assuming mean velocity 5 km/s. To convert time to approximate depth in kilometres multiply seconds by 3 (in the crust) or by 4 (in the mantle). The lines are drawn through prominent correlations observed on the records; apart from this the only interpretation is implied by the naming of features. For location of profiles see Fig. 1. HF, Haig Fras; SCSB, South Celtic Sea Basin. Vertical lines across profiles 4 and 5 mark location of photographs of original records shown in Figs 3 and 6 respectively.

Variscan or Cadomian (650–590 Ma) in age (Autran *et al.* 1980). We have not yet devised an experiment to choose between possible explanations of the shallow reflections beneath the granites. Nor have we been able to image the batholith, the Blackstones Gabbro crossed on WINCH, or the sources of gravity and magnetic anomalies crossed in mid-channel. COCORP in the USA have been no more successful in imaging major igneous intrusions (Nelson *et al.*, in press; Cheadle *et al.*, in press).

Reflections from the lower crust dominate the records drawn in Figs 2 and 4. They are absent along a 50 km section off the coast of Wales (profile 2, Fig. 2) but are ubiquitous elsewhere. They are numerous, short (3–10 km), and subhorizontal (Fig. 7). Similar reflections have been seen on BIRPS profiles north of Scotland, across the Caledonides from the Hebrides to Wales, and on the ECORS line across the Paris basin (Bois *et al.*, in press). They have also been reported from Germany (Meissner & Wever, in press), Australia (Mathur 1983), and the USA (Hauser *et al.* 1984) and their origin has been hotly debated in recent meetings (Hall, in press; Barazangi, in press). Evidence is accumulating that the Moho, defined by wide-angle refraction/reflection experiments, coincides with the bottom of the reflective zone (Barton *et al.* 1984; Matthews, in press). The relation between the normal incidence reflections described here and the wide-angle reflections described by Brooks *et al.* (1984) will be discussed elsewhere.

The appearance of the reflective lower crust varies with azimuth: sections in the strike direction have more reflections, perhaps from off-line (see for example profile 1 in Fig. 2) which is sub-parallel to the Caledonian strike and perpendicular to profile 2 (Fig. 1). (Two other examples occur on WINCH: in Brewer *et al.* 1983, Fig. 2 where the southern end of the line crosses SWAT profile 1; and between HG and EF.) The appearance also varies from place to place along the profiles. We do not think that the variation within the SWAT profiles over Variscan crust is less than the variation within the WINCH profiles over Caledonian crust, and we do not find evidence that Variscan

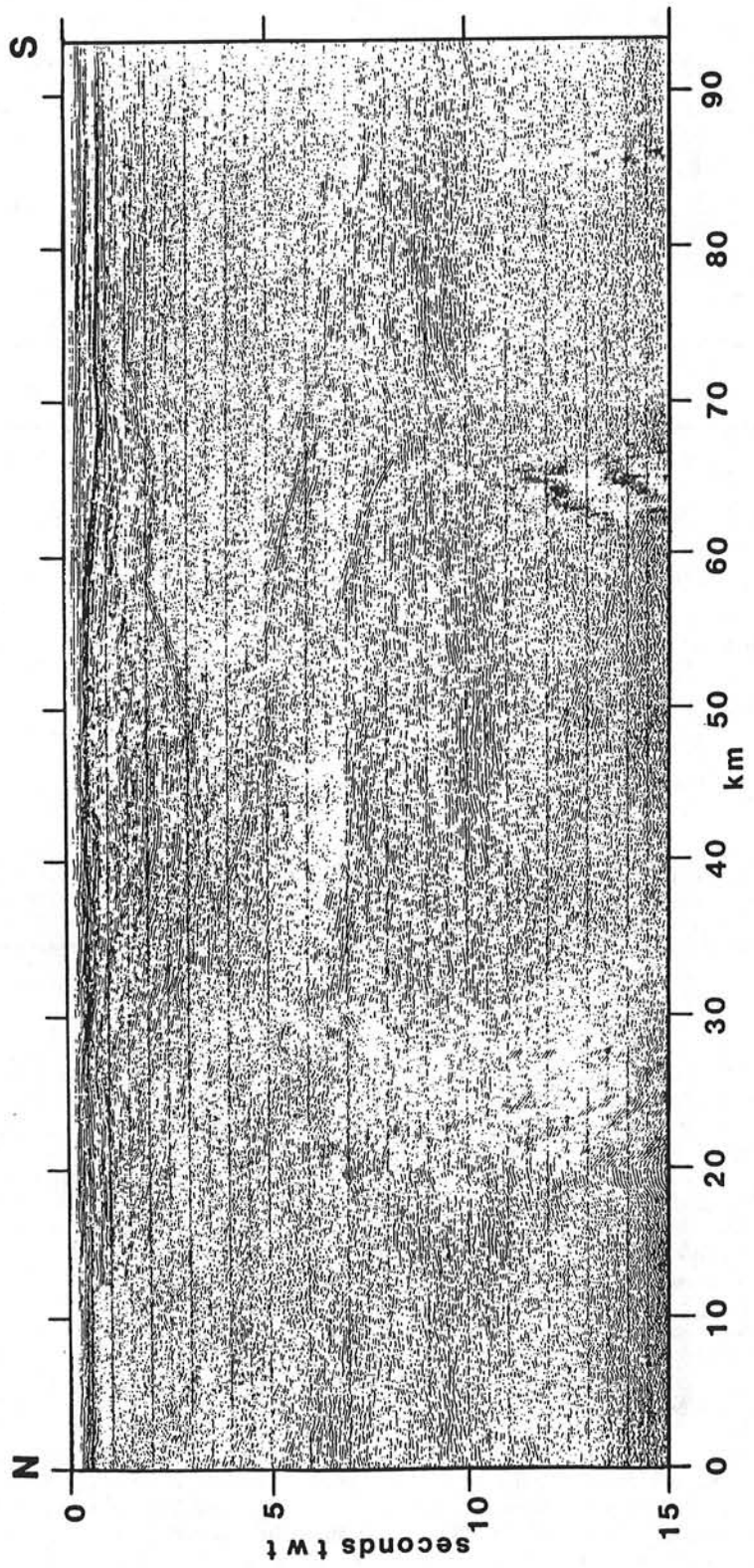


**Fig. 3.** Photograph of seismic record of part of profile 4 showing the Variscan front; for location see Fig. 2.

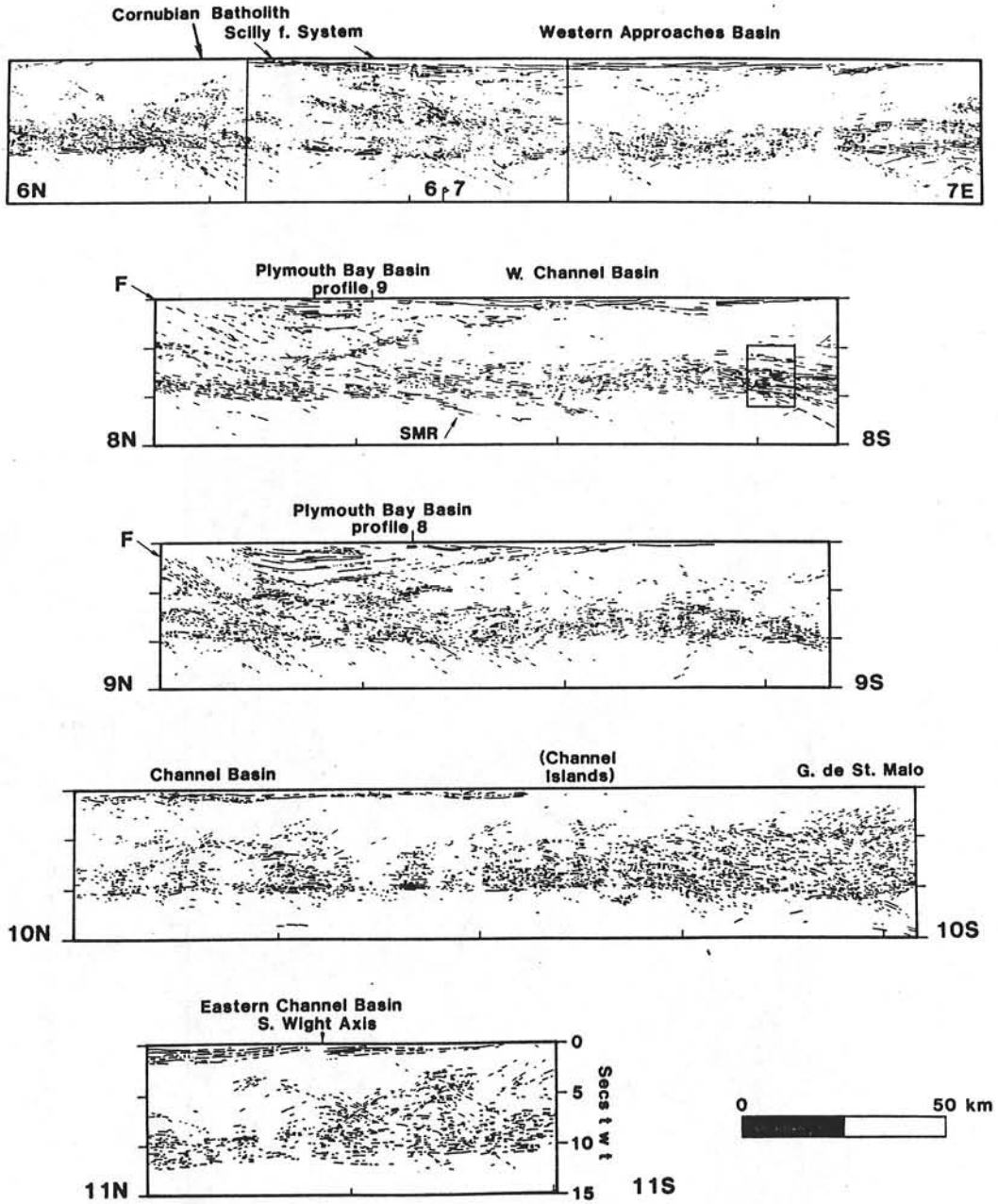


**Fig. 4.** Line drawings of unmigrated time sections of SWAT profiles 6–11. See caption to Fig. 2. Intersection of profiles 8 and 9 marked by a numbered tick. Vertical lines across profile 6/7 mark location of Fig. 5. Rectangle on profile 8 is location of Fig. 7. SMR, Sub-Moho Reflection.

and Caledonian crust can be distinguished by reflection character.

The reflection time to the Moho, identified as the base of the layering, is curiously constant over all the profiles seen in Figs 2 and 4 (except at the northern end of line 11). The larger basins appear not to influence the reflection time to the Moho. A preliminary depth migration of the line drawing suggests that the Moho rises only about 3 km under the Plymouth Bay basin, although the total thickness of the crystalline crust beneath the sediments is reduced from about 30 km to about 21 km. Likewise, the reflection time to the top of the reflective lower crust appears surprisingly

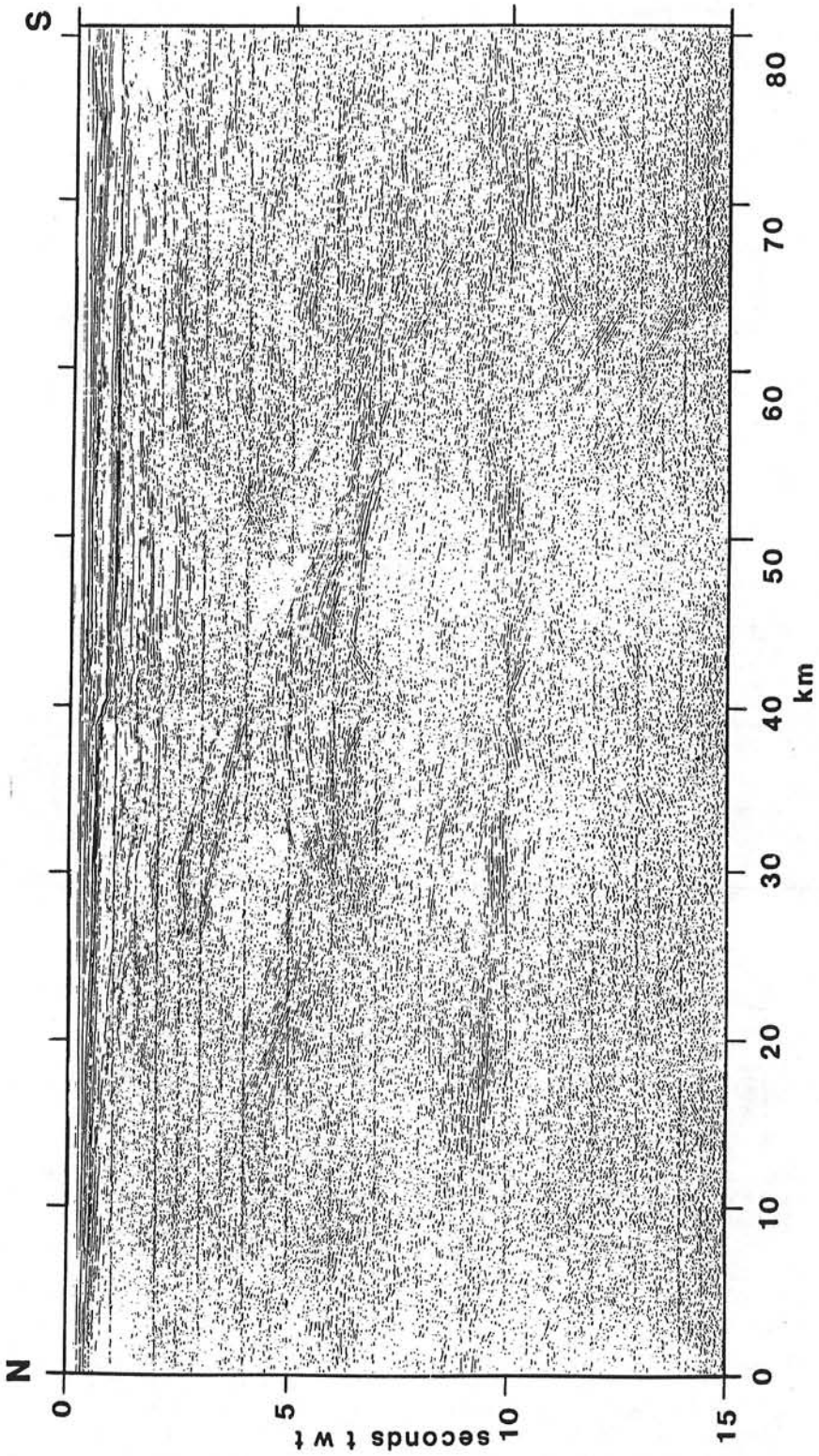


**Fig. 5.** Photograph of part of profile 6/7 showing Scilly Fault system. For location see Fig. 4.

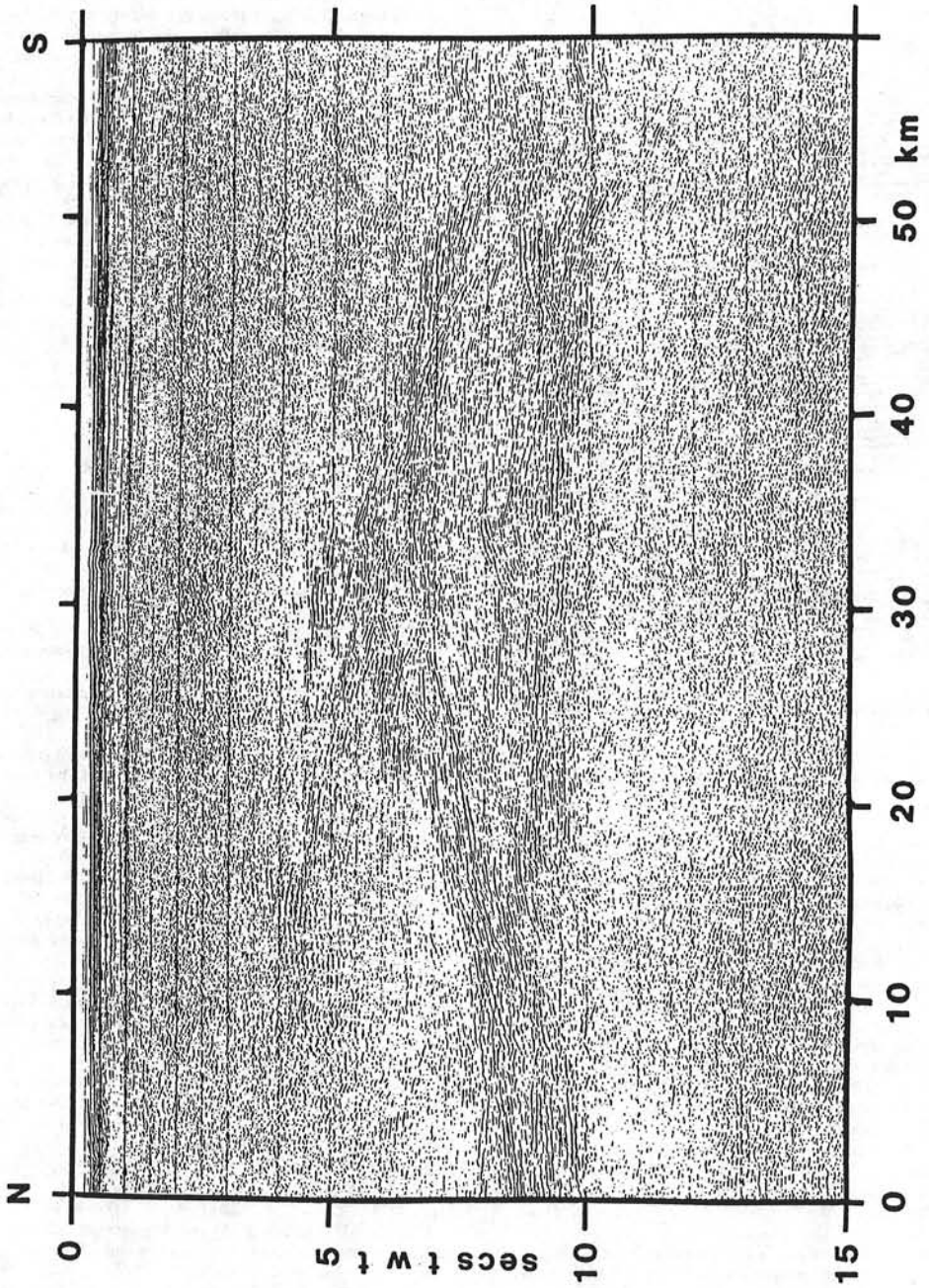


**Fig. 6.** Photograph of seismic record of part of profile 5 across the Haig Fras granite. For location see Fig. 2.

constant. Several sub-Moho events can be seen on the unmigrated profiles shown in Figs 2 and 4. Most of them resemble diffractions and collapse after 2-D depth migration of the line drawings, but two, on profiles 4 and 8, remain as events in the upper mantle and lower crust similar to the Flannan Fault seen on MOIST and WINCH.

The records and tapes of the SWAT lines can be obtained at the cost of reproduction by writing to the Programme Manager, Marine Geophysics Research Programme, British Geological Survey, Murchison House, West Mains Road, Edinburgh EH9 3LA, UK. Telex 727343.

BIRPS is funded by the Natural Environment Research Council. Twenty five per cent of the cost of SWAT was paid by the ECORS group (INAG, IFP, Elf-Aquitaine, IFREMER). Scientists from British Geological Survey and Universities visiting the BIRPS core group to work on the data in Cambridge, were supported respectively by the Department of Energy (London) and by Shell Expro (UK) Ltd.

## References

AUFFRET, G. A., PASTOURET, L., CASSAT, G., DE CHARPAL, O., CRAVETTE, J. & GUENNOC, P. 1979. Dredged rocks from the Armorican and Celtic

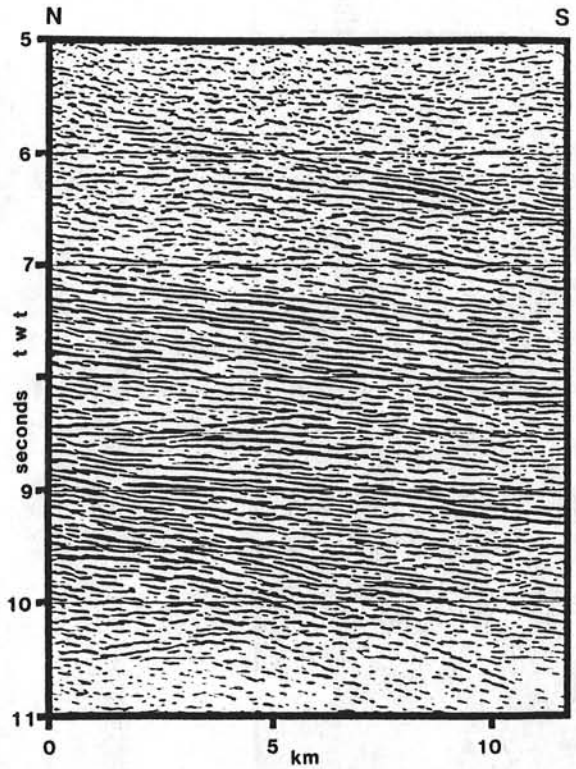


**Fig. 7.** Photograph of part of the seismic record of profile 8 showing reflective lower crust. For location see Fig. 4.

margins. *In*: MONTADERT, L. & ROBERTS, D. G. *et al. Initial Reports of the Deep Sea Drilling Project* **48.** U.S. Govt. Printing Office, Washington, D.C. 995–1014.

AUTRAN, A., BRETON, J.-P., CHANTRAINE, J. & CHIRON, J.-C. 1980. *Carte tectonique de la France. 1:1,000,000.* Bureau de Recherches Géologiques et Minières.

BARAZANGI, M. (ed.) In press. *Deep Structure of the Continental Crust.* American Geophysical Union. Geodynamics Series.

BARR, K. W., COLTER, V. S. & YOUNG, R. 1981. The geology of the Cardigan Bay–St. George's Channel Basin. *In*: ILLING, L. V. & HOBSON, G. D. (eds) *Petroleum Geology of the Continental Shelf of North–West Europe.* Heyden, London. 432–43.

BARTON, P. J., MATTHEWS, D. H., HALL, J. & WARNER, M. 1984. Moho beneath the North Sea compared on normal incidence and wide angle seismic records. *Nature, London.* **308,** 55–6.

BOIS, C., DAMOTTE, B., MASCLE, A., CAZES, M., TORREILLES, G., GALDEANO, A., HIRN, A., MATTE, P. & RAOULT, J. F. In press. Deep seismic profiling of the crust in Northern France: programme ECORS. *In*: BARAZANGI, M. (ed.) *Deep Structure of the Continental Crust.* American Geophysical Union, Geodynamics Series.

BREWER, J. A., SMITHSON, S. B., OLIVER, J. E., KAUFMAN, S. & BROWN, L. D. 1980. The Laramide orogeny: evidence from COCORP deep crustal seismic profiles in the Wind River Mountains, Wyoming. *Tectonophysics.* **62,** 165–89.

——, MATTHEWS, D. H., WARNER, M. R., HALL, J. R., SMYTHE, D. K. & WHITTINGTON, R. J. 1983. BIRPS deep seismic reflection studies of the British Caledonides. *Nature, London,* **305,** 206–10.

—— 1984. Clues to the deep structure of the European Variscides from crustal seismic profiling in North America. *In*: HUTTON, D. H. W. & SANDERSON, D. J. (eds) *Variscan Tectonics of the North Atlantic Region.* Special Publication of the Geological Society, London, **14,** 253–64.

—— & SMYTHE, D. K. 1984. MOIST and the continuity of crustal reflector geometry along the Caledonian–Appalachian orogeny. *Journal of the Geological Society, London,* **141,** 105–20.

BROOKS, M., MECHIE, J. & LLEWELYN, D. J. 1983. Geophysical investigations in the Variscides of south–west Britain. *In*: HANCOCK, P. L. (ed.) *The Variscan Fold Belt in the British Isles.* Adam Hilger, Bristol. 186–97.

——, DOODY, J. J. & AL-RAWI, F. R. J. 1984. Major crustal reflectors beneath SW England. *Journal of the Geological Society, London,* **141,** 97–103.

CHEADLE, M. J., CZUCHRA, B. L., BYRNE, T., ANDO, C. J., OLIVER, J. E., BROWN, L. D., KAUFMAN, S., MALIN, P. E. & PHINNEY, R. A. In press. The deep crustal structure of the Mojave Desert, California, from COCORP seismic reflection data. *Tectonics.*

DAY, G. A. & WILLIAMS, C. A. 1970. Gravity compilation in the NE. Atlantic and interpretation of gravity in the Celtic Sea. *Earth and Planetary Science Letters,* **8,** 205–13.

—— & EDWARDS, J. W. H. 1983. Variscan thrusting in the basement of the English Channel and Southwest Approaches. *Proceedings of the Ussher Society,* **5,** 432–6.

DUNNING, F. W. 1977. Caledonian–Variscan relations in North–West Europe. *In*: *La Chaîne Varisque d'Europe Moyen et Occidentale.* Colloque International du Centre National de la Recherche Scientifique, Paris, **243,** 165–80.

EDWARDS, J. W. F. 1984. Interpretations of seismic and gravity surveys over the eastern part of the Cornubian platform. *In*: HUTTON, D. H. W. & SANDERSON, D. J. (eds) *Variscan Tectonics of the North Atlantic Region.* Special Publication of the Geological Society, London, **14,** 119–24.

HALL, J. (ed.). In press, 1985. *Nature of the Lower Continental Crust.* Special Publication of the Geological Society, London.

HAUSER, E. *et al.* 1984. The COCORP 40°N transect of the North American Cordillera: Part 2. *Geological Society of America. Abstracts with Programs,* **16,** 532.

HOLDER, A. P. & BOTT, M. H. P. 1971. Crustal structure in the vicinity of south–west England. *Geophysical Journal of the Royal Astronomical Society,* **23,** 465–89.

HUTTON, D. H. W. & SANDERSON, D. J. (eds) 1984. *Variscan Tectonics of the North Atlantic Region.* Special Publication of the Geological Society, London, **14.**

LALAUT, P., SIBUET, J. -C., WILLIAMS, C. J. 1981. *Carte gravimétrique de l'Atlantique Nord–est.* Centre National pour l'Exploitation des Océans, Paris.

LEVERIDGE, B. E., HOLDER, M. T. & DAY, G. A. 1984. Thrust nappe tectonics in the Devonian of South Cornwall and the western English Channel. *In*: HUTTON, D. H. W. & SANDERSON, D. J. (eds) *Variscan Tectonics of the North Atlantic Region.* Special Publication of the Geological Society, London, **14,** 103–12.

MATHUR, S. P. 1983. Deep reflection probes in Eastern Australia reveal differences in the nature of the crust. *First Break,* **1,** 9–16.

MATTHEWS, D. H. In press. Seismic reflections from the Lower crust around Britain. *In*: HALL, J. (ed.) *Nature of the Lower Continental Crust.* Special Publication of the Geological Society, London.

MEISSNER, R. & WEVER, T. In press. Nature and development of the crust according to deep reflection data from the German Variscides. *In*: BARAZANGI, M. (ed.) *Deep Structure of the Continental Crust.* American Geophysical Union. Geodynamics Series.

NAYLOR, D. & SHANNON, P. M. (eds) 1982. *Geology of Offshore Ireland and West Britain.* Graham & Trotman, London.

NELSON, K. D., ZHU, T. F., GIBBS, A. K., HARRIS, R. A., OLIVER, J. E., BROWN, L. D., KAUFMAN, S. AND SCHWEIKERT, R. In press. COCORP Deep seismic reflection profiling in the Northern Sierra Nevada Mountains, California. *Tectonics.*

SHACKLETON, R. M., RIES, A. C. & COWARD, M. P. 1982. An interpretation of the Variscan structures in south west England. *Journal of the Geological Society, London,* **139,** 533–41.

SMITH, A. J. & CURRY, D. 1975. The structure and geological evolution of the English Channel. *Philosophical Transactions of the Royal Society, London,* A **279,** 3–20.

ZIEGLER, P. A. 1982. *Geological Atlas of Western and Central Europe.* Shell International Petroleum, Maatshappij B. V.

Received 16 August 1985; revised typescript accepted 3 October 1985.

Reprinted from Sibuet, J.-C., Ryan, W.B.F., et al., 1979.
*Initial Reports of the Deep Sea Drilling Project*, Volume XLVII, Part 2, Washington (U.S. Government Printing Office)

# 38. SITE 398: EVOLUTION OF THE WEST IBERIAN PASSIVE CONTINENTAL MARGIN IN THE FRAMEWORK OF THE EARLY EVOLUTION OF THE NORTH ATLANTIC OCEAN[1]

Jean-Claude Sibuet, Centre Océanologique de Bretagne, B.P. 337, 29273, Brest, Cedex, France
and
William B.F. Ryan, Lamont Doherty Geological Observatory, Palisades, New York

## INTRODUCTION

DSDP Site 398 is located on the West Iberian passive continental margin, south of Galicia Bank, 20 km to the south of Vigo Seamount (Figure 1). The kinematic evolution of the Iberian plate is closely controlled by the relative motions of the African, European, and North American plates. A study based on magnetic data and land data was undertaken to better define the relative motion of Iberia with respect to these main plates (Sibuet et al., in preparation). Trapped between these plates, microcontinents such as Galicia Bank and Flemish Cap (located between Iberia and North America) assumed their own relative motions with respect to Iberia and North America during the early evolution of the North Atlantic. Consequently, the initial oceanic circulation between small basins corresponding to the Bay of Biscay and the North Atlantic west of Iberia and Europe is closely controlled by relative positions and movements of these microcontinents. Site 398 paleoenvironment data, therefore, are of crucial interest in understanding the early evolution of the North Atlantic and the vertical evolution of continental margins.

## ACOUSTIC STRATIGRAPHY

Site 398 was drilled about 400 meters laterally off the IFP-CNEXO Flexichoc seismic line GP 19 near shotpoint 440 (Figure 2, see location on Figure 1), in a water depth of 3900 meters. A total penetration of 1740 meters was obtained. Four main acoustic units (Figure 2) lie over the acoustic basement (Groupe Galice, this volume).

The acoustic basement is clearly of sedimentary origin on this profile. It is highly diffractive in most places and shows strong relief either as broad undulations or as sharp crests corresponding to buried highs. Some of these highs may even outcrop as shown on some seismic profiles. Sharp crests and strongly dipping layers in the basement suggest the presence of tilted fault blocks frequently observed over passive margins. On some profiles, several highs are flat-topped and covered by a thin sedimentary blanket which suggests that they have been affected by subaerial erosion.

Formation 4, which is a moderately to strongly layered formation, is separated from the overlying Formation 3 by a strong reflector. Formation 4 lies in troughs between horsts and tilted blocks. Layering is quite conformable between its base and the top of the basement in the lowest part of the fill. At the top, it can be almost flat. This indicates that sedimentation occurred as basement blocks were being tilted.

Formation 3 is generally transparent or slightly layered. It fills depressions similar to Formation 4, but actually differs from it by its less inclined or even horizontal bedding. It may be absent on top of some structural highs.

Formation 2 often seems to have been deposited on an almost flat topography. It is a layered sequence marked by several good reflectors. Bedding is generally flat and conformable with the lower boundary.

Formation 1 is acoustically transparent on top (acoustic Unit 1A). Layering increases towards the base (acoustic Unit 1B) where it merges into Formation 2.

## STRATIGRAPHY FROM PISTON CORES, DREDGE SAMPLES, AND HOLE 398D CORES

The acoustic formations just described can be related to the lithologic column of Site 398 and to the stratigraphy obtained from core and dredge samples (Dupeuble et al., 1976 and this volume; Site 398 Report; Groupe Galice; de Graciansky and Chenet; Sigal; Maldonado; all, this volume).

Based upon correlations between lithologic and acoustic units, stratigraphic and seismic hiatuses, physical properties, mineralogical composition of sediments, and acoustic impedance, the proposition has been made that the lowermost 73 meters were drilled into acoustic basement (Site 398 Report; Bouquigny and Willm, both, this volume). This lowermost section consists of a complex sequence of marlstone, siltstone, and white indurated limestone of late Hauterivian to early Barremian age. The white indurated limestones were deposited under pelagic conditions, whereas marlstones and siltstones could have been emplaced by low-density turbidity currents in a quiet-water environment. Limestones were deposited above the CCD but probably at depths reaching 2 km at the site (Site 398 Report, this volume).

Acoustic Formation 4, corresponding to upper Barremian to latest uppermost Aptian, consists of sand-silt-clay graded sequences interbedded with thick (1 to 10m) slumped beds or debris flows. These sequences resulted from the redeposition of older deposits on submarine slopes and on a subsiding sea floor (de Graciansky et

[1]Contribution 616 of the Scientific Department of the Centre Océanologique de Bretagne.

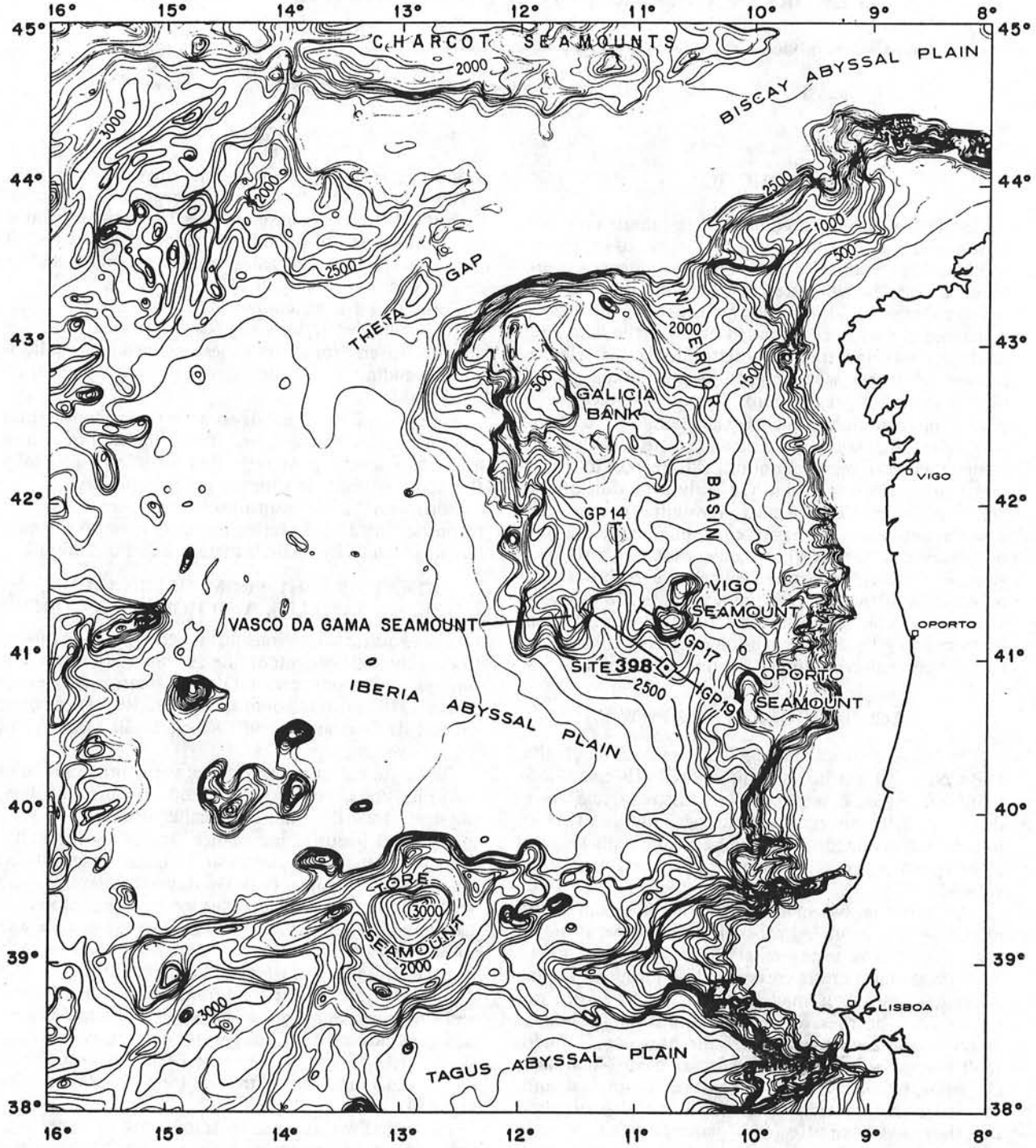


Figure 1. *Location of Site 398 and bathymetric map of the Galicia Bank area (Laughton et al., 1975) in corrected fathoms.*

al., in press). A stratigraphic break exists in the uppermost Aptian which corresponds both to a sharp lithological change and to a major reflector between Formations 4 and 3.

Acoustic Formation 3 corresponds to lower Albian to middle Cenomanian. At its base, lower to middle Albian laminated dark shales, mostly of continental provenance, are succeeded by interbedded dark shales

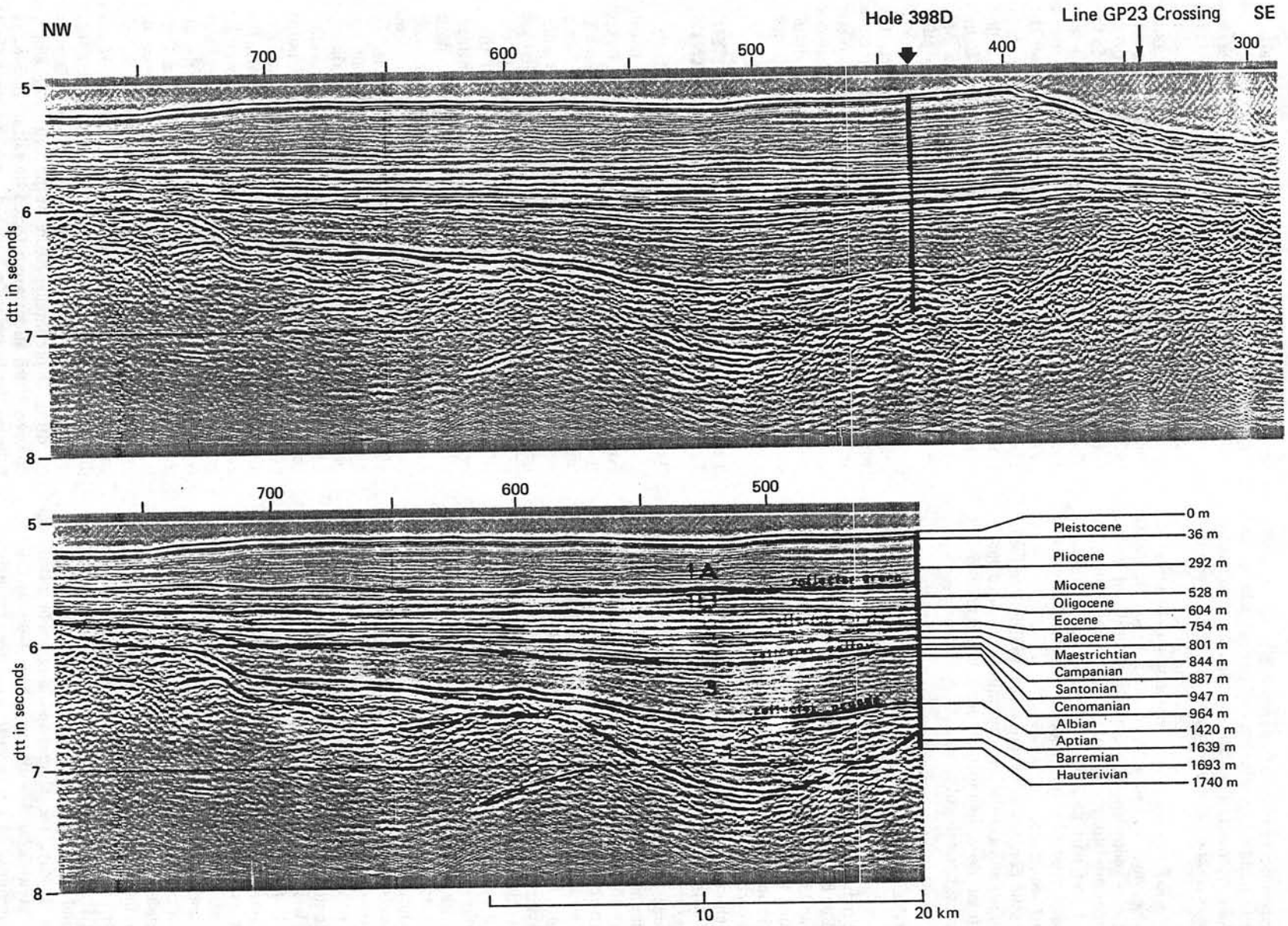


Figure 2. *Migrated section of the Flexichoc seismic profile GP 19 (IFP-CNEXO-CEPM) located on Figure 1. Shot numbers are at the top of the profile. Shot spacing: 50 meters. Horizontal scale is in the lower part; vertical scale, in seconds of double travel time. The main seismic reflectors and acoustic units are shown on the interpreted profile. Limits and depths of geological stages (based on Site 398 results) are on the right side.*

and marlstones of middle to upper Albian and by upper Albian to middle Cenomanian redeposited pelagic marl and chalk. Acoustic Formations 3 and 2 are separated by the well-known Cenomanian to lower Senonian hiatus.

Acoustic Formation 2, corresponding to Senonian to upper Eocene, consists of two main lithologic units. Reddish to yellowish brown marly nannofossil chalk, calcareous mudstone, claystone, and siliceous mudstone in the lower part underly siliceous marly nannofossil chalk and mudstone interbedded with turbiditic sand-silt-marl sequences.

Acoustic Formation 1 spans recent to Oligocene sedimentation, and consists of rhythmically bedded marly nannofossil ooze, nannofossil ooze, marly nannofossil chalk, and nannofossil chalk.

## MAGNETIC DATA: THE EARLY EVOLUTION OF THE NORTH ATLANTIC

The sedimentary evolution of this continental margin should be considered in the general context of the kinematic and tectonic evolution of the North Atlantic. All published kinematic solutions for the evolution of the Atlantic north of the Azores-Gibraltar line, and also all reconstructions of continents before their separation (Le Pichon, 1968; Pitman and Talwani, 1972; Laughton, 1972; Le Pichon et al., 1977; Groupe Galice, this volume), are based on magnetic lineations and/or fracture zone trends. As a general rule, the fit of corresponding magnetic anomaly lineations, on each side of the spreading ridge axis, from anomaly 32 (Upper Cretaceous) to the present gives a good idea of the kinematic evolution of the North Atlantic (Pitman and Talwani, 1972; Laughton, 1972). No magnetic data were available to provide other kinematic constraints between the anomaly 32 fit and the pre-opening positions of the continents. These positions were deduced from the shape of the continental margins, the correspondence of trends of the oldest oceanic portions of fracture zones, and of pre-rift linear markers on land (Le Pichon et al., 1977).

Figure 3 presents a new map of magnetic lineations in the northeast Atlantic based on a compilation of published data north of the Charlie-Gibbs fracture zone (Pitman and Talwani, 1972; Kristoffersen and Talwani, 1977), west of anomaly 25 (Williams and McKenzie, 1971; Pitman and Talwani, 1972; Williams, 1975; Laughton et al., 1975; Cande and Kristoffersen, 1977), and on a new re-examination of magnetic profiles east of anomaly 25 (Sibuet et al., in press). Magnetic anomalies 33 and 34 have been identified using the proposed criterion of Cande and Kristoffersen (1977).

A triple junction point probably existed west of the Bay of Biscay at the time of anomalies 33 and 34, as proposed by Williams (1975). Although Late Cretaceous to late Eocene compressive movements have affected the initial configuration of anomalies 33 and 34 in the Bay of Biscay, the shape and amplitude of these anomalies associated with the Charcot-Biscay-Cantabria seamounts do not seem to have been strongly affected by this compressive episode. (Sibuet et al., in preparation).

In the Iberian Abyssal Plain, west of the Iberian Peninsula and east of anomaly 34, magnetic anomalies reach about 150 nT. The size and spacing of these anomalies are similar to those of the Cretaceous quiet zone west of North Africa (Hayes and Rabinowitz, 1975). From south to north, the eastern limit of the domain outlined by these anomalies corresponds to the Tore-Madeira rise along the *J* anomaly (Pitman and Talwani, 1972; Olivet et al., 1976; Rabinowitz et al., 1979), then to a positive anomaly which continues the Tore-Madeira rise to the 41 °N parallel and which could Correspond to the *M*0 anomaly, and finally to a line which bounds the northwest corner of Galicia Bank. The *J* anomaly has been identified with the *M*0-*M*1 anomaly (Rabinowitz et al., 1979) dated as late Aptian (Leg 53, Francheteau, personal communication; van Hinte, 1976). If those assumptions are correct, the wide area located between anomaly 34 and this feature should correspond to the Cretaceous quiet magnetic zone. East of this feature, the *M* sequence would not exist. Nevertheless, this should not necessarily imply that oceanic crust created by sea-floor spreading is lacking east of the *J* anomaly.

## LEG 47B RESULTS IN THE FRAMEWORK OF THE EARLY EVOLUTION OF THE NORTH ATLANTIC

### Triassic-Liassic or Older Tensional Episode

The first epoch of rifting of continents in the North Atlantic is still being debated. It is thought to be linked to several tensional phases occurring from Permian to late Lias in the continental Eurasian-American framework (e.g., Arthaud and Matte, 1975; Groupe Galice, this volume) and to the early history of the Mesogea (e.g., Aubouin, 1977). Generally, the existence of this rifting eposide is supported by the presence of thick evaporitic series linked to a fast subsidence of continental blocks. Reliable age data around the Iberian Peninsula and Grand Banks exist, especially for the Triassic-Lias episode. On the Grand Banks, Jurassic and older formations are presented in structural basins bounded by block-faulted basement structures and display salt diapirism (Daily Oil Bulletin, 1973). In Aquitaine, Triassic-Liassic sedimentation is characteristic of a subsiding basin filled with thick detrital and evaporitic deposits (Winnock, 1971; Dardel and Rosset, 1971; Winnock et al., 1973). In initial reconstructions of continents, the Aquitaine basin could be continued towards the west by grabens and basins related to the Labrador-Biscay Fault (Laughton, 1972; Le Pichon et al., 1971a). In the interior basin (Figure 1) between Galicia Bank and Iberia, the deep sedimentary layers may be Jurassic or older (Groupe Galice, this volume). Nevertheless, the very thick sedimentary series shows no evidence of salt diapirism on seismic profiles and does not indicate that this area has been affected by a Triassic-Liassic episode of rifting. In the smaller basins of the continental slope, however, formations are affected by salt diapirism, as between the Porto seamount and the Portuguese shelf

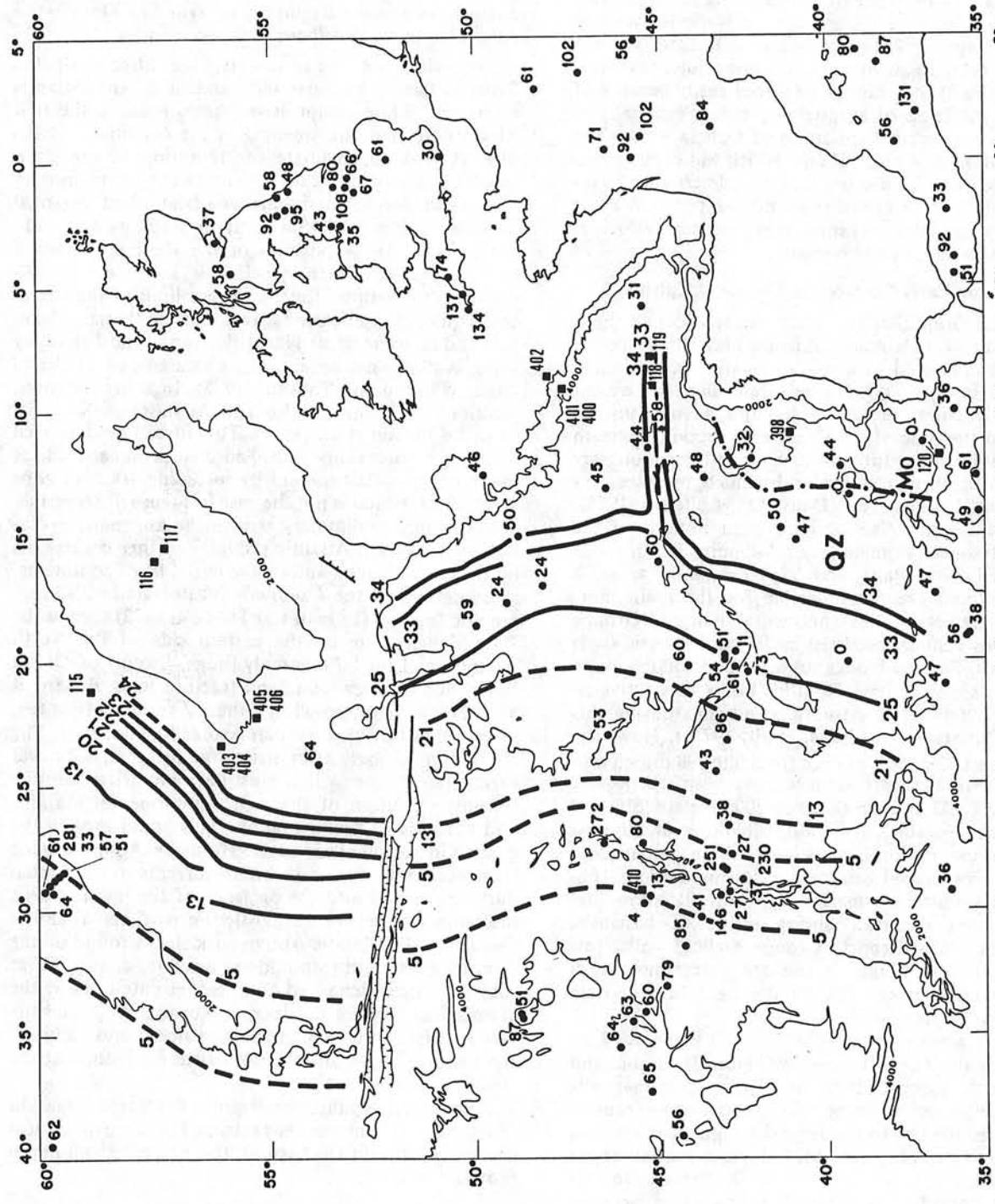


Figure 3. *Magnetic lineations in the northeast Atlantic. See text for data sources. Numbered squares correspond to locations and numbers of DSDP sites.*

(Montadert et al., 1974; Wilson, 1975; Groupe Galice, this volume). Consequently, numerous studies support the hypothesis that the initial Eurasian-American continent has been affected, at least locally, by intense fracturing and by an episode of rifting giving rise to subsiding basins filled with Triassic-Liassic evaporites and/or clastic sediments. The westernmost extension of these basins is located east of the Cretaceous quiet magnetic zone (Figure 3), but cannot be traced easily because of the great thickness of sedimentary cover, especially in the Iberian Abyssal Plain south of Galicia Bank. The amount of oceanic crust, if any, which was created during this tensional episode cannot be determined. This crust is probably a mixed type, neither purely oceanic nor purely continental as supported by seismic velocities in similar zones of early opening.

### Late Jurassic-Early Cretaceous Tensional Episode

South of Grand Banks, on the western Scotian shelf, a Berriasian/Valanginian hiatus has been discovered in sediments deposited in a shallow marine environment (Gradstein et al., 1975). On the Grand Banks, the most striking structural feature is a major angular unconformity at the base of the Cretaceous section. Beneath this unconformity, Jurassic and older formations are preserved in structural basins bounded by basement block-faulted structures (Daily Oil Bulletin, 1973). Coeval tensional episodes have been noticed in the Alpine-Mesogean domain (e.g., Aubouin, 1977).

In the Galicia Bank and Vigo Seamount areas, a major tectonic event responsible for the main morphologic trends of the continental margin (Groupe Galice, this volume) occurred in the Late Jurassic-Early Cretaceous. Faulted blocks subsided and rotated along faults of Panamean type. Rotating faults were active on both the Iberian and Armorican margins during this episode (Montadert, Roberts, et al., 1977a). However, since the last 73 meters of core from Site 398 drilled into a half-graben structure seem to have been redeposited above the CCD at a depth up to 2000 meters (Site 398 Report, this volume), it is impossible to evaluate how much vertical motion is associated with each tensional episode. Fan-shaped sedimentary accumulations, observed in acoustic Formation 4 (Figure 2), show that sedimentation occurred during tilting of basement blocks (Site 398 Report; Groupe Galice; both, this volume). Latest Aptian is the age determined from borehole data for the end of the Late Jurassic-Late Cretaceous episode.

The Cretaceous magnetic quiet zone is bounded on the east by the *J* or *M*0 anomaly (Figure 3). East of this limit, the *M* sequence is lacking, but a quiet magnetic domain exists and could be related either to a continental subsided area or to the Jurassic magnetic quiet zone (Sibuet et al., in preparation). If these assumptions are correct, this would mean that either the Permian to Lias tensional episode has affected a large area between North America and the Iberian peninsula with oceanization of continental crust, or, more probably, that an early opening of limited extent occurred during the Middle Jurassic after the Permian to Lias tensional episode. In both hypotheses, as the *M* sequence is lacking, there is no creation of typical oceanic crust between North America and the Iberian Peninsula in the Early Cretaceous before the late Aptian.

### *J* Anomaly and the Beginning of True Sea-Floor Spreading in the Northern Atlantic

Following the above events, the history of the Tethyan Ocean becomes independent of the Atlantic evolution. While compressive phases induced the first Alpine deformations, opening of the Atlantic is occurring. A first approximate configuration of the landmasses is given in Figure 4. The relative positions of Africa and North America are well established (personal communication from Shouten, *in* Rabinowitz et al., 1979). The relative position of the Iberian Peninsula with respect to North America is based on a well-documented position for the eastern limit of the Cretaceous quiet magnetic zone seaward of the Iberian Peninsula and on some limited identification of the *J* anomaly using available magnetic profiles located east of Grand Banks (Pitman and Talwani, 1972). In a first attempt, positions of Europe and Rockall are those of the initial fit of Le Pichon et al. (1977). This fit can be improved by using a better shape of *M*0 anomalies on each side of the northern Atlantic and by including fracture zone constraints, which is not the case in Figure 4. Nevertheless, this new preliminary step in the kinematic evolution of the North Atlantic provides further constraints on the early opening and on the initial fit of continents.

By definition, the *J* anomaly is associated with topographic features (Pitman and Talwani, 1972) such as the Tore-Madeira rise on the eastern side of the North Atlantic and the "*J*-Anomaly Ridge," south of Grand Banks and the Newfoundland fracture zone. Ballard et al. (1976) have proposed that these *J* anomaly twin features were associated with an Azores-like hot spot. The formation of these twin structural features, whatever their mode of formation, must have modified both the tectonic evolution of the nearby continental margins and the style of sedimentation. This could explain the change in sedimentation type from the Aptian graded sequences emplaced by turbidity currents to the Albian dark shales and also the presence of the main seismic discontinuity between acoustic Formations 4 and 3 (Figure 2). The middle Aptian dark shales found on the Armorican margin (Montadert, Roberts, et al., 1977a) may have been deposited at an earlier date because the connection between the Iberian Abyssal Plain and the Bay of Biscay was not established north and south of the Flemish Cap-Galicia Bank structural feature at the time of anomaly *J*.

Since latest Aptian, the western continental margin of the Iberian Peninsula has subsided because of vertical cooling of the lithosphere as the accreting boundary moved westward.

### Anomaly 34: A Step in the Opening of the North Atlantic

The trend and length of anomaly 34 on each side of the North Atlantic have been defined from numerous

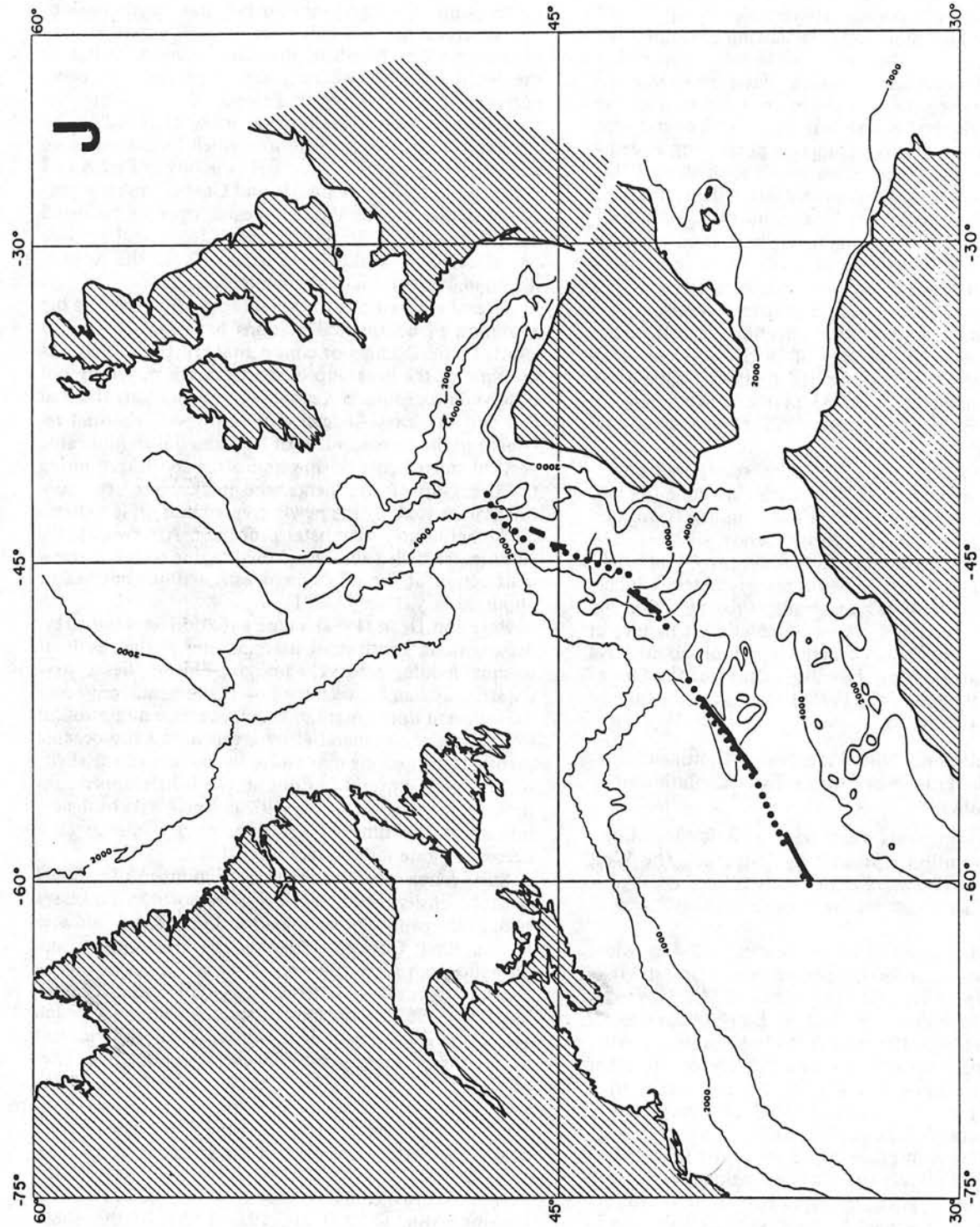


Figure 4. *Tentative reconstruction of the positions of the continents at the time of* J *anomaly (uppermost Aptian). Bathymetric contours are in meters. America is kept fixed.* J *anomaly is represented by the dotted line on the eastern side and by the continuous line on the western side of the North Atlantic.*

data. Between the Charlie-Gibbs fracture zone and the Azores-Gibraltar line, it is impossible, using the constraints of these two fracture zones, to match the corresponding plate boundaries at the time of anomaly 34 (upper Santonian in the van Hinte scale [1976]).

Le Pichon and Sibuet (1971), having examined the kinematics of the Eocene episode of compression between the Iberian and European plates, show that the boundary between the two plates extended west of the Pyrenees, along the Spanish marginal trench to end west of King's Trough at a triple junction point. Consequently, the positions of anomalies 34 on each side of this plate boundary have been shifted after their creation. Segments of anomalies 34, located north and south of the Charcot and Biscay seamounts, have been matched without any ambiguity with anomaly 34 on the American side, using the trend constraints of the Charlie-Gibbs fracture zone and the Azores-Gibraltar line. One of the main kinematic implications is that at the time of anomaly 34, the Bay of Biscay was not completely created. This is supported by the possible presence of anomalies 34 and 33 in the central part of the Bay of Biscay (Williams, 1975; Sibuet et al., in preparation).

In late Santonian time, the open sea is well developed south of the Charlie-Gibbs fracture zone (53 °N). The sudden occurrence of primary minerals formed in upstream soils (illite, chlorite, sandy silicate, kaolinite) from late Santonian to at least early Maestrichtian is probably due to the supply of minerals inherited from high latitudes and transported by the newly established north-south oceanic circulation (Chamley et al., this volume). This oceanic circulation could have been established during the early opening of the Labrador Sea (Le Pichon et al., 1971b) which is at the time of anomaly 34 (Figure 5).

### General Evolution of the West Iberian Continental Margin in the Framework of the Early Evolution of the North Atlantic

Based on arguments which have been developed, the following evolution is tentatively proposed. The West Iberian continental margin was likely created during the Permian Triassic-Lias rifting episode (280 to 174 m.y. B.P.).

A limited oceanic domain (about 100 km wide) opened between the Iberian peninsula and Grand Banks in the Middle Jurassic (174 to 150 m.y. B.P.). However, no oceanic opening occurred in Late Jurassic-Early Cretaceous (150 to 109 m.y. B.P.) but, simultaneously, a second tensional episode would be responsible for fault-block subsidence and tilting on the West Iberian continental margin. In latest Aptian (109 m.y. B.P.), the main features of the continental margin morphology would have been in place. Since then (109 m.y. B.P.), the continental margin has subsided regionally except in a few zones such as the northern part of Galicia Bank where Late Cretaceous-Tertiary compressive movements have occurred. The decisive opening of the northern Atlantic dates from that time.

## MECHANISMS OF FORMATION AND EVOLUTION OF PASSIVE CONTINENTAL MARGINS

To estimate vertical movements, one must consider the structural and tectonic evolution of a passive continental margin. North of the Azores-Gibraltar line in the North Atlantic where graben-type subsidence occurred prior to splitting in Permian to Lias time, the vertical evolution of continental margins is hidden by the complex posterior evolution which has taken place since Early Cretaceous. Indeed, in the Bay of Biscay and between the Iberian peninsula and Grand Banks, a possible Middle Jurassic limited oceanic opening followed by a Late Jurassic-Early Cretaceous tensional episode has affected the vertical evolution of both the Armorican and West Iberian continental margins.

Several mechanisms to explain the formation and the evolution of continental margins have been proposed (Bott, 1976). Doming of continental crust before and at the time of the break-up of continents is generally not observed according to Kent (1977) except along the Red Sea and the East African rifts. However, thermal response to the emplacement of hot material should cause vertical movements during and after splitting. During the break-up of continents, the thickness of the continental crust along the newly created margin is reduced by subaerial and subcrustal processes. Afterwards, the continental shelf subsides, probably due to the thermal contraction of the lithosphere with a time constant of about 50 m.y. (Sleep, 1971).

Bott and Dean (1972) suggest that differential stress occurs along continental margins and is the result of unequal loading across the margin. This implies a varying stress system between the lower continental crust and the adjacent upper mantle, which causes a migration of lower continental material by creep in the sub-oceanic mantle. This process may cause subsidence of the shelf, which favors normal faulting in the brittle upper continental crust (Bott 1971, 1973). Such a subsidence, intense at the time of splitting, may continue at a decreasing rate indefinitely thereafter.

Subsidence may also occur in response to increased crustal density produced by metamorphic processes such as the gabbro to eclogite transition (Ringwood and Green, 1966; Collette, 1968), or the greenshist to amphibolite transition (Falvey, 1974), or by intrusions of basic or ultrabasic igneous rocks (Beloussov, 1960; Sheridan, 1969). Lithosphere should respond to such variation of the density structure by a lithospheric flexure involving margin subsidence (Walcott, 1972). Recently, Foucher and Sibuet (in press) questioned the validity of this last mechanism and proposed an interpretation of heat-flow data from the Armorican margin compatible with a thinning of the continental crust by creep in the lower part of the crust, the upper brittle part of the crust being affected by Panamean or normal faulting (Montadert et al., 1977b). All of the above mechanisms may contribute to margin subsidence; the problem is to assess their relative importance.

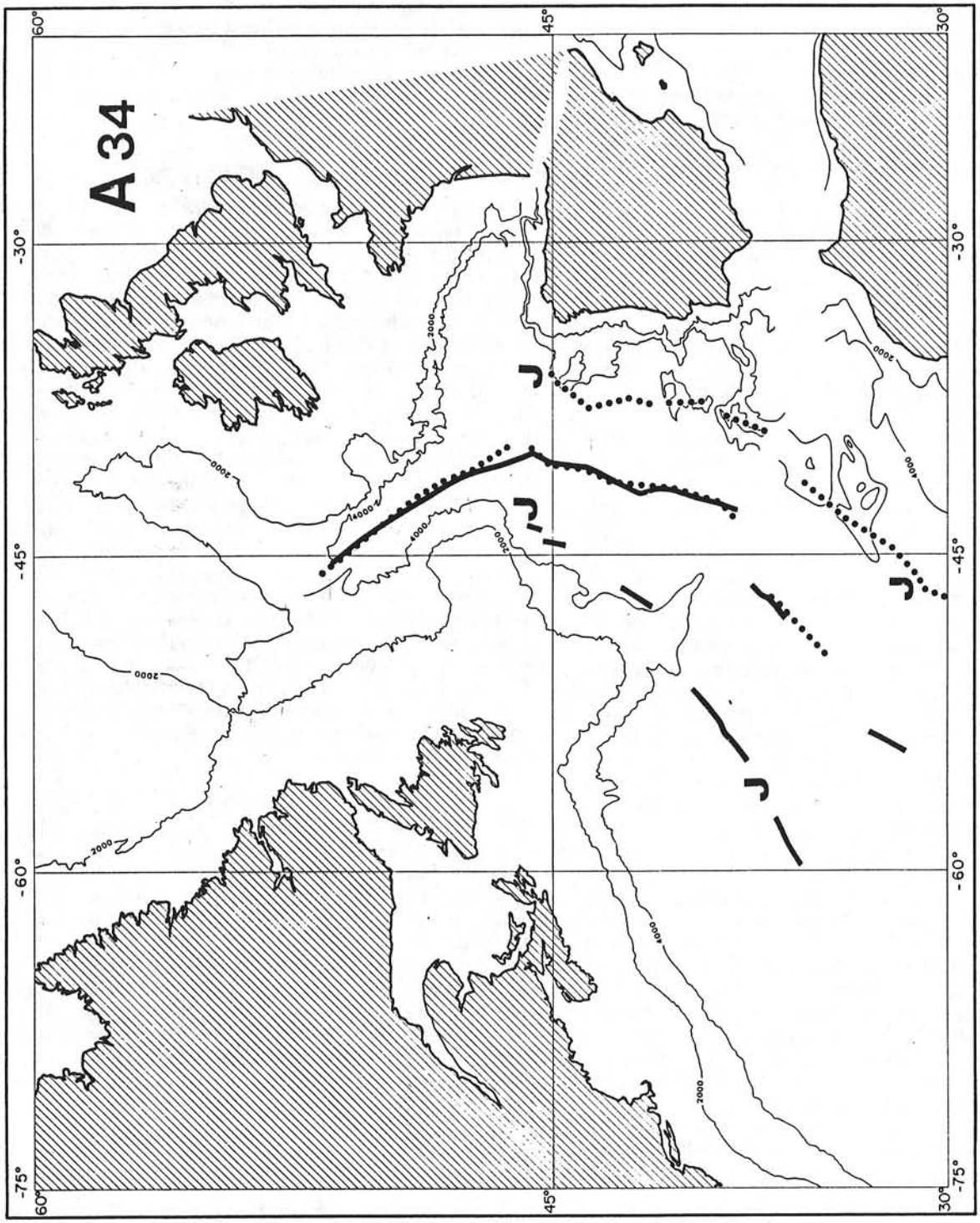


Figure 5. *Reconstruction of the position of continents at the time of anomaly 34 (late Santonian). Bathymetric contours are in meters. America is kept fixed. Magnetic anomalies J and A-34 are represented by the dotted line on the eastern side and by the continuous line on the western side of the North Atlantic. Using conventions of Le Pichon et al. (1976), parameters of rotation are: Europe/North America – 63.0°N 149.3°E –19.0°; Iberian peninsula/North America – 82.8°N 121.3°E –22.5°.*

## VERTICAL MOVEMENTS AT THE LEVEL OF SITE 398

The complexity and diversity of proposed mechanisms to explain the formation of continental margins are partly due to the fact that paleodepths across continental margins are unknown. The history of subsidence remains to be unraveled using sedimentological patterns on the sea floor depending on, for example, dissolution and productivity for opal and carbonate, and of surface and deep water circulation. The vertical distribution of benthic faunas allows paleodepth estimation as follows: continental shelf (0 to 200 m), upper bathyal (200 to 500 m), middle bathyal (500 to 1000 m), and lower bathyal (1000 to 2000 m). In the abyssal domain (>2000 m), depth distinctions are often impossible.

We will try to show how the Site 398 results, placed in the general context of the West Iberian continental margin evolution can provide constraints about the vertical evolution at Site 398 (Sibuet et al., in press).

Eroded surfaces 2.5 km deep, unaffected by the Late Jurassic-Early Cretaceous tensional episode, exist both on the Armorican and West Iberian continental margins. Site 398 paleodepth will be estimated using data concerning the vertical evolution of these eroded surfaces.

### Eroded Surfaces

Flat surfaces covered with post-latest Aptian sediments have been identified on the Armorican and West Iberian continental margins at depths ranging from 1.5 to 2.8 km (Figure 6). These surfaces are horizontal or dip gently toward the ocean. We interpret them as relics of subaerially eroded areas which were at zero depth in pre-latest Aptian time. They are identified on Galicia Bank, on Vigo and Vasco da Gama seamounts (Figure 1), and between these features. The depth of these surfaces is at 1.5 km on Galicia Bank and 2.5 to 2.8 km elsewhere. Because a subduction zone functioned in the Bay of Biscay, north of Iberia, from Late Cretaceous to Eocene time (Sibuet and Le Pichon, 1971; Le Pichon and Sibuet, 1971; Choukroune et al., 1973), the northern border of Galicia Bank could have been affected by this compressive phase. Depths of these surfaces are consequently constant on the Armorican (Montadert et al., 1977b) and West Iberian continental margins, but not on Galicia Bank itself.

These eroded surfaces have subsided on a regional scale from zero level to their present depth since the beginning of the real opening of the North Atlantic, which is dated as latest Aptian. Isostatic readjustment due to local or flexural loading is minor; sediment cover on the eroded surfaces (Figures 6 and 7) does not exceed 0.8 km. Consequently, the subsidence could be related to the thermal cooling of the lithosphere as the spreading axis moved away.

Several authors suggest that the subsidence of the entire continental margin follows the thermal oceanic subsidence curve since the creation of oceanic domain (Watts and Ryan, 1976; Montadert et al., 1977b). Seismic reflection profiles show that the whole fault pattern of the West Iberian continental margin was sealed up since latest Aptian (Groupe Galice, this volume), except locally where tertiary compressive phases took place. Consequently, either the whole margin subsides globally, the vertical motion being consumed at the level of a vertical fault pattern parallel to the margin trend, or the continental margin was flexured, continental and oceanic plates being coupled or not (Figure 8). Because such a fault pattern has not been noted, the second hypothesis seems more probable.

### Vertical Evolution at the Level of Site 398

We have supposed that the subsidence curve of the eroded surface was an exponential type (Figures 9 and 10) and that at the level of Site 398, located 20 km south of such an eroded surface, the same subsidence curve could be applied, even if the drill site is 2 km deeper than the present depth of the eroded surface. Consequently, the paleodepth of the acoustic basement should be at least 2 km in the Lower Cretaceous, which is compatible with the paleodepth of sediment emplaced at this time (Site 398 Report). The local isostatic readjustment has been calculated using shipboard density measurements (Site 398 Report) (Figure 9). Compaction has been taken into account to calculate the Site 398 paleodepth (Figure 10). The extremes of the CCD curve, superimposed on the paleodepth curve in Figure 10, are arbitrary.

During the ante-latest Aptian evolution, we presume that the acoustic substratum was affected by the two episodes of rifting of Permian-Triassic-Lias and Late Jurassic-Early Cretaceous ages, without knowledge of the relative subsidence contribution of each phase. Between these two phases, during the Middle Jurassic, the West Iberian continental margin could regionally subside by thermal cooling linked to the removal of the heat source (Figure 10).

## CONCLUSION

The paleodepth at the level of a drilling site can only give local information on the vertical evolution of a passive continental margin. Only biostratigraphic data from wells belonging to a transect of the margin linked to structural and tectonic processes could permit quantification of the vertical evolution of a continental margin and the understanding causes of subsidence. If the thermal subsidence seems to be the main cause of the vertical evolution of a continental margin, subsidence due to sediment and water load including sea-level changes must be taken into account.

## ACKNOWLEDGMENTS

Vincent Renard critically reviewed the manuscript and made helpful suggestions.

## REFERENCES

Arthaud, F. and Matte, P., 1975. Late Hercynian wrench faults in Southern Europe and Northern Africa: geometry and nature of deformation, *Tectonophysics*, v. 25, p. 139-171.

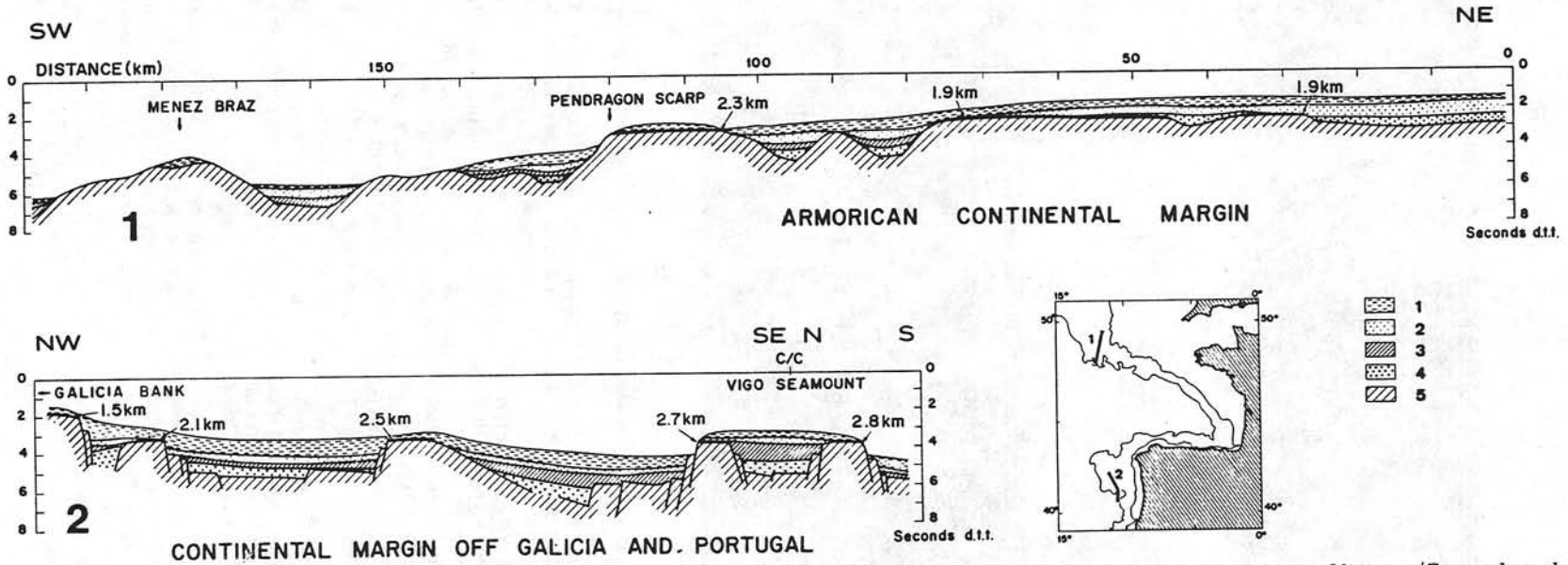


Figure 6. *Interpreted seismic profiles obtained on the Armorican and West Iberian continental margins. 1: acoustic Unit 1 (present to Oligocene/Eocene boundary); 2: acoustic Unit 2 (Oligocene/Eocene boundary to Santonian); 3: acoustic Unit 3 (Santonian to latest Aptian); 4: acoustic Unit 4 (ante-latest Aptian); 5: acoustic basement. Eroded surfaces are marked with thick lines and their depths indicated.*

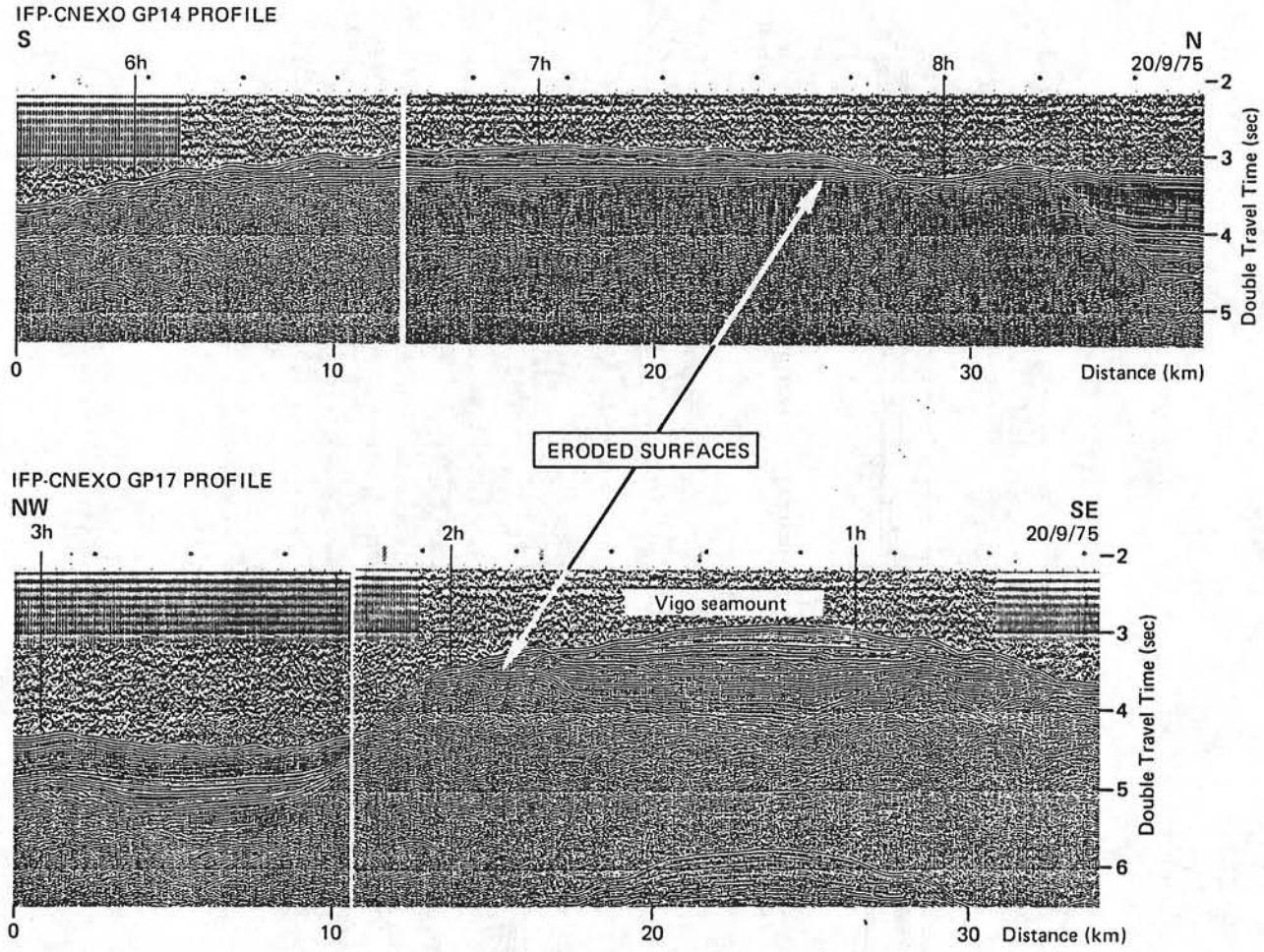


Figure 7. *Examples of eroded surfaces at a depth of 2.4 km. Locations of profiles are shown in Figure 1.*


Aubouin, J., 1977. Téthys, Atlantique et Pacifique: regard tectonique. *Bull. de la Société Géologique de France,* v. 4, p. 170–179.

Ballard, J.A., Vogt, P.R., and Egloff, J., 1976. The magnetic "*J*-Anomaly" and associated structures in the North Atlantic (abstract), *EOS*, v. 57, p. 264.

Beloussov, V.V., 1960. Development of the earth and tectogenesis. *J. of Geophys. Res.*, v. 65, p. 4127-3146.

Bott, M.H.P., 1971. Evolution of young continental margins and formation of shelf basins, *Tectonophysics,* v. 11, p. 319-327.

_____, 1973. Shelf subsidence in relation to the evolution of young continental margins. *In* Tarling, D.H. and Runcorn, S.K. (Eds.), *Implications of continental drift to the earth sciences:* London and New York (Academic Press), v. 2, p. 675-683.

_____, 1976. Problems of the formation and geodynamic development of Atlantic-type continental margins, *Anais da Academia Brasileira de Ciencias,* v. 48, p. 37-42.

Bott, M.H.P. and Dean, D.S., 1972. Stress systems at young continental margins, *Nature Physical Science,* v. 235, p. 23-25.

Cande, S.C. and Kristoffersen, Y., 1977. Late Cretaceous magnetic anomalies in the North Atlantic, *Earth and Planet. Sci. Lett.*, v. 35, p. 215-224.

Choukrone, P., Le Pichon, X., Séguret, M., and Sibuet, J.C., 1973. Bay of Biscay and Pyrenees, *Earth and Planet. Sci. Lett.*, v. 18, p. 109-118.

Collette, B.J., 1968. On the subsidence of the North Sea area. *In Geology of shelf seas:* Edinburg and London (Donovan, Oliver and Boyd), p. 15-30.

Daily Oil Bulletin, 1973 (April 23). *Regional Geology of the Grand Banks,* p. 1-5.

Dardel, R.A., and Rosset, R., 1971. Histoire géologique et structurale du Bassin de Parentis et de son prolongement en mer. *In Histoire structurale du golfe de Gascogne:* Paris (Technip), v. 2, p. 1-28.

de Graciansky, P.C., Müller, C., Réhault, J.P., and Sigal, J., in press. Reconstruction de l'évolution des milieux de sédimentation sur la marge continentale ibérique: le flanc sud du haut-fond de Vigo et le forage DSDP IPOD 398. Problèmes de surface de compensation des carbonates. *In Séance specialisée de la Société Géologique de France,* 12-13 décembre 1977.

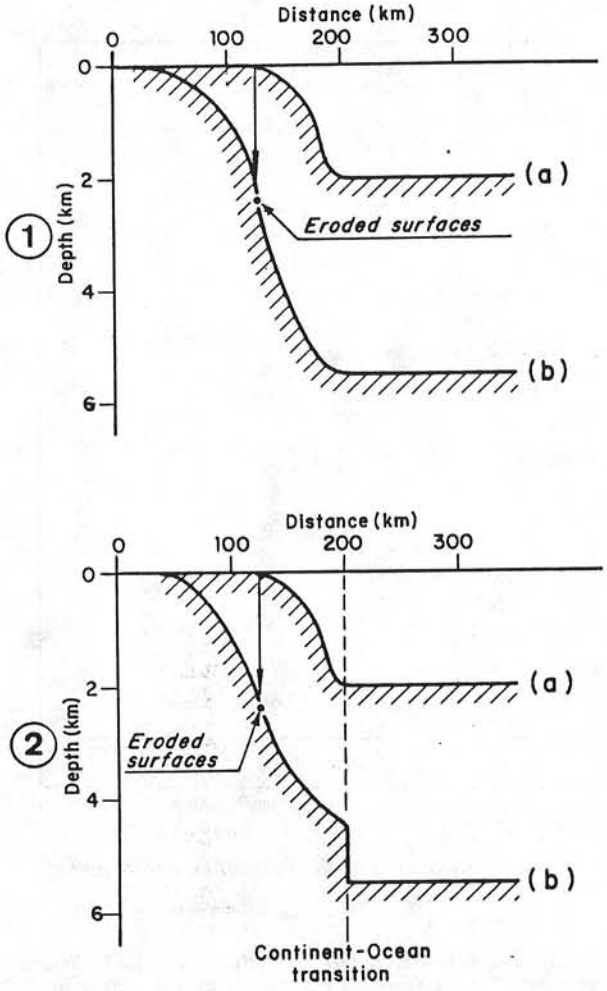


Figure 8. *Diagrams showing the vertical evolution of the Armorican and West Iberian continental margin since latest Aptian (a) to the present time (b) in the hypothesis of a flexuring of the continental margin with (1) or without (2) coupling of oceanic and continental crusts. Eroded surfaces at zero level in the Early Cretaceous are actually at 2.4 km.*

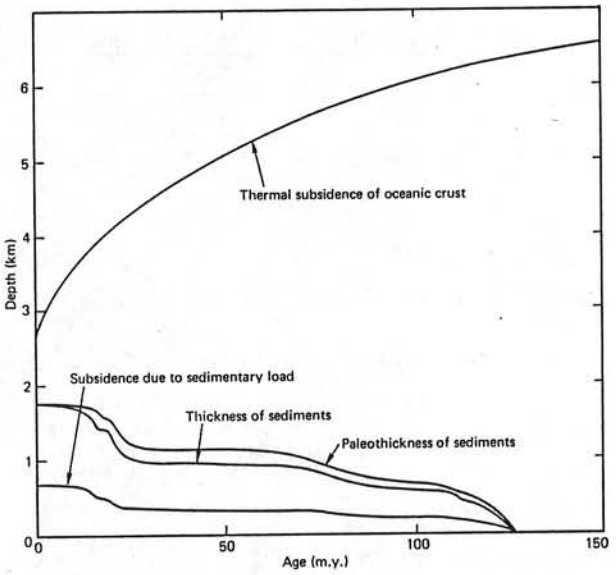


Figure 9. *Oceanic subsidence curve after Le Pichon et al. (1976). Sediment thickness, paleothickness of sediments taking into account the compaction of sediments, and local isostatic readjustment due to sedimentary load are calculated as a function of time at the level of Site 398.*

*continental margins and offshore petroleum exploration:* Canadian Society of Petroleum Geologists, Calgary, Alberta, Canada, p. 103-131.

Dupeuble, P.A., Réhault, J.P., Auxiétre, J.L., Dunand, J.P., and Pastouret, L., 1976. Résultats de dragages et essai de stratigraphie des bancs de Galice et des montagnes de Porto et de Vigo (marge occidentale ibérique), *Marine Geology,* v. 22, p. M37-M49.

Falvey, D.A., 1974. The development of continental margins in plate tectonic theory, *Australian Petrol. Explor. Assoc.*, v. 14, p. 95-106.

Foucher, J.P., and Sibuet, J.C., in press. Thermal models of passive margin evolution, *Phil. Trans. of the Roy. Soc. of London.*

Gradstein, F.M., Williams, G.L., Jenkins, W.A.M., and Ascoli, P., 1975. Mesozoic and Cenozoic stratigraphy of the Atlantic continental margin, Eastern Canada. *In* Yorath, C.J., Parker, E.R., and Glass, D.J. (Eds.), *Canada's*

Hayes, D.E. and Rabinowitz, P.D., 1975. Mesozoic magnetic lineations and the magnetic quiet zone off northwest Africa, *Earth and Planet. Sci. Lett.*, v. 28, p. 105–115.

Jansa, L.F. and Wade, J., 1975. Geology of the continental margin off Nova Scotia and Newfoundland. Offshore Geology of Eastern Canada, *Canadian Geological Survey Paper 74-30,* v. 2, p. 51-105.

Kent, P.E., 1977. Vertical tectonics associated with rifting and spreading (abstract). *In The evolution of passive continental margins in the light of recent deep drilling results*: Meeting of the Royal Society, London, December 19-20.

Kristoffersen, Y. and Talwani, M., 1977. Extinct triple junction south of Greenland and the Tertiary motion of Greenland relative to North America, *Geol. Soc. of Am. Bull.*, v. 88, p. 1037-1049.

Laughton, A.S., 1972. The southern Labrador Sea: a key to the Mesozoic and early Tertiary evolution of the North Atlantic. *In* Berggren, W.A., Laughton, A.S., et al., *Initial Reports of the Deep Sea Drilling Project,* v. 12: Washington (U.S. Government Printing Office), p. 1155–1179.

Laughton, A.S., Roberts, D.G., and Graves, R., 1975. Bathymetry of the northeast Atlantic: Mid-Atlantic Ridge to southwest Europe, *Deep-Sea Research,* v. 22, p. 791-810.

Le Pichon, X., 1968. Sea-floor spreading and continental drift, *J. of Geophys. Res.*, v. 73, p. 3661-3697.

Le Pichon, X. and Sibuet, J.C., 1971. Western extension of boundary between European and Iberian plates during the Pyrenean orogeny, *Earth and Planet. Sci. Lett.*, v. 12, p. 83-88.

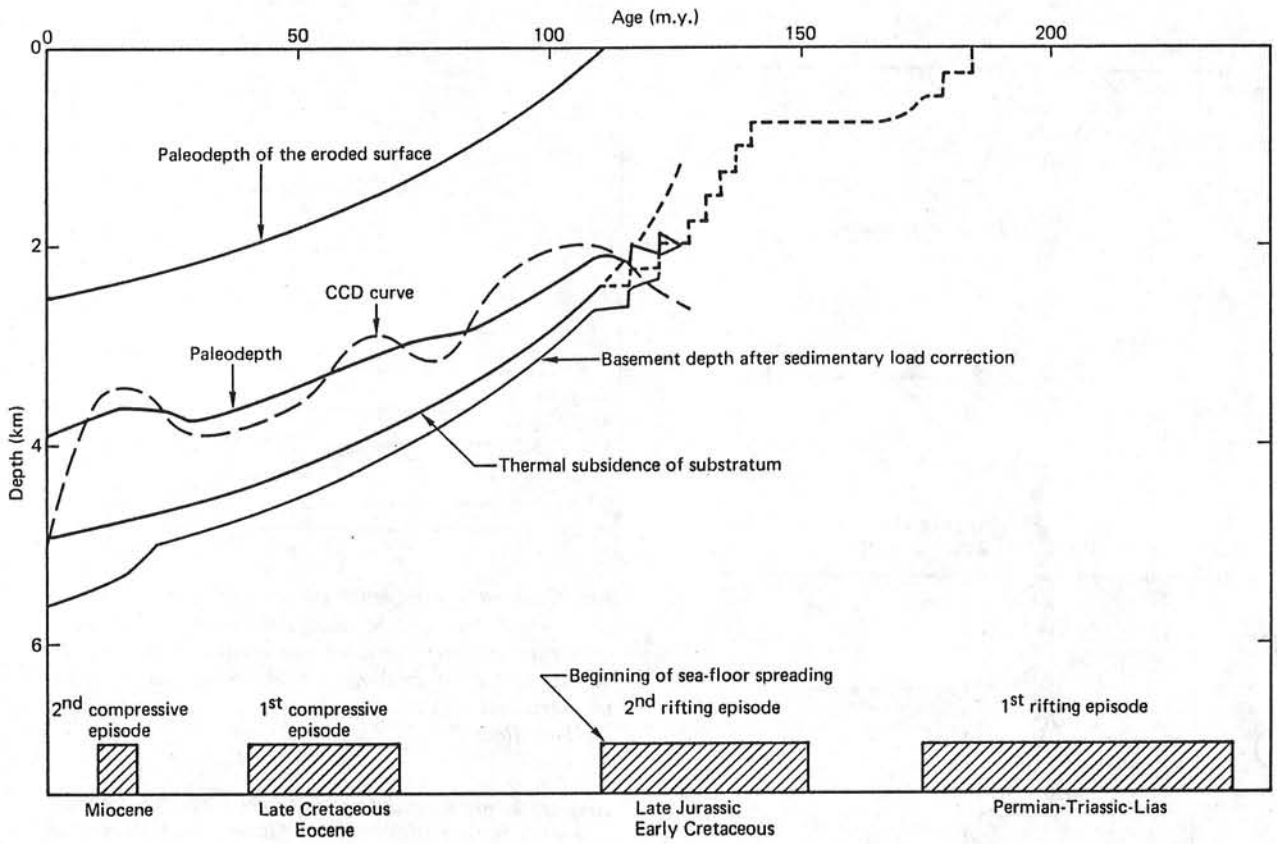


Figure 10. *Paleodepth of eroded surfaces since the Early Cretaceous. Proposed paleodepth of the substratum before and after sedimentary load correction and paleodepth at the level of Site 398.*


Le Pichon, X., Bonnin, J., Francheteau, J., and Sibuet, J.C., 1971a. Une hypothése d'évolution tectonique du golfe de Gascogne. *In* Debyser, J. et al. (Eds.), *Histoire structurale du Golfe de Gascogne:* Paris (Technip), v. 2, p. 1-44.

Le Pichon, X., Hyndman, R., and Pautot, G., 1971b. Geophysical study of the opening of the Labrador Sea, *J. of Geophys. Res.*, v. 76, p. 4724-4743.

Le Pichon, X., Francheteau, J., and Bonnin, J., 1976. Plate tectonics. *In Developments in Geotectonics:* Amsterdam, (Elsevier), v. 6, p. 1-300.

LePichon, X., Sibuet, J.C., and Francheteau, J., 1977. The fit of the continents around the North Atlantic ocean, *Tectonophysics,* v. 38, p. 169-209.

Montadert, L., Winnock, E., Delteil, J.R., and Grau, G., 1974. Continental Margins of Galicia—Portugal and Bay of Biscay. *In* Burk, C.A., and Drake, C.L. (Eds.), *The geology of continental margins:* New York (Springer-Verlag), p. 323-342.

Montadert, L., Roberts, D.G., Auffret, G.A., Bock, W.O., Dupeuble, P.A., Hailwood, E.A., Harrison, W., Kagami, H., Lumsden, D.N., Müller, C., Schnitker, D., Thompson, R.W., Thompson, T.L., and Timofeev, P.P., 1976. *Glomar Challenger* sails on Leg 48, *Geotimes,* v. 21, p. 19-23.

Montadert, L., Roberts, D.G., et al., 1977a. The nature of the continent-ocean boundary, Biscay and Rockall (abstract). Meeting on the Evolution of passive margins in the light of recent deep drilling results, London, October 19-20.

Montadert, L., Roberts, D.G., Auffret, G.A., Bock, W., Dupeuble, P.A., Hailwood, E.A., Harrison, W., Kagami, H., Lumsden, D.N., Müller, C., Schnitker, D., Thompson, R.W., Thompson, T.L., and Timofeev, P.P., 1977b. Rifting and subsidence on passive continental margins in the North-East Atlantic, *Nature,* v. 268, p. 305-309.

Olivet, J.L., Pastouret, L., Auzende, J.M., and Auffret, G.A., 1976. Armorican margin evolution in relation with the Bay of Biscay genesis (abstract), *Coll. IUSGS Durham,* April 1976.

Pitman, W.C., III, and Talwani, M., 1972. Sea-floor spreading in the North Atlantic, *Geol. Soc. of Am. Bull.*, v. 83, p. 619-646.

Ringwood, A.E. and Green, D.H., 1966. An experimental investigation of the gabbro-eclogite transformation and some geophysical consequences, *Tectonophysics*, v. 3, p. 383-427.

Rabinowitz, P.D., Cande, S.C., and Hayes, D.E., 1979. The *J* anomaly in the Central North Atlantic Ocean. *In* Tucholke, B., Vogt, P. et al., *Initial Reports of the Deep Sea Drilling Project*, v. 43: Washington (U.S. Government Printing Office), p. 879-886.

Sheridan, R.E., 1969. Subsidence of continental margins, *Tectonophysics,* v. 7, p. 219-229.

Sibuet, J.C. and Le Pichon, X., 1971. Structure gravimétrique du golfe de Gascogne et le fossé marginal nord-espagnol. *In* Debyser, J. et al. (Eds.), *Histoire structurale du Golfe de Gascogne:* Paris (Technip), v. 9, p. 1-27.

Sibuet, J.C., Ryan, W.B.F., Arthur, M., Barnes, R., Blechsmidt, G., de Charpal, O., de Graciansky, P.C., Habib, D., Iaccarino, S., Johnson, D., Lopatin, B.F., Mal-

donaldo, A., Montadert, L., Moore, D.G., Morgan, G.E., Mountain, M., Réhault, J.P., Sigal, J., and Williams, C.A., in press. Deep drilling results of Leg 47B (Galicia Bank area) in the framework of the early evolution of the North Atlantic ocean, *Phil. Trans. of the Roy. Soc. of London.*

Sibuet, J.C., de Charpal, O., Montadert, L., and Ryan, W.B.F., in press. Mouvements verticaux dans le région des bancs de Galice (Atlantique Nord-Est) d'après les résultats du Leg 47B. *In* Séance spécialisée de la Société Géologique de France, 12-13 décembre 1977.

Sleep, N.H., 1971. Thermal effects of the formation of Atlantic continental margins by continental break up, *Geophys. J. of the Roy. Astron. Soc.*, v. 24, p. 325-350.

van Hinte, J.E., 1976. A Cretaceous time scale, *Am. Assoc. of Petrol. Geol. Bull.*, v. 60, p. 498-516.

Walcott, R.I., 1972. Gravity, flexure and the growth of sedimentary basins at a continental edge, *Geol. Soc. of Am. Bull.*, v. 83, p. 1845-1848.

Watts, A.B. and Ryan, W.B.F., 1976. Flexure of the lithosphere and continental margin basins, *Tectonophysics,* v. 36, p. 25-44.

Williams, C.A., 1975. Sea-floor spreading in the Bay of Biscay and its relationship to the North Atlantic, *Earth and Planet. Sci. Lett.*, v. 24, p. 440-456.

Williams, C.A. and McKenzie, D.P., 1971. The evolution of the North-East Atlantic, *Nature,* p. 232, p. 168-173.

Wilson, R.C.L., 1975. Atlantic opening and mesozoic continental margin basins of Iberia, *Earth and Planet. Sci. Lett.*, v. 25, p. 33-43.

Winnock, E., 1971. Géologie succincte du Bassin d'Aquitaine (contribution à l'histoire du Golfe de Gascogne). *In* Debyser, J. et al. (Eds.), *Histoire structurale du Golfe de Gascogne*: Paris (Technip), v. 1, p. 1-30.

Winnock, E., Fried, E., and Kieken, M., 1973 Les caractéristiques des sillons aquitains, *Bulletin de la Société Géologique de France,* v. 1, p. 1-76.

Reprinted from Boillot, G., Winterer, E. L., Meyer, A. W., et al., 1987
*Proceedings, Initial Reports (Part A), of the Ocean Drilling Program*, Vol. 103

# 5. PHYSIOGRAPHY AND STRUCTURE OF THE WESTERN IBERIAN CONTINENTAL MARGIN OFF GALICIA, FROM SEA BEAM AND SEISMIC DATA

Jean-Claude Sibuet,[1] Jean-Pierre Mazé,[1]
Philip Amortila,[1, 2] and Xavier Le Pichon[3]

**ABSTRACT**

A new bathymetric map, based on Sea Beam data, was compiled for the continental margin south of Galicia Bank, in the area of Ocean Drilling Program (ODP) Leg 103 drilling. Using a new series of 12 single-channel seismic profiles oriented perpendicularly to the continental margin and multichannel seismic profiles previously acquired in the area, we constructed a detailed map of the surface of the tilted fault blocks and half grabens formed during the Early Cretaceous phases of rifting. Tilted fault blocks 13–18 km apart and oriented roughly north–south, are continuous over distances of as great as 60 km. We divided the upper and lower parts of the margin on the basis of magnetic data, distance between tilted fault blocks, nature of sediments involved in the rifting processes (pre- and syn-rift or only syn-rift sediments). This report also discusses the significance of the S reflector located below the tilted fault blocks.

## INTRODUCTION

In early 1982, the Seagal cruise was conducted by IFREMER (Institut Français de Recherche pour l'Exploitation de la Mer) on the *Jean Charcot* to collect Sea Beam and single-channel seismic-reflection data to investigate the early geologic history of rifting, subsidence, and sedimentation of the western Galicia continental margin. With two 90-in.$^3$ water guns and four 540-in.$^3$ air guns, 1800 km of seismic data were acquired. Sea Beam coverage was designed to avoid any ambiguity concerning lateral extension or correlation of morphologic features between profiles over the entire surveyed area (Fig. 1). Because the post-rift sedimentary cover is thin, most of the basement-rock features have bathymetric expression, and their trends are clearly established by Sea Beam data.

In this chapter, we present a new bathymetric map based on these Sea Beam data. This map has been integrated into the general bathymetric map of the northeast Atlantic Ocean, recently published by Lallemand et al. (1985a and b) (Fig. 1). The data are examined in the context of preliminary drilling results of ODP Leg 103 (Boillot, Winterer, et al., 1985, 1986; see site chapters, this volume). We also discuss these data within a geological framework, which indicates that the western Iberian continental margin was formed in an area previously affected by the late Hercynian orogeny and subsequent tensional phases (Fig. 2).

## METHODS

### Sea Beam Data Processing

The new bathymetric map of southwest Galicia margin presented in this paper was compiled exclusively from Sea Beam data. Basic data are those of the Seagal cruise, but all available Sea Beam transits acquired in the area have been used. The Sea Beam system is a multibeam echo-sounder, comprising 16 adjacent narrow beams. Width of the mapped swath beneath the track is approximately two-thirds of the water depth (Renard and Allenou, 1979). The track control of Sea Beam data used to compile the bathymetric map is shown in Figure 3.

During the Seagal cruise, twelve N95°E parallel profiles, each about 150 km long, were acquired perpendicular to the trend of the tilted fault blocks formed during the Early Cretaceous rifting episode. Profile spacing was 5.5 km. Sea Beam transverse profiles are important because they cut the Seagal N95°E profiles and provide improved navigation through bathymetric constraints. The REGINA (Recalage Graphique Interactif de la Navigation à partir du Sea Beam) software package developed by IFREMER allowed us to fit the Sea Beam bathymetric contours of two crossing lines by moving one line with respect to another. This was done on a color screen in a normal or automatic mode. If the bathymetry was not flat, each crossing gave a navigation constraint (i.e., two points corresponding to the same position). Then, this new set of Sea Beam navigation constraints was merged with the conventional navigation data set to provide a new navigation data set. The transit satellite navigation was consequently improved, and distortions owing to automatic contouring procedures were avoided near crossings. Several types of interpolation procedures could be used to create a regular grid. The size of the grid net and the smoothing rate of Sea Beam data were chosen as a function of both the navigation accuracy and the Sea Beam coverage. The resulting bathymetric contour map appears in Figure 4. The Sea Beam coverage is about 50% in the western part of the study area but only about 30% in the upper part of the margin to the east. The accuracy of the bathymetric map consequently diminishes slightly eastward. Depths are in uncorrected meters (assuming a water velocity of 1500 m/s), and the bathymetric contour interval is 50 m. Detailed maps having 10-m isobath spacing are shown near ODP Leg 103 sites.

A three-dimensional bathymetric diagram was also constructed (Fig. 5; see frontispiece, this volume), presenting a viewpoint, vertical exaggeration, and smoothing rate that give the best exhibition of the Galicia margin morphologic trends.

### Seismic-Refraction and -Reflection Velocities

Three seismic-refraction profiles using sonobuoys were acquired in the abyssal domain during the Seagal cruise (location in Fig. 3). The seismic source was four 940-in.$^3$ air guns towed 10 m below sea surface at a speed of 6 kt. Shots were spaced every 25 s. Velocities and thicknesses were calculated from both wide-angle reflection and refraction arrivals (Le Pichon et al.,

[1] IFREMER Centre de Brest, B.P. 337, 29273 Brest cédex, France.
[2] Now at Geophysical Company of Norway (U.K.), The GECO Centre, Knoll Rise, Orpington, Kent BR6 OXG, England.
[3] Ecole Normale Supérieure, Département de Géologie, 24, rue Lhomond, 75231 Paris cédex 05, France.

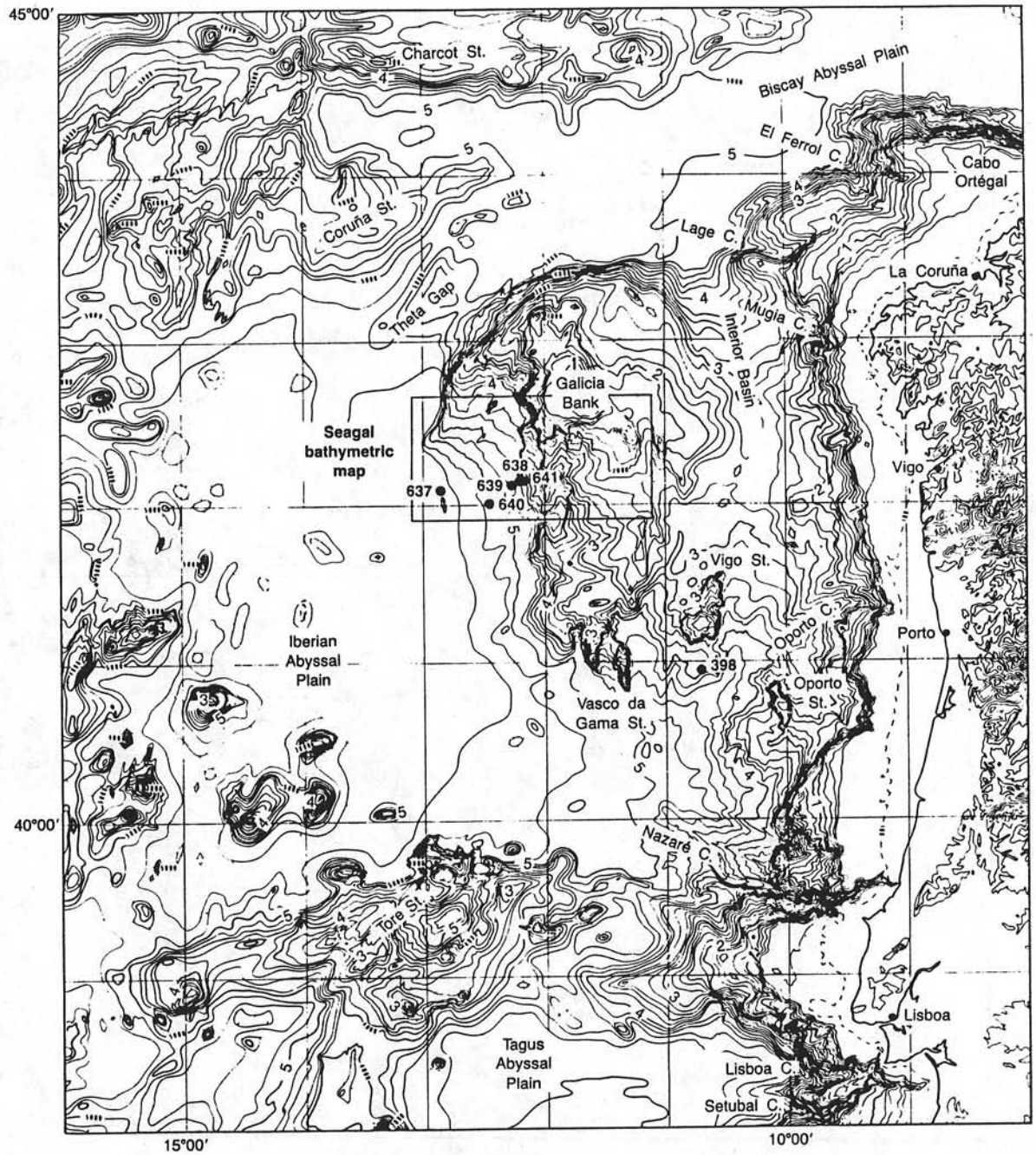


Figure 1. Bathymetric map of the Galicia Bank area (after Lallemand et al., 1985a and b). Contour spacing 200 m; for ease of identification, contours are labeled in both meters (smaller numbers) and kilometers (larger numbers). ODP sites are located within the box showing the limits of the Seagal bathymetric map.

1968). Table 1 lists sonobuoy refraction and reflection velocities based on the assumption of a surface-sound-channel velocity of 1.51 km/s. Because the refraction profiles were not reversed and were shot perpendicularly to the basement features, velocities determined for the tilted fault blocks and the lower crust are not precise. Nevertheless, these results are consistent with the compressional wave velocities (Fig. 6) obtained by the Dix relation from root mean square (rms) velocity spectra after processing the multichannel seismic profile GP-08 located near the refraction profiles (Groupe Galice, 1979; Fig. 3).

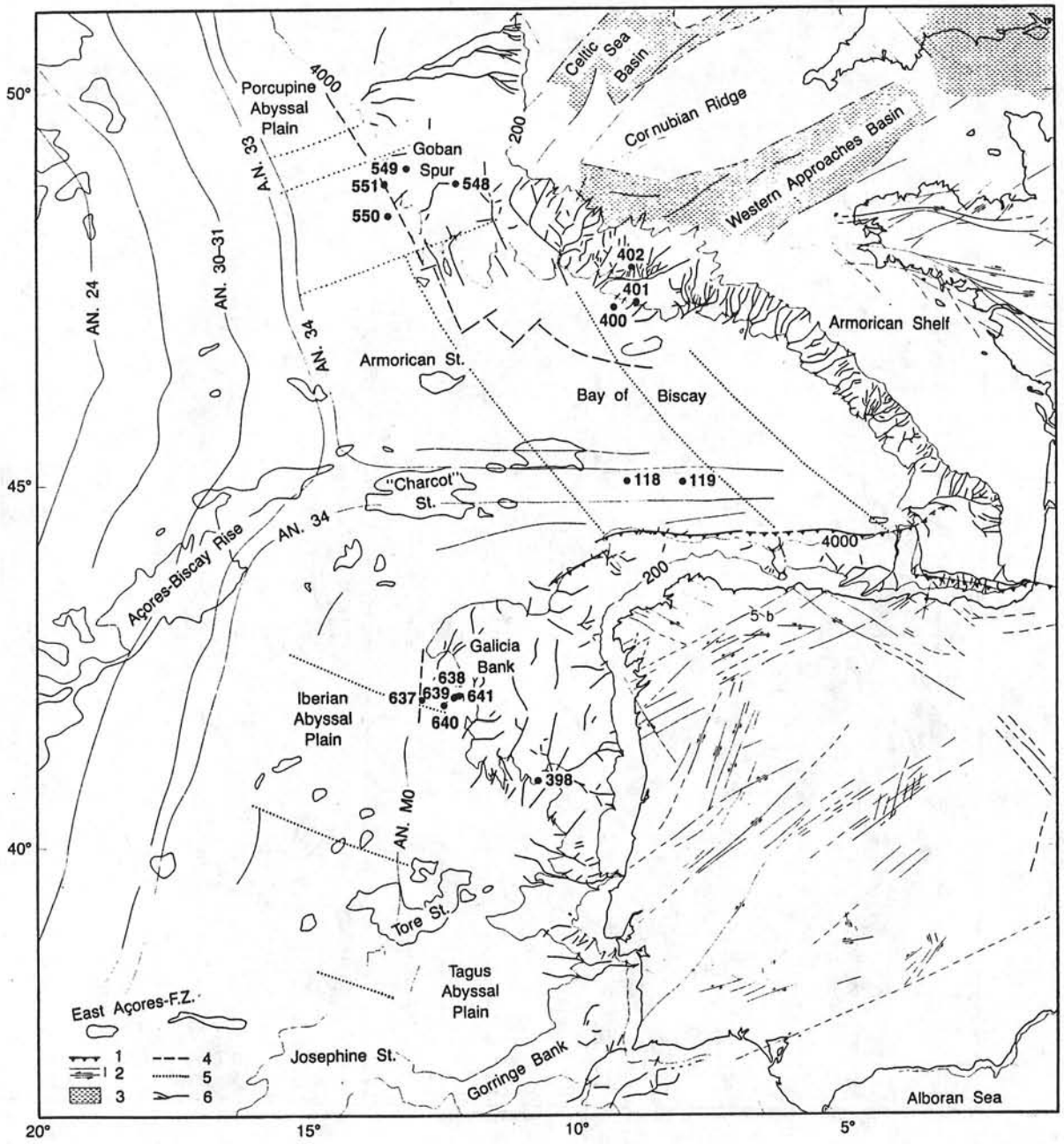


Figure 2. General structural map of the northeast Atlantic, showing identified magnetic anomalies (Guennoc et al., 1978, 1979; Sibuet and Ryan, 1979a; Verhoef et al., 1986). Canyon trends are shown on the continental margins (Lallemand and Sibuet, in press): (1) north Iberian Paleogene thrusting front; (2) late Hercynian faults on land and continental shelves, after Parga (1969), Arthaud and Matte (1975), Montadert et al. (1979d), and Sibuet et al. (1985); (3) approximate present limit of Jurassic sediments in the Western Approaches and Celtic Sea Basins (Pegrum and Mountenay, 1978); (4) continent/ocean boundary (Sibuet et al., 1985); (5) flow lines of initial opening of Bay of Biscay and northeast Atlantic Ocean (Olivet et al., 1984; Savostin et al., 1986); (6) directions of canyon orientations on the continental margins (Lallemand and Sibuet, in press).

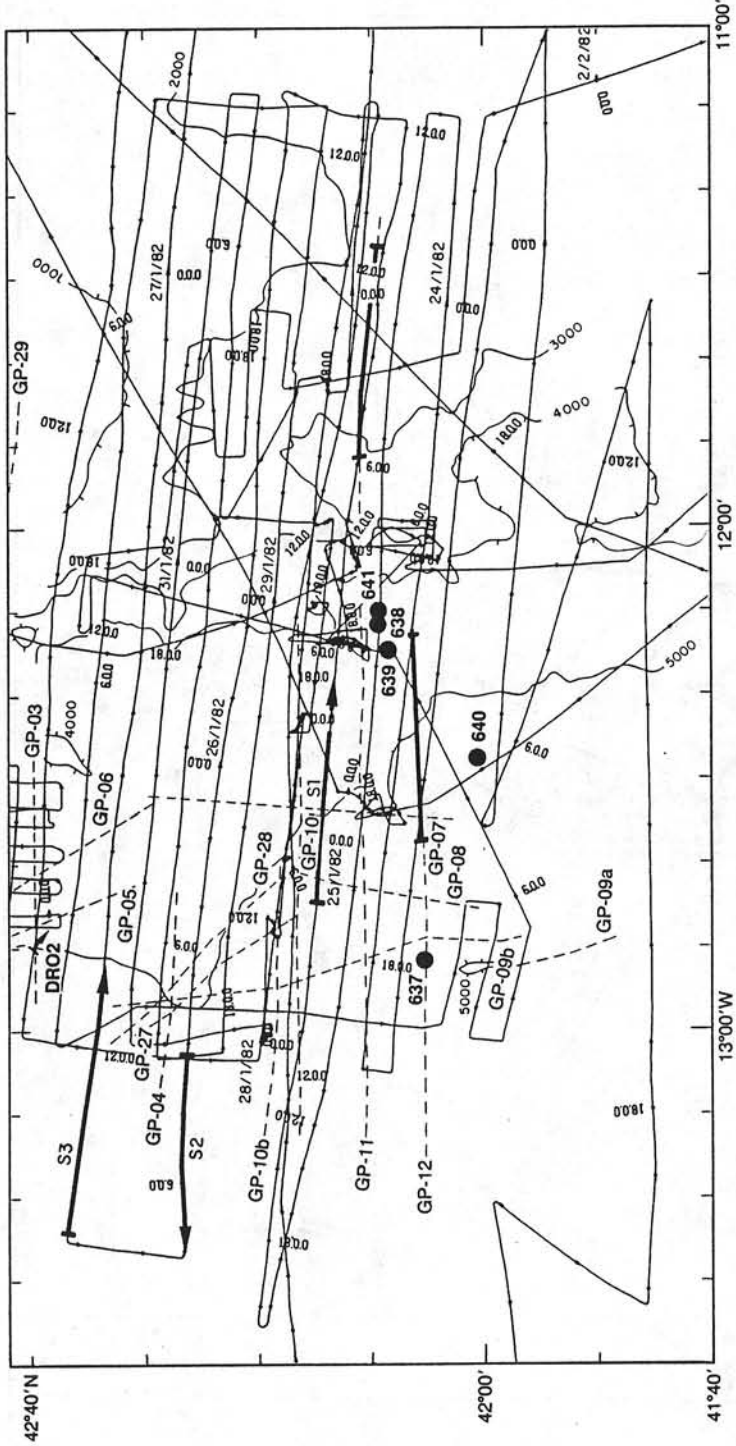


Figure 3. Location map of the Sea Beam and single-channel seismic profiles acquired during the Seagal cruise (continuous lines) and IFP-CNEXO multichannel seismic profiles (dashed lines). Location of refraction sonobuoys S1, S2, and S3 and the parts of multichannel lines GP-11 and GP-12 shown in Figure 10 are indicated. Location of sites drilled during ODP Leg 103 are also shown.

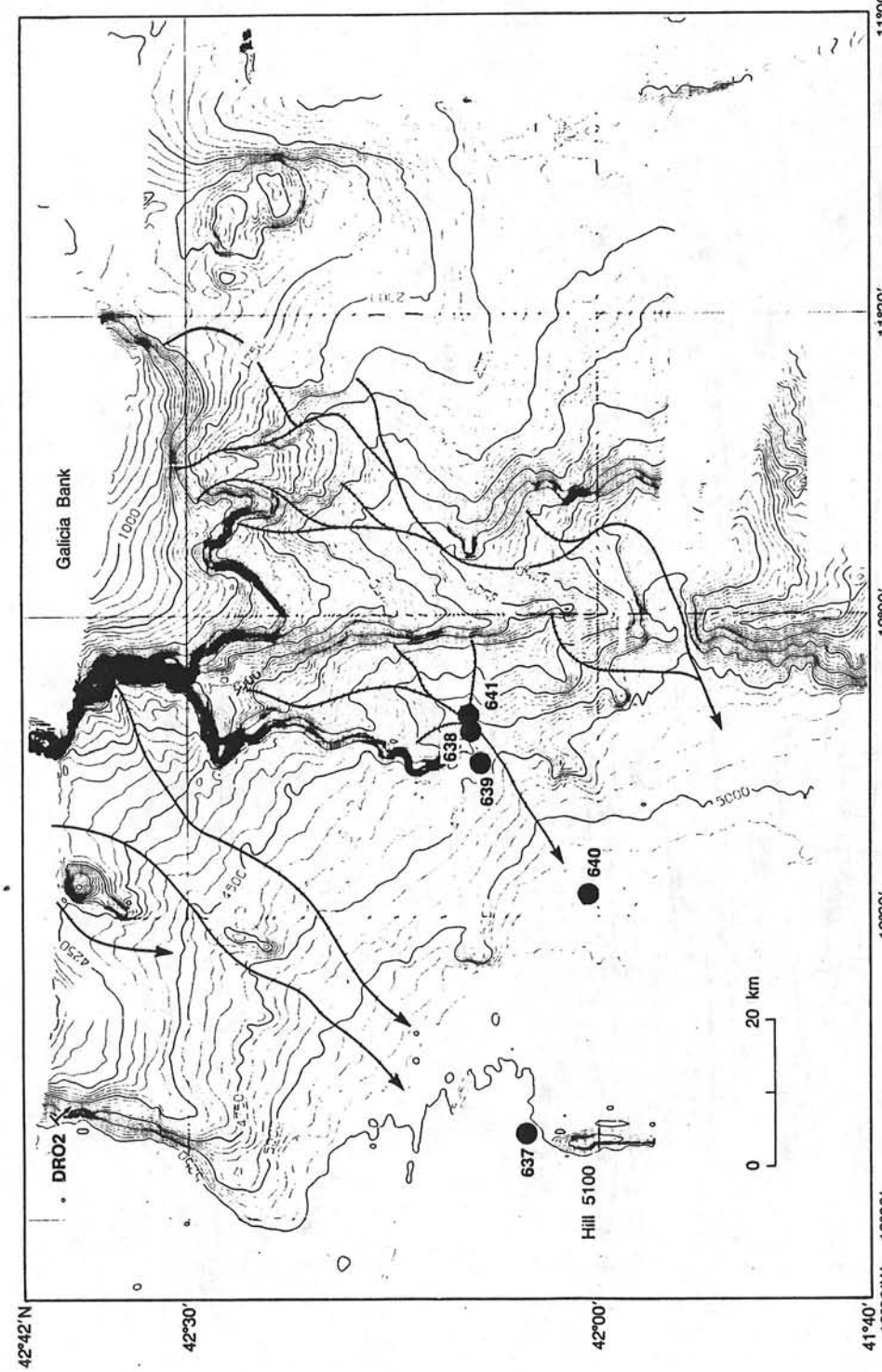


Figure 4. Sea Beam bathymetric map, in Mercator projection, of southwest Galicia margin, established using Sea Beam data (location of tracks in Fig. 3). Depths are in uncorrected meters (water velocity 1500 m/s). Contour spacing, 50 m. ODP sites drilled during Leg 103 and DR02 dredge are located. Main canyon trends are highlighted.

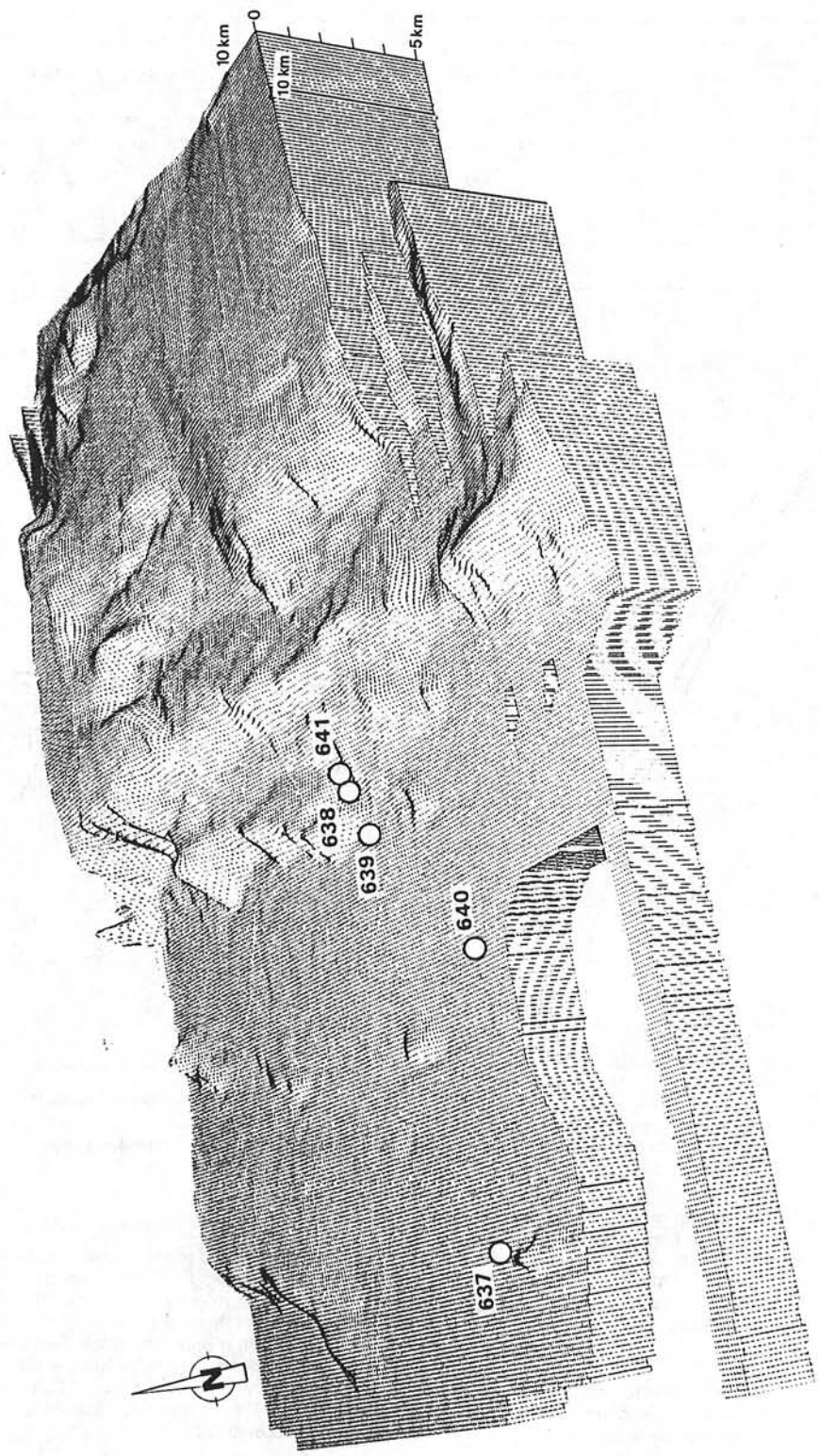


Figure 5. Block diagram showing the bathymetry of southwest Galicia margin. Vertical exaggeration, ×5. Grid dimension, 500 m. Point of view was chosen to highlight the north–south basement structures. Diagram provided by G. Riou and A. Normand of the IFREMER ATDO (Assistance et Traitement des Données Océaniques). See frontispiece (this volume) for a color version of this diagram.

**Table 1. Refraction and wide-angle reflection results from sonobuoy data.**

| Refraction profile | Position of the ends of profiles | | Velocity of layers (in km/s) | | | | | | | Thickness of layers (in km) | | | | | |
|---|---|---|---|---|---|---|---|---|---|---|---|---|---|---|---|
| | Latitude | Longitude | Water | A | B | C | D | E | F | Water | A | B | C | D | E |
| S1 | 42°15'N<br>42°13'N | 12°46'W<br>12°19'W | 1.51 | 2.05 | 2.55 | 2.9 | 4.33 | 6.1 | 8.01 | 5.175 | 0.595 | 1.02 | 0.373 | 0.97 | 1.47 |
| S2 | 42°26'N<br>42°27'N | 13°03'W<br>13°27'W | 1.51 | 2.36 | | 3.12 | 4.2 | 5.87 | 7.8 | 5.287 | 1.12 | | 0.5 | 1.06 | 0.93 |
| S3 | 42°37'N<br>42°34'N | 13°24'W<br>12°53'W | 1.51 | 2.36 | | 3.14 | 4.3 | 5.8 | — | 5.280 | 1.64 | | 1.1 | 0.31 | — |

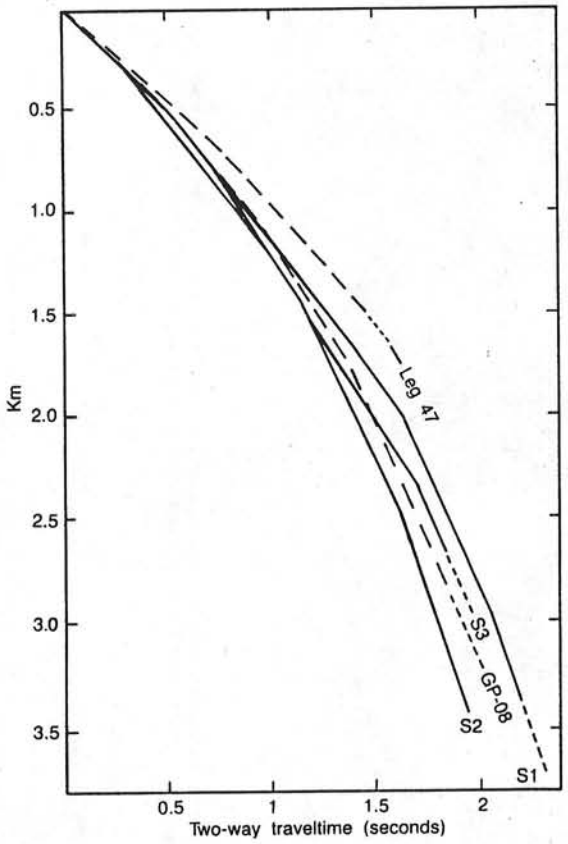


Figure 6. Results of the three sonobuoy profiles listed in Table 1, compared with velocities calculated from multichannel seismic profile GP-08 (Groupe Galice, 1979) and Leg 47B results (Sibuet, Ryan, et al., 1979b).

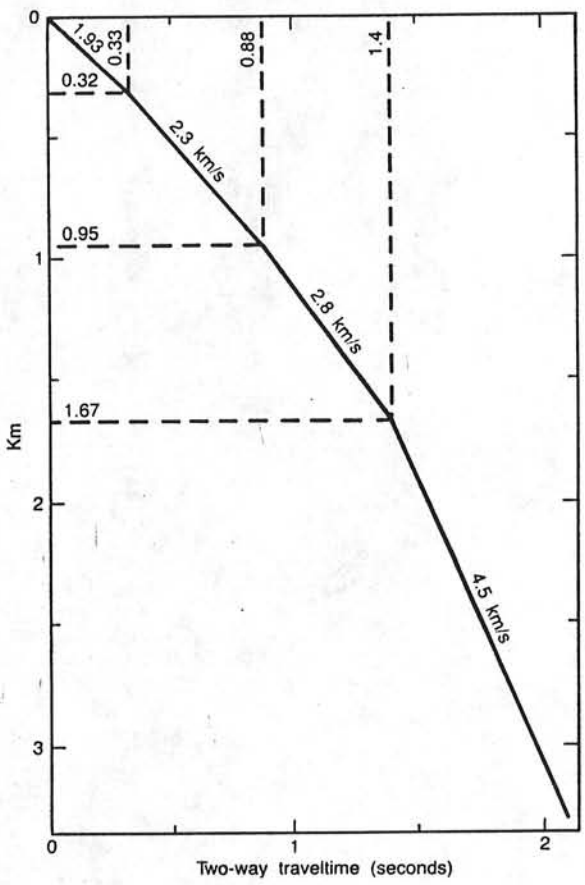


Figure 7. Depth-velocity profile adopted to compute basement depths on southwestern Galicia margin.

Results of the velocity-depth correlation at Site 398 (Sibuet, Ryan et al., 1979a) are also reported. A fair agreement exists between the different data. We adopted the velocity-depth profile of Figure 7 to compute the thickness of the post-rift sediment layers and to deduce the depth of sediments affected by rifting for the entire southwestern Galicia margin.

## REGIONAL TECTONIC SETTING

The starved continental margin of western Galicia Bank was formed during several phases of extension since the Permian and was affected by early Tertiary and Miocene compressions.

### Permian to Lias Phases of Distension

The Permian to Triassic phase of distension documented in northwest Europe (Ziegler, 1978, 1981) and in Morocco (Manspeizer et al., 1978) is interpreted as being the first phase of doming before rifting in the western Iberian Peninsula (Mougenot et al., 1979). Extension is indicated in late Triassic-early Liassic time by the large basins occurring in Algarve (Mougenot et al., 1979) and probably in the eastern part of the Tagus Abyssal Plain (Olivet et al., 1984) where thick Liassic and Dogger sedimentary strata accumulated.

Only during the Liassic did the large subsidence rates occur that are observed in narrow and deep basins, for example, as in Portugal. This Liassic phase of distension, which is also marked by large volcanic emissions, is associated with the first rifting phase (Mougenot et al., 1979). Sibuet and Ryan (1979) emphasized this phase in their interpretation of the subsidence history at Deep Sea Drilling Project (DSDP) Site 398 (Sibuet, Ryan et al., 1979a). During the Middle Jurassic, marine sediments deposited in Portugal (Lusitanian Basin, Mougenot et al., 1979) suggest the existence of a regional subsidence that we associate with the thermal cooling of the lithosphere after the late Triassic–Liassic phase of rifting.

### Latest Jurassic to Early Cretaceous Phases of Distension

The latest Jurassic to Early Cretaceous phases of distension resulted in the formation of the present-day continental margins of the North Atlantic Ocean north of the Azores-Gibraltar fracture zone. These phases affected the entire northwest European and Arctic–North Atlantic rift system. The timing and geometry of this rifting phase have been well established both from the interpretation of seismic data and from DSDP and ODP holes drilled on the eastern North Atlantic continental margins during DSDP Legs 47B, 48, 80, 81, and ODP Leg 103 (Sibuet, Ryan, et al., 1979b; Montadert, Roberts, et al., 1979a; de Graciansky, Poag, et al., 1985; Roberts, Schnitker, et al., 1984; Boillot, Winterer, et al., 1985, 1986).

From Goban Spur to Gibraltar (Fig. 2), the overall tectonic style of continental-margin deformation is characterized by a series of tilted fault blocks bounded by normal or listric faults, which delineate half grabens. Tilted fault blocks developed within the Jurassic sedimentary cover. Western Galicia margin is the most spectacular example of this tilted fault-block geometry. One of the most important results of ODP Leg 103 was to show that the extension and deepening of the western Galicia continental margin occurred in several stages. The Jurassic carbonate platform faulted and subsided during the latest Tithonian–earliest Valanginian. Depressions were partly buried by Valanginian and Hauterivian interbedded turbidite sandstones and claystones, themselves affected until the Aptian by normal faulting and rotation of fault blocks (Boillot, Winterer, et al., 1985, 1986). Consequently, faulting and tilting began at least as early as Early Cretaceous and continued episodically until late Aptian. A comparison with the land and shelf geology shows that the latest Jurassic–Early Cretaceous phase is in fact a succession of tectonic phases, the main one being the Austrian phase (Baranyi et al., 1976; Kamerling, 1979).

### Onset of Seafloor Spreading

The initiation of seafloor spreading in the northeast Atlantic is well documented in DSDP and ODP data by both dating of the first oceanic crust and dating of the regional unconformity that marks the end of the rifting phase on continental margins. The oldest oceanic magnetic anomalies identified are M0 (late Aptian) west of Galicia Bank and 34 (late Santonian) in the Bay of Biscay and west of the British Isles (Fig. 2; e.g., Guennoc et al., 1978, 1979; Sibuet and Ryan, 1979). From drilling results, the first appearance of oceanic crust was dated to be late-early Albian at Goban Spur (Masson et al., 1985), early Albian near the Meriadzek Terrace in the Bay of Biscay (Montadert et al., 1979c; Groupe Cymor, 1981), and late Aptian west and south of Galicia Bank (Sibuet and Ryan, 1979; Boillot, Winterer, et al., 1985, 1986). This indicates that the initial formation of oceanic crust after the Late Jurassic–Early Cretaceous rifting phase propagated from south to north.

### Cenozoic Compressive Phases

From Late Cretaceous to late Eocene, compressive movements resulted in uplift of the Pyrenees, the maximum tectonic activity being during the Eocene. The Pyrenees, the northern Spanish marginal trough, the Açores-Biscay Rise, and the King's Trough complex have been interpreted, according to distribution of magnetic anomalies in the North Atlantic, as features created at the plate boundary between Iberia and Europe (Le Pichon and Sibuet, 1971) and resulting from a counterclockwise rotation of Iberia with respect to Europe around a pole located west of Morocco (Olivet et al., 1984).

In the oceanic area, maximum deformation occurred near the north Iberian–European plate boundary. Numerous areas were uplifted during late Eocene, including both the oceanic domain and the continental margins (Montadert et al., 1979d; Groupe Galice, 1979; Groupe Cybère, 1984; Sibuet et al., 1985). In the Galicia Bank area, the large faults that run along the northwest edge of Galicia Bank continue to the southwest, where large deformations with clear reverse faulting affect the Mesozoic and Eocene sedimentary layers (Montadert et al., 1979d; Réhault and Mauffret, 1979; Groupe Cybère, 1984). Contemporaneous movements occurred in the Interior Basin, between Galicia Bank and the continent.

Numerous studies show that deformation occurred on land in the whole continental domain of North Africa, Iberia, and Europe (de Charpal et al., 1974; Letouzey and Trémolières, 1980; Bergerat, 1985). The stress field is characterized by a north–south horizontal compression, in agreement with the relative north–south compressive motion of Africa with respect to Europe (Savostin et al., 1986), which resulted in a transcurrent tectonic regime from northeastern Iberia to the Rhine graben and the Bohemian Massif.

The Miocene compressive episodes mostly affected the Tore–Madeira Rise, the Gorringe and Ampère Banks, and the adjacent continental margins, as well as the Betic and Rif System on land. North of this deformation belt and up to the northern Bay of Biscay margin, hiatuses reveal Miocene movements (Site 398, Sibuet, Ryan, et al., 1979a) and a slight angular unconformity (Olivet et al., 1976; Groupe Galice, 1979).

## MORPHOLOGY OF THE SOUTHWEST GALICIA BANK CONTINENTAL MARGIN

Detailed bathymetric Sea Beam surveys were performed on the western Iberian continental margin north of Cap Ortegal (Groupe Cybère, 1984), north (Groupe Transmarge, 1984) and east (this study) of Galicia Bank, on Vigo, Oporto, and Vasco da Gama Seamounts south of Galicia Bank (Mougenot et al., 1984), in Nazaré Canyon (Groupe Transmarge, 1982), and on Tore Seamount (J. L. Olivet, personal communication, 1985). These features were included in the bathymetric map by Lallemand et al. (1985a and b, Fig. 1), which provides a more precise morphologic depiction than does the Laughton et al. (1975) document.

The roughly north–south continental margin west of Iberia consists of two contrasting physiographic provinces north and south of 40°N latitude. Galicia Bank lies in the northern province, which also includes several other seamounts such as Vigo, Porto, and Vasco da Gama. The margin is separated from the narrow continental shelf by the Interior Basin, a large sediment-filled depression, which trends generally north–south and stretches from the southern Bay of Biscay to Vigo Seamount. The seamounts may represent either horsts formed during the Early Cretaceous rifting episode (Laughton et al., 1975; Groupe Galice, 1979; Montadert et al., 1979d) or uplifted Eocene struc-

tures (Boillot et al., 1979; Mougenot et al., 1984). South of 40°N latitude, large prominent canyons (Nazaré, Lisboa, Setubal, and Saõ Vicente Canyons) appear to be controlled by the late Hercynian fracture pattern (e.g., Boillot et al., 1974; Sibuet and Berthois, 1979).

The Seagal Sea Beam survey was restricted to the part of the continental margin south of Galicia Bank from the typical oceanic crust east of 13°W longitude to the first tilted fault block facing the Interior Basin at 11°25′W longitude (Figs. 1 and 4). The principal morphologic trends are the roughly north–south tilted fault block features, which correspond either to ridges (e.g., at 12°W longitude), to steep bathymetric gradients (e.g., at 12°12′W longitude), to a line of elongated seamounts (e.g., at 12°30′W longitude), or to a combination of steep gradients and elongated seamounts (e.g., at 12°50′W longitude). We interpret these features as having resulted from progressive westward burial below sediment of tilted north–south basement fault blocks.

Canyons can be traced continuously throughout the study area (Figs. 4, 8, and 9). A dendritic pattern with primary and secondary tributaries is observed on steep slopes between 11°40′ and 12°12′W longitude, whereas such canyons are absent or poorly defined when slope gradients decrease. The trends of the major canyons roughly follow the north–south basement structures and are bayonet-shaped where they pass through the north–south basement structures. The main canyons are fed from the north–south basement highs located on each of their sides (Fig. 9). ODP Site 641 is at the intersection of one main canyon and two tributaries just at the edge of the only observed depression in the area (Fig. 9). This depression, about 1 km in diameter and 20 m deep, is at a major slope break (7° to 2°). Such depressions, called "splash pools" by Le Pichon and Renard (1982), are commonly observed on Sea Beam or Gloria records (Le Pichon and Renard, 1982; Kenyon et al., 1978) acquired on continental margins. Surveys made from a submersible of the Provence lower continental-slope canyons demonstrate that deep-water transport can carry large boulders, which tend to accumulate where the slope flattens out. Dams are thus built across the canyons, creating bathymetric depressions (Le Pichon and Renard, 1982). Slumped sediments, including Upper Cretaceous debris were recovered in the upper section of ODP Hole 641 (Site 641 chapter, this volume); ODP Site 641 is probably located on such a dam.

## STRUCTURE OF THE SOUTHWEST GALICIA BANK CONTINENTAL MARGIN

The rift structures are illustrated by seismic profiles GP-11 and GP-12, which show a series of tilted fault blocks that delineate half grabens (Fig. 10). Normal faults bound the western side of these blocks. These structures on Galicia margin are even more impressive than the structure of two tilted fault blocks described south of the Meriadzek Terrace on the northern Bay of Biscay margin (Site 400, Montadert, Roberts, et al., 1979b). These latter two blocks display internal deformation and secondary faults, which fostered a debate about the estimated amount of extension (Le Pichon et al., 1983; Chenet et al., 1983).

One of the main results of ODP Leg 103 was to show that faulting and tilting occurred during several stages from very early Cretaceous to late Aptian (Boillot, Winterer, et al., 1985, 1986). The basement rock is composed of conglomerates with low-grade metamorphosed sedimentary rocks of possible Paleozoic age and altered volcanic rocks. Near Sites 638, 639, and 641, the upper section of the tilted fault blocks includes Tithonian and Lower Cretaceous limestones, probably resting directly on the basement rock. Syn-rift deposits probably include Valanginian and Hauterivian turbidite sandstones and claystones overlain by Barremian to Aptian limestones, thin turbidites, and debris flows.

At Site 640, located at the base of the margin, west of the previous sites, the upper section of a tilted fault block composed of Lower Cretaceous sandstones was drilled. This suggests that a second phase of rifting affected syn-rift deposits. Consequently, the 25-m.y.-long rifting, depending on the geometry of syn-rift deposits and on the position on the continental margin, affects both the pre-rift Jurassic and the syn-rift Lower Cretaceous deposits. In the following sections, we will refer to the surface lying at the top of both pre- and syn-rift sediments deformed during the different stages of the rifting phase as the *rifting surface*.

Figure 11 shows an interpretation of the composite multichannel seismic profiles GP-11 and GP-12 across the entire margin. Figure 11A is a line drawing in two-way traveltime (in seconds). Figure 11B is a depth profile without vertical exaggeration drawn from the velocity-depth profile shown in Figure 7. S1, S2, and S3 are the locations of the refraction profiles. The position of the Mohorovičić discontinuity is shown below the oceanic domain (S2) and the possibly thinned continental crust (S1).

The location of the seismic-transition zone (Fig. 11) was inferred from seismic-reflection and -refraction data, magnetic data, and ODP Site 637 results (see Site 637 chapter, this volume). The zone is probably located just west of Hill 5100, where serpentinized peridotite were dredged (Boillot et al., 1980) and drilled (Boillot, Winterer et al., 1985, 1986).

The profile presented here can be considered as a typical section across a tilted fault-block margin. Rotated fault blocks are well expressed in the upper part of the margin. In contrast, in the lower part of the margin, extending east of the Hill 5100 for more than 30 km, the top of the rifted series is highly irregular. Faulting and tilting in that region affect the Lower Cretaceous syn-rift sediments deposited during the early phases of rifting (ODP Site 640; Boillot, Winterer, et al., 1985, 1986). Below the syn-rift series, a strong reflector, named the S reflector (Figs. 10 and 11), shows undulations, which are mainly due to a pull-up effect below the tilted blocks. This reflector, however, is not strictly planar. The seismic velocity below the S reflector is about 6.1 km/s, and the Mohorovičić discontinuity is roughly 2 km below it. We shall discuss this later.

Figure 12 displays the Seagal east–west profiles in which only the topography of the top of the rifted series is shown. Profiles are represented in the east–west vertical plane without vertical exaggeration. The basement depth was calculated using the velocity–depth profile of Figure 7. The profile-to-profile correspondence of tilted fault blocks can easily be followed on the block diagram of Figure 12, which outlines the lateral extension of tilted fault blocks. The topographic map of the tilted fault blocks (Fig. 13) was established using all available seismic data (Fig. 3) and indicates the following:

1. The roughly north–south tilted fault blocks are continuous for as much as 60 km.

2. A change of about 10° in the direction of the crest and valley system is observed at 42°15′N latitude. As in the northern Bay of Biscay (Montadert et al., 1979d), a possibly transecting N100°E fault does not show any lateral displacement. On the other hand, a slight slope change is observed along the strike of the features. A similar boundary also oriented N100°E limits the southern part of Galicia Bank.

3. The tilted blocks and half-graben features dip southward about 3° west of 12°15′W longitude and about 6° east of this longitude and south of Galicia margin, as apparent in the seafloor morphology (Fig. 5).

4. The spacing between consecutive fault-block crests varies systematically between 9 and 18 km (Figs. 13 and 14). East of 12°15′W longitude, tilted fault blocks consist mostly of pre-rift

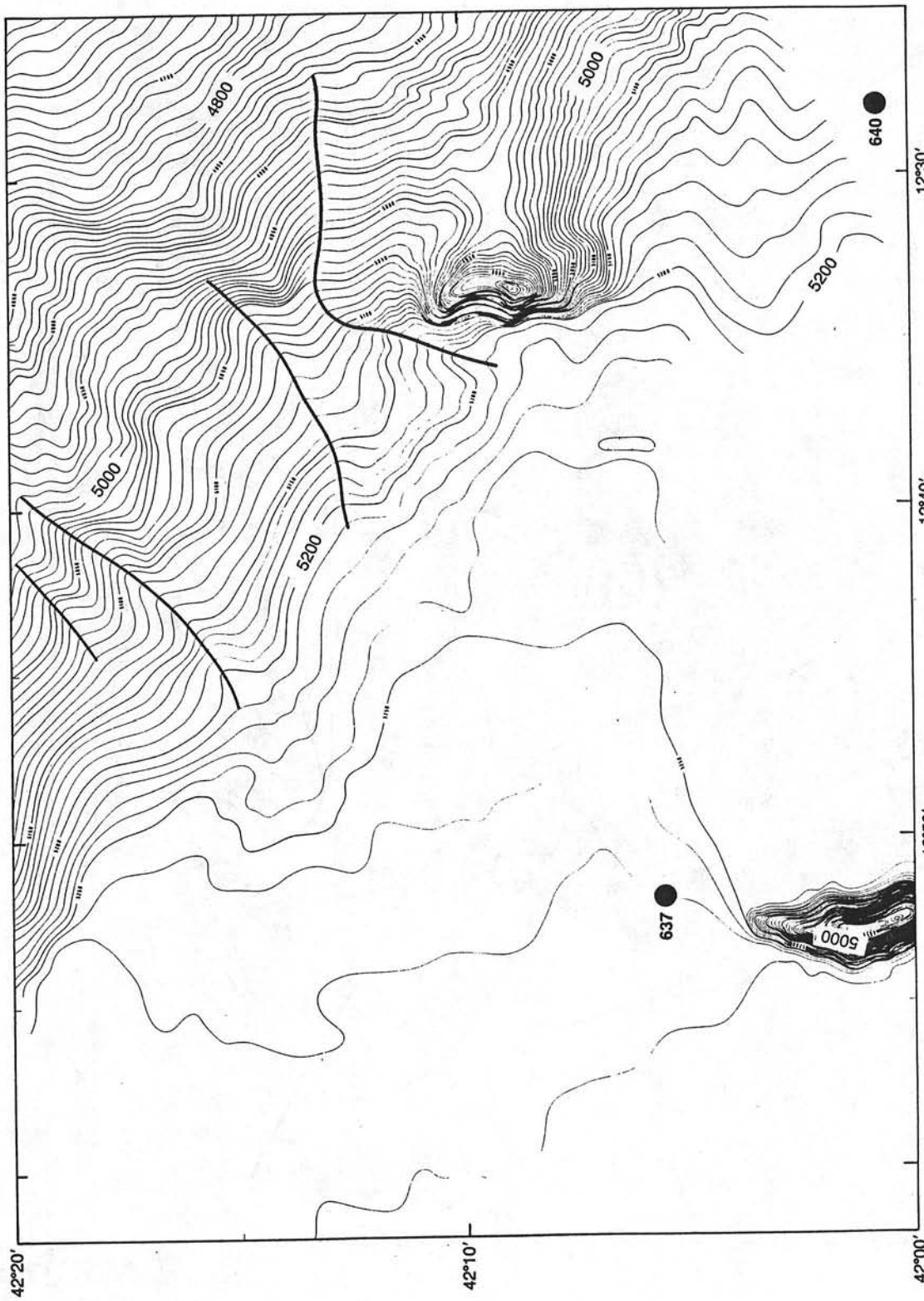


Figure 8. Detailed Sea Beam bathymetric map of the vicinity of ODP Sites 637 (north of Hill 5100) and 640 (tilted fault block). Contour spacing every 10 m. Axes of canyons are highlighted.

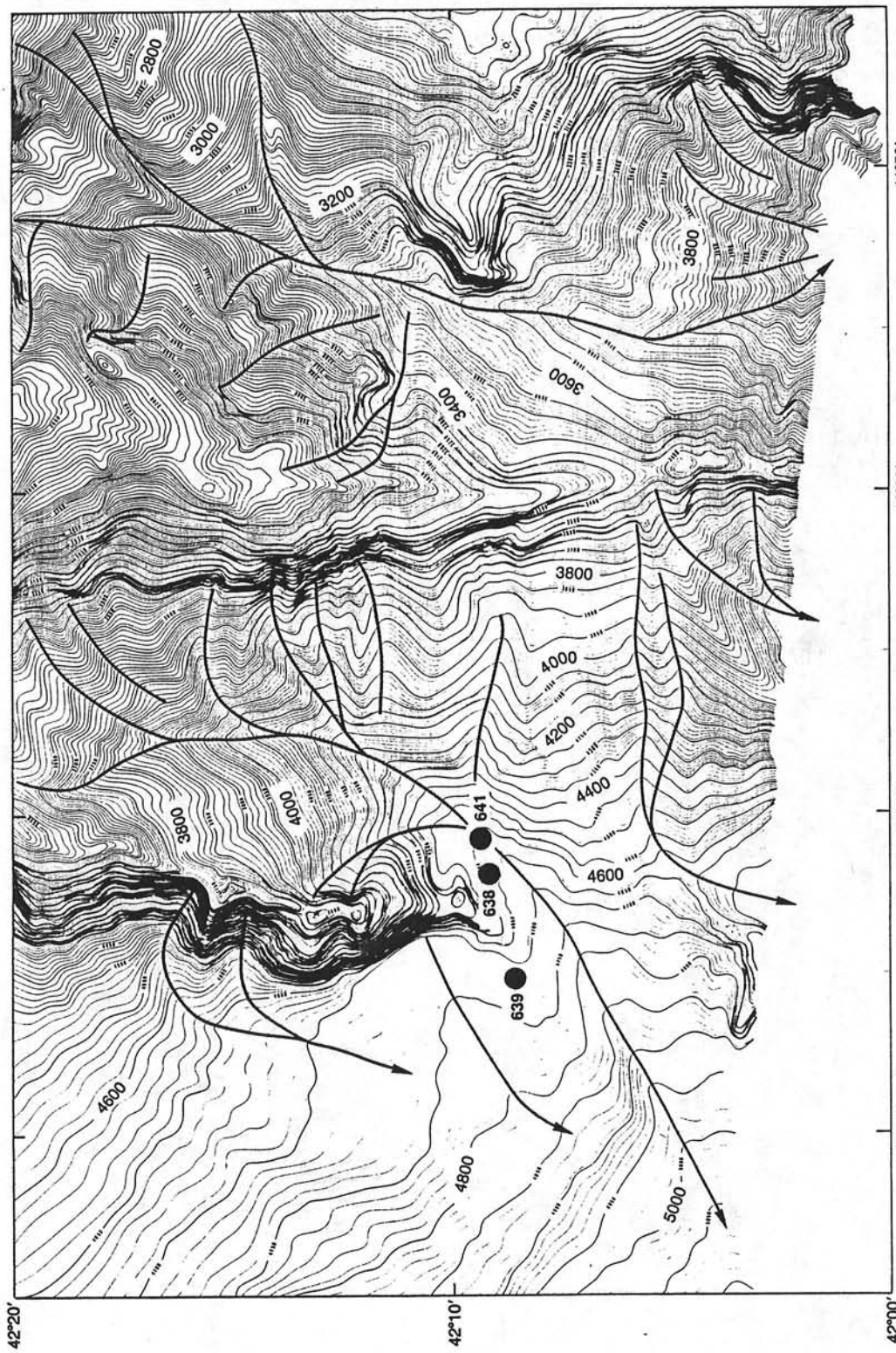


Figure 9. Detailed Sea Beam bathymetric map of the vicinity of ODP Sites 638, 639, and 641 drilled on the same tilted fault block. Contour spacing every 10 m. Main canyons and tributaries are highlighted.

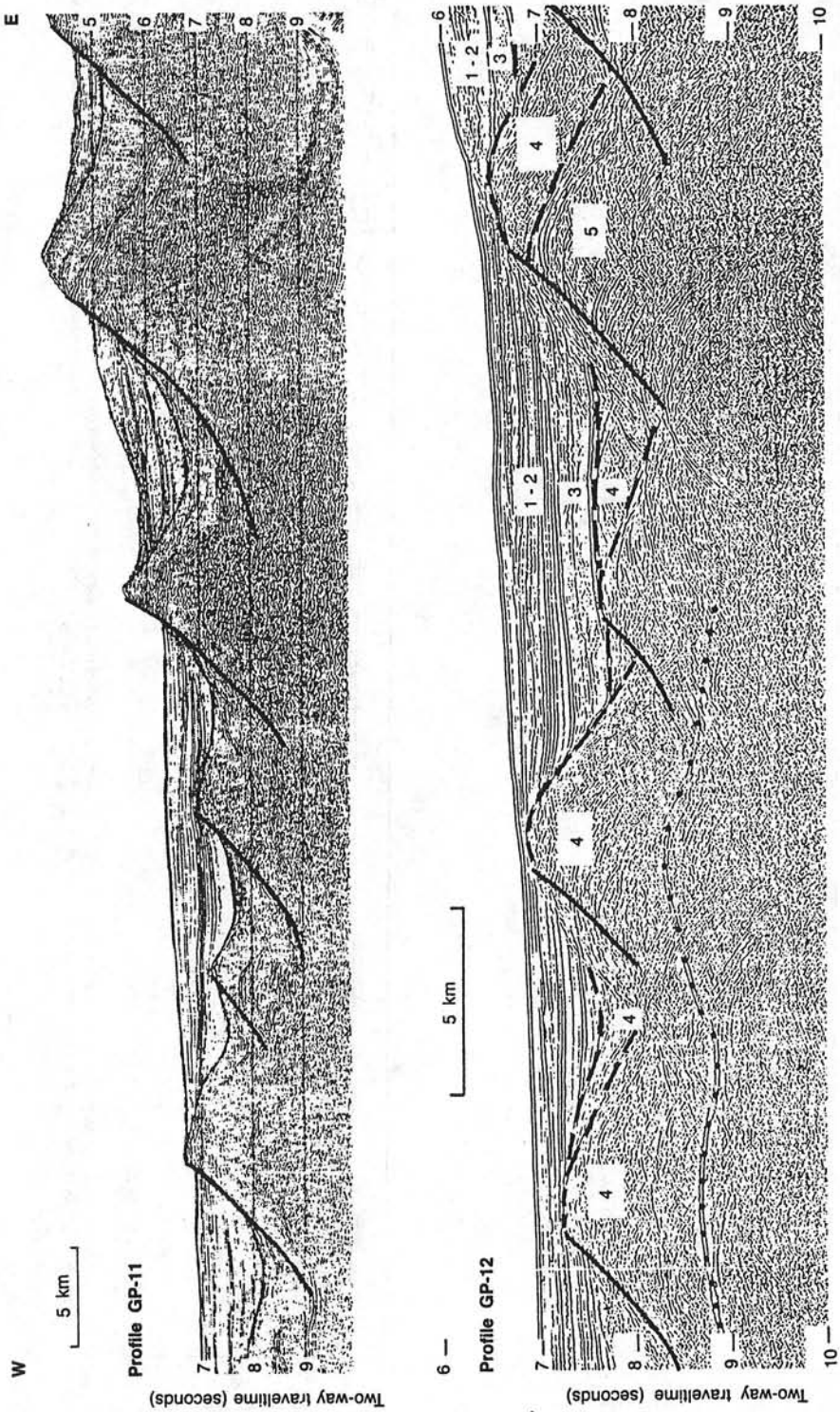


Figure 10. IFP-CNEXO multichannel seismic profiles GP-11 and GP-12 located in the upper and lower parts of Galicia margin (see Fig. 3 for profile locations). Migrated section in profile GP-11 is interpreted in terms of listric faults (after Montadert, 1982), but there is no seismic evidence for the curvature of the lower part of those faults. Profile GP-12 shows the S reflector (dotted line) below the syn-rift sediments affected by faulting and tilting during the latest phases of the Early Cretaceous rifting. Variation of traveltime shows a "pull-up" effect below the crest of the blocks, mainly owing to the difference in velocities within the blocks and sediments infilling half grabens. In the eastern part of the GP-12 profile, the tilted fault blocks include both pre- and syn-rift deposits, and the upper parts of the blocks consist of Valanginian syn-rift deposits, which were eroded during and after tilting: (1) Oligocene to Holocene; (2) Senonian to late Eocene; (3) early Albian to middle Cenomanian post-rift deposits; (4) Early Cretaceous syn-rift deposits involved or not in the tilting and faulting of blocks; (5) pre-rift sediments (Late Jurassic and older).

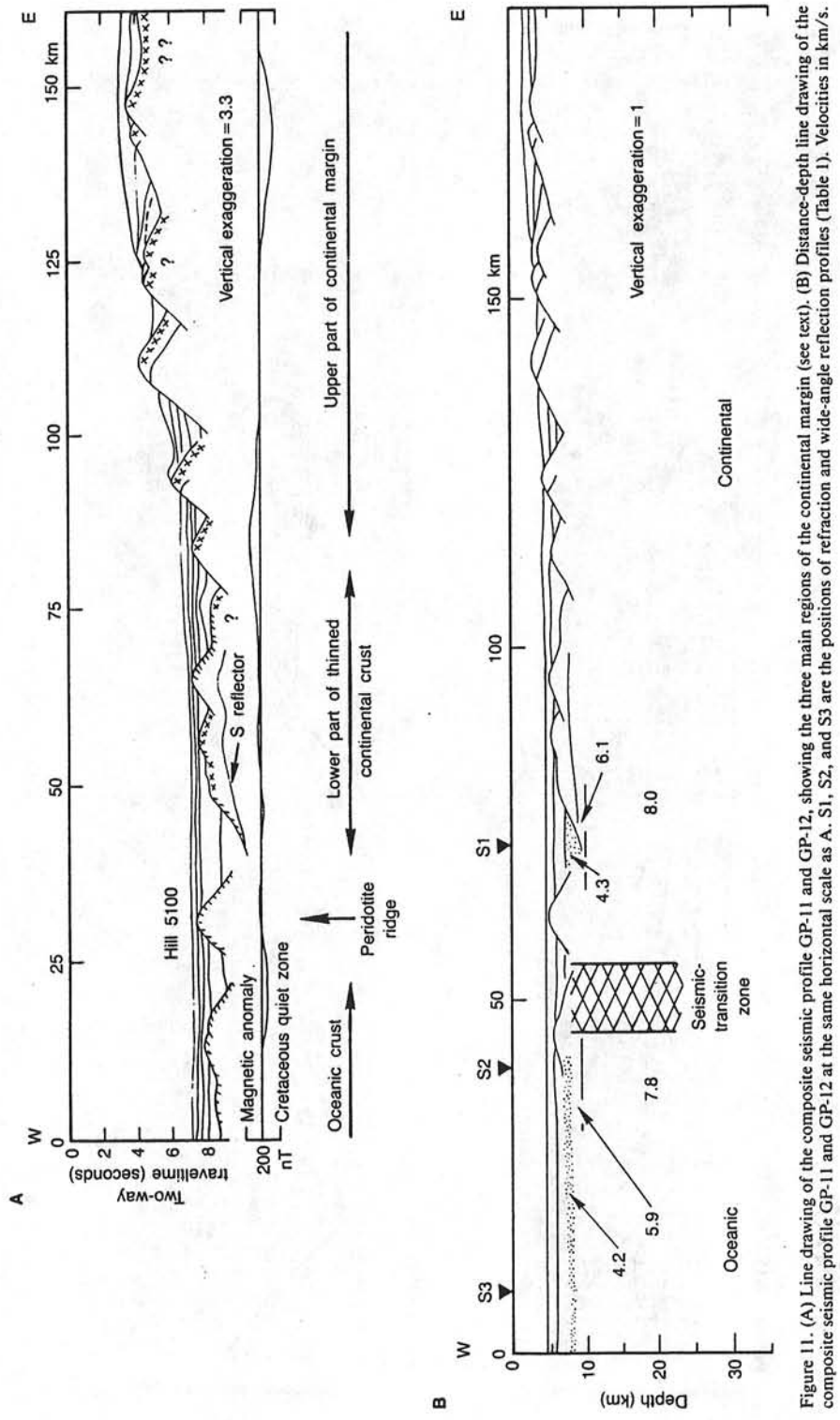


Figure 11. (A) Line drawing of the composite seismic profile GP-11 and GP-12, showing the three main regions of the continental margin (see text). (B) Distance-depth line drawing of the composite seismic profile GP-11 and GP-12 at the same horizontal scale as A. S1, S2, and S3 are the positions of refraction and wide-angle reflection profiles (Table 1). Velocities in km/s.

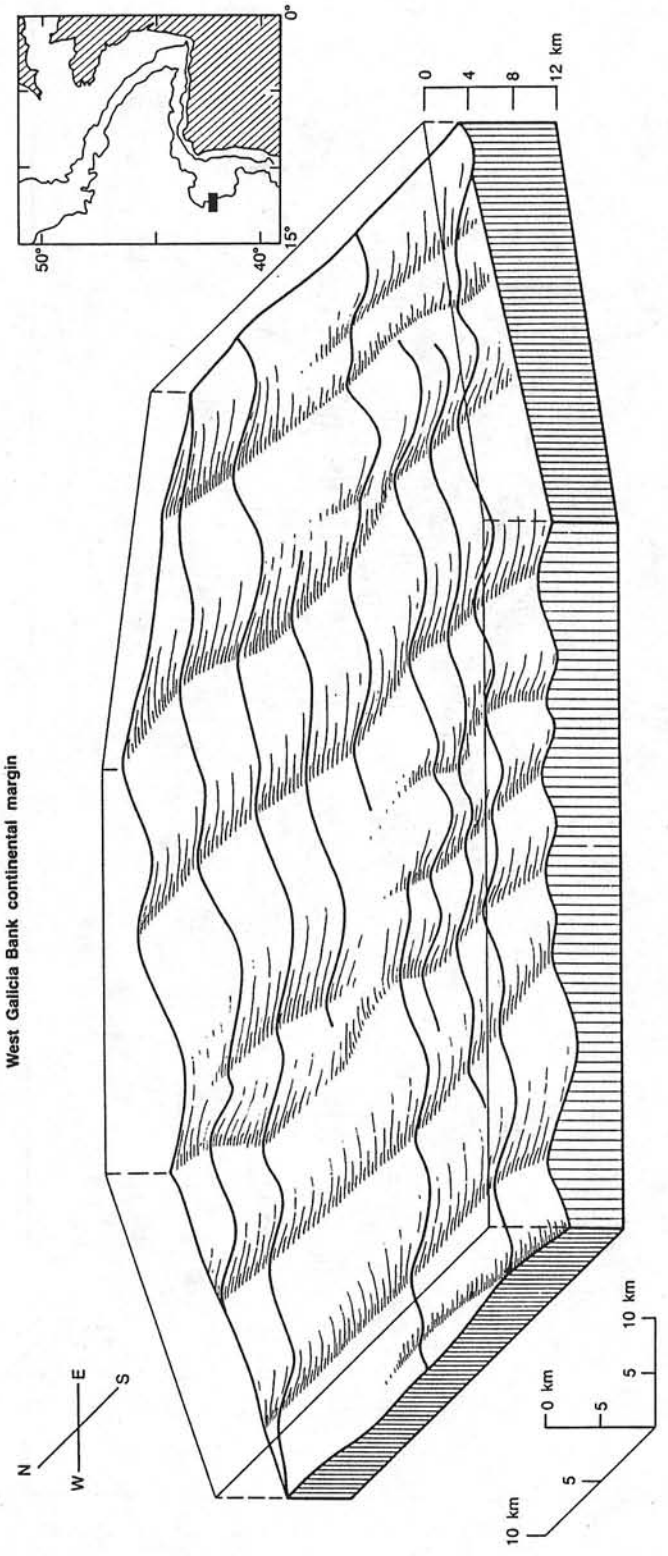


Figure 12. Block diagram of the surface of tilted fault blocks, showing the lateral continuity of blocks and half grabens. Seagal profiles were used to construct the block diagram.

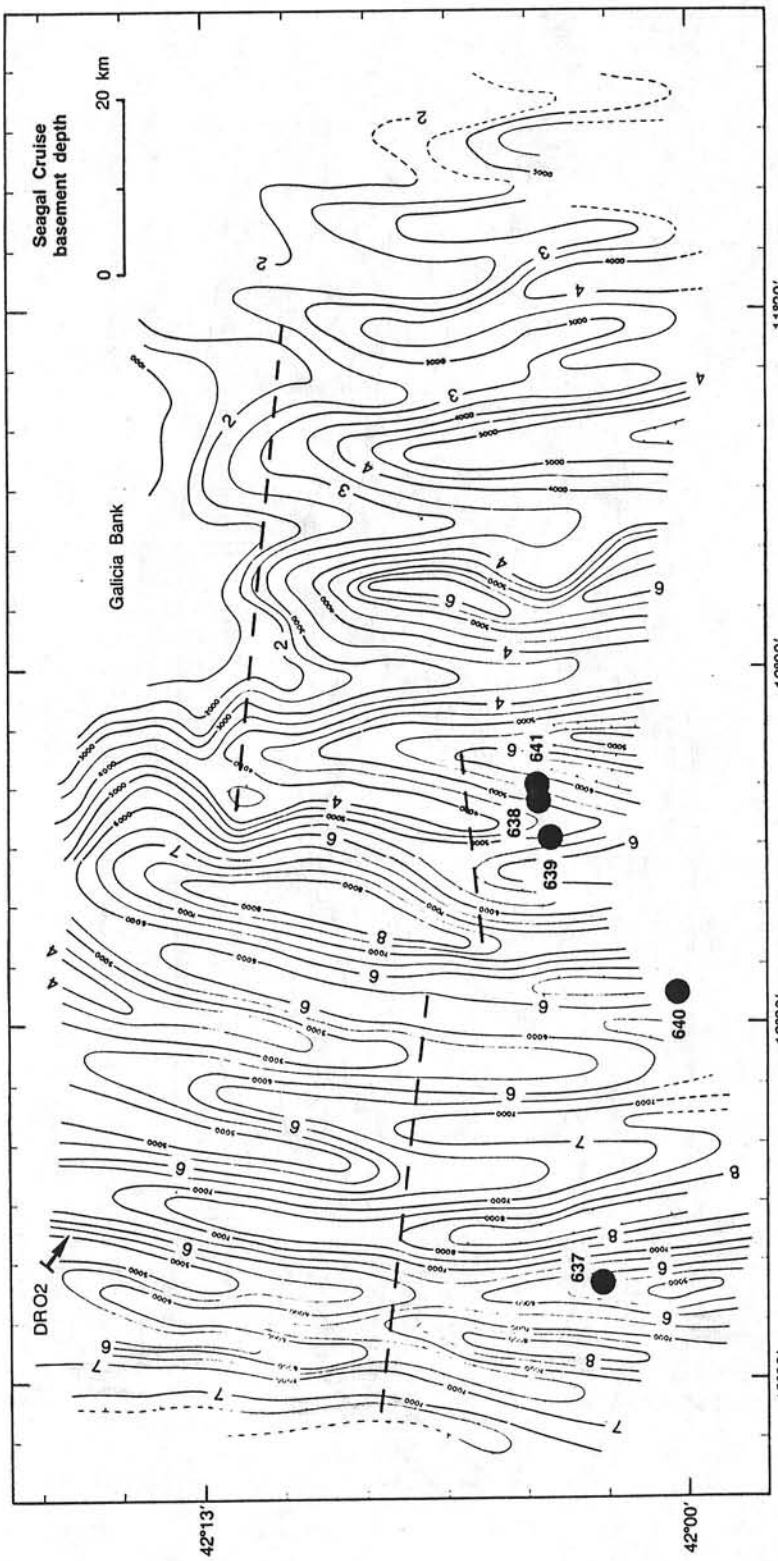


Figure 13. Topographic map of the surface of tilted faulted blocks in kilometers established from all available seismic data in Figure 3. Isobath spacing is 0.5 km for ease of identification, they are labeled in both meters (smaller numbers) and kilometers (larger numbers). Sediment thicknesses were computed from the depth-velocity profile of Figure 7. Dashed lines are possible transverse fault, southern edge of the Galicia Bank *sensu stricto*, and location of the slight 10° change in the trend of tilted fault blocks. DR02 dredge and ODP Leg 103 drill sites are indicated.

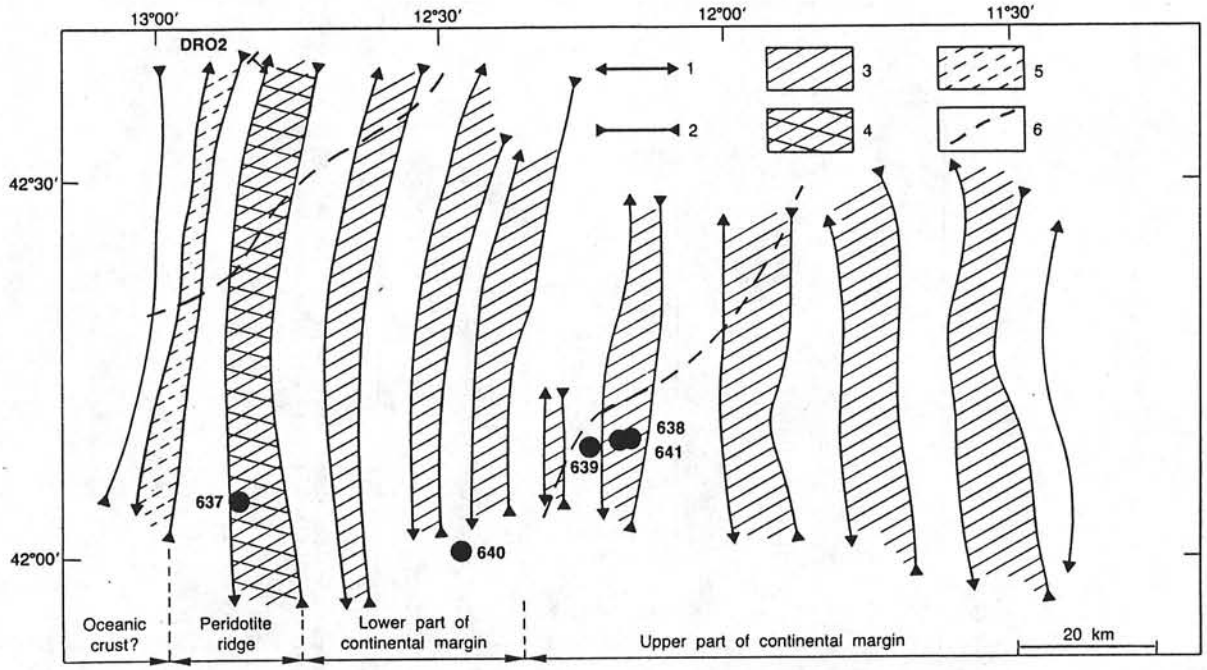


Figure 14. Distribution of crest and depression axes: (1) crests, (2) axes of half grabens or depressions, (3) subsiding part of tilted fault blocks. Blank areas correspond to the exposed part of normal faults along which tilted fault blocks glide, (4) eastern side of the peridotite ridge, (5) eastern side of oceanic ridges, (6) lower and upper parts of the continental margins, distinguished by the block spacing, the presence of the S reflector, and the magnetic data.

material and display a regular seaward increase in tilt. Their crest spacing is 13–18 km. Between 12°15′W longitude and the serpentinized peridotite ridge, syn-rift deposits appear to constitute the main part of tilted fault blocks above the S reflector. Tilting is irregular, and crest spacing is only 9–13 km.

To conclude, seismic data allow us to distinguish three main domains on southwestern Galicia margin:

1. *East of 12°15′ W longitude.* The upper part of the margin is characterized by a series of tilted fault blocks, which include syn-rift deposits. ODP Sites 638, 639, and 641 were drilled here (see site chapters, this volume).

2. *Between 12°15′ W longitude and the peridotite ridge.* The lower part of the margin is characterized by less well-defined tilted fault blocks created within syn-rift deposits. ODP Site 640 was drilled in this region (see Site 640 chapter, this volume).

3. *The peridotite ridge and the probable oceanic domain west of the ridge.* ODP Site 637 was drilled on this ridge (see Site 637 chapter, this volume).

Magnetic anomalies (Fig. 15) were mapped during the *Jean Charcot* survey. Diurnal variations were not removed. The map has an overall accuracy of about 30 gammas (nT), on the basis of intersections between tracks. Because the amplitudes of the anomalies are about 100 nT peak to peak, this is a significant limitation to the accuracy of the contours and the trends. In the upper part of the margin, the morphology of the blocks is an obvious control on the trends of the linear anomalies. Quasi-circular anomalies are superposed on these linear anomalies. In the lower part of the margin, the anomalies have a lower amplitude, which may be explained by the larger depth to basement (6 instead of 4 km, resulting in a ratio of 1:2 for linear anomalies and 1:3 for point anomalies). However, the anomaly trends do seem to diverge from the block trends, and their wavelengths are significantly larger than the spacing between blocks. Finally, the edge of the oceanic domain is associated with a large anomaly, identified as the J anomaly (Sibuet and Ryan, 1979; Tucholke and Ludwig, 1982). Thus, the magnetic anomalies confirm the proposed subdivision of the margin into three domains.

## NATURE AND ORIGIN OF HILL 5100

Several seismic profiles were obtained across the north-trending Hill 5100 and its north–south prolongation below the Iberian Abyssal Plain. ODP Site 637 recovered 74 m of serpentinized peridotite (see Site 637 chapter, this volume), confirming the previous results of dredging (Boillot et al., 1980). Figure 16 shows the Sea Beam bathymetric map and single-channel seismic data collected over this feature during the Seagal cruise. The feature acted as a dam, at least during the Cenozoic Period, which corresponds to the upper 0.7 s (two-way traveltime) of sediments. Although seismic profiles are extremely short, the interpretation of the large seismic coverage (e.g., profile GP-12, Fig. 16) calibrated at DSDP Site 398 (Groupe Galice, 1979) shows that horizons A and B correspond to main discontinuities linked to the compressive late Eocene and middle to late Miocene movements. At the contact of Hill 5100, an upward curvature of the reflectors increases downward and can be interpreted either as a 150-m uplift of the ridge during the late Eocene or, more probably, as differential compaction on the flanks of the ridge (Fig. 16, profile GP-2).

About 50 km north of ODP Site 637, we recovered alkali basalt and serpentinized peridotite rocks in the same DR02 dredge station (from latitude 42°39.7′N, longitude 12°50.0′W to latitude 42°38.9′N, longitude 12°49.0′W; from 4800 to 4500 m water depth). Dredged samples belong to outcrops because of the high tension (7 tons) recorded during the operation. The serpentinized peridotite is characterized by an abundance of chrysotile, antigorite, and olivine minerals. The chemical composition

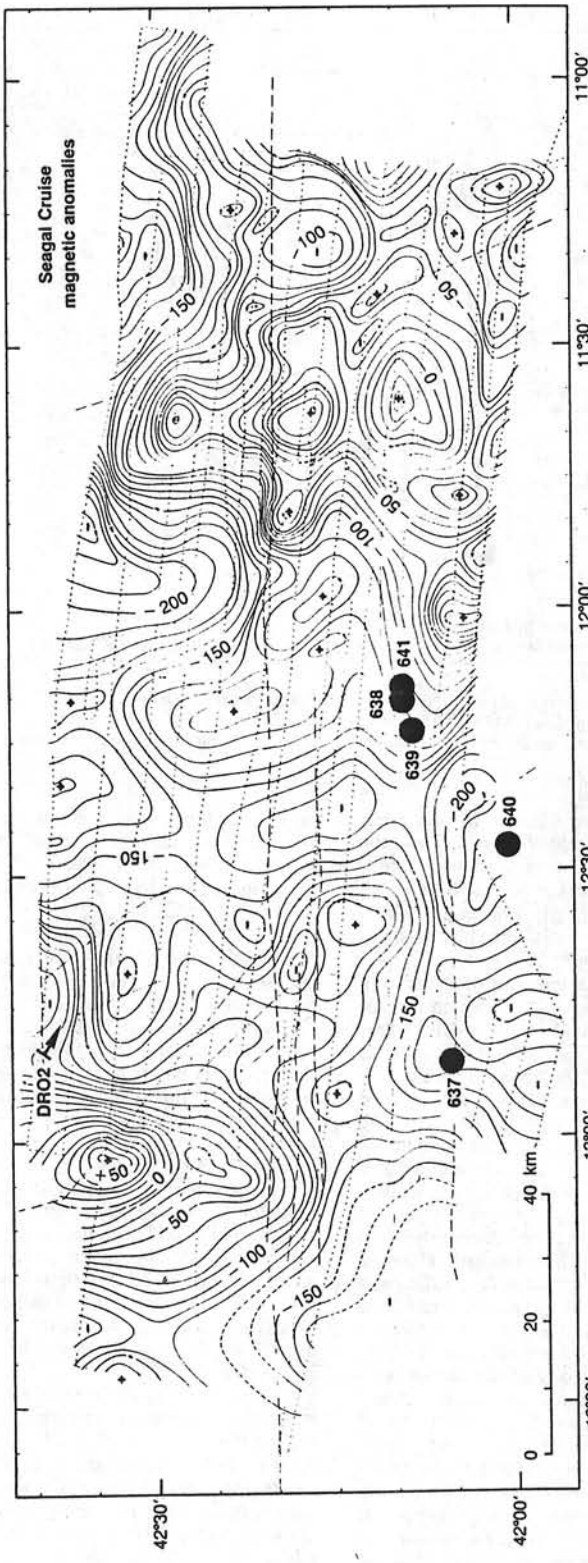


Figure 15. Magnetic anomalies in gammas (nT), established from Seagal data (dotted lines) and other available data (dashed lines). Contour interval, 10 nT. The upper and lower parts of the continental margin are distinguished by the change in the amplitude of magnetic anomalies. The peridotite feature (ODP Site 637) is marked only by a faint roughly north–south magnetic anomaly. The J anomaly corresponds to the large magnetic anomaly west of 13°W longitude.

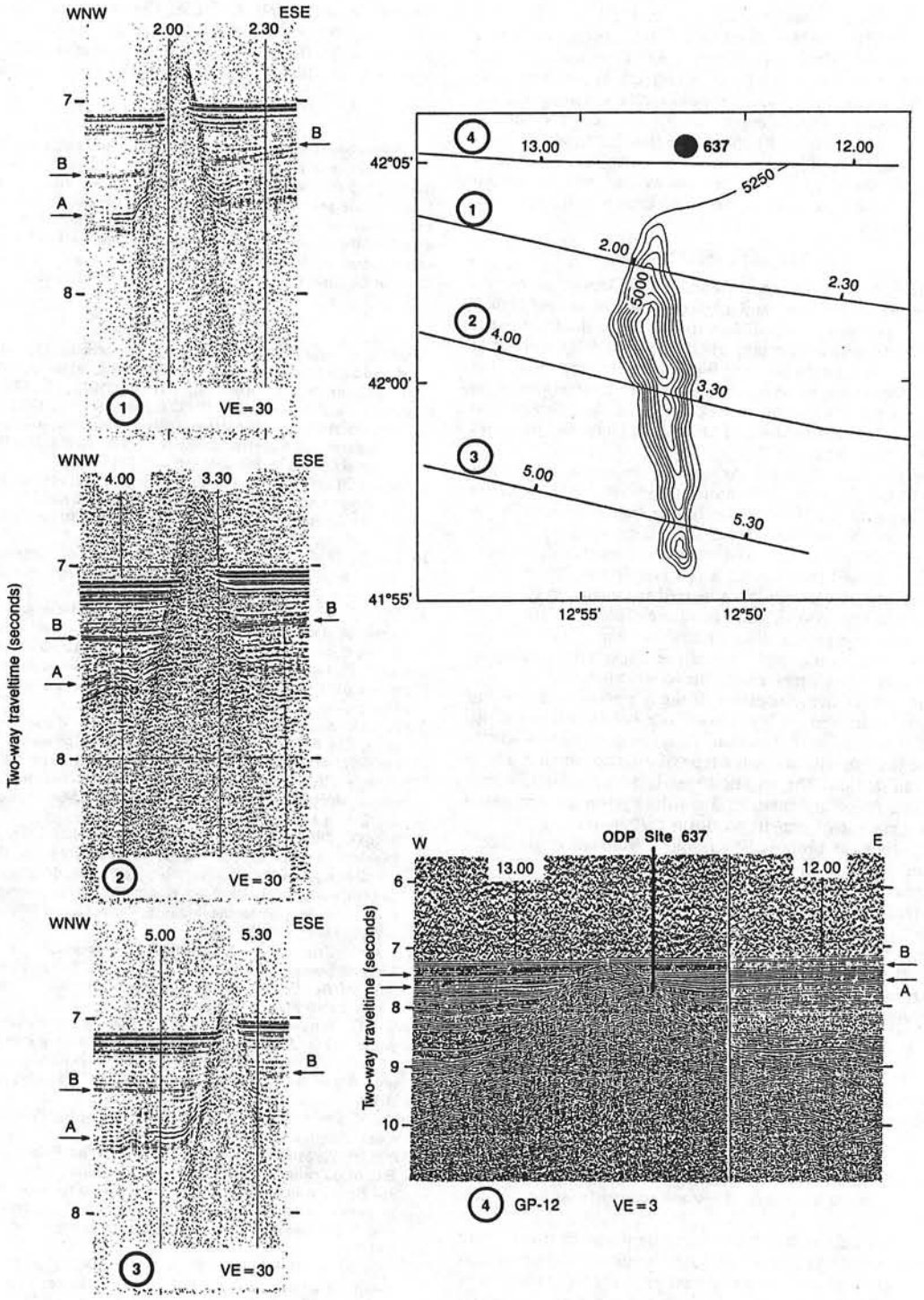


Figure 16. Bathymetric map of Hill 5100 established from Sea Beam data and seismic profiles over that feature. Isobath spacing is 50 m. Location of single-channel seismic profiles 1, 2, 3 (Seagal cruise), and 4 (IFP-CNEXO multichannel seismic profile GP-12) shown on Sea Beam map. Late Eocene (A) and middle Miocene (B) unconformities are shown by arrows on the four seismic sections.

characterized by high water (23.3% at 1050°C) MgO (20.2%) and CaO (19.4%) contents agrees well with the presence of these minerals. Dredge DR02 and ODP Site 637 belong to the same north–south basement ridge (Figs. 4 and 13). It is tempting to suggest that the peridotite ridge should extend northward along the base of western Galicia margin over a distance of about 100 km (Fig. 1). Nevertheless, we must note that the structural context differs considerably along this trend; the Hill 5100 basement feature seems to deepen northward and then to rise up again, becoming part of the lower steep continental slope west of Galicia Bank.

## DISCUSSION

We previously noted that the lower margin blocks are mostly made of syn-rift sediments and apparently do not include "true" upper crust basement rock. This is similar to the situation at the base of the Armorican margin, where Barbier (1986), Barbier et al. (in press), and Le Pichon and Barbier (in press) reported that the lower blocks are made entirely of layered sediments and do not contain 6-km/s basement rock. They further showed that the restored vertical thickness of blocks systematically increases toward the continent.

Below the blocks, in the Armorican margin area, Barbier (1986) and Barbier and Le Pichon (in press) mapped the depth of a reflector at the base of the blocks that progressively increases toward the continent. Using the refraction results of Ginzburg et al. (1985) and their own wide-angle velocity determinations, they showed that the 6.5-km/s layer below the reflector lies immediately below 4.6-km/s layered sediments on the lower margin but below 6.0-km/s basement rock further inland. They consequently interpreted this reflector as being a tectonic discontinuity, cutting obliquely across the upper crust, its upper part being in direct contact with the lower crust.

In the Galicia area, the extent of the intermediate S reflector is much more limited, as it has been followed far below the upper part of the continental margin. Thus, we do not know whether we are dealing with the same type of reflector as that on the Armorican margin. The question then is does the 6-km/s layer below the S reflector consist of 2-km-thick lower crust material or does it consist of pre-rift platform carbonates or crystalline basement rock, as proposed by Boillot, Winterer, et al. (1985, 1986) and Meyer et al. (1985).

In either instance, the extreme thinning of the crust in the lower margin (2 km, exclusive of the syn-rift sediment thickness) clearly cannot be accounted for by the relatively modest stretching that affected the block layer itself (Le Pichon and Sibuet, 1981; Chenet et al., 1983). Note that, with such extreme thinning, local outcrop of serpentinized peridotite ridges across the remaining thin veil of crust is not unusual.

## CONCLUSIONS

Data acquired during the *Jean Charcot* Seagal cruise allow us to establish a Sea Beam bathymetric map of the ODP Leg 103 drilling area and to compare the morphology with tilted blocks seen on single-channel and multichannel seismic profiles. Following are the main findings of this study:

1. North–south tilted fault blocks are continuous over distances of as much as 60 km. They are spaced from 9 to 18 km apart.

2. The margin southwest of Galicia Bank can be divided into three main areas: (A) East of 12°15′W longitude, the upper part of the margin is characterized by a series of regularly tilted fault blocks 13–18 km apart, which include syn-rift deposits in their upper section. Magnetic anomalies appear to be partly controlled by basement faulting. (B) Between 12°15′W and Hill 5100, the lower part of the margin is characterized by irregularly tilted fault blocks formed mainly of syn-rift deposits. The distance between blocks is only 9–13 km. The deep S reflector underlies this area. Magnetic anomalies have an orientation different from orientation of the blocks. (C) The oceanic domain is located west of Hill 5100 and is associated with the J anomaly.

## ACKNOWLEDGMENTS

The authors express their gratitude to G. Boillot and E. Winterer, co-chief scientists of Leg 103, who asked us to prepare this contribution for the Leg 103 Part A volume. Fruitful discussions with G. Boillot and J. L. Olivet are acknowledged. G. Auffret made the first description and analyses of the dredge DR02 samples. P. Miles and J. Gardner reviewed a draft of this paper and offered helpful suggestions. We thank the officers and crew of the *Jean Charcot* during the Seagal cruise, in particular Captain G. Girard. This is IFREMER contribution 66.

## REFERENCES

Arthaud, F., and Matte, P., 1975. Les décrochements tardi-hercyniens du Sud-Ouest de l'Europe. Géométrie et essai de reconstitution des conditions de la déformation. *Tectonophysics*, 25:139–171.

Avedik, F., and Howard, D., 1979. Preliminary results of a seismic refraction study in the Meriadzek-Trevelyan area, Bay of Biscay. *In* Montadert, L., Roberts, D. G., et al., *Init. Repts. DSDP*, 48: Washington (U.S. Govt. Printing Office), 1015–1023.

Baranyi, I., Lippolt, J. J., and Todt, W., 1976. Kalium-Argon Altersbestimmungen an Tertiärten Vulkaniten des Oberrhein-graben-Gebites: II. Die Alterstraverse vom Hegau nach Lothringe. *Oberrheinische Geol. Abh.*, 35:41–62.

Barbier, F., 1986. Etude de la structure profonde de la marge Nord-Gascogne. implications sur la formation des marges passives [Thesis]. Université Pierre et Marie Curie, Paris.

Barbier, F., Le Pichon, X., and Duvergé, J., in press. Structure profonde de la marge Nord-Gascogne, implications sur le mécanisme de rifting et de formation de la marge continentale. *Bull. Soc. Géol. Fr.*

Bergerat, F., 1985. Déformations cassantes et champs de contraintes tertiaires dans la plateforme européenne [Thesis]. Université Pierre et Marie Curie, Paris.

Boillot, G., Auxiètre, J., Dunand, J., Dupeuble, P., and Mauffret, A., 1979. The northwestern Iberian margin: a Cretaceous passive margin deformed during Eocene. *In* Talwani, M., Hay, W., and Ryan, W. B. F. (Eds.), *Deep Drilling Results in the Atlantic Ocean: Continental Margins and Paleoenvironment, M. Ewing Series 3*: Washington D.C. (Am. Geophys. Union), 138–153.

Boillot, G., Dupeuble, P. A., Hennequin-Marchand, I., Lamboy, M., Leprêtre, J.-P., and Muselec, P., 1974. Le role des décrochements "tardi-hercyniens" dans l'évolution structurale de la marge continentale et dans la localisation des grands canyons sous-marins à l'Ouest et au Nord de la péninsule ibérique. *Revue Géogr. Phys. Géol. Dyn.*, XVI(1):75–86.

Boillot, G., Grimaud, S., Mauffret, A., Mougenot, D., Kornprobst, J., Mergoil-Daniel, J., and Torrent, G., 1980. Ocean-continent transition off the Iberian margin: a serpentinite diapir west of Galicia Bank. *Earth Planet. Sci. Lett.*, 48:23–34.

Boillot, G., Winterer, E., et al., 1985. Résultats préliminaires de la campagne 103 du *JOIDES Resolution* (Ocean Drilling Program) au large de la Galice (Espagne): sédimentation et distension pendant le "rifting" d'une marge stable—hypothèse d'une dénudation tectonique. *Acad. Sci. Paris, C. R.*, 301:627–632.

Boillot, G., Winterer, E., et al., 1986. ODP Leg 103 drills into rift structures. *Geotimes*, 31(1):15–17.

Chenet, P.-Y., Montadert, L., Gairaud, H., and Roberts, D. G., 1983. Extension ratio measurements on the Galicia, Portugal and Northern Biscay continental margins: implications for evolutionary models of passive continental margins. *In* Watkins, J. S., and Drake, C. L. (Eds.), Studies in Continental Margin Geology. *AAPG Mem.*, 34: 703–715.

de Charpal, O., Trémolières, P., Jean, F., and Masse, P., 1974. Un exemple de tectonique de plateforme, les causses majeurs. *Inst. Fr. Pet. Rev.*, 29:715–732.

de Graciansky, P.-C., Poag, C. W., et al., 1985. *Init. Repts. DSDP*, 80: Washington (U. S. Govt. Printing Office).

Ginzburg, A., Whitmarsh, R. B., Roberts, D. G., Montadert, L., Camus, A., and Avedik, F., 1985. The deep seismic structure of the

northern continental margin of the Bay of Biscay. *Ann. Geophys.*, 3, 4:499–510.

Groupe Cybère (Malod, J.-A., Témine, D., Boillot, G., Capdevila, R., Cousin, M., Dupeuble, P.-A., Gonzalez-Ladeiro, F., Herbin, J.-P., Lamboy, M., Lepvrier, C., Martinez-Catalan, J., Mascle, G., Muller, C., Pastouret, L., Rojouan, F., Taugourdeau-Lantz, J., and Vanney, J.-R.), 1984. La marge déformée du Nord-Ouest de l'Espagne. *Publ. du CNEXO, Résultats des Campagnes à la mer*, 29.

Groupe Cymor (Pastouret, L., Auffret, G. A., Auzende, J.-M., Beuzart, P., Dubois, P., Séguret, M., Sigal, J., and Vanney, J.-R.), 1981. La marge continentale armoricaine, résultats d'observation en submersible et de dragages dans le canyon Shamrock. *Acad. Sci., Paris, C. R.*, 292:741–748.

Groupe Galice (Auzende, J.-M., Jonquet, H., Olivet, J.-L., Sibuet, J.-C., Auxiètre, J.-L., Boillot, G., Dunand, J.-P., Mauffret, A., de Charpal, O., Apotolescu, V., and Montadert, L.), 1979. The continental margin off Galicia and Portugal: acoustical stratigraphy, dredge stratigraphy, and structural evolution. *In* Sibuet, J.-C., Ryan, W. B. F., et al., *Init. Repts. DSDP*, 47, Pt. 2: Washington (U.S. Govt. Printing Office), 633–662.

Groupe Transmarge (Vanney, J.-R., Mougenot, D., Galisson, H., Gosselin, J., Hardonnière, C., Leuridan, J., Pigeon, P., Regnauld, H., El Robrini, M., Rojouan, F., Rothwell, G., and Virlogeux, P.), 1982. Levé bathymétrique de précision à l'aide du sondeur multifaisceaux Sea-Beam du canyon de Nazaré (marge continentale du Portugal). *Acad. Sci. Paris, C. R.*, 294:1099–1102.

Groupe Transmarge (Vanney, J.-R., Mougenot, D., Galisson, H., Gosselin, J., Hardonnière, C., Leuridan, J., Pigeon, P., Regnauld, H., El Robrini, M., Rojouan, F., Rothwell, G., and Virlogeux, P.), 1984. Levé bathymétrique à l'aide du sondeur multifaisceaux "Sea-Beam" du versant septentrional du banc de Galice (marge continentale ouest ibérique). *Acad. Sci. Paris, C. R.*, 299, II(3):115–120.

Guennoc, P., Jonquet, H., and Sibuet, J.-C., 1978. Carte magnétique de l'Atlantique nord-est. anomalies du champ total. Échelle 1/2400000. *In* CNEXO (Ed.), Paris (BRGM, Service Promotion et Vente).

Guennoc, P., Jonquet, H., and Sibuet, J.-C., 1979. Présentation d'une carte magnétique de l'Atlantique nord-est. *Acad. Sci. Paris, C. R.*, 288(D):1011–1013.

Kamerling, P., 1979. The geology and hydrocarbon habitat of the Bristol Channel basin. *J. Pet. Geol.*, 2:75–93.

Kenyon, N. H., Belderson, R. H., and Stride, A. H., 1978. Channels, canyons and slump folds on the continental slope between southwest Ireland and Spain. *Oceanol. Acta*, 1(3):369–380.

Lallemand, S., Mazé, J.-P., Monti, S., and Sibuet J.-C, 1985a, Présentation d'une carte bathymétrique de l'Atlantique Nord-Est. *Acad. Sci. Paris, C. R.*, 300, II(4):145–149.

Lallemand, S., Mazé, J.-P., Monti, S., and Sibuet, J.-C., 1985b. Carte bathymétrique de l'Atlantique Nord-Est. Échelle 1/2400000. *In* CNEXO (Ed.) Paris (BRGM, Service Promotion et Vente).

Lallemand, S., and Sibuet, J.-C., in press. Tectonic implications of canyon directions over the northeast Atlantic continental margin. *Tectonics.*

Laughton, A. S., Roberts, D. G., and Graves, R., 1975. Bathymetry of the northeast Atlantic: Mid-Atlantic Ridge to southwest Europe. *Deep-Sea Res.* 22:791–810.

Le Pichon, X., Angelier, J., and Sibuet, J.-C., 1983. Subsidence and stretching. *In* Watkins, J. S., and Drake, C. L. (Eds.), Studies in Continental Margin Geology. *AAPG Mem.* 34:731–741.

Le Pichon, X., and Barbier, F., in press. Passive margin formation based on the Bay of Biscay study. *Tectonophysics.*

Le Pichon, X., Ewing, J., and Houtz, R., 1968. Deep-sea sediment velocity determination made while reflection profiling. *J. Geophys. Res.*, 73:2597–2614.

Le Pichon, X., and Renard, V., 1982. Avalanching: a major process of erosion and transport in deep-sea canyons: evidence from submersible and multinarrow beam surveys. *In* Scrutton, R. A., and Talwani, M. (Eds.), *The Ocean Floor:* New York (Wiley), 113–128.

Le Pichon, X., and Sibuet, J.-C., 1971. Western extension of boundary between European and Iberian plates during the Pyrenean orogeny. *Earth Planet. Sci. Lett.*, 12:83–88.

Le Pichon, X., and Sibuet, J.-C., 1981. Passive margins: a model of formation. *J. Geophys. Res.*, 86:3708–3720.

Letouzey, J., and Trémolières, P., 1980. Paleo-stress fields around the Mediterranean since the Mesozoic derived from microtectonics: comparison with plate tectonic data. Geologie des chaînes alpines issues de la Téthys. *Mem. BRGM*, 26th C.G.I., Paris, 115:261–273.

Masson, D. G., Montadert, L., and Scrutton, R. A., 1985. Regional geology of the Goban Spur continental margin. *In* de Graciansky, P.-C., Poag, C. W., et al., *Init. Repts. DSDP*, 80, Pt. 2: Washington (U.S. Govt. Printing Office), 1115–1140.

Manspeizer, W., Puffer, J. H., and Cousminer, H. L., 1978. Separation of Morocco and eastern North America: a Triassic-Liassic stratigraphic record. *Geol. Soc. Am. Bull.*, 89:901–920.

Meyer, A., Boillot, G., Winterer, E., et al., 1985. Early Cretaceous rifting and origin of the "S reflector" : preliminary results of Ocean Drilling Program Leg 103. *Eos*, 66(46):917 (Abstract).

Montadert, L., Roberts, D. G., et al., 1979a. *Init. Repts. DSDP*, 48: Washington (U.S. Govt. Printing Office).

Montadert, L., Roberts, D. G., et al., 1979b. Sites 399, 400, and Hole 400A. *In* Montadert, L., Roberts, D. G., et al., *Init. Repts. DSDP*, 48: Washington (U.S. Govt. Printing Office), 35–71.

Montadert, L., Roberts, D. G., et al., 1979c. Site 401. *In* Montadert, L., Roberts, D. G., et al., *Init. Repts. DSDP*, 48: Washington (U.S. Govt. Printing Office), 73–124.

Montadert, L., de Charpal, O., Roberts, D. G., Guennoc, P., and Sibuet, J.-C., 1979d. Northeast Atlantic passive continental margins: rifting and subsidence processes. *In* Talwani, M., Hay, W., and Ryan, W. B. F. (Eds.), *Deep Drilling Results in the Atlantic Ocean: Continental Margins and Paleoenvironment, M. Ewing Series 3:* Washington (Am. Geophy. Union), 154–186.

Montadert, L., 1982. Les marges continentales passives. *La Recherche*, 13:730–742.

Mougenot, D., Monteiro, J. H., Dupeuble, P.-A., and Malod, J.-A., 1979. La marge continentale sud-portugaise: évolution structurale et sédimentaire. *Ciencias da Terra*, 5: Lisboa (Univ. Nov. Lisboa), 223–246.

Mougenot, D., Kidd, R. B., Mauffret, A., Regnauld, H., Rothwell, R. G., and Vanney, J.-R., 1984. Geological interpretation of combined Sea Beam, gloria and seismic data from Porto and Vigo Seamounts, Iberian continental margin. *Mar. Geophys. Res.*, 6:329–363.

Olivet, J.-L., Bonnin, J., and Auzende, J.-M., 1976. Manifestations des phases de compression tertiaire dans l'Atlantique du Nord-Est. *4th Réunion Sci. Terre*, Paris, 311 (Abstract).

Olivet, J.-L., Bonnin, J., Beuzart, P., and Auzende, J.-M., 1984. Cinématique de l'Atlantique Nord et Central. Paris (Publications du CNEXO).

Parga, J.-R., 1969. Sistemas de fracturas tardihercinicas del macizo hesperico. *Trabajos del Lab. Geol. de Lage*, 37:1–15.

Pegrum, R. M., and Mountenay, N., 1978. Rift basins flanking North Atlantic Ocean and their relation to North Sea area. *AAPG Bull.*, 62:419–441.

Réhault, J.-P., and Mauffret, A., 1979. Relationships between tectonics and sedimentation around the northwestern Iberian margin. *In* Sibuet, J.-C., Ryan, W. B. F., et al., *Init. Repts. DSDP*, 47, Pt. 2: Washington (U.S. Govt. Printing Office), 663–681.

Renard, V., and Allenou, J.-P., 1979. Le Sea Beam, sondeur à multifaisceaux du N/O *Jean Charcot:* description, évaluation et premiers résultats. *Rev. Hydrographique Internationale*, Monaco, 56:35–71.

Roberts, D. G., Schnitker, et al., 1984. *Init. Repts. DSDP*, 81: Washington (U.S. Govt. Printing Office).

Savostin, L. A., Sibuet, J.-C., Zonenshain, L. P., Le Pichon, X., and Roulet, M.-J., 1986. Kinematic evolution of the Tethys Belt from the Atlantic Ocean to the Pamirs since the Triassic. *Tectonophysics*, 123: 1–35.

Sibuet, J.-C., and Berthois, L., 1979. Dominant structural trends on the western continental margin of Iberia: implications of initial rifting. *In* Sibuet, J.-C., Ryan, W. B. F., et al., *Init. Repts DSDP*, 47, Pt. 2: Washington (U.S. Govt. Printing Office), 753–760.

Sibuet, J.-C., Ryan, W. B. F., et al., 1979a. Site 398. *In* Sibuet, J.-C., Ryan, W. B. F., et al., *Init. Repts. DSDP*, 47, Pt. 2: Washington (U.S. Govt. Printing Office), 25–233.

Sibuet, J.-C., Ryan, W. B. F., et al., 1979b. *Init. Repts. DSDP*, 47, Pt. 2: Washington (U.S. Govt. Printing Office).

Sibuet, J.-C., and Ryan, W. B. F., 1979. Site 398: evolution of the west Iberian passive continental margin in the framework of the early evolution of the North Atlantic Ocean. *In* Sibuet, J.-C., Ryan, W. B. F., et al., *Init. Repts. DSDP*, 47, Pt. 2: Washington (U.S. Govt. Printing Office), 761–775.

Sibuet, J.-C., Mathis, B., Pastouret, L., Auzende, J.-M., Foucher, J.-P., Hunter, P. M., Guennoc, P., de Graciansky, P.-C., Montadert, L.,

and Masson, D. G., 1985. Morphology and basement structures of the Goban Spur continental margin (northeastern Atlantic) and the role of the Pyrenean orogeny. *In* de Graciansky, P.-C., Poag, W., et al., *Init. Repts. DSDP*, 80: Washington (U.S. Govt. Printing Office), 1153–1165.

Tucholke, B. E., and Ludwig, W. J., 1982. Structure and origin of the J anomaly ridge, western North Atlantic Ocean. *J. Geophys. Res.*, 87: 9389–9407.

Verhoef, J., Colette, B. J., Miles, P. R., Searle, R. C., Sibuet, J.-C., and Williams, C. A., 1986. Magnetic anomalies in the northeast Atlantic Ocean (35°–50°N). *Mar. Geophys. Res*, 8:1–25.

Ziegler, P. A., 1978. Northwestern Europe: tectonics and basin development. *Geol. Mijnbouw*, 57:589–626.

Ziegler, P. A., 1981. Evolution of sedimentary basins in northwest Europe. *Petroleum Geology of the Continental Shelf of Northwest Europe:* London (Institute of Petroleum), 9–39.

(10) Montadert L., de Charpal O., Roberts D., Guennoc P., et Sibuet J.-C., 1979. Northeast Atlantic passive margins : rifting and subsidence processes. In Deep Drilling results in the Atlantic Ocean : continental margins and paleoenvironment, M. Talwani, W.W. Hay, et W.B.F. Ryan (eds), M. Ewing Series 3, American Geophysical Union, Washington, p. 164-186.

(11) Lallemand S., et Sibuet J.-C., 1986. Tectonic implications of canyon directions over the northeast Atlantic continental margins. Tectonics, 5, p. 1125-1143.

(12) Diament M., Sibuet J.-C., et Hadaoui A., 1986. Isostasy of the northern bay of Biscay continental margin. Geophys. J. R.A.S., 86, p. 893-907.

# NORTHEAST ATLANTIC PASSIVE CONTINENTAL MARGINS: RIFTING AND SUBSIDENCE PROCESSES

Lucien Montadert and Olivier de Charpal

Institut Français du Pétrole, 92506 Rueil, Malmaison, France

David Roberts

Institute of Oceanographic Sciences, Wormley, Surrey, England

Pol Guennoc and Jean-Claude Sibuet

Centre Océanologique de Bretagne, 29273 Brest, France

Abstract. From geophysical data and DSDP drilling results (Legs 47B and 48) in the NE Atlantic (Galicia-Portugal and Northern Bay of Biscay), a model for rifting, attenuation and subsidence of a passive continental margin is proposed.

## Introduction

The northern margin of the Bay of Biscay and the Galicia marginal plateau were selected for drilling during I.P.O.D., because they offer one of the unique areas in the Atlantic Ocean, where drilling could reach easily layers deposited during the early stages of the evolution of a passive continental margin. The four sites drilled, 398, 400, 401, 402 did not attain all the objectives ; nevertheless, complemented by intensive multichannel seismic reflection profiling and dredgings, they allow us to propose a model of evolution of a passive continental margin. The geological structure of this part of the N.E. Atlantic and of their continental margins is complex because it results not only from rifting and drifting of Europe, Iberia and North America, but also from convergence between Europe, Iberia and Africa. The age and kinematics of the opening of the Bay of Biscay is still matter of controversy. If one accepts identification of anomalies 33 - 34 following CANDE et al (1977), the creation of Oceanic Crust in Biscay finished before anomalies 33 - 34 or eventually terminated just after, if these anomalies are also recognized in the axis of the Bay (triple junction during anomalies 33 - 34, Williams, 1975). The beginning of accretion is most probably intra Aptian (see Section III). One must thus distinguish (MONTADERT et al, 1974) the western part of Galicia Bank area and the Northern Bay of Biscay margin with its onshore prolongation in the Aquitaine basin which remained essentially stable during their entire history, and the North Spanish margin including the northern part of Galicia bank which was active almost since the opening of the Bay of Biscay (Cenomanian movements recorded in the Pyrenées) and at least until the Eocene-Oligocene.

Bathymetry of the part of the Northeast Atlantic considered in this paper shows clearly different provinces (fig. 1, 2) (BERTHOIS et al 1966, 1968) :

1. From Nazare canyon to the latitude of Porto offshore from the Portugal sedimentary basin, the continental shelf 40 to 50 km wide is linked to the Iberian Abyssal Plain by a relatively narrow continental slope.

2. Farther North, all the way to Cape Finisterre, the continental shelf is about 30 km wide and is bounded in the East by the Hercynian basement of Galicia. In the West as opposed to the preceeding zone, it is prolonged for nearly 200 km by a marginal plateau. This plateau comprises the large Galicia Bank whose top is 600 m deep, and several other seamounts (Vigo, Vasco de Gama) ; it is separated from the shelf by an Interior Basin running in a North-South direction from the Biscay Abyssal Plain to Porto Seamount. DSDP site 398 is located 20 km to the South of Vigo Seamount (fig.1,2).

3. The northern steep margin of Spain which had been strongly affected by the Pyrenean orogeny.

4. The Armorican margin from Aquitaine to the western Approaches basin is narrow and steep and bounded to the west by the deep and thick Mesozoïc-Cenozoïc Armorican marginal basin. It corresponds on the shelf to a Hercynian basement covered by a thin wedge of sediments.

5. The Western Approaches margin is broader with several large topographic features e.g. the Meriadzek Terrace, the Trevelyan escarpment, the Shamrock Canyon. It intersects the NE-SW Western Approaches Mesozoic-Cenozoïc basin on the shelf. Its SE boundary with the Armorican margin is very sharp near the Black Mud Canyon and is controlled by a NE-SW fault zone known also on the shelf.

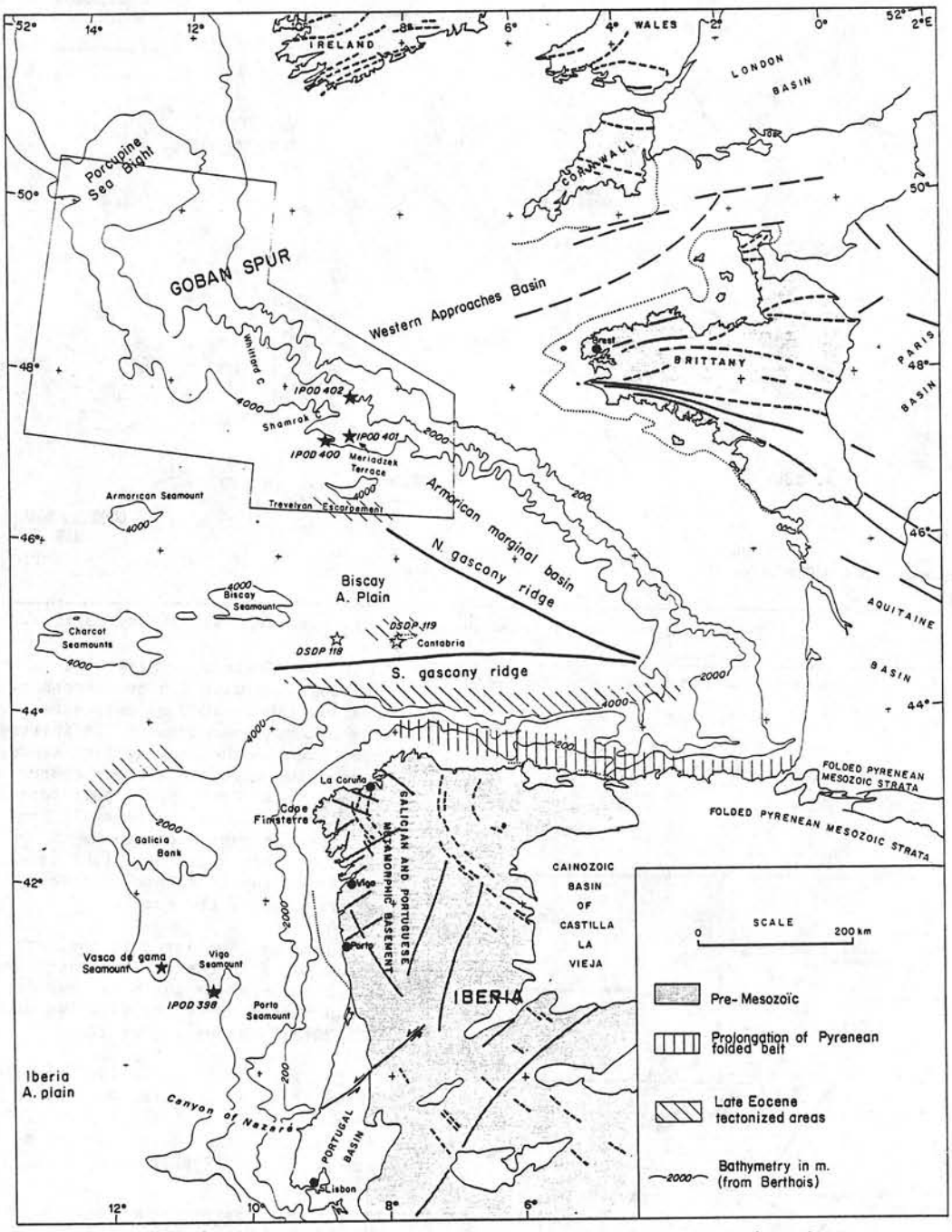


Fig. 1. General physography of SW Europe. Continental margins with DSDP drilling sites.

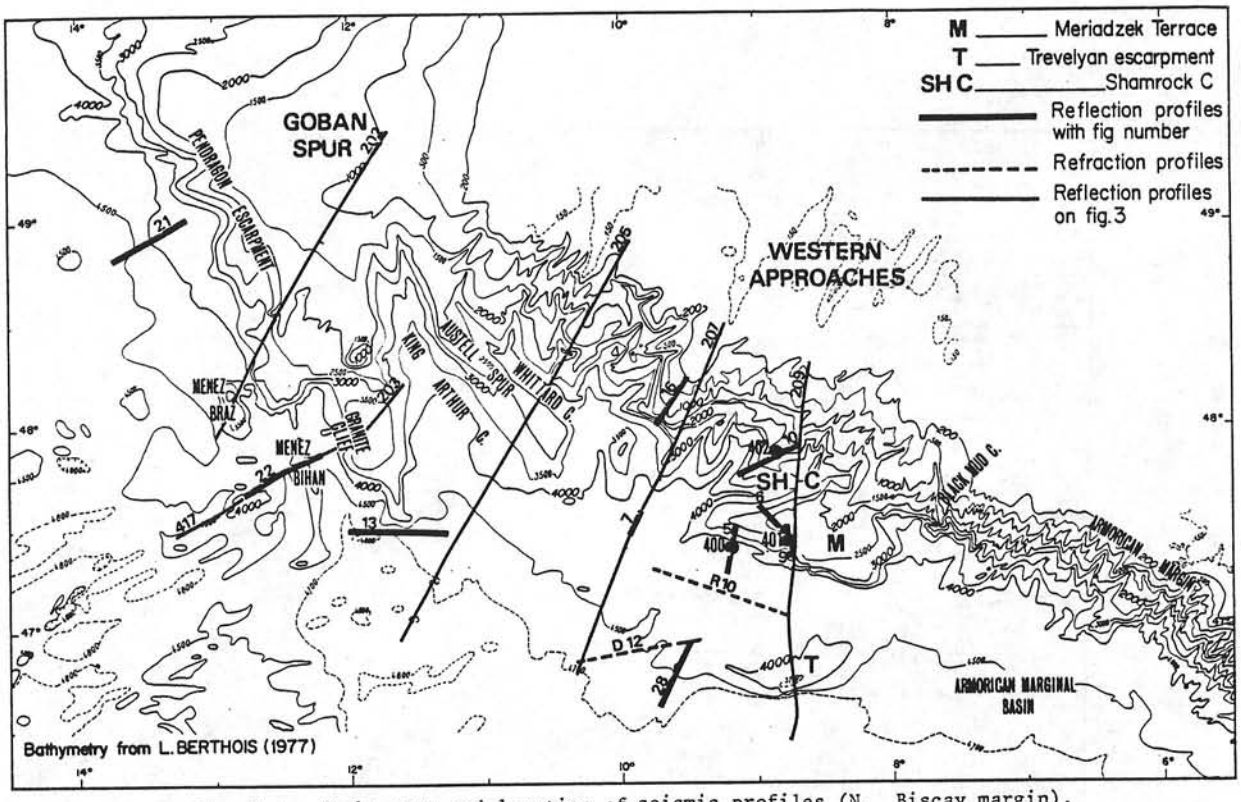


Fig. 2 A. Bathymetry and location of seismic profiles (N. Biscay margin).

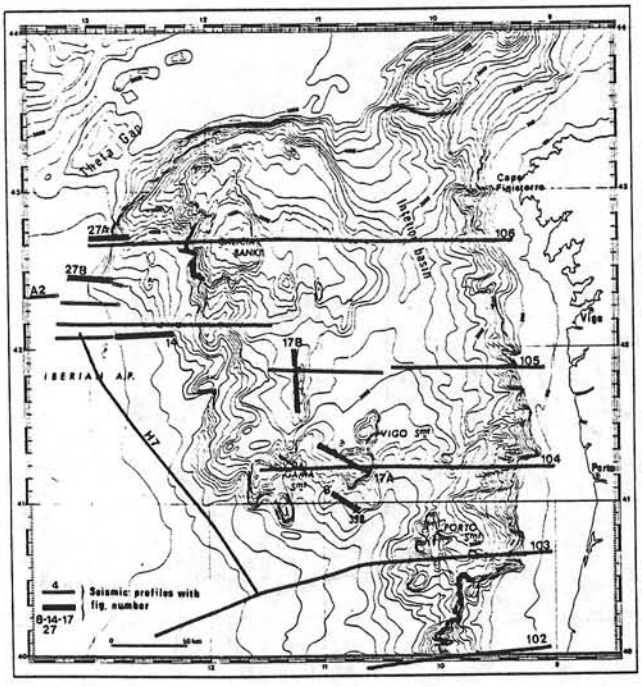


Fig. 2 B. Bathymetry and location of seismic profiles (W. Galicia margin).

6. The Goban Spur margin has a quite different physiography with a broad smooth rise relatively shallow (above 2000 m) deepening abruptly along the Pendragon escarpment. It intersects a basement high in the prolongation of Cornwall. The connection with the Western Approaches margin is marked by several topographic features like the Granite Cliff, and the Austell Spur separated by large canyons trending NW-SE.

7. The Porcupine Sea Bight is a depression corresponding to a thick Mesozoïc-Cenozoïc basin intersected by the margin.

The area considered in the Northern Biscay corresponds to the Western Approaches margin where sites 400 - 401 - 402 have been drilled, and the Goban Spur margin. Its detailed bathymetry by BERTHOIS is shown figure 2A.

Previous published seismic reflection data in these areas of drilling were scarce. In the Galicia Bank area, BLACK et al. (1964), FUNNEL et al. (1969) carried out geophysical surveys and got numerous dredge data. IFP-SNPA carried out a regional multi-

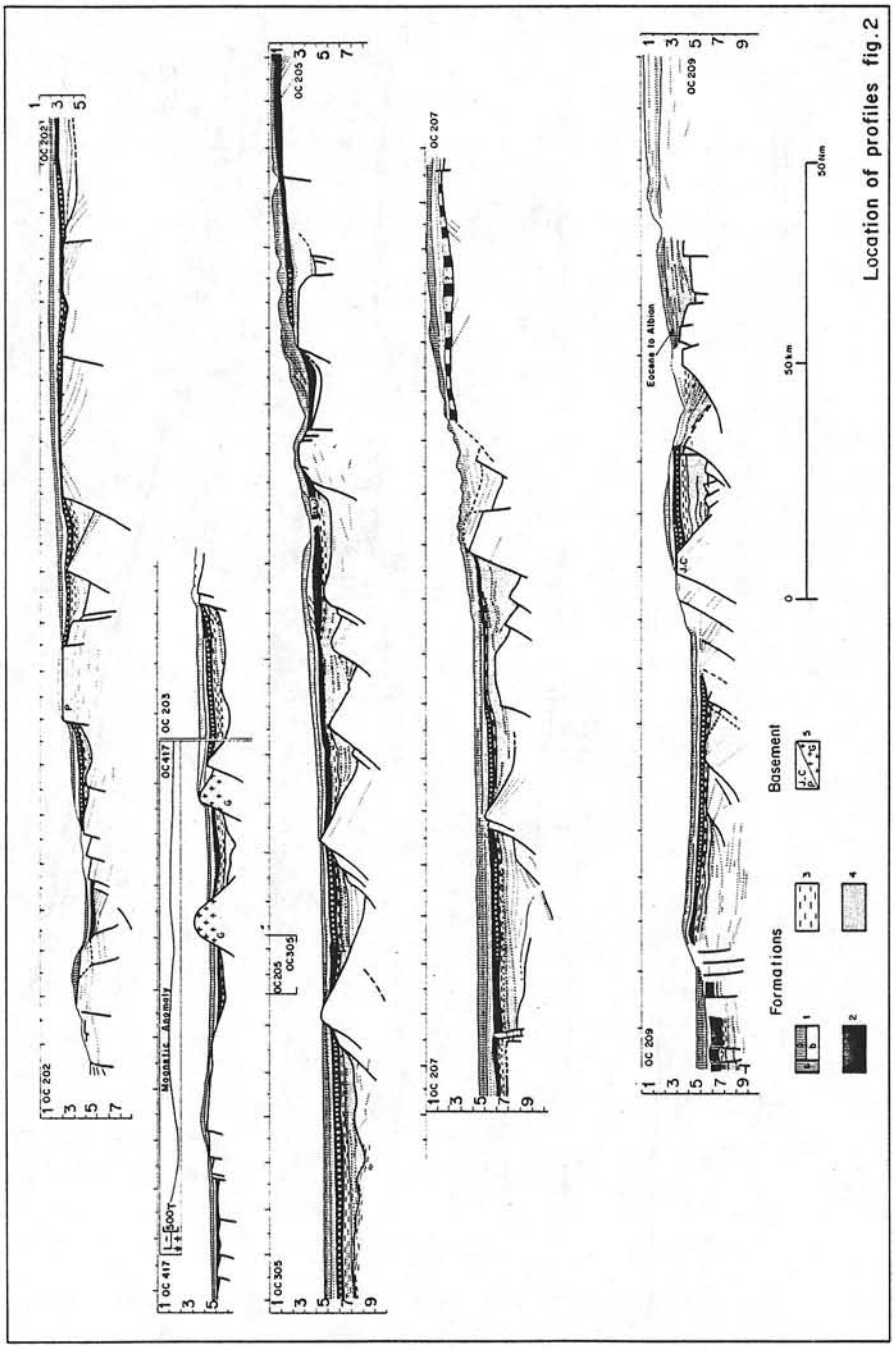


Fig. 3. Depth sections across N. Biscay margin.

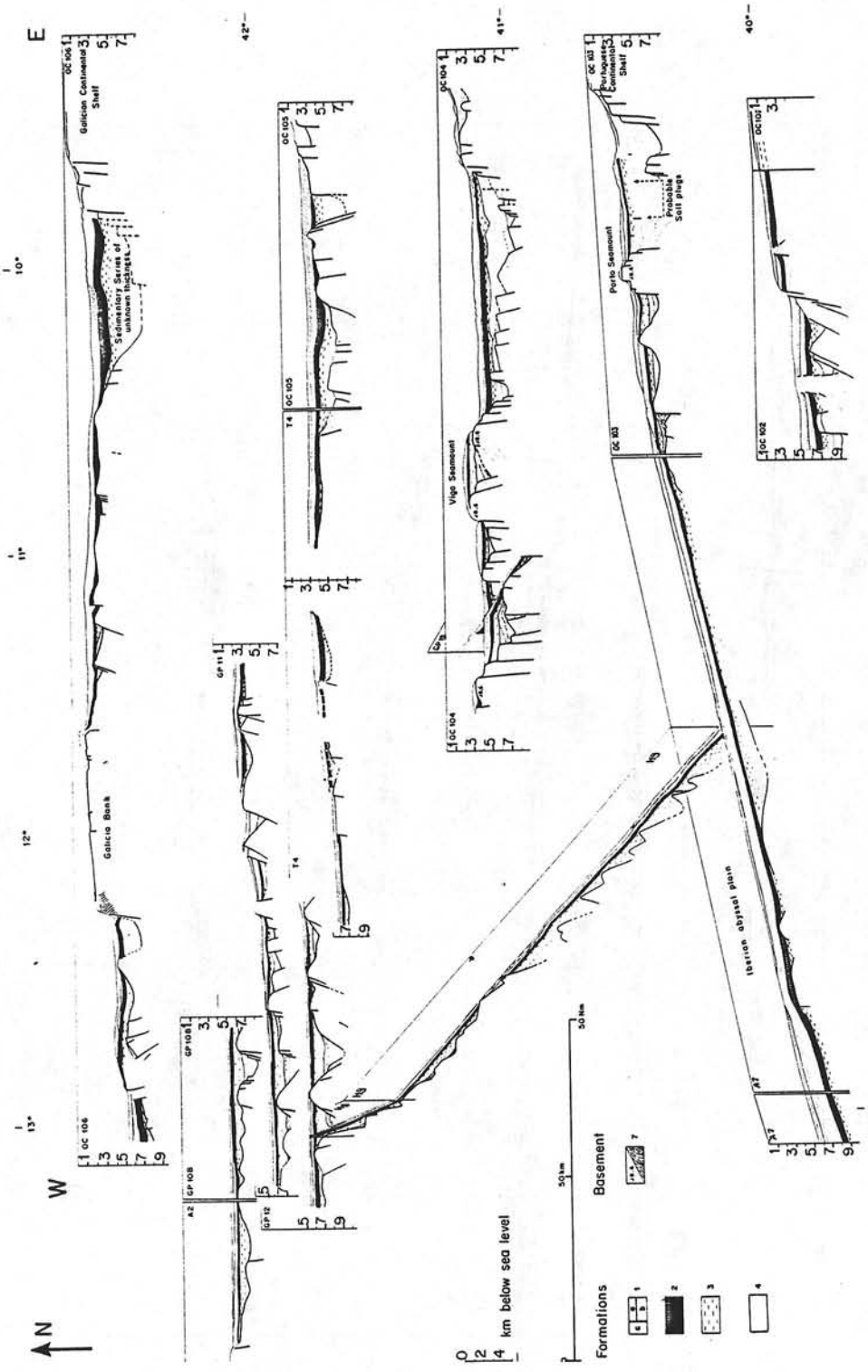


Fig. 4. Depth sections across W. Galicia margin

channel seismic reflection survey (MONTADERT et al, 1974). For the leg 47B (Groupe Galice, in press), CNEXO-IFP shot 2600 km of additional multichannel seismis reflection profiles while CNEXO and University of Paris (Laboratoire de Géologie Dynamique) carried out several cruises with single channel seismic reflection profiling (5800 km) and numerous dredgings. In northern Biscay, single channel profiles (STRIDE et al 1968, DINGLE and SCRUTTON 1977, C.O.B. unpublished profiles) and multichannel profiles (MONTADERT et al. 1971, 1974) have shown the existence of horst and graben structures and of Cenozoïc and Mesozoïc sediments. To prepare Leg 48 drilling sites, French institutions (Institut Français du Pétrole, CNEXO, CEPM) made 3600 km of multichannel seismic profiles. After the Leg, these institutions carried out a new survey with 1300 km of multichannel seismic profiles completed by high resolution multichannel seismic on the three sites. The Institut of Oceanographic Sciences (U.K.) made also about 2000 kms of multichannel seismic profiles in this area.

## Stratigraphy

This section will be devoted mainly to the seismic stratigraphy calibrated by boreholes and dredge data.

### Acoustic stratigraphy (Fig. 3 and 4)

The seismic sections show in most cases 4 main sedimentary units over an acoustic basement.

Acoustic basement. The "basement" is distinguished from overlying sediments either by its diffractive character or by dipping reflectors. Folding is present locally (Devonian, Carboniferous ?). A strong reflector defines the basement surface and is characterized by a strong relief consisting of sharp crests, undulations, flat horizontal surfaces that comprise the buried relief (fig. 3, 4). The basement itself appears to be divided by faults into blocks (horsts and half grabens) of different heights, very frequently tilted along rotational faults (fig. 5). Where the "basement" is also composed of sedimentary rocks, their thickness may reach two seconds, or more than 3 kilometers assuming a mean sound velocity of 3,5 km/sec (fig. 5). In the Galicia area, where the acoustic basement is of sedimentary nature, it seems generally not so well layered (fig. 8) as in the upper part of the Biscay margin. The dips and faults show that it was fractured and displaced prior to the deposition of most of the overlying sedimentary cover.

Formation 4 (fig. 3, 4, 5, 6). Formation 4, which is a moderately to strongly layered formation, is separated from the overlying formation 3 by a strong reflector. Formation 4 lies in troughs between horsts and tilted blocks. Layering is quite conformable at the base with the top of the basement in the lowest part of the fills and at the top can be almost flat. This indicates that sedimentation occurred as basement blocks were being tilted.

Formation 3 (fig. 3, 4, 6). Formation 3 is in most cases transparent or slightly layered. It is thickest in the deep troughs between large tilted blocks (e.g. 800 m in Meriadzek) (fig. 6) but in the abyssal plain it appears as a thin continuous layer (about 200 m thick) overlying Formation 4 (fig. 7). Bedding may be slightly inclined in troughs and basins but dips are much less than in Formation 4. In general, the Formation appears to be absent on the structural highs, and its upper boundary lies well below the highs ; however very condensed equivalents may be present on some high points (site 401). Deposition of Formation 3 infilled the depressions between the fault blocks resulting in a subdued but not totally buried topography. Dips within Formation 3 between tilted blocks reflects only differential compaction. In contrast to Formation 4, deposition took place after the basement had ceased to move actively.

Formation 2 (fig. 3, 4, 5, 6, 7). The sequence above Formation 3 consists in several strong reflectors separated by finely layered strata. It cannot be considered as a single unit since a structural or erosional unconformity frequently occurs within the sequence. Its lower part has been called Formation 2 and is distinguished easily from the upper part called Formation 1b where these two units are unconformable (fig. 8). Elsewhere, the units are identified only on the basis of layer-to-layer correlation. Generally Formation 2 contains more reflectors than 1b, except in areas of thick distal deposition (the abyssal plain), where it may be the contrary. It should be noted that Formation 2 is layered in most areas. In those cases where post-rift deformation is observed, Formation 2 is always affected but not 1b. Thickness of Formation 2 is between 200 to 800 meters thick, reaching its maximum beneath the abyssal plain but it may be condensed into a single reflector. On Biscay margin (Meriadzek Terrace), it may be completly eroded (fig. 6).

Formation 1. Formation 1 is the most recently deposited sequence and is weakly layered. Often, it can be divided into two members, 1a and 1b, the latter one being more intensely layered. If high resolution seismic profiles are considered, a higher member of subunits can be locally distinguished but their correlation throughout the area is very difficult. The lower member 1b is often unconformable on Formation 2, but may be conformable over large areas. Member 1a is almost everywhere conformable with 1b. The whole Formation 1 is 600 to 900 meters thick, and its thickness is greatest beneath the abyssal plain and the Continental slope (1200 to 1400 m). This formation is characterized by large scale sedimentary features.

### Correlation of formations with the lithological units of the holes

Detailed correlations between seismic units and major lithologic changes on the holes are

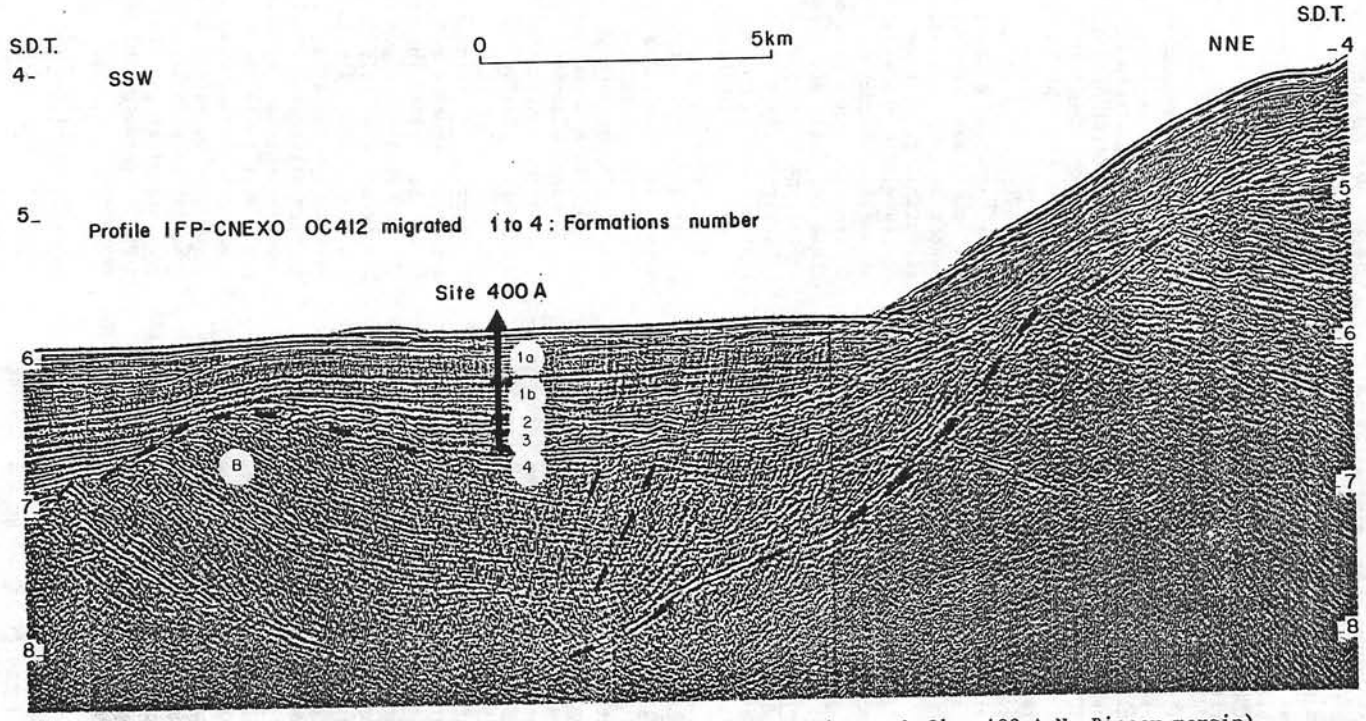


Fig. 5. Example of tilted black bounded by listric fault (through Site 400 A,N. Biscay margin)

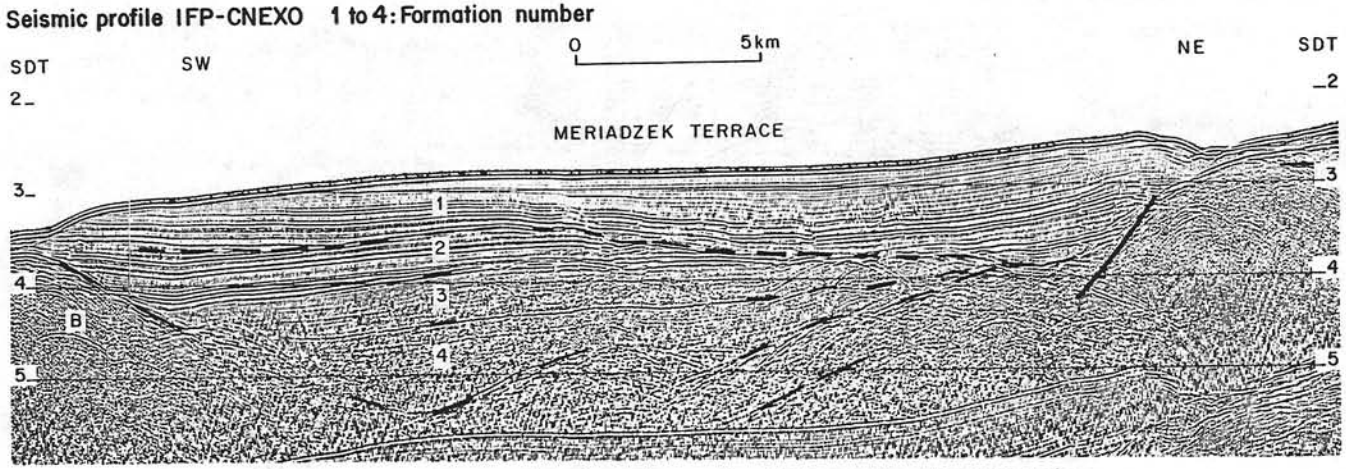


Fig. 6. Acoustic stratigraphy and unconformities on N. Biscay margin.

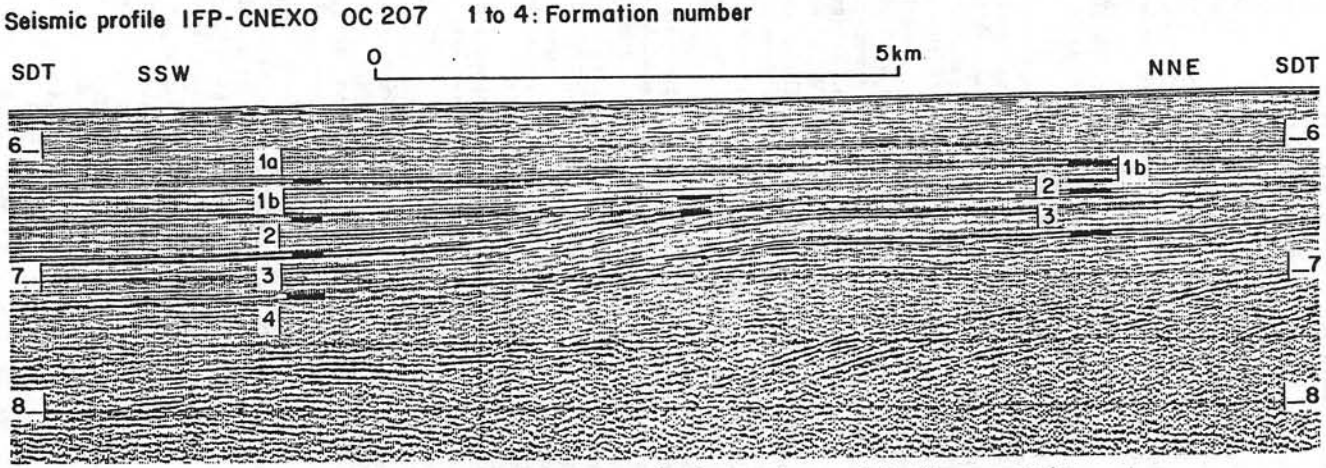


Fig. 7. Acoustic stratigraphy on the lower slopes of N. Biscay margin.

always one of the major problems for extending regionally results of DSDP holes. At site 398, correlations have been improved by computation of synthetic seismogram, using acoustic impedance values deduced from core measurements and computation of acoustic impedance pseudologs (BOUQUIGNY and WILLM, in press). In Biscay, density and velocity logging obtained in holes 401 and 402 permit a good correlation, especially because high resolution seismic reflection profiling have been carried out on the sites after leg 48. (Site chapters 401, 402, leg 48, in press). A summary of these correlations is given below :

Hole 398 (fig. 8) (Site chapter 398, leg 47B, in press, Groupe Galice, in press). Acoustic formation 1 is of Oligocene age to present and is essentially constituted by nanno ooze and chalk. Acoustic formation 2 corresponds to Senonian to Upper Eocene. It consists of two main lithological units : brown marly nanno chalk, calcareous mudstone, claystone and siliceous mudstone in the lower part which underlies siliceous marly nannochalk and mudstone interbedded with turbiditic sand-silt-marl sequences. Acoustic formation 3 corresponds to Lower Albian to Middle Cenomanian. At its base, Lower to Middle Albian laminated dark shales mostly of continental provenance are followed by interbedded dark shales and marlstones from Middle to Late Albian and by Late Albian to Middle Cenomanian redeposited marl and chalk of pelagic origin. Acoustic formation 4 corresponds to Late Barremian to Uppermost Aptian. It is constituted of sand-silt-clay graded sequences interbedded with thick (1 to 10 m) slumped beds of debris flows. A stratigraphical break exists in the Uppermost Aptian and corresponds both to a sharp lithological change and to a major reflector between formations 4 and 3. The acoustic basement is clearly of sedimentary origin on this profile. It is highly diffractive in most places and shows strong reliefs either as broad undulations or as sharp crests corresponding to buried highs. At hole 398, it consists of marlstone, siltstone and white indurated limestone of late hauterivian to early Barremian age.

Holes 400 - 400A (fig. 5) (400, Site Chapter, leg 48, in press). Formation 1a corresponds to Quaternary, Pliocene and Upper-Middle Miocene oozes and chalk. 1b is the underlying layered sequence whose base is the Oligocene/middle Eocene hiatus. This sequence is composed of an upper slightly layered member and a lower more strongly stratified member and corresponds to lower Miocene, Oligocene oozes, nannofossils chalks and marly chalks with mudstone layers. Although well defined in the Site 400 area, this sequence is not easily correlated far from the hole, because it is very similar in appearance to Formation 2 and the boundary between the two Formations may be not clear where the formations are conformable. In some cases, Formations 1b and 2 have not been distinguished. Formation 2 corresponds in the hole to the sequence defined at the top by the Oligocene/

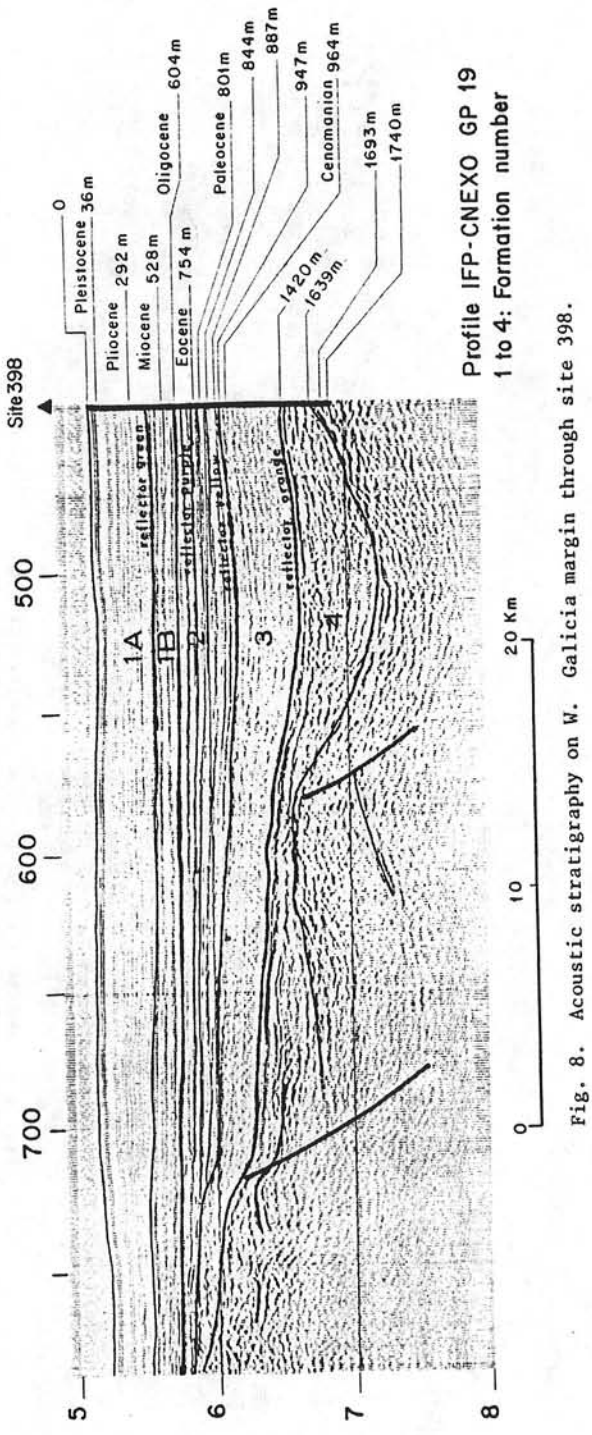


Fig. 8. Acoustic stratigraphy on W. Galicia margin through site 398.

middle Eocene hiatus and its base by the Upper/ Lower Cretaceous hiatus. This sequence is composed of alternating marly chalks and mudstones. Formation 3 was drilled in part and is composed of carbonaceous mudstones, marly chalks and limy claystones of Albian to Aptian age. This sequence is correlated with all the transparent or slightly layered sequences underlying Formation 2 observed on the profiles at depths below two and half seconds beneath sea level. In many places, these layers are characterized by low interval velocity although this is not the case at Site 400. Formation 4 was not reached and is assumed to be of pre-Aptian Early Cretaceous age.

Hole 401 (fig. 9) (401 Site Chapter, leg 48, in press). Formation 1 was partly drilled and corresponds with the Quarternary to Oligocene sequence. The top of Formation 2 has been correlated with the Late Eocene unconformity (Reflector 1 in the hole) that is clearly seen in the right part of the profile in fig. 9. Formation 2 is composed of siliceous nannochalk and marly nannochalk of Middle Eocene to late Cretaceous age. Formation 3 is not visible on the profiles near site 401, where very thin Upper Aptian chalks were drilled. It is well developped to the North of the site where it is characterized as elsewhere by weak layering and low sound velocity. The acoustic basement drilled at hole 401 consists of Late Jurassic to possible lowermost Cretaceous shelf bioclastic limestones.

Hole 402 (fig. 10) (402 Site Chapter, leg 48, in press). The upper formation 1 is constituted by Quaternary muds and oozes with ice-rafted pebbles. Neogene is very reduced. The layered sequence (formation 2) comprises late Eocene oozes and Middle Eocene siliceous nanno chalks and limestones, above a series of carbonaceous calcareous mudstones, and limestones of Albian and Aptian age (formation 3). The top of the almost transparent lower formation 4 has probably been attained (lower Aptian Nannoconus limestone). It must represent essentially pre-Aptian Early Cretaceous sediments contemporaneous with the rifting. The acoustic basement is interpreted as pre-rifting Mesozoïc platform carbonates.

The stratigraphic controls provided by dredgings will be discussed later but generally support the seismic interpretation.

The main unconformities

Several unconformities are observed on the North Biscay and Galicia continental margins. Some are related to tectonic movements, others to paleo-oceanographic events.

The first unconformity of structural origin separates the post-rifting sediments (formation 3) from the underlying sediments (formation 4 or

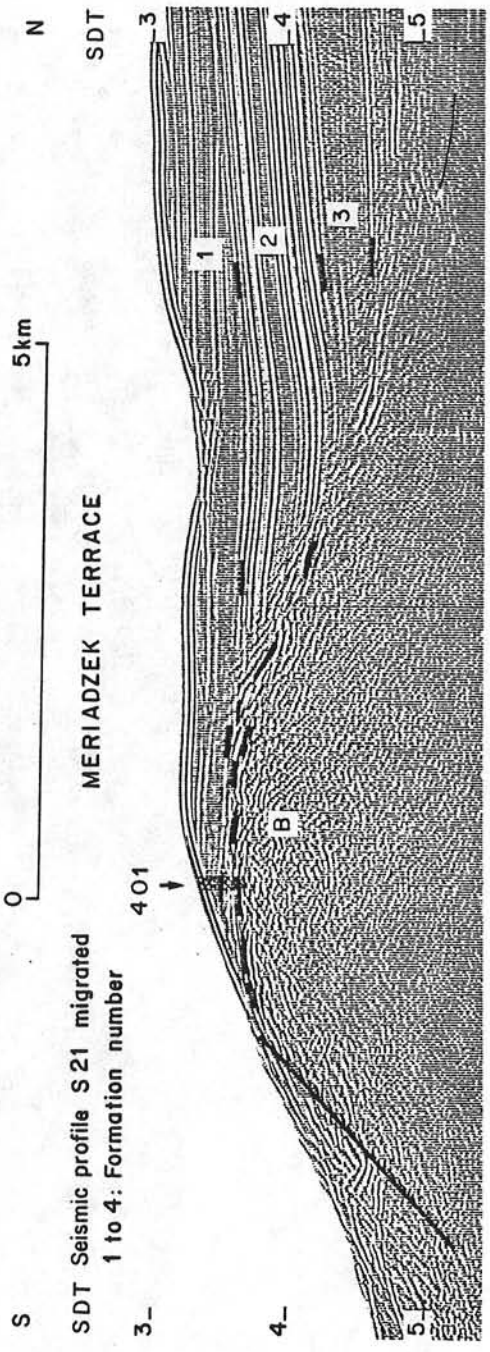


Fig. 9. Acoustic stratigraphy on N. Biscay margin through site 401.

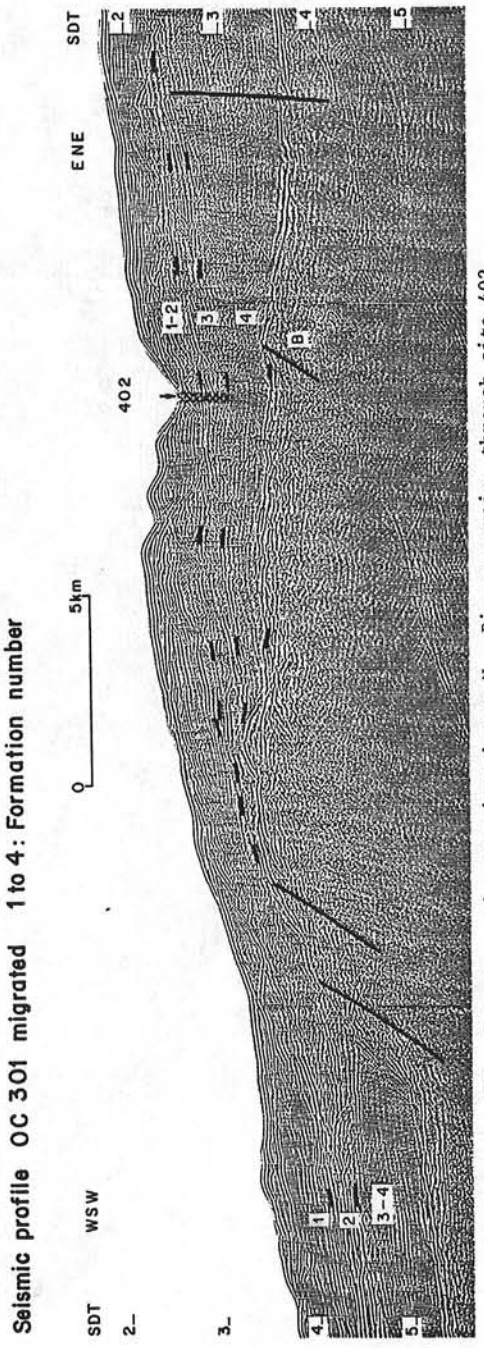


Fig. 10. Acoustic stratigraphy on N. Biscay margin through site 402.

acoustic basement) which were affected by rift tectonics. Since the paleotopography created by rifting was very pronounced (fig. 3, 4) and the post-rift sediments are very thin, every situation is present from no visible unconformity in a half graben to non deposition of post-rifting sediments on the crest of a tilted block ; fault block crests even outcrop on the sea bottom. However beneath large parts of the margin, the change in regime from rifting to subsidence occurred in deep waters so that deep syn-rift sediments grade without interruption to deep post-rift sediments in half grabens. In these cases one cannot observe a continuous break-up unconformity.

Another unconformity of structural origin is observed locally in areas which were affected by late Eocene compressional movements. This is particularly clear along the Trevelyan escarpment which was largely created at that time and along the northern flank of Galicia Bank (see last section).

Another unconformity separates the upper Cretaneous chalks from the Aptian-Albian "black shales". A large hiatus of Cenomanian to Santonian age in Biscay and of Mid Cenomanian to early Senonian in Galicia separates the two formations (389 Site chapter, leg 47B, in press). The unconformity is emphasized by the change of seismic facies between the transparent formation 3 and the strongly layered formation 2. Angular truncation of the black shales below formation 2 at the unconformity is due to differential compaction of the black shales in the half graben during a period of non deposition and bottom current activity. This hiatus is known in many parts of the Atlantic and is due to a major paleo-oceanographic event synchronous with the global Cenomanian-Turonian transgression.

Between Formation 2 (Upper Cretaceous to late Eocene) and Formation 1, an unconformity is also often visible and associated with strong erosion (fig. 6, 9). This event which occurred between the Late Eocene and Oligocene has not been dated with great precision, but it clearly post dates the middle Eocene paleo-oceanographic change that is marked by a sharp increase of silica production. This paleo-oceanographic event which resulted of a change in plate tectonic motions is linked to the onset of a strong bottom water circulation that caused erosion, sediment drift, dunes, sediment waves, resulting in a seismic facies very different from Formation 2 which is in contrast mainly characterized by pelagic draping. This event very probably affected the whole Atlantic and could be synchronous of the "great sculptural event" described on the western Atlantic margin (TUCHOLKE, 1978).

Formation 1 is also composed of different depositional sequences separated by unconformities

that are particularly visible on the upper slope, and possibly related to eustatic changes in sea level (VAIL et al., 1977). They are however difficult to pick on the whole margin.

## The structural evolution of the continental margin

### The rifting phase

Pre-rifting geology and beginning of rifting. In Biscay, seismic reflection profiles show that the fault blocks (fig. 3, 4, 5) contain either thick layered sediments whose parallel inclined reflectors are clearly seen in front of the Western approaches basin, or basement with a thin sedimentary cover in the area of Goban Spur. Data on the age and nature of these rocks are rather scarce. At Site 401, on Meriadzek Terrace, late Jurassic and possibly earliest Cretaceous calcarenites were penetrated below an horizontal erosional surface. These sediments may represent a pre-rift carbonate platform. Late Jurassic Calpionellid limestones dredged on the Meriadzek Terrace (PASTOURET et al., 1976) support this interpretation, but indicates also more open sea conditions. Since the exact age for beginning of the rifting phase is not known, an alternative hypothesis is that the late Jurassic shallow water Carbonates found at Site 401 are geographically restricted to the highest point of previously faulted blocks. Several dredges in the Goban Spur area, (Granite Cliff, Menez Bihan, fig. 2) recovered granitoïdes whose ages vary from 251 MY to 290 MY, indicating an hercynian basement (PAUTOT et al., 1976). Metamorphic rocks have also been dredged as well as sedimentary rocks as shallow water carbonate of probable Carboniferous age and sandstones (AUFFRET et al., in press). These lithologic data confirms the seismic reflection data, and demonstrate the existence of two geological provinces prior to rifting i.e. one with thick mesozoïc deposits in front of the western Approaches basin, and another on Goban Spur that corresponds to a regional basement high with a thin Mesozoïc sedimentary cover. These geological realms are known on the shelf as the western Approaches mesozoïc basin and the basement high running from Cornwall to Goban Spur and are intersected by the present margin and the initial rift.

On Galicia plateau, numerous dredges recovered schists, phyllads, gneiss, granulite and granite on the escarpments of Galicia Bank, Vigo Seamount and Vasco da Gama Seamount (DUPEUBLE et al., 1976) (Groupe Galice, in press) indicating the presence of a continental basement of probably same nature than known on land in Galicia. The oldest sedimentary rocks, obtained by dredgings on the continental slope and on the marginal banks of Vigo, Porto and Vasco da Gama, are bioclastic limestones with algae dated Late Kimeridgian to Berriasian and Calpionella pelagic micrites dated Late Tithonian to early Berriasian (Groupe Galice, in press). This means that at the end of Jurassic times there was a shallow epicontinental sea communicating with an open sea connected to the Mesogea. These samples seem to come either from the acoustic basement or perhaps from formation 4. There is no direct evidence on the margin of sedimentary rocks older than Late Jurassic but on the continental shelf of Portugal, a complete mesozoïc series exists including evaporites of Triassic age. Seismic reflection surveys in the deep basin between Porto Seamount and the continental shelf show diapiric structures, probably linked to these Triassic evaporites (MONTADERT et al. 1974). In the area of site 398 (fig. 8), the acoustic basement is constituted of tilted faulted blocks clearly of sedimentary origin. It has been proposed that the lowermost 73 meters were drilled in the acoustic basement (Site 398 chapter, in press). This lowermost section consists of a complex sequence of marlstone, siltstone and white indurated limestone of Late Hauterivian to Early Barremian age. The white indurated limestones were deposited under pelagic conditions whereas marlstones and siltstones could have been emplaced by low density turbidity currents in a very quiet environment. Limestones have been deposited at a depth shallower than the CCD but probably at depths reaching 2 kilometers at the site (site 398 chapter, in press). If this interpretation is correct, the initiation of rifting in this area would have been early Barremian. Nevertheless, the acoustic basement being steep and irregular, and taking in account the uncertainty of hole location with respect to the seismic profile, it is possible that site 398 did not penetrate in the pre-rift formations but bottomed in the syn-rift formations.

It is clear that pre-rifting geology in North Biscay and Galicia are similar. In both cases, rifting occurred on a pre-existing marine mesozoic basin.

The pre-rift paleogeography is still disputable because of the lack of deep stratigraphic data on the margins, and uncertainties on the pre-rift reconstructions of Biscay. The Hercynian basement was subjected to a first phase of tensional tectonics during Triassic-lower Liassic time with evaporite deposition that is well known in Aquitaine and part of Galicia-Portugal (WINNOCK 1971 - ROSSET et al., 1971 - MONTADERT et al., 1971 - 1974 - BRGM et al., 1974). The western Approaches basin could also have been initially structured by this distension. It is noteworthy that in the Aquitaine, the northern boundary of the thick Triassic deposits is a fault system (the Celtaquitaine flexure of WINNOCK, 1971) which is exactly in the prolongation of the present armorican continental margin. These tensional movements ceased in Aquitaine as well as in Galicia-Portugal during most of the Jurassic when marine epicontinental sediments were depo-

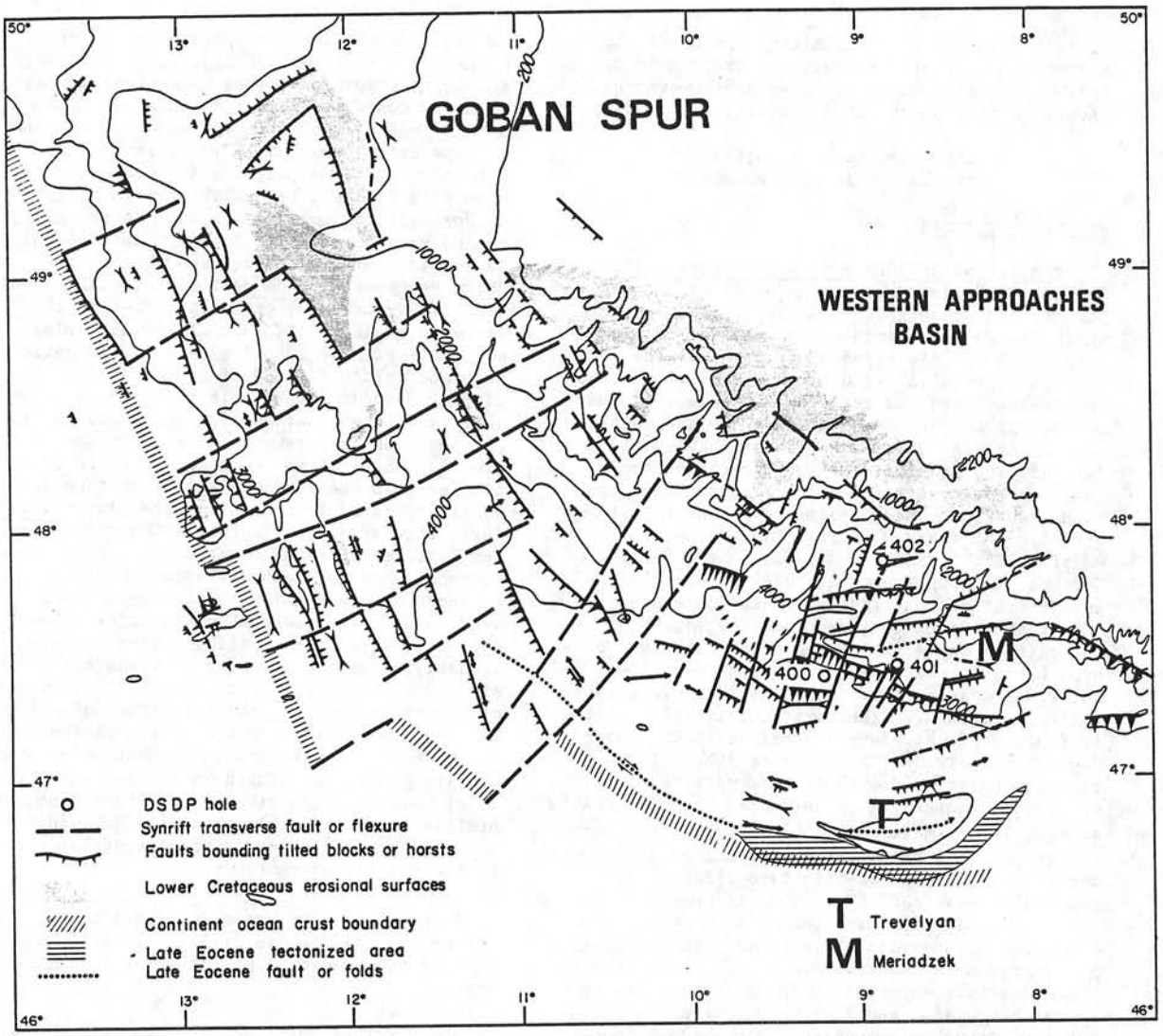


Fig. 11. Schematic tectonic pattern of the rift system on N. Biscay margin.

sited indicating an open sea. The bathymetry of this Mesozoïc sea is not well established offshore, but calpionellid limestones are known all around Biscay and Galicia. In northern Biscay, seismic reflection profiles consistently show a downslope facies variation of the pre-rift mesozoïc, with the developement of a well layered series perhaps indicating more basinal deposits. This change is examplified by figure 10 upslope and by figure 5 downslope. After this quiet Jurassic period, tensional tectonism occurred again at the end of the Jurassic all over the Europe-America plate, creating a complex system of rifts. Some of these subsequently aborted like in the North sea or in the Western Approaches but others evolved to form a passive continental margin with accretion of new oceanic crust. In Northern Biscay, the start of this rifting episode is not well documented. In the Western Approaches basin, results of the exploration wells have not been published but in the Celtic Sea the break up unconformity is of Aptian age. In Aquitaine it is particularly well documented for the Parentis Basin which opens directly westward into Biscay. Detailed maps based on drilling results (BRGM et al., 1974) indicate that the Parentis Basin is first identifiable in late Oxfordian time as an area of slightly more rapid subsidence. During the Neocomian the Parentis Basin became a large graben, indicating a period of active rifting. Since the northern boundary of the Parentis Basin is in continuity with the Armorican margin, the timing may

be extrapolated to the Northern Biscay and is not in contradiction with our observations. Site 398 results (see above) could indicate a starting of the rifting episode or an episode in the rifting process in Lower Barremian time.

It is thus concluded that in this part of the Northeast Atlantic, active rifting took place in Lower Cretaceous time, in a preexisting marine basin in contrast to other rift systems which were subaerial.

The tectonic style of the rift system. The tectonic style of rifting is examplified by several interpretative depth sections across both margins based on seismic reflection profiles (fig. 3, 4). The overall tectonic style is characterized by a series of tilted blocks bounded by faults which in many cases are clearly listric faults. These blocks delineate half grabens. True horsts are rare on the Biscay margin. Some of these blocks are cut by erosional surfaces, which on too highly exaggerated profiles give the misleading appearence of horsts. There is a clear polarity of the dip of faults towards the axis of the rift system in Northern Biscay and in the western part of the Galicia Plateau.

A schematic fault pattern of the rift system developped during lower Cretaceous has been mapped from the seismic profiles in North Biscay (fig. 11). The pattern is best documented in the area of Meriadzek where the spacing of the profiles is less than 10 km. However, delineation of fault trends is often uncertain and more so in the area of Goban Spur. Spacing between consecutive fault block crests varies from a few kilometers to 30 kilometers and the length of individual blocks is limited to between several and 20 - 30 kilometers by transecting normal faults that do not show horizontal displacement. These faults are often delineated by the lack of continuity of tilted blocks. The apparent throw can vary along these faults since crests and half grabens do not coincide on both sides. Comparable patterns have been described on intracontinental rift system such as the southern Ethiopian rift system (MOORE et al. 1978). The trend of the tilted blocks generally follows the strike of the margin and changes between the Goban Spur (150° E) and the Meriadzek area to more variable trends of 80° to 130° E. Transecting faults oriented almost perpendicular to the margin, vary in direction from 60° E in Goban Spur area to 15° - 30° E in the Meriadzek area where trends are again more variable. If, as is probable, faulting during rifting accomodated previous fractures or inhomogeneities in the Hercynian basement, the observed differences in fault orientation suggests that the Hercynian basement in the areas of Goban Spur and Meriadzek is different on both lithology and structure. In any case, the faults trending at 80° E in the Meriadzek area and controlling in particular the Shamrock

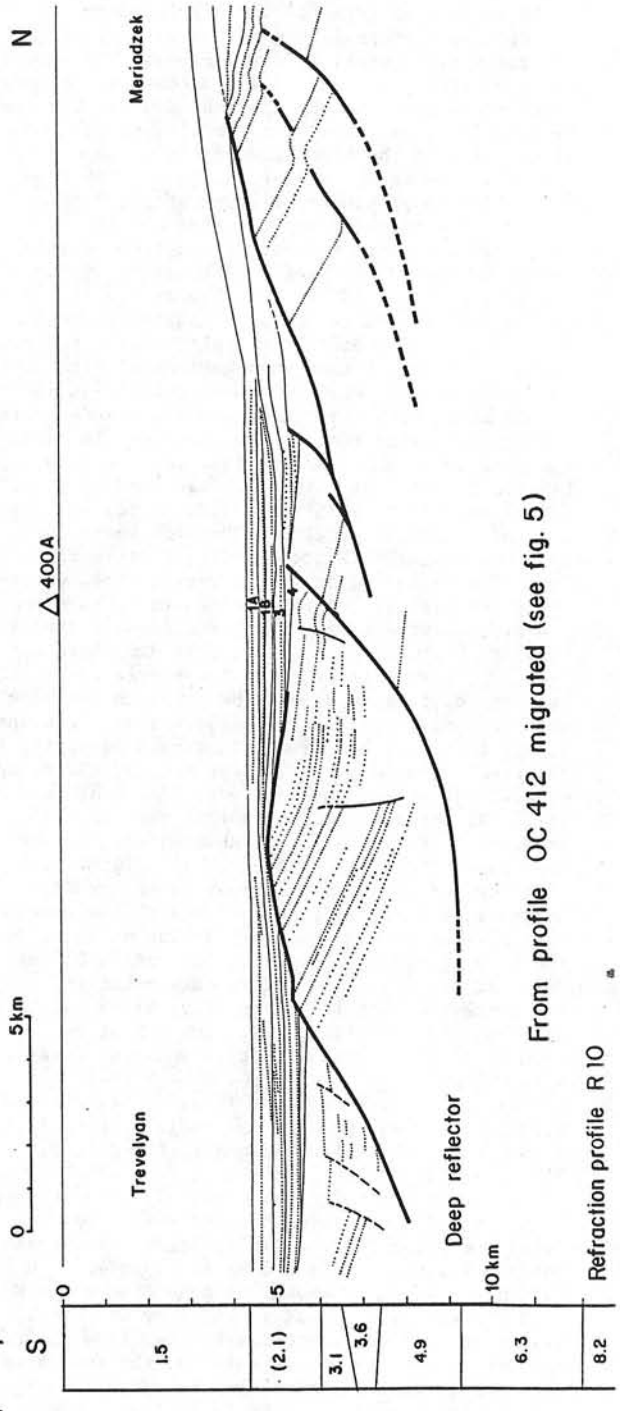


Fig. 12. Geological cross section through tilted blocks at site 400 A and comparison with seismic refraction data (N. Biscay margin).

canyon, have clearly the same orientation as the Hercynian shear zones of Brittany (fig. 1).

Of particular interest and significance for the rifting process is the nature of listric faults created during rotation of the blocks. The base of the syn-rifting sediments is a datum which allows determination of the throw of the faults. For listric faults this throw is a function of the amount of rotation of the block and of the width of the block. It may be as much as 3 to 4 kms for some large individual blocks. Tilting of the blocks involves their rotation about axes parallel to their strike. Depth reconstruction from seismic profiles (fig. 3, 4) show that rotation of the block is commonly 20° to 30°. The change of dip of the faults with depth which characterized listric faults is especially visible beneath the rise, where the faults become near horizontal with depths below the blocks. Figure 5 shows details of individual block with listric faults and figure 12 is a depth reconstruction of the same profile with the same horizontal and vertical scales. Such listric faults have been also described by BLAIR (1975) and BOWEN (1975) in the North Sea and postulated by LOWELL et al. (1972-1975) in the Red Sea and by GARFUNKEL and BARTOV (1977) in the Suez Rift. A reflector, often very strong, underlying the base of the listric faults is seen beneath the rise (fig. 13). Variations in travel time to this reflector are visible and shown as a "pull up" below the crest of the blocks due to the velocity difference between beds within the blocks and sediments infilling the adjacent half grabens. It may therefore be assumed that this reflector is relatively flat and thus independent of the tectonised layer above. An exactly similar feature (fig. 14) observed at the foot of the western escarpment of the Galicia Bank area (fig.2B) demonstrates that it is not of local origin. Such a strong reflector must correspond to a sharp contrast in acoustic impedance and should therefore correspond also to a refraction horizon. On the N. Biscay margin, refraction profile D12 of Ewing et al. (1959) is unfortunately located at the western end of Trevelyan (fig.2A) on both continental and oceanic crusts, thus making the results of little value in this respect. However a recent profile(n° 10) using O.B.S. parallel to the Meriadzek escarpment (fig.2A) (AVEDIK and HOWARD, in press) crosses the reflection profile shown figure 12. Below sediments with 2,1, 3,1 and 3,6 km/sec velocities there is a 2 km thick layer of 4,9 km/sec velocity whose base is situated near 9,500 km below sea level, almost exactly at the level where the listric faults become near horizontal. Below there is a 3 km thick layer with 6,3 km/sec velocity above the Moho discontinuity (8,2 km/sec) situated at 12 km below sea level. Computing vertical sound travel time from the seismic refraction data shows that the interface between 4,9 and 6,3 km/sec layers would lie at 9,2 sec two way travel time in good agreement with the observed travel time of the horizontal

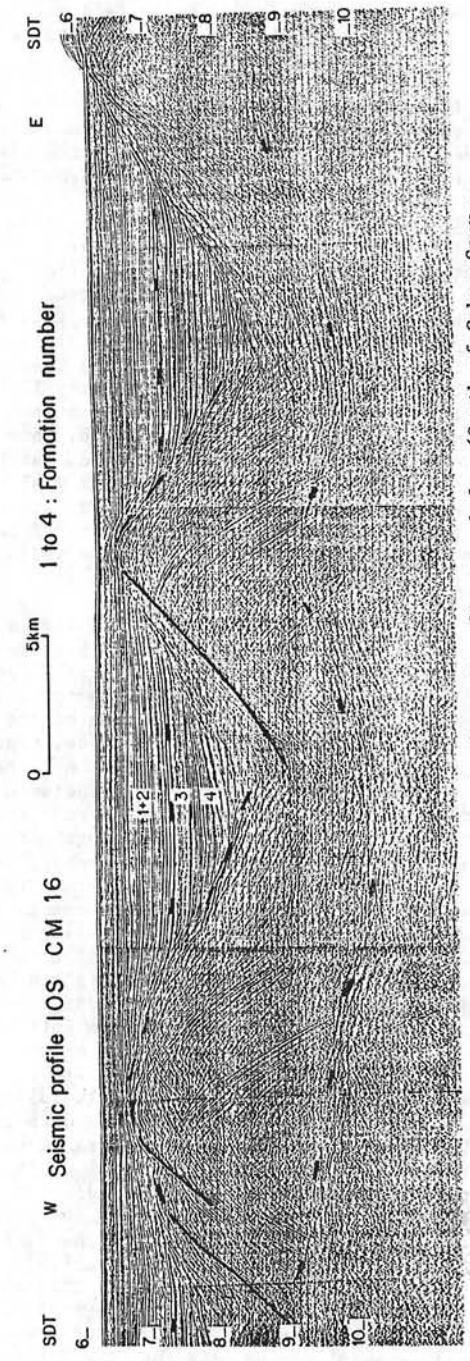


Fig. 13. Tilted blocks and the deep horizontal reflector below (South of Goban Spur - N. Biscay margin).

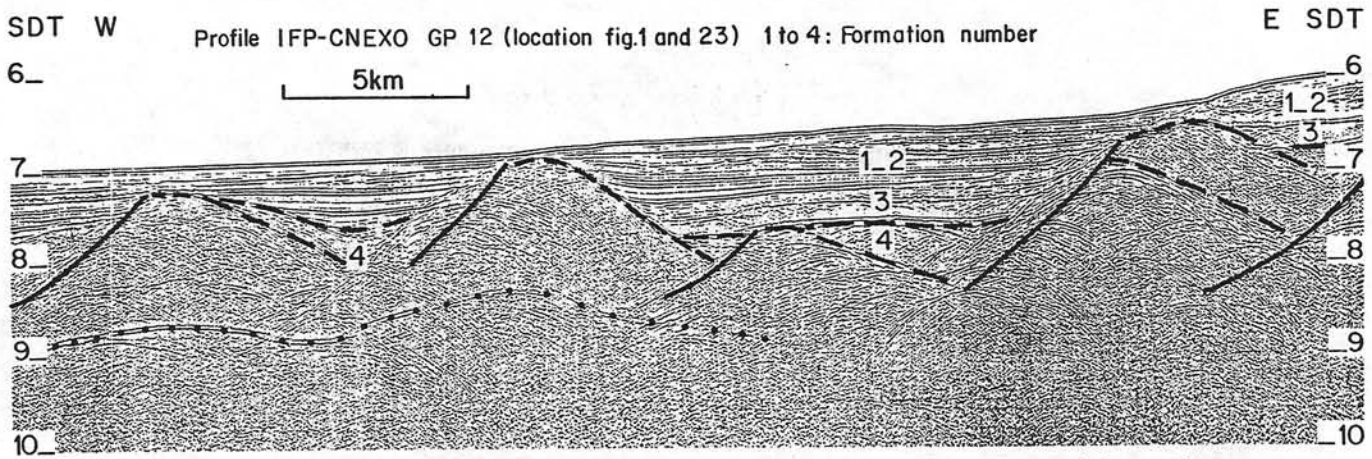


Fig. 14. Tilted blocks and the deep horizontal reflector below (S.W. of Galicia Bank).

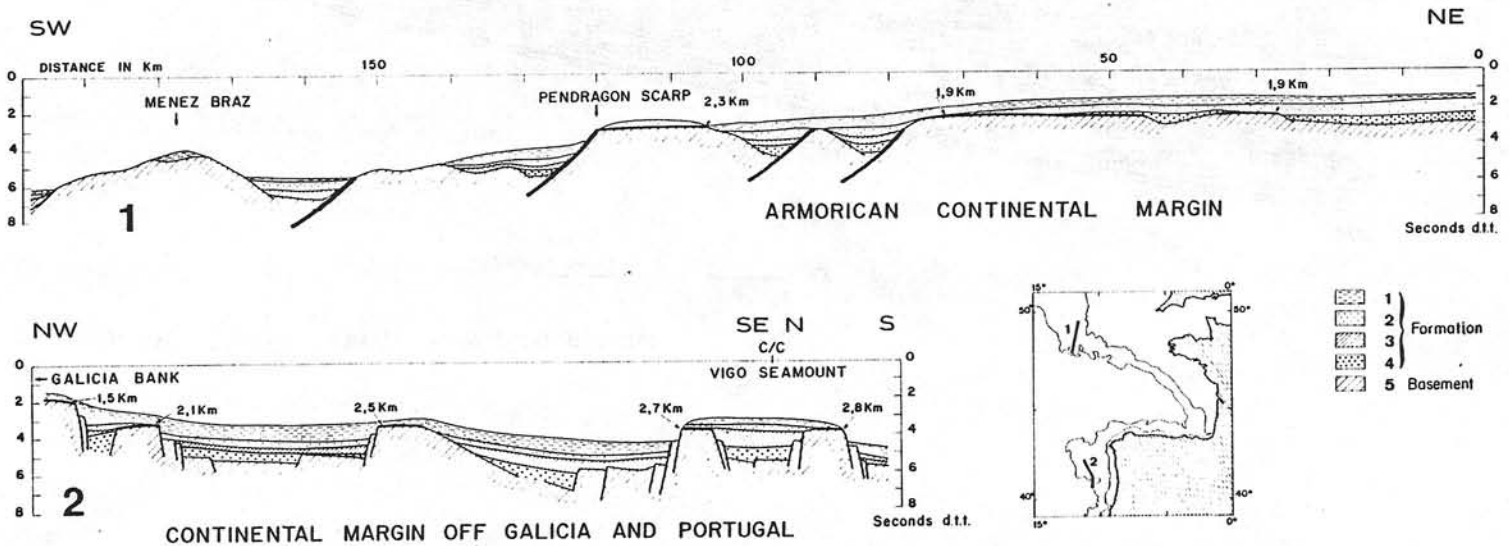


Fig. 15. Lower Cretaceous erosional surfaces truncating faulted blocks on N. Biscay and W. Galicia margins.

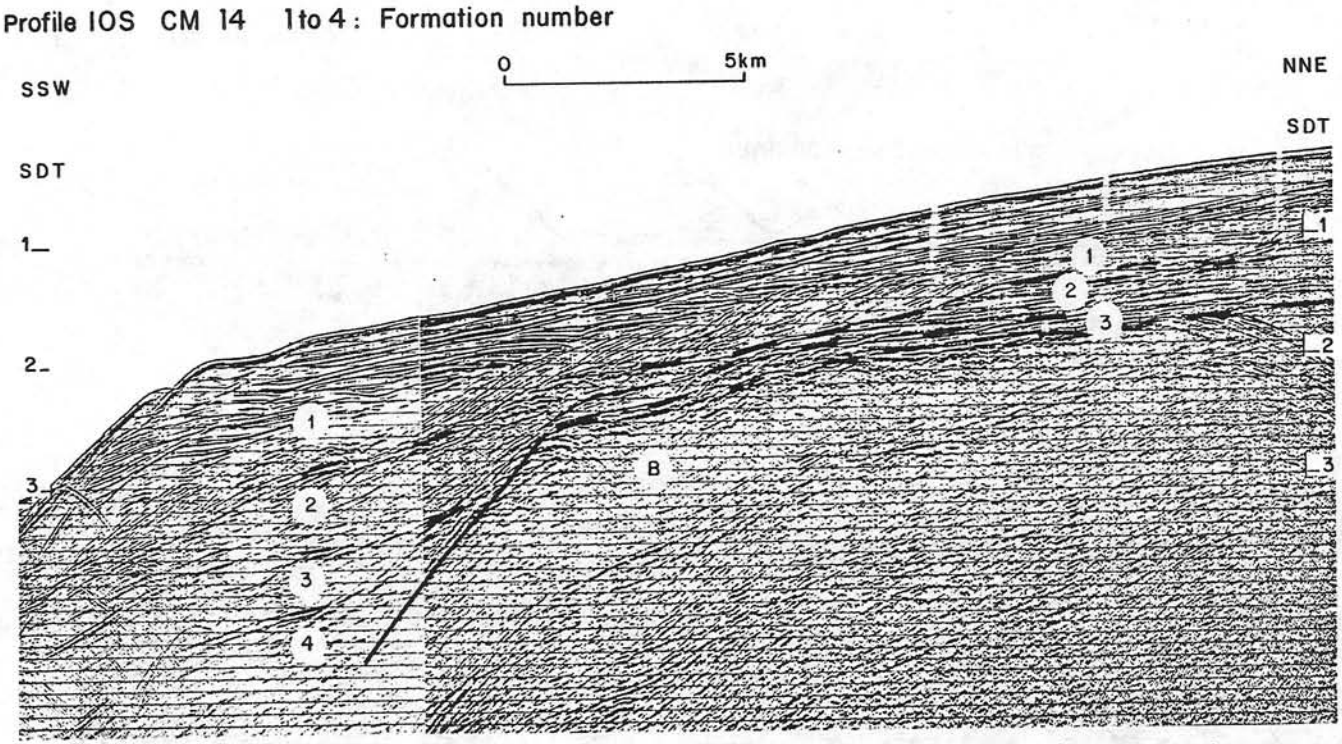


Fig. 16. Lower Cretaceous erosional surface truncating a tilted block on N. Biscay Upper slope.

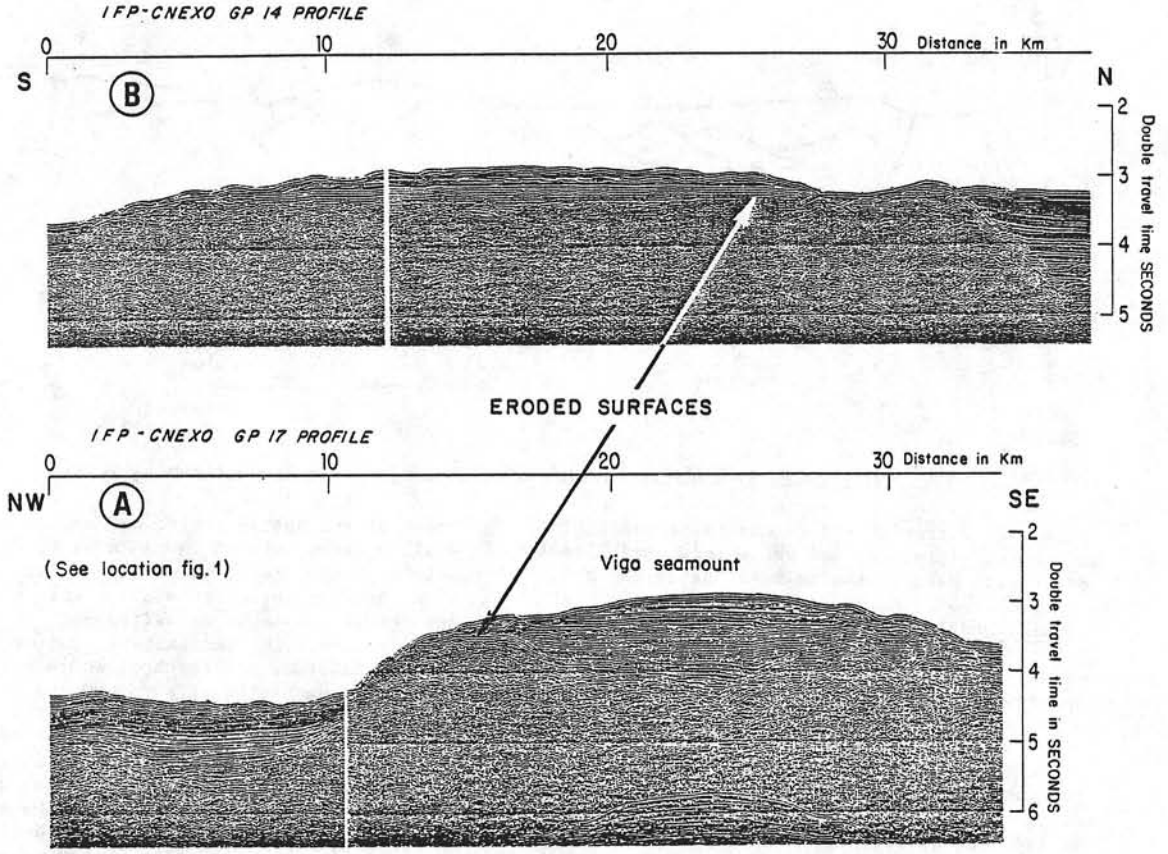


Fig. 17. Lower Cretaceous erosional surfaces truncating faulted blocks on W. Galicia margin.

reflector below the tilted blocks. Drill and dredge data show that tilted blocks include Mesozoïc sediments, and others Hercynian basement showing that the tectonised layer includes continental basement as well as sedimentary rocks. The geological and refraction data thus show that the boundary defined by the near horizontal base of the listric faults and the reflector does not correspond to a particular geological horizon in sedimentary rocks allowing decollement but merely to a mechanical discontinuity within the upper part of the continental crust. This discontinuity which clearly existed at the time of rifting, was situated at around 6 to 8 km below sea level in the central part of the rift South of Meriadzek as calculated from the depth section (fig. 12).

The Syn-rifting sediments. Sediments deposited during rifting (Formation 4) are generally well characterized by convergence of the reflectors towards the crest of the block indicating contemporaneous deposition during tilting. Due to the complex fault block pattern the distribution of the syn-rifting sediments is complex and they may be thin or absent on top of the blocks, and very thick in the half grabens behind large tilted blocks. In some grabens the upper part of the syn-rifting sediments do not show any evidence of tectonic influence on their deposition and seems only to infill a pre-existing depression. This may indicate that rotation of the blocks could have stopped at different periods in different areas. Nevertheless, the latest activity which is probably intra-Aptian without precision in Biscay is very well defined in Galicia and dated latest Aptian (site 398 chapter, in press, SIBUET and RYAN, in press) (fig. 8).

No precise stratigraphic data are available in Northern Biscay because leg 48 drilling was not able to penetrate below the Aptian in a half graben. Some dredgings (AUFFRET et al., in press) found Barremian micritic limestones or marly chalks deposited at shelf or outer shelf depths in the Shamrock Canyon, and Valanginian to Barremian shallow water limestones or chalks on Meriadzek escarpment. On the contrary, in Galicia, the hole 398 penetrated a syn-rift section of sand-silt-clay graded sequences interbedded with thick (1 to 10 m) slumped beds or debris flows dated

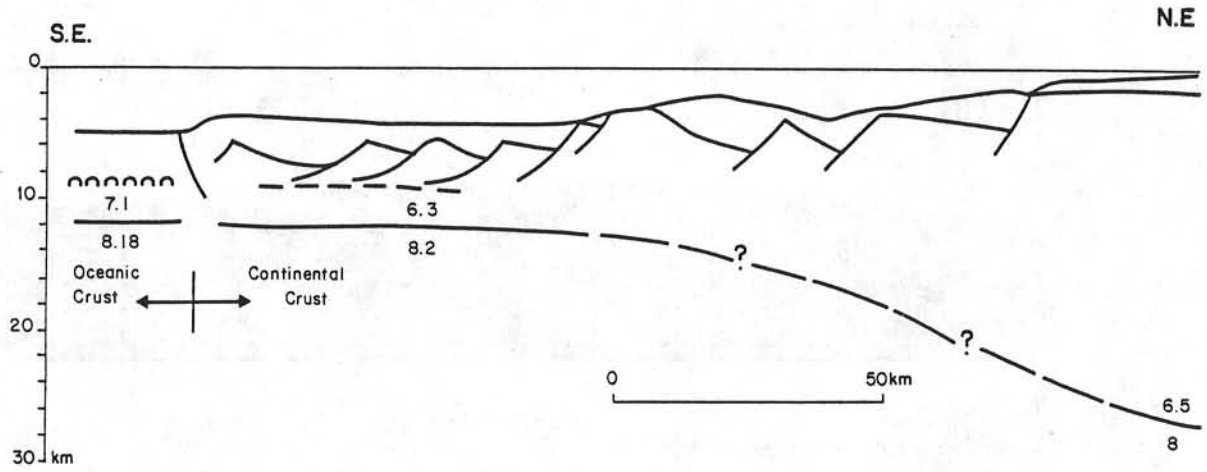


Fig. 18. Schematic crustal section through the N. Biscay continental margin.

Aptian and Barremian and a complex sequence of marlstone, siltstone, and white indurated limestones of Late Hauterivian to Early Barremian age.

The submarine topography at the end of rifting. In Biscay, the drill and dredge data and seismic reflection profiles allow reconstruction of the topography of the sea floor at the end of rifting in Aptian time.

The most striking feature allowing this reconstruction are horizontal planes which cut, in some areas, the crest of the tilted blocks (fig. 15), and indicate subaerial or shallow submarine erosion. These erosional surfaces are shown on fig. 11 in grey. They extend much closer to the ocean-continent boundary off Goban Spur than in the Meriadzek-Trevelyan area where the closest point to the boundary is near site 401.

The age of this erosional event is given by hole 401 and by data on the shelf. At site 401 (fig. 9) outershelf chalks of upper Aptian age rest above shallow water carbonates of late Jurassic and possibly lowermost Cretaceous age ; this demonstrates that erosion occurred during pre-Aptian time while rifting was active, i.e. while blocks were rotating. Near the shelf edge, (fig. 16) calibration of seismic lines from data of the western Approaches basin demonstrate also that the Aptian (pro-parte)-Albian rests on the erosional surfaces cutting the faulted blocks. The seismic profiles therefore delineate areas on the continental margin which were at zero level during rifting. Fig. 11 shows that a large part of the margin in front of the western Approaches basin was below this level. However results from dredging and hole 402 show areas where no erosion occurred but were nevertheless under shallow water during Aptian time. At site 402 Aptian-Albian black shales were deposited as a prograding shelf on a subsiding shallow platform. It appears that in front of the Aptian shelf, one or several isolated shallow banks existed in the area of Meriadzek. Outside these areas, water was deeper. At site 400A, Aptian-Albian sediments are interpreted as deep water sediments deposited not far above the CCD. Since post-rifting sediments including formation 3 are not faulted, the depth at which Aptian sediments were deposited at site 400 can be estimated from the throw of the faults along the Meriadzek escarpment, i.e. from the difference of altitude between the Aptian at site 401 and site 400. A depth of 1500-2000 m is indicated for the area of site 400A on Trevelyan plateau at the end of rifting. In front of the western Approaches basin, large areas of the submarine rift system were deep and a central trough existed of about 2000 m depth. At the same time most of the Goban Spur area was much shallower since erosional surfaces are observed relatively close to the continental-oceanic boundary (fig. 11). Only a narrow deep trough existed there at the end of rifting. This change of style between the two areas may be explained by the difference in nature of the pre-rift rocks. On Goban Spur rifting affected an hercynian granitic basement without sedimentary cover, but in the Meriadzek area rifting affected an hercynian basement probably of a different nature and covered by a thick mesozoïc sequence. This would suggest that the physiography of a rift system may be largely controlled by the nature of the pre-rift rocks.

In Galicia, the same erosional surfaces are observed (fig. 15, 17 ) but no hole had been drilled through. Hole 398 which was drilled in a low demonstrated that syn-rift sediments were deposited in a deep water environment above the CCD during Hauterivian and Lower Barremian and clearly beneath the CCD after Mid Aptian times. Even, if the CCD on margins could be different from oceanic basins, an estimate of water depth during Aptian time is given by several authors (LE PICHON et

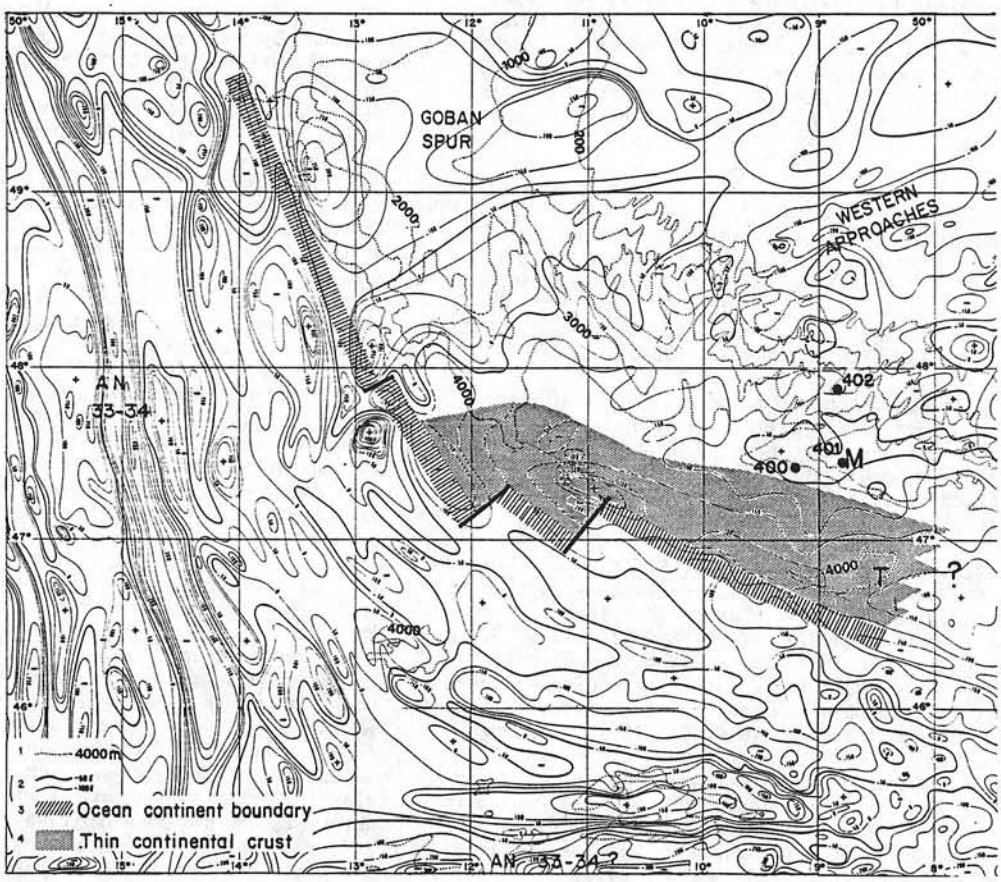


Fig. 19. Magnetic anomalies, and oceanic-continental crusts boundary (N. Biscay margin).

al. in press, VAN ANDEL et al. 1977) around 1500-2000 meters. An independent estimate of the water depth at the end of rifting is given by the difference of levels between the Aptian depth at site 398 and the erosional surface evidenced on Vigo Seamount and supposed to be of Lower Cretaceous age as in Biscay ; the value obtained is around 2500 meters. Such result is in a good agreement with the estimation made in Biscay (1500-2000 m). The higher value for Galicia is in agreement with the fact that there, the Aptian was deposited below CCD, while in Biscay at site 400 it was deposited slightly above. The major consequence of these observations is that on the Northeast Atlantic during Aptian, at the end of rifting, large submarine troughs as deep as 2500 m existed.

## Discussion on rifting and thinning of the crust

Although rift tectonics are relatively simple, there is continuing controversy about their nature and development. Structural models are based mainly on the studies of continental subaerial rift systems like the East African rifts, the Rhine Graben, the Suez rift,...

The different hypothesis. A common hypothesis is that intracontinental rifts are related to doming of the continental crust (CLOSS 1939) and the following stages have been recently proposed (NEUGEBAUER 1978) : 1. upwarping of the crust 2. incipient volcanic activity 3. formation of faults and increasing volcanic activity 4. subsidence of graben. BURKE and WHITEMAN (1973) considered also that rifts developed on crest of uplifts interpreted as isostatic responses to mass deficiencies produced by partial melting of the mantle above rising plumes at the base of the lithosphere. FREUND (1965) pointing out the difference in width between the different rifts, the presence or absence of a swell, proposed a necking hypothesis with thinning of the crust below accompanied by rising of the mantle. He also raised the question of the spatial and temporal relations between the rifts and the orogenies. ARTEMJEV and ARTYUSHKOV (1971) from a study of

the Baïkal rift proposed a mechanism resulting from crustal extension when neck shaped strains in the crust are developed. The lower part of the crust is plastically attenuated and faults occur in the upper layer of the crust where the viscosity is too high. FUCHS (1974) proposed a somewhat similar model for the Rhine Graben.

The cause of crustal extension is also a matter of controversy. HEISKANEN and VENING-MEINESZ (1958) proposed large scale movements in the mantle created by thermal convection, while ARTEMJEV and ARTYUSHKOV (1971) suggest gravity convection. Others relate rifting to the stress field existing inside plates as a consequence of collisions (ILLIES 1975 - GARFUNKEL and BARTOV 1977).

Data on rifting from the study of continental margins are relatively scarce because the rift structures are often covered by a very thick sedimentary overburden hiding the deep structures. This difficulty is partly overcome on the starved North Biscay and Galicia margins.

Rifting and attenuation in Biscay and Galicia. Legs 47B and 48 results and seismic reflection profiles demonstrated that on this area rifting was submarine (MONTADERT, ROBERTS et al. 1977, de Charpal et al. 1978) in contrast to many rifts and occurred on a pre-existing mesozoïc sedimentary basin perhaps shaped during an earlier Triassic tensional episode (WINNOCK, 1971). Although the onset of rifting is not well established, comparison with Aquitaine basins suggests it may have begun by late Jurassic but was probably mainly active during Neocomian. The end of rifting and the onset of spreading is very probably late Aptian. As demonstrated in the previous section, broad 2500 m deep troughs existed at that time. This fact and the tectonic style observed with tilted blocks including the upper part of the continental crust, bounded by listric faults, is characteristic of an extension of the crust with the synchronous development of a central trough. Under continuing extension the fault blocks can rotate only because the central trough is subsiding so that individual blocks dip away from the axis. In the trough, the continental crust affected by listric faults was about 6 to 8 km thick ; the rotation of the blocks reduced this thickness to about 4 - 5 kms (fig. 12).

We suggest that the mechanical discontinuity which controlled the level above which continental crust was faulted during rifting corresponds to the transition between the upper brittle and the lower ductile continental crust (GRIGGS, 1960).This boundary is close to a strong horizontal reflector situated at about 10 km below sea level. This reflector corresponds to an increase of velocities from 4,9 km to 6,3 km/sec as shown by refraction data (fig. 18). (AVEDIK and HOWARD, in press - BOTT and WATTS, 1971). The Moho discontinuity was determined at 12 km below sea level. These results demonstrate an almost complete thinning of the ductile continental crust, reduced to 3 km as a maximum, by some subcrustal process, while it was probably around 15 - 20 km away from the rift (fig. 18). Recent heat flow data obtained in North Biscay margin (FOUCHER and SIBUET, in press) support this mechanism of thinning of the ductile part of the continental crust. Phase changes or intrusion in the lower part of the ductile continental crust could be mechanisms which played a part in crustal attenuation. Nevertheless, as the layer affected by these processes does not contain radiogenic elements, it is still necessary to explain the amount of crustal attenuation and heat flow data, to invoke another process for thinning of the almost entire ductile crust.

The amount of horizontal extension can be estimated approximately for the upper part of the continental crust. For rotation of 20° to 30° of the blocks the extension of the area between the present shelf edge and the oceanic-continental crusts boundary is around 10 - 15 % of the previous width.

Also relevant to the rifting process is the fact that no erosion occurred before and during rifting in the central trough of the rift system. In this case rifting was not preceded by and therefore is not a consequence of a large doming. The same observation was made in the Rhine Graben and in the Suez rift where more or less complete pre-rift sedimentary layers are preserved. The uplifting of the shoulders of the rift there postdates the initiation of the graben. Such uplifting occurred also in Biscay away from the rift trough but is not expressed in the topography since erosion kept pace with the uplift and maintained the area at the level of the sea. The cause of the uplift of the shoulders of the rift could well be regional isostatic adjustment.

Speculation on the mechanism of rifting. From our observations, therefore, the most appealing mechanism for rifting would be stretching of the lithosphere as a response to intraplate stresses. These stresses could be due to the difference between the absolute velocities of plate boundaries or consequences of continental collisions. (FORSYTH and UYEDA, 1975). These stresses were applied to a crust made of two layers of completely different mechanical properties. As shown above, the extension is limited, but the thinning of the ductile part of the crust is much more important than the thinning of the brittle part by rotation of blocks. Rock mechanics experiments (POULET, 1976) show that strain of ductile material increases continuously when a certain level of stress is attained (viscous behavior). On the contrary, the continuous strain of brittle material is relatively limited for increasing stress until a fracture is created which releases the stress. One must therefore conclude that there was mechanical decoupling between the two sections of the crust. For this reason, it is quite possi-

ble that thinning of the ductile part of the crust began before the creation of the first fault in the brittle crust. Then speculating that tensile stresses are the same at the lateral boundaries of the whole lithosphere, the extension will be more important in the lower ductile part by continuous viscous flow starting at a low level of stress accumulation and stress relaxation by faulting until complete break up of the lithosphere. The continuous necking of the lower ductile part of the crust is accompanied by rising of the mantle and a depression in the upper brittle crust (the rift trough) which allows rotation of blocks along listric faults.

The post rifting history

Complete rupture of the lithosphere occurred at the end of rifting in latest Aptian time and new oceanic crust accreted in deep waters along the young Continental margin which began to subside.

The different mechanisms for subsidence. Several mechanisms have been proposed for explaining this subsidence of the continental margins. SLEEP (1971, 1973), SLEEP and SNELL (1976) suggested that post-rifting subsidence could be related to thermal contraction of the lithosphere which occurred when the heat source moves away the margin after onset of spreading. BOTT (1971, 1973), BOTT and DEAN (1973) suggested that accompanying or following the thermal contraction of the lithosphere, subsidence could occur as an isostatic response to crustal thinning caused by hot creep of lower continental crustal material towards the suboceanic mantle. This would be due to instability of young continental margins because of gravitational energy associated with the junction between oceanic and continental crust that would create wedge subsidence in the upper brittle layer. Finally WALCOTT (1970 - 1972) explained subsidence of the continental margin under loading by sediments by flexure of the lithosphere.

On the starved North Biscay and Galicia margins, the post rifting sediments are so thin that the influence of loading on subsidence is negligible, so that the fundamental mechanism of subsidence of a passive continental margin can be directly studied.

Transition between continental and oceanic crusts. In Biscay, the transition between continental crust and oceanic crust is relatively well documented by geophysical data. The magnetic anomaly map of the total field (fig. 19) (SIBUET et al., in preparation) covers an area from the shelf of the western Approaches to the center of the Bay of Biscay. The continental shelf is characterized by strong amplitude anomalies (HILL and VINE, 1965 - SEGOUFIN, 1975 - LE BORGNE and LE MOUEL, 1970) which do not extend off the shelf break. On the continental slope, anomalies of generally small amplitude are oriented parallel to the margin with some transverse discontinuities which can be linked with transverse faults of the rift pattern. Northward, gravity and magnetic anomalies show the extension of the batholitic axis of SW England until the shelf break (HILL and VINE, 1965 - DAY and WILLIAMS, 1970 ; SIBUET, 1972). The map shows that this axis extends until the foot of the continental slope where a late hercynian granodioritic complex have been found by dredgings (PAUTOT et al. 1976). The oceanic domains of the Porcupine abyssal plain and of the Bay of Biscay are characterized by magnetic anomalies often of strong amplitude and small wave length, shown as well marked lineations respectively oriented SSE-NNW and E. - W. to ESE - WNW. In the Porcupine abyssal plain the first clearly identified anomalies may be anomalies 33 - 34 (CANDE and KRISTOFFERSEN, 1977) of late Upper Cretaceous age (VAN HINTE, 1976). Although interpretation of magnetic anomalies in Biscay is still under discussion, it seems that the central anomalies of the Bay, oriented E.W. and superimposed on the N. ans S CHARCOT and Biscay seamounts can be identified as anomalies 33 - 34 (CANDE and KRISTOFFERSEN, 1977 - SIBUET et al., in press). This would imply that a triple point was active during the last phase of opening of the Bay (WILLIAMS, 1975 - SIBUET et al., in preparation). However the Biscay seamounts are extensively tectonised and this interpretation may not be correct (ROBERTS, to be published). Lineations existing between the anomalies 33 - 34 and the margin indicate the existence of an oceanic crust of pre-Senonian age (An 34, 80 MY) (ALVAREZ et al., 1977 - Van HINTE, 1976). These lineations are not very continuous but they exist. They have been delineated mainly from the correlation between profiles of 3 small positive anomalies. These anomalies inside the "quiet zone" may be small reversals as observed for example in the Albian of Site 400 A (HAILWOOD et al., in press). This is in good agreement with geological data on the margin that indicates an Aptian age for the end of rifting. Nevertheless it must be pointed out that anomaly MO of Aptian age is not found along the margin and accretion of new oceanic crust just after anomaly MO cannot be excluded. At the foot of the margin the transition from continental crust to oceanic crust is delineated from the gravity and magnetic profiles (fig. 20) and from seismic reflection profiles (fig. 21, 22). In the NW part of the margin, this boundary follows the base of the continental slope from Porcupine Sea Bight as far as Southern end of Goban Spur. The boundary is linear and very sharp along Goban Spur (fig. 21). South of Goban Spur, the transition is also sharp (fig. 22) since Hercynian granites have been dredged on the last tilted block and oceanic crust is seen about 10 km to the SW. In this case, magnetic anomalies amplitude begin to increase already below the very attenuated continental crust. South eastwards, the boundary is shifted northward and it is close a localized positive magnetic anomaly and a strong amplitude (more than 400 $\gamma$). Along the Trevelyan

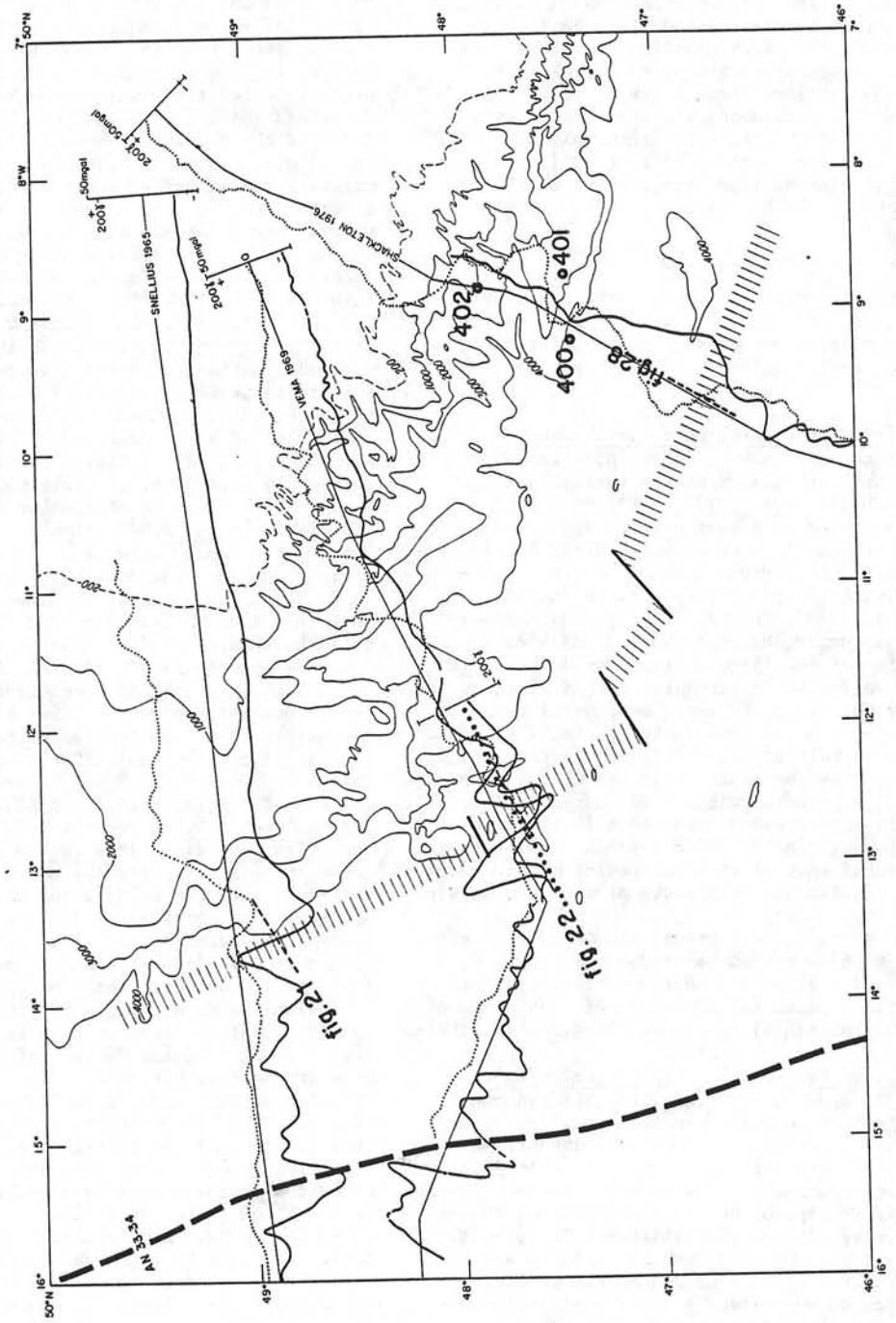


Fig. 20. Magnetic and gravity profiles through the continental-oceanic crusts boundary (N. Biscay margin).

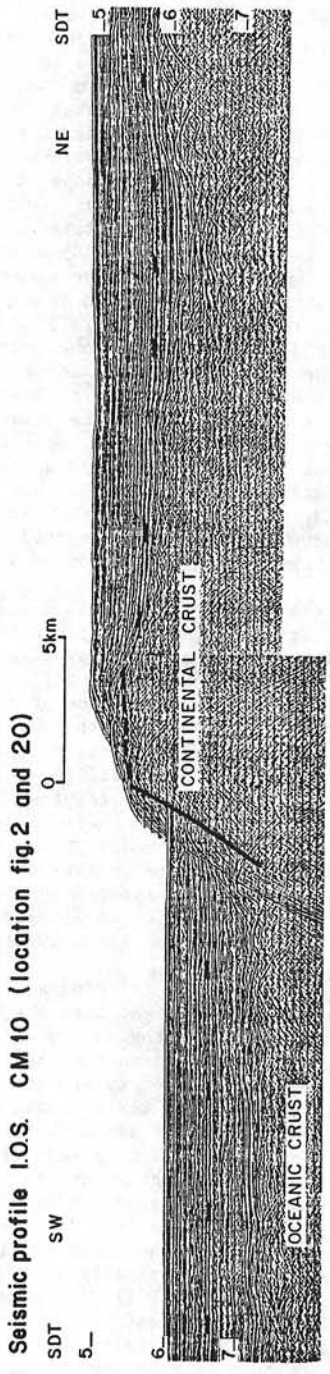


Fig. 21. Continental-Oceanic crusts boundary on Goban Spur (N. Biscay margin).

escarpment, it follows a large negative magnetic anomaly (250 γ) which extends far to the SE where it is superimposed on the north Gasgony ridge (GRAU et al., 1973 - MONTADERT et al., 1975) which is the Southern limit of the deep thick Armorican marginal basin. Seismic reflection data do not show evidence of formation 3 (Aptian-Albian) on the oceanic crust west of Goban Spur, but it is present along Trevelyan (fig. 27). This may indicate that the opening along Goban Spur was slightly younger than to the South. The nature and origin of the Armorican marginal basin north of the North Gasgony ridge is also raised by these results. It is either a piece of pre-Aptian oceanic crust covered by a thick mesozoïc sediment or it may be thinned continental crust as at Trevelyan covered by a much thicker layer of lower cretaceous sediments.

In the Galicia area, the magnetic anomaly map of the total field (fig. 23) (SIBUET et al., in preparation - Groupe Galice, in press) covering the western Iberian continental part of Galicia including Galicia bank, Vigo, Porto and Vasco de Gama Seamounts, is characterized by magnetic anomalies of ± 150 gammas without an obvious grain direction, typical of continental areas. Westwards, a north-south positive feature has been interpreted, South of 41°N, as the MO anomaly (Groupe Galice, in press). The MO anomaly cannot be traced northwards. Between MO and the well defined 34 anomalies exist a series of positive and negative anomalies of ± 150 gammas more or less continuous and similar to the magnetic quiet zone anomalies described in the Bay of Biscay. Some of these magnetic lineations correspond probably to an isochron in the quiet magnetic zone and could be associated with the small reversals observed by Hailwood et al. (in press). Northwards of 41°N, where the MO anomaly is not defined, the transition between continental and oceanic crusts is evidenced by steep gradients in magnetic anomalies and is well defined on seismic profiles as in North Biscay. Southwards of 41°N and East of anomaly MO, the Iberian abyssal plain has the same magnetic character than the surroundings continental area. It could be either oceanic crust older than Aptian either subsided thin continental crust. The beginning of oceanic crust formation is clearly dated Latest Aptian (MO anomaly) in perfect agreement with the age of the end of rifting phase of the margin as shown by site 398 results.

The post-rifting subsidence. Significant faulting of the post-rifting sediments is absent and only local cenozoïc deformations are observed. Post-rifting subsidence is thus characterized by an overall tilting of the margin in post Aptian time with coupling between the oceanic and continental crust. The absolute subsidence of the margin after rifting can be therefore estimated by the difference between the altitude of the Aptian horizon at the end of rifting and today.

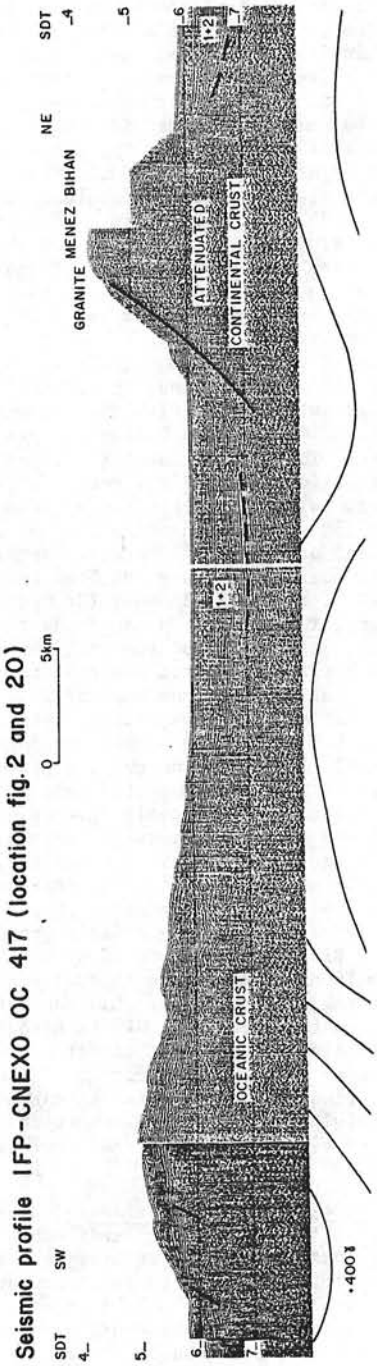


Fig. 22. Continental-oceanic crusts boundary S.W. of Goban Spur (N. Biscay margin).

In Galicia, subsidence cannot be determined on a transect of the margin by lack of data but can be estimated in the area of site 398 (SIBUET and RYAN, in press). Since at site 398 we have no precise paleodepths, we first determined the subsidence curve (fig. 24) of a subaerial early cretaceous erosional surface on the top of Vigo Seamount (fig. 15, 17) located 20 km north of the site. This surface which was at the sea-level at the end of rifting in Latest Aptian time is presently 2,5 km deep. We supposed that the subsidence is related to the thermal cooling of the lithosphere since the opening of the North Atlantic, and we have drawn (figure 24) a subsidence curve of exponential type. We have supposed that the same subsidence curve could be applied to the site area if the site location is 2 km deeper than the present depth of the erosional surface. Consequently, the paleodepth of the acoustic basement should be at about 2,5 kilometers in Lower Cretaceous time, which is compatible with the paleodepth of sediment emplaced at this time. The local isostatic readjustment has been calculated using shipboard density measurements. Compaction has been taken into accound to calculate the site 398 paleodepth. The CCD curve have been superimposed on the paleodepth curve. Extrema of the CCD curve are arbitrary.

On the contrary, in North Biscay, data from leg 48 drillings, dredgings and constraints from seismic reflection profiles allow reconstruction of the topography of the sea floor at the end of rifting, and by substraction of the present depth of Aptian calculation of the absolute subsidence along a transect trough the margin. The results are presented on a simplified section (fig. 25) through the best documented area of the margin from the shelf edge to the continental-oceanic crusts boundary. Although post-rifting sediments are only a few hundred meters thick, an isostatic correction has been applied to the Aptian horizon for a local loading on an Airy-type crust (see for example WATTS and RYAN, 1976).

From fig. 25, it is inferred that the present depth attained by a point on the margin depends on its altitude at the end of rifting and on its distance from the ocean-continent boundary, while the absolute value of subsidence depends only on the distance to the ocean-continent boundary. It should be noted that estimation of the subsidence of a margin requires knowledge of the topography at the end of rifting which may be difficult to determine. This diagram confirms that a good coupling existed between the continental and oceanic crusts since near the boundary, the continental crust subsided practically as much as the adjacent oceanic crust. SLEEP (1971) suggested that due to cooling of the lithosphere the subsidence rate would decay exponentially with time and that the time constant of subsidence would be similar to the time constant of subsidence of mid-ocean ridges, i.e. 50 M.Y. Fig. 25 shows that, for the

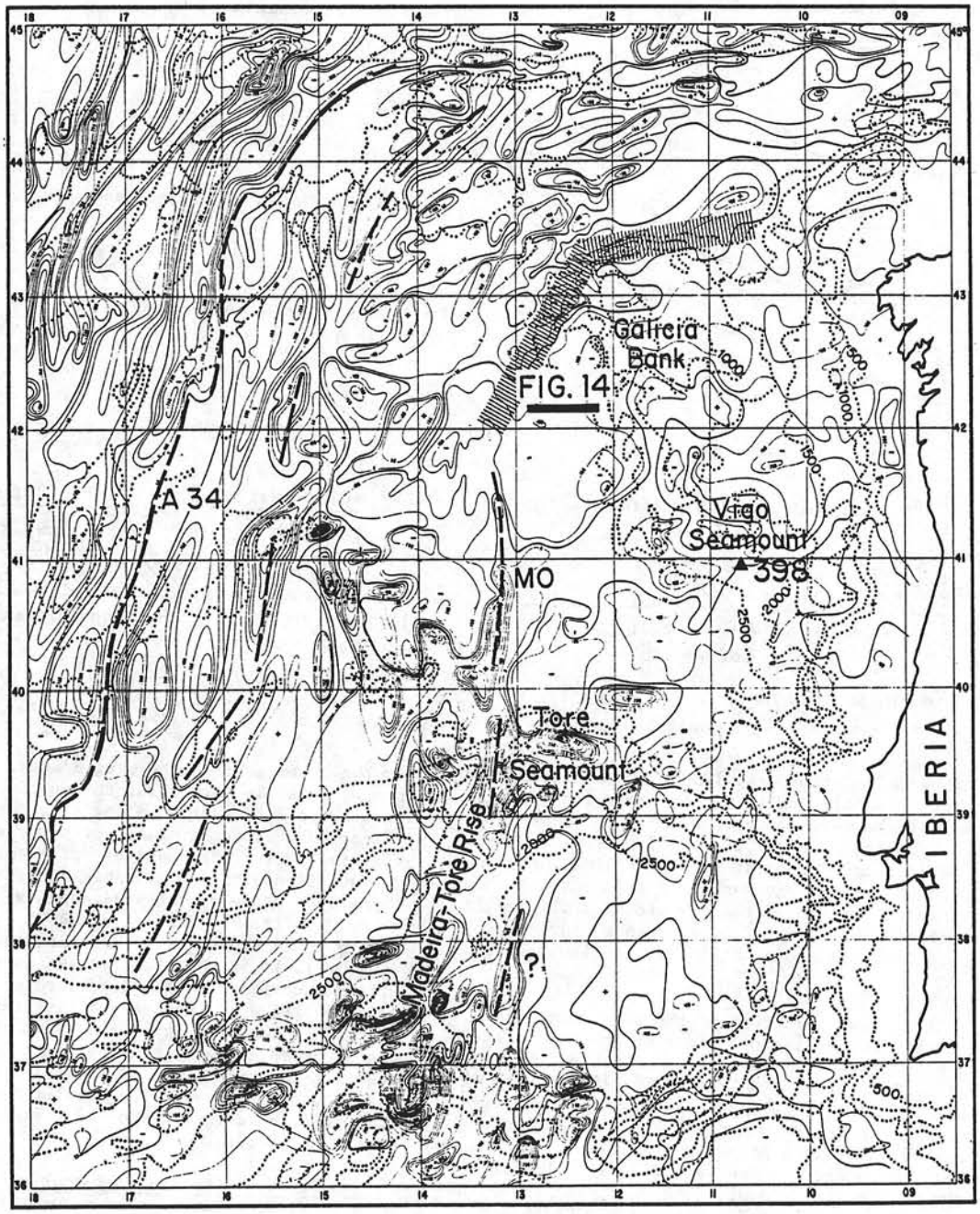


Fig. 23. Magnetic anomalies W. of Iberia.

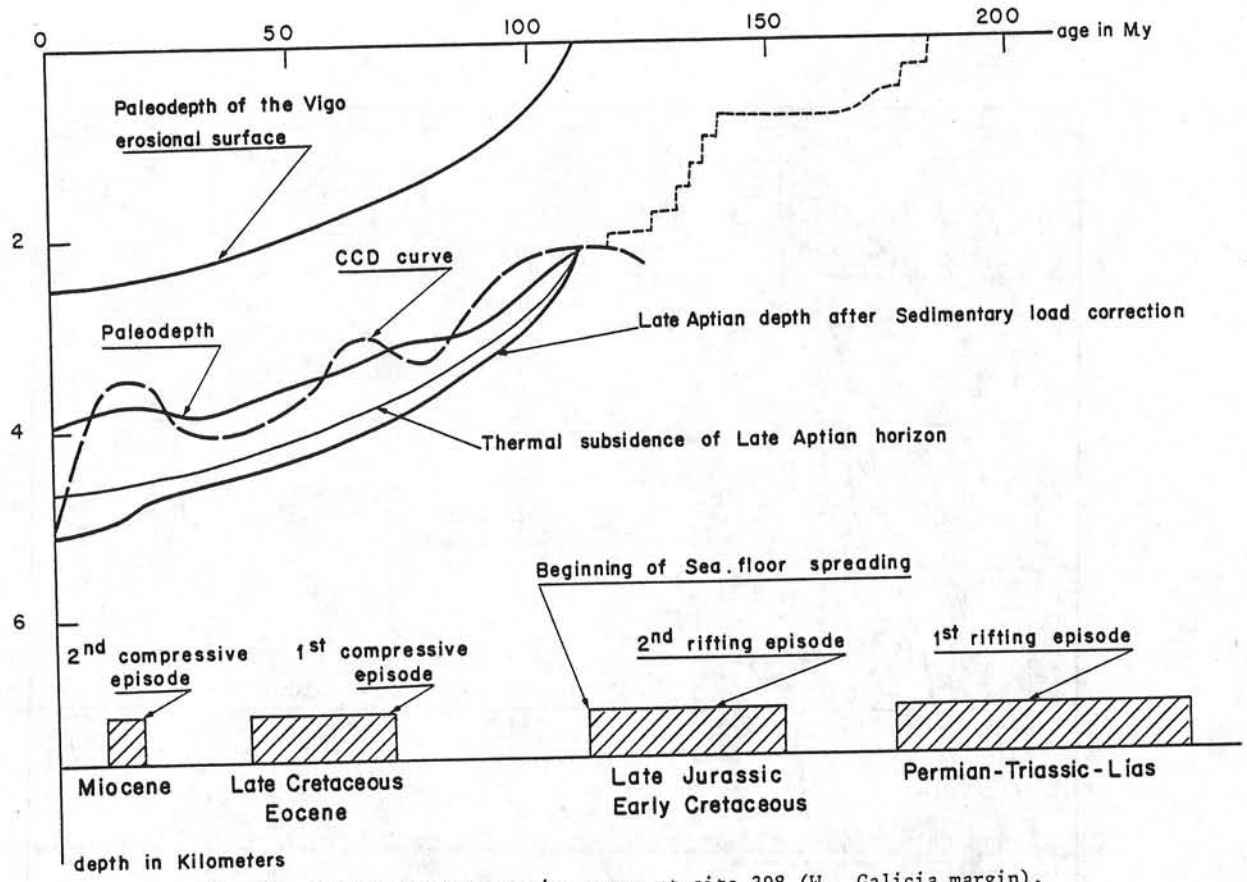


Fig. 24. Subsidence versus time curve at site 398 (W. Galicia margin).

same period of time, say 120 MY since Aptian, the amount of subsidence is not the same for every point of the margin, so that the time constant cannot be the same for the whole margin if subsidence decreased exponentially with time. Only in the lower part of the margin is the constant similar to the one of the oceanic crust. There is therefore not a single law that characterizes the subsidence of a whole margin but one law for each point.

The exponential decay of the subsidence rate with time for different points on the margin can can be checked from paleodepth estimate for different periods of time after Aptian. In the case of Biscay, these curves cannot be drawn with precision since paleodepth estimates from paleontological data are less and less precise for increasing water depths and for increasing ages. Paleodepths estimate for the Mesozoïc (DUPEUBLE, in press) and for Cenozoïc (SCHNITKER, in press - DUCASSE and PEYPOUQUET, in press) nevertheless support an exponential decay especially at site 401, although elsewhere there is no contradiction with the paleontological and sedimentological data (fig. 26).

In the lower part of the margin where the continental crust is very thin, the subsidence rate is not too different from the subsidence rate of the adjacent oceanic crust but towards the shelf, with increasing thickness of continental crust, the subsidence rate diminishes considerably. Changes of slope on the subsidence versus distance curve (fig. 25) reflect probably a sharper change in thickness of the continental crust (fig. 18). It is therefore suggested that post rifting subsidence without influence of loading is essentially an isostatic adjustment to cooling of the lithosphere in which the continental crust has been previously thinned during the rifting process. In that case, one can expect a relationship between the absolute subsidence of a point on a margin and the thickness of the continental crust.

The Cenozoic (Eocene) deformations. In N. Biscay, we observed that after rifting of the margin, subsidence occurred tilting regionally the margin. Rejuvenation of the rift faults is not observed during this period, although it may occur on other margins due to differential loa-

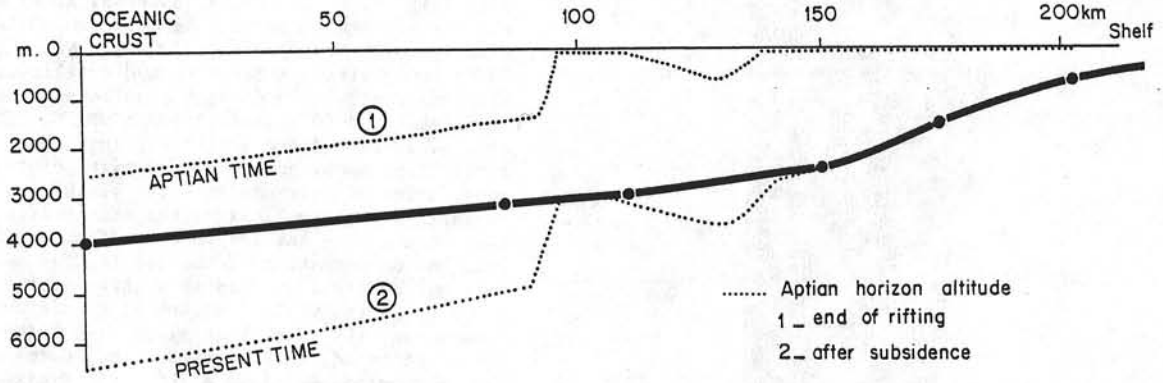


Fig. 25. Absolute amount of subsidence (full line) after rifting on a transect through N. Biscay margin.

ding under a thick sedimentary cover. The absence of tectonic activity is in good agreement with the position of the North Biscay margin within the European plate during Cenozoïc. Nevertheless to the South, the northern edge of Iberia including Galicia Bank area was a plate boundary where some subduction of Biscay oceanic floor occurred at least until late Eocene-Oligocene. Intense deformations linked to this compression phase occur all along the Northern boundary of Iberia and Galicia Bank area (Pyrenean foldings) (fig. 1). Eastwards, towards the Mediterranean area, Europe-Iberia was in collision with Africa. In such conditions, intraplate deformations can occur and indeed have been described both in the oceanic and continental parts of the European and Iberian plates. Moreover, South of Iberia along Betics and Magrebian ranges, intense early to middle Miocene tectonics occurred. Some deformations of this age can be observed northwards until the southern part of Galicia Bank area.
In the Galicia area (Groupe Galice, in press) the large faults which runs along the northwest edge of Galicia Bank continues in the southwest as a flexure which affects the Mesozoïc and Eocene layers without disturbing more recent deposits. Movements of the same age are also visible in the Interior basin. At the foot of the northwestern Galicia bank, the deformations are much more intense with clear reverse faults linked with some overthrusting of Galicia Bank over the oceanic crust (fig. 27).

Another way to quantify cenozoïc deformations on the continental margin is to follow the shape, slope and altitude of the lower Cretaceous erosional surfaces. Figure 17 shows significant difference in the altitude of these surfaces between the southern part (2,5 - 2,8 km) and the Galicia Bank (1,5 km). This could be explained by uplifting of Galicia Bank during the Eocene compressional events. Nevertheless, if one takes into account the relationship between subsidence and thickness of continental crust as established in N. Biscay, the higher level of the surface of Galicia Bank s.s. could be explained also by thicker continental crust there than southwards.

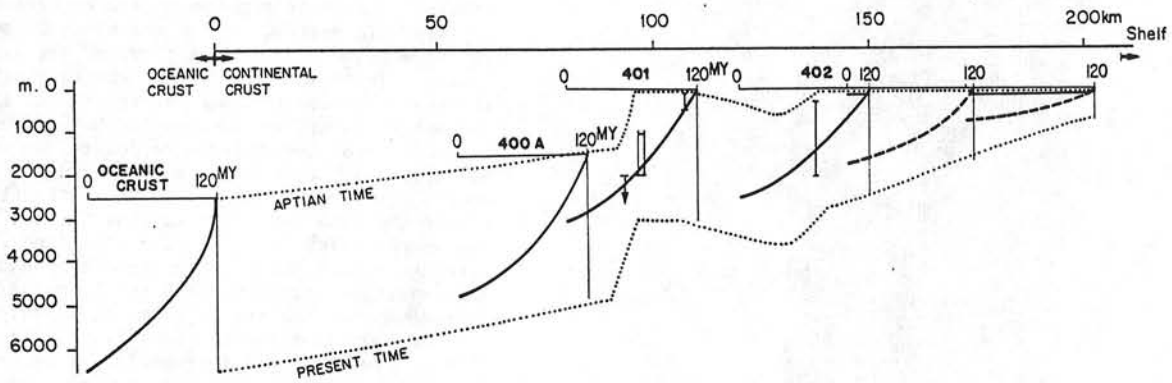


Fig. 26. Hypothetic subsidence versus time curves for different points on a transect through N. Biscay margin (compare with fig. 18).

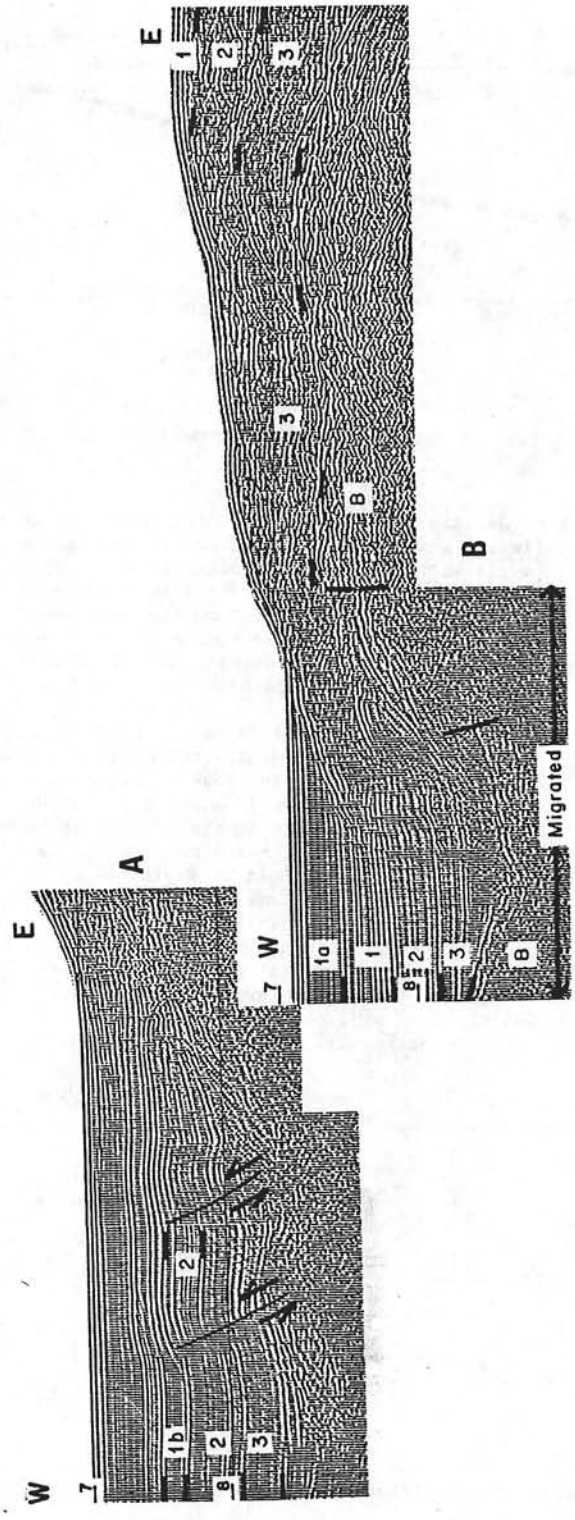


Fig. 27. Late Eocene compression N.W. of Galicia Bank.

In the oceanic area, to the north the tectonized area (fig. 1) along Iberia, numerous areas uplifted during late Eocene can be defined (MONTADERT et al., 1971 - GRAU et al., 1972 - MONTADERT et al., 1974) from seismic reflection and drilling. On uplifted areas, thin pelagic post Eocene sediments were deposited (DSDP site 119, LAUGHTON, BERGGREN et al., 1972) and are easily distinguished from turbidites deposited around the high points. Numerous faults of this age are also visible in the abyssal plain as well as on the continental margin. Their occurrence has led to overestimates of their role on the formation of the continental margin. On land, numerous studies show that deformation occurred in the whole continental domain at the same period (DE CHARPAL et al., 1974, TREMOLIERES, to be published) in France, England, Germany, linked to compression along a 10° - 20° E direction. Another compressional event occurred since Miocene time but seems to be restricted mainly to the Southeastern part of the Paris basin. The whole European plate was submitted during late Eocene-Oligocene to compression in the oceanic domain as well as in the continental one. Following orientation of the pre-existing structures, this compression created strike-slip faults, reverse faults, folds, etc...

On the North Biscay margin, the new seismic profiles allows a better estimate of the Cenozoïc deformations. Faults are relatively restricted to some areas (fig. 11) and the most striking features are observed along the Trevelyan escarpment. Along an E.W. belt, numerous faults, including reverse faults, affected the series including Formation 2 (fig. 28). The faulting caused uplift that created the Trevelyan escarpment. This strongly tectonized E.W. belt disappears progressively towards the N.W., as indicated by the disappearance of the escarpment, and merges into almost a single fault system oriented NW-SE which can be followed as far as the south of Goban Spur (fig. 11). This fault is interpreted as a strike slip fault because of absence of vertical throw and deformation of layers on both sides as in drag folds. Other effects of late Eocene deformations include maybe narrow elongated folds, broadly oriented EW, on top and along Trevelyan escarpment and Meriadzek escarpment. In a few cases, rejuvenation of rift faults is visible. The Cenozoïc deformations observed in this part of the margin accord with an almost N.S. direction of Eocene lateral compression as determined on land. Reverse faults and even some thrusting is observed when a pre-existing almost EW discontinuity existed in the basement. This is true for the Trevelyan escarpment which is situated at the junction between the oceanic-continental crusts boundary and the important structural boundary separating the western Approaches margin from the Armorican margin and the Armorican marginal basin (fig. 1). This is true also for the uplifted area oriented E.W. in the center of Biscay with some features like Cantabria Seamount, which are controlled by

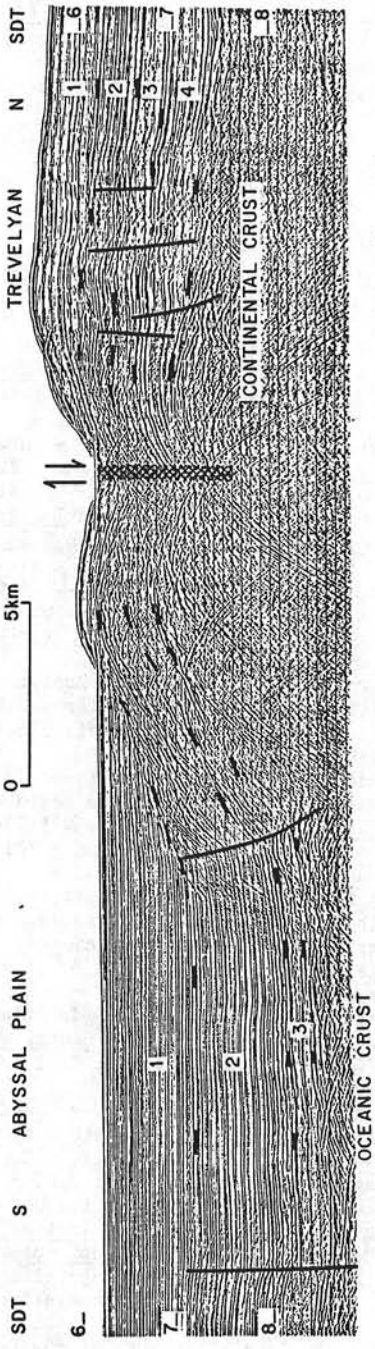


Fig. 28. Late Eocene compression along Trevelyan escarpment (N. Biscay margin) (see fig. 11).

a very sharp rise, oriented E.W., of the Ocean crust. When the discontinuities or inhomogeneities in the basement are oriented differently for example NW-SE like the North Biscay and Armorican margins or the North Gascony ridge in the central part of Biscay, the Eocene compression is marked essentially by faults with a strike slip component.

## Conclusion

A scheme of the structural evolution of a starved passive continental margin can be proposed from DSDP drilling results combined with intensive geophysical surveys. Environment and tectonics of the rifting phase has been established : active rifting took place in Lower Cretaceous time in a pre-existing marine basin and with no volcanic activity in contrast to many subaerial rift systems. The overall tectonic style is characterized by a series of tilted fault blocks bounded in many cases by listric faults. The rotation of the blocks (20-30°) along listric faults reduced the thickness of the upper continental crust from 6-8 km to 4-5 km. Close to the near horizontal base of the listric faults, a strong horizontal reflector corresponding to the 6,3-4,9 km/s refraction interface has been interpreted as the boundary between the upper brittle and the lower ductile continental crusts. The Moho discontinuity 25 km deep in the vicinity of the shelf break is 12 km deep in the lower part of the margin. In this area the ductile part of the crust (6,3 km/s) is only 3 km thick. Drill dredge and seismic reflection data allow to reconstruct the topography of sea floor at the end of rifting in Aptian time. In the axis of the rift system, submarine troughs 2,5 km deep existed. The thinning of the continental crust cannot be explained by the 10-15 % of extension estimated for the upper brittle part. One suggests that the ductile part of the crust is thinned by creep in response to tension in the continental plate. Rift would not be related to doming of the continental crust but merely to stretching of the lithosphere as a response to intraplate stresses. Knowing the topography of the sea-floor at the end of rifting and the present depth of the Aptian datum, one can determine the absolute amount of subsidence on a transect of the margin after the beginning of accretion (late Aptian time). This value decreased continuously from the oceanic-continental crust boundary (4000 m) to the shelf break. For each point of the margin, the subsidence versus time curve is an exponential whose time constant increases with depth. This suggests that post rifting subsidence was essentially an isostatic adjustment to cooling of the lithosphere in which the continental crust has been previously thinned during the rifting process.

Acknowledgments. L.M, D.G.R and J.C.S whish to acknowledge the U.S. National Science Foundation, the international JOIDES institutions and D.S.D.P-

IPOD who made legs 47B and 48 and their participation possible. L.M, O.C, P.G and J.C.S are indebted to Institut Français du Pétrole, CNEXO and CEPM (IFP, SNEA(P), CFP) which permitted the acquisition of data, and their participation to Leg 47B and 48 studies. They are particularly grateful to the geophysicists (J.P. FAIL, R. DONATIEN, J. CASSAND) and Crew of the M.S Florence of the Institut Français du Pétrole which collected the geophysical data in Galicia plateau and in the Bay of Biscay before and after Leg 47B and 48 of the Glomar Challenger. D.G.R. whishes to acknowledge the Department of Energy supporting acquisition of the seismic data after Leg 48 and his participation with Leg 48 studies. The authors are grateful to M. POULET (IFP) for his many helpful suggestions and discussions and to P. VAIL (Exxon Research) and J.GROW (U.S.G.S.) for their critical review of the manuscript.

## References

Alvarez W.A., Fisher A.G., Lowrie W., Napoleone G., Premoli Silva I., Roggenthen W.M. - Upper Cretaceous-Paleocene magnetic stratigraphy at Gubbio, Italy - V - Type section for the late Cretaceous-Paleocene magnetic time scale. Geol. Soc. America Bull, 88, 367-389, 1977.

Artemjev, M.E. and Artyushkov, E.V. Structure and isostasy of the Baikal rift and the mechanism of rifting. J. Geophys. Res., 76 : 1197-1211, 1971.

Auffret G.A., Pastouret L., Cassat G., de Charpal O., Cravatte J., Guennoc P. - Dredged rocks from the Armorican and Celtic Margins. In Initial Reports of the Deep Sea Drilling Project, volume 48, Washington (U.S. Government Printing Office). In press.

Avedik F., Howard D. - Preliminary results of a seismic refraction study in the Meriadzek - Trevelyan area, Bay of Biscay. In Initial Reports of the Deep Sea Drilling Project, volume 48, Washington (U.S. Government Printing Office). In press.

Berthois L. and Brenot R. - Cartes bathymétriques du talus du plateau continental en onze feuilles éditées par Berthois L. avec le concours du CNRS. 1966.

Berthois L., Brenot R. et Debyser J. - Remarques sur la morphologie de la marge continentale entre l'Irlande et le cap Finisterre. Rev. Inst. Franç. du Pétrole, vol. XXIII, n° 9, p. 1046-1049, 1968

Black M., Hill M.N., Laughton A.S., Matthews D.H. Three non magnetic seamounts off the Iberian coast. Geol. Soc. London Quart. Jour, v. 120, p. 477-517, 1964.

Blair D.G. - Structural styles in North Sea Oil and Gas Fields. In Petroleum and the continental shelf of North-West Europe. Vol. 1 Geology - Ed. A.W. Woodland. Applied Science Publishers Ltd 327-338, 1975.

Bott, M.H.P. - Evolution of young continental margins and formation of shelf basins - Tectonophysics, 11, 5, 319-327, 1971.

Bott, M.H.P. and Dean, D.S. - Stress systems at young continental margins. - Nature phys. Sci. 235, 23-25, 1972.

Bott, M.H.P. - Shelf subsidence in relation to the evolution of young continental margins. - In : Tarling, D.H. & Runcorn, S.K. (eds) : Implications of Continental Drift to the Earth Sciences. Academic Press, London, 2, 675-683, 1973.

Bott, M.H.P. and Watts A.B. - Deep structure of the continental margin adjacent to the British Isles. In : The Geology of the East Continental Margin - 2 - Europe. Ed. F.M. Delany Report n° 70/14 Institute of Geological Sciences - p. 93-109, 1971.

Bouquigny R. and Willm, C. - Tentative Calibration of Site 398 and special processing of part of lines GP19 and GP23. In Initial Reports of the Deep Sea Drilling Project, volume 47B. Washington (U.S. Government Printing Office), in press.

Bowen J.M. - The Brent oil field. In : Petroleum and the continental shelf of North-West Europe. Vol 1 Geology. Ed. A.W. Woodland. Applied Science Publishers Ltd 353-362, 1975.

BRGM - ELF Re - ESSO REP - SNPA - Géologie du Bassin d'Aquitaine. Editions : BRGM Paris, 1974.

Burke K. and Whiteman A.J. - Uplift, rifting and the break-up of Africa. In Implication of Continental drift to the earth Sciences, D.H. Tarling and S.K. Runcorn. Eds. V. 2, p. 735-756, 1973.

Charpal O. de, Trémolières P., Jean F. et Masse P.- Un exemple de tectonique de plate-forme. Les Causses majeurs. Rev. Inst. Franç. du Pétrole, XXIX-5, p. 715-732, 1974.

Charpal O. de, Guennoc P., Montadert L., Roberts D.G. Rifting, crustal attenuation and Subsidence in the Bay of Biscay. Nature. Vol. 275. n° 5682, 26 octobre 1978.

Cande S.C., and Kristoffersen Y. - Late Cretaceous magnetic anomalies in the North Atlantic. Earth Planet. Sci. Letters, 35, 215-224, 1977.

Cloos H. - Hebung - Spaltung - Vulkanismus. Geol. Rundsch., 30 : 405-527, 1939

Day G.A., Williams C.A. - Gravity compilation in the northeast Atlantic and interpretation of gravity in the Celtic Sea. Earth Planet. Sc. Letters, 8, 207, 213, 1970.

Dardel R.A., and Rosset R. - Histoire géologique et structurale du bassin de Parentis et de son prolongement en mer; in Histoire structurale du golfe de Gascogne. t. I-II : Paris, Ed. Technip p. IV.2-1-IV.2-28, 1971

Dingle R.V., Scrutton R.A. - Continental margin fault pattern mapped South West of Ireland. Nature vol. 268 - 25 Aug. 1977 p. 720-723, 1977.

Ducasse O., and Peypouquet J.P. - Cenozoïc Ostracoda : their importance for bathymetry, hydrology and biogeography. In Initial Reports of the Deep Sea Drilling Project, volume 48 - Washington (U.S. Government Printing Office). In press.

Dupeuble P. - Mesozoïc Foraminifera and microfacies from sites 400 A, 401 and 402 A of the DSDP Leg 48. In Initial Reports of the Deep Sea Drilling Project, volume 48 - Washington (U.S. Government Printing Office). In press.

Ewing J. and Ewing M. - Seismic refraction measurements in the Atlantic Ocean basins, in the Mediterranean Sea, on the Mid-Atlantic Ridge, and the Norwegian Sea, Bull. Geol. Soc. Am. 70, 291, 1959.

Forsyth D. and Uyeda S. - On the relative importance of the driving forces of the plate motion. Geophs. J.R. Astr. Soc. 43, p. 163-200, 1975

Foucher J.P. and Sibuet J.C. - Thermal regime of the Northern Bay of Biscay Continental margin in vicinity of the DSDP sites 400 to 402. In Initial Reports of the Deep Sea Drilling Project, volume 48 - Washington (U.S. Government Printing Office). In press.

Freund R. - Rift Valleys. Can. Geol. Surv. Pap., Paper 64-14, p. 330-344, 1965.

Fuchs K. - Geophysical contributions to taphrogenesis. In : J.H. Illies and K. Fuchs (Editors), Approaches to Taphrogenesis. Schweizerbart, Stuttgart, p. 420-432, 1974.

Funnel, B.M., Friend J.K. and Ramsey A.T.S. - Upper Maestrichtian planktonic foraminifera from Galicia Bank, West of Spain, Paleontology, 12, part 1, 19-42, 1969.

Garfunkel Z., Bartov Y. - The Tectonics of the Suez Rift. Geol. Surv. Israel Bull n° 71, 1977.

Grau G., Montadert L., Delteil R., and Winnock E. - Structure of the European continental margin between Portugal and Ireland, from seismic data, in Mueller, S., ed., The structure of the earth's crust : Tectonophysics, v. 20, no. 1-4, p. 319-339, 1973.

Griggs D.T. and Handin J. (Editors) - Rock deformation. Geol. Soc. Am., Mem., 79 : 1-382, 1960.

Groupe GALICE. The continental margin off Galicia Bank and Portugal : acoustical stratigraphy and structural evolution. In Initial Reports of the Deep Sea Drilling Project, volume 47B, Washington (U.S. Government Printing Office), in press.

Hailwood E.A., Schnitker D., Bock W., Costa L., Muller C., and Dupeuble P.A. - Northeast Atlantic magnetobiostratigraphy. In Initial Reports of the Deep Sea Drilling Project, volume 48 - Washington (U.S. Government Printing Office), in press.

Heiskanen W.A. and Vening-Meinesz F.A. - The Earth and its Gravity Field. 470 pp. Mc Graw-Hill, New-York, 1958.

Hill M.N. and Vine F.J. - A preliminary magnetic survey of the western Approaches to the English Channel. Quart. Jl. Geol. Soc. London, 121, 463-465, 1965.

Illies J.H. - Recent and paleo-intraplate tectonics in stable Europe and the Rhine graben rift system. Tectonophysics, 29 - 251 - 264, 1975.

Laughton A.S., Bergen W.A., et al. - Initial reports of the Deep Sea Drilling Project, v. XII : Washington (U.S. Govt. Printing Office) Site 118 and 119, 1972.

Le Borgne E. and Le Mouël J. - Cartographie aéromagnétique du Golfe de Gascogne. C.R. Acad. Sc. Paris, 271 - D, 1167-1170.

Lowell J. and Genik G. - Sea-floor spreading and structural evolution of the southern Red Sea, Am. Ass. Petroleum Geol. Bull., 56, 247-59, 1972.

Lowell J.D., Genik G.J., Nelson T.H. and Tucker P.M. - Petroleum and plate tectonics of the southern Red Sea. In : Petroleum and Global Tectonics. Ed. A.G. Fischer and S. Judson. Princeton University Press. p. 129-153, 1975.

Montadert L., Damotte B., Delteil J.R., Valéry P. and Winnock E. - Structure géologique de la marge continentale septentrionale du golfe de Gascogne (Bretagne et Entrées de la Manche), in Histoire structurale du golfe de Gascogne, t. I-II: Paris, Ed. Technip, p. III. 2-1-III. 2-22, 1971).

Montadert L., Roberts D.G., Auffret G.A., Bock W.O., Dupeuble P.A., Hailwood E.A., Harrison W., Kagami H., Lumsden D.N., Muller C., Schnitker D., Thompson R.W., Thompson T.L., Timofeev P.P. - Glomar Challenger sails on Leg 48. Geotimes, 21, 12, 19-23, 1976.

Montadert L., Roberts D.G., Auffret G.A., Bock W.O., Dupeuble P.A., Hailwood E.A., Harrison W., Kagami H., Lumsden D.N., Muller C., Schnitker D., Thompson R.W., Thompson T.L., Timofeev P.P. - Rifting and subsidence on passive continental margins in the North East Atlantic. Nature vol. 268 n° 5618 p. 305-309, 1977.

Montadert L., and Winnock E. - L'histoire structurale du golfe de Gascogne, in Histoire structurale du golfe de Gascogne, t. I-II : Paris, Ed. Technip, p. VI.16-1-VI.16-18, 1971.

Montadert L., Winnock E., Delteil J.R., and Grau G. Continental Margins of Galicia - Portugal and Bay of Biscay. In the Geology of Continental Margins, C.A. Burk and C.L. Drake, eds.,Springer-Verlag, New-York, 323-342, 1974.

Montadert L., Roberts D.G., De Charpal O., Guennoc P. Rifting and Subsidence of the northern continental margin of the Bay of Biscay. In Initial Report of the Deep Sea Drilling Project, volume 48 - Washington (U.S. Government Printing Office), in press.

Moore J.M., Davidson A. - Rifting Structure on Southern Ethiopa. Tectonophysics 46 (1978) 159-173, 1978.

Neugebauer H.J. - Crustal doming and the mechanism of rifting Part I : Rift formation. Tectonophysics, 45. n° 2-3. 159-186, 1978.

Pastouret L., Auffret G.A. - Observations sur les microfaciès des roches sédimentaires prélevées sur la marge armoricaine. Rev. Inst. Français du Pétrole, vol. XXXI, n° 3, p. 401-425, 1976.

Pautot G., Renard V., de Charpal O., Auffret G.A., Pastouret L. - A granite cliff deep on the North Atlantic. Nature, 263, 1976, p. 669-672, 1976.

Poulet M. - Apport des expériences de mécanique des roches à la géologie structurale des bassins sédimentaires. Rev. Inst. Français du Pétrole. XXXI, n° 5 p. 781-822, 1976.

Schnikter D. - Cenozoic deep-water benthic Foraminifera. Bay of Biscay. In Initial Reports of the Deep Sea Drilling Project, volume 48 - Washington (U.S. Government Printing Office), in press.

Segoufin J. - Structure du plateau continental armoricain. In : A discussion on the geology of the English Channel. Phil. Trans. R. Soc. London, A 279 p. 109-121, 1975.

Sibuet J.C. - Contribution de la gravimétrie à l'étude de la Bretagne et du plateau continental adjacent. C.R. Somm. Soc. Geol. France, 24 avril 1972, 124-129, 1972.

Sibuet J.C., Ryan W.BF - Site 398 : Evolution of the West Iberian Passive Continental Margin in the framework of the early evolution of the North Atlantic Ocean - In Initial Reports of the Deep Sea Drilling Project, volume 47B - Washington (U.S. Government Printing Office), in press.

Site chapter 398 - In Initial Reports of the Deep Sea Drilling Project, volume 47B - Washington (U.S. Government Printing Office), in press.

Site chapters 400, 401, 402 - In Initial Reports of the Deep Sea Drilling Project, volume 48 - Washington (U.S. Government Printing Office) in press.

Sleep N.H. - Thermal effects of the formation of Atlantic Continental Margins by continental break-up. Geophys. J.R. Astron. Soc., 24, 325-350, 1971.

Sleep N.H. - Crustal Thinning on Atlantic Continental Margings : evidence from older margins. - In : Tarling D.H. & Runcorn S.K. (eds) : Implication of Continental Drift to the Earth Sciences. Academic Press, London, 2, 685-692, 1973.

Sleep N.H. and Snell N.S. - Thermal Contraction and flexure of Mid-Continent and Atlantic marginal basins. - Geophys. J.R. Astron. Soc., 45, 125-143, 1976.

Stride A.H., Curray J.R., Moore D.G. and Belderson R.H. - Marine geology of the Atlantic Continental margin of Europe, Phil. Trans. Roy. Soc. (London) A264 31, 1969.

Tremolieres P. - Les mécanismes de déformation à l'échelle d'un bassin. To be published.

Tucholke B.E., Mountain G.S. - Lithologic correlation and significance of major seismic reflectors in the Western North Atlantic. The 2d Ewing M. Memorial Symposium. March 19-25-1978, 1978.

Van Andel T.H., Thiede J., Sclater J.G., Hay W.W. Depositional history of the South Atlantic Ocean during the last 125 million years. J. of Geology, vol. 85 n° 6 Nov. 77 p. 651-699, 1977.

Van Hinte J.E. - A Cretaceous Time Scale. Am. Ass. Petr. Geol. Bull., 60, 4, 498-516, 1976.

Vening-Meinesz F.A. - Les "graben" africains, résultats de compression ou de tension dans la croûte terrestre. Bull. Inst. R. Colonial Belge, 21 : 539-552, 1950.

Walcott R.I. - Flexural rigidity, thickness and viscosity of the lithosphere - J. Geophys. Research, 75, 10, 3941-3954, 1970.

Walcott R.I. - Gravity flexure and the growth of sedimentary basins at a continental edge. - Bull. geol. Soc. Amer., 83, 6, 1845-1848, 1972.

Watts A.B. and Ryan W.B.F. - Flexure of the lithosphere and continental margins basins. Tectonophysics n° 36 p. 25-44, 1975.

Williams C.A. - Sea-floor spreading in the Bay of Biscay and its relationship to the North Atlantic. Earth Planet. Sci. Letters, 24, 440-456, 1975.

Winnock E. - Géologie succincte du Bassin d'Aquitaine (contribution à l'histoire du Golfe de Gascogne).In Histoire Structurale du Golfe de Gascogne, Technip, Paris, IV, 1, 1-30, 1971.

TECTONICS, VOL. 5, NO. 7, PAGES 1125-1143, DECEMBER 1986

# TECTONIC IMPLICATIONS OF CANYON DIRECTIONS OVER THE NORTHEAST ATLANTIC CONTINENTAL MARGIN

Serge Lallemand[1]

Laboratoire de Géodynamique, Département des Sciences de la Terre, Université d'Orléans, France

Jean-Claude Sibuet

Département des Géosciences Marines, IFREMER, Centre de Brest, France

Abstract. The basis of this study is a new bathymetric map of the northeast Atlantic compiled from previously published maps made from conventional echosounder data, plus all Sea Beam data acquired on board the R/V JEAN CHARCOT since 1977. As most of the Sea Beam data have been obtained on the continental margin from Porcupine Seabight to the south of the Iberian Peninsula, a precise picture of the continental slope is given. A statistical analysis of the canyons, based on 750 measurements, reveals that many of the canyons present sharp changes in their direction, indicating a structural control mainly linked to the late Hercynian trends, especially around the Iberian Peninsula. Nevertheless, the paths of canyons may merely reflect recent gravity processes, as in the Porcupine Seabight. Canyons locally follow the directions of listric and associated transecting faults (Permian to Triassic and upper Jurassic to lower Cretaceous), as on the Celtic margin, and every type of tectonic lineament--for example, the North Pyrenean Paleogene thrust front which fringes the Gouf of Cap Breton. A comparison of diagrams for the northern and southern Bay of Biscay margin (especially trends predating the opening) is compatible with a 25° rotation of Iberia with respect to Europe.

[1]Now at Ecole Normale Supérieure, Département de Géologie, Paris.



Paper number 6T0399.
0278-7407/86/006T-0399$10.00

## INTRODUCTION

Reliable bathymetric maps of the northeast Atlantic Ocean have been available since the early 1960s. The continental margins, largely cut by down slope canyons, were systematically surveyed by Berthois, who implemented tracklines in a direction parallel to the continental margin trends [e.g., Berthois and Brenot, 1960, 1964; Berthois et al., 1968]. Then an exhaustive compilation of conventional data in the northeast Atlantic was done by Laughton et al. [1975]. Ten years after, continental margins from the Porcupine Seabight to Gibraltar were largely surveyed by the Institute of Oceanographic Sciences (IOS) using the GLORIA Mark II [e.g., Kidd and Roberts, 1982], a dual-scan sonar towed at shallow depths with a maximum scanning range of 30 km on each side of the fish track [Somers et al., 1978] and by the R/V JEAN CHARCOT equipped with a multibeam echo sounder [Renard and Allenou, 1979] since 1977. Both Sea Beam and GLORIA are

tools which provide precise information on morphologic trends. Twenty Sea Beam cruises or transits have been carried out, mainly on continental margins, which allow us to produce a new detailed bathymetric map (Plate 1) [Lallemand et al., 1985 a,b]. Most of the Sea Beam data have been acquired along the continental margins (Plate 2), which provides a fairly good picture of the morphology of the northeast Atlantic continental margins, especially along the slopes. Many of the canyons cross the margins obliquely and present sharp changes in their directions. This indicates that the canyon trends are not only controlled by gravity processes, but they are also largely influenced by the structural pattern [e.g., Boillot et al., 1974; Kenyon et al., 1978; Sibuet and Berthois, 1979]. We propose to perform a statistical study of the direction of canyons and to correlate these directions with the structural pattern known on land and on the continental shelf.

## GEOLOGICAL EVOLUTION OF THE NORTH ATLANTIC OCEAN

Tensional episodes occured from Permian to Lias in the areas of the future plate boundaries between Europe, North America, and Iberia. The continental crust was thinned, sometimes with formation of very limited amount of oceanic crust [e.g., Foucher et al., 1982], but the complete structural outline of all continental margins of the northeast Atlantic Ocean was mainly acquired during the late Jurassic-early Cretaceous phase of rifting which occured simultaneously with the opening of the central Atlantic Ocean.

The oldest magnetic anomalies identified in the northeast Atlantic Ocean are M0 (late Aptian) west of Galicia Bank and 34 (upper Santonian) in the Bay of Biscay and west of the British Isles [Sibuet and Ryan, 1979; Guennoc et al., 1978, 1979] (Figure 1). Nevertheless, oceanic crust still exists between the oldest identified magnetic anomalies and the continent-ocean boundary. From drilling results the first appearance of oceanic crust has been dated lower Albian at Goban Spur [Masson et al., 1984], early Albian near the Meriadzek terrace in the northern Bay of Biscay [Montadert et al., 1979a,b; Pastouret et al., 1981] and late Aptian west of Galicia Bank [Sibuet and Ryan, 1979]. This indicates that the initial emplacement of oceanic crust propagated from south to north.

The formation of the Bay of Biscay results from the rotation of Iberia with respect to Europe around a pole located in southwest Europe [Le Pichon et al., 1971; Olivet et al., 1984] from late Jurassic-early Cretaceous to the time of anomaly 33 (Campanian) [Sibuet and Ryan, 1979] or during the Cretaceous Quiet Magnetic Zone (Albian to Santonian) for Olivet et al. [1984]. No conclusive evidence from land geology in the Pyrénées and Aquitaine Basin allows us to discriminate between these two hypotheses. Simultaneously, the North Atlantic opening was going on. From late Cretaceous to late Eocene, the compressive movements resulted in the uplift of Pyrénées and the formation of the North Spanish subduction zone with a paroxysmal phase during Eocene [Sibuet and Le Pichon, 1971; Le Pichon and Sibuet, 1971a].

## MAIN PHYSIOGRAPHIC PROVINCES ON CONTINENTAL MARGINS

The northeast Atlantic continental margins can be divided into six main domains (Figure 1) on the basis of the following criteria: (1) general trend of the margin; (2) structural and kinematic arguments; and (3) orientation of canyons.

The presence of specific trends families of canyons allows us to distinguish several subzones in areas 2, 3, 5, and 6.

Area 1. The Goban Spur continental margin, oriented N330°, was formed in lower Cretaceous during the separation of Europe and north America along a N70° direction [Masson et al., 1984; Sibuet et al., 1984a,b].

Area 2. The Celtic continental margin, oriented approximately N110°, resulted from the southeastward movement of Iberia with respect to Eurasia in lower Cretaceous [e.g., Le Pichon et al., 1971].

Area 3. The Armorican continental margin, oriented N135°, was also formed during the rotation of Iberia but corresponds to a sheared continental margin [Le Pichon et al., 1971]. It presents a narrower continental slope than the Celtic margin.

Area 4. The Landes Plateau is bounded to the north and south by the Cap Ferret Canyon and the Gouf of Cap Breton, respectively, which are both oriented

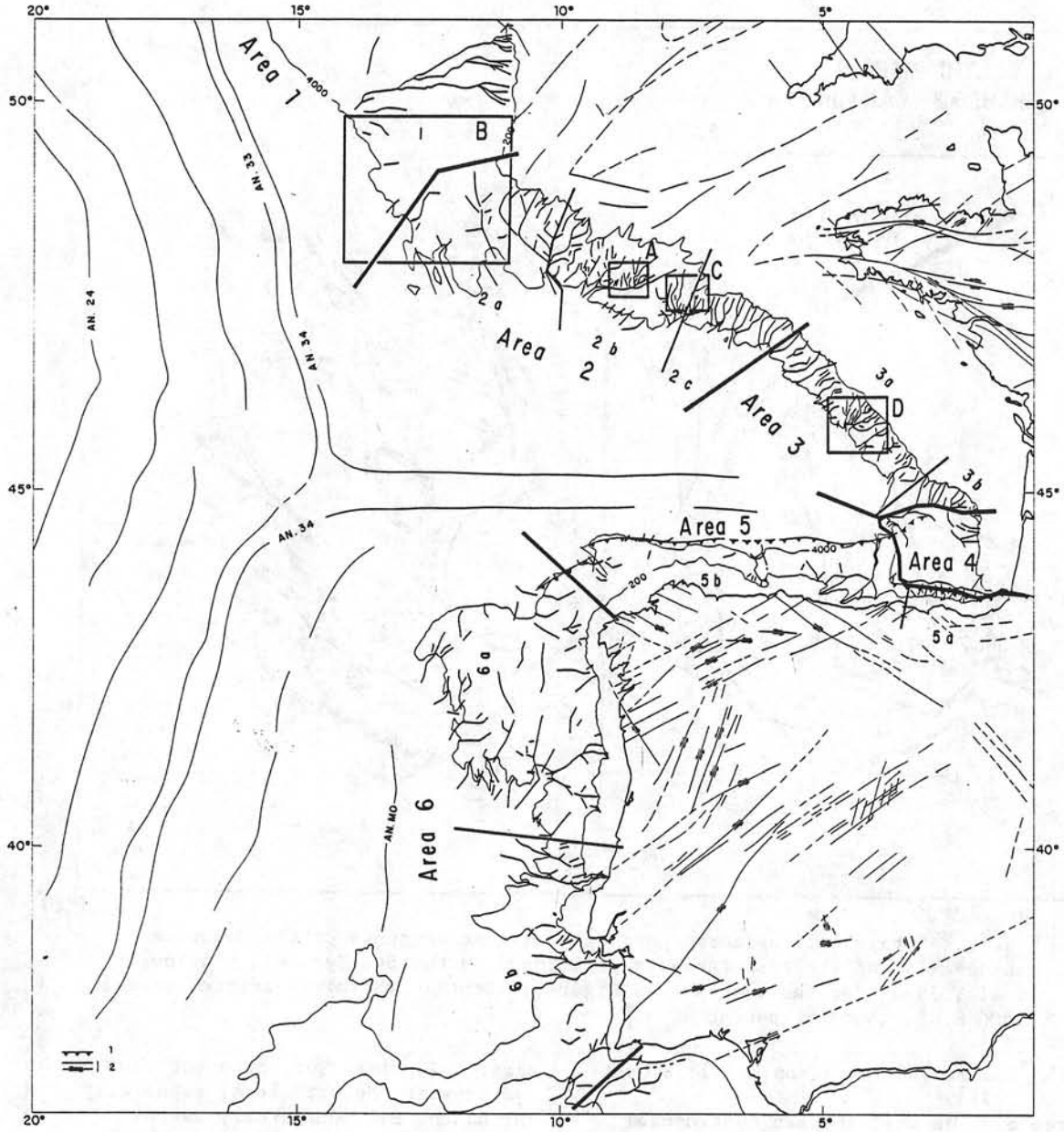


Fig. 1. Simplified structural map of the northeast Atlantic region. The main physiographic provinces of the continental margin and the location of canyons and their tributaries used in this study are shown. Identified magnetic anomalies from Guennoc et al. [1978, 1979]. 1, North Iberia Paleogene thrusting front; 2, Late Hercynian faults [Parga, 1969; Arthaud and Matte, 1975; Pegrum and Mounteney, 1978; Montadert et al., 1979a; Sibuet et al., 1948b].

N100°, and to the west by the Santander Canyon which is roughly north-south in trend.

Area 5. The North Spanish continental margin is the counterpart of the Celtic margin but was largely tectonized during the lower Tertiary compressive phase (100-150 km of amplitude) which gave rise to the formation of the North Spanish marginal

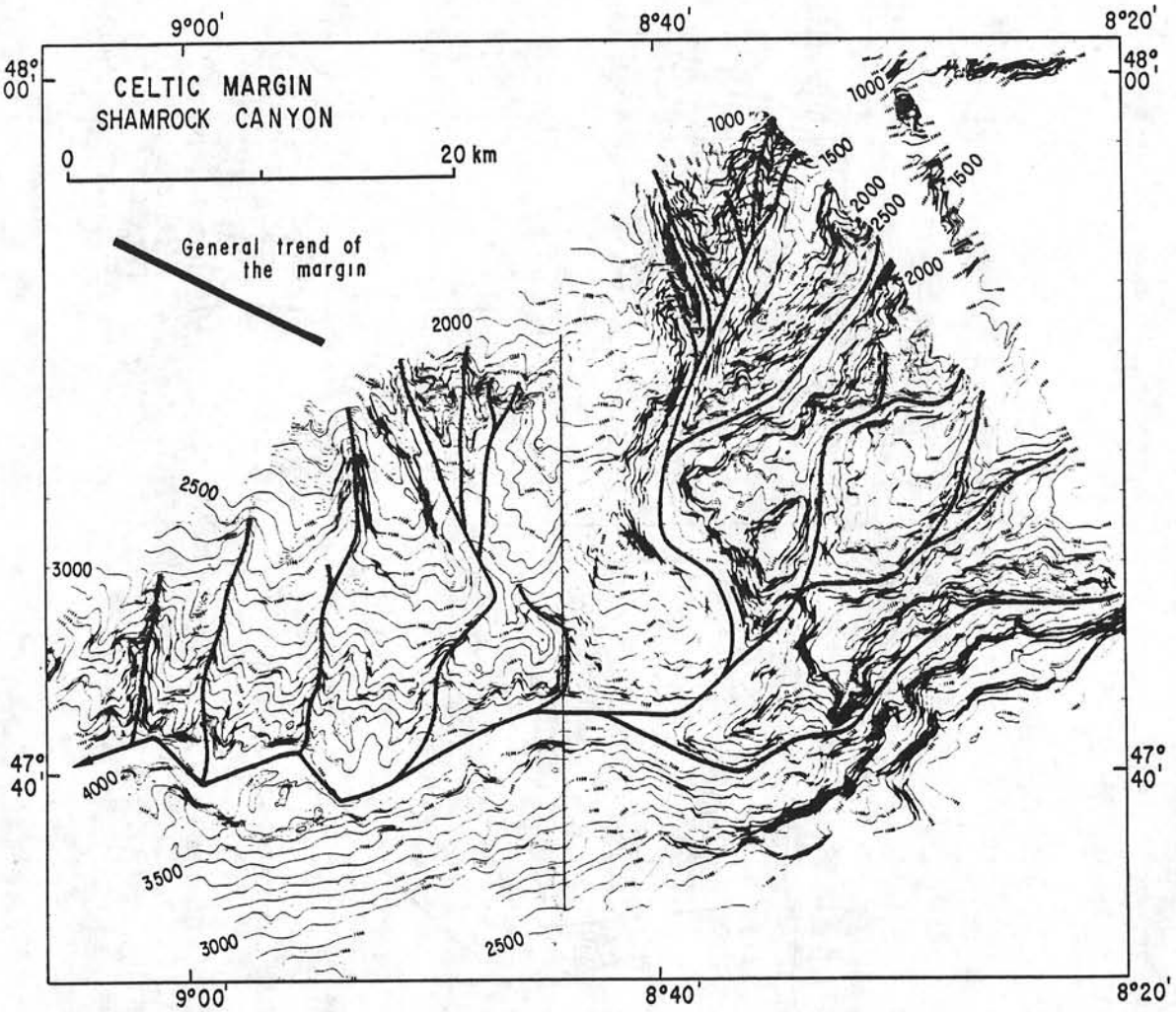


Fig. 2. Straight lines corresponding to linear segments of the Shamrock canyon axis and its tributaries superimposed on the Sea Beam map [Pastouret et al., 1982] located as box A on Figure 1. Depths are in uncorrected meters (1500 m/s). Isobath spacing 20 m.

trough [Sibuet and Le Pichon, 1971; Sibuet et al., 1971].

Area 6. The west Iberian continental margin which is roughly oriented north-south presents, in its northern portion, a large promontory named Galicia Bank (subarea 6a) that is separated from the continental shelf by the Interior Basin filled up with sediments [Auzende et al., 1979].

## METHODOLOGY

Most of the tectonic lines which appeared during the formation of the continental margins represent preferential erosional guides for incipient channels and canyons. Nevertheless, especially during the Plio-Quaternary period, important sedimentary gravity processes occured along the major gradient of slopes, giving rise to canyons oriented perpendicularly to the margin. A statistical analysis of the orientation of the canyons was undertaken in order to discriminate between tectonic and gravity directions and to compare these tectonic trends with onland and offshore structural trends.

Seven hundred and fifty measurements of orientation and length of segments of canyon axes have been made along the whole continental margin. Accuracy of

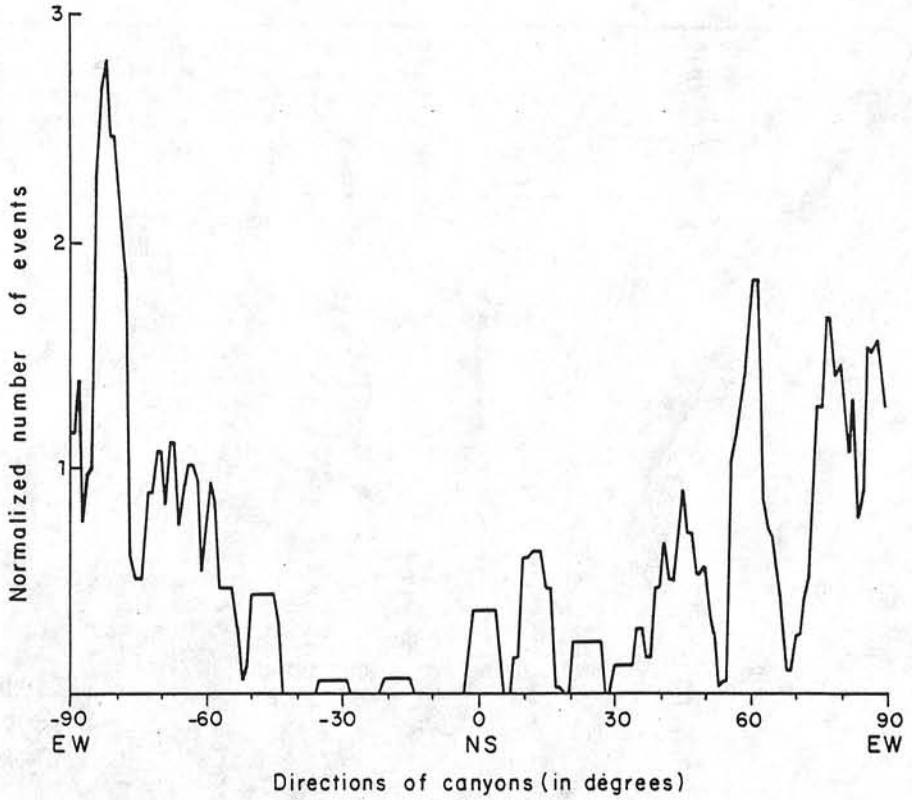


Fig. 3. Diagram of normalized number of events as a function of the direction of canyons, for area 1 defined in Figure 1.

measurements is about 3° for the orientation and about 2 km for the length of segments. Generally, this precision is better when measurements have been carried out on Sea Beam bathymetric maps. If the canyon is sinuous, we divide it into short segments taking into account the surrounding morphological directions if necessary. Thus each measurement corresponds to a portion of canyon and not to the entire canyon (see the example of the Shamrock canyon, Figure 2). Data have been normalized as follows in order to compare them between areas.

If Li is the cumulative length of canyons following the i direction (expressed in degrees from -89° to +90°)

$$\text{in an area, } Fi = \left(Li \Big/ \sum_{i=-89}^{+90} Li\right) \times 100$$

Fi being the frequency of cumulated length of canyons following the i direction.

Curves have been then smoothed using mobile averaging over 7°.

Results appear in a set of six diagrams (Figures 3, 5, 8, 9, 10, and 11) showing the distribution of canyons for each of the six areas. Superimposed on the curves are the directions of onland structural trends likely to extend offshore and gravitational directions perpendicular to the local trend of continental slopes. For example, if the trend of the continental slope is N120°±10°, the gravity direction of the main canyons would be N30°±10°.

## DISCUSSION OF RESULTS

### Area 1: Porcupine and Goban Spur Margins

The presence of channels on the eastern slope of the Porcupine Seabight was first suggested by Berthois and Brenot [1960]

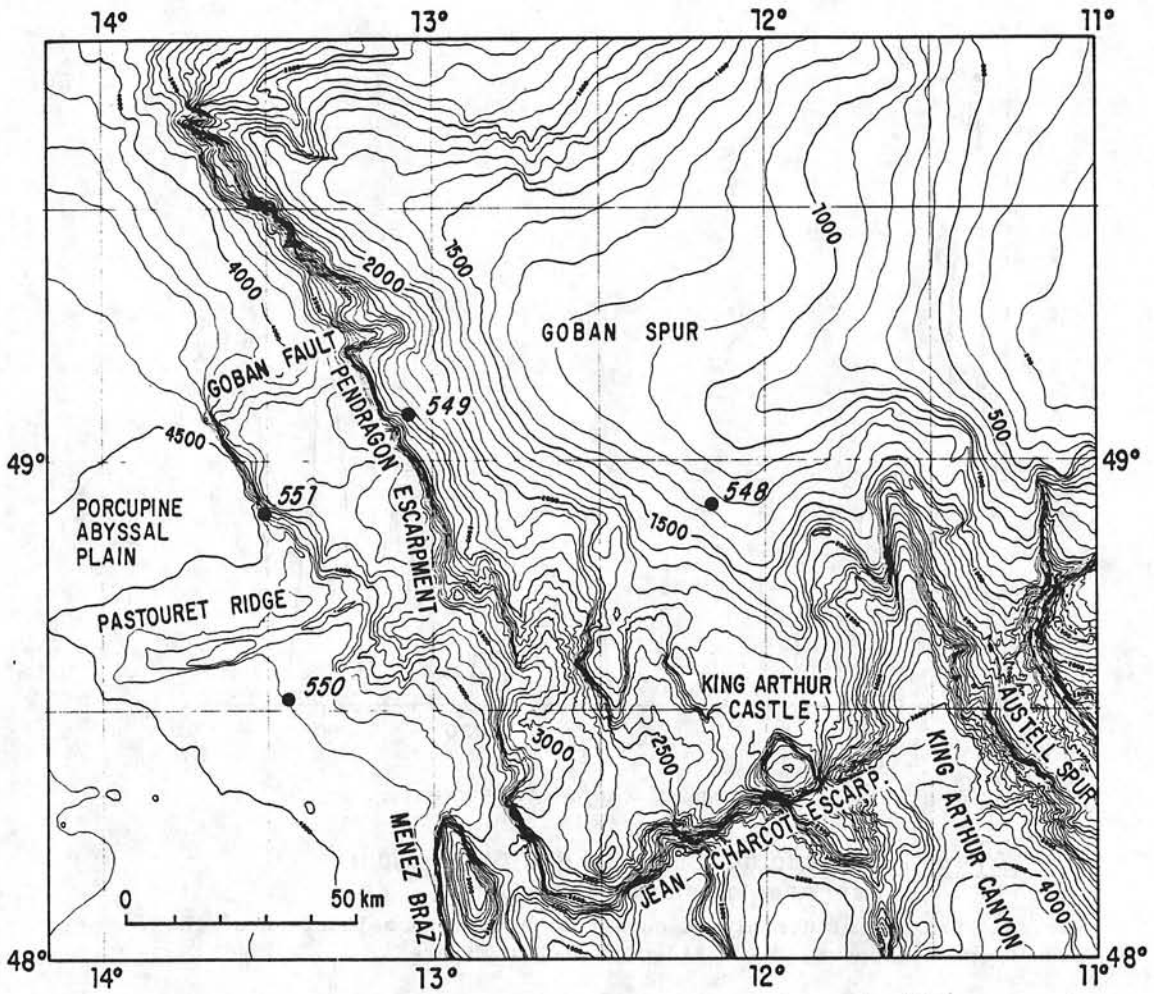


Fig. 4. Bathymetric map of the Goban Spur continental margin [Sibuet et al., 1984a, b] established from Sea Beam, conventional and unpublished GLORIA data and located as box B in Figure 1. Depths are in uncorrected meters (1500 m/s). Contour spacing every 100 m. Locations of DSDP leg 80 drilling sites are shown. The JEAN CHARCOT escarpment and the Goban fault are late Hercynian features oriented N70° and reactivated during the lower Cretaceous rifting phase. Between these two features, the NNW-SSE trending Pendragon escarpment and another parallel escarpment on which DSDP site 551 is located correspond to the crest and oceanward side of tilted fault block created during the rifting phase.

and then confirmed by the side-scan sonar survey of Kenyon et al. [1978]. The system, roughly E-W oriented, was named the Gollum Channel system and corresponds to the main contribution to Figure 3. Inasmuch as numerous slump folds are observed in the vicinity of these channels (N.H. Kenyon, personal communication, 1985) and as the heads of canyons are mainly oriented perpendicularly to the subcircular shape of the upper slope (see the main peak on Figure 3), these trends are likely close to gravity directions and do not suggest any tectonic control.

On the Goban Spur continental margin (Figure 4), the NW-SE trending Pendragon Escarpment and another parallel escarpment located 35 km southwestward correspond to the fault planes which limit the tilted fault blocks. They are offset or interrupted by ENE-WSW trending faults such as the Goban fault and the JEAN CHARCOT escarpment [Sibuet et al., 1984b]. Nevertheless, as almost no canyon exists


Plate 1. Bathymetric map of the northeast Atlantic. Mercator projection (W.G.S. 72 ellipsoid). Contour spacing 200 m [Lallemand et al., 1985b].

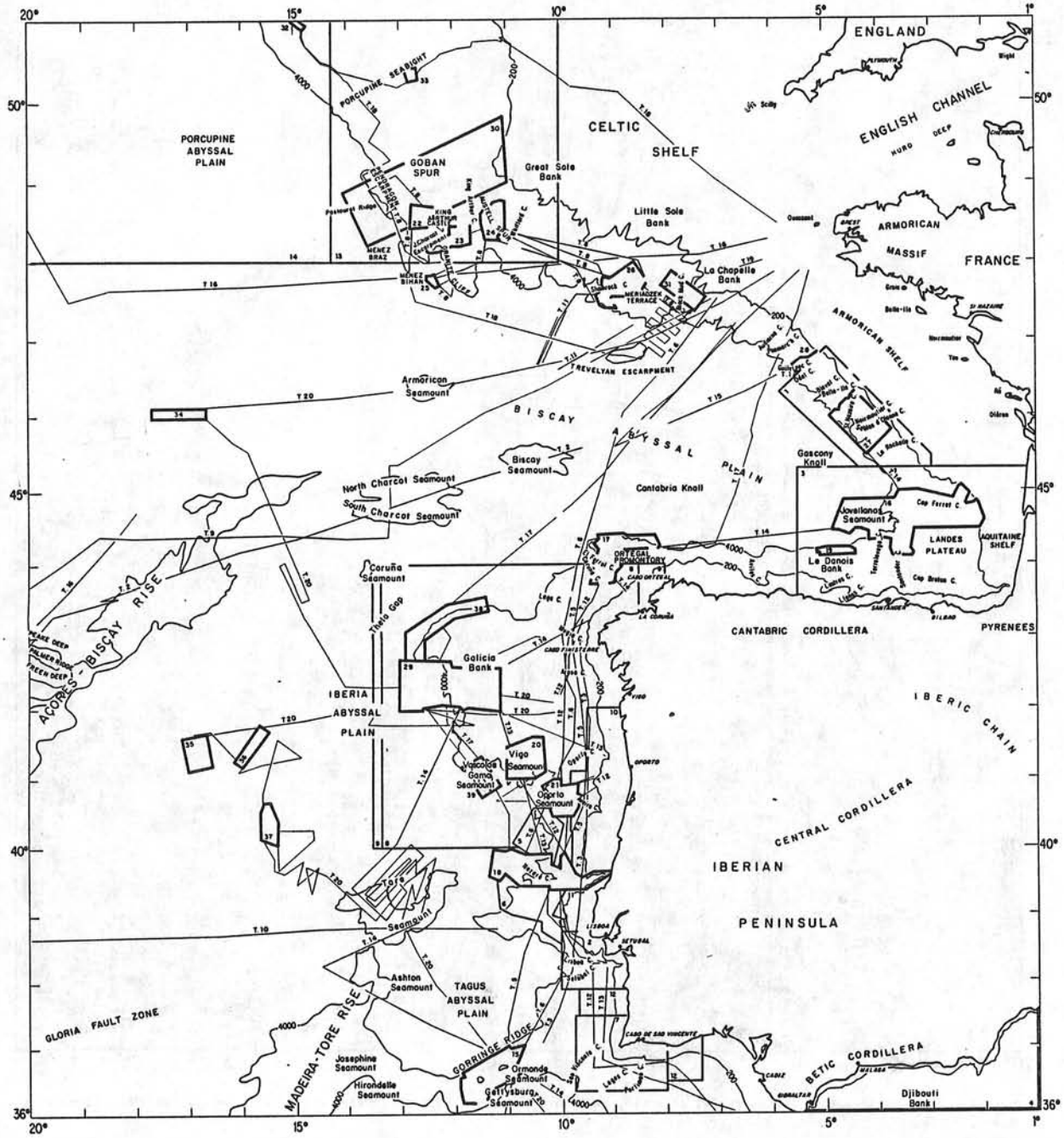


Plate 2. Location of recent conventional maps, Sea Beam detailed maps and transits used to establish the bathymetric map of Plate 1. (See Lallemand et al. [1985a, b] for references.) Toponymy of features is given.

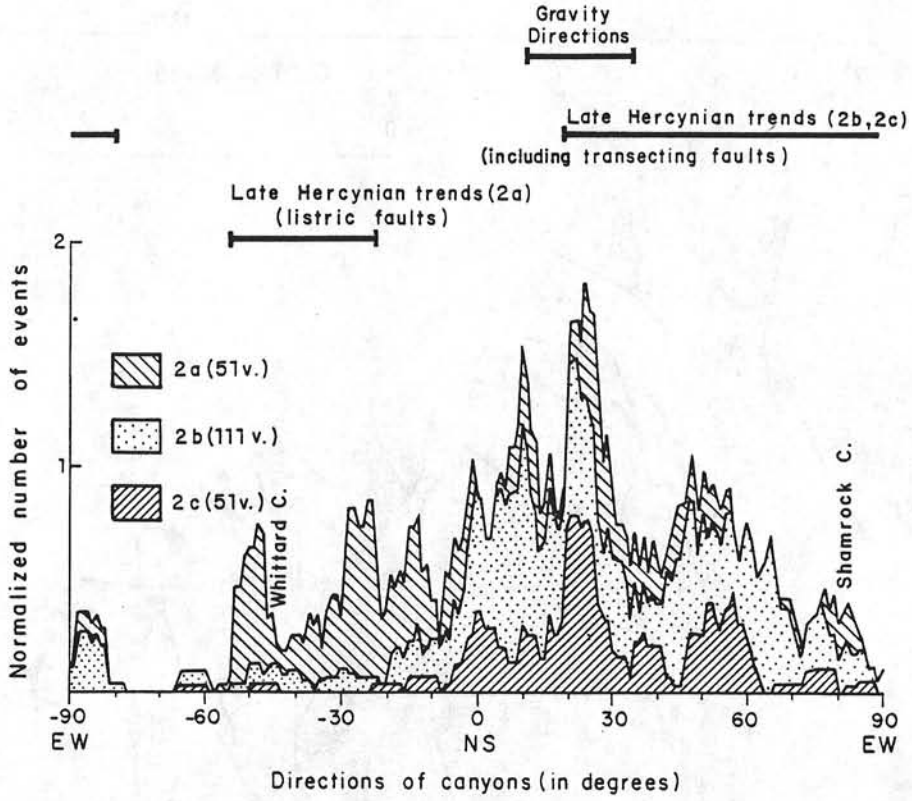


Fig. 5. Diagram of normalized number of events as a function of the direction of canyons for area 2 defined in Figure 1.

along this margin (Figure 4), there is no contribution to the diagram of these Caledonian or late Hercynian tectonic trends reactivated during the late Jurassic-early Cretaceous rifting phase.

Area 2: Celtic Margin

Subzone 2a represents the connection between the Goban Spur and Celtic margins and is marked by several topographic features such as Granite Cliff, Menez Braz, Menez Bihan, and Austell Spur, separated by large NW to NNW trending canyons (Plates 1 and 2 and Figure 4). Three peaks at -15°, -25°, and -50° appear in Figure 5 (Subzone 2a). For both the Goban Spur margin and the transition zone 2a, the trends of the listric faults along which the tilted blocks glide are oriented -25° (e.g., the Pendragon Escarpment, Figure 4) and follow the strike of the margin [Montadert et al., 1979a; Sibuet et al., 1984b]. The -50° direction is mainly due to the contribution of the Whittard canyon and its tributaries (Plates 1 and 2 and Figure 1). This canyon continuously changes of direction from 60° in its upper portion to -45° along its main course and cuts the Tertiary sedimentary cover.

Subzone 2b presents large topographic features such as the Meriadzek terrace, the Trevelyan escarpment, and the Shamrock canyon. Subzone 2c has the same regular slope as the Armorican margin (subzone 3a), but its general direction is clearly linked to that of the Celtic margin. Figure 5 shows that the main peaks occur from -5° to 40° and from 45° to 65° for both subzones 2b and 2c. These peaks are linked to the directions of late Hercynian faults in Brittany and on the continental shelf, directions which vary from NNE-SSW to E-W in azimuth. The major peak at N20° corresponds to the gravity trends but also to the direction of transecting faults located in the Meriadzek area by Montadert et al. [1979a] and reactivated during the

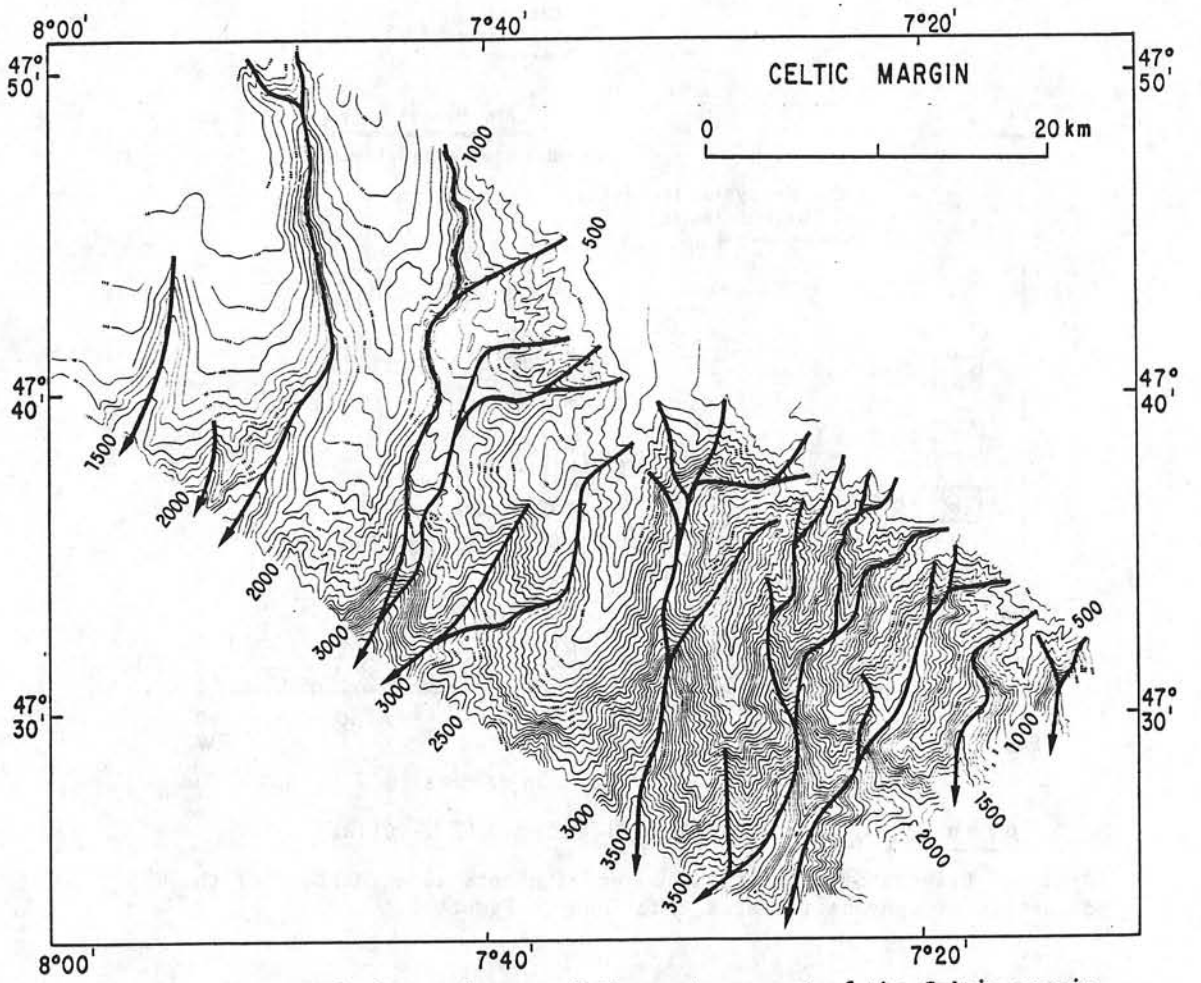


Fig. 6. Sea Beam bathymetric map of the eastern part of the Celtic margin located as box C in Figure 1. Depths are in uncorrected meters (1500 m/s). Isobath spacing is 100 m. Note the N20°-30° general trend of canyons corresponding to the main peak in Figure 5.

lower Cretaceous rifting phase. Figure 6 displays the Sea Beam bathymetry of the upper part of the Celtic margin (subzone 2c). The general N20° orientation of the numerous canyons illustrate that it is a major contribution to Figure 5. Nevertheless, the degree of downcutting and the path of canyons also depend of the lithology as it was demonstrated for the Shamrock canyon notching the chalk and calcareous marl and changing of directions in the vicinity of horsts [Auzende et al., 1981; Pastouret et al., 1982] (Figure 2). Our conclusion is that in any case, even if gravity processes exist, as shown by the presence of the N25° peak, the structural control remains for the major canyons such as the Shamrock canyon which is clearly oblique (N80°) to the slope trend and presents sharp changes in directions which are compatible with the late Hercynian trends.

Area 3: Armorican Margin

In contrast with the Celtic margin, the Armorican margin is a linear, narrow, steep margin oriented N135° which follows the early Cretaceous transform direction of opening of the Bay of Biscay [e.g., Le Pichon et al., 1971; Olivet et al., 1984]. The overall dendritic canyon pattern is due to the numerous secondary valleys and side-gulleys as evidenced on the detailed

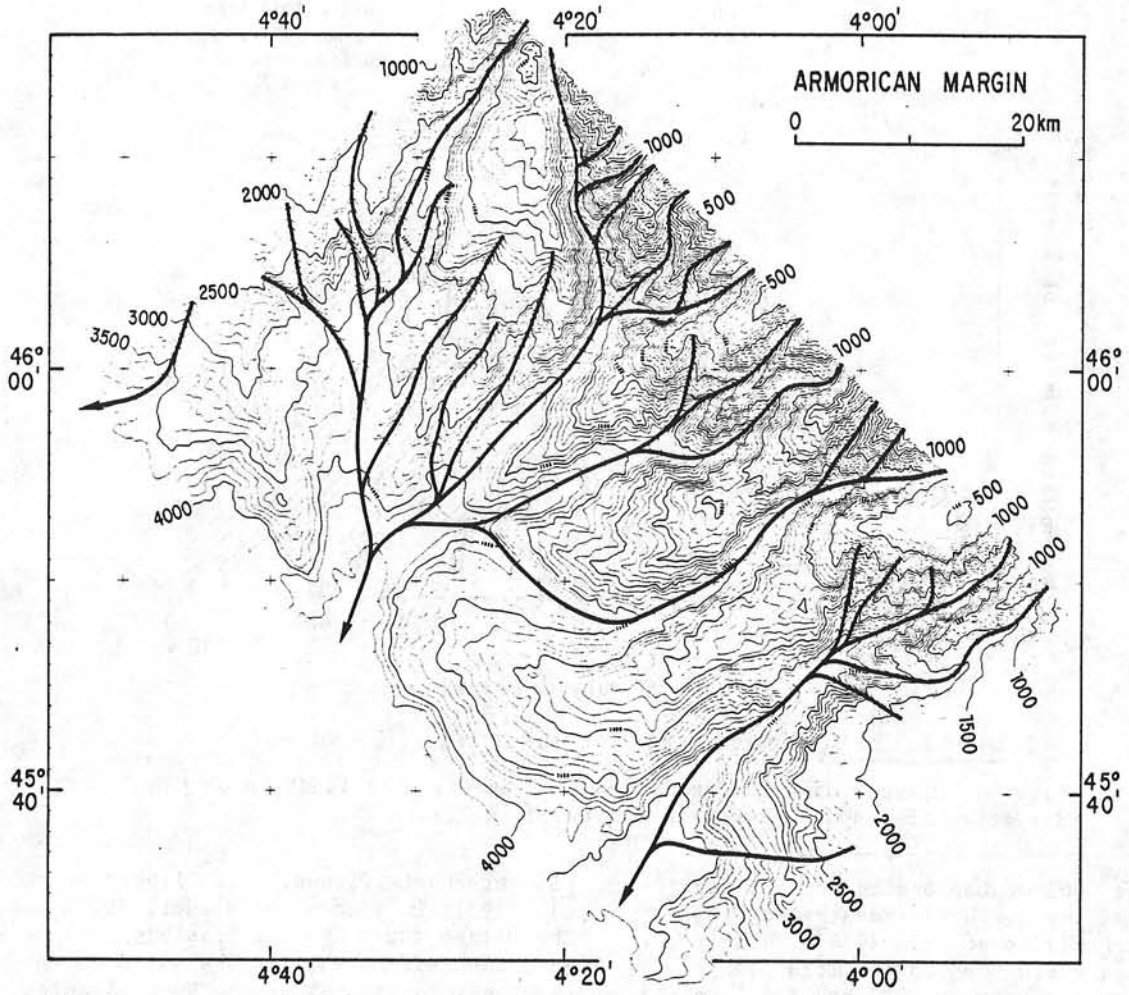


Fig. 7. Sea Beam bathymetric map of a portion of the Armorican margin located as box D in Figure 1 [Pastouret, 1984]. Depths are in uncorrected meters (1500 m/s). Isobath spacing is 100 m. The canyon pattern is characterized by numerous tributaries.

Sea Beam bathymetric map of Figure 7. The canyon axes themselves change from sinuous to straight and present frequent sharp turns (Figures 1 and 7). Figure 8 shows that the directions of canyons vary from N-S to N100°, with a major peak which corresponds to the general gravity trend between N40° and N50° for subzone 3a and between N-S and N30° for subzone 3b. On the continental shelf, most of the faults are oriented N55° to N65° (Figure 1). They are conjugated faults of the large shear system which affects the Hercynian basement of the Armorican massif. Their orientations correspond to the major N55° to N65° peak appearing on the diagram (subzone 3a).

Area 4: Landes Plateau

In the southeast corner of the Bay of Biscay, the Landes Plateau lies on the prolongation of the Aquitaine basin and can be considered as a prograding Tertiary structure over a promontary that includes Triassic to Mesozoïc terranes [Valéry et al., 1971; Derégnaucourt and Boillot, 1982]. It is limited to the north and south by the Cap Ferret canyon and the Gouf of Cap Breton respectively. Both show a structural control: the Cap Ferret canyon following normal faults reactivated during Tertiary [Derégnaucourt and Boillot, 1982] corresponds to the extension of the onland Parentis basin,

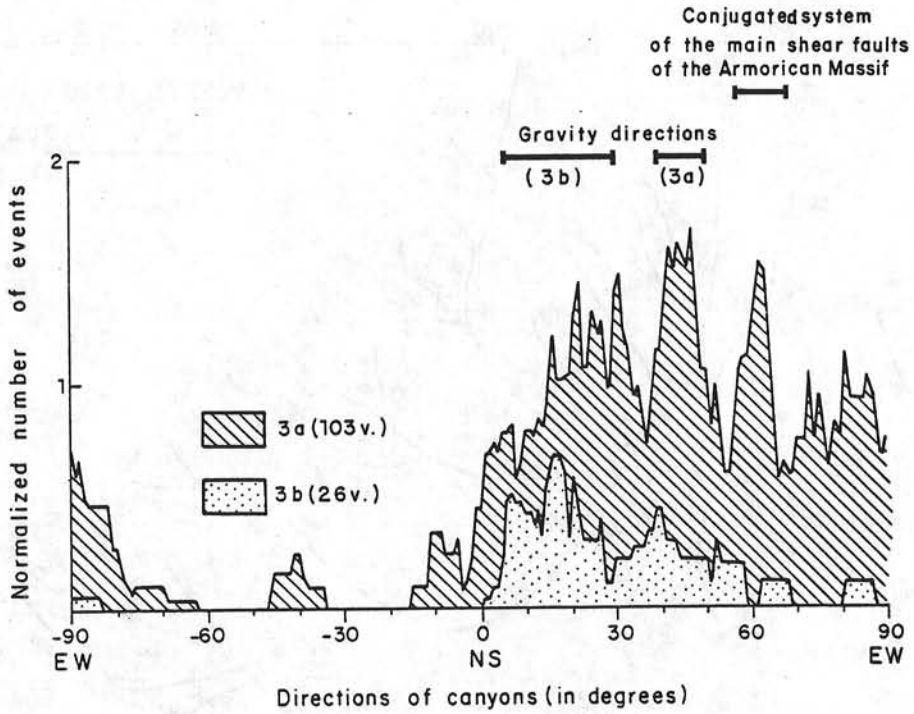


Fig. 8. Diagram of normalized number of events as a function of the direction of canyons, for area 3 defined in Figure 1.

and the Gouf of Cap Breton fringes the front of the North Pyrenean Paleogene thrust [Boillot et al., 1974]. These features correspond to the main peaks which appear between N70° and N110° on the diagram (Figure 9). The NW-SE lower Cretaceous dextral faults, located on the plateau itself and south of it (such as the Bilbao fault trending NW-SE from Bilbao) [Derégnaucourt and Boillot, 1982], were reactivated during the lower Tertiary Pyrenean phase of compression and may have controlled the canyon pattern corresponding to the -40° peak of Figure 9.

Area 5: North Spanish Margin

The North Spanish margin, which consists of a narrow shelf (30-40 km) and a steep slope (17°) rising directly from the Bay of Biscay, was largely tectonized during the late Cretaceous to late Eocene phase of compression resulting in the formation of the North Spanish marginal trough presently filled up with sediments [Sibuet and Le Pichon, 1971; Sibuet et al., 1971; Le Pichon and Sibuet, 1971a]. The Bilbao fault and its possible extension offshore limit the two domains (subzones 5a and 5b) of the North Spanish continental margin, characterized by an oceanic subduction to the west and a continental collision with two overthrusting fronts to the east [Boillot and Capdevilla, 1977].

Subzone 5a includes tributaries of the southern flank of the Gouf of Cap Breton. The main peaks occuring between -40° and -30° and between 0° and 30° (Figure 10) are linked to the presence of early Cretaceous and early Tertiary tectonic features [Groupe Cybère, 1984] but also to gravity processes for the second family of canyon trends.

Within subzone 5b, the North Spanish margin is globally oriented E-W, and no major peak corresponds to the gravity directions. This area displays a broad variety of canyon trends (Figure 10).

From the Cybère diving cruise, performed in 1982 on the western part of the North Spanish margin, five principal

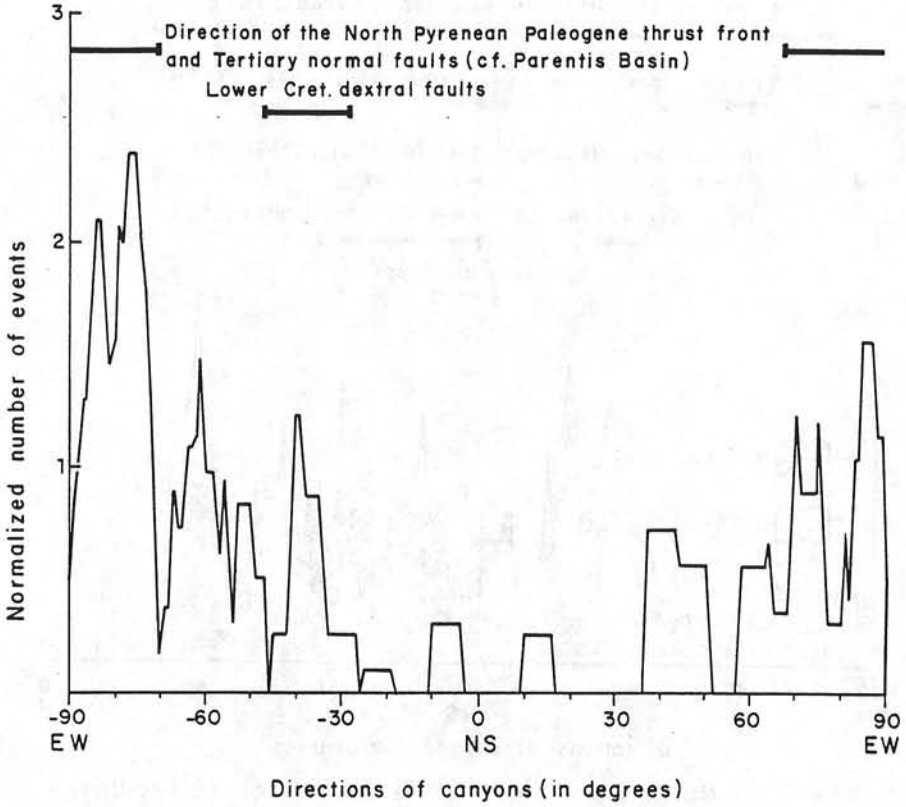


Fig. 9. Diagram of normalized number of events as a function of the direction of canyons, for area 4 defined in Figure 1.

directions of fracturing were observed in the Mesozoïc terranes: 0°, 20°, 50° to 70°, 90° and -50° to -60° [Groupe Cybère, 1984]. Directions of fracture observed in the Eocene terranes are 0°, 50°, 90° and -60°. As both sets of directions are similar (except N20°), this suggests that the same net of fracturing was reactivated during the Eocene compressive phase. The 20°, 50° to 70°, and -50° to -60° directions are parallel to those measured in the Mesozoïc basement of Galicia and attributed to the Hercynian and late Hercynian tectonics [Parga, 1969; Arthaud and Matte, 1975]. Consequently, it seems that the formation of the margin and the succeeding Tertiary deformation mainly occur along previous fractures in the substratum [Boillot et al., 1974; Groupe Cybère, 1984]. Figure 10 clearly shows all these structural directions. The major N60° peak corresponds to one of the well-known late Hercynian tectonic lines of Parga [1969] reactivated during Cenozoïc time [Boillot et al., 1974].

Area 6: West Iberian Margin

The west Iberian margin can be considered as two contrasting physiographic provinces divided at 40°N. North of this latitude lies a large continental plateau which includes the Galicia bank sensus-stricto, but also several other seamounts such as Vigo, Porto, and Vasco da Gama which may represents horsts formed during the early Cretaceous rifting episode [Auzende et al., 1979; Montadert et al., 1979a].

On the Galicia bank s.s. the major directions of faults at -30°, 20°, and 50° [Grimaud, 1981] correspond to the late Hercynian directions (Figure 11). On the southern Portuguese margin, Mougenot et al. [1979] and Sibuet et al. [1986] have shown that the late Hercynian fracture

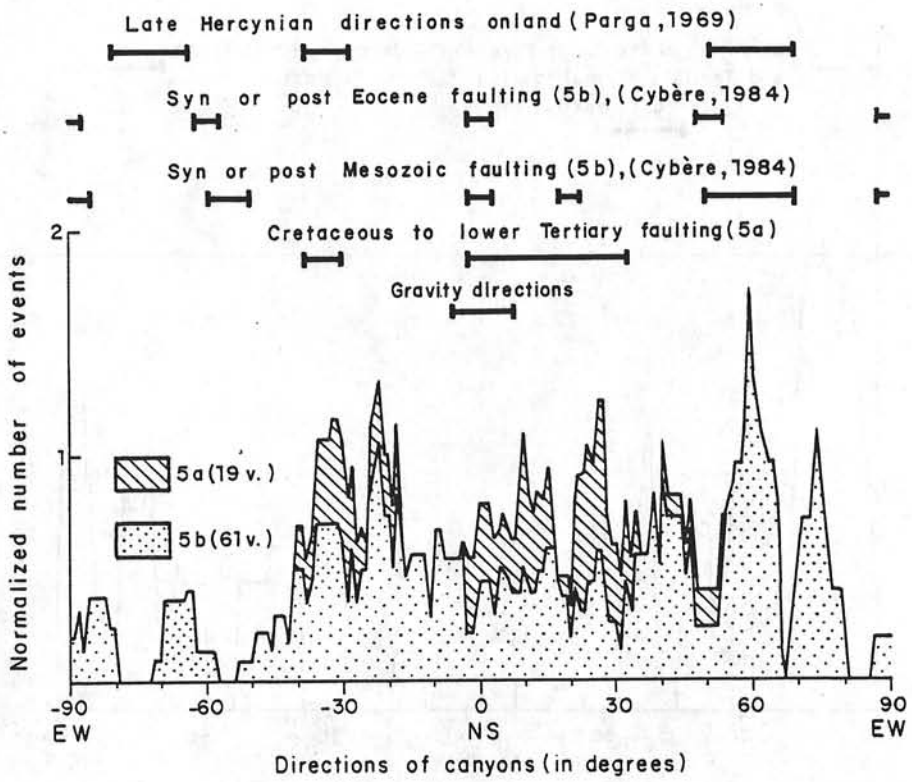


Area 5: North Spanish continental margin (80 values)

Fig. 10. Diagram of normalized number of events as a function of the direction of canyons, for area 5 defined in Figure 1.

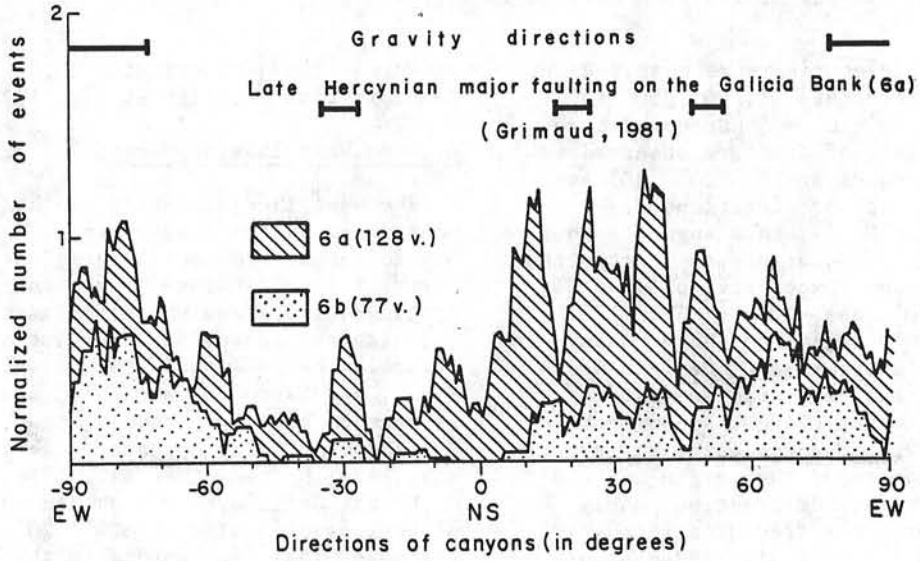


Area 6: West Iberian continental margin including Galicia Bank (205 values)

Fig. 11. Diagram of normalized number of events as a function of the direction of canyons, for area 6 defined in Figure 1.

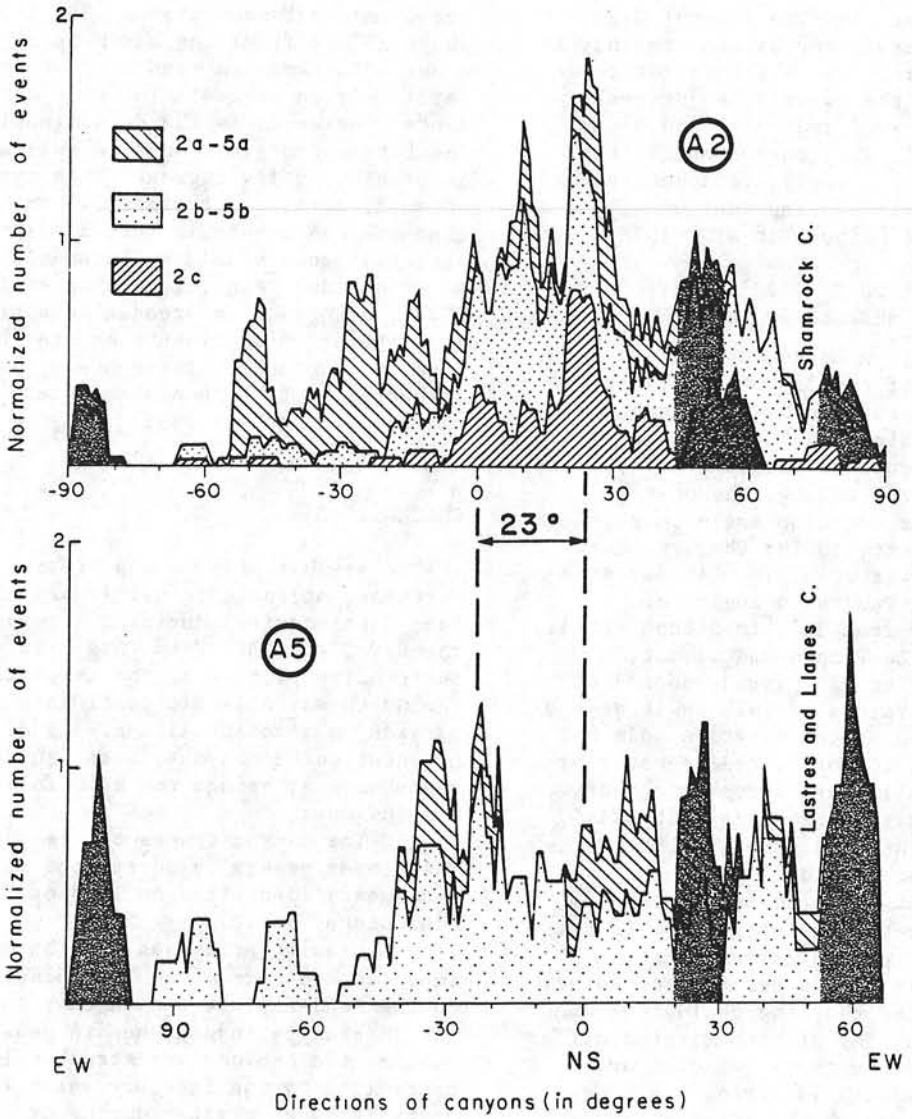


Fig. 12. Correspondence of diagrams of the Celtic and north Spanish margins based on a 23° rotation of Iberia with respect to Europe in order to illustrate the match between the late Hercynian fracture patterns of each side of the Bay of Biscay. The dark peaks underline three main late Hercynian structural directions followed by canyons.

pattern have been reactivated several times since the first Permo-Triassic tensional episode, along the NE-SW, ENE-WSW, and NW-SE strike-slip directions. Thus the large prominent Nazaré, Lisboa, Setubal, and Sao Vicente canyons (subzone 6b) are obviously controlled by the late Hercynian fracture pattern [e.g., Boillot et al., 1974], at least in their upper portion.

Figure 11 shows a great variety of directions which reflects the influence of a complex tectonic pattern, largely similar north and south of 40°N latitude in subzones 6a and 6b, while the physiographic character of these two subzones

differs considerably. The general N-S trend of the margin corresponds roughly to E-W gravity directions which do not come out clearly in the diagram. Major peaks appear between -90° and -55°, and 5° and 70° and at -30°. They correspond to the late Hercynian and early Cretaceous set of faults reactivated during the post tectonic phases [Sibuet et al., 1986].

## ARGUMENTS IN FAVOR OF A 23° ROTATION OF IBERIA WITH RESPECT TO EUROPE

The currently accepted hypothesis about the formation of the Bay of Biscay is the one initially proposed by Le Pichon et al. [1970, 1971]. Since that time, several authors have proposed slight modifications which concern the timing, the pole position or the rotation angle [e.g., Le Pichon and Sibuet, 1971b; Choukroune et al., 1973; Olivet et al., 1984; Savostin et al., 1986]. Published angles of rotations vary from 30° [Le Pichon et al., 1971] to 23° [Le Pichon and Sibuet, 1971b]. Olivet et al. [1984] adopted an angle of 24°. Values of this angle depend on the position of the rotation pole but also on the choice of fitted isobaths or features. In all these reconstructions, the North Spanish margin was initially connected to the Celtic margin. It is tempting to look at the angular correlation between lineaments predating the opening of the Bay of Biscay: in this case, the late Hercynian fracturation pattern even if it was reactivated later.

We saw indeed that the geological and tectonic evolutions of both margins differ considerably after their creation and separation, especially during the Eocene compressive phase which affected the southern margin. Consequently, correlation between peaks must not be done on a criterion of amplitude, but on a criterion of global correspondence of peaks without the influence of gravity processes.

Figure 12 shows such a correspondence between peaks belonging to the late Hercynian fracture pattern on both the Celtic and North Iberian Peninsula margins. Each dark peak represents identified late Hercynian trends (Figure 5 and 10). Peaks in subzones 2c and 2a, 2b correspond respectively to peaks in subzones 5a and 5b. The peak at 55° (with respect to area 2) is common between subzones 2c and 5a and three peaks at -85°, 50° and 82° (with respect to area 2) are common between subzones 2a, 2b, and 5b. A 23° shift of the North Spanish margin diagram with respect to that of the Celtic margin accounts for this correspondence. The error in the determination of the rotation angle cannot be evaluated but is probably a few degrees. This type of attempt, derived for example from the idea that one can constrain initial fits by the correspondence of older lineaments located on both sides [e.g., Le Pichon et al., 1977], brings an independent constraint to the fitting of continents before the initiation of the rifting phase, as discussed by Le Pichon and Sibuet [1981] and Savostin et al. [1986].

## CONCLUSIONS

The new bathymetric map of the northeast Atlantic is mainly based on Sea Beam data acquired during 20 cruises on the R/V JEAN CHARCOT in this area. From the precise picture of the morphology of the northeast Atlantic continental margins, a statistical analysis of the orientation of canyons, based on 750 measurements, brings the main following conclusions:

1. The canyon trends of the continental slopes generally correspond to lineaments identified on land or on the continental shelf.
2. Gravity processes play a more important role from the Porcupine Seabight to the Landes plateau than they do around the Iberian peninsula, but in general, most of the canyons are structurally controlled by the late Hercynian features or by features created during or after the formation of these continental margins.
3. A 23° rotation of Iberia with respect to Europe is in good agreement with the correspondence of identified late Hercynian lineaments on both sides of the Bay of Biscay.

Acknowledgements. We greatly acknowledge the captains and the crews of the R/V JEAN CHARCOT and the chief scientists of the 20 oceanographic cruises during which Sea Beam data were collected. J.-P. Cadet and N. H. Kenyon critically reviewed the manuscript and offered helpful suggestions. S. Monti and J.-P. Mazé drew all the bathymetric maps. IFREMER contribution 70.

REFERENCES

Arthaud, F., and P. Matte, Les décrochements tardi-hercyniens du Sud-Ouest de l'Europe. Géométrie et essai de reconstitution des conditions de la déformation, Tectonophysics, 25, 139-171, 1975.

Auzende, J.-M., H. Jonquet, J.-L. Olivet, J.-C. Sibuet, J.-L. Auxiètre, G. Boillot, J.-P. Dunand, A. Mauffret, O. de Charpal, V. Apotolescu, and L. Montadert, The continental margin off Galicia and Portugal: Acoustical stratigraphy, dredge stratigraphy and structural evolution, Initial Rep. Deep Sea Drill. Proj., 47 (2), 633-662, 1979.

Berthois, L., and R. Brenot, La morphologie sous-marine du talus du plateau continental entre le sud de l'Irlande et le Cap Ortegal (Espagne), J. Cons. Cons. Int. Explor. Mer, 25, 111-114, 1960.

Berthois, L., and R. Brenot, Bathymétrie du Golfe de Gascogne et de la côte du Portugal, I, Commentaires sur le levé complémentaire des feuilles 9 et 10 des abords du plateau continental; II, Bathymétrie du talus du plateau continental à l'Ouest de la péninsule ibérique du Cap Finisterre au Cap St-Vincent, paper presented at the 52nd meeting, Cons. Int. pour l'Explor. de la Mer, Sept.-Oct. 1964.

Berthois, L., R. Brenot, and J. Debyser, Remarques sur la morphologie de la marge continentale entre l'Irlande et le Cap Finisterre, Rev. Inst. Fr. Pet. Ann. Combust. Liq., 23, 1046-1049, 1968.

Boillot, G., and R. Capdevilla, The Pyrénées: Subduction and collision?, Earth Planet. Sci. Lett., 18, 151-160, 1977.

Boillot, G., P.-A. Dupeuble, I. Hennequin-Marchand, M. Lamboy, J.-P. Leprêtre, and P. Muselec, Le rôle des décrochements "tardi-hercyniens" dans l'évolution structurale de la marge continentale et dans la localisation des grands canyons sous-marins à l'Ouest et au Nord de la péninsule ibérique, Rev. Géogr. Phys. Géol. Dyn., 16 (1), 75-86, 1974.

Choukroune, P., X. Le Pichon, M. Séguret, and J.-C. Sibuet, Bay of Biscay and Pyrénées, Earth Planet. Sci. Lett., 18, 109-118, 1973.

Derégnaucourt, D., and G. Boillot, Structure géologique du Golfe de Gascogne, Bull. Bur. Rech. Géol. Min., 2, I, 3, Géol. Gites Miner. Fr., 149-178, 1982.

Foucher, J.-P., X. Le Pichon, and J.-C. Sibuet, The ocean-continent transition in the uniform stretching model: role of partial melting in the mantle, Phil. Trans. R. Soc. London, Ser.A, 305, 27-43, 1982.

Grimaud, S., La marge ibérique au Nord et à l'Ouest du banc de Galice (Espagne), thesis, 90 pp., Paris VI Univ., Paris, 1981.

Groupe Cybère, La marge déformée du Nord-Ouest de l'Espagne, Publ. Cent. Natl. Exploit. Océans, Résultats Campagnes Mer, 29, 135 pp., 1984.

Guennoc, P., H. Jonquet, and J.-C. Sibuet, Carte magnétique de l'Atlantique nord-est, anomalies du champ total; échelle 1/2.400.000 CNEXO, Paris, 1978. (Available from BRGM, Serv. Promotion et Vente, Orléans, France.)

Guennoc, P., H. Jonquet, and J.-C. Sibuet, Présentation d'une carte magnétique de l'Atlantique nord-est, C. R. Acad. Sci., sér.D, 288, 1011-1013, 1979.

Kenyon, N.H., R.H. Belderson, and A.H. Stride, Channels, canyons and slump folds on the continental slope between southwest Ireland and Spain, Oceanol. Acta, 1 (3), 369-380, 1978.

Kidd, R.B., and D.G. Roberts, Long-range sidescan sonar studies of large-scale sedimentary features in the North Atlantic, Bull. Inst. Géol. Bassin Aquitaine, 31, 11-29, 1982.

Lallemand, S., J.-P. Mazé, S. Monti, and J.-C. Sibuet, Présentation d'une carte bathymétrique de l'Atlantique nord-est, C. R. Acad. Sci., sér.2, 300, 145-149, 1985a.

Lallemand, S., J.-P. Mazé, S. Monti, and J.-C. Sibuet, Carte bathymétrique de l'Atlantique nord-est, scale 1/2.400.000, IFREMER, Paris, 1985b. (Available from BRGM, Serv. Promotion et Vente, Orléans, France.)

Laughton, A.S., D.G. Roberts, and R. Graves, Bathymetry of the northeast Atlantic: Mid-Atlantic Ridge to southwest Europe, Deep Sea Res., 22, 791-810, 1975.

Le Pichon, X., and J.-C. Sibuet, Western extension of boundary between European and Iberian plates during the Pyrenean orogeny, Earth Planet. Sci. Lett., 12, 83-88, 1971a.

Le Pichon, X., and J.-C. Sibuet, Comments

on the evolution of the northeast Atlantic, Nature, 233, 257-258, 1971b.

Le Pichon, X., and J.-C. Sibuet, Passive margins: A model of formation, J. Geophys. Res., 86, 3708-3720, 1981.

Le Pichon, X., J. Bonnin, and J.-C. Sibuet, La faille nord-pyrénéenne: Faille transformante liée à l'ouverture du Golfe de Gascogne, C. R. Acad. Sci., 261, 1941-1944, 1970.

Le Pichon, X., J. Bonnin, J. Francheteau, and J.-C. Sibuet, Une hypothèse d'évolution tectonique du Golfe de Gascogne, in Histoire structurale du Golfe de Gascogne, edited by J. Debyser et al., pp. 1-44, Technip, Paris, 1971.

Le Pichon, X., J.-C. Sibuet, and J. Francheteau, The fit of the continents around the North Atlantic Ocean, Tectonophysics, 38, 169-209, 1977.

Masson, D.G., L. Montadert, R.A. Scrutton, and J.-P. Gruvel, Evolution of the Goban Spur: History of a starved passive margin, Initial Rep. Deep Sea Drill. Proj., 80, 115-140, 1984.

Montadert, L., O. de Charpal, D. Roberts, P. Guennoc, and J.-C. Sibuet, Northeast Atlantic passive continental margins: Rifting and subsidence processes, in Deep Drilling Results in the Atlantic Ocean: Continental Margins and Paleoenvironment, Maurice Ewing Ser., vol.3, edited by M. Talwani et al., pp. 154-186, AGU, Washington D.C., 1979a.

Montadert, L., et al., Site 401, Initial Rep. Deep Sea Drill. Proj., 48, 73-124, 1979b.

Mougenot, D., J.H. Monteiro, P.-A. Dupeuble, and J.-A. Malod, La marge continentale sud-portuguaise; évolution structurale et sédimentaire, Cienc. Terra, 5, 223-246, 1979.

Olivet, J.-L., J. Bonnin, P. Beuzart, and J.-M. Auzende, Cinématique de l'Atlantique Nord et Central, Pub. Centr. Natl. Exploit. Océans, 108 pp., 1984.

Parga, J.-R., Sistemas de fracturas tardihercinicas del macizo hesperico, Trab. Lab. Geol. Lage, 37, 1-15, 1969.

Pastouret, L., Carte bathymétriques des canyons sud-armoricains de St-Nazaire, de Noirmoutier, des Sables d'Olonne et d'Oléron, CNEXO, Paris, 1984. (Available from BRGM, Serv. Promotion et Vente, Orléans, France.)

Pastouret, L., G.A. Auffret, J.-M. Auzende, P. Beuzart, P. Dubois, M. Séguret, J. Sigal, and J.-R. Vanney, La marge continentale armoricaine, résultats d'observation en submersible et de dragages dans le canyon Shamrock, C. R. Acad. Sci., Sér.2, 292, 741-748, 1981.

Pastouret, L., P. Beuzart, and S. Monti, Présentation de cartes bathymétriques de la marge continentale armoricaine et celte, Golfe de Gascogne, Bull. Soc. Geol. Fr., 24, 407-411, 1982.

Pegrum, R.M., and N. Mounteney, Rift basins flanking North Atlantic Ocean and their relation to North Sea area, Am. Assoc. Petrol. Geol. Bull., 62, 419-441, 1978.

Renard, V., and J.-P. Allenou, Le Sea Beam, sondeur à multifaisceaux du N/O JEAN CHARCOT: Description, évaluation et premiers résultats, Rev. Hydrogr. Int., 56, 35-71, 1979.

Savostin, L.A., J.-C. Sibuet, L.P. Zonenshain, X. Le Pichon, and M.-J. Roulet, Kinematic evolution of the Tethys belt from the Atlantic Ocean to the Pamirs since the Triassic, Tectonophysics, 123, 1-35, 1986.

Sibuet, J.-C., and L. Berthois, Dominant structural trends on the western continental margin of Iberia: Implications on initial rifting, Initial Rep. Deep Sea Drill. Proj., 47 (2), 753-760, 1979.

Sibuet, J.-C., and X. Le Pichon, Structure gravimétrique du Golfe de Gascogne et le fossé marginal nord-espagnol, in Histoire structurale du Golfe de Gascogne, 9, edited by J. Debyser et al., pp. 1-18, Technip, Paris, 1971.

Sibuet, J.-C., and W.B.F. Ryan, Site 398: Evolution of the west Iberian passive continental margin in the framework of the early evolution of the north Atlantic Ocean, Initial Rep. Deep Sea Drill. Proj., 47 (2), 461-475, 1979.

Sibuet, J.-C., G. Pautot, and X. Le Pichon, Interprétation structurale du Golfe de Gascogne à partir des profils de sismique, in Histoire structurale du Golfe de Gascogne, 10, edited by J. Debyser et al., pp. 1-32, Technip, Paris, 1971.

Sibuet, J.-C., B. Mathis, and P.M. Hunter, La ride Pastouret (plaine abyssale de Porcupine): Une structure éocene, C. R. Acad. Sci., Ser.2, 299, 1391-1396, 1984a.

Sibuet, J.-C., B. Mathis, L. Pastouret, J.-M. Auzende, J.-P. Foucher, P. M.

Hunter, P. Guennoc, P.-C. de Graciansky, L. Montadert, and D.G. Masson, Morphology and basement structures of the Goban Spur continental margin (northeastern Atlantic) and the role of the Pyrenean orogeny, in Initial Rep. Deep Sea Drill. Proj., 80, 1153-1165, 1984b.

Sibuet, J.-C., J.-P. Mazé, P. Amortila, and X. Le Pichon, Physiography and structure of the western Iberian continental margin off Galicia from Sea Beam and seismic data, leg 103, Ocean Drilling Program, part A, in press, 1986.

Somers, M.L., R.M. Carson, J.A. Revie, R.H. Edge, B.J. Barrow, and A.G. Andrews, Gloria II: An improved long-range sidescan sonar, in Oceanology International, 78, Technical Session J, pp. 16-24, B.P.S. Exhibitions Ltd, London, 1978.

Valery, P., J.-R. Delteil, A. Cottençon, L. Montadert, B. Damotte, and J.-P. Fail, La marge continentale d'Aquitaine, in Histoire structurale du Golfe de Gascogne, 8, edited by J. Debyser et al., pp. 1-24, Technip, Paris, 1971.

S. Lallemand, Ecole Normale Supérieure, Département de Géologie, 24 rue Lhomond, 75231 Paris Cédex 05, France.

J.-C. Sibuet, Département des Géosciences Marines, IFREMER, Centre de Brest, BP 337, 29273 Brest Cédex, France.

(Received September 20, 1985;
revised June 10, 1986;
accepted June 26, 1986.)

*Geophys. J. R. astr. Soc.* (1986) **86**, 893–907

# Isostasy of the Northern Bay of Biscay continental margin

Michel Diament *Laboratoire de Géophysique (U.A. du CNRS no. 730). Bât. 509, Université Paris-Sud, 91405 Orsay cedex, France*

Jean-Claude Sibuet *IFREMER Centre de Brest, BP 337, 29273 Brest cedex, France*

Ahmed Hadaoui *Laboratoire de Géophysique (U.A. du CNRS no. 730), Bât. 509, Université Paris-Sud, 91405 Orsay cedex, France*

Accepted 1986 March 3. Received 1986 March 3; in original form 1985 March 15

**Summary.** Spectral analysis of eight marine gravity profiles and seven *SEASAT* profiles, combined with corresponding bathymetric data over the Northern Bay of Biscay origin, yield identical admittance functions for wavelengths greater than 120 km. The resulting admittance function has been interpreted in terms of an Airy model of compensation for wavelengths greater than 250 km and in terms of an elastic plate model of compensation for shorter wavelengths. The Airy model corresponds to a crustal thickness variation across the margin. The plate model with an elastic thickness of 8 km is associated with the regional compensation of a sedimentary load which was probably emplaced during and just after rifting.

**Key words:** continental margin, Bay of Biscay, marine gravity, satellite altimetry, admittance

## Introduction

To explain the gravity or geoid anomalies which are observed across continental margins it has often been assumed in many studies that the topography of continental margins represents a stated isostatic equilibrium and that the Airy model of compensation is applicable (e.g. Haxby & Turcotte 1978, Rabinowitz 1982). In this case the gravity signal is completely controlled by the crustal thickness variation, even though a so-called Airy isostatic anomaly often exists across continental margins (Rabinowitz 1982). Karner & Watts (1982) and Louden (1983) used the spectral analysis approach, which characterizes the isostatic response (admittance) without any *a priori* choice of a model (McKenzie & Bowin 1976), and concluded that the admittance must be interpreted in terms of a flexure model of isostasy (elastic plate model). This type of model explains satisfactorily the Airy isostatic anomaly. Karner & Watts (1982) also discussed the long wavelength effect in the gravity

signal due to the thermal isostasy (i.e. the effect due to the transition from oceanic to continental lithosphere) and concluded that the thermal gravity effect decays rapidly with time after the initial rifting and that the gravity signal is dominated by the crustal structure. In fact, in order to study the lithospheric transition, geoid anomalies are better suited than gravity anomalies because the geoid is much more sensitive to deep sources of anomalies than gravity data and also because the geoid anomalies provided by altimetric satellites have a better signal to noise ratio in the long wavelength domain (Chapman & Talwani 1979). On the other hand, gravity anomalies are better suited for the investigation of crustal isostasy.

In this paper we present the results of an analysis of altimetry and gravity anomalies in connection with bathymetry carried out in order to quantify the isostatic equilibrium of an extensional continental margin. We choose to analyse the Northern Bay of Biscay margin for three reasons: (a) a good set of marine data are available in this area (gravity, bathymetry, seismic reflection and refraction); (b) the main trend of this margin is perpendicular to the descendant *SEASAT* track directions; (c) the observations of listric faults (Montadert *et al.* 1979) and tilted blocks (Le Pichon & Sibuet 1981) were used to propose models of formation and evolution of this starved continental margin which have time control through DSDP holes (Montadert *et al.* 1979). These models are based on the assumption of local isostasy through a plastic behaviour of the lithosphere during the rifting and post-rifting stages.

## Geological setting

The present structure of the Northern Bay of Biscay margin (Fig. 1) is dominated by a tensional phase during Lower Cretaceous time which lasted 20–40 Myr (Montadert *et al.* 1979; Sibuet & Ryan 1979). Le Pichon & Sibuet (1981) and Le Pichon, Angelier & Sibuet (1983) have shown that extensional values as large as 3 are calculated from the geometry of tilted blocks. A model of formation of this continental margin by simple stretching has been proposed and takes into account both refraction and heat flow data. The assumption of local isostasy in this model of a margin starved of sedimentary loading suggests that the flexural rigidity of the lithosphere decreased dramatically during the rifting phase and later returned to a typical value for a lithosphere of this age. Watts & Ryan (1975) also used a similar model for the Gulf of Lion.

A deep basin, the Armorican basin, located on the thinned continental crust, is observed along the Armorican margin (Fig. 2, between 300 and 390 km) but is absent along the Celtic margin. The edge effect, seen on Fig. 3 from the free-air anomaly map (Lalaut, Sibuet & Williams 1981a, b), is due to the juxtaposition of two different vertical distribution of densities and partially hides deep structures. Nevertheless, two maximas of 30 and 60 mgal on the gravity map, which correspond to the Meriadzek Terrace and the Trevelyan Escarpment, respectively, cannot be explained simply by the morphology. These two maxima limit the Celtic and Armorican margins which are characterized by a different gravimetric pattern.

## Data reduction

Eight profiles combining bathymetric, free-air anomaly and seismic reflection data acquired by IFREMER (Institut Français de Recherche pour l'Exploitation de la Mer) have been used in this study. They are located in Figs 1 and 3. In order to analyse the gravity edge effect associated with the continental margin, each profile has been centred on the continental slope. For this purpose, original data have been extended on the continental shelf using the gravity map of Lalaut *et al.* (1981a, b) and the bathymetric map of Lallemand *et al.* (1985a, b). The data have been projected normal to the trend of the continental margin and the

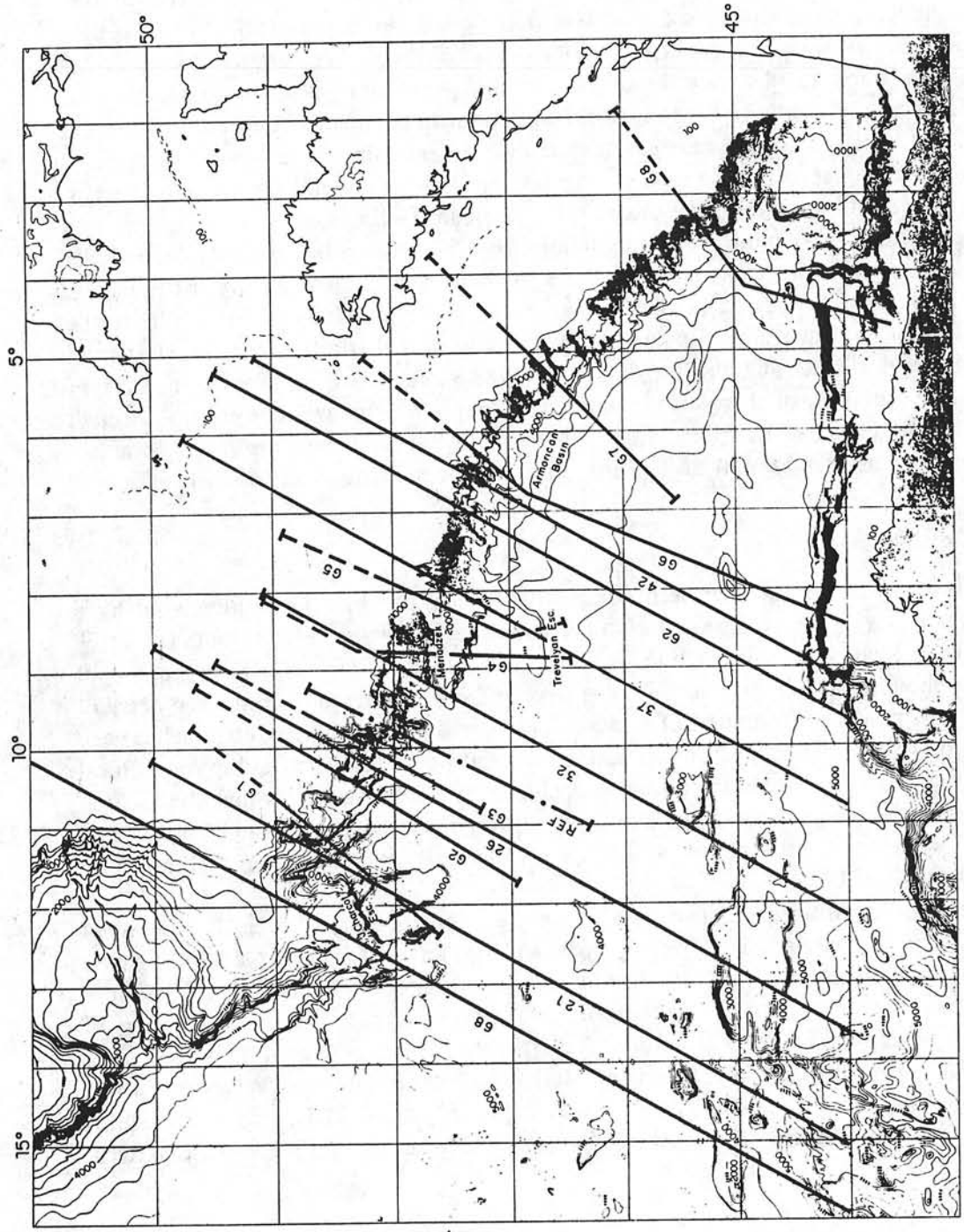


**Figure 1.** Location of *SEASAT* tracks (numbered from 21 to 68) and marine tracks (G1 to G8) on the north-east Atlantic bathymetric map of Lallemand *et al.* (in press). Dotted lines correspond to the extension of marine data (see text). REF is the seismic reflection and refraction line obtained by Avedick *et al.* (1982). Note that the bathymetry is dominated by two-dimensional features but that some three-dimensional structures exist which affect the gravity signal, particularly in the short wavelength domain as visible on profiles G1 and G2, for example.

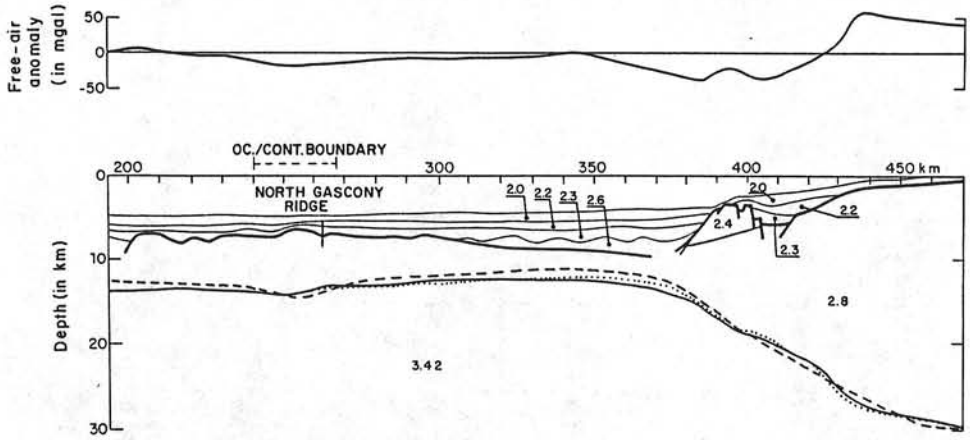


**Figure 2.** Free-air anomaly profile G6 and seismic structure (Foucher *et al.* 1982). Densities in g cm$^{-3}$. The base of the crust is obtained assuming local (solid line), regional (dotted line) and best-fitting model (broken line).

lengths of the eight working profiles have been reduced to 350 km (Fig. 4). Finally, in order to use a Fast Fourier Transform (FFT), the data have been linearly interpolated with a step of 2.75 km.

As previously mentioned, the direction of *SEASAT* tracks is approximately normal to the margin. We have chosen to analyse profiles 600 km long. The corresponding bathymetry has been taken from the topographic map of Lallemand *et al.* (1985a, b). The global spherical harmonics up to degree and order 10 of the geoid were removed in order to subtract the long wavelength anomalies which are not correlated with the topography. For that purpose, the GRIM 3 model developed by Reigber *et al.* (1983) has been used. The profiles obtained appear to show a good correlation with the topography (Fig. 5). The step of altimetric data is about 5–6 m across the Northern Bay of Biscay margin and is similar to observations on other margins (Haxby & Turcotte 1978; Kogan *et al.* 1985). There is also a small depression in the altimetric data at the foot of the continental slope. That can be related to the flexure of the lithosphere under the sedimentary load associated to the deep basin. Such an effect is much more pronounced on continental margins loaded with major sedimentary deposits such as the Bering Sea (A. Cazenave, private communication).

The altimetric data and the corresponding gravity data have been linearly interpolated with a step of 4.75 km. This interpolation step is larger than the one used for gravity data only because the original sampling interval of altimetry is larger (7 km instead of about 1 km).

The correlation between the *SEASAT* altimetric geoid corrected for the GRIM (10, 10) long wavelentth model and the topography can also be seen on Fig. 6. This figure was obtained using all of the descending and ascending *SEASAT* tracks in the area after minimization of the cross-over differences using the method described by Balmino, Brossier & Moynot (1977).

## Results

Admittances have been computed for both sets of data (gravity and altimetry) using the method proposed by McKenzie & Bowin (1976). The response function obtained from the altimetry data has been normalized for comparison by multiplying by $gk$ where $k$ is a wave-number and $g$ is normal gravity (Chapman 1979). It is important that the value for

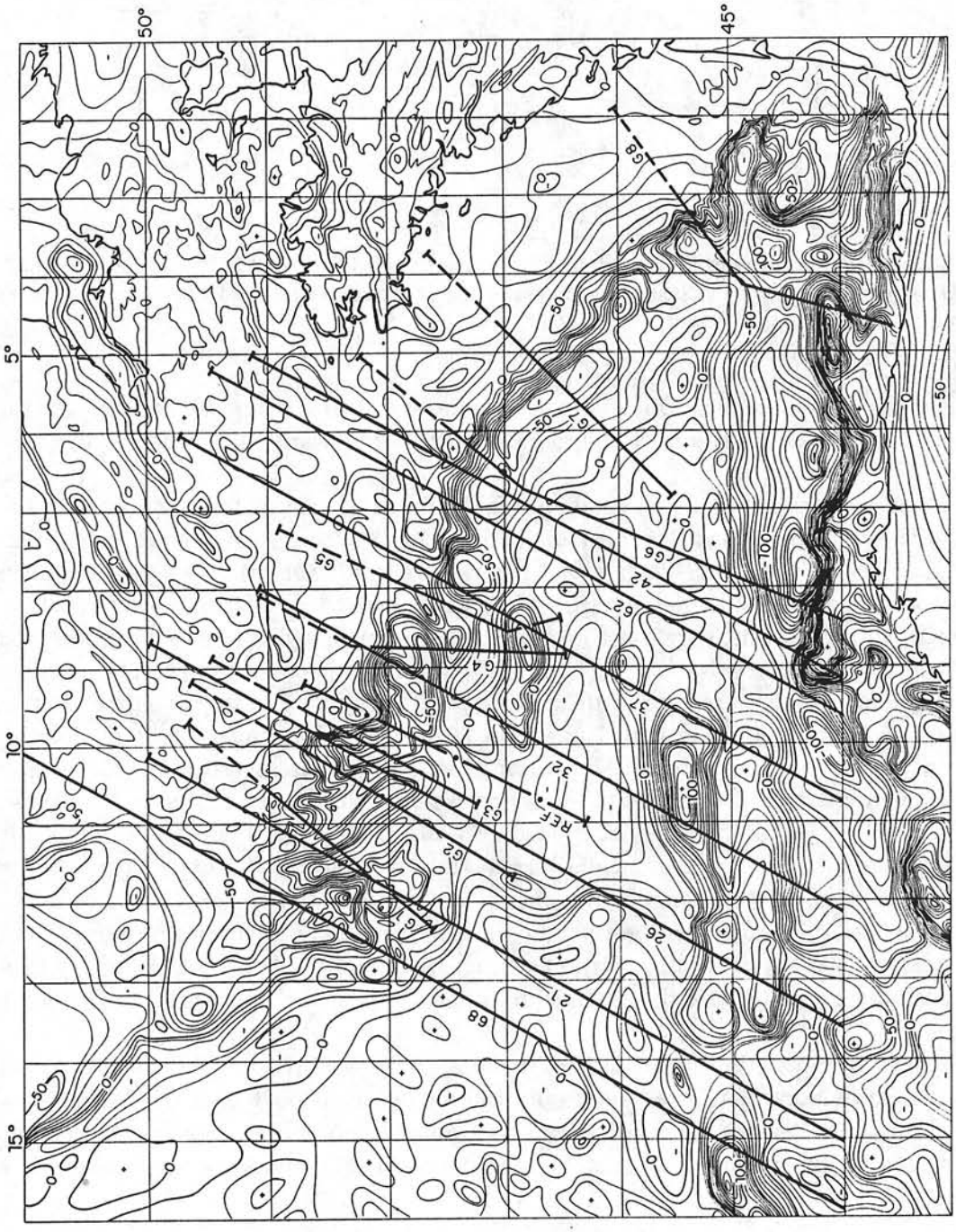


**Figure 3.** Free-air anomaly map of the north-east Atlantic Ocean from Lalaut *et al.* (1981b) on which are located *SEASAT* tracks (number from 21 to 68), marine tracks (G1 to G8) and the REF seismic reflection and refraction line (Avedik *et al.* 1982). Contour interval 10 mgal.

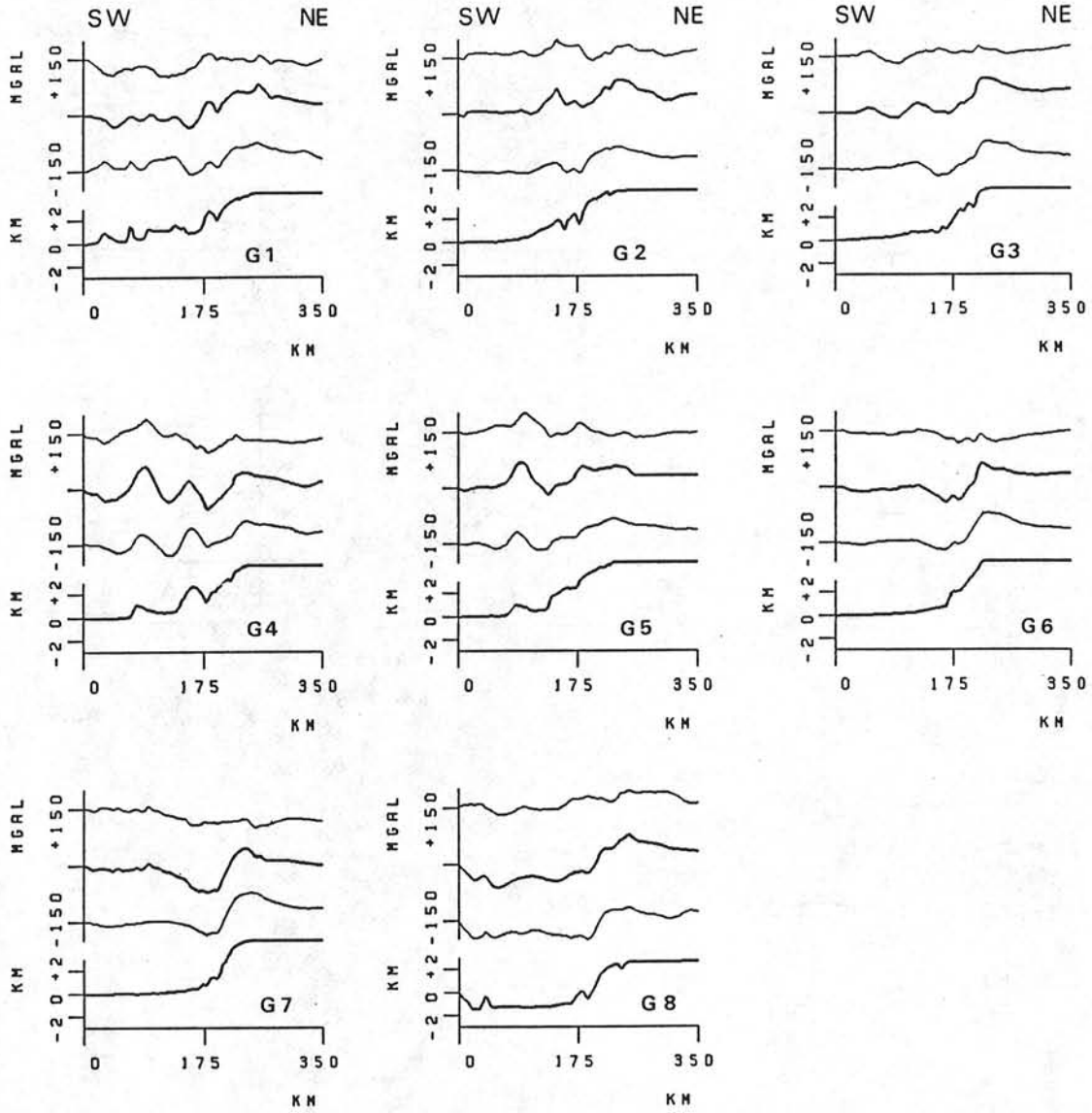


**Figure 4.** Marine data used in this study. Profile locations were given in Figs 1 and 3. Each graph plots four data sets. From bottom to top they are: bathymetry (km); computed gravity (mgal); observed free-air anomaly (mgal) and residual anomaly (mgal).

admittance at the longest wavelength (i.e. profile length) be reliable without loss of the information in the short wavelength domain by possible aliasing caused by tapering the ends of the profiles. The question of aliasing has been analysed by Diament (1985), who demonstrated that the present method, based on the use of the spatial derivatives on profiles with large gradients in the data, is appropriate for continental margins.

Fig. 7 displays the various parameters computed with both the altimetry/topography and gravity/topography transfer functions. The results obtained with the gravity data for wavelengths greater than 33 km (wavenumbers smaller than 0.03) show that the phase is close to zero and that coherence is high. This demonstrates that the gravity in this waveband is controlled by the topography and its isostatic response. As expected, there is a linear decay of the logarithm of the admittance for the short wavelength corresponding to the exp $(-kd)$ attenuation due to the water layer ($d$ is the water layer thickness). The statistical parameters

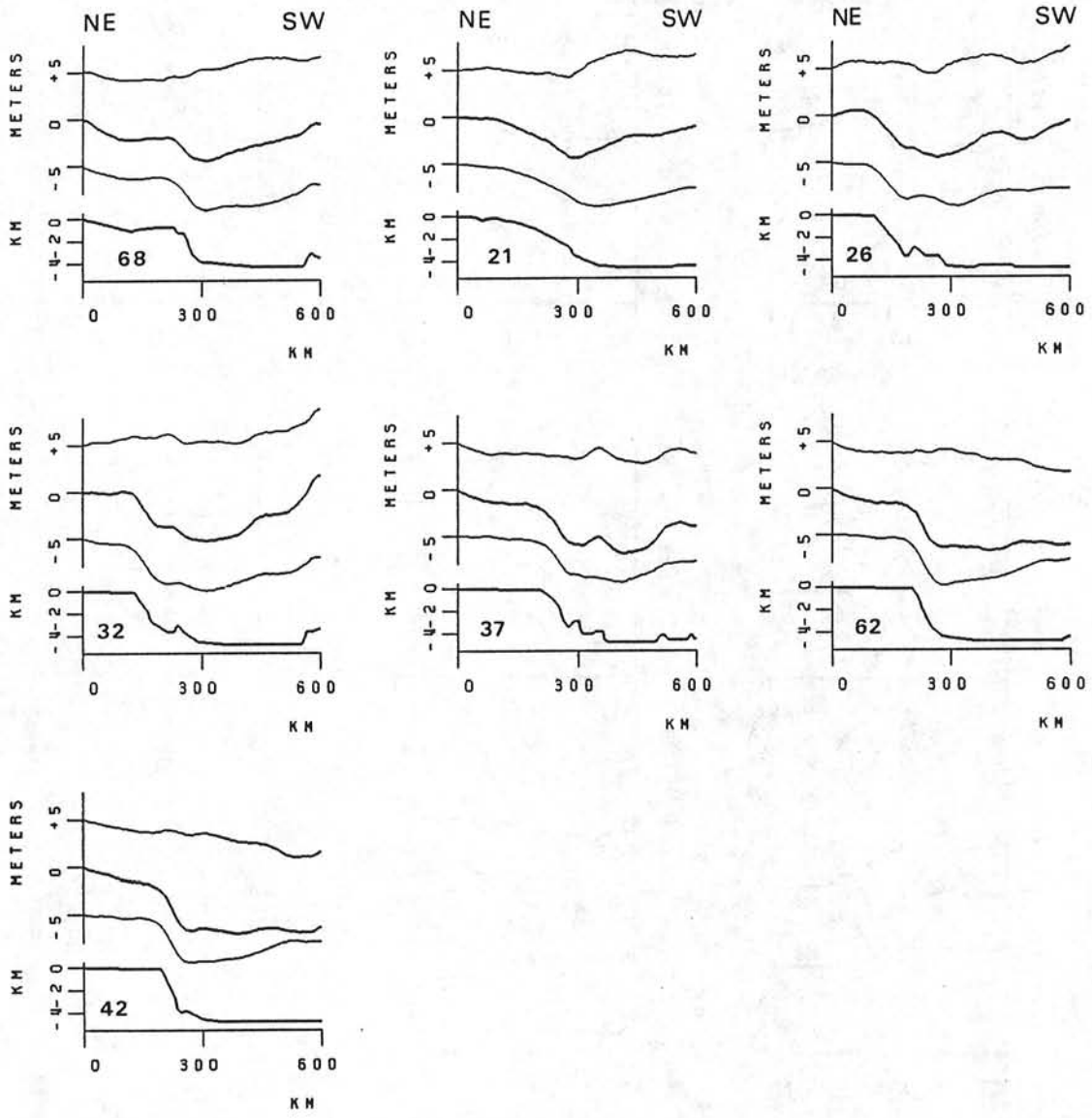


**Figure 5.** *SEASAT* data used in this study. Profile locations were given in Figs 1 and 3. Each graph plots four data sets. From bottom to top they are: bathymetry (km); computed geoid (m); observed *SEASAT* altimetry minus the long wavelength geoid given by GRIM 3 (10, 10) model (m) and residual anomaly (mm).

associated with the altimetric data set indicate that the admittance is reliable for wavelengths greater than 100 km (wavenumbers smaller than 0.01). For shorter wavelengths, the estimates of the admittances are not significant because the coherence is low and the values of the phase are important. This loss of information at short wavelengths is related to: (a) the use of altimetry data which does not contain information in the short wavelength domain; (b) the power spectrum decrease of the bathymetry at short wavelengths due to chosen linear interpolation step which is much smaller than the one used to digitize the bathymetric data on the original map (Kogan & Kostoglodov 1981; Ribe 1982); (c) the altimetry and topographic profiles are out of phase because they were obtained separately, while each measure of marine gravity is associated with a topographic value recorded simultaneously.

Thus for wavelengths between 350 and 100 km, reliable transfer functions can be com-

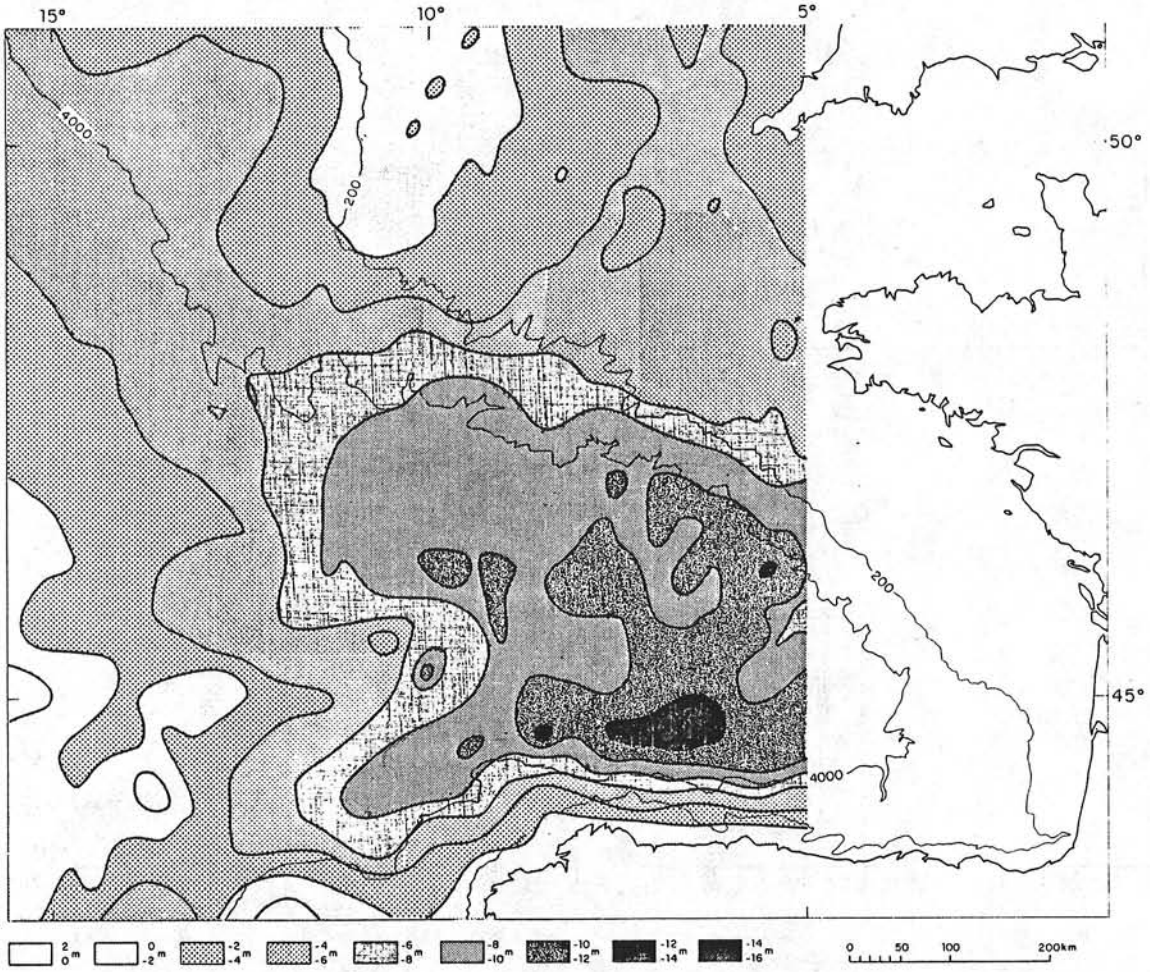


**Figure 6.** *SEASAT* altimetric geoid superimposed on the simplified bathymetric map. The long wavelength geoid (GRIM 3 (10, 10)) has been removed.

puted from the two sets of data. This waveband contains information on the mechanical properties of the lithosphere (Sandwell 1982).

The resulting admittances are plotted in Fig. 8 together with some theoretical curves. Let us first examine the experimental values. For wavelengths greater than 100 km, the values of the altimetry/bathymetry admittance are consistent with those of the gravimetry/bathymetry admittance. For short wavelengths, the values of the gravimetry/bathymetry admittance are scattered with respect to the expected exponential decay. This could be due to:

(a) Bathymetric features are not always two-dimensional features perpendicular to the direction of profiles. Profile G1, for example, cuts into the eastern prolongation of the Jean–Charcot escarpment, a major fault oriented N 70°, which is an old Caledonian and/or Late Hercynian feature reactivated during the Lower Cretaceous rifting phase. Also, the Celtic continental margin is cut by canyons characterized by numerous changes in direction which individualizes three-dimensional morphologic features;

(b) Local crustal heterogeneities vary from profile to profile as shown by the residual gravity on Fig. 4. Lalaut (1980) has shown the presence of low density bodies within the upper thinned continental crust on the Celtic continental margin with density contrasts of $-0.2$ to $-0.4$ g cm$^{-3}$ with respect to the crust.

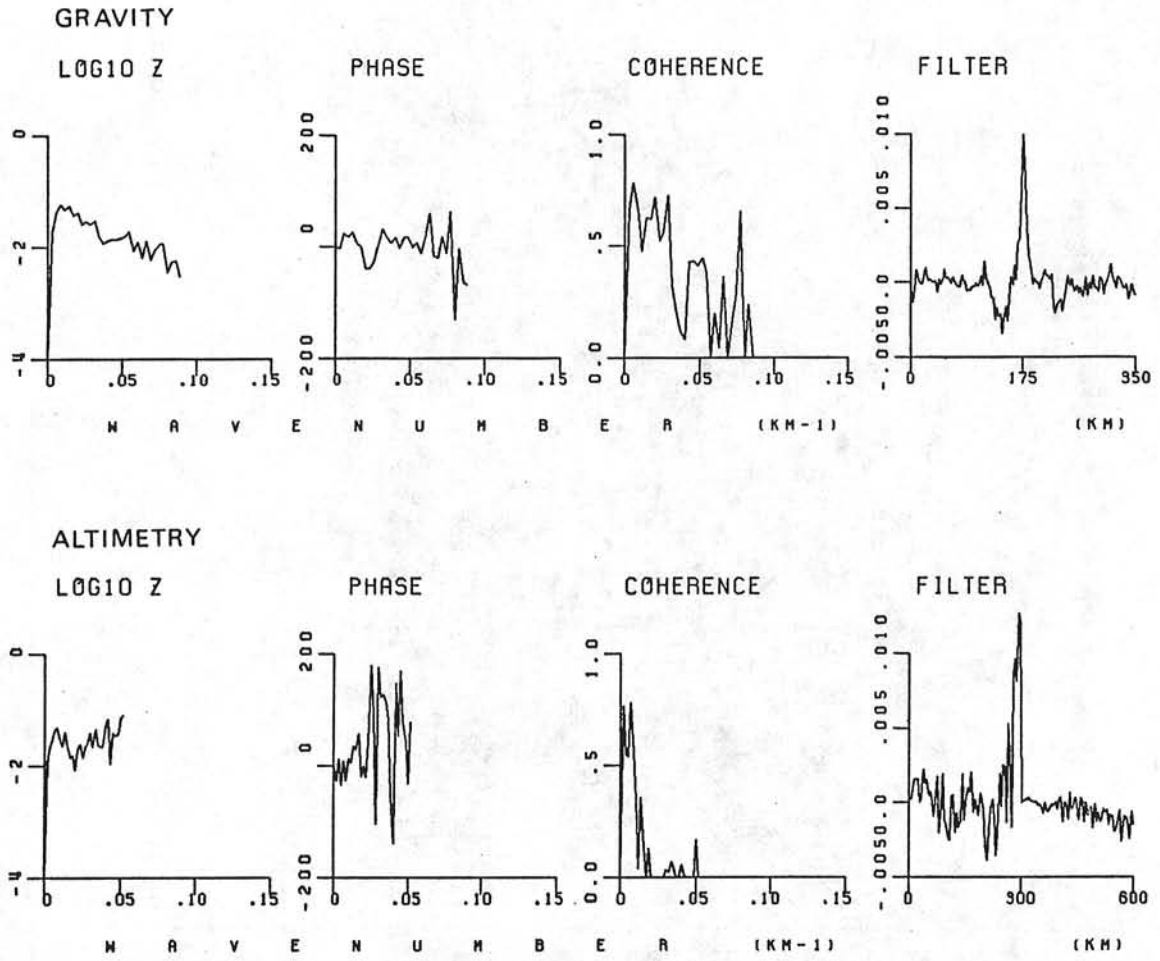


**Figure 7.** Logarithm of the admittances and associated statistical parameters computed with marine gravity data (upper part) and altimetry data (lower part). The phase of the admittance must be close to zero to infer the admittance reliably. The coherence is a measure of the fraction of the power spectrum of gravity related to the topography. The filter is the inverse Fourier transform of the admittance. It appears from this figure that the gravity admittance can be interpreted for wavelengths greater than 30 km and that the altimetric admittance can be interpreted for wavelength greater than 100 km.

Nevertheless, no attempt was made to correct these two effects since deviations between the experimental values and the theoretical curve are not critically large.

As the two separate sets of data processed independently yield the same response for wavelengths between 100 and 600 km, we conclude that as far as mechanical isostasy is concerned, either gravity or altimetry can be used. Nevertheless the use of gravity gives additional information in the short wavelength domain (i.e. $\lambda \leqslant 80$ km) which can be used to determine the basement density (e.g. McKenzie & Bowin 1976).

### Interpretation of the transfer function

The interpretation of the short wavelength domain in terms of the effect of uncompensated topography yields a basement density of 2.75 g cm$^{-3}$ and an equivalent water depth of 5500 m. This estimate is higher than the mean observed water depth on the topographic profiles (2470 m) but is close to the depth observed in the abyssal plain ($\simeq$ 4800 m). Since the computed density is close to the value for crustal density, we assume that the short

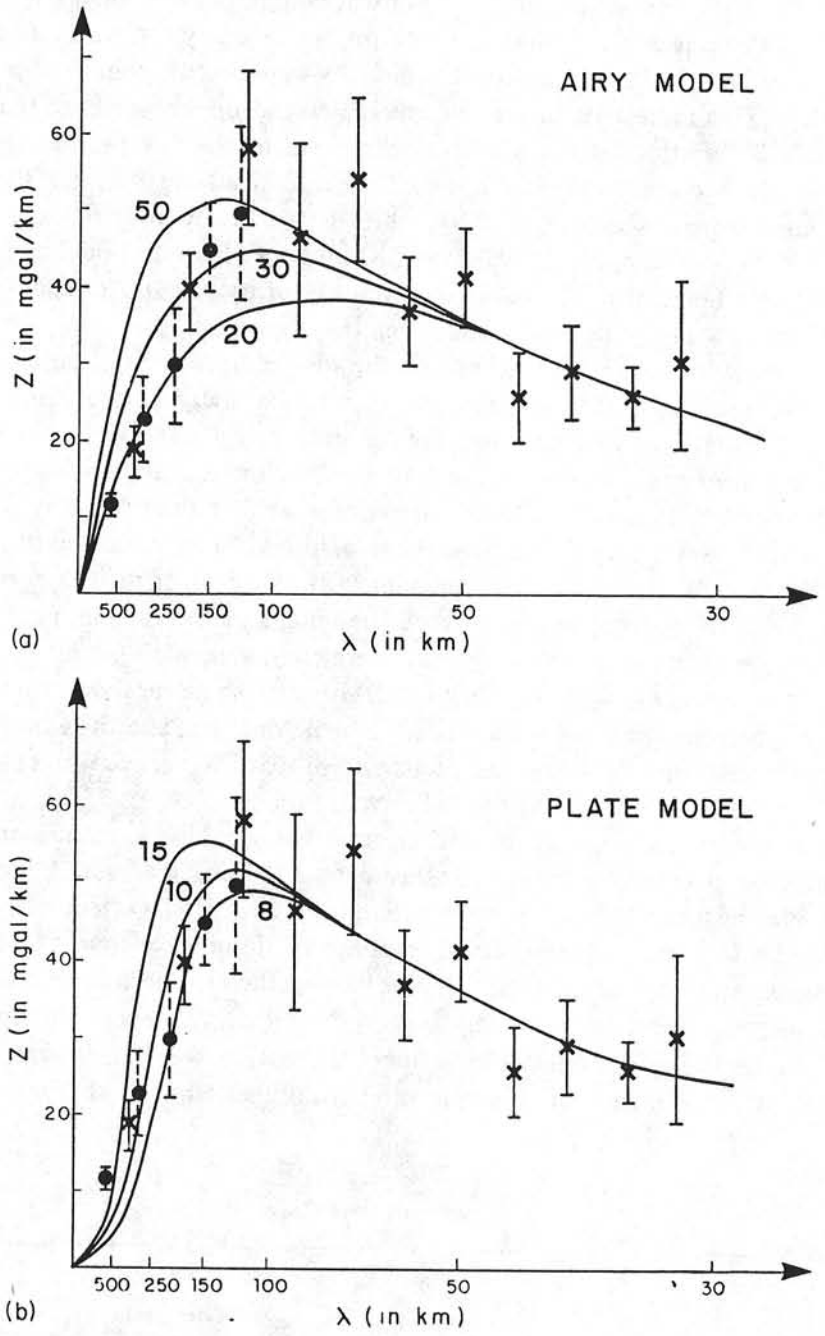


**Figure 8.** (a) Fit of an Airy model of compensation to the computed admittance for depths of compensation of 20, 30 and 50 km, respectively. The adopted basement density is 2750 kg $m^{-3}$ and water layer thickness is 5500 m. Crosses are the admittance values computed with gravity data and points are the admittance values computed with altimetry data and then normalized. (b) Fit of a plate model of compensation to the computed admittances. Curves correspond to an elastic thickness of 8, 10 and 15 km, respectively. Crosses are the admittance values computed with gravity data and points are the admittance values computed with altimetry data and then normalized.

wavelength domain of the observed admittance is controlled by the main density interface between seawater and the crust with no specific effect due to the thin sedimentary layer. At longer wavelengths (70 km $\leq \lambda \leq$ 600 km), the comparison between the observed values of admittance and the curves computed for either the flexural model of isostasy (elastic plate model) or an Airy type model (Fig. 8a, b) indicate that neither model satisfactorily explains

the data across the entire waveband studied. For wavelengths smaller than 250 km, the data are well fitted by the elastic plate model but are poorly fitted by the Airy model. Thus, the topography in this waveband appears to be regionally supported by an elastic plate whose thickness is 8 km. This represents in fact an average elastic thickness across the margin and does not exclude a variation of the elastic thickness from the oceanic to the continental domain. This result is consistent with that of Karner & Watts (1982) for the Southwest African continental margin which, like the Northern Bay of Biscay margin, was formed in the early Cretaceous. For wavelengths larger than 250 km, the flexural model does not fit the observed admittance (Fig. 8b). The data are fitted better by an Airy model with a crustal thickness of 20 km. Two possible explanations can be proposed:

(a) The transfer function in this waveband is dominated by the variation of crustal thickness (from 5 to more than 30 km) across the continental margin. According to Haxby & Turcotte (1978), isostatic equilibrium must be achieved at the base of the crust. Due to the narrowness of the deep basin loaded at the foot of the Northern Bay of Biscay continental margin, the sedimentary load only affects wavelengths smaller than 250 km. The thickness of this sedimentary load is much less than those of the US East Coast continental margin analysed by Karner & Watts (1982) or Louden (1983). If we reject the values of admittance plotted for wavenumbers associated with twice the length of the original profiles in Karner & Watts (1982) (see Diament 1986), their results are consistent with the plate model for the entire studied waveband ($\lambda \leqslant 400$ km) they used, although some local deviations larger than the plotted error bars are present for the eastern North American and the Coral Sea margins. Consequently the difference between our results and those of Karner & Watts (1982) may be related simply to the different sizes of the sedimentary loads.

(b) The continental margin, as a transition zone between the oceanic and continental lithosphere, may be affected by thermal isostasy. If so, the observed admittance would be a mixture of mechanical and thermal responses (Sandwell 1982). The effect of a deep thermal anomaly would be to increase the observed response for long wavelengths compared to the mechanical response (Kogan *et al.* 1985). In the case of the Northern Bay of Biscay margin, however, the thermal effect has probably been removed completely by lateral conduction (Louden & Forsyth 1976; Watremez 1980) since its creation about 110 Myr ago. A simple computation of a two-dimensional isostatic model, compensated at the base of the crust,

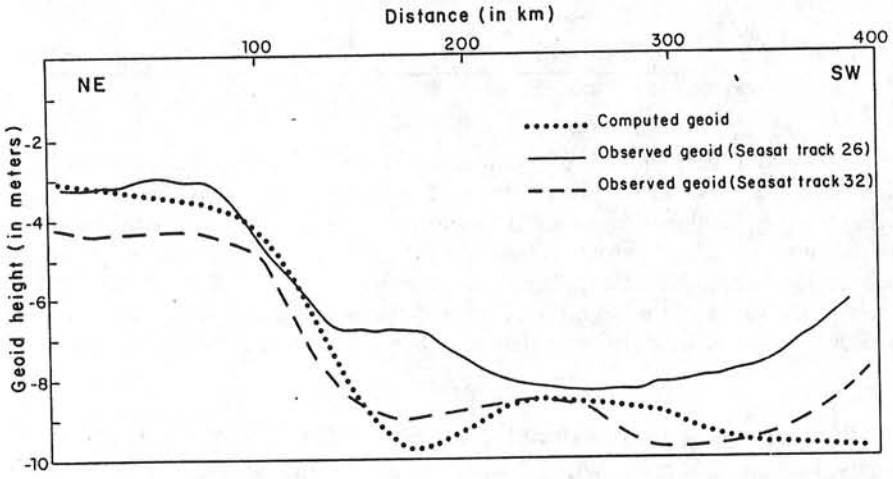


**Figure 9.** Computed geoid anomaly across the margin and along the REF seismic line (Avedik *et al.* 1982) compared to the two neighbouring (26 and 32) *SEASAT* tracks. Isostasy is assumed to be achieved at the base of the crust (see text).

shows that it is not necessary to invoke deeper sources of anomalies. For this computation, the density structure of the crust and of the overlying sedimentary layers have been inferred from seismic reflection and refraction data (Avedik *et al.* 1982) obtained both along and perpendicular to the REF line (Fig. 1). The computed geoid anomaly is similar to the observed geoid anomalies along the adjacent tracks 26 and 32 (Fig. 9).

## Discussion

Direct modelling of the geoid anomaly, combined with the results of the interpretation of the transfer function, implies that the isostatic equilibrium of the Bay of Biscay margin is controlled by both variation of the crustal thickness and by the flexure of the crust under the sedimentary load. Each process dominates in a different waveband (Fig. 10). Bodine, Steckler & Watts (1981), considering seamounts emplaced over lithospheres of different age, have proposed a square root relationship between the effective elastic thickness ($T_e$) and the age ($t$) of the lithosphere at the time of loading

$$T_e = (4.3 \pm 0.5)\sqrt{t}.$$

This relationship has been confirmed in other studies (e.g. Cazenave *et al.* 1980; McAdoo & Martin 1984). A simplistic application of this relationship to the Bay of Biscay data implies an age of about 3.5 Myr. This would mean that the sedimentary load had been emplaced on a 3.5 Myr old lithosphere which is presumed to be at 0 age at the end of the rifting phase. The reality of the situation, however, is much more complex. Beaumont, Keen & Bouteiller

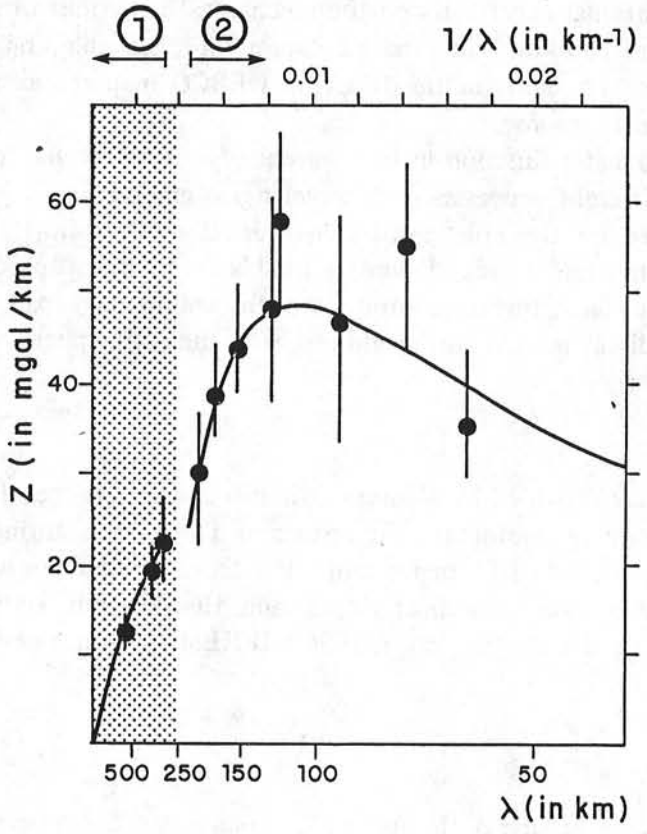


**Figure 10.** Best adjustment of the two models as a function of wavelength. Area (1) corresponds to the crustal thickness variation and area (2) to the flexure model under the sedimentary load.

(1982), expressing the same idea as Le Pichon & Sibuet (1981), stated that 'all the models of evolution of margins which assume a local isostatic equilibrium may be approximately correct for hot extending regions soon after rifting, but are increasingly in error in late stages of evolution, when the cooling and thickening lithosphere becomes stronger and exhibits significant bending or flexural charactersitics'. As noted previously, the Northern Bay of Biscay rifting phase lasted 20–40 Myr ago. Synrift sediments were deposited during the creation of half grabens between tilted fault blocks, based on the existence of fan-shaped acoustic reflectors (Montadert *et al.* 1979). Synrift sediments were consequently deposited on a lithosphere characterized by an elastic plate thickness which decreased when thinning increased. At the end of the rifting phase, the morphology of the margin was acquired. Sediments, consisting mainly of turbidites, preferentially fill depressions associated with half grabens and the depression at the base of the continental slope (Foucher, Le Pichon & Sibuet 1982). Since the end of the rifting phase, the equivalent elastic plate thickness has increased due to the cooling of the lithosphere. As depressions have been filled, the sedimentation becomes more uniform (Sibuet & Ryan 1979) corresponding roughly to the emplacement of a uniform load over the whole margin.

Consequently, the estimate of an age of 3.5 Myr for the lithosphere on which the sedimentary load was emplaced gives a value which integrates over several phenomena. It must be only considered as an indication for the deposition of the sedimentary load during and just after the rifting phase.

## Conclusion

(1) The use of a combined set of marine gravity and *SEASAT* altimetry data with bathymetry data yields additional constraints on the mechanical behaviour of the lithosphere for wavelengths larger than 100 km. When marine data are not available, the altimetry data can be combined with general bathymetric data (the GEBCO map for example) in order to quantify this mechanical response.

(2) The observed transfer function in two wavebands across the Bay of Biscay margin is dominated by two different processes. For wavelengths greater than 250 km, the transfer function is dominated by the crustal thickness variation. For shorter wavelengths, the flexure of the lithosphere under the sedimentary load is the dominant process.

(3) The value of the elastic thickness implies that the sedimentary load was emplaced over the Northern Bay of Biscay margin during and just after the rifting phase.

## Acknowledgments

The *SEASAT* data were provided by Georges Balmino and we are grateful to Nicole Vales who made their preliminary treatments. Comments of Tony Watts during the early stage of this study were very useful. This paper benefited from discussions with Paul Beuzart, Jacques Dubois, Luce Fleitout, Mikhael Kogan and Henri-Claude Nataf. This work was supported by CNEXO under contract no. 81/6669. IFREMER Centre de Brest, contribution 35.

## References

Avedik, F., Camus, A. L., Ginzburg, A., Montadert, L., Roberts, D. G. & Whitmarsh, R. B., 1982. A seismic refraction and reflection study of the continent-ocean transition beneath the North Biscay margin, *Phil. Trans. R. Soc. A*, **305**, 5–25.

Balmino, G., Brossier, C. & Moynot, B., 1977. Prétraitement des mesures altimétriques de GEOS 3; description du logiciel développé, *Tech. Rep. B/CB/BM/NS/7.089/CTG – GRGS.*

Beaumont, C. Keen, C. E. & Bouteiller, R., 1982. On the evolution of rifted continental margins: comparison of models and observations for the Nova-Scotia margin, *Geophys. J. R. astr. Soc.*, **70**, 667–712.

Bodine, J. H., Steckler, M. S. & Watts, A. B., 1981. Observations of flexure and the rheology of the oceanic lithosphere, *J. geophys. Res.*, **86**, 3695–3707.

Cazenave, A., Lago, B., Dominh, K. & Lambeck, K., 1980. On the response of the ocean lithosphere to seamount loads from *GEOS 3* satellite radar altimeter observations, *Geophys. J. R. astr. Soc.*, **63**, 233–254.

Chapman, M. E., 1979. Techniques for interpretation of geoid anomalies, *J. geophys. Res.*, **84**, 3793–3801.

Chapman, M. E. & Talwani, M., 1979. Comparison of gravimetric geoid with GEOS 3 altimetric geoid, *J. geophys. Res.*, **84**, 3803–3816.

Diament, M., 1985. Influence of data analysis on admittance computation, *Annls. Géophys.*, **3**, 6, 785–792.

Foucher, J.-P., Le Pichon, X. & Sibuet, J.-C., 1982. The ocean-continent transition in the uniform lithospheric stretching model: role of partial melting in the mantle, *Phil. Trans. R. Soc. A*, **305**, 27–43.

Haxby, W. F. & Turcotte, D. L., 1978. On isostatic geoid anomalies, *J. geophys. Res.*, **83**, 5473–5478.

Karner, G. D. & Watts, A. B., 1982. On isostasy at Atlantic type continental margins, *J. geophys. Res.*, **87**, 2923–2948.

Kogan, M. & Kostoglodov, V., 1981. Isostasy of fracture zones in the Atlantic Ocean, *J. geophys. Res.*, **86**, 9248–9258.

Kogan, M., Diament, M., Bulot, A. & Balmino, G., 1985. Thermal isostasy in the South Atlantic Ocean from geoid anomalies, *Earth planet. Sci. Lett.*, **74**, 280–290.

Lalaut, P., 1980. Contribution à l'étude de la structure profonde du Golfe de Gascogne par méthodes gravimétriques, *Thèse de 3ème cycle*, Université Pierre et Marie Curie.

Lalaut, P., Sibuet, J.-C. & Williams, C., 1981a. Présentation d'une carte gravimétrique de l'Atlantique Nord-Est, *C.r. Acad. Sci., Paris*, **292**, 597–600.

Lalaut, P., Sibuet, J.-C. & Williams, C., 1981b. *Carte gravimétrique de l'Atlantique Nord-Est*, CNEXO, Paris (Ed.).

Lallemand, S., Mazé, J.-P., Monti, S. & Sibuet, J.-C., 1985a. Présentation d'une carte bathymétrique de l'Atlantique Nord-Est, *C.r. Acad. Sci., Paris*, **300**, 145–149.

Lallemand, S., Mazé, J.-P., Monti, S. & Sibuet, J.-C., 1985b. *Carte bathymétrique de l'Atlantique Nort-Est.*, IFREMER, Paris (Ed.).

Le Pichon, X., Angelier, J. & Sibuet, J.-C., 1983. Subsidence and stretching, in *Studies on Continental Margin Geology*, eds Watkins, J. S. & Clarke, C. L., *Mem. Am. Ass. Petrol. Geol. Tulsa*, **29**, 731–741.

Le Pichon, X. & Sibuet, J.-C., 1981. Passive margins: a model of formation, *J. geophys. Res.*, **86**, 3708–3720.

Louden, K. E., 1983. Time-series analysis of gravity anomalies and topography across the Nova-Scotian continental margin (abstract), *EOS Trans. Am. geophys. Un.*, **64**, 676.

Louden, K. E. & Forsyth, D., 1976. Thermal conduction across fracture zones and the gravitational edge effect, *J. geophys. Res.*, **81**, 4869–4874.

McAdoo, D. C. & Martin, C. F., 1984. *SEASAT* observations of lithospheric flexure seaward of trenches, *J. geophys. Res.*, **89**, 3201–3210.

McKenzie, D. P. & Bowin, C. O., 1976. The relationship between bathymetry and gravity in the Atlantic Ocean, *J. geophys. Res.*, **81**, 1903–1915.

Montadert, L., Roberts, D. G., de Charpal, O. & Guennoc, P., 1979. Rifting and subsidence of the Northern continental margin of the Bay of Biscay, *Init. Rep. Deep Sea drill. Proj.*, **48**, 1025–1060.

Montadert, L., de Charpal, O., Roberts, D., Guennoc, P. & Sibuet, J.-C., 1979. Northeast Atlantic passive continental margins: rifting and subsidence processes, in *Deep Drilling Results in the Atlantic Ocean: Continental Margins and Paleo-environment*, eds Talwani, M., Hay, W., & Ryan, W., *M. Ewing Series*, **3**, 154–186, American Geophysical Union.

Rabinowitz, P. D., 1982. Gravity measurements bordering passive continental margins, in *Dynamics of Passive Margins*, ed. Scrutton, R. P., American Geophysical Union.

Reigber, C., Balmino, G., Moynot, B. & Mueller, H., 1983. The GRIM 3 earth gravity field model, *Mar. Geod.*, **8**, 93–138.

Ribe, N. M., 1982. On the interpretation of frequency response functions for oceanic gravity and bathymetry, *Geophys. J. R. astr. Soc.*, **70**, 273–294.

Sandwell, D. T., 1982. Thermal isostasy: response of a moving lithosphere to a distributed heat source, *J. geophys. Res.*, **87**, 1001–1014.

Sibuet, J.-C. & Ryan, W. B. F., 1979. Site 398: evolution of the West Iberian passive continental margin in the framework of the early evolution of the North Atlantic Ocean, in *Init. Rep. Deep Sea drill. Proj.*, 47, part 2, 761–776, eds Sibuet, J.-C., Ryan, W. B. F. *et al.*, US Government Printing Office, Washington.

Watremez, P., 1980. Flux de chaleur sur le massif armoricain et sur la marge continentale: essai de modélisation de l'évolution thermique de la marge continentale, *Thèse de 3éme cycle*, Université de Bretagne Occidentale, Brest.

Watts, A. B. & Ryan, W. B. F., 1975. Flexure of the lithosphere and continental margin basins, *Tectonophys.*, **36**, 25–44.

(13) Foucher J.-P., et Sibuet J.-C., 1980. Thermal regime of the northern bay of Biscay continental margin in the vicinity of the D.S.D.P. sites 400 -402. In the evolution of passive continental margins in the light of recent Deep Drilling Results, P. Kent, A.S. Laughton, D.G. Roberts, et E.W.J. Jones (eds), The Royal Society, London, p. 157-167.

(14) Le Pichon X., et Sibuet J.-C., 1981. Passive margins : a model of formation. J. Geophys. Res., 86, p. 3708-3720.

(15) Foucher J.-P., Le Pichon X., et Sibuet J.-C., 1982. The ocean-continent transition in the uniform lithospheric stretching model : role of partial melting in the mantle. Phil. Trans. R. Soc. Lond., A 305, p. 27-43.

(16) Le Pichon X., Angelier J., et Sibuet J.-C., 1983. Subsidence and stretching. In Studies in continental margin geology, Watkins J.S., et Drake C.L. (eds), AAPG Memoir 34, Tulsa, p. 731-741.

*Phil. Trans. R. Soc. Lond.* A **294**, 157–167 (1980) [ 157 ]
*Printed in Great Britain*

# Thermal régime of the northern Bay of Biscay continental margin in the vicinity of the D.S.D.P. Sites 400–402†

By J.-P. Foucher and J. C. Sibuet
*Centre Océanologique de Bretagne, B.P.* 337, 29273 *Brest, France*

Average heat flow values on land in western Europe are about 2 h.f.u., whereas recently acquired surface-ship measurements and the downhole heat flow determinations at D.S.D.P. Site 402 indicate that the heat flow is only about one-half of this value over the continental slope and rise of the adjacent northern Bay of Biscay margin in the vicinity of the D.S.D.P. Sites 400–402. Assuming that both the margin and the adjacent continental area are close to steady state thermal conditions, we suggest that the observed heat flow contrast reflects different radioactive crustal contributions to the surface heat flow in the two areas. Under the margin, the crust is thinner and would have a smaller radioactive contribution, the decrease in the contribution being related to the nature of the crustal thinning process under the margin.

The heat flow data are compatible with a model of crustal thinning that considers this to be mainly a result of mechanical deformation of the crust through extension.

## Introduction

Ten conventional oceanic surface heat flow measurements were made over the northern margin of the Bay of Biscay in the vicinity of the D.S.D.P. sites 400–402 during the RV Suroit–SU 01 (December 1975) and RV Jean Charcot–CH 66 (February 1976) cruises of C.N.E.X.O. These measurements, complemented by the heat flow determination made at Site 402 during Leg 48 of the Deep Sea Drilling Project (Erickson *et al.* 1979) provide information on the thermal régime of the margin. The main observation is that the regional heat flow over the margin is substantially lower than over the adjacent Western European continental area. We suggest in this report that the observed heat flux contrast provides constraints on the debatable nature of the crustal thinning processes under the margin.

## Regional setting

The study area lies north of the Bay of Biscay over the Western Approaches margin, in the vicinity of the D.S.D.P. Sites 400–402 (figure 1). Extensive geological and geophysical work (e.g. Auffret *et al.*, Montadert *et al.*, Avedik & Howard, all 1979) as well as drilling results have provided detailed information on the structure of the margin. Under a thin upper Cretaceous to Cainozoic sediment cover of 1–2 km thickness, a series of tilted fault blocks extends from the mid-continental slope to the abyssal plain down to the Trevelyan Escarpment at a depth of about 4 km (figure 2). The fault blocks trend subparallel to the margin controlling the relief of the Meriadzek Terrace and are bounded by listric faults that become near horizontal at a depth of about 4–5 km below the sediment surface (Montadert *et al.* 1979). They consist of Mesozoic sediments drilled at Site 401, and/or Hercynian basement rocks

† Contribution no. 654 of the Scientific Department of the Centre Océanologique de Bretagne.

dredged at the base of Goban Spur at about 4 km depth (Pautot *et al.* 1976). It is now widely agreed that the fault block structure of the margin was mainly shaped during the rifting episode that is dated as Late Jurassic – Early Cretaceous and preceded the onset of the opening of the Bay of Biscay in the Upper Aptian. Structural interpretation and geophysical results suggest that the continental oceanic crust boundary lies south of the Trevelyan Escarpment (figure 1) (Montadert *et al.*, Avedik & Howard, both 1979). Under Trevelyan seismic refraction data indicate that the Moho lies at a depth of 12–13 km compared with 27–30 km under the continental shelf (Avedik & Howard 1979), implying a considerable thinning of the original continental crust.

Six of the ten surface heat flux measurements reported here form a transect from the mid-

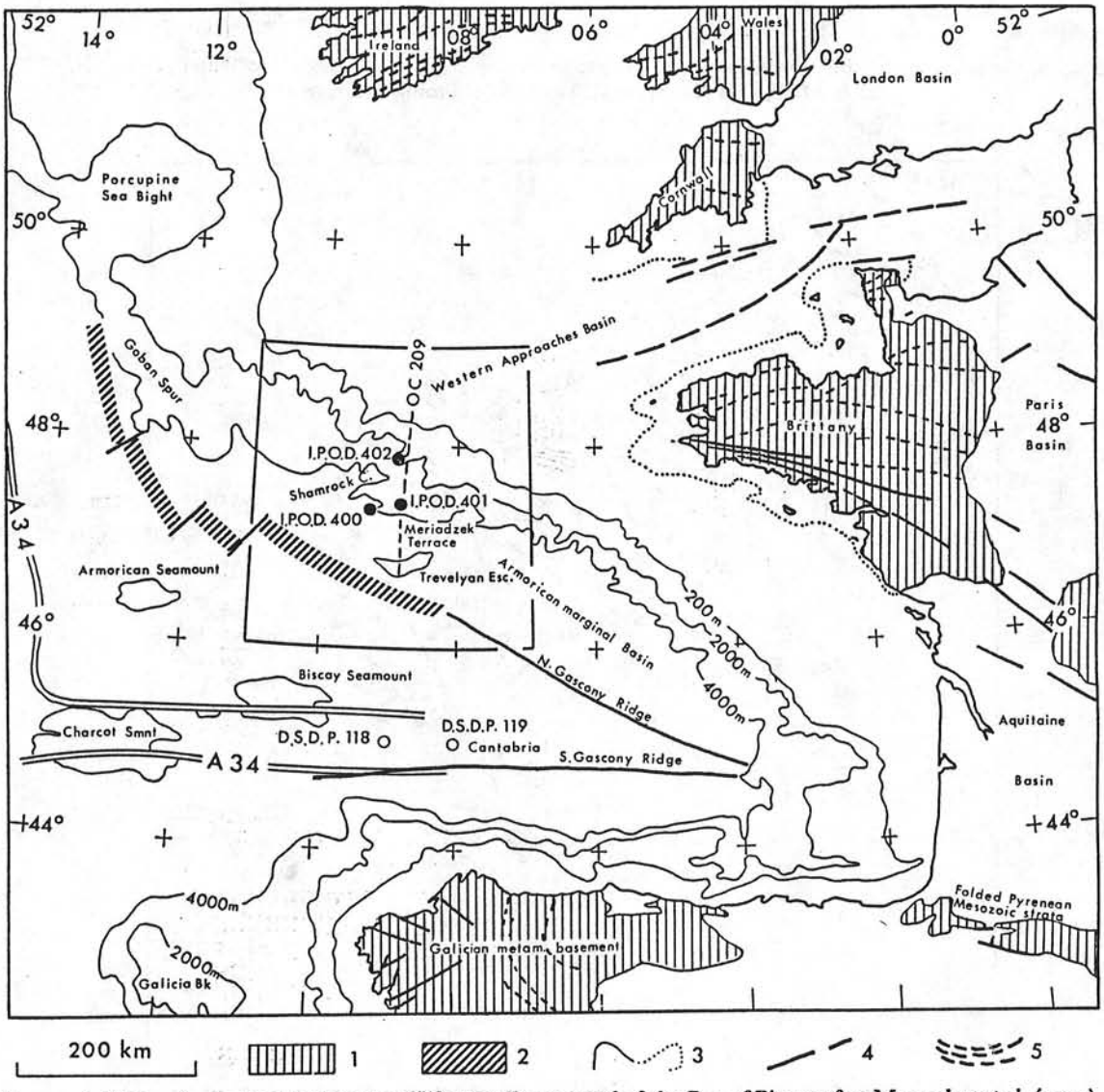


FIGURE 1. Main physiographic features of Western Europe and of the Bay of Biscay after Montadert *et al.* (1979). Magnetic anomaly 34 after Sibuet *et al.* (this volume). The hatched area shows the continental – oceanic crust boundary (Montadert *et al.* 1979). (1) Hercynian ranges and Palaeozoic basins. (2) Continent–ocean boundary (Montadert *et al.* 1979). (3) Boundaries of inshore basins. Blank areas inland represent the Mesozoic and Cainozoic basins. (4) Main fractured zones and faults. (5) Main Hercynian fold trends.

continental slope to the abyssal plain across the Meriadzek Trevelyan area; the four other measurements are located over the North Western termination of the Meriadzek Terrace known as the Aegis Ridge. The D.S.D.P. Site 402 heat flux determination was located slightly higher on the slope (figure 3).

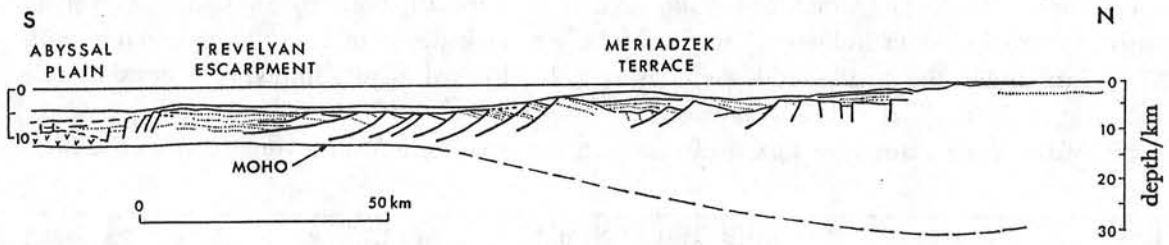


FIGURE 2. Cross section of the Western Approaches continental margin along seismic reflexion profile OC 209 after Montadert *et al.* (1979). Location of profile in figure 1.

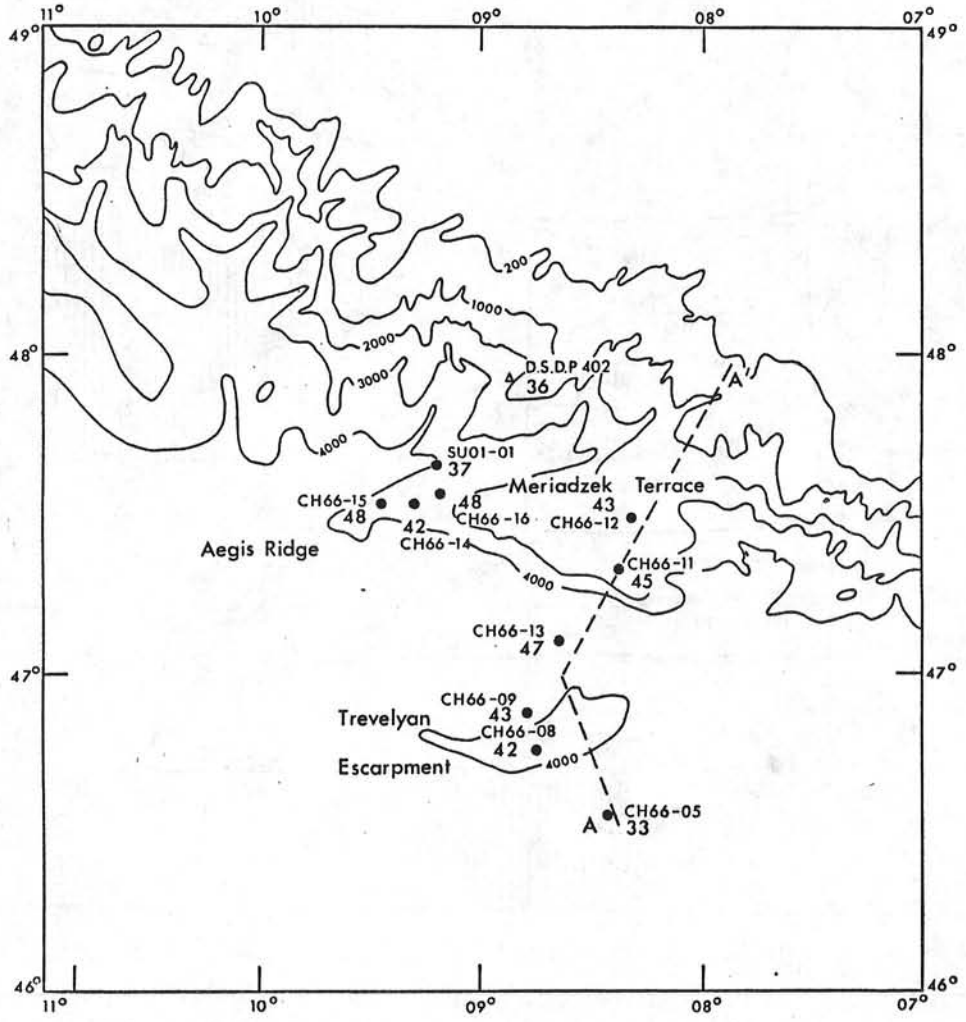


FIGURE 3. Location map of the C.N.E.X.O. heat flow measurements over the Western Approaches continental margin. The D.S.D.P. Site 402 heat flow determination is shown by a triangle. The heat flow values are in mW $m^{-2}$.

## Surface geothermal data

The temperature gradients were determined from the temperatures measured at up to five different depths in the upper 2–10 m of sediment by means of thermistor temperature probes attached at known vertical distances along the 10 m long barrel of a piston corer (Gerard *et al.* 1962). At each site, the temperature of each probe was measured about every 10 s for a total period of about 6 min, during which the corer was left undisturbed in the sediment. The recording device, of the Wheatstone bridge and film recording (Lamont) type described by Langseth (1965), was housed in a pressure vessel at the top of the corer. Equilibrium temperatures in the sediment were extrapolated from the temperature transients recorded, by linear fitting of the temperatures against the reciprocal of time (Bullard 1954). The accuracy of the temperatures determined in the sediment with respect to the bottom water temperature is better than 0.005 °C.

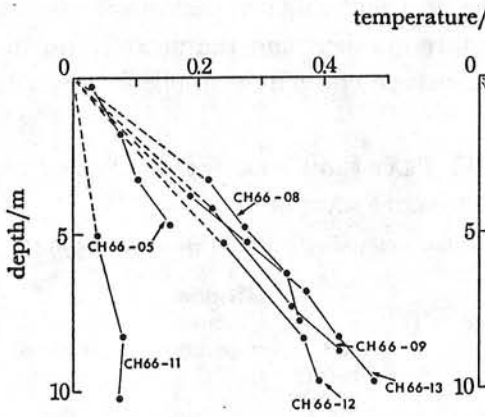


Figure 4

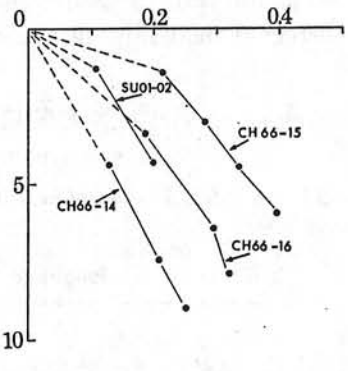


Figure 5

Figure 4. Temperature profiles in sediment at stations located along profile AA′ (figure 3). Note the anomalously low gradient at station CH 66–11. Temperatures are relative to the bottom water temperature at each station.

Figure 5. Temperature profiles in sediment for the four stations over the Aegis Ridge. Temperatures are relative to the bottom water temperature at each station.

The thermal conductivity of the sediment was measured on board the ship at several points along each core recovered, in most cases every 50 cm, by using the transient needle probe technique (Von Herzen & Maxwell 1959) and correcting the values to *in situ* temperature and pressure conditions (Ratcliffe 1960). The accuracy of the needle probe technique has been estimated to 3–4 % (Von Herzen & Maxwell 1959). Larger errors can, however, occasionally occur, owing to mechanical disturbances of the sediment either during the coring operation itself or afterwards during handling the core on board the ship. In practice, conductivity values departing significantly from the trend defined by the other values were eliminated in the absence of notable apparent changes in the lithology of the sediment.

The temperature profiles in the sediment are linear to a first approximation (figures 4 and 5). The linearity is in particular indicated by the agreement between the extrapolated surface sediment temperatures and the measured bottom water temperatures (table 1). Pronounced curvatures downwards were, however, observed at station CH 66–08 over Trevelyan (figure 4) and stations CH 66–14, CH 66–15 and CH 66–16 over the Aegis ridge (figure 5). Bottom

water temperature fluctuations may be one possible explanation of the curvature (see, for example, Pugh 1975) but, in the absence of available long-term bottom-water temperature records, this explanation remains hypothetical. However, at station CH 66–15 where the maximum difference between the extrapolated and measured bottom water temperatures occurs, the four temperature points at depths in the sub-bottom between 1.5 and 5.9 m are nearly perfectly aligned. If the curvature of the temperature profile at station CH 66–15 results from bottom water temperature fluctuations, the shape of the temperature profile then suggests that these fluctuations are of short periods (periods of a few days or weeks) penetrating only to small depths in the sediment (Pugh 1975). The occurrence of short-term bottom-water temperature fluctuations may be related to instability of the water masses along the slope of the margin. In the absence of any evidence on which to rely on to apply corrections to the observed temperature profiles, no correction has been made. We consider the stations where pronounced curvature of the temperature profiles are observed as being of moderate quality.

Table 1 summarizes the data obtained. The heat flux value at each station is simply taken as the product of the mean vertical temperature gradient and the mean harmonic thermal conductivity. The corrected heat flux values include corrections applied to account for the

TABLE 1. SUMMARY OF THE C.N.E.X.O. HEAT FLOW MEASUREMENTS OVER THE WESTERN APPROACHES MARGIN

(Included is the D.S.D.P. site 402 heat flow determination (Erickson *et al.* 1979.)

| station | position latitude N | position longitude W | water depth/m | bottom water temperature °C | penetration/ m | no. of temp. in sed. |
|---|---|---|---|---|---|---|
| SU01–01 | 47° 39.6′ | 9° 13.8′ | 3826 | 2.52 | 4.3 | 2 |
| CH66–05 | 46° 32.5′ | 8° 26.5′ | 4732 | 2.54 | 4.7 | 4 |
| CH66–08 | 46° 44.5′ | 8° 44.9′ | 3641 | 2.58 | 7.7 | 4 |
| CH66–09 | 46° 51.5′ | 8° 48.7′ | 4081 | 2.53 | 8.7 | 3 |
| CH66–11 | 47° 18.1′ | 8° 23.1′ | 2789 | 2.89 | 10.2 | 3 |
| CH66–12 | 47° 28.3 | 8° 19.3′ | 2095 | 3.52 | 9.7 | 3 |
| CH66–13 | 47° 05.8′ | 8° 40.9′ | 4378 | 2.52 | 9.7 | 5 |
| CH66–14 | 47° 31.3′ | 9° 19.9′ | 3304 | 2.65 | 8.8 | 3 |
| CH66–15 | 47° 32.0′ | 9° 28.6′ | 4052 | 2.52 | 5.9 | 4 |
| CH66–16 | 47° 33.5′ | 9° 12.2′ | 2972 | 2.83 | 7.7 | 3 |
| IPOD Site 402 | 47° 52.5′ | 8° 50.4′ | 2339 | 3.40 | | |

| station | temperature gradient/km$^{-1}$ (B.W.T. extrapolated) | no. of conductivity measurements | thermal conductivity/ W m$^{-1}$ K$^{-1}$ | heat flow/mW m$^{-2}$ | topographical correction (%) | sediment correction (%) | corrected heat flow/ mW m$^{-2}$ |
|---|---|---|---|---|---|---|---|
| SU01–01 | 30 (2.59) | 7 | 1.22 ± 0.18 | 37 | −5 | 5 | 37 |
| CH66–05 | 28 (2.56) | 4 | 1.17 ± 0.05 | 33 | −4 | 5 | 33 |
| CH66–08 | 34 (2.69) | 13 | 1.09 ± 0.07 | 37 | 7 | 5 | 42 |
| CH66–09 | 38 (2.60) | 19 | 1.05 ± 0.10 | 40 | 4 | 5 | 43 |
| CH66–11 | < 13 (2.90) | 15 | 1.09 ± 0.04 | < 14 | 0 | 5 | < 15 |
| CH66–12 | 32 (3.60) | 12 | 1.25 ± 0.16 | 40 | 4 | 5 | 43 |
| CH66–13 | 47 (2.55) | 11 | 1.06 ± 0.04 | 50 | −11 | 5 | 47 |
| CH66–14 | 28 (2.63) | 7 | 1.31 ± 0.05 | 37 | 10 | 5 | 42 |
| CH66–15 | 40 (2.68) | 6 | 1.14 ± 0.10 | 46 | 0 | 5 | 48 |
| CH66–16 | 31 (2.90) | 12 | 1.35 ± 0.23 | 42 | 10 | 5 | 48 |
| IPOD Site 402 | 28.5 | | 1.26 ± 0.07 | 36 | | | |

effects upon the near-surface temperature gradients of the large-scale topographic variations across the margin (topographic corrections in table 1) and of the sedimentation (sedimentary corrections in table 1). Topographic corrections were computed by solving the two dimensional steady state heat conduction equation (Sclater & Miller 1970) applied to topographic profiles across the margin (see, for example, figure 6). Topographic corrections are typically 5 %, with a maximum of 11 % at station CH 66–13 at the top of the Aegis Ridge. Sedimentary corrections

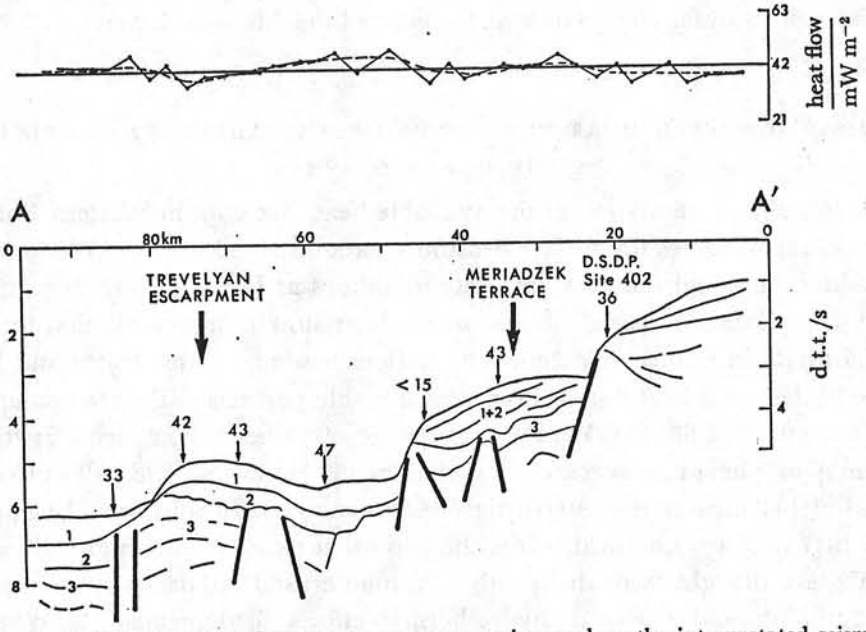


FIGURE 6. (Bottom.) Corrected heat flow measurements superimposed on the interpretated seismic profile AA' from Montadert *et al.* (1974) located in figure 3. Sedimentary units as follows: (1) post-Eocene; (2) Cainomanian to Eocene; (3) Aptian–Albian. (Top.) Effects of the topography on the surface heat flux assuming a constant heat flux at depth of 42 mW $m^{-2}$. The dotted line is a smoothed curve.

were calculated by using the Von Herzen & Uyeda (1963) procedure, adopting a thermal diffusivity value of $3 \times 10^{-3}$ $cm^2$ $s^{-1}$ (Von Herzen & Maxwell 1959). For a total sedimentary thickness of 1–2 km, assumed to have been deposited at a uniform rate over the Meriadzek Trevelyan area since the end of rifting (110 Ma), the correction amounts to 3.3–6.6 %. Over the Aegis Ridge, sediments are lacking or reduced for the period ranging from 110–60 Ma. Assuming then that the *ca.* 1 km thick sediments have been deposited over the last 60 Ma, the correction amounts to 4.5 %. A 5 % average correction was applied to all measurements (table 1). The total correction at each station does not exceed 15 %, which justifies the simple correction procedures adopted above. The uncertainty on the corrected heat flux values is estimated to ± 20 %

## RESULTS

Excluding station CH 66–11, where we have measured an abnormally low conductive heat flux, the mean conductive heat flux value calculated for the nine other stations is 43 ± 5 (s.d.) mW $m^{-2}$. There is no apparent trend in the heat flow distribution across the margin, with the exception, however, of a slightly lower value of 33 mW $m^{-2}$ at station CH 66–05 at the foot of the Trevelyan Escarpment, in close proximity of the oceanic crust, which requires

confirmation by further measurements. The surface heat flux data are in good agreement with the heat flow determination of $36 \pm 14$ mW m$^{-2}$ reported for the D.S.D.P. Site 402 located slightly higher on the slope (Erickson *et al.* 1979). The thermal régime of the Western Approaches continental slope and rise appears then to be characterized by a low and fairly uniform regional heat flux of the order of 36–43 mW m$^{-2}$. The exceptionally low conductive heat flux measured at station CH 66–11 may indicate that conduction is not the dominant heat transfer process in the vicinity of this station. One may therefore suggest the occurrence of convective heat transfer along faults at the edge of the Meriadzek Terrace.

## Comparison with heat flux data of the adjacent continental and oceanic areas

Figure 7 shows the compilation of the available heat flux data in Western Europe and the Bay of Biscay. Included are the surface heat flow data obtained over the Western Approaches margin reported here and the heat flow determinations at D.S.D.P. Site 402 (Erickson *et al.* 1979). The compilation is based on the world heat flow data compilation by Jessop *et al.* (1976) and for data in France on recent compilations made by Gable (1977) and Bertaux *et al.* (1978). The background heat flux in France over stable portions of the Hercynian continental crust is of the order of 65–85 mW m$^{-2}$. This range of values is comparable with the $72.5 \pm 19.8$ (s.d.) mW m$^{-2}$ heat flux average calculated for the Hercynian fold belt in Central Europe from a total of 147 measurements (Hurtig & Oelsner 1977). In southwest England, a similar value of 67 mW m$^{-2}$ was obtained, while the two other exceptionally high values, of 134 and 137 mW m$^{-2}$, are thought to be due partly to a high crustal radioactivity associated with the Cornwall batholith and partly to hydrothermal effects (Tammemagi & Wheildon 1974). Compared to the background heat flux in Western Europe, the heat flux over the Western Approaches margin then appears to be reduced by a factor of nearly two. In contrast, heat flow values over the margin are similar to those in the Bay of Biscay. The average of the five available heat flux values in the Bay of Biscay is $45 \pm 10$ (s.d.) mW m$^{-2}$.

## Implications

We note first that the elapsed time since the last major thermal event to have affected the Western Approaches margin (dated at 100 Ma, corresponding to the end of rifting before the onset of opening of the Bay of Biscay in Upper Aptian), is considerably more than the thermal time constant of the lithosphere, i.e. a few tens of millions of years. This implies that the Western Approaches margin is close to thermal equilibrium. This is true *a fortiori* for the stable Hercynian continental area where the time since the last major thermal event to have affected the lithosphere (*ca.* 280 Ma) is still larger. Nearly steady state thermal conditions therefore characterize the thermal regime of both the Western Approaches margin and the adjacent Western European continental area. The steady state surface heat flow $Q_s$ can be seen as the sum of two components, the crustal radioactive heat production $Q_c$ and the heat flux from the mantle $Q_m$. If one neglects the lithospheric mantle radioactive heat production, which is unlikely to exceed a few mW m$^{-2}$ (see, for example, Bickle 1978) the mantle heat flux is, to a first approximation, the heat flux at the base of lithosphere. Consequently, the heat flux contrast observed between the Western Approaches margin and the adjacent stable Hercynian Western European continental

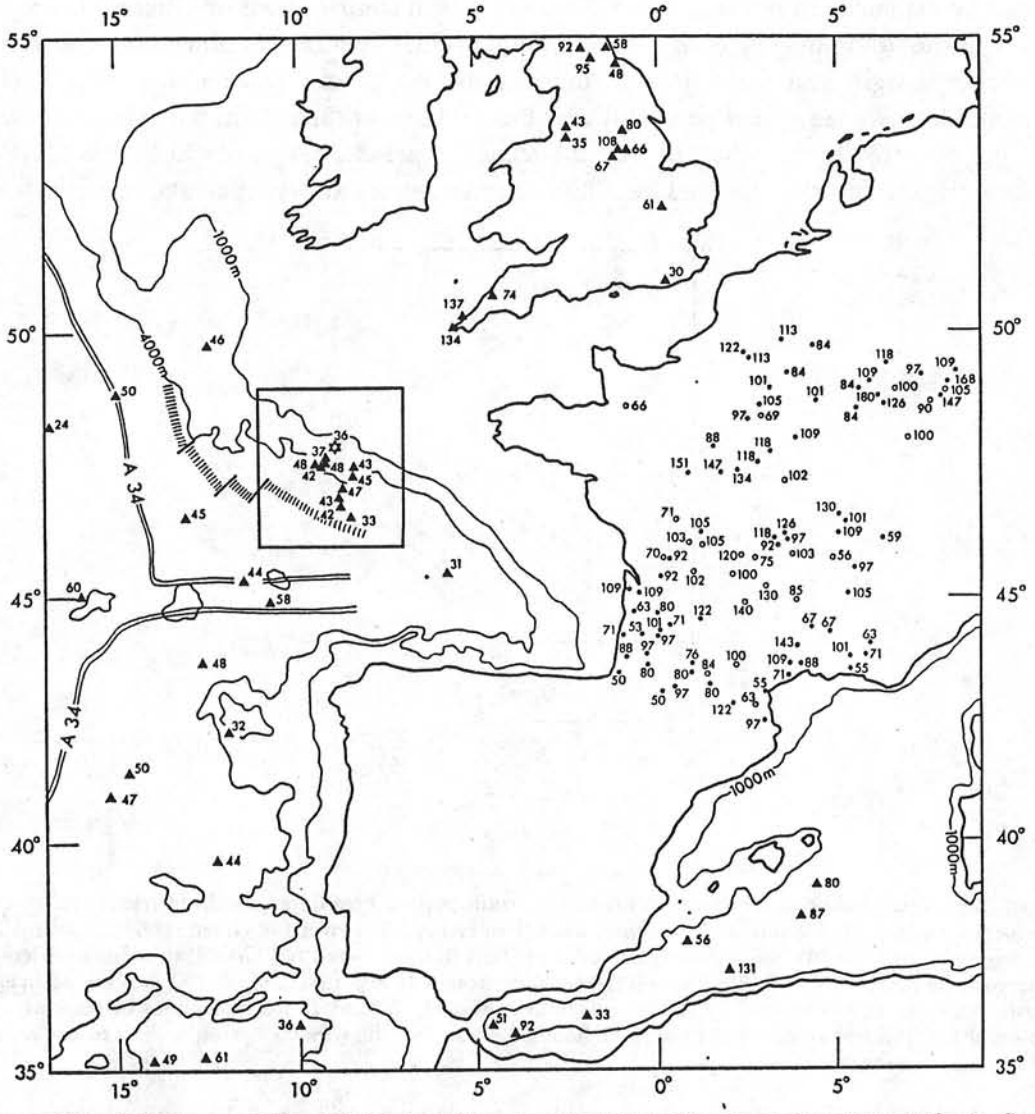


FIGURE 7. Compilation map of the available heat flow data in Western Europe and the Bay of Biscay. Sources: Jessop *et al.* (1976) (triangles); Gable (1977) (full circles); Bertaux *et al.* (1978) (open circles); Erickson *et al.* (1979) (star); this study (triangles in the box). The hatched area shows the continental–oceanic crust boundary.

TABLE 2. ESTIMATES OF THE SURFACE HEAT FLOW $Q_s$, THE CRUSTAL CONTRIBUTION $Q_c$ AND THE MANTLE HEAT FLUX $Q_m$ FOR THE WESTERN APPROACHES CONTINENTAL SLOPE AND RISE AND THE ADJACENT OCEANIC AND CONTINENTAL AREAS

(The 25 mW m$^{-2}$ $Q_m$ value given for the Bay of Biscay is a mean estimate for the oceanic regions (Kono & Yoshii 1975).)

| | Bay of Biscay oceanic crust | Western Approaches continental slope | West European Hercynian continental crust |
|---|---|---|---|
| age of last thermal event/Ma | 70–110 | 110 | 280 |
| $Q_s$/(mW m$^{-2}$) | 35–55 | 36–43 | 65–85 |
| $Q_m$/(mW m$^{-2}$) | (25) | 24–30 | 24–30 |
| $Q_c$/(mW m$^{-2}$) | (10–30) | 6–19 | 35–61 |
| $Q_c(L)/Q_c(L_0)$ | — | 0.11–0.46 | |

area can be explained in terms of either different crustal contributions or different heat flux at the base of the lithosphere or even a combination of these two causes. Since both the Western Approaches margin and the adjacent continent belong to one same stable portion of the European plate, we see *a priori* no reason why the heat flux at the base of the lithosphere would vary from one area to the other, so that the second explanation appears to be less likely. We therefore suggest that the observed heat flux contrast reflects different crustal contributions.

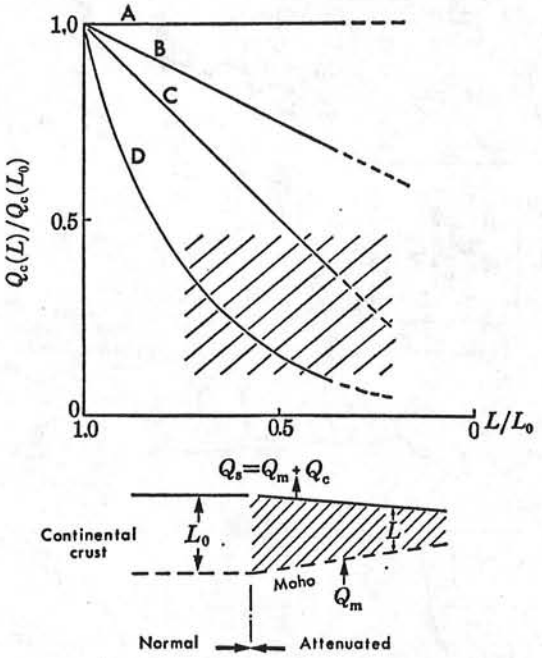


FIGURE 8. Predicted change in the crustal contribution to the surface heat flow assuming various mechanisms of crustal thinning. (A) Deep crustal metamorphism (Falvey 1974; Ringwood & Green 1966; Colette 1968). (B) Creep in lower crust (Artemjev & Artyushkov 1971; Bott & Dean 1972). (C) Crustal stretching (Artemjev & Artyushkov 1971; Morton & Black 1975). (D) Surface erosion (Sleep 1971). $Q_c$ and $Q_m$ are respectively the crustal and mantle contributions to the surface heat flow $Q_s$. $L_0$ and $L$ are thicknesses of respectively the normal and thinned continental crust. The hatched area gives the window corresponding to the heat flow constraints (see text).

Table 2 illustrates our approach in providing tentative estimates of the crustal contributions $Q_c$ and the mantle heat flux $Q_m$ for the Western Approaches margin and the adjacent continental and oceanic areas. The 24–30 mW m$^{-2}$ $Q_m$ value used for Western Europe, also adopted for the Western Approaches margin, is the estimate derived by Daignères & Vasseur (1979) for the Bournac site in the Central Massif in France. At this site, the measured surface heat flow is 85 mW m$^{-2}$, so that about two thirds of the surface heat flux would be accounted for by crustal radioactivity. Based on the 24–30 mW m$^{-2}$ $Q_m$ value derived at the Bournac site, which is to our knowledge the only $Q_m$ estimate available in Western Europe, the crustal contribution for the Western Approaches margin would therefore be only a fraction composed of between 0.11 and 0.46 of the crustal contribution for Western Europe (table 2). Allowing for some uncertainty in the $Q_m$ value, since the regional validity of the Bournac site estimate may be questioned, a higher $Q_m$ value would still increase the amount of reduction of the crustal contribution, while an upper limit of the possible amount of reduction is given by the case of the mantle heat flux taken equal to zero; $Q_c(L)/Q_c(L_0)$ would be then equal to $Q_s(L)/Q_s(L_0)$ and would occur between 0.42 and 0.66.

If the above approach is correct, one important implication of the heat flow results is to require crustal thinning processes under the margin capable of producing a large reduction of the crustal radioactive heat production. Figure 8 illustrates schematically the possibility of four main types of crustal thinning to decrease the crustal radioactive heat production. One fundamental preliminary observation is then that if crustal thinning reflects only an upward migration of the Moho as a result of deep metamorphic changes such as gabbro to eclogite (Ringwood & Green 1966; Colette 1968) or Greenshist to amphibolite (Falvey 1974), no variation is expected in the steady state surface heat flux in so far as each lithospheric column can be considered as a closed system for the radiogenic sources contained in this column, which is assumed here (figure 8, curve A). In other words, we assume that there is no lateral migration of the radiogenic sources and no input of new radiogenic sources from below. Applied to the Western Approaches margin, this means that deep metamorphism processes are unlikely to be the dominant cause of the crustal thinning since these processes would not account for the large reduction of the surface heat flow. In contrast to deep metamorphism, the three other processes considered in figure 8 can produce a significant decrease of the crustal radioactive contribution. One of these processes is surface erosion, generally related to doming of the continental crust in the early stage of formation of a rifted margin (Closs 1939; Sleep 1971). If radiogenic sources are mainly concentrated in the upper crustal material, as generally believed (see, for example, Roy *et al.* 1968; Lachenbruch 1968), surface erosion is expected to cause a rapid decrease of the crustal contribution since it would remove the more radiogenic crustal material (figure 8, curve B). However, the loss of radiogenic sources during erosion can be compensated to some extent by the radioactive contribution of the sediments deposited after erosion. The two other processes considered in figure 8 involve a purely mechanical deformation of the crust under tensional forces developed either during rifting (Artemjev & Artjuskyov 1971; Morton & Black 1975) or in the early stage of opening of a new ocean, in this latter case as a result of unequal loading and associated isostatic compensation across the margin (Bott 1971; Bott & Dean 1972). The extension would then occur through brittle faulting of the upper crust and ductile deformation of the lower crust. If the amount of extension is, to a first approximation, constant with depth through the whole thickness of the crust, the crustal radioactive contribution would decrease linearly with the amount of crustal thinning, whatever the radiogenic sources distribution model adopted (figure 8, curve C). If the extension affects mainly the deep crust (Bott 1971; Bott & Dean 1972), the decrease in the crustal radioactive contribution is difficult to assess since it depends largely on the crustal deformation and radiogenic source distribution models adopted, but in any case would be less than for the case of a uniform extension of the crust (figure 8, curve D).

Surface erosion must be eliminated as a possible process of crustal thinning under the Western Approaches margin, since there is evidence that no erosion occurred before and during rifting in the central trough of the rift system (Montadert *et al.* 1979). Then, one possible explanation of the large reduction of the surface heat flux is to presume that the dominant process of crustal thinning under the margin was crustal extension. In this respect, assuming that the one half reduction of the crustal thickness under the continental slope and rise of the Western Approaches margin is a result of a purely extensive deformation uniformly affecting the whole thickness of the crust, the predicted change in the crustal contribution $Q_c$ is a reduction also of about one half (applying curve C in figure 8), which is within the range of the estimated reduction values in table 2. Such a large extension of the original continental

crust suggested by the interpretation above is much more than the 15% extension estimated by Montadert *et al.* (1979) from a reconstruction of the displacements of the tilted fault blocks along fault planes.

We thank J. Francheteau for a critical reading of the manuscript, D. Roberts and L. Montadert for their encouragement, and D. Carré and Y. Potard for technical assistance.

## References (Foucher & Sibuet)

Artemjev, M. E. & Artjuskyov, E. V. 1971 *J. geophys. Res.* **76**, 1197–1211.
Auffret, G. A., Pastouret, L., Cassat G., De Charpal, O., Cravatte, J. & Guennoc, P. 1979 In *Init. Rep. D.S.D.P.* vol. 48 (in the press).
Avedik, F. & Howard, D. 1979 In *Init. Rep. D.S.D.P.* vol. 48 (in the press).
Bertaux, M. G., Bienfait, G., Bottinga, Y., Fontaine, J., Guyot, G., Jolivet, J., Kast, Y., Meunier, J., Ottlé, J., Perrier, G., Poupinet, G. & Vasseur, G. 1978 *C. r. hebd. Séanc. Acad. Sci., Paris* **286**, 933–936.
Bickle, M. J. 1978 *Earth planet. Sci. Lett.* **40**, 301–315.
Bott, M. H. P. 1971 *Tectonophysics*, **11**, 319–327.
Bott, M. H. P. & Dean, D. S. 1972 *Nature, Lond.* **235**, 23–25.
Bullard, E. C. 1954 *Proc. R. Soc. Lond.* A **222**, 408–429.
Closs, H. 1939 *Geol. Rdsch.* **30**, 405–527.
Colette, B. J. 1968 In *Geology of shelf areas* (ed. Donavan), pp. 15–30. Edinburgh: Oliver & Boyd.
Daignères, M. & Vasseur, G. 1979 *Ann. Géophys.* **35**, 1–9.
Erickson, A. J., Avera, W. E. & Byrne, R. 1979 In *Init. Rep. D.S.D.P.* vol. 48 (in the press).
Falvey, D. A. 1974 *Aust. Petrol. Exploration Ass.* **14**, 95–106.
Gable, R. 1977 *Edn. Bur. Rech. géol. miner., Paris* 121–122.
Gerard, R., Langseth, M. G. & Ewing, M. 1962 *J. geophys. Res.* **67**, 785–803.
Hurtig, E. & Oelsner, C. 1977 *Tectonophysics* **41**, 147–156.
Jessop, A. M., Hobart, M. A. & Sclater, J. G. 1976 *The world heat flow data collection* 1975. Geothermal service of Canada; Energy, Mines and Resources Canada, Earth Physics Branch, Ottawa, vol. 5, pp. 1–125.
Kono, Y. & Yoshii, J. 1975 *J. phys. Earth* **23**, 63–75.
Lachenbruch, A. H. 1968 *J. geophys. Res.* **73**, 6977–6989.
Langseth, M. G. 1965 In *Terrestrial heat flow* (ed. W. H. K. Lee), vol. 8, pp. 58–77. Geophysical Monograph series, American Geophysical Union.
Montadert, L., Winnock, E., Delteil, J. R. & Grau, G. 1974 In *The geology of continental Margins* (ed. C. A. Burk & C. L. Drake), pp. 323–342. New York: Springer–Verlag.
Montadert, L., De Charpal, O., Roberts, D., Guennoc, P. & Sibuet, J. C. 1979 In *M. Ewing Symposium II proceedings* (in the press).
Morton, W. H. & Black, R. 1975 In *Afar Depression of Ethiopia* (ed. Pilger & Rösler) vol. 1, pp. 55–65. Stuttgart: Schweizerbart'sche Verlagsbuchlandlung.
Pautot, G., Renard, V., Auffret, G. A., Pastouret, L. & De Charpal, O. 1976 *Nature, Lond.* **263**, 669–672.
Pugh, D. T. 1975 *Earth and planet. Sci. Lett.* **27**, 121–126.
Ratcliffe, E. H. 1960 *J. geophys. Res.* **65**, 1535–1541.
Ringwood, A. E. & Green, D. H. 1966 *Tectonophysics* **3**, 383–427.
Roy, R. F., Blackwell, D. D. & Birch, F. 1968 *Earth planet. Sci. Lett.* **5**, 1–12.
Sclater, J. G. & Miller, S. P. 1970 *Tectonophysics* **10**, 283–300.
Sleep, N. H. 1971 *Geophys. J. R. Astr. Soc.* **24**, 325–350.
Tammemagi, H. Y. & Wheildon, J. 1974 *Geophys. J. R. Astr. Soc.* **38**, 83–94.
Von Herzen, R. P. & Uyeda, S. 1963 *J. geophys. Res.* **68**, 4219–4250.
Von Herzen, R. & Maxwell, A. E. 1959 *J. geophys. Res.* **64**, 1557–1563.

JOURNAL OF GEOPHYSICAL RESEARCH, VOL. 86, NO. B5, PAGES 3708–3720, MAY 10, 1981

# Passive Margins: A Model of Formation

XAVIER LE PICHON

*Laboratoire de Géodynamique, Université Paris VI, 75230 Paris Cedex 05, France*

JEAN-CLAUDE SIBUET

*Centre Océanologique de Bretagne, B.P. 337, 29273 Brest Cedex, France*

The stretching model of McKenzie is applied to the formation of passive continental margins, assuming local isostatic equilibrium. We present the quantitative implications of the model; we then discuss its fit to the IPOD data on the Armorican and Galicia continental margins of the northeast Atlantic. The amount of brittle stretching observed in the upper 8 km of the prestretched continental crust reaches a maximum value of about 3. This large amount of thinning is comparable to the thinning of the whole continental crust observed by seismic refraction measurements and required by the model for the whole lithosphere. This agreement suggests that the simple stretching model is a good first approximation to the actual physical process of formation of the margin. It is thus possible to compute simply the thermal evolution of the margin and to discuss its petrological consequences. It is also possible to obtain a quantitative reconstruction of the edge of the continent prior to breakup. Finally, the large slope of the base of the lithosphere during the formation of the margin results in a force similar but opposite to the 'ridge-push' force acting on accreting plate boundaries.

## INTRODUCTION

The purpose of this paper is to apply the stretching model of *McKenzie* [1978*a*, *b*] to the formation of passive continental margins. We first present the implications of the model; we then discuss its fit to the data obtained on the Armorican and Galicia continental margins of the northeast Atlantic Ocean [*Montadert et al.*, 1979*a*, *b*; *Foucher and Sibuet*, 1979; *Avedik and Howard*, 1979] (see Figure 1). Finally, we discuss some consequences of this model.

## THE MODEL

We use the simplest stretching model proposed in Figure 1 of *McKenzie* [1978*a*, *b*]. A lithosphere of thickness $h_l$ with a continental crust of thickness $h_c$ is in thermal equilibrium at time $t = 0$. Production of heat by radioactivity is ignored, and the temperature at the base of the lithosphere is equal to the temperature of the asthenosphere $T_a$; $\rho_m$ is the density of mantle material at 0°C, $\rho_{c0}$ the density of continental crust at 0°C, $\rho_w$ the density of water, and $\alpha$ the coefficient of thermal expansion. Isostatic local compensation is assumed at all times. Let us call $\rho_l$ the average density of the mantle part of the lithosphere, $\rho_c$ the average density of the crust before stretching and $\rho_a$ that of the asthenosphere.

### *Initial Subsidence*

If stretching of the whole lithosphere occurs instantaneously at time $t = 0$ in such a way that the thickness of the lithosphere becomes $h_l/\beta$, $\rho_l$ and $\rho_c$ will not change, and thus the average density of the whole lithosphere will not change either. If this average density is smaller than $\rho_a$, the positive buoyancy of the lithosphere will be reduced by a factor $\beta$, and its surface will subside. If it is larger, the negative buoyancy will be reduced by the same factor, and its surface will rise. Taking the $Z$ axis positive downward and the starting elevation equal to 0, we have the initial subsidence (supposed to be under water):

$$Z_i = \frac{h_l\rho_a - h_c\rho_c - (h_l - h_c)\rho_l}{\rho_a - \rho_w}(1 - 1/\beta)$$

with

$$\rho_a = \rho_m(1 - \alpha T_a)$$

$$\rho_c = \rho_{c0}\left(1 - \frac{\alpha}{2} T_a \frac{h_c}{h_l}\right)$$

$$\rho_l = \rho_m\left(1 - \frac{\alpha}{2} T_a - \frac{\alpha}{2} T_a \frac{h_c}{h_l}\right)$$

Thus

$$Z_i = \frac{h_l\{(\rho_m - \rho_{c0})(h_c/h_l)[1 - (\alpha/2)T_a(h_c/h_l)] - \rho_m(\alpha/2)T_a\}}{\rho_m(1 - \alpha T_a) - \rho_w} \cdot \left(1 - \frac{1}{\beta}\right) \quad (1)$$

The expression for $Z_i$ is linear in $1 - (1/\beta)$. The condition for subsidence to occur is that the numerator be positive, which expresses that the lithosphere has a positive buoyancy

$$\frac{h_c}{h_l} > \frac{\rho_m(\alpha/2)T_a}{(\rho_m - \rho_{c0})[1 - (\alpha/2)T_a(h_c/h_l)]}$$

Note that we have neglected the effect of compressibility on density, as most authors have done [e.g., *McKenzie*, 1978*a*]. First, this effect is quite smaller than the temperature effect. Second, as we really are interested in the variation of density between two columns where the distribution of pressure is the same and only the distribution of temeprature differs, it is justified to neglect the pressure effect in a first approximation.



Paper number 80B1662.
0148-0227/81/080B-1662$01.00

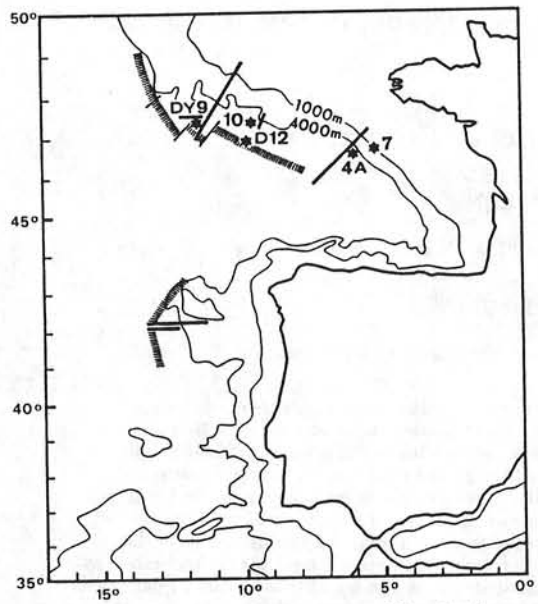


Fig. 1. Location map of the two areas providing the data used in this study, the northern Bay of Biscay margin to the north and the Galicia margin to the south. The continental crust-oceanic crust limit is identified by hachures as well as the refraction profiles (stars) used in this study after *Bott and Watts* [1971] and *Avedik and Howard* [1979]. The lines are the main seismic reflection profiles.

*Subsidence at Time t Infinite*

In this section it will be shown that the subsidence at time $t$ infinite $Z_\infty$ can also be expressed as a linear function of $1 - (1/\beta)$. Let $\rho_l'$ and $\rho_c'$ be the average densities of the mantle part of the lithosphere and crust at time $t$ infinite; then

$$Z_\infty = \frac{h_l(\rho_l' - \rho_l) + h_c[\rho_l - (\rho_l'/\beta) + (\rho_c'/\beta) - \rho_c]}{\rho_a - \rho_w}$$

with

$$\rho_l' = \rho_m\left(1 - \frac{\alpha}{2}T_a - \frac{\alpha}{2}T_a\frac{h_c}{\beta h_l}\right)$$

$$\rho_c' = \rho_{c0}\left(1 - \frac{\alpha}{2}T_a\frac{h_c}{\beta h_l}\right)$$

Thus

$$Z_\infty = h_c\left(1 - \frac{1}{\beta}\right)\frac{\rho_l - \rho_c + \rho_m(\alpha/2)T_a + \epsilon}{\rho_a - \rho_w}$$

where

$$\epsilon = -\frac{\rho_m - \rho_{c0}}{\beta}\left(\frac{\alpha}{2}T_a\frac{h_c}{h_l}\right)$$

or

$$Z_\infty = h_c\left(1 - \frac{1}{\beta}\right)\frac{(\rho_m - \rho_{c0})[1 - (\alpha/2)T_a(h_c/h_l)] + \epsilon}{\rho_a - \rho_w} \quad (2)$$

Neglecting $\epsilon$ introduces an error which is not larger than 5 parts per thousand.

The difference between $Z_\infty$ and $Z_l$ is due to the progressive return to thermal equilibrium. It is the thermal subsidence $Z_t$ which follows the initial subsidence due to stretching $Z_i$:

$$Z_t = Z_\infty - Z_l$$

Note that the value of the subsidence at infinite time is independent of the cooling history and consequently of the lateral variation in temperature. It only depends on a unique equilibrium value $h_l$ for the thickness of the lithosphere at infinite time. Similarly, the initial subsidence $Z_i$, supposed to have been produced in a very short period of stretching, is not affected by lateral variations of temperature. Thus the values obtained for $Z_l$ and $Z_\infty$ are rigorous within the assumptions made. Recently, *Jarvis and McKenzie* [1980] have shown that the instantaneous stretching model is adequate provided the duration of stretching is less than 20 Ma.

On the other hand, the evolution of the thermal subsidence with time will be affected by lateral variations of temperature. Thus the solution proposed by *McKenzie* [1978*a*, *b*] cannot be applied rigorously here but provides a somewhat lower estimate of this thermal subsidence, since the effect of lateral conduction should be to produce a faster cooling than computed by McKenzie, except near the zone of oceanic crust accretion, where the opposite effect might be expected.

## APPLICATION TO THE NORTHERN BAY OF BISCAY AND GALICIA CONTINENTAL MARGINS

*Choice of the Constants*

We next examine whether this model fits the northern Bay of Biscay and Galicia continental margins using three complete and two incomplete multichannel reflexion profiles across the margin (Figure 1) obtained in these areas by the Centre National pour l'Exploitation des Oceans/Institut Français du Pétrole [*Montadert et al.*, 1979*a*, *b*]. In order to apply (1) and (3) we need to define the values of constants $h$, $h_c$, $\rho_m$, $\rho_{c0}$, $\rho_w$, $\alpha$, and $T_a$. The values of $h_l$, $h_c$, and $\rho_{c0}$ will not be similar for all margins, and fairly large variations might consequently be expected. On the other hand, less variations might be expected in the values of $\rho_m$, $\rho_w$, $\alpha$, and $T_a$.

We know that mid-ocean ridge crests usually have a depth close to 2.5 km provided the asthenosphere is neither unusually hot nor cold. This implies that a so-called standard continental lithospheric column is in equilibrium with a zero age oceanic lithosphere under 2.5 km of water.

The following tabulation gives the constants chosen to fit the Armorican and Galicia data; they are slightly modified from *McKenzie* [1978*a*, *b*]:

| Parameter | Value |
|---|---|
| $h_l$ | 125 km |
| $h_c$ | 30 km |
| $\rho_m$ | 3.35 g cm$^{-3}$ |
| $\rho_{c0}$ | 2.78 g cm$^{-3}$ |
| $\rho_w$ | 1.03 g cm$^{-3}$ |
| $\alpha$ | $3.28 \times 10^{-5}$ °C$^{-1}$ |
| $T_a$ | 1333°C |

The zero-age oceanic lithosphere is supposed to be at a uniform temperature $T_a$ and to have an oceanic crust 5.5 km thick with the same average $\rho_{c0}$ as the continental crust of 2.78 g cm$^{-3}$. It could, for example, correspond to a crust composed of a 2-km-thick layer 2 of density 2.57 g cm$^{-3}$ and a 3.5-km-thick layer 3 of density 2.9 g cm$^{-3}$, which seems quite reasonable. The thickness of continental crust $h_c$ is imposed by re-

fraction data which suggest a value of 29–30 km. The thickness of lithosphere $h_l$ is the one suggested by the results of *Parsons and Sclater* [1977]. We also adopt the values of $\alpha$ and $T_a$ given by *Parsons and Sclater* [1977]. The set of constants then is entirely determined, the value of the last constant being 3.35 g cm$^{-3}$ for $\rho_m$.

Equation (1) becomes

$$Z_i = 3.61\left(1 - \frac{1}{\beta}\right) \text{ km} \tag{3}$$

The condition for initial subsidence to occur is

$$h_c/h_l > 0.13 \qquad h_c > 16 \text{ km}$$

Equation (2) becomes

$$Z_\infty \sim 7.83\left(1 - \frac{1}{\beta}\right) \text{ km} \tag{4}$$

$$Z_t \sim 4.21\left(1 - \frac{1}{\beta}\right) \tag{5}$$

however, in the case of the Bay of Biscay the lapse of time since the formation of the margin in Albian time is not infinite but about 120 m.y. [*Montadert et al.*, 1979*a*, *b*]. *McKenzie* [1978*a*, *b*] has shown that to a first approximation, thermal subsidence follows an exponential law with a time constant equal to the time constant of the oceanic lithosphere, which is 62.8 m.y. according to *Parsons and Sclater* [1977]. The interval of time since Albian is equivalent to twice the time constant, and thermal subsidence has thus reached approximately 87%, $(1 - 1/e^2)$ of its maximum value. Consequently,

$$Z_{t=120} \sim 3.64\left(1 - \frac{1}{\beta}\right)$$

and

$$Z_{120} \sim 7.23\left(1 - \frac{1}{\beta}\right)$$

The effect of lateral conduction tends to increase the rate of cooling over most of the margin, and consequently, $Z_{120}$ is probably somewhat underestimated. Furthermore, we have an additional constraint which is given by the relation between subsidence $Z_{120}$ and thinning of continental crust as obtained by seismic refraction and gravity measurements across the margin. This is because in the model the amount of thinning is the same for the whole crust as for the whole lithosphere. Thus $\beta$ is given by the ratio between the present thickness of crust and its original thickness (30 km). $Z_{120}$ is given by the present depth corrected for any postrifting sedimentary load, assuming local isostatic equilibrium. It will be seen that on the Armorican continental margin the continental crust thickness data suggest a linear relationship of the type

$$Z_{120} = 7.5\left(1 - \frac{1}{\beta}\right)$$

We consequently adopt

$$Z_{120} = 7.5\left(1 - \frac{1}{\beta}\right) \text{ km}$$

*The Continent-Ocean Transition*

Figure 2 shows the resulting linear relationships between relative thinning $1 - (1/\beta)$ and subsidence immediately after rifting and after an infinite time. Note that a depth of 2.5 km is reached for $1 - 1/\beta = 0.69$ and $\beta = 3.24$ immediately after rifting. The asthenosphere will not be able to break through the thinned continental lithosphere as long as $Z_l$ is smaller than 2.5 km, since its isostatic equilibrium level is 2.5 km. This equilibrium level is called mantle geoid by *Turcotte et al.* [1977]. However, Turcotte et al. do not take into account the presence of crust, and their geoid is consequently deeper (3.6 km). But a situation in which the asthenosphere would rise to 3.6 km without segregating an oceanic crust by partial fusion is not realistic. This is why the 2.5-km level should be adopted.

On the other hand, once $\beta$ has reached this value of 3.24, the continental crust is reduced to a thickness of 9.25 km and is highly fractured. The lithosphere-asthenosphere limit is less than 40 km away from the surface, and a fair amount of partial fusion may be expected. Thus it is likely that in general the asthenosphere will be able to break through to the surface when this depth is reached, although occasionally, thinning larger than 3.24 may occur along portions of the margin, producing extremely thinned continnental crust with a deeper surface than the adjacent oceanic crust. In the Bay of Biscay, $Z_{120}$ for $\beta = 3.24$ is 5.2 km and $Z_\infty$ 5.4 km. The maximum value reached by $Z_\infty$ for $\beta$ infinite is 7.83 km. This is larger than the maximum depth of the oceanic lithosphere because it assumes that the thickness of crust is zero, which is of course an impossible situation. Thus in general, one should expect to find continental crust down to a depth of 5.2 km in the absence of sedimentation in the Bay of Biscay. With sedimentation the corresponding maximum possible thickness of sediment is 15 to 20 km.

To summarize, this model predicts that the limit between continental and oceanic crust should occur, in general, at an initial depth of 2.5 km, corresponding in the Bay of Biscay to

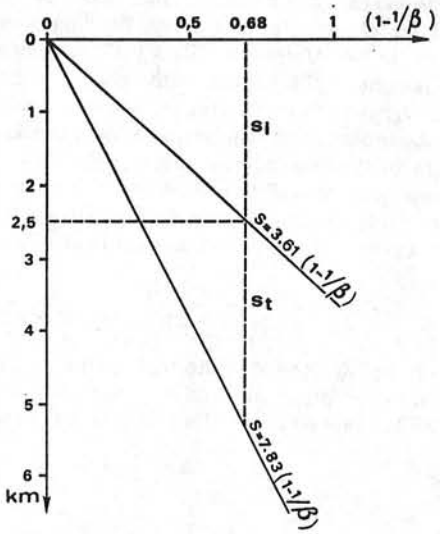


Fig. 2. Relationship between relative thinning $(1 - (1/\beta))$ and subsidence. The first line is the relationship immediately after stretching. The second line is the relationship at time infinite. A depth of 2.5 km is reached immediately after stretching for a thinning of $1 - (1/\beta) = 0.68$.

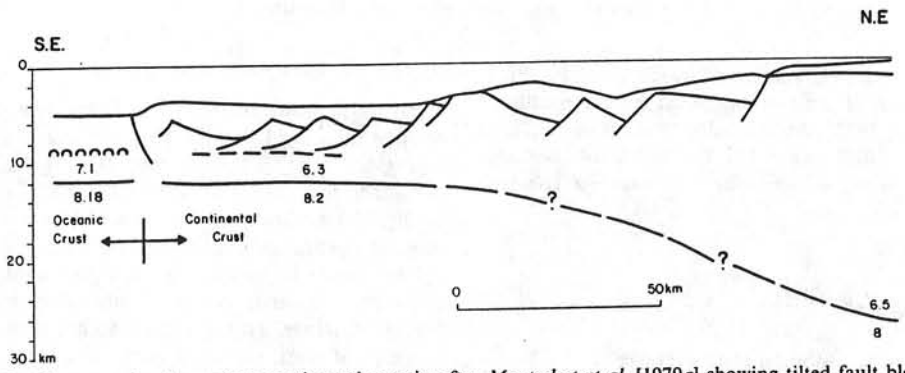


Fig. 3. Profile across the Armorican continental margin after *Montadert et al.* [1979a] showing tilted fault blocks. The vertical exaggeration is 2.5.

a $\beta$ close to 3.2 and a present water depth of 5.2 km. Thinned continental crust may be found occasionally at a lower depth if the thinning exceeded 3.2 without the asthenosphere being able to break through, but oceanic crust should not be found at smaller depths.

*Geometry of Extension of Upper Layer*

We now have a model which predicts the amount of thinning for a given subsidence. Montadert et al. have shown that 'the overall tectonic style of the continental margin is characterized by a series of tilted blocks bounded by faults which in many cases are clearly listric faults.' We ask the following question in this section: Is the geometrical extension produced by these faults compatible with the model we just developed?

As shown in Figure 3, there are typically 8 to 10 blocks about 20 km wide each which are tilted inward toward the margin, the angle of tilt increasing to about 30° in the deepest portion. However, although the faults flatten with depth by 10° to 15° at least in the deepest portion, the rotation of any block with respect to the adjacent one is very small, and consequently, the faults bounding the blocks can be considered as plane in a first approximation.

*Morton and Black* [1975] have discussed a similar configuration of faulting in the Danakil horst. They have shown that the extension can reach a value as high as $\beta = 3$. However, in this case the observed tiltings of the bedding planes are as high as 60° to 70°. *Morton and Black* [1975] conclude that the average reduction of thickness in the crust is about 10% by 10° of tilting, and this result has been widely quoted in the literature. According to this analysis we should expect a 30% reduction in the thickness of crust, that is, a $\beta$ of only about 1.4.

We consequently need to look in more detail at the actual geometric configuration. Figure 4 shows schematically two such blocks offset along a plane normal fault. We have

$$\beta = \frac{L}{l} = \frac{\sin(\alpha' + \theta' - \theta)}{\sin(\alpha' + \theta')} - \frac{h}{l \operatorname{tg}(\alpha' + \theta')} \tag{7}$$

where $\alpha$ is the supplement of the angle of the fault plane with respect to the bedding plane and $\theta$ is the present angle of tilting of the bedding plane: $\alpha' \sim \alpha$ and $\theta' \sim \theta$; then if $h = 0$,

$$\beta \sim \frac{\sin \alpha}{\sin(\alpha + \theta)} \tag{8}$$

which is equivalent to $\beta = 1/\cos\theta$ when $\alpha = 90°$. As $\theta$ has a maximum value of 30°, $\beta \leq 1.15$. But $\alpha$ is not equal to 90°. For normal faults, the original dip angle should be close to 60° at the surface and $\alpha = 120°$. Then $\beta \leq 1.73$. Morton and Black have observed an original dip angle of 60° to 70°, equivalent to 120° to 110°. In addition, they assume that a second generation of faulting appears when $\theta$ increases beyond 20°–30°, the initial generation of rotated fault planes being too shallow. This explains why they need very high values of $\theta$ to produce a $\beta$ of 3.

*Proffett* [1977] has discussed the amount of extension produced by normal faulting in the Yerington district (Nevada) of the Basin and Range province. Locally, he measures a stretching factor ($\beta$) as high as 2.4, which is a value similar to the ones found by Morton and Black in the Danakil horst. Stretching is obtained by low-angle normal faults which have been cut by a younger generation of higher-angle normal faults. The original surface dip angle of faulting was 40°–70°, and the faults shallow with depth to 40°–50° at a depth of 8–10 km. Thus the present low angle of dip (0° to 10°) results from the tilting of the fault planes by an angle $\theta$ of up to 60°. However, $\theta$ does not show any large increase from one fault to the other. Consequently, the fault planes can be considered parallel in a first approximation. With the values of $\alpha$ and $\theta$ suggested by the data of Proffett, it is clear that a very high stretching factor should indeed be measured.

Figure 5 is a migrated section without vertical exaggeration of one block on the Armorican continental margin which has been published by *Montadert et al.* [1977a], and Figure 6 shows the main parameters necessary to compute the extension. The main block in the central part of the section (A'B)

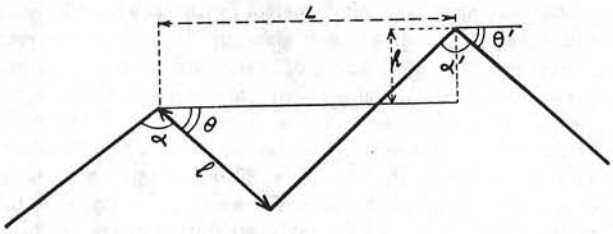


$$\beta = \frac{L}{l} = \frac{\sin(\alpha'+\theta'-\theta)}{\sin(\alpha'+\theta')} - \frac{h}{l \operatorname{tg}(\alpha'+\theta')}$$

$$\sim \frac{\sin\alpha}{\sin(\alpha+\theta)} - \frac{h}{l \operatorname{tg}(\alpha+\theta)}$$

$$\sim \frac{\sin\alpha}{\sin(\alpha+\theta)}$$

Fig. 4. Computation of the geometrical extension for tilted blocks separated by plane normal faults.

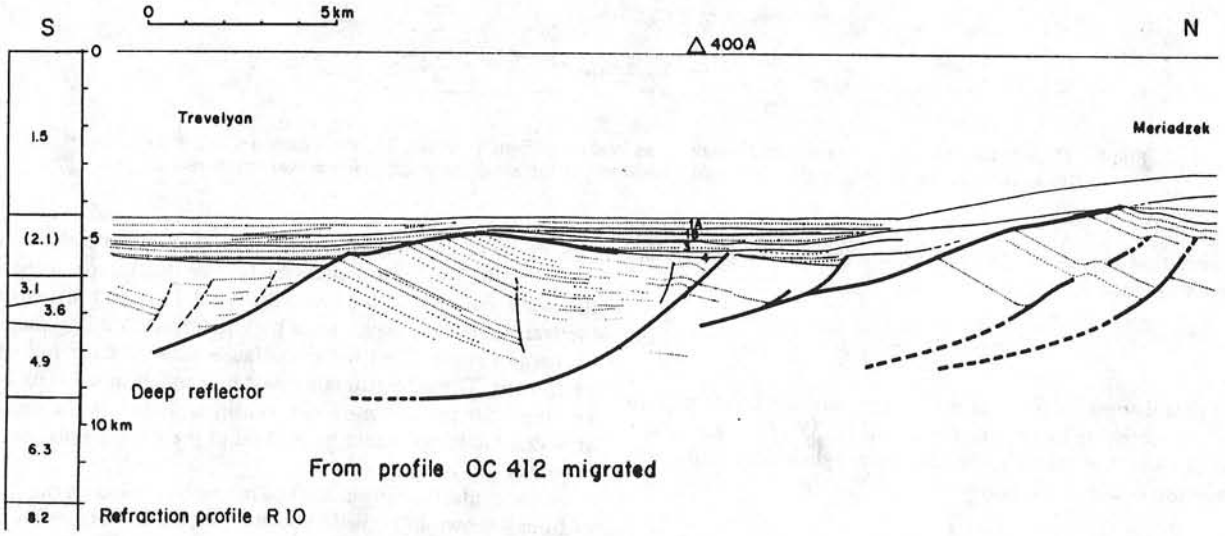


Fig. 5. Interpretation of a migrated multichannel seismic reflection profile across the lower portion of the Armorican continental margin after *Montadert et al.* [1979*a*].

has been tilted by an angle $\theta$ of 26.5°, while the right-hand block is tilted by an angle $\theta'$ of 28°; thus $\theta$ is equivalent to $\theta'$, and there has been no rotation of the central block with respect to the upper block, which implies that the fault surface along AA′ is plane. Thus the angle BA′A, which is equal to 136°, is very close to $\alpha'$ (133°). AB′ ($h$) is equal to 0.8 km, and BA′($l$) to 7 km. Using (7), we have $\beta = 2.5$. This can be checked by measuring directly the ratio of BB′ ($L$) to BA′ ($l$), which is equal to 2.6. The present depth of the upper surface of the block is 5.2 km and is 4.6 km after isostatic readjustment for the postrift sedimentary cover. Using (6), we have a water depth of 4.6 km for this value of $\beta$. We conclude that the amount of mechanical thinning in the upper layer is equivalent to the thinning of the whole lithosphere predicted by the model. However, Figure 5 shows that the refraction results of profile R10 indicate a thinner crust and consequently a higher $\beta$ than the one predicted by the model. We shall come back to this point later.

We see in Figure 5 and 6 that this high value of $\beta$ can be obtained because the average original dip angle of the fault plane was 45° and not 60°. Thus after rotation by 28° the fault plane lies at an angle of only 17° with the horizontal, which allows for this very large extension and explains the difference with Morton and Black's findings. However, Morton and Black work on the superficial tectonics, whereas the reflection profile gives us the deep tectonics and cannot resolve the tectonics of the uppermost layer. There is clearly a large amount of complex deformation in the upper part of the block near the main fault plane, possibly caused by drag along the fault plane. This deformation must be extensional and may be in detail quite similar to the one observed by Morton and Black. But small blocks and high angles of tilt will never be resolved by seismic reflection.

The process of brittle stretching then involves faulting of a 7-km-wide block along 45° faults with simultaneous tilting of the block and fault plane by 28°. This high angle of tilting re-

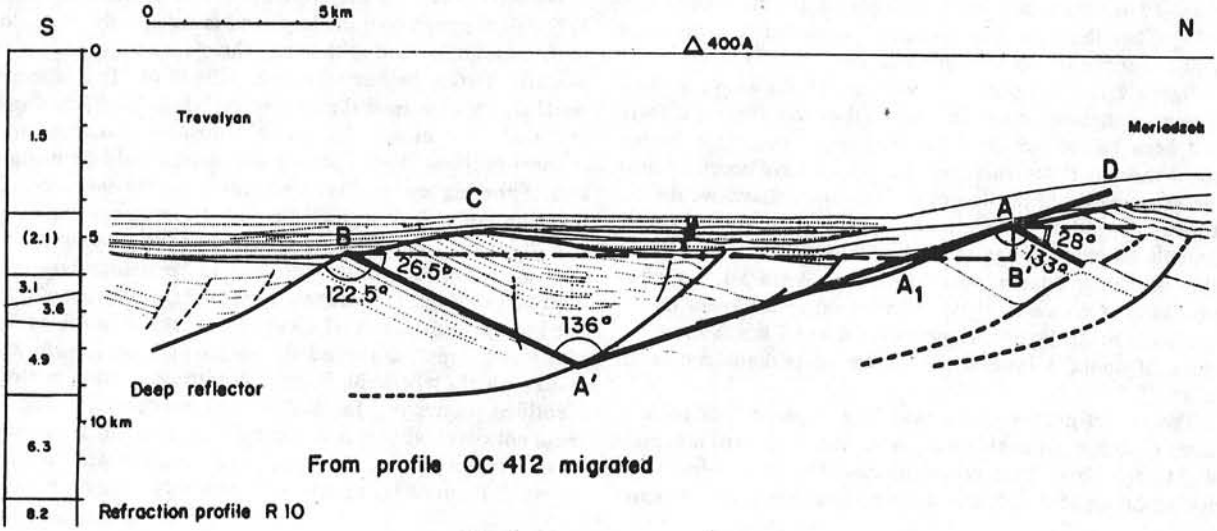


Fig. 6. Parameters of Figure 5.

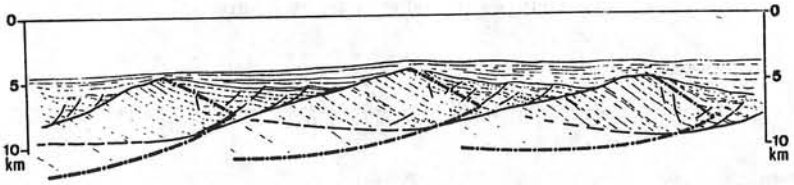


Fig. 7. Hypothetical geometry of three tilted blocks in the lower continental margin. The thick dash-dot line is the geometry in the absence of deformation. The thin dashed line is the actual geometry. No vertical exaggeration.

quires that the block glides along the fault plane by a minimum amount of

$$g = \frac{l \sin \theta}{\sin (\alpha + \theta)} \tag{9}$$

so that its upper surface is not higher than the upper surface of the preceding block. For $\theta = 30°$, $\alpha = 135°$, $l = 7$ km, and $g = 13.5$ km. But actually, the block must glide deeper to reach isostatic equilibrium, and

$$g = \frac{l \sin \theta}{\sin (\alpha + \theta)} + \frac{h}{\sin (\alpha + \theta)}$$

From (3) we have

$$h = 3.6 \frac{d\beta}{\beta^2}$$

if local isostatic equilibrium is preserved from block to block, which gives us the means of modeling the topography of the margin knowing $\alpha$ and $\theta$.

Actually, on Figures 5 and 6, $g = 12$ km. Thus the fault plane is affected by a very large amount of motion which is accompanied by important deformation by drag along the fault plane. The original thickness of the fault block is probably close to 8–9 km, and the fault tends to flatten by about 10°–15° below an original depth of about 7 km. This suggests that the transition brittle ductile occurs near 8–10 km at a probable temperature of about 200°C, which is not unreasonable. It is well known that most earthquakes in areas of extension, as in Aegea, occur above 10 km [*McKenzie*, 1978*b*, and personal communication, 1980]. McKenzie has also noted that on the basis of earthquake mechanisms, fault planes apparently tend to flatten at depth, although this flattening is rarely observed at the surface, even in highly eroded areas [*Angelier*, 1979]. Thus the flattening probably occurs below 6- to 8-km depth near the brittle-ductile transition.

Figure 7 is a cartoon of three such blocks showing their present configuration and the shapes they should have if there had been no deformation. Seismics give us no information about the actual deformation which must have occurred near the lower flattened portion of the fault plane, and we do not attempt to model it. Everything happens as if the blocks were actually barely touching each other, 'floating' on the presumably originally ductile material of the 6.3-km/s lower layer [*Avedik and Howard*, 1979]. The resulting thickness of the originally brittle layer varies between 4 and 2 km, with an average of about 3 instead of 7–8 km or perhaps somewhat more.

The model proposed can thus be compared to a pack of cards resting at an angle on a plane, with each card making a slight angle $d\theta$ with the preceding one. The tilt $\theta$ is due to the accumulation of the $d\theta$, and the horizontal extension increases very rapidly as $\theta$ approaches 30°. Note that in this case, faulting and tilting occur simultaneously. For this reason, even if the faults flatten out to become horizontal at the brittle-ductile transition, they never were parallel to the bedding plane, as it was already tilted when the faults reached their full development. Thus the estimate made by Proffett of a 13- to 16-km depth for the brittle-ductile transition, based on the depth at which the faults would be parallel to the bedding planes, is probably too large.

To conclude, the only published migrated section on the Bay of Biscay shown in Figure 5 shows a mechanical extension by a factor of 2.6, which is close to the one predicted by our model. This high $\beta$ value is similar to values of 3 measured by Morton and Black in the Danakil horst and 2.4 measured by Proffett in the Basin and Range province. We have shown that these values can be obtained with a simple geometrical model of plane normal faulting in which tilting occurs simultaneously with faulting. Although listric faulting does occur, it is not an essential part of our model.

On the other hand, Morton and Black as well as Proffett show that as tilting flattens the fault planes, a new generation of higher-angle normal faults occur. We believe that these high-angle faults only characterize the shallower levels and that the low-angle fault planes are still active at deeper levels, where the lithostatic pressure is higher. The new generation of high-angle normal faults, together with the deformation produced in the upper layer near the fault plane (see Figure 5), bias the interpretation toward lower $\theta$ and larger $l$, unless high-quality data are available. This fact may explain why many workers have obtained rather low values of $\beta$.

### *Variation of β With Z*

We have seen that the mechanical extension in the upper brittle portion can be quite large and is apparently quite close to the amount needed to thin the whole crust according to the isostatic relation between $\beta$ and $Z$ given in (4). In this section we shall try to extend the test to the whole northern Biscay and Galicia continental margins using the available multichannel profiles. Ideally, the sections used should be migrated and of the highest quality. Unfortunately, the migrated sections are not always available, and it is sometimes quite difficult to obtain a reasonable evaluation of the probable extension. Although this work will have to be redone later with migrated sections, the results are, however, quite encouraging. We have measured $\theta$ on 31 blocks as a function of the equivalent water depth, corrected for sediment loading. We have chosen blocks where the original prerifting layering could be identified, correcting for the vertical exaggeration and for sediment cover whenever it is significant. Individual measurements are not precise, but the overall variation with depth as shown in Figure 8 is unlikely to be seriously in error. Figure 8

shows that the measured $\theta$ does tend to systematically increase with water depth from less than 5° to a maximum of 30°.

To measure $\beta$, we have used two methods. The first is very simple: we simply measure the ratio $L/l$. The second one is based on (7), assuming that $\alpha' = \alpha$ and $\theta' = \theta$. Both methods yield equivalent results. The sections are not migrated and are simply approximately converted to depths: individual errors can be quite large. The main difficulty comes into the actual definition of a block. For example, in Figure 5, if the data were not so good, one could argue that the northern end of the left block lies near hole 400 A and not further north at the base of the main slope, as imposed by the stratigraphic continuity. With such an interpretation the $\beta$ measured would be much lower.

We have consequently made two successive attempts with two different sets of blocks. In a first attempt, with 22 blocks, shown in Figure 9, we have assumed that the data were biased toward low $\beta$ values and tried to take that into account. In a second attempt, with 24 blocks, shown in Figure 10, we have tried to be quite conservative in the choice of the blocks. Three different categories of blocks have been identified according to the quality of the interpretation.

A first conclusion appears by looking at the distribution of the 5 points corresponding to seismic refraction stations. Although there is some scatter and although $\beta$ as large as 7.5 have been measured on the deepest stations which have a water depth of 6.5 km, the overall thinning of continental crust varies linearly with water depth and follows a relation close to

$$Z = 7.5\left(1 - \frac{1}{\beta}\right)$$

As previously mentioned, this is the reason why we chose to adopt 7.5 and not 7.2 in the relationship, although both values would be acceptable. The main point we wish to emphasize is that one should not discuss the results of individual stations separately from the others but should on the contrary consider the relationship best fitting the set of stations over the maximum range of water depth. It is well known that results of adjacent refraction stations may have significant differences due either to local variability or to imprecise measurements.

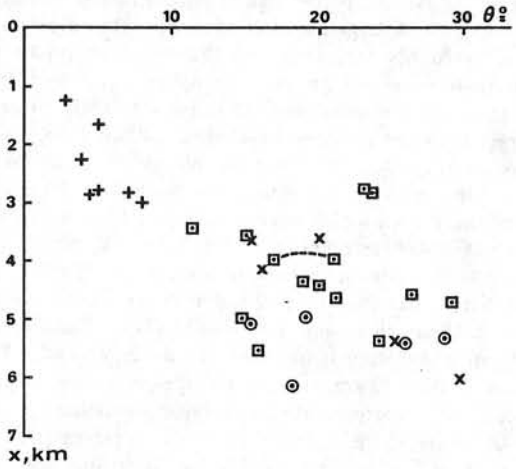


Fig. 8. Angle of tilt $\theta$ versus equivalent water depth for the northern Bay of Biscay and Galicia continental margins. Squares, crosses, and circles are data from tilted faulted blocks of good, medium, and bad quality, respectively.

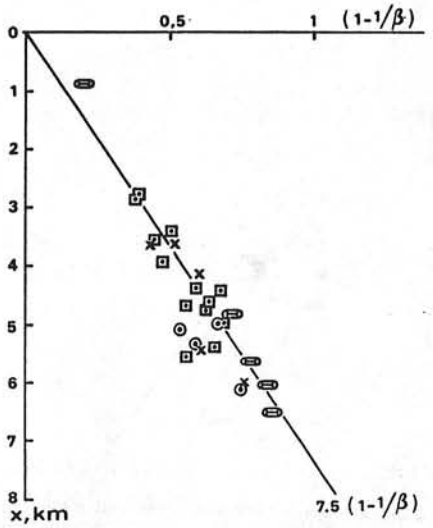


Fig. 9. Relationship between thinning of crust and equivalent water depth: probable interpretation. The refraction stations (ovals) are the ones identified in Figure 1. Squares, crosses, and circles are data from tilted fault blocks of good, medium, and bad quality, respectively.

A second conclusion is that in Figure 9 but also in Figure 10, stretching in the upper crustal layer reaches values which have, as an upper limit, the values derived for the thinning of the whole lithosphere. In addition, the best measurements tend to fall quite close to the predicted relationship. Note that the deepest blocks, immediately before the continental-oceanic crust transition, which is well defined here, have an equivalent water depth of 5 to 6 km, close to the predicted value of 5.2 km.

We conclude that with the present quality of data available, there is no need to advocate the use of more complex models, as our model seems to provide a fair approximation to the subsidence, the continental crust thinning, and the depth of the continental-oceanic crust transition.

It is actually quite surprising that the very crude approximation of perfect local isostasy on which this model is built seems to be upheld by the data. This is probably due to the fact that during the phase of rapid stretching the flexural rigidity of the lithosphere decreases dramatically, as has been shown by *Watts and Ryan* [1976] for the continental margin of the Gulf of Lyon. Some preliminary computations based on the effect of the relatively small post-rift sedimentary load suggest that the flexural rigidity is now back to a value typical for a lithosphere of that age.

It should be pointed out that *Watts* [1980] has recently examined the rates of subsidence in the Gulf of Lyon and concluded that they were too high to be explained by a simple stretching model. However, the conclusion reached depends on the date chosen for the end of the stretching phase. If, as we believe, this date is later than proposed by Watts, it is easy to reconcile his data with the stretching model.

## GEOLOGICAL EVOLUTION OF THE MARGIN

We now examine whether the early geological evolution of the margin, as described by *Montadert et al.* [1979*a*, *b*], is compatible with the model. The remarkable quality of geological and geophysical data obtained in these areas provides a clear picture of the early geological history. Active extensional tec-

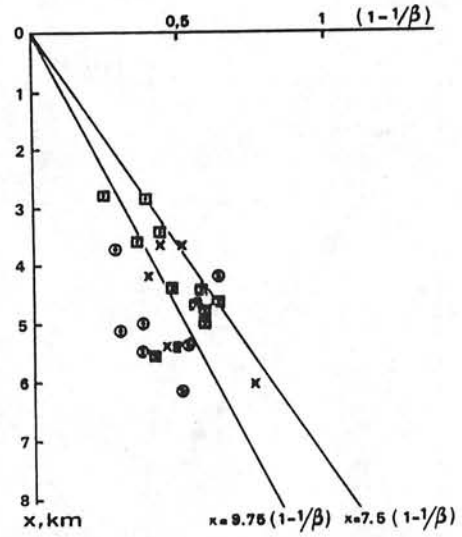


Fig. 10. Same as Figure 9 but with conservative interpretation.

tonics started sometime in late Jurassic–early Cretaceous (140 m.y. ago?) and created a faulted subsiding graben. A difficult question to answer is whether the graben progressively expanded in width as it deepened or whether the width kept constant through time. The existence of eroded summits of faulted blocks on the shallowest portion of the margin [*Montadert et al.*, 1979*a*] suggests the first part of the alternative. As the extensional zone progressed outward, new faulted blocks were created and were simultaneously progressively tilted. However, if the offsets $g$ (see (9)) on the fault planes did not progress fast enough, the outer ends of the shallowest blocks might have been raised above the erosion level. Later on, the whole graben subsided below sea level. In any case, when the oceanic crust was emplaced 120 m.y. ago, the trough had reached a depth of approximately 2.5 km, which is what is predicted by our model. At this time, active extensional tectonics ceased as the first oceanic crust accretion was occurring, and the following subsidence was purely thermal.

The fact that extensional tectonics ceased when accretion started is fairly critical. It renders rather difficult the mechanism proposed by *Bott* [1971, 1973] of hot creep of the lower crust toward the oceanic mantle which should be quite efficient after accretion has begun. If on the other hand, it is assumed that the thinning of the lower crust and lithosphere was much larger than the thinning of the upper crust during the rifting stage, then one should assume the existence of a major level of décollement between the two portions of lithosphere with quite different strain distribution patterns within both portions. In any case, *Foucher and Sibuet* [1979] have shown that thinning of the lower crust and lithosphere keeping intact the upper crust is difficult to reconcile with the measured fairly low heat flow. We conclude that the simple stretching model best accounts for the presently available data.

Figure 11 summarizes the crustal structure across the Bay of Biscay margin, based on refraction data with interpolation based on continuous two-dimensional gravity computations. According to our model, mass and consequently volume of crust are conserved. Thus it is easy to estimate the original continent limit, which is 120 km further inland than the present continental-oceanic crust limit.

Although our model is based on the data obtained in the Bay of Biscay, a 'starved' margin where the total thickness of sediments is limited, it can account for a margin which would have received a considerable amount of sedimentation both during the early phase of rifting and later during the thermal subsidence. The east American continental margin is an example of this type. Figure 12 shows, as an exercise, a possible interpretation of a profile of this margin (based on *Grow et al.* [1979]) according to this model. The limit of continental-oceanic crust and the sedimentary data used for the isostatic correction are after *Grow et al.* [1979]. It is seen that the maximum predicted initial subsidence is about 2.5 km, which is reasonable. Note that the model predicts that the initial altitude of the continent was close to the zero level before stretching started.

## IMPLICATIONS OF THE MODEL

In this section we briefly discuss some implications of the simple stretching model. However, we do not discuss here its thermal consequences concerning the distribution of radiogenic heat and the evolution of continental margin sedimentary basins [*Foucher and Sibuet,* 1979; *Christie and Sclater,* 1980; *Royden et al.,* 1980].

### *Petrological Implications*

The petrological consequences will be explored qualitatively with the constants determined for the Bay of Biscay using as a guide the estimation made by *Ahern and Turcotte* [1979] for the production and migration of the liquid phase under a mid-ocean ridge. Significant partial fusion will start when the temperature of the lithosphere-asthenosphere limit increases beyond the solidus, at a depth of 70 to 60 km corresponding to a $\beta$ of about 2. The percentage of partial fusion will first be less than 5%, and the volume of magma very small. Thus although liquid basalt has a density of 2.6 g cm$^{-3}$ and could theoretically migrate to the surface, a successful eruption is unlikely. If it occurs, it should be of the highly alkaline type.

As stretching increases and the depth of the lithosphere-asthenosphere limit decreases, partial fusion increases as well as the total volume of magma produced. Successful eruptions become more likely, and the corresponding alkalinity of the magma should tend to decrease. As $\beta$ increases beyond 3, the average depth of production of magma becomes less than 50 km, and the average percentage of partial fusion becomes at least 5 to 10%. A large quantity of magma thus accumulates below the highly fractured and thinned lithosphere. One might then expect in general the asthenosphere to break through to the seafloor as soon as the water depth is equal to or larger than the asthenosphere geoid, although locally, exceptions might occur on numerous places along the margin. As the asthenosphere is able to break through to the seafloor, most of the magma which has been produced by partial fusion in the asthenosphere, on both sides of the break, might be able to migrate laterally and escape to the surface. If this is so, a somewhat thicker than normal initial oceanic crust might be expected [*Rabinowitz and Labrecque,* 1977]. Finally, when steady state accretion is installed, the average depth of production is about 30 km, and the average percentage of partial fusion 10–15%, corresponding to a typical tholeiite.

In summary, the probability of eruptions increases as $\beta$ increases from 2 to beyond 3.2. During the rifting episode or just after, the early eruptions should be highly alkaline, but

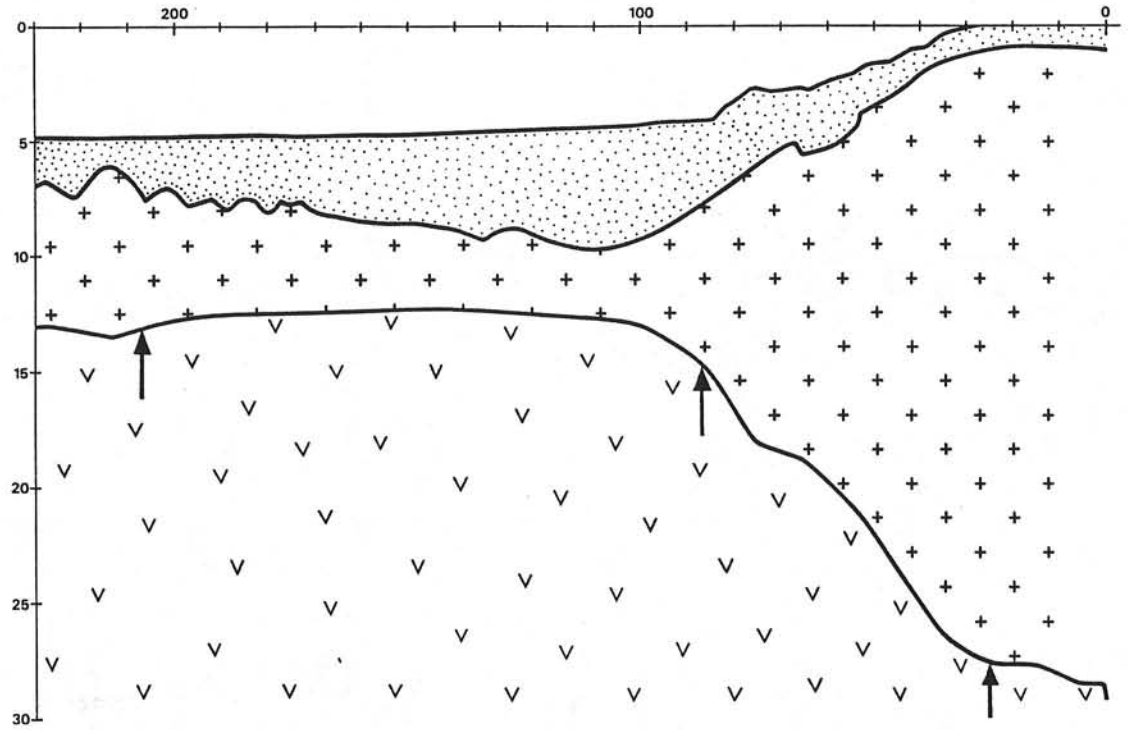


Fig. 11. Profile across the Armorican continental margin (see location in Figure 1). The sedimentary cover is dotted. The leftmost arrow marks the present oceanic crust limit; the middle arrow marks the reconstructed position of this limit before stretching, assuming no thinning beyond the rightmost arrow.

the alkalinity tends to decrease as $\beta$ increases. When the asthenosphere first reaches the seafloor, the crust first produced should still be quite alkaline and might be unusually thick. It should progressively change to a tholeiitic type and a normal thickness as steady state is reached.

The previous discussion assumes a normal temperature and homogeneous asthenosphere. If the temperature of the asthenosphere is unusually high, the percentage of partial fusion will be much higher, and tholeiitic material might be produced as soon as the magma is able to reach the surface. This is obviously the case near 'hot spots.' In addition, heterogeneities in the asthenosphere may considerably modify this highly simplified model. In any case this process could explain the presence of some magnetic anomalies of limited extension (20 km) located on the thinned continental crust of the northern Bay of Biscay, which do not correspond to associated morphological or gravimetric features [*Guennoc et al.*, 1979].

### *Roles of Nonzero Initial Elevation and of Unusual Asthenosphere Conditions*

If the asthenosphere has an abnormally high average temperature, the level of equilibrium of the zero-age oceanic lithosphere is smaller than 2.5 km and may even reach zero as in Iceland and Afar. The amount of stretching necessary to reach the steady state accretionary stage is much smaller provided the initial elevation of the continent is zero. If, on the other hand, the initial elevation of the continent is higher than sea level, due to increased continental crust thickness, but the asthenosphere has a normal average temperature, the amount of stretching necessary does not change significantly. This is because although the amount of subsidence necessary is larger, the rate of subsidence is also larger. Clearly, many variations are possible by combining anomalies of average temperature of asthenosphere with anomalies of crustal thickness. In addition, for a given thickness of crust $h_c$ the variation in the thickness of prerifting lithosphere $h_l$ introduces a large variation in the initial subsidence relation (1). As $h_l$ increases, the initial subsidence $Z_i$ decreases. On the contrary, as $h_l$ decreases, $Z_i$ increases. Thus the model can fit a very wide range of geological cases. In this paper we limit the discussion to the case described by the given constants, which is believed to account approximately for the northern Biscay continental margin.

### *Kinematics*

The present variation of thickness of continental crust across the margin directly reflects the amount of stretching during the initial phase. Figure 14 shows the variation of thickness of crust across the profiles of Figures 12 and 13. This variation is roughly linear between 26 and 5 km and can be approximated within this portion of curve by $h = 26 - x/3$ for Figure 11 (Bay of Biscay) and $h = 26 - x/7.5$ for Figure 12 (eastern North America), where $h$ and $x$ are in kilometers. Most of the stretching occurs over a present width of 60 km for the Bay of Biscay and 150 km for eastern North America before reaching maximum thinning.

Assuming this linear relation, it becomes easy to compute the initial width $X_i$ of the portion of continental margin of present width $X$. We have

$$Z = Kx$$

$$Z = 7.8[1 - (1/\beta)]$$

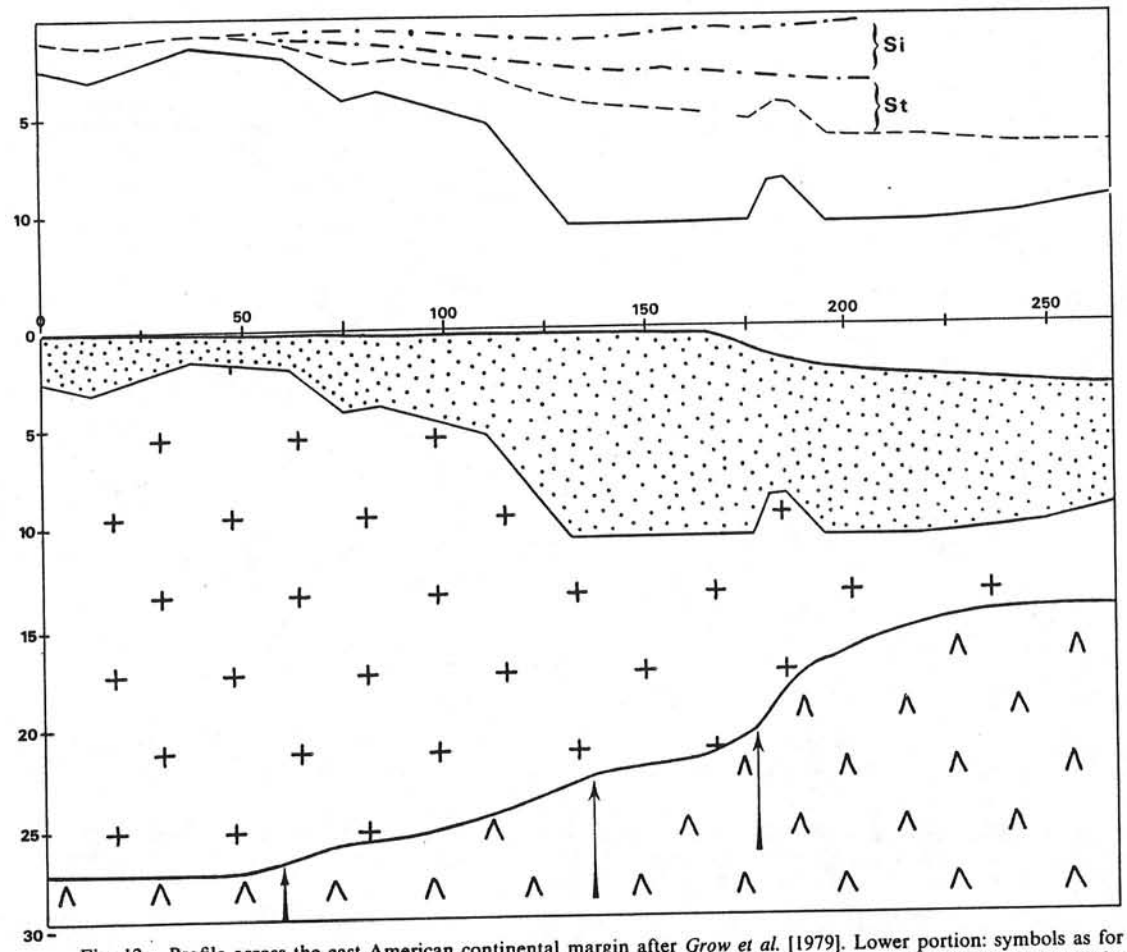


Fig. 12. Profile across the east American continental margin after *Grow et al.* [1979]. Lower portion: symbols as for Figure 11. Upper portion: the solid line is the present depth of basement, the dashed line the equivalent water depth, $S_t$ the thermal subsidence, and $S_i$ the initial subsidence based on a stretching model.

thus

$$X_i = \int_0^x (1 - kx/7.8)\, dx = X - KX^2/15.6$$

or, more generally,

$$X_i = \frac{X}{2}\left(1 + \frac{1}{\beta_x}\right) \qquad Z \leq 5.4 \text{ km}$$

taking the origin of the $x$ at the point where linear thinning of crust starts. Beyond the depth of 5.4 km, the stretching factor $\beta$ is constant and equal to 3.24; any additional $dX$ is such that

$$dXi = dX/3.24$$

It is consequently ideally possible to make an evaluation of the original width of crust before stretching, and one can, in principle, make accurate prerift continental reconstruction. This solves the difficult problem of continental fit which is otherwise untractable in detail [*Bullard et al.*, 1965; *Le Pichon et al.*, 1973].

We have seen that although the variation of thickness of crust is linear both on the Biscay margin and on the U.S. margin, there is a difference by a factor of 2.5 in the amount of thinning per kilometer between the two margins. Although one might not expect such large variations along the same margin, small variations might be expected. Let us assume for example $K = 1/10$ in one section of the margin and $1/15$ in another one. Then the widths of the basin at the time oceanic crust accretion becomes possible are $2 \times 52$ and $2 \times 78$ km, respectively. The corresponding amounts of extension are 36 and 54 km. Thus oceanic accretion may start in the first section after 36 km of extension occurred between the two plates, while continental stretching will continue in the second section until the total extension exceeds 54 km.

This may well be what happens now in the Red Sea, which is about 200–250 km wide and at the axis of which new oceanic crust is just being emplaced in the southern portion at 2000- to 2500-m depth. The southern portion, which is farther away from the pole of rotation, has been submitted to a larger amount of extension than the northern portion (see, for example, *Le Pichon and Francheteau* [1978]). Thus the northern portion is still in the continental stretching stage, while the southern portion reached the oceanic stage 3 to 5 m.y. ago. The stretching interpretation explains why the oceanic crust emplacement is not continuous at the present axis, as the distribution of strain may vary slightly according to the varying crustal strength. This interpretation is quite close to the one proposed by *Lowell and Genik* [1972]. It suggests that the stretching factor is of the order of 3 over the axial part of the Red Sea. The relatively high crustal velocities measured by

*Tramontini and Davies* [1969] might perhaps be explained by volcanic extrusives. A preliminary study shows that this model may be reconciled with the kinematic interpretation proposed for the Red Sea by *Le Pichon and Francheteau* [1978].

Another interesting kinematic consequence of this model is the existence of a special type of transform fault in the pre-accretionary extension basin (Figure 14). *Le Pichon and Hayes* [1971] and *Le Pichon and Fox* [1971] have discussed the importance of offsets in the initial break for the structuration of the margin. Such offsets are inherited from the pre-accretionary stage. In this case the sense of motion is opposite to the topographic offset, as in the classical *Wilson* [1965] transform faults. But the offset changes continuously along the fault depending on the way strain is distributed along the section. In addition, this type of transform fault may even appear where there is no offset of the initial break if strain is distributed in a different manner in two adjacent sections. Note that these offsets may reach tens of kilometers locally, as seems to be the case on the Armorican continental margin (see Figure 17 of *Montadert et al.* [1979*a*]).

The range of width of thinned continental crust basins before oceanic crust accretion starts seems to be 150 to 350 km. It is then significant that the history of mountain belts (The Alpine belt, for example) is often marked by a period of extension which creates marine basins of limited width. For example, the Triassic to Jurassic basins of the western alpine belts may not have been more than 300 km wide [e.g., *Le Pichon and Blanchet*, 1978]. These basins may thus have been entirely floored by thin continental crust, although they may have reached depths as large as 5 km by late Cretaceous time. Later shortening may have reactivated the faulted blocks as nappes 20 km wide and 2–4 km thick, whereas the portion of crust which has been stretched by ductile flow may be easily subducted. Although we cannot develop here these considerations, it is obvious that our model has predictive values for both paleogeographic and tectonic conditions. The width of the thinned continental crust basins, on the other hand, is significantly larger than the one characteristic of continental rifts. For example, in Albian time, 120 m.y. ago, just before oceanic accretion started, the Bay of Biscay was a 2.5-km-deep, 300-km-wide basin floored by stretched thin continental crust affected by very active extensional tectonics. Some limited alkaline volcanism may have affected the deepest portion of the basin. The original width of this portion of crust before stretching was probably about 150 km (Figure 11). The tectonic situation of the Bay of Biscay in early Cretaceous time is thus quite different from the one characteristic of the Rhine graben, Baïkal graben, or the African Rift valleys [*Le Pichon et al.*, 1973]. These are typically 50 to 75 km wide and have been affected by a limited amount of extension (10% for the Rhine graben). On the other hand, it can be compared to the one of the present Aegean Sea [*McKenzie*, 1978*b*; *Le Pichon and Angelier*, 1979], which is affected by extensional tectonics over a width of about 300 km with a $\beta$ of up to 2. This analogy suggests that stretching may be relatively evenly distributed in the initial stage over a wide surface, as in the Basin and Range province [*Proffett*, 1977; *Wright*, 1976], until stress release tends to concentrate itself in a narrow area, perhaps because of an effect of strain softening.

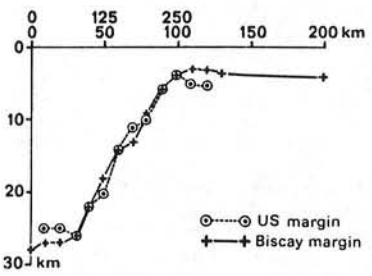


Fig. 13. Profiles of continental crust thickness against distance for the northern Bay of Biscay and northeastern U.S. continental margins based on Figures 11 and 12. The lower horizontal scale is for the Bay of Biscay, and the upper one for the U.S. margin.

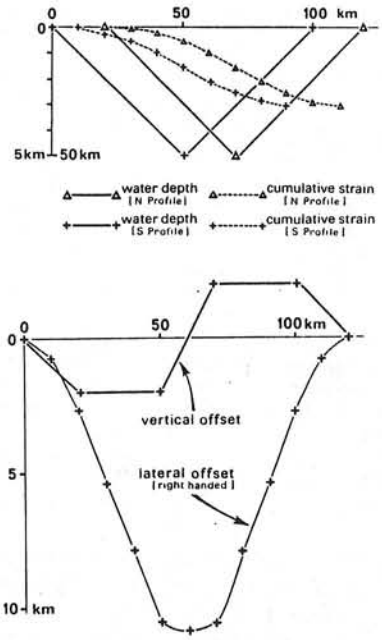


Fig. 14. Effect of an offset of a 5-km-deep rifted basin in which $Z = 0.1x$ on the lateral and vertical offsets across the fault separating the two offset portions of margin. The northern portion of margin is assumed to be right laterally offset by 20 km. (Top) The two offset bathymetric profiles are shown as well as the cumulative strain curves. (Bottom) The vertical and lateral offsets are presented.

*Dynamics*

Consequently, the concentration of strain in a relatively narrow area is the phenomenon which leads to the formation of a deep basin. An important factor in the concentration of strain is the following. Once the lithosphere has started to thin locally, a new force tends to pull material from the thicker toward the thinner lithosphere, thus increasing the extensional stresses within the rift. This force is equivalent to the ridge push force [e.g., *Souriau*, 1980] but is acting in the opposite direction because of the positive buoyancy of the lithosphere on the margin. However, because of the much steeper slope of the asthenosphere-lithosphere boundary, and consequently the much larger lateral density gradients, this force increases more rapidly with horizontal distance than on the mid-ocean ridge. Assuming that a solid lithosphere is floating on a fluid asthenosphere, the situation can be compared to a heavy liquid drop inserted within a light solid (see Figure 15). The solid tends to spread with the space occupied by the liquid. How-

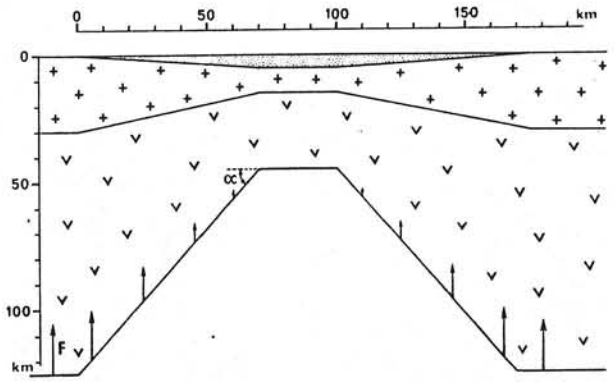


Fig. 15. Geometry of a rifted basin immediately prior to the accreting stage and corresponding distribution of the buoyancy force of the lithosphere. Note the very steep angle $\alpha$ of the asthenosphere-lithosphere boundary.

ever, if the density of the solid increases and becomes equal to the density of the liquid, the force decreases and becomes null.

In the case we are considering, the difference between the average density of the lithosphere and that of the asthenosphere is proportional to the buoyancy divided by the thickness of the lithosphere. As the water depth drops below the asthenosphere geoid (2.5 km), the buoyancy becomes negative and the total force ceases to increase but rather decreases. This may be an additional reason why thinning does not in general extend beyond this limit.

If the extensional forces which produce the overall extension cease, this gravitational force still exists. However, in the absence of overall extension its net result is a compression which tends to suppress the thinned lithospheric basin. It may be the driving force which eliminates intracontinental thinned crust basins in the later stage of evolution of mountain belts.

## CONCLUSIONS

We have presented a simple stretching model for the northern Bay of Biscay and Galicia continental margins in the northeast Atlantic. This model is based on *McKenzie*'s [1978*a*] stretching model assuming local isostasy. It is quantitative and predictive and seems to account for the available data. In particular, it explains the relationship between initial subsidence, thermal subsidence, and continental crust thinning, and it gives the reason for the transition from continental stretching to oceanic accretion.

This model has many implications which have been barely touched upon in this paper. We think that it can probably explain the evolution of most nontransform passive continental margins.

*Acknowledgments.* This paper is an obvious outcome of the IPOD Northeast Atlantic Drilling Program. It would have been impossible without the extremely high quality of the analysis of data made by many scientists. It was presented at the Wegener symposium in Berlin in February 1980, and the first author is grateful to the organizers of this meeting who initiated this study. We thank J. P. Foucher and A. Tarantola for fruitful discussions and F. Avedik, who permitted the use of unpublished refraction data on the Armorican continental margin. We thank two anonymous reviewers for useful suggestions. Contribution 695 of the Centre Océanologique de Bretagne.

## REFERENCES

Ahern, J. L., and D. L. Turcotte, Magma migration beneath an ocean ridge, *Earth Planet. Sci. Lett., 45,* 115–122, 1979.

Angelier, J., Néotectonique de l'Arc égéen, *Publ. 3,* Soc. Géol. Nord, Lille, France, 1979.

Avedik, F., and D. Howard, Preliminary results of a seismic refraction study in the Meriadzek-Trevelyan Area, Bay of Biscay, *Initial Rep. Deep Sea Drill. Proj., 48,* 1015–1024, 1979.

Bott, M. P. H., Evolution of young continental margins and formation of shelf basins, *Tectonophysics, 11,* 319–327, 1971.

Bott, M. H. P., Shelf subsidence in relation to the evolution of young continental margins, in *Implication of Continental Drift to the Earth Sciences,* edited by D. H. Tarling and S. K. Runcorn, vol. 2, pp. 675–683, Academic, New York, 1973.

Bott, M. P. H., and A. B. Watts, Deep structure of the continental margin adjacent to the British Isles, The Geology of the east Atlantic continental margin, *Rep. 70/14,* pp. 89–109, Inst. of Geol. Sci., London, 1971.

Bullard, E., J. E. Everett, and A. G. Smith, The fit of the continents around the Atlantic, Symposium on continental drift, *Philos. Trans. R. Soc. London, 258,* 41–51, 1965.

Christie, P. A. F., and J. G. Sclater, An extensional origin for the Buchan and Witchground Graben in the North Sea, *Nature, 283,* 729–732, 1980.

Foucher, J. P.,asnd J. C. Sibuet, Thermal regime of the Northern Bay of Biscay continental margin in the vicinity of DSDP sites 400 to 402, *Initial Rep. Deep Sea Drill. Proj., 48,* 289–296, 1979.

Grow, J. A., C. O. Bowin, and D. R. Hutchinson, The gravity field of the U.S. Atlantic continental margin, *Tectonophysics, 59,* 27–52, 1979.

Guennoc, P., H. Jonquet, and J. C. Sibuet, Présentation d'une carte magnétique de l'Atlantique Nord-Est, *C. R. Acad. Sci., 288,* 1011–1013, 1979.

Jarvis, J. G., and D. P. McKenzie, Sedimentary formation with finite extension rates, *Earth Planet. Sci. Lett., 48,* 42–52, 1980.

Le Pichon, X., and J. Angelier, The Hellenic arc and trench system: A key to the neotectonic evolution of the Eastern Mediterranean area, *Tectonophysics, 60,* 1–42, 1979.

Le Pichon, X., and R. Blanchet, Where are the passive margins of the Western Tethys Ocean?, *Geology, 6,* 597–600, 1978.

Le Pichon, X., and J. P. Fox, Marginal offsets, fracture zones, and the early opening of the North Atlantic, *J. Geophys. Res., 76,* 6294–6308, 1971.

Le Pichon, X., and J. Francheteau, A plate-tectonic analysis of the Red Sea–Gulf of Aden area, *Tectonophysics, 46,* 369–406, 1978.

Le Pichon, X., and D. E. Hayes, Marginal offsets, fracture zones, and the early opening of South Atlantic, *J. Geophys. Res., 76,* 6283–6293, 1971.

Le Pichon, X., J. Francheteau, and J. Bonnin, *Plate Tectonics,* vol. 6, *Developments in Geotectonics,* 300 pp., Elsevier, New York, 1973.

Lowell, J. A., and G. Genik, Sea-floor spreading and structural evolution of the Southern Red Sea, *Am. Assoc. Pet. Geol. Bull., 56,* 247–259, 1972.

McKenzie, D., Some remarks on the development of sedimentary basins, *Earth Planet. Sci. Lett., 40,* 25–32, 1978*a*.

McKenzie, D., Active tectonics of the Alpine Himalayan belt: The Aegean Sea and surrounding regions, *Geophys. J. R. Astron. Soc., 55,* 217–254, 1978*b*.

Montadert, L., D. G. Roberts, O. De Charpal, and P. Guennoc, Rifting and subsidence of the Northern Continental Margin of the Bay of Biscay, *Initial Rep. Deep Sea Drill. Proj., 48,* 1025–1060, 1979*a*.

Montadert, L., O. De Charpal, D. C. Roberts, P. Guennoc, and J. C. Sibuet, Northeast Atlantic passive margins: Rifting and subsidence processes, in *Deep Drilling Results in the Atlantic Ocean: Continental Margins and Paleoenvironment, Maurice Ewing Ser.,* vol. 3, edited by M. Talwani, W. W. Hay, and W. B. F. Ryan, pp. 164–186, AGU, Washington, D. C., 1979*b*.

Morton, W. H., and R. Black, Crustal attenuation in Afar, in *Afar Depression of Ethiopia,* vol. 1, edited by A. Pilger and A. Rösler, pp. 55–65, Schweizerbart'sche Verlagsbuchlandlung, Stuttgart, 1975.

Parsons, B., and J. G. Sclater, An analysis of the variation of ocean floor bathymetry and heat flow with age, *J. Geophys. Res., 82,* 803–827, 1977.

Proffett, J. M., Jr., Cenozoic geology of the Yerington district, Nevada, and implications for the nature and origin of Basin and Range faulting, *Geol. Soc. Am. Bull., 88,* 247–266, 1977.

Rabinowitz, P. D., and J. L. Labrecque, The isostatic gravity anomaly: Key to the evolution of the ocean-continent boundary at passive continental margins, *Earth Planet. Sci. Lett., 35,* 145–150, 1977.

Royden, L., J. G. Sclater, and R. P. Von Herzen, Continental margin subsidence and heat flow: Important parameters in formation of petroleum hydrocarbons, *Am. Assoc. Pet. Geol. Bull., 64,* 173–187, 1980.

Souriau, M., Dynamics of the lithosphere-asthenosphere system for oceanic plates, preprint, Groupe de Rech. Spatiales, Toulouse, France, 1980.

Tramontini, C., and D. Davies, A seismic refraction survey in the Red Sea, *Geophys. J. R. Astron. Soc., 17,* 225–242, 1969.

Turcotte, D. L., W. F. Haxby, and J. R. Ockendow, Lithospheric instabilities, in *Island Arcs, Deep Sea Trenches and Back-Arc Basins, Maurice Ewing Serv.,* vol. 1, edited by M. Talwani and W. C. Pitman III, pp. 63–69, AGU, Washington, D. C., 1977.

Watts, A. B., Sediment loading and its relation to the subsidence and tectonics of Atlantic-type continental margins (abstract), *Int. Geol. Congr. 26th, 3,* 1354, 1980.

Watts, A. B., and W. B. F. Ryan, Flexure of the lithosphere and continental margin basins, *Tectonophysics, 36,* 25–44, 1976.

Wilson, T., A new class of faults and their bearing on continental drift, *Nature, 207,* 343–347, 1965.

Wright, L., Late Cenozoic fault patterns and stress fields in the Great Basin and westward displacement of the Sierra Nevada block, *Geology, 4,* 489–494, 1976.

(Received May 9, 1980;
revised September 22, 1980;
accepted October 3, 1980.)

*Phil. Trans. R. Soc. Lond.* A **305**, 27–43 (1982) [ 27 ]
*Printed in Great Britain*

# The ocean–continent transition in the uniform lithospheric stretching model: role of partial melting in the mantle*

By J.-P. Foucher†, X. Le Pichon‡ and J.-C. Sibuet†
† *Centre Océanologique de Bretagne, B.P. 337, 29273 Brest cédex, France*
‡ *Université Pierre et Marie Curie, Laboratoire de Géologie dynamique, 4 place Jussieu, 75230 Paris cédex 5, France*

The role of partial melting in the uniform lithospheric stretching model of continental margin formation is explored. It is shown that the transition from continental lithosphere stretching to oceanic accretion is most probably controlled by the production of a significant amount of partial melting in the asthenosphere immediately below the lithosphere, which requires stretching factors larger than 3. It is also shown that, at stretching factors exceeding 2, the law of subsidence is significantly changed by the presence of partial melt in the underlying asthenosphere. The implications for the existence of deep continental margin basins on thinned continental crusts are examined. The Armorican deep continental margin basin is taken as an example.

## Introduction

A simple uniform stretching model of subsidence (McKenzie 1978*a*, *b*) has been applied at various continental margins (see, for example, Royden & Keen 1980; Royden *et al.* 1980; Cochran 1981; Le Pichon & Sibuet 1981). We use this model to discuss more specifically the nature and mode of transition from the stretched continental lithosphere to the accreted oceanic lithosphere. In particular, we examine whether the stretching model can account for the existence of deep continental margin basins. The Armorican deep continental margin basin is taken as an example.

The method proposed by Le Pichon *et al.* (1982) for the simple stretching model is adopted, which allows us to ignore the density stratification of the lithosphere. This is because, as a first approximation, the lithosphere is floating on top of the asthenosphere, and hence subsidence is controlled by the existence of two reference levels, one near 3.6 km and the other near 7.8 km water depth. These are the levels that would be reached by the asthenosphere in the absence of lithosphere and of formation of oceanic crust. The first one is for hot asthenosphere; the other one for asthenosphere cooled to thermal equilibrium. The instantaneous ($Z_1$) as well as the total subsidence after an infinite time ($Z_t$) can then be expressed simply as a function of the difference of elevation between the starting level and the 3.6 and 7.8 km reference levels, respectively. Thus confining ourselves for simplification to basins below water, we have

$$Z_1 = \gamma(3.6 - E)$$

and

$$Z_t = \gamma(7.8 - E)$$

where $E$ is the starting water depth, $\gamma = 1 - 1/\beta$ and $\beta$ is the stretching factor (see figures 1 and 2).

In the continental margin model discussed by Le Pichon & Sibuet (1981) and Le Pichon *et al.* (1982), the amount of stretching increases from no stretching ($\beta = 1$, $\gamma = 0$) on the continental shelf to a maximum value, $\beta_{max}$, beyond which oceanic lithosphere accretion starts. It was argued by Le Pichon & Sibuet (1981) that, although instantaneous subsidence can theoretically

* Contribution no. 754, Centre Océanologique de Bretagne.

reach a limit value of 3.6 km for infinite stretching, oceanic accretion will probably start much earlier and will be increasingly likely to occur once the water depth exceeds 2.5 km, which is the level reached by new oceanic crust at mid-ocean ridge crests. However, it was proposed that stretching may occasionally exceed the value corresponding to 2.5 km subsidence, thus producing stretched continental crust that is deeper than the adjacent oceanic crust. As a result, a deep continental margin basin will be created.

The amount of uniform stretching necessary to bring the surface of the lithosphere in isostatic equilibrium from sea level to 2.5 km water depth is 3.2 ($\gamma = 0.69$; see figure 2). It has been shown by Le Pichon & Sibuet (1981) and Le Pichon *et al.* (1982) that such large values of stretching are

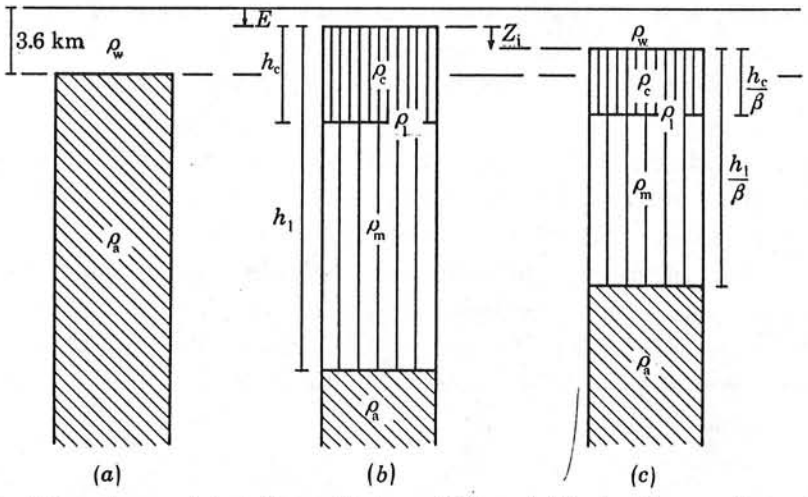


FIGURE 1. Initial stretching phase and isostatic equilibrium. Oblique hatched pattern, asthenosphere; vertical hatched pattern, lithosphere. Average densities are $\rho_a$ (asthenosphere), $\rho_m$ (mantle portion of lithosphere), $\rho_c$ (crust), $\rho_l$ (whole lithosphere), $\rho_w$ (water). (*a*) Hypothetical column with lithosphere entirely replaced by asthenosphere (which is isostatically equivalent with $\rho_a = \rho_l$). This enables definition of the reference levels (mantle geoid and asthenosphere geoid) at 3.6 and 7.8 km respectively. (*b*) Lithosphere before stretching: $h_c$ and $h_l$ are thicknesses of crust and lithosphere respectively. $E$ is the starting water depth. (*c*) Lithosphere just after instantaneous stretching by a factor $\beta$. The subsidence relative to (*b*) is $Z_i$.

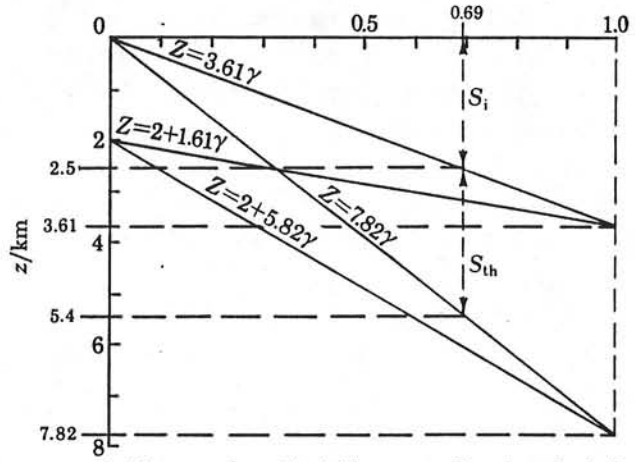


FIGURE 2. Initial instantaneous subsidence and total subsidence as a function of relative thinning of the lithosphere for two different starting elevations: 2 km above sea level and sea-level. $S_i$ and $S_{th}$ are the initial and thermal subsidences. The 2.5, 3.61 and 7.82 km levels are identified.

indeed measured on the deeper portion of the Armorican continental margin and that consequently the model could be accepted at least as a first approximation.

The reason why the transition from continental lithosphere stretching to oceanic accretion should occur for a given stretching factor $\beta$ was, however, not discussed in detail by Le Pichon & Sibuet (1981). They did mention the probable role played by the increase in the amount of partial melting as the base of the lithosphere is raised by stretching but did not try to discuss it quantitatively. That this transition does not occur randomly at widely different stretching factor values is proved by the fact that the transition from stretched continental crust to oceanic crust, where this is documented, does not seem to be marked by a significant topographic step (see, for example, Montadert *et al.* 1971*a*, *b*). Thus, it can be concluded that in general the stretched continental crust had reached a level within 500 m or less of the level of emplacement of early oceanic crust when this transition occurred. Such a coincidence is unlikely to be fortuitous and should be controlled by a physical mechanism. Small differences of 500 to 1000 m, when they occur, however, are geologically very significant since they control the existence of early deep continental margin basins. It is consequently necessary to examine the mechanisms that control the transition from the stretching mode to the accreting mode to be able to discuss possible variations at the origin of the basins. In the following, we briefly present the geology and geophysics of the Armorican deep continental margin basin, then we discuss how partial melting may be the mechanism playing the dominant role in provoking the transition from stretching to accretion. We show that taking into account this partial melting introduces significant modifications in the curves of figure 2. We then discuss the possible origin of deep continental margin basins based on this mechanism.

## The northern Bay of Biscay continental margin

Over the past 10 years, a considerable number of data have been acquired including those of *Glomar Challenger* Legs 48 and 80. The structure of the northern Bay of Biscay margin is featured by a series of horsts, graben and tilted fault blocks buried beneath a thin sedimentary cover that has been only slightly affected by post-rifting tectonics (Roberts & Montadert 1980). The fault blocks parallel to the margin occupy the area between the shelf edge and the ocean–continent boundary. They affect either the Hercynian basement in the western part of the Celtic margin (Pautot *et al.* 1976) or a pre-existing continental basin as shown by the presence of reflectors within the blocks (Montadert *et al.* 1979*a*, *b*) and the results of Hole 401 drilled in a tilted fault block (Montadert *et al.* 1979*a*). The present structure of the margin is mainly the result of a tensional phase 20–40 Ma long occurring in a submarine environment during Lower Cretaceous time (Montadert *et al.* 1979*b*; Sibuet & Ryan 1979). Le Pichon & Sibuet (1981) and Le Pichon *et al.* (1982) have shown that extensional values as large as 3 are calculated from the geometry of tilted fault blocks. The calculated amount of thinning for the brittle portion of the crust is comparable with the tinning of the whole continental crust deduced from seismic refraction measurements and required by the uniform stretching model for the whole lithosphere.

A deep margin basin, located on the thinned continental crust, is observed along the northern Bay of Biscay (figure 3) except in the western part of the Celtic margin, where the oceanic crust is directly in contact with the continental slope, a 0.5–1.0 km vertical offset being often observed. From refraction data (Avedik & Howard 1979) and density data from Leg 48, the interpreted profile of figure 3 is shown in figure 4. If the whole sedimentary cover, taken to be in local isostatic

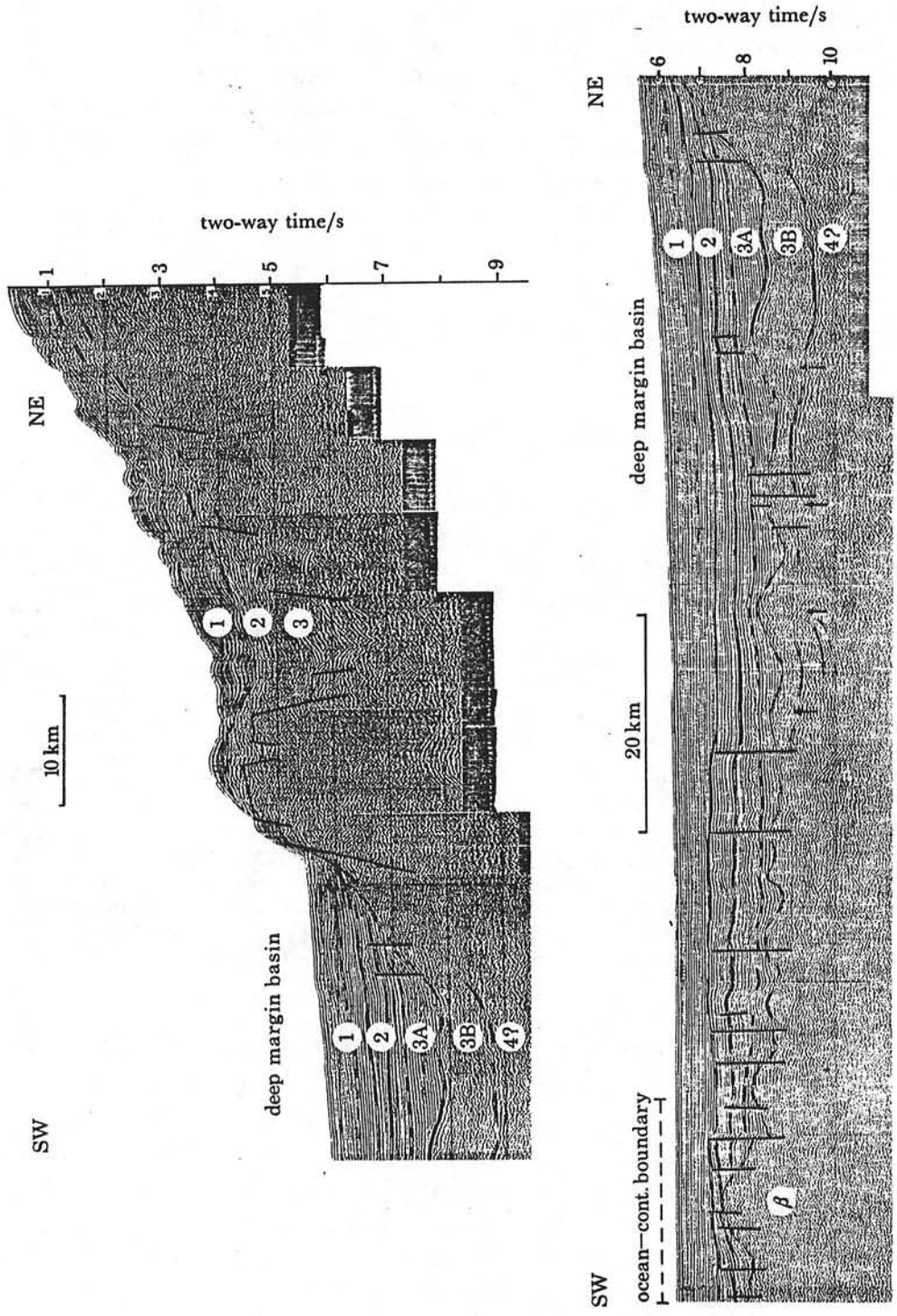


FIGURE 3. C.E.M. 017 seismic reflexion section across the Armorican margin (from Montadert *et al.* 1971*a*, *b*). The location of the seismic section is shown in the inset to figure 4. Note the rough topography of the reflector at the top of the lower sedimentary unit 3 B.

equilibrium, is removed, a slight deep-margin basin, about 0.5 km deep, remains on the thinned continental crust and is fringed by the oceanic crust or by a small dam generally less than 0.5 km high. Below the deep margin basin, the inferred thickness of the thinned continental crust, based on the interpretation of free-air anomalies in terms of local as well as regional isostatic equilibrium (Lalaut 1980), is about 3 km. This value is in agreement with the interpretation of a refraction line shot in the deep margin basin about 50 km southweastwards of the seismic section of figure 3 (Limond *et al.* 1974). In summary, the deep margin basin, located on a greatly thinned continental crust about 3 km thick, is, in the absence of sediments, a slight geological feature 0.5 km or less deeper than the adjacent oceanic crust.

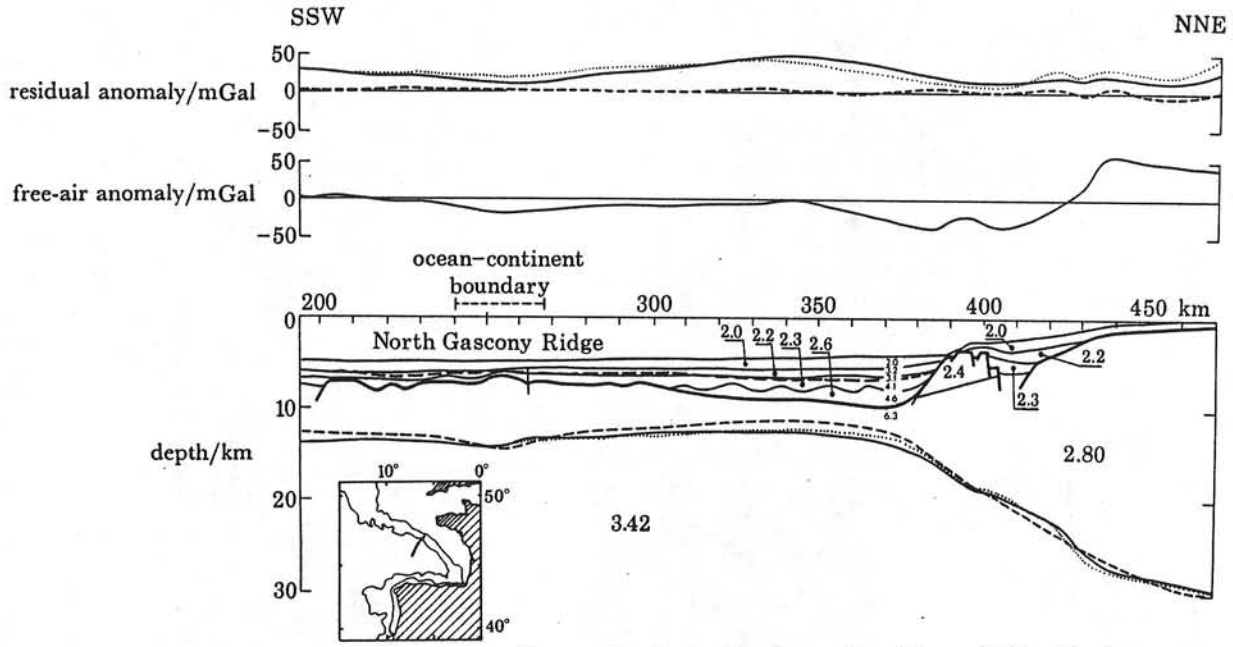


FIGURE 4. Free-air anomaly profile corresponding to the seismic reflexion profile of figure 3. Densities in grams per cubic centimetre. Oblique numbers are seismic refraction velocities (Avedik & Howard 1979). The base of the crust is obtained assuming local (solid line) and regional (dotted line, with flexural parameter $\alpha = 50$ km) isostatic equalibrium. The broken line corresponds to the best-fitting model. The position of the basement after correction for the effect of the sedimentary load is shown by a broken line.

## PARTIAL MELTING IN THE UPPER MANTLE AT LARGE STRETCHING FACTORS

The base of the lithosphere rises from $h_1$ to $h_1/\beta$ during extension by a factor $\beta$, which results in the ascent between $h_1$ and $h_1/\beta$ of hot upper mantle material at the temperature of the asthenosphere, $T_a$, which we take as the temperature at depth $h_1$ in the mantle (figure 1). At small stretching factors, the pressure drop in the ascending hot upper mantle remains insufficient to produce partial melting, which means that the ascending upper mantle does not cross its solidus. This is not so at large stretching factors when the ascending upper mantle crosses the solidus, then producing partial melting. The critical extension value $\beta_c$, beyond which the stretching process produces partial melting as well as the amount of partial melting in the upper mantle at a given stretching factor $\beta$, $\beta > \beta_c$, is primarily controlled by the law assumed to describe the dependence of partial melting on temperature and pressure in the upper mantle. Although this law is poorly

known, for discussion purposes we adopt that proposed by Ahern & Turcotte (1979) as it has a simple analytical expression:

$$f = A\{\exp[B(T - Cz - D)] - 1\}, \quad (1)$$

where $f$ is the degree of partial melting, $T$ is temperature, $z$ is depth and $A$, $B$, $C$, $D$ are constants with values given in table 1. The empirical equation (1) accounts to a fairly good approximation for the experimental data with 0.01 % water reported by Ringwood (1975) (see also fig. 2 in Ahern & Turcotte 1979). Thus, in the following section, we propose to apply the equation of Ahern & Turcotte (1979) to illustrate quantitatively how partial melting in the upper mantle varies as a function of the stretching factor $\beta$.

TABLE 1. VALUES OF PARAMETERS

| parameter | | value |
|---|---|---|
| $\rho_w$ | density of water | 1.0 g cm$^{-3}$ |
| $\rho_a$ | density of upper mantle at $T_a$ | 3.3 g cm$^{-3}$ |
| $G$ | adiabatic temperature gradient | 0.3 K km$^{-1}$ |
| $A$ | constant in (1) | 0.4 |
| $B$ | constant in (1) | $3.65 \times 10^{-3}$ K$^{-1}$ |
| $C$ | constant in (1) | $3.0 \times 10^{-5}$ K cm$^{-1}$ |
| $D$ | constant in (1) | 1100 °C |
| $L$ | latent heat of fusion | 334 J g$^{-1}$ |
| $C_p$ | specific heat | 1.05 J g$^{-1}$ K$^{-1}$ |
| $\alpha$ | thermal expansion coefficient | $3.28 \times 10^{-5}$ K$^{-1}$ |
| $\rho_{al}$ | density of melt fraction (liquid basalt) | 2.6 g cm$^{-3}$ |
| $\rho_{as}$ | density of melt fraction after solidification | $2.85 + 0.00833z$ ($z$ in kilometres; see figure 6) |

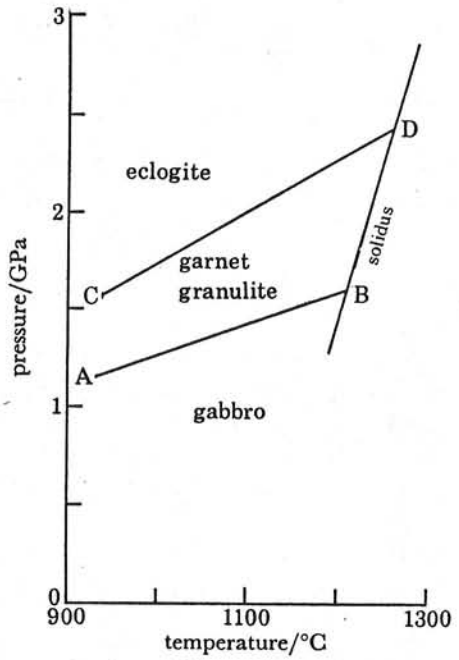


FIGURE 5. Experimental $P$–$T$ diagram showing stability fields of eclogite, garnet granulite and gabbro (from Green & Ringwood 1967). The transition from gabbro to eclogite is not sharp but occurs through a 400–800 MPa garnet granulite interval.

Given a stretching factor $\beta$ and assuming no partial melting ($\beta < \beta_c$), the initial temperature distribution is given by

$$\left.\begin{aligned} T &= (T'_a\beta/h_1)\,z \quad \text{for} \quad 0 \leqslant z \leqslant h_1/\beta \\ \text{and} \quad T &= T'_a + G(z - h_1/\beta) \quad \text{for} \quad h_1/\beta \leqslant z \leqslant h_1, \end{aligned}\right\} \tag{2}$$

with $T'_a = T_a - G(h_1 - h_1/\beta)$.

In (2) we have introduced the adiabatic temperature gradient $G$, generally ignored in previous developments of the stretching model, but which should be considered in an approach including a description of partial melting effects because of the high sensitivity of the degree of melting to small changes in temperature. This high sensitivity is illustrated by the steep slope of the solidus (figure 5).

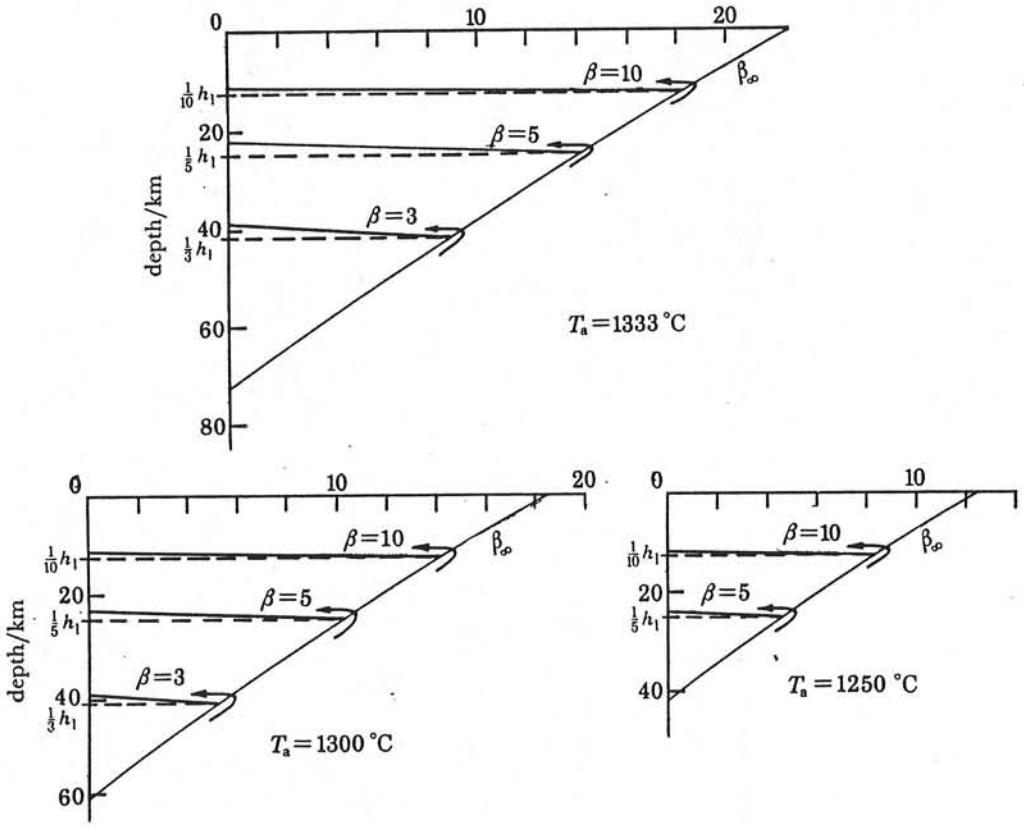


FIGURE 6. Partial melting as a function of depth at various stretching factors (3, 5 and 10) and for three different values of $T_a$, 1250, 1300 and 1333 °C.

Introducing now partial melting ($\beta > \beta_c$), equations (2) become

$$\left.\begin{aligned} T &= (T'_a\beta/h_1)\,z - fL/C_p \quad \text{for} \quad 0 \leqslant z \leqslant h_1/\beta \\ \text{and} \quad T &= T'_a + G(z - h_1/\beta) - fl/C_p \quad \text{for} \quad h_1/\beta \leqslant z \leqslant h_1, \end{aligned}\right\} \tag{3}$$

where the term $fL/C_p$ is the temperature decrease due to the extraction of latent heat of fusion, $L$ is the latent heat of fusion and $C_p$ is the specific heat capacity at constant pressure (table 1). Thus, the degree of melting, $f$, can be calculated from (1) with $T$ in (1) given by (3). The solution can be obtained from simple numerical calculations. Figure 6 displays the results obtained. Partial

melting is nearly restricted to the upper mantle underlying the stretched lithosphere. The top of the zone of melting is near $h_1/\beta$, its base is at depth $z_f$ obtained from (1), making $f$ equal to zero.

$$z_f = \frac{T_a - Gh_1 - D}{C - G} \quad \text{for} \quad \beta > \frac{h_1}{z_f}. \tag{4}$$

Through the zone of melting, the degree of melting $f$ decreases nearly linearly with depth so that to a good approximation the degree of melting $f$ is given by

$$f = f_0(1 - z/z_f), \tag{5}$$

where $f_0$ is the degree of melting in upper mantle material ascending adiabatically from the base of the lithosphere to the surface.

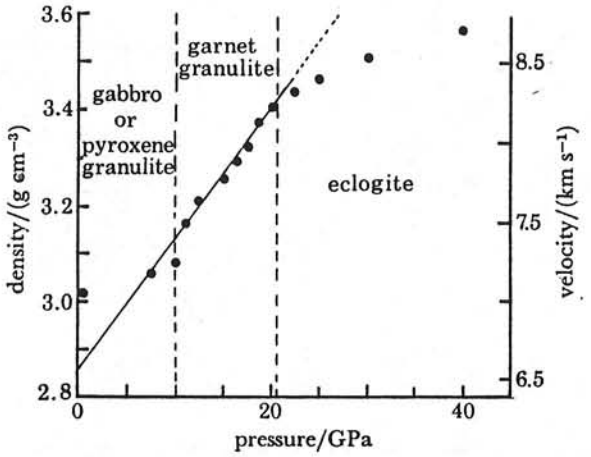


FIGURE 7. Experimental data points reported by Green & Ringwood (1967), showing the increase in density with pressure of alkali basalts. We approximate the density variation with $\rho = 2.85 + 0.00833\,z$ (solid line; $z$ in kilometres, $\rho$ in grams per cubic centimetre).

Thus, partial melting is predicted to occur as soon as the base of the stretched lithosphere is raised to $z_f$, i.e. corresponding to a critical extension value $\beta_c = h_1/z_f$.

Taking $h_1 = 125$ km and $T_a = 1300$ °C, then $z_f = 60.2$ km and $\beta_c = 2.1$. For $T_a = 1333$ °C, $z_f = 72.4$ km and $\beta_c = 1.7$. For $T_a = 1250$ °C, $z_f = 41.7$ km and $\beta_c = 3$. It will be noted that partial melting begins at relatively moderate extension values, from 1.7 to 2.1 for usually assumed temperatures at the base of the lithosphere, 1333 and 1300 °C respectively.

Equation (5) is convenient for deriving some quantities of interest to a discussion of the effects of partial melting, in particular the maximum degree of melting, $f_{max}$, which occurs at $h_1/\beta$, is given by

$$f_{max} = f_0(1 - \beta_c/\beta), \tag{6}$$

and the total equivalent thickness, $h_b$, of liquid basalt produced is given by

$$h_b = \frac{\rho_a}{\rho_{al}} \int_{h_1/\beta}^{z_f} f_0(1 - z/z_f)\,dz;$$

$$h_b = \frac{\rho_a}{\rho_{al}} f_0 z_f / 2(1 - \beta_c/\beta)^2. \tag{7}$$

From (6), taking $T_a = 1333$ °C, $f_{max}$ reaches 5 % at $\beta = 2.9$, and 10 % at $\beta = 3.1$. For $T_a = 1300$ °C, the 5 and 10 % levels are reached at $\beta = 2.9$ and 4.6 respectively. For $T_a = 1250$ °C, $\beta = 5.0$ and 16.0 respectively. Again, the high sensitivity of the results to the assumed temperature $T_a$ at the

base of the lithosphere is illustrated. However, it must be emphasized that for reasons of continuity in the application of (1) at the transitions from the stretched continental crust to the oceanic crust, the value of $T_a$ is constrained by the requirement that at $\beta$ tending to infinity the amount of liquid basalt produced by partial melting is capable of accounting for the creation of a normal 5.5 km thick oceanic crust. From (7), taking $T_a = 1333\,°C$, $h_b = 10.4\,km$ when $\beta$ tends to infinity, while for $T_a = 1300\,°C$, $h_b = 7.0\,km$, and for $T_a = 1250\,°C$, $h_b = 3.2\,km$. Thus, we suggest that realistic descriptions of the partial melting in the upper mantle in the present approach are for values of $T_a$ between 1333 and 1300 °C, the exact value depending on whether it is considered that nearly all of the liquid basalt produced migrates to the surface to form the oceanic crust, or whether only part of it is involved (Ahern & Turcotte 1979; Sleep 1974).

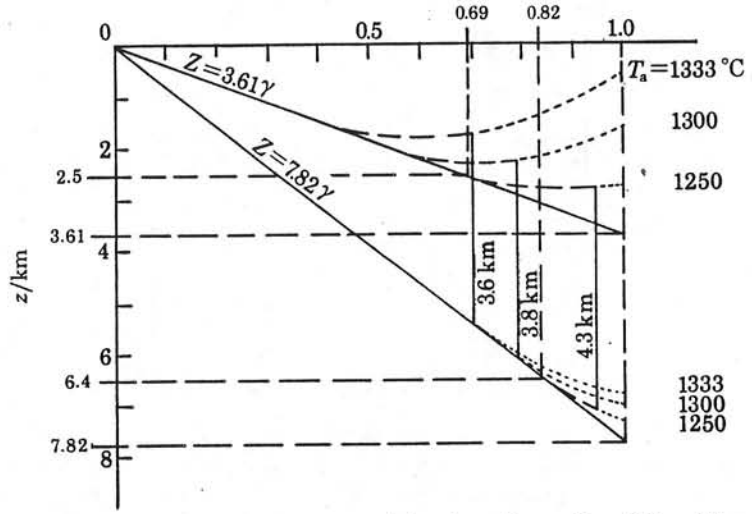


FIGURE 8. Subsidences of figure 2 (solid lines) corrected for the effects of partial melting (broken lines, then dotted lines). Broken lines are for degrees of melting less than 10 %. Dotted lines are for degrees of melting exceeding 10%. Vertical bars show the amount of thermal subsidence at $\beta$ corresponding to a degree of melting of 10%.

Further partial melting introduces significant changes in the mean density of the upper mantle, which result in considerable modifications of the subsidence curves of figure 2. If $\rho_{a1}$ is the density of the melt fraction (liquid basalt), the mean density change $\Delta\rho_1$ at $t = 0$, introduced over the whole thickness of the melting zone, i.e. from $h_1/\beta$ to $z_f$, is given by

$$\Delta\rho_1 = \frac{\int_{h_1/\beta}^{z_f} \rho_{a1} - \rho_a/\rho_{a1} f\,dz}{z_f - h_1/\beta}\,\rho_a, \tag{8}$$

which implies a correction $\Delta S_1$ ($\Delta S_1 < 0$ since $\rho_{a1} < \rho_a$) to be applied to the initial subsidence $S_1$:

$$\Delta S_1 = \frac{\rho_a}{\rho_a - \rho_w}\frac{\Delta\rho_1}{\rho_a}(z_f - h_1/\beta),$$

or

$$\Delta S_1 = \frac{\rho_a}{\rho_a - \rho_w}\int_{h_1/\beta}^{z_f} \frac{\rho_{a1} - \rho_a}{\rho_{a1}} f\,dz. \tag{9}$$

In (9) we have assumed that local isostatic conditions prevail at depth $h_1$. Similarly, if $\rho_{as}$ is the density of the melt fraction after cooling and solidification, a correction $\Delta S_\infty$ is predicted at

thermal equilibrium, which is given by

$$\Delta S_\infty = \frac{\rho_a}{\rho_a - \rho_w} \int_{hl/\beta}^{zf} \frac{\rho_{as} - \rho_a}{\rho_{as}} f \, dz, \tag{10}$$

where $\rho_{as} = 2.85 + 0.00833\, z$, taking into account the change in density due to pressure (see figure 7 and table 1).

Figure 8 shows the resulting subsidence curves after corrections have been applied by adopting numerical values in table 1. We have neglected, in the calculation of the corrections above at $t = 0$, the effects of the temperature drop $\Delta T$ due to the extraction of the latent heat of melting,

$$\Delta T = Lf/C_p,$$

which introduces a density change, $\rho_a \alpha \Delta T$, that is $\rho_a \alpha Lf/C_p$, about $0.03\, f$, adopting values in table 1. This density change can be ignored in comparison with the much larger density change $(\rho_{a1} - \rho_a)\, \rho_a/\rho_{a1} f$, about $0.9\, f$, involved in (8).

## General implications

As is seen from the previous description, and limiting ourselves to the most realistic range of cases of $T_a = 1333$ °C and $T_a = 1300$ °C within our set of assumptions, partial melting is predicted to occur in the upper mantle beginning at relatively small stretching factors, of the order of 2, then reaching 10 % at the base of the stretched lithosphere at $\beta = 3.1$ for $T_a = 1333$ °C or $\beta = 4.6$ for $T_a = 1300$ °C. Thus, a considerable amount of melt is predicted to be present in the upper mantle at moderately large values of $\beta$. We suggest that the transition from the stretching process to oceanic accretion is controlled to a large extent by the ability of the large volume of melt produced to migrate and erupt to the sea floor.

Melt migration models have been proposed to account for the segregation of an oceanic crust from a partly molten mantle at mid-oceanic ridges (see, for example, Sleep 1974; Ahern & Turcotte 1979). The first melt produced forms on grain boundary intersections (Waff & Bullau 1979), then with the amount of melt increasing, intersections become interconnected, which makes the matrix more permeable and favours migration due to the buoyancy of the melt fraction. It has been inferred from geochemical studies that migration begins above about 10 % melting at mid-oceanic ridges (Kay *et al.* 1970). A 10 % melt fraction is produced at extensions from 3.1 ($T_a = 1330$ °C) to 4.6 ($T_a = 1300$ °C), as discussed above. Such extension values may then be minimum estimates required to initiate oceanic accretion. It should be noted from (7) that, with $\beta$ increasing beyond the critical value $\beta_c$ at which partial melting begins, the volume of melt produced will increase rapidly, as illustrated by the fact that at $\beta = 2\beta_c$, one-quarter of the total volume of melt predicted at $t_\infty$ would be produced. As a result, the probability for the transition from stretching to oceanic accretion process will increase rapidly with $\beta$, which suggests that the transition will probably not occur at $\beta$ greatly in excess of the minimum estimates given above. However, it will be noted that unlike at mid-oceanic ridges the zone of melting in the stretching model does not extend up to the surface but remains confined to the upper mantle underneath the stretched lithosphere. Presumably then, migration will bring the melt material to the base of the lithosphere, where it may accumulate. Large accumulations, however, would be unstable because of the high buoyancy of the melt material. Possible mechanisms for the ascent of the melt material through the thinned lithosphere are propagation along fractures or

elastic cracks, and diapiric intrusion. The melt material could ascend and erupt rapidly to the sea floor once it has reached the base of the lithosphere. It follows that the transition to oceanic accretion would then be primarily controlled by the volume of partial melt produced in the upper mantle and its ability to migrate to the base of the lithosphere. If so, previous estimates of minimum extension values required to initiate oceanic accretion remain valid.

Important implications arise from the modified subsidence curves of figure 8, which permit a discussion of the relative subsidence of the stretched continental crust and the adjacent oceanic crust at large stretching factors, when accounting for the effects of partial melting. As is seen from figure 8, for the values of $T_a$ between 1300 and 1333 °C that we considered to be realistic, the stretched continental crust is not expected to subside below 2.5 km during extension, which means, if 2.5 km is taken as the depth of the zero age oceanic crust (Parsons & Sclater 1977), that the stretched continental crust remains shallower than the level of emplacement of the oceanic crust. This is because it is assumed that the melted portion does not solidify rapidly as long as it does not erupt to the surface to form the oceanic crust. Its cooling is controlled by the overall cooling of the lithosphere. This seems to remove the possibility that deep continental margin basins may develop on a stretched continental lithosphere deeper than the adjacent oceanic lithosphere in the early stages of oceanic accretion. Assuming that the maximum depth reached by the oceanic crust is 6.4 km (Parsons & Sclater 1977), it is also seen that the stretched continental crust remains shallower than the oceanic crust for $\beta \lesssim 5$. Further, the total amount of thermal subsidence can be inferred directly from the curves in figure 8. At the 10 % melt fraction produced at the base of the lithosphere, which we considered as a minimum degree of melting required to initiate oceanic accretion, the total thermal subsidence predicted on the stretched continental crust is 3.6 km assuming that $T_a = 1330$ °C, and 3.8 km assuming that $T_a = 1300$ °C. These values would be slighly increased for slightly higher $\beta$, but in all cases remain close to the expected thermal subsidence of the oceanic lithosphere, which is about 3.9 km. An important consequence is that no major differential vertical movements at the transition from the stretched continental crust to the oceanic crust are expected to occur during the return to thermal equilibrium after the phase of active extension.

## Extension of finite versus instantaneous duration

In the preceding discussion, we have assumed that stretching is instantaneous, i.e. no significant cooling of the stretched lithosphere occurs during the tectonic phase. Jarvis & McKenzie (1980) have shown that this is a reasonable approximation provided the duration of this tectonic phase does not exceed $60\gamma^2$ Ma for $\beta \geqslant 2$. With large stretching factors, as involved in the deeper parts of the stretched continental crust, and for a duration of extension of the order of megayears as may be realistically assumed, the cooling occurring during the tectonic phase cannot be ignored if topographic differences as small as 500 m are significant to the creation of deep basins.

Let us consider, for example, a phase of active extension $\Delta t$ Ma long. If the extension were instantaneous, the subsidence after a time $t$ would be $S_1$ plus a small portion of the thermal subsidence $S_{th}$ ($S_{th} = S_t - S_1$), which can be approximated by

$$S_t = S_1 + S_{th}(1 - e^{-t/62.8}),$$

assuming an exponential decay and a thermal time constant of 62.8 Ma for the lithosphere (Parsons & Sclater 1977). As the extension is not instantaneous, cooling starts before the end of

the tensional phase. At constant extensional rate, one might approximate the effect by taking a new time $t' = t + \frac{1}{2}\Delta t$ for computing $S_{th}$. As the stretching factor actually changes continuously from 1 to a maximum value, the effect will be about one-half and an order of magnitude estimate can be obtained by choosing $t' = t + \frac{1}{4}\Delta t$. This was checked by numerical computations by Angelier *et al.* (1982) for the Aegean sea, where $\Delta t = 13$ Ma and $\beta = 1.5$ to 2.

As a consequence, the actual curves computed in the preceding section for instantaneous stretching should be corrected at $t = 0$ by adding a term $\Delta S$ of the order of

$$S_{th}(1 - e^{-\Delta t/4\times 62.8}).$$

With $\Delta t = 20$ Ma, $S_{th} = 3900$ m and $\Delta S = 300$ m; with $\Delta t = 40$ Ma, $\Delta S = 600$ m.

Thus the subsidence curves as a function of $\gamma$ now reach a level deeper than the level of implacement of new oceanic crust because the stretched lithosphere has already began to cool when the oceanic lithosphere is emplaced. Such an effect is thus necessarily implied if the stretching is not instantaneous. Simultaneously, another mechanism, the transfer of heat by lateral conduction, also generates a relative cooling at the base of the continental slope with respect to the seaward stretched continental crust and results in the creation of a depression (Watremez 1980).

Note, on the other hand, that the effect on the amount of melting produced will be much smaller and can probably be neglected. This is because cooling by conduction from the surface is unable to penetrate deep to the lower boundary of the lithosphere, below which most of the melting occurs. Consquently, if the transition to accretion is controlled by the amount of partial melting, it will occur at the same value of $\beta$ but for a larger subsidence; thus a basin can be created. This difference of level will disppear progressively with time as cooling proceeds, but the basin may be preserved if it has been loaded with sediments.

## Application: the origin of the deep Armorican basin

As seen previously, if our density estimates are correct, a slight unloaded basin 0.5 km deep exists on the greatly thinned continental crust of the deep Armorican margin. The boundary of the basin is marked by a little basement offset 0.5 km high in the vicinity of the ocean–continent transition. The uniform stretching model, including the effects of partial melting, accounts for the formation of an early basin if we include the effect of an extensional phase about 40 Ma long. However, this model does not explain that, at infinite time and after isostatic correction, the basement depth appears to be larger than that of the oceanic crust.

At this point, it should be noted that the law of partial melting in the mantle is poorly known and that, in any case, it is extremely sensitive to variations in temperature. Thus, one could obtain rather different results with relatively slight changes in the physical parameters. Further, we have not taken into account the compressibility of the melted portion. Stolper *et al.* (1981) argue that because the compressibility of basaltic melt is much higher than that of mantle minerals, the density contrast between melt and the solid phase should decrease with increasing source region depth. This effect would tend to increase the likeliness of formation of deep early basins on thinned continental crust.

On the other hand, if the igneous crust is indeed only 3 km thick, this model cannot account for such a large extension factor ($\beta = 10$). A possible explanation, compatible with the stretching

model, could then be that the Neocomian phase of extension affected a pre-existing basin (the double rifting phase model).

Montadert *et al.* (1979*a*, *b*) have clearly shown the existence of such a pre-existing basin on the Celtic margin northwest of the Meriadzek Terrace, for example, at Site 401 (Montadert *et al.* 1979*a*), which was drilled in 2500 m water depth through a tilted fault block, where the existence of a shallow water Jurassic carbonate platform is suggested. On the other hand, several authors (e.g. Winnock 1971; Dardell & Rosset 1971; Mattauer & Séguret 1971; Olivet 1978) have proposed that the Permian to Lias tensional phase led to the formation of a depression partly filled with Jurassic sediments along the present day Northern Bay of Biscay margin. Without entering into a debate about the nature and origin of the lowest sedimentary layer identified as 3 B on figure 3 and in which velocities of 4.4 km $s^{-1}$ (Bacon *et al.* 1969) and 4.6 km $s^{-1}$ (Avedik & Howard 1979) have been found, we suggest that, at the level of the Armorican margin, this layer 3 B could correspond to the infilling of a pre-existing depression that has been stretched during the Neocomian phase. If the thickness of the continental crust is reduced to 3 km beneath the deep Armorican Basin, an explanation could be that this portion of the crust has been stretched twice by a global stretching factor reaching 10. In that case, if the interval between the two phases of extension is long enough to cool the lithosphere sufficiently, the base of layer 3 B after the second tensional episode should be at a depth greater than that of the new oceanic crust emplaced at 2.5 km deep, more or less at the level of the top of the stretched sediments. The resulting basin would consequently be created at the end of the second tensional phase, the newly emplaced oceanic crust acting as a dam for already emplaced sediments.

## Conclusion

Adopting the simple analytical expression proposed by Ahern & Turcotte (1979) for the degree of partial melting in the mantle as a function of temperature and depth, we have determined the amount of partial fusion produced in the formation of a continental margin by using the uniform lithospheric model. Although the law is poorly known and is highly sensitive to slight changes in the physical parameters, our study demonstrates the importance of this phenomenon and indicates that the transition from stretching to accretion most probably occurs once the amount of melt produced in the asthenosphere below the stretched lithosphere becomes large enough.

Using an adiabatic temperature of 1262.5 °C (actual temperature 1300 °C) and 1295.5 °C (actual temperature 1333 °C) at the base of the 125 km thick lithosphere before thinning, we have derived the corrected curves of subsidence. As long as the melt does not migrate to the surface to form the oceanic crust, it will cool very slowly within the lithosphere and consequently will take several tens of megayears to solidify completely. Thus, the difference of density between liquid and solid phases leads to a smaller subsidence, the difference in the initial subsidence being several hundred metres, depending on the actual amount of stretching reached. Melting begins at a stretching factor of about 2 and becomes significant (maximum of 10 %) at a stretching factor of 3–4. Thus it is at this large stretching factor that the transition to oceanic crust becomes possible.

A significant feature of the new curves of subsidence is that the thinned continental lithosphere, in the initial subsidence stage, is always shallower than new oceanic lithosphere. However, as the process of extension is not instantaneous but takes several tens of megayears, cooling has already

affected the thinned continental lithosphere when accretion starts. As a result, the depth reached may be larger than the depth of the mid-ocean ridge and a deep continental margin basin may thus exist in the initial stage of sea-floor accretion. However, the difference of elevation should progressively disappear with age, although sedimentary loading will maintain the depressed basement.

Although this study was initiated to explain the presence of the deep Armorican continental margin basin, the process just described does not seem to be able to explain it. This is because the crust of the basin appears to be extremely thin according to gravity estimates (3 km, requiring $\beta = 10$). Such a large thinning, if it is confirmed, may perhaps be explained within the framework of this model by a double-rifting stage.

N. Guillo-Uchard and A. Grotte helped with the preparation of the paper and illustrations.

## References (Foucher *et al.*)


Ahern, J. L. & Turcotte, D. L. 1979 *Earth planet. Sci. Lett.* **45**, 115–122.

Angelier, J., Lyberis, N., Le Pichon, X., Barrier, E. & Huchon, P. 1982 *Tectonophysics* (In the press.)

Avedik, F. & Howard, D. 1979 *Init. Rep. D.S.D.P.* **48**, 1015–1024.

Bacon, M., Gray, F. & Matthews, D. H. 1969 *Earth planet. Sci. Lett.* **6**, 377–385.

Cochran, J. R. 1981 *J. geophys. Res.* **86**, 263–287.

Dardell, R. A. & Rosset, R. 1971 In *Histoire structurale du Golfe de Gascogne* (ed. J. Debyser, X. Le Pichon & L. Montadert), vol. 4, pt 2, pp. 1–28. Paris: Éditions Technip.

Green, D. H. & Ringwood, A. E. 1967 *Contr. Miner. Petr.* **15**, 103–190.

Jarvis, J. G. & McKenzie, D. P. 1980 *Earth planet. Sci. Lett.* **48**, 42–52.

Kay, R., Hubbard, N. & Gast, P. 1970 *J. geophys. Res.* **75**, 1585–1613.

Lalaut, P. 1980 Thèse de 3ème cycle, Université Pierre et Marie Curie, Paris (131 pages.)

Le Pichon, X. & Sibuet, J.-C. 1981 *J. geophys. Res.* **86**, 3708–3720.

Le Pichon, X., Sibuet, J.-C. & Angelier, J. 1982 In *A.A.P.G. Proceedings of the Hedberg Conference, Galveston,* January 1981. (In the press.)

Limond, W. Q., Gray, F., Grau, G., Fail, J. P., Montadert, L. & Patriat, P. 1974 *Earth planet. Sci. Lett.* **23**, 357–368.

McKenzie, D. 1978*a* *Earth planet. Sci. Lett.* **40**, 25–32.

McKenzie, D. 1978*b* *Geophys. Jl R. astr. Soc.* **55**, 217–254.

Mattauer, M. & Séguret, M. 1971 In *Histoire structurale du Golfe de Gascogne* (ed. J. Debyser, X. Le Pichon & L. Montadert), vol. 4, pt 4, pp. 1–24. Paris: Éditions Technip.

Montadert, L., Damotte, B., Delteil, J. R., Valéry, P. & Winnock, E. 1971*a* In *Histoire structurale du Golfe de Gascogne* (ed. J. Debyser, X. Le Pichon & L. Montadert), vol. 3, pt 2, pp. 1–22. Paris: Éditions Technip.

Montadert, L., Damotte, B., Fail, J. P., Delteil, J. R. & Valéry, P. 1971*b* In *Histoire structural du Golfe de Gascogne* (ed. J. Debyser, X. Le Pichon & L. Montadert), vol. 6, pt 14, pp. 1–42. Paris: Éditions Technip.

Montadert, L., Roberts, D. G., de Charpal, O. & Guennoc, P. 1979*a* *Init. Rep. D.S.D.P.* **48**, 1025–1060.

Montadert, L., de Charpal, O., Roberts, D. G., Guennoc, P. & Sibuet, J.-C. 1979*b* In *Deep-drilling results in the Atlantic Ocean: continental margins and paleoenvironment* (ed. M. Talwani, W. W. Hay & W. B. F. Ryan) (Maurice Ewing series, vol. 3), pp. 164–186. Washington, D. C.: American Geophysical Union.

Olivet, J. L. 1978 Thèse de Doctorat d'État, Université de Paris 7. (200 pages.)

Parsons, B. G. & Sclater, J. G. 1977 *J. geophys. Res.* **82**, 803–827.

Pautot, G., Renard, V., de Charpal, O., Auffret, G. A. & Pastouret, L. 1976 *Nature, Lond.* **263**, 669–672.

Ringwood, A. E. 1975 *Composition and petrology of the Earth's mantle.* McGraw-Hill. (618 pages.)

Roberts, D. G. & Montadert, L. 1980 *Phil. Trans. R. Soc. Lond.* A **294**, 97–103.

Royden, L. & Keen, C. E. 1980 *Earth planet. Sci. Lett.* **51**, 343–361.

Royden, L., Sclater, J. G. & von Herzen, R. P. 1980 *Bull. Am. Ass. Petrol. Geol.* **64**, 173–187.

Sibuet, J.-C. & Ryan, W. B. F. 1979 *Init. Rep. D.S.D.P.* **47** B, 761–775.

Sleep, N. H. 1974 *Bull. geol. Soc. Am.* **85**, 1225–1232.

Stolper, E., Walker, D., Hager, B. H. & Hays, J. F. 1981 *J. geophys. Res.* **86**, 6261–6271.

Waff, H. S. & Bulau, J. R. 1979 *J. geophys. Res.* **84**, 6109–6114.

Watremez, P. 1980 Thèse de 3ème cycle, Université de Bretagne Occidentale. (108 pages.)

Winnock, E. 1971 In *Histoire structurale du Golfe de Gascogne* (ed. J. Debyser, X. Le Pichon & L. Montadert), vol. 4, pt 1, pp. 1–30. Paris: Éditions Technip.

*Discussion*

D. G. ROBERTS. It is difficult to estimate the amount of extension in an area. To carry out this type of investigation you need migrated seismic sections with very good control on the interval velocities, as well as refraction control. To estimate the extension we have concentrated on those blocks where we can see the basement reflexion. The values of the extension ($\beta$) that we obtain vary from about 1.1 to 1.45. The block to the west of the one that Foucher showed has extended by 1.45, and the basement reflexion is clear. But it is by no means straightforward to interpret the section, and the value obtained for the extension depends on your assumptions about the geometry of the faulting.

J.-P. FOUCHER. Why I explained in some detail how we obtained our estimates of the extension was to answer some of the points that Roberts has raised. The estimates in question were all obtained from the interpreted seismic section of Montadert *et al.* They are the measured ratios between the present total length of the profile and the lengths of different layers. Where the geometry is ambiguous we have used the minimum amount of extension.

P.-Y. CHÉNET. Dr Foucher has remarked that the estimate of the amount of extension obtained from the shallow brittle deformation differs from that at depth. In the Meriadzek–Trevelyan region it is about 1.5 near the surface and increases to 2 at a depth of 6–8 km. I have obtained the same values for the same blocks, which is encouraging. But Dr Foucher said that this difference should be produced by greater brittle deformation at the shallow levels. This would mean a thinning of the upper layers by about 30 % by brittle failure, and none at depth. I have never seen an outcrop that shows 30 % thinning produced by internal deformation. I think a more reasonable model is one in which the extension throughout is about 1.5, which is taken up by brittle failure at shallow depths and by creep at deeper levels. The creep may cause lateral offsets in deep layers and therefore may be responsible for the difference between the extension determined from the geometry of shallow and deep layers respectively.

A. W. BALLY. I should like to comment on the cross section showing layers marked A to D. Judging from the slide, it looks as if the cross section is not balanced, since the length of layer A appears to be much longer than that of layer D. Balanced cross sections have served as useful approximations in the reconstruction of folded belts. The same method can be used on sections displaying normal faulting. Thus you can only speculate that layer A has been thinned. Such thinning would prevent you from making an accurate estimate of the extension, if you do not know what the original thickness of the layer was.

J.-P. FOUCHER. As I said, if you wish to balance the cross section you have to allow layer A to have been thinned by internal deformation. I agree that this introduces some difficulty in measuring the extension from the geometry of the uppermost strata, which we assume in our interpretation to have been disturbed.

A. W. BALLY. But then the reasoning may be circular. First you draw a cross section that is not balanced, then you conclude that because the section is not balanced, stretching must occur. However, you cannot show which layers have been thinned during the extension and which other layers have not. Also, there is no way that such thinning can be detected on the reflexion section only.

J.-P. Foucher. It seems to us reasonable to assume that the uppermost layers could deform during the gliding of the blocks to their present position, especially if these layers were poorly consolidated, as seems likely. The available seismic data do not permit the detection of such small-scale deformation, though field observations support this interpretation. Clearly, when measuring extension, care should be taken to measure it over the whole thickness of the brittle layer, and not just over the uppermost layer, which is often disturbed.

E. R. Oxburgh, F.R.S. It is only possible to carry out the type of reconstruction shown in both of the previous papers if the sections are obtained normal to the strike of the faults. There has recently been considerable debate on how the Bay of Biscay opened, and it is not yet generally agreed in what direction the relative motion occurred. I would therefore like to ask the authors of both papers how well they can constrain the strikes and the dips of the faults in the region? If these constraints are not good, then the types of calculations that they have described may only put rather broad limits on the amount of extension.

D. G. Roberts. There is a very great deal of seismic data available in the area, and as far as possible the lines have been run normal to the faults separating the blocks. We believe that a more important source of error is the absence of accurate seismic velocities. It is not possible to estimate the extension until the diffractions have been removed and the time section converted into a depth section by using the interval velocities. Since the dip of both the faults and the blocks is controlled by the velocities used in this conversion, the extension estimates are dependent on accurate velocities.

Sir Peter Kent, F.R.S. One of the maps shows a considerable amount of dip faulting, as well as strike faulting, which presumably makes extension estimates even harder to obtain.

D. G. Roberts. On the floor of the Bay of Biscay and close to the ocean junction between the ocean and the continent there are a number of inversion structures related to the late stages of the Pyrenean orogeny in the Eocene and Oligocene. One of the sections clearly shows such a inversion on the ocean side of the continental ocean boundary. In making estimates of the extension we have tried to avoid such places and have concentrated on those areas dominated by listric normal faults. For this reason we chose to carry out the experiment west of the Trevelyan Escarpment because of the clear evidence of inversion there in the Eocene and Oligocene.

P.-Y. Chénet. I believe that it is important to test whether a simple stretching model, with the same extension at all depths, can produce the main features of this continental margin. I do not believe that it can account for the observed geometry of the listric normal faults, and think that we need a model with at least two layers, each of which undergoes different amounts of extension.

J. F. Dewey. I do not believe that it is possible to use the geometry of the listric faults alone to make accurate estimates of the amount of extension. Where such features have been studied in the field, there is clear evidence for a considerable amount of internal deformation within the blocks on either side of the faults, by movement on joint planes, faults, fissures and other processes, none of which would be visible on a seismic record, and all of which would contribute to the strain.

D. G. Roberts. I agree that such processes would not be visible on a seismic section, which can only resolve the large structures. But none the less the estimates of extension that we have obtained are considerably smaller than those obtained by Le Pichon and Sibuet using the same seismic lines. In any case our values are maximum ones.

J. F. DEWEY. But I do not believe that it is possible to use the geometry of the brittle faulting of the upper part of the crust to make accurate estimates of the extension. All that such studies can provide is a lower limit on the amount of extension. A better way to estimate the extension is to use the change in crustal thickness, which avoids the problems caused by internal deformation of the sediments.

M. H. P. BOTT, F.R.S. It is only possible to stretch the upper crust by jointing by about 5 % before the density becomes too low to be compatible with the gravity observations. But this is far from the 100 % required to make the geometric deformation compatible with the crustal thinning.

J. F. DEWEY. But this argument does not apply if the holes are filled with carbonate or some other cement!

J. A. JACKSON. Another type of observation that is relevant to Dewey's suggestion is the observed strain release following large normal faulting earthquakes. Though many small aftershocks occur within the blocks on either side of the main fault plane, the displacements involved in these shocks are small compared with that on the main fault plane. These observations suggest that the internal deformation occurs because of the geometry of the main fault.

If the dip of the main fault changes with depth, motion can only occur if the blocks on one or other side deform internally. But there is no seismic evidence that this internal deformation makes an important contribution to the total strain.

M. F. OSMASTON. The lithosphere-stretching hypothesis, discussed in both the preceding papers to account for the observed faulting, has the essential property that the duration of lithosphere stretching at depth must exactly match the period or periods of apparently extensional surface faulting. If the latter were to occur without the former, even for a short time, décollement of fault slices would be implied and this would put in question whether *any* of the faulting is a measure of lithosphere stretching. A duration of stretching from the Triassic until some time in the Cretaceous seems plate-tectonically unlikely; so too would be a continuance of stretching after the locus of ocean floor genesis had moved away from the margin. Therefore, how precisely at present can one define the period or periods of apparent extensional faulting and how does the date of its final cessation compare with independent evidence of the age of the ocean floor at this margin?

D. L. TURCOTTE. There are two other mechanisms of thinning crust that have received rather little attention today. The first is uplift followed by erosion. There is no doubt that this process has recently occurred along the East African rift system, where there is also evidence of crustal thinning. Presumably this region will later subside to form a basin. The other possibility is that phase changes occur in the lower crust. It is important that these alternatives to the crustal stretching model should continue to be discussed.

# Subsidence and Stretching

**Xavier Le Pichon**
**Jacques Angelier**
*Université Pierre et Marie Curie*
*Paris, France*

**Jean-Claude Sibuet**
*Centre Océanologique de Bretagne*
*Brest, France*

**We present a new formulation of McKenzie's simple uniform stretching model that is based on two reference levels, one near 3.6 km and the other near 7.8 km below sea level. In the absence of lithosphere, the asthenosphere would reach these levels if no oceanic crust were formed. The first level is for hot asthenosphere, the other is for asthenosphere cooled to thermal equilibrium. The instantaneous motion as well as the total vertical motion, produced by uniform stretching of the lithosphere, is expressed simply as a function of the elevation difference between the starting level and respectively the 3.6 and 7.8 km reference levels. In addition, we show that the behavior of the lithosphere under extensional strain is different above and below the 2.5 km-deep asthenosphere geoid. Below this level, oceanic accretion starts rapidly; above it, extensive thinning of the lithosphere produces subsidence until the asthenosphere geoid level is reached, enabling the asthenospheric material to break through to the surface. At low strain rate, pieces of the lower lithosphere may detach and sink in the asthenosphere. This process results in uplift and is taken into account in the formulation proposed.**

This paper, following an earlier and shorter presentation made elsewhere (Le Pichon, Angelier, and Sibuet, 1982),presents and discusses a new formulation of the simple uniform stretching model of subsidence proposed by McKenzie (1978a, 1978b). The main advantage of McKenzie's model is its simplicity, which leads to a simple formulation and the use of a minimum number of parameters. We demonstrate that as the lithosphere, to a first approximation, is floating on top of the asthenosphere, the subsidence is controlled by the existence of two reference levels, one near 3.6 km and the other near 7.8 km water depth. That subsidence can be expressed as a function of the difference of elevation between the starting level and the reference levels.

To apply these models to active extensional areas, it is necessary to demonstrate that extensions as large as those predicted by the model do exist in the upper part of the crust. The model was first developed for the Aegean area by McKenzie. There, the surface extension produced by normal faulting is in fair agreement with the extension predicted by the model (Angelier, 1979; Le Pichon and Angelier, 1981; Angelier, 1981). However, the largest measured coefficient of surface extension $\beta$ is only 1.4 to 1.5. The areas presumably affected by larger extension lie under water, where adequate field observations have not been made. Even in these submerged areas, the predicted $\beta$ is generally smaller than 2.

The model has since been applied quite successfully to the formation of passive continental margins by Royden, Sclater, and von Herzen (1980) and Royden and Keen (1980). There, the predicted extension exceeds 3 in the deepest portions; the sedimentary thickness is too large to check whether such a large extension does indeed exist within the upper crustal layer. Le Pichon and Sibuet (1981) have independently applied this model to the Armorican continental margin. Using data of Montadert et al (1979a, 1979b), they made a quantitative analysis of the extension within the upper brittle layer and showed that it is compatible to a first approximation with the uniform stretching model. However, using the same data, Montadert et al (1981) made much lower estimates of the

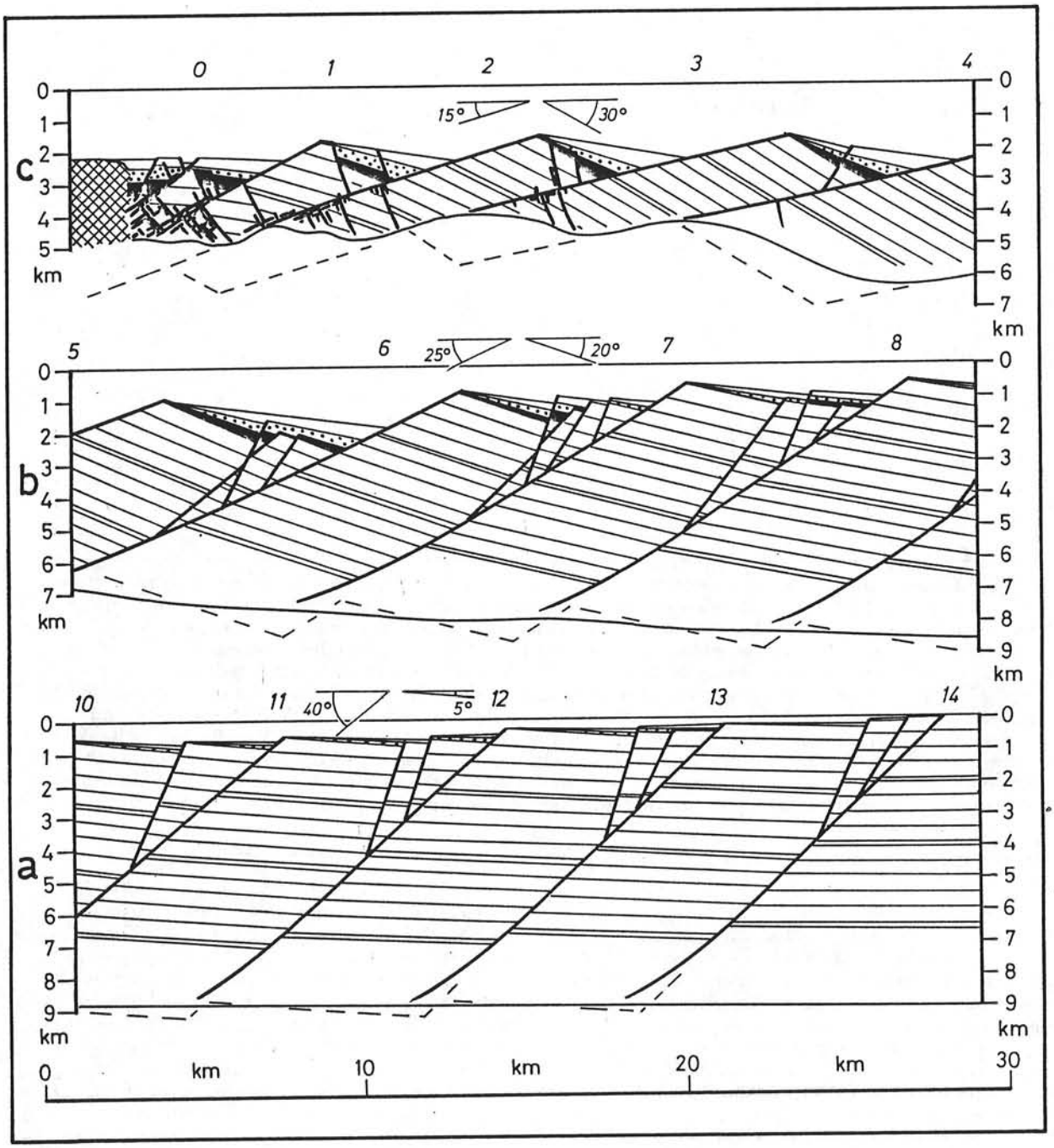


**Figure 1** — Simplified geometric model of a continental margin, based on the interpretation of the Armorican margin by Le Pichon and Sibuet (1981), without vertical exaggeration. The volume remains constant during extension. Plastic deformation may occur only in the lower layers (in white), whereas upper layers (stratified) are faulted. Different parts of the margin from the continent toward the ocean are shown as *a*, *b*, *c*, with increasing extensional rates. Faults are plane, except for their lower part where plastic deformation occurs. As the tilt of blocks slightly increases from continent to ocean, the existence of steeper normal faults is geometrically indispensable. Together with the lower parts of main faults, these faults may resemble concave listric faults. The deformation is more complex in *c*. The thinning is increased by the interfingering of the two sets of normal faults with opposite dips. In addition, oceanic crust is created where $\beta$ is greater than 3.3.

upper crustal extension. It is consequently necessary to discuss estimates by Le Pichon and Sibuet before going further.

## EXTENSION WITHIN THE UPPER CRUSTAL LAYERS

Figure 1 is a theoretical model without vertical exaggeration proposed by Le Pichon, Angelier, and Sibuet (1982) on the basis of the interpretation of the Armorican continental margin of Le Pichon and Sibuet. This model illustrates the main features of their interpretation. The faulting pattern can be compared to a pack of cards resting at an angle on a plane, with each card (tilted block) forming a slight angle with the preceding one. The two critical factors are the original angle ($\alpha$) of the fault plane with the bedding plane and the angle ($\theta$) of tilting of the bedding plane. If the height of the two blocks is the same, then this equation is true:

$$\beta = \frac{\sin \alpha}{\sin (\alpha - \theta)}$$

In the lower portion of the northern Bay of Biscay continental margin, $\alpha$ and $\theta$ are remarkably constant when measured on the largest best defined blocks (Montadert et al, 1979a, 1979b).

Le Pichon and Sibuet obtain $\alpha \sim 45°$, $\theta \sim 30°$, thus $\beta \sim 2.7$; this is close to the value predicted by the simple stretching model.

The proposed model is valid if the tilted blocks are contiguous and share the same fault plane. If they are not, much lower extension factors may be measured. It becomes very difficult to explain why the blocks are tilted in such a uniform manner if they do not share common fault planes. Clearly, then, the pack of cards model does not work and each block must be tilted independently of the others. Le Pichon and Sibuet discussed the fact that this model is substantiated by Morton and Black (1975) in the Danakil and Aisha areas near Djibouti and by Proffett (1977) in the Basin and Range province. There, contiguous fault blocks which have been tilted in the pack of cards manner result in extension factors as large as 3.

In contrast to a pack of cards, voids are not permitted so that the increase in $\theta$ from one block to the other, as the process begins, is accommodated by deformation through additional conformal normal faulting as shown in Figure 1 where an extension factor larger than 3 is obtained in this manner at the base of ther continental margin. This phenomenon reduces the apparent fault offset and tends to bias the estimate of surface extension toward lower values when they are based on actual measurements of the original length of the surface layer. In a zone of extension of this type, it is more reasonable to expect the deformation to be absorbed by extension in the upper surface layer than by compression in the lower ones. And this is what is observed in the field (Angelier, 1979). We believe that this is the origin of the discrepancy between Le Pichon and Sibuet estimates of $\beta$ and those made by Montadert et al. (1979a, 1979b, 1981). Since the difference in estimates is very large we will discuss it in more detail on the single migrated section published to date by Montadert et al, which served as the type example to Le Pichon and Sibuet.

## TYPE-SECTION OF THE ARMORICAN MARGIN

Figure 2 is the interpretation of the seismic section through the Armorican margin published by Montadert et al (1979a). To estimate the extension, we need to correlate the geological horizons throughout the section. We did this by correlating two levels of reflectors, shown shaded in Figure 1, on the basis of acoustic similarities suggested by the Montadert et al

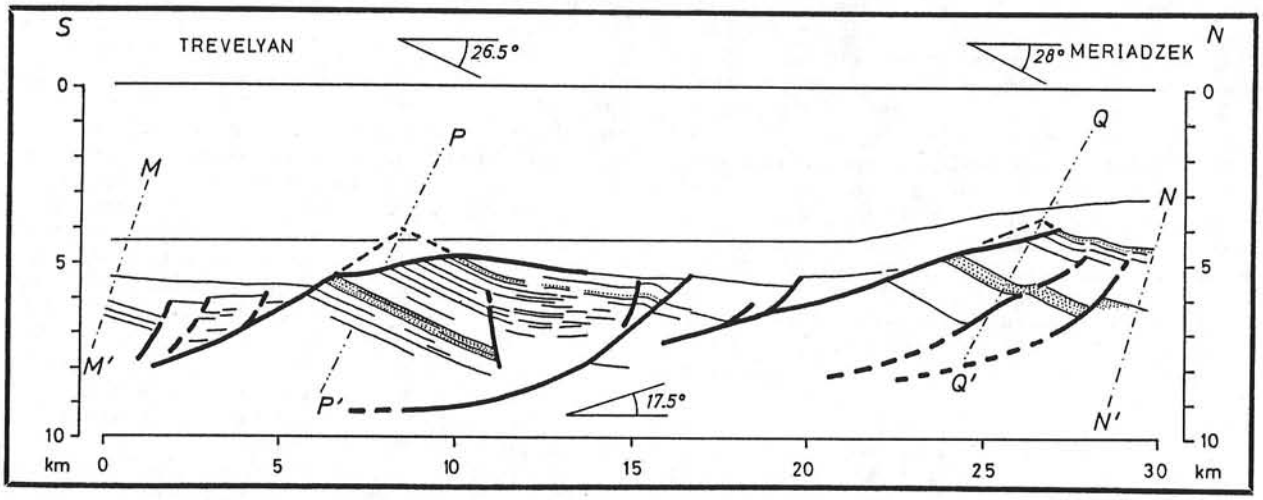


**Figure 2** — Geological cross section through tilted blocks of the Armorican margin based on a migrated seismic profile. The interpretation was published by Montadert et al (1979a). Two equivalent stratigraphic levels are shaded. The angles of tilting and of the major fault plane are also indicated.

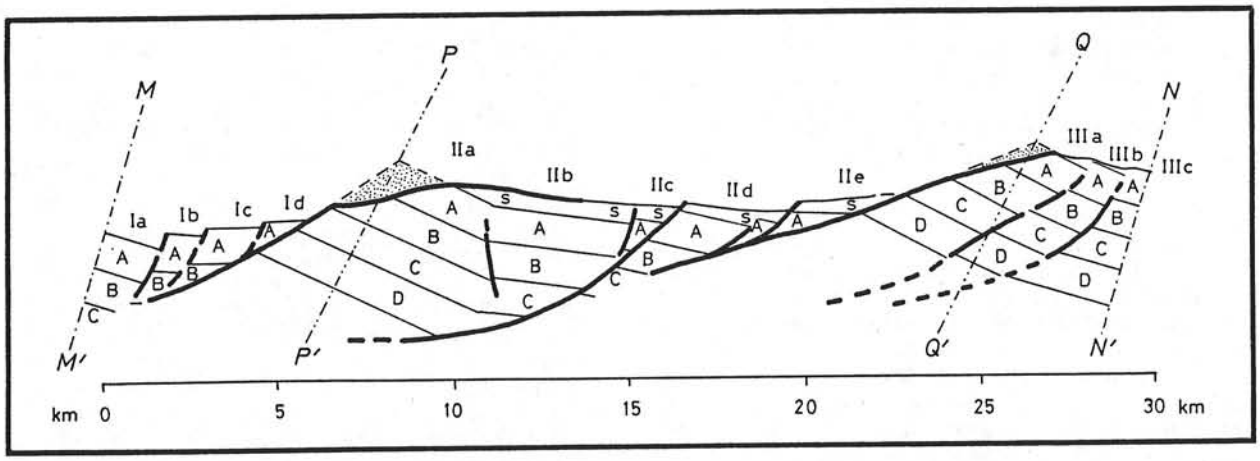


**Figure 3** — The section of Figure 2 is modified here by four additional main layers A to D, one km thick each, for retrotectonic analysis purposes. The different blocks are numbered and the limits of the sections on which the extension is measured are also indicated (MM′ to NN′ and PP′ to QQ′).

(1979a) interpretation. Now we can estimate the extension, provided we can assume that no significant extension occurred perpendicular to the section and that the thicknesses of the layers did not change. The first assumption is quite reasonable because all the tilted blocks are parallel. We discuss the validity of the second assumption later.

It is then possible to divide the original section into stratigraphic levels (Figure 3). For convenience, we chose four layers, each 1 km-thick, called A to D. The two shaded reflectors correspond respectively to the top of layers A and C. These layers were presumably horizontal before the faulting and related block tilting occurred. A thin layer (Figure 3) lies on top of layer A in the central block (II), whereas it seems absent on the top of block III. The nature of blocks Ib, Ic, Id, IId, and IIe is uncertain. Since the hypothesis of their nature has noticeable effect on the computations, this problem is discussed later. Note the absence of the crests of faulted blocks (shaded areas of blocks IIa and IIIa) which may be explained by erosional processes or by tectonic deformation; this alternative is also important in the computation of β and is taken into account.

It is important to define the extremities of the section along which β is computed. Taking into account the relative homogeneity of the fault patterns and tilted blocks across the margin, these extremities must be chosen among homologous portions of the fault pattern. This is clearly the case for lines PP′ and QQ′ passing by the crests of the two adjacent main blocks. It is probably the case for lines MM′ and NN′, which cut similar portions of two main blocks. Consequently, the computations are made for both sections.

To estimate β, measure the total length of various levels on the sections of Figure 3. For example, the total length of layer A on MM′ to NN′ varies from 19 km (top) to 16 km (bottom), assuming deformation removed dotted portions in Figure 2. If erosion removed the dotted portions, the total original length is increased. Also, if we assume that layer *s* is absent on top of the small intermediate blocks (II d and e) and that the tops of these blocks are the top of layer A, we obtain the greatest possible estimate for the original length of layer A: 22 km (top) and 18 km (bottom). As the present length of section MM′ to NN′ is 29.5 km, β is 1.3 to 1.6 at the top of layer A and 1.6 to 1.8 at its bottom. The same computations made for section PP′ to QQ′ (18 km long) give β equal to 1.4 to 1.7 at the top of layer A and to 1.7 to 1.9 at its bottom. Regardless of assumptions, there is a systematic increase of computed β from top to bottom of layer A.

Let us now complete the stretching factor β for the deepest layer D. We have no problems about possible erosion and about the nature of the small intermediate blocks. The original length on MM′ to NN′ is 14 km (top) and 13 km (bottom), and 8.5 and 7 km respectively on PP′ to QQ′. The corresponding β is 2.1 at the top, in both cases, and 2.3 and 2.6 respectively at the bottom.

The discrepancy between the estimates made for layers A and D is important and suggests that the upper layers were noticeably elongated during rifting and that consequently their thickness did not remain constant. Figure 4 shows measured ratios between the present total length of the profile and the length of the different layers (described in Figure 3). The results differ slightly near the surface depending on the assumptions made (compare Figures 4a and 4b). In general, the ratio progressively increases with depth from about 1.5 at the surface to values between 2 and 2.5 below B (these ratios are slightly greater if we use PP′ to QQ′ instead of MM′ to NN′). Although the structure is not well controlled at depth, there is little doubt that the apparent stretching factor increases with depth to values close to 2.2 to 2.5.

This may take place for two reasons. First, it is likely that the uppermost layers of the tilted blocks were extensively deformed while gliding along the great normal faults with a *minimum* offset to 5 km; such deformation is commonly observed on land and

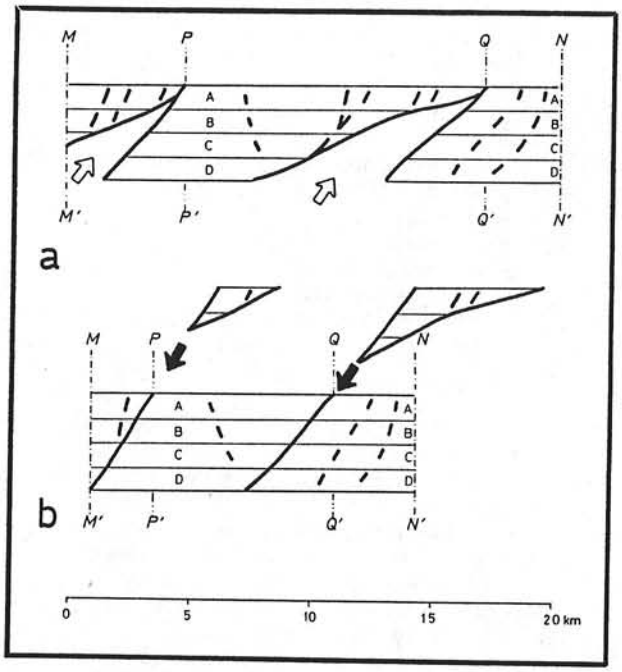


**Figure 4** — Measured ratios versus depth of present length of profile MM′ to NN′ and profiles PP′ to QQ′ on original lengths of different strata as defined in Figure 3 assuming constant thickness of the layers. In *a*, erosion is assumed for the shaded areas in Figure 3; in *b*, deformation is assumed to explain this geometry.

results in strata thinning, especially in poorly consolidated sediments (corresponding small-scale normal faults and cracks as well as the continuous deformation remain undetected by seismics). Second, the identification of the acoustic stratigraphy of the small intermediate blocks is hypothetical. We chose the hypothesis leading to the minimum amount of extension. For example, parts of these blocks could correspond to synrift sedimentary deposits, as suggested by increased thickness in the lowermost areas.

Figure 5 is a simple geometric reconstruction of the initial configuration (a retrotectonic profile). It clearly illustrates the alternative: deformation by extension in the upper layers or deformation by compression in lower layers. In the first hypothesis (Figure 5a), we chose to insure the continuity of layer A and large gaps are present at depth. The corresponding extension coefficient is 1.45. The large shortening of the lower layers cannot be explained reasonably within an extensional framework. A possible explanation is that the major fault plane, with a shallow dip between blocks II and III, intersects older steeply dipping normal faults of the southern part of block III; thus, the older fault pattern is now masked by intermediate blocks II c and II d. This rather complex hypothesis, which assumes a two-phase evolution of the margin, is supported by no data and does not explain the regularity of the youngest fault pattern observed over the whole margin.

In the second hypothesis, the continuity of layer D is maintained, but larger overlaps exist for layer A and a smaller one for layer B. Earlier we pointed out that reasonable geological explanations may be found for this overlap. The corresponding values of the stretching factor are 2.2 for MM′ to NN′ and 2.4 for PP′ to QQ′. These estimations are minimum values; reconstruction assumes that the thickness of layer D remained constant and consequently ignores any possible small-scale extensional deformation. However, geological analyses of fault blocks on land suggest that small-scale faulting and continuous deformation have little effect on large blocks, except in the vicinity of large faults (e.g. Angelier, 1979). Thus, the geometrical analysis of Figures 2 to 5 leads to β values which are certainly larger than 2.2 but probably do not exceed 2.6.

This compares to the evaluation by Le Pichon and Sibuet, using a large fault block geometry with no internal deformation, which is $\beta = 2.5$. Le Pichon and Sibuet show that this stretching factor is the one predicted by the uniform stretching model to obtain the present water depth by subsidence from a sea-level pre-stretching state.

We conclude that the safest way to evaluate the extension of the upper crustal layer is to assume that it is the result of tilted blocks. Then, you need only to evaluate the angle of tilting and the angle of the fault plane with the bedding plane on the best defined blocks, thus avoiding the difficulties related to the deformation of the uppermost layer. Otherwise, use great care to make complete retrotectonic analysis of the whole thickness of the observed section and not only the uppermost layer.

Evidence now available to us indicates that the simple uniform stretching model is a good approxi-

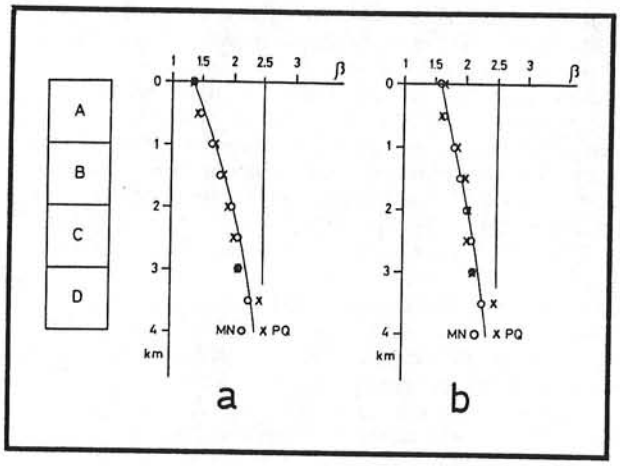


**Figure 5** — Retrotectonic profiles reconstructed from Figure 3 assuming constant thickness layers. In *a*, continuity of layer A is insured. The corresponding extension is 1.45. In *b*, continuity of layer D is insured. The corresponding extension is 2.2 to 2.4 depending on the section chosen. In *a*, there are large gaps at depth (open arrows). In *b*, there is a large overlap for layer A and a smaller one for B (black arrows).

mation to the actual geological situation both in Aegea and on the Armorican continental margin. Next, we explore this uniform stretching model.

## NEW FORMULATION OF THE SIMPLE STRETCHING MODEL

Consider a lithosphere of thickness $h_L$, composed of a crust portion of thickness $h_c$ and of average density $\rho_c$ and a mantle portion of average density $\rho_m$ (Figure 6). $\rho_c$ and $\rho_m$ relate to the densities $\rho_{co}$ and $\rho_{mo}$ at 0°C through the actual distribution of temperature within the crust and mantle. We call $\rho_L$ the average density of the lithosphere $\rho_L = f(h_c/h_L, \rho_c, \rho_m)$, as $\rho_c < \rho_m$, then $\rho_c < \rho_L < \rho_m$.

The lithosphere lies on the asthenosphere of average density $\rho_a$. The asthenosphere is made of the same material as the mantle portion of the lithosphere and has a constant temperature $T_a$, which is higher than the lithosphere average temperature so that $\rho_c < \rho_a < \rho_m$. The lithosphere floats in isostatic equilibrium on top of the asthenosphere and we define a reference level (L) as the level which the asthenosphere reaches in the absence of lithosphere. The surface elevation (E) of the lithosphere, with respect to this reference level (L), is determined by the buoyancy (B) of the lithosphere; $B = h_L(\rho_a - \rho_L)$. The sign of B depends on whether $\rho_a$ is larger or smaller than $\rho_L$, which is determined primarily by the ratio between $h_c$ and $h_L$. If B is positive, that is if $\rho_a$ is larger than $\rho_L$, then E is positive and the lithosphere stands above the reference level and vice versa.

We can determine rather precisely the reference level depth with respect to the crest of the mid-ocean ridge, as was first proposed by Turcotte, Ahern, and Bird (1977) who call this reference level the mantle geoid. Adopting the constants of Le Pichon and Sibuet (in press), who balanced a ridge crest column with 30 km continental lithosphere column, we choose an oceanic crust 5.5 km thick with an average density of 2.765 g-cm$^{-3}$ on top of asthenospheric material at temperature, $T_a$. The adopted density for mantle material at 0° C, $\rho_{mo}$, is 3.35 g-cm$^{-3}$. Finally, we adopt the values for the thermal expansion coefficient $\alpha$ and the temperature of the asthenosphere $T_a$ proposed by Parsons and Sclater (1977); $\alpha = 3.28 \times 10^{-5}$ °C$^{-1}$, and $T_a$ = 1 333° C. We take 2.5 km as the water depth of the ridge crest.

By removing the oceanic crust and balancing the columns, we find that the reference level lies 3.61 km below sea level. Turcotte, Ahern, and Bird, choosing what we consider less realistic constants, obtain 3.25 km. Thus, this reference level is probably known with a precision of 300 to 400 m wherever the asthenosphere is not unusually hot (as under Iceland or Afar).

The elevation (E) of the lithosphere above this level is $E = B/(\rho_a - \rho_w)$ when it is under water, and $E = (B + 3.61\ \rho_w)/\rho_a$ when it is above water.

If uniform stretching of the whole lithosphere occurs instantaneously at time t = 0 in such a way that the thickness of the lithosphere becomes $h_L/\beta$, the average density $\rho_L$ does not change and the buoyancy is reduced in the same ratio. The new elevation becomes $E_n = B/[\beta(\rho_a - \rho_w)]$ if $E_n$ is below water, and $E_n = (B/\beta + 3.61\ \rho_w)/\rho_a$ if it is above water. In the simplest case where E is at or below sea level, $E_n = E/\beta$.

The instantaneous change in surface elevation is $Z_i = E - E_n$. When E is at or below sea level $Z_i = E(1 - 1/\beta)$, or $Z_i = \gamma E$ where $\gamma = 1 - 1/\beta$.

There is uplift instead of subsidence if E is negative ($\rho_L > \rho_a$), which reflects the fact that $E_n$ is 0 when the stretching factor is infinite and the lithosphere is completely replaced by hot asthenosphere (Figure 6a).

The proportion of original thickness which is taken away by thinning is $\gamma$. Thus, we find the linear relationship in relative thinning coefficient first proposed by McKenzie (1978a). In this formulation, the amount of subsidence ($Z_i$) is entirely determined by the elevation (E) of the surface of the lithosphere with respect to the reference level and the thinning coefficient ($\gamma$). It does not depend explicitly on the thickness, composition, and density distributions within the lithosphere; this is important as these parameters are poorly known, whereas the starting elevation is generally much better known.

Let us take as an example a starting elevation at sea level (E = 3.61 km). We have $Z_i = 3.61\ \gamma$, which is the exact relationship found by Le Pichon and Sibuet (1981) for the Armorican continental margin. To obtain this relationship, they used the formulation proposed by McKenzie which requires defining the density distribution within the lithosphere. Thus, they chose a $\rho_{co}$ of 2.78 g-cm$^{-3}$, an $h_c$ of 30 km for the continental crust, an $h_L$ of 125 km for the lithosphere, and a linear temperature distribution. The two methods of computation agree because they balanced their continental lithosphere column with the same ridge crest column. One could use different densities, thicknesses, and temperature distribution for the continental lithosphere. Provided the columns are balanced, which they must be, the formula for the subsidence is the same.

It follows that the higher the starting elevation, the larger the amount of subsidence for a given stretching factor. To reach the same level, the stretching factor must increase with the initial elevation.

The surface of the lithosphere is at the 3.6 km water depth reference level (L) when $\rho_L = \rho_a$. Adopting a linear temperature distribution and the constraints defined above, $\rho_c = \rho_L$ when $h_c/h_L = 0.13$. When $h_L$ = 125 km, $h_c$ = 16 km. A critical level in geodynamics is 3.6 km because it is the boundary between a lithosphere lighter than the asthenosphere, which can only be forcibly subducted, and a lithosphere denser than the asthenosphere, which is in a state of gravitational instability and should tend to subduct by itself.

However, as pointed out by Le Pichon and Sibuet, the actual hydrostatic level to which the asthenosphere rises by itself is 2.5 km and not 3.6 km. This is because as the asthenosphere rises, partial fusion occurs resulting in segregation of an oceanic crust. Consequently, the 2.5 km level is the real "asthenosphere geoid." The asthenosphere may not break to

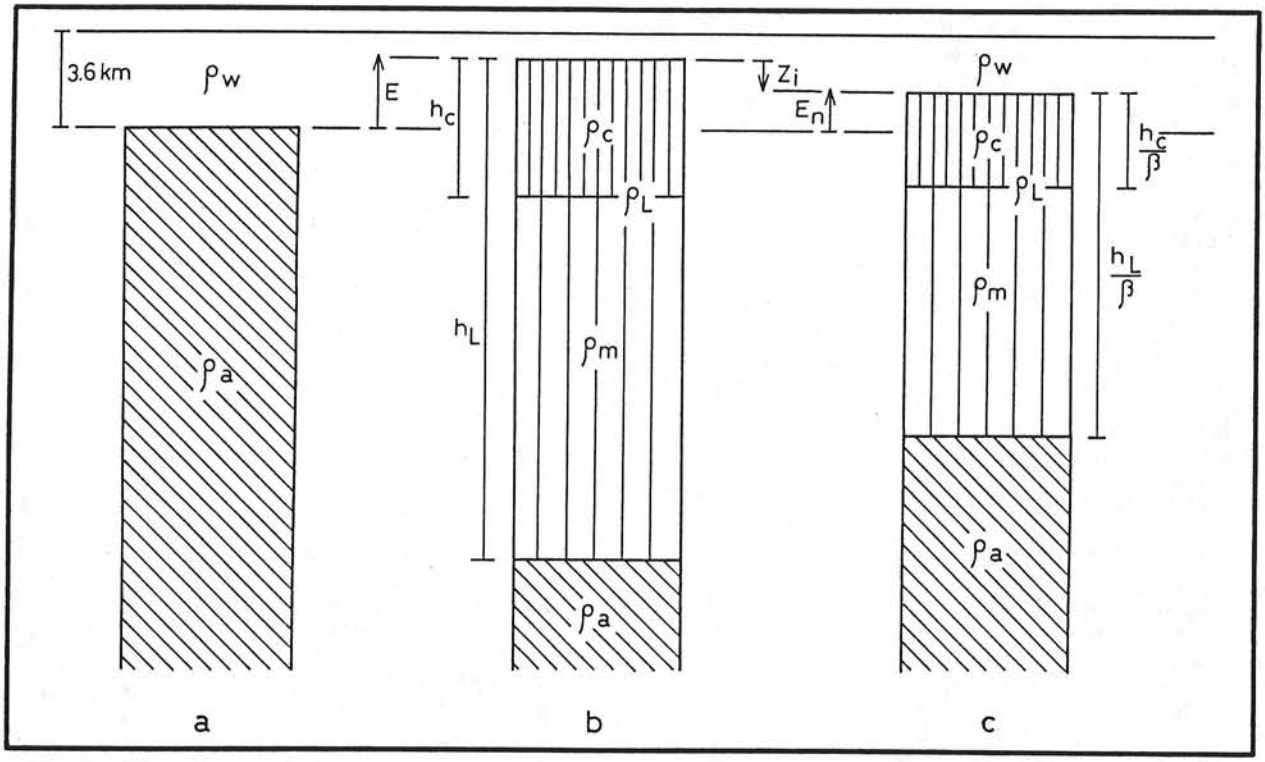


**Figure 6** — Initial stretching phase and isostatic equilibrium. Oblique hatchured pattern: asthenosphere. Vertical hatchured pattern: lithosphere. Average densities are $\rho_a$ (asthenosphere), $\rho_m$ (mantle portion of lithosphere), $\rho_c$ (crust), $\rho_L$ (whole lithosphere), $\rho_w$ (water). *a*: hypothetic column with lithosphere entirely replaced by asthenosphere (which is isostatically equivalent with $\rho_a = \rho_L$). This enables to define the "mantle geoid" and the "asthenosphere geoid". *b*: lithosphere before stretching ($h_c$ and $h_L$: thicknesses of crust and lithosphere, respectively). The surface elevation with respect to *a* is E. *c*: lithosphere just after instantaneous stretching by a factor $\beta$. The new surface elevation with respect to *a* is $E_n$. The subsidence relatively to *b* is $Z_i$.

the surface while the level of the previous lithosphere remains above 2.5 km; this is the minimum depth at which new oceanic lithosphere may form. It follows that the higher the starting elevation, the larger the stretching factor must be before oceanic accretion starts and the more difficult it is to pass from continental extension to oceanic accretion.

The above considerations lead us to recognize two quite different behaviors for lithosphere under extensional strain, depending on whether the lithosphere surface is above or below the asthenosphere geoid. Below this level, the asthenospheric material tends to rise to the surface as soon as stretching proceeds. The ascension is furthered helped by the buoyancy of the melted portion produced by partial fusion. This phenomenon increases rapidly as any possible intrusion rises and consequently the crust is invaded by magma and breaks apart. Thus, no significant thinning of the lithosphere is likely to occur and the transition to accretion should be rather sharp.

On the other hand, if the surface of the lithosphere stands above the 2.5 km deep asthenosphere geoid, then the asthenospheric material cannot reach the surface level and break the continuity of the lithosphere. In addition, as crust-mantle interface is situated deeper, its density contrast is a more efficient barrier, with respect to any possible asthenospheric intrusion into which the proportion of partial fusion is much less than in the previous case. Thus stretching may proceed until subsidence reaches a water depth of 2.5 km. It is unlikely that it will greatly exceed this value as the likelihood of the asthenosphere breaking to the surface increases rapidly beyond this depth.

## THE THERMAL SUBSIDENCE PHASE

As pointed out by McKenzie (1978a, 1978b), the initial stretching phase results in a crowding of the isotherms near the surface and consequently in a subsequent cooling phase which produces thermal subsidence. The asymptotic equilibrium state to which the infinitely thinned cooling lithosphere should tend is the one corresponding to a hypothetical outcropping asthenosphere cooled to a steady thermal state. Accepting an equilibrium value of 125 km for the oceanic lithosphere (Parsons and Sclater, 1977) and using a linear distribution of temperature, we find that the 3.61 km deep hot asthenosphere deepens to 7.82 km. Thus, 7.82 km is the value which should be reached asymptotically after an infinite amount of

time in the zero thickness crust case; 3.61 km is the value corresponding to the same zero thickness crust case immediately after stretching. For reasons developed above, such a case is not possible and the maximum water depth is unlikely to significantly exceed the maximum depth for oceanic lithosphere, which is 6.4 km.

The role of the 7.82 km level for the steady thermal state reached after an infinite amount of time is equivalent to the role of the 3.61 km reference level for the instantaneously thinned lithosphere. The difference is that the law of subsidence at infinite time as a function of thinning cannot be determined unless the altitude of the unthinned lithosphere *at thermal equilibrium* is known. A special case exists when the thermal equilibrium prior to thinning is obtained for the same 125 km thickness of lithosphere with a linear distribution of temperature. Then the buoyancy (B′) of the initial state of unthinned lithosphere at thermal equilibrium, with respect to the 7.82 km reference level, is $B' = h_c (\rho_{mo} - \rho_{co}) (1 - 2\, T_a\, h_c/h_L)$. Its elevation E′ above the 7.82 km level is $E' = B' / (\rho_a - \rho_w)$ under water and $E' = (B' + 7.82\, \rho_w) / \rho_a$ above water.

In the simplest case where the initial pre-stretching level is at or below sea level, the final subsidence at infinite time is: $Z_\infty = (1 - 1/\beta)(E' + \varepsilon) = \gamma\ (E' + \varepsilon)$; where $\varepsilon = -(\alpha/2\,\beta)\, T_a\, (h_c^2 / h_L)\, (\rho_{mo} - \rho_{co}) / (\rho_a - \rho_w)$; as $h_c < 60$ km, $\varepsilon < E'/100\,\beta$; and in general $h_c \sim 30$ km, $\varepsilon \sim E'/200\,\beta$. Thus, within the precision of determination of the different constants $Z_\infty = \gamma E'$. This result could be obtained directly from the equation giving B′, noting that $\alpha\, T_a\, h_c/2h_L \sim 1$ % ($h_c < 60$ km) and, in general, of the order of 0.5 % ($h_c \sim 30$ km). Neglecting this term, $B' = h_c (\rho_{mo} - \rho_{co})$ and the new buoyancy at thermal equilibrium (infinite time) after thinning, $B'_n$ is equal to $B'_n = h_c (\rho_{mo} - \rho_{co}) / \beta = B'/\beta$.

The simple formulas developed in the first section can be applied, replacing B by B′ and E by E′. In particular, when the initial stage is under water, $Z_\infty = \gamma E'$. Putting the initial stage at sea level, we find the result obtained by Le Pichon and Sibuet for the Armorican margin, $Z_\infty = 7.82\ \gamma$, which applies to any margin in which the initial pre-stretched level at equilibrium was sea level, assuming a linear distribution of temperature over a thickness of 125 km.

## GENERALIZED FORMULATION

The easiest way to deal with the air-water interface discontinuity in the formulation is to convert the altitudes A above sea level to virtual water depth ($D^\chi$) by multiplying it by the isostatic factor under water: $D^\chi = -A\, \rho_a/(\rho_a - \rho_w) = -1.47\ A$. Then, the virtual elevation ($E^\chi$) above the 3.61 km level is always $E^\chi = 3.61 - D^\chi$ in km, where $D^\chi$ is either the true water depth (below water) or the virtual water depth which is negative (above water). Similarly the virtual elevation (E′) above the 7.82 km level is $E^{\chi\prime} = 7.82 - D^\chi$. The instantaneous virtual subsidence is (1) $Z^\chi_i = (3.61 - D^\chi)\, \gamma$, and the total virtual subsidence is (2) $Z^\chi_\infty = 7.82 - D^\chi)\, \gamma$. The thermal virtual subsidence ($Z^\chi_t$) at any given time (t) can be estimated using the 62.8 million year thermal time constant proposed by Parsons and Schlater (1977); (3) $Z^\chi_t \sim (Z^\chi_\infty - Z^\chi_i)\,(1 - e^{-t/62.8})$. Formulas (2) and (3) are only valid if the initial pre-stretching state is at thermal equilibrium and can be described in a first approximation by a linear distribution of temperature over a thickness of 125 km. Then, the virtual subsidence can be converted back into a real subsidence: $Z_i = Z^\chi_i$ if $Z^\chi_i \leq 3.61$; $Z_i = (Z^\chi_i - 3.61)\,(\rho_a - \rho_w)/\rho_a + 3.61$ if $Z^\chi_i > 3.61$. Similarly: $Z_\infty = Z^\chi_\infty$ if $Z^\chi_\infty \leq 7.82$; $Z_\infty = (Z^\chi_\infty - 7.82)\,(\rho_a - \rho_w)/\rho_a + 7.82$ if $Z^\chi_\infty > 7.82$.

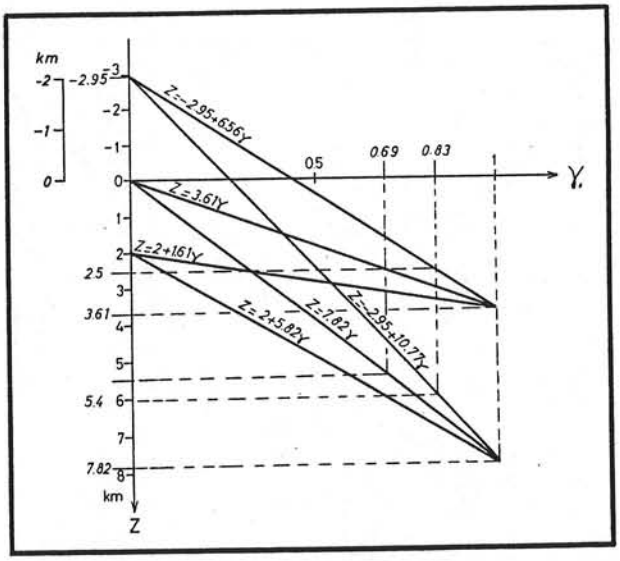


**Figure 7** — Initial virtual instantaneous subsidence ($Z^\chi_i$) and virtual total subsidence ($Z^\chi_\infty$) as a function of relative thinning of the lithosphere for three different starting elevations: 2 km above sea level, sea level, and 2 km below sea level. A change of scale is used above sea level to convert virtual water depth into actual altitude, by multiplying the scale by $\rho_a / (\rho_a - \rho_w)$. The 2.5, 3.61, and 7.82 km levels are identified.

Figure 7 illustrates this generalized formulation. The air-water discontinuity is taken care of by a change in vertical scale. Three different cases are shown with starting elevations 2 km above sea level, sea level, and 2 km below sea level. The streching factor required to reach a water depth of 2.5 km, immediately after stretching at which oceanic accretion starts is respectively 5.91, 3.25, and 1.45. Thus, the higher the initial elevation, the larger the amount of stretching necessary before oceanic accretion starts. The final water depth reached at infinite time is respectively 6.0, 5.4, and 3.8 km. Thus the maximum depth at which thinned continental crust should be expected on old continental margins, in the absence of sedimentation, is about 5.5 km if the initial steady state was close to sea level (slightly more or quite less if it was above or below sea level). Note that "old" means an age large with respect to 62.8 million years (more than 120 million years); "instantaneous" means an amount of time small with respect to 62.8 million years, (less than 20

million years Jarvis and McKenzie, 1980).

Figure 6 shows that the depth of 3.61 km at which the lithosphere is neutrally buoyant corresponds to an initial depth immediately after stretching of 1.04, 1.66, and 2.44 km and a stretching factor ($\beta$) of 2.56, 1.86, and 1.38, respectively. It is important level, as the thinned and cooled lithosphere below it may be easily subducted whereas it resists subduction above this depth. Thus, if an old marginal basin is subducted, one expects the subduction of the continental rise and slope to a depth of about 1.5 km water depth. If it is recent, only the lower portion of the continental rise is subducted.

## CONTINENTAL MARGINS AND CONTINENTAL RIFTS

Since Heezen (1962), it has been explicitly assumed that the basic genetic sequence is one which evolves from a continental rift valley, similar to the African ones, to an open ocean continental margin. This leads to a major difficulty: although the measured extension in the upper brittle layer of Rift Valleys is small (a few kilometers) it is accompanied by an important thinning of the lithosphere but not apparently of the continental crust. As a result, the lower part of the lithosphere is replaced by hot asthenosphere and the continental crust is uplifted. If, following Artemjev and Artyushkov (1971) and Bott (1971), a process of necking with brittle behavior in the upper crustal layer and plastic behavior in the lower one is invoked, then it is necessary to assume a larger amount of stretching in the lower than in the upper layer, as proposed by Bott (1971) and many authors since. In any case, it is clear that the simple model of uniform stretching cannot produce continental rifts.

A significant difference between continental rifts and regions where the uniform stretching model has been applied is the strain rate. The amount of extension across continental rifts is a few kilometers over 100 km, about 10%. The extension typically has been acting for several tens of million years. Choosing 10% and 20 million years as typical values, the strain rate is $\beta_{inst} = 16 \times 10^{-17}$ sec $^{-1} \sim 10^{-16}$ sec$^{-1}$. In the Aegean Sea, following Le Pichon and Angelier (1979), the average surface extension is 1.4 (40%) and has been obtained over 13 million years. Thus, $\beta_{inst} = 8 \times 10^{-16}$ sec$^{-1} \sim 10^{-15}$ sec$^{-1}$. On the Armorican margin, the largest total extension is 3.24 according to the model of Le Pichon and Sibuet (1981) and the average one is $\beta = 2\,\beta_{max}/(1 + \beta_{max}) = 1.53$. It was obtained over a period of about 20 million years. The maximum $\beta_{inst} = 5 \times 10^{-15}$ sec$^{-1}$ and the average one is $7 \times 10^{-16}$ sec$^{-1}$, that is of the order of $10^{-15}$ sec$^{-1}$.

In Afar, the largest measured $\beta$ is 3 (Morton and Black, 1975) over a time span of about 20 million years, and in the Basin and Range it is 2.4 (Profett, 1977) over a time span of about 7 to 13 million. The maximum strain rate is about $2 \times 10^{-15}$. In all these regions where stretching was very large, the instantaneous strain rate is, as an average, of the order of $10^{-15}$ sec$^{-1}$. It is an order of magnitude lower in the continental Rift domain.

A second significant difference is the distribution of major faults. Continental rifts have the structure of a large graben with two major faults. On the contrary, regions where a large extension was measured have numerous large faults. For example, in Crete, which is part of the Aegean extensional domain (Angelier, 1979), the largest fault delimitate blocks typically 30 km across. In the Basin and Range, Afar, and on the Armorican continental margins, tilted blocks are a few kilometers to at most 20 to 30 km across.

Another important observation is that there is no indication, in continental rifts, that the lower continental crust was thinned to a greater extent than in the upper brittle portion. For example, in the Rhine graben, which is probably the best studied continental rift, the total surface extension is about 4 to 5 km (Sittler, 1974). This gives a surface extension rate of 1.12 over the 40 km width of the central valley. The surface extension cannot be measured over the eroded uplifted shoulders of the central valley. The crust has an average thickness of about 26 km over the entire 100 to 150 km width of the rift system, instead of about 29 to 30 km on each side (Werner and Kahle, 1980). This is an average extension rate of 1.12 to 1.15, quite comparable to the measured surface extension rate. On the other hand, Werner and Kahle (1980) show that gravity requires the lithosphere to be thinned by a factor of about 1.8 from an assumed original thickness of 135 to about 75 km. Thus, everything happens as if the lower portion of lithosphere was replaced totally by hot asthenosphere whereas the upper one was only slightly extended, mostly through a set of deep master faults.

We suggest that at low strain rates, near $10^{-16}$ sec$^{-1}$, the limited extension in the upper brittle portion is mostly absorbed in the main graben structure over two large master faults, whereas it results in the lower lithosphere in the detachment and sinking of large pieces replaced by hot asthenosphere, in a manner similar to the one suggested by McKenzie (1978b). This process might be triggered by the intrusion of asthenospheric material in narrow zones immediately below the rift where the totality of the strain is being released.

Although we do not know the actual process through which the gravitationally unstable portions of lithosphere sink in the asthenosphere, our hypothesis explains rather well the present structure of the Rhine graben or African rift valley which we may schematize by a normal thickness crust (30 km) overlying a greatly thinned portion of mantle lithosphere (30 km or less). This results not in subsidence but in an uplift of about 1.0 km, making further evolution to an oceanic stage even more difficult, as pointed out earlier. At higher strain rates, the extension distributed over a much larger surface in the upper brittle portion and the entire lithosphere appears to be thinned at a uniform rate. Intermediate cases might occur at intermediate stages. In addition, a zone of low strain rate may convert later into a zone of high strain rate. Thus, extremely complex evolutions may

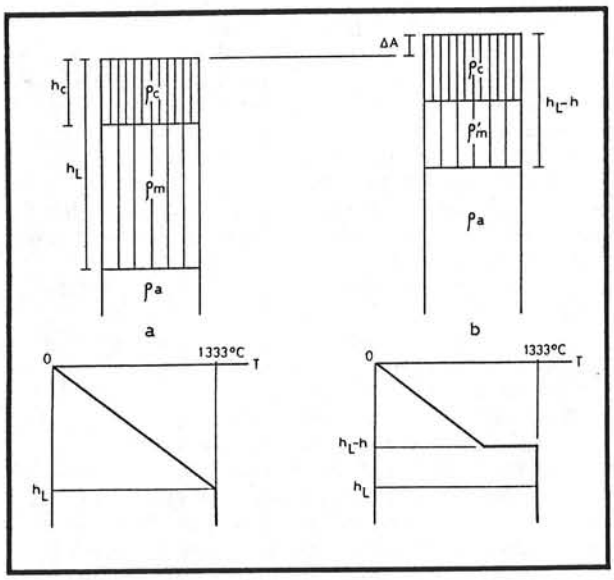


**Figure 8** — Sinking of a lower portion of lithosphere of thickness h and its replacement by hot asthenosphere resulting in an uplift Δ A.

result from varying levels of stresses being applied to a given area, even if unusual asthenosphere or lithosphere conditions are absent.

Next compute the uplift due to the replacement of the lower portion of the lithosphere of thickeness h, at thermal equilibrium, by hot asthenosphere. The resulting uplift (ΔA; A is the altitude) is $\Delta A = + \alpha h^2 T_a / (2 h_L) = 1.75 h^2 \times 10^{-4}$, where h is in km. The maximum uplift is 1.58 km if the entire mantle portion (95 km) is replaced by hot asthenosphere. The change of depth under water should be multiplied by the isostatic factor $\rho_a / (\rho_a - \rho_w)$, and consequently $\Delta D^x = 2.57 h^2 \times 10^{-4}$ km where $D^x$ is the virtual water depth and $\Delta D^x$ the part of this virtual water depth produced by the lower part of the lithosphere sinking.

Compute the subsidence resulting from thinning of this truncated lithosphere of virtual water depth $D^x$, situated — $\Delta D^x$ above the thermal equilibrium stage (see Figure 8), using formulas (1), (2), (3). The formula for the instantaneous subsidence does not change because the average density, and consequently the buoyancy, is not modified by thermal processes during the subsidence. The total virtual subsidence becomes (4) $Z^x_\infty = [7.82 - (D^x - \Delta D^x)] \gamma - \Delta D^x$, and the thermal virtual subsidence is (5) $Z^x_t = [\gamma (4.21 + \Delta D^x] (1 - e^{-t/62.8})$. An example is a lithosphere, in thermal equilibrium at sea level, in which the whole mantle portion sinks and is replaced by asthenosphere. Then, the uplift $D^x = \Delta D^x = - 2.32$ km ($\Delta A = 1.58$ km). Thus $Z^x_i = 5.93 \gamma$. The instantaneous subsidence is larger, but the depth reached is less important than it would have been prior to the uplift for the same value of β. To reach the water depth of 2.5 km at which oceanic accretion may start, we need a β of 5.3 instead of 3.25. $Z^x_\infty = 7.82 \gamma + 2.32$. Thus, the total virtual subsidence corresponding to the 2.5 km water depth instantaneous subsidence level is: $Z^x_\infty = 8.68$ km and the actual depth reached is 6.36 km (8.68 − 2.32). Finally, $Z^x_t = [1.89 \gamma + 2.32] (1 - e^{-t/62.8})$, and for the 2.5 km instantaneous level $Z^x_t = 3.86 (1 - e^{-t/62.8})$.

This case quantitatively corresponds to a prolonged period of low strain rate, producing a continental rift stage, followed by a high strain rate period then producing continental margin stage. The results of Royden and Keen (1980) for the eastern Canada margin might be interpreted in this way. Royden and Keen use a model in which the mantle portion of the lithosphere may be stretched by a factor which is equal to, or larger than, the one applied to the continental crust. When it is larger, this is equivalent to the sinking of the lower lithosphere model although the uplift they obtain is somewhat larger. The temperature at the base of the thinned lithosphere is in their case $T_a$ and not $T_a (1 - h/h_L)$. Royden and Keen find that uniform stretching over the entire lithosphere fits data on the subsidence of eight wells on the Nova Scotia margin. However, on the Labrador margin they need to use a mantle portion which is more highly stretched than the crust. Our hypothesis indicates that the Labrador region started as a continental rift with uplift during a low strain rate phase which was followed by a higher strain rate phase with uniform stretching. We believe that formulas (1) and (5) could fit the Royden and Keen data probably as well as they did within the accuracy of the measurements; the parameters to be fitted being $D^x$, $\Delta D^x$, and γ.

## CONCLUSIONS

We have confirmed the geometrical analysis of surface faulting in highly strained extensional areas, made by Le Pichon and Sibuet (1981). The geometry of faulting in the upper brittle layer, 8 to 10 km thick prior to extension, can be compared to a pack of cards resting at an angle on a plane, with each card making a slight angle with the preceding one. However, be careful to measure the extension over the entire thickness of the brittle layer, rather than on the uppermost, often disturbed layer.

We showed that the behavior of the lithosphere under extensional strain is controlled by the existence of two reference levels, one near 3.6 km and the other near 7.8 km water depth. These are the levels which would be reached by the asthenosphere in the absence of lithosphere and of formation of oceanic crust. The first one is for hot asthenosphere, the other one for asthenosphere cooled to thermal equilibrium. The instantaneous as well as total vertical motion after an infinite time produced by uniform stretching of the lithosphere is then expressed simply as a function of the difference of elevation between the starting level and respectively the 3.6 and 7.8 km reference levels.

We also showed that the behavior of the lithosphere under extensional strain is quite different above and below the 2.5 km deep asthenosphere geoid. Below this level, continuity of the old lithosphere is likely to be rapidly broken and, as a consequence, oceanic ac-

cretion begins rapidly. Above this level, the old lithosphere is thinned extensively until it reaches the level of the asthenosphere geoid, thus enabling the asthenospheric material to break through to the surface.

We suggested that the behavior of the lithosphere under extensional strain is quite different at low ($10^{16}$ sec $^{-1}$) and high ($10^{15}$ sec $^{-1}$) strain rates. The low strain rate situation is considered typical of the continental rifts, similar to the African rifts or the Rhine graben. The lower lithosphere is thinned by simultaneous diapiric asthenospheric instrusions and lithospheric sinking; the upper one is only slightly thinned. For high strain rates, the whole lithosphere is apparently thinned rather uniformly, as in Aegea and probably on many continental margins. Thus, the continental rift stage, as typified by the Rhine graben and African rifts, is not necessarily the early stage of evolution of a continental margin. Present day Aegea may be a better example of an early stage of passive continental margin revolution. However, composite cases may occur and we provide a simple method to quantitatively account for them.

## ACKNOWLEDGMENTS

The CNRS (ATP IPOD n. 4228) and the Centre National pour l'Exploitation des Océans (contrat CNEXO No. 79-5929) supported this work. Contribution number 720 du Centre Océanologique de Bretagne.

## REFERENCES CITED

Angelier, J., 1979, Néotectonique de l'Arc égéen: Société Géologique du Nord, publication n. 3, 418p.

Angelier, J., 1981, Analyse quantitative des relations entre déformation horizontale et mouvements verticaux: l'extension égéenne, la subsidence de la mer de Crète et la surrection de l'arc héllénique: Annales de Géophysique, v. 37, p. 327-346.

Artemjev, M. E., and E. V. Artyushkov, 1971, Structure and isostasy of the Baikal rift and the mechanism of rifting: Journal of Geophysical Research, v. 76, p. 1197-1212.

Bott, M. P., 1971, Evolution of young continental margins and formation of shelf basins: Tectonophysics, v. 11, p. 319-327.

Heezen, B. C., 1962, The deep-sea floor, *in* Runcorn, ed., Continental drift: New York, Academic Press, p. 235-288.

Jarvis, J. G., and D. P. McKenzie, 1980, Sedimentary formation with finite extension rates: Earth and Planetary Science Letters, v. 48, p. 42-52.

Le Pichon, X., and J. Angelier 1979, The Hellenic arc and trench system — a key to the neotectonic evolution of the eastern Mediterranean area: Tectonophysics, v. 60, p. 1-42.

———, and ———, 1981, The Aegean Sea: Proceedings, Royal Society of London, A 300, p. 357-372.

———, and J. C. Sibuet, 1981, Passive margins, a model of formation: Journal of Geophysical Research, v. 86, p. 3708-3720.

———, J. Angelier, and J. C. Sibuet, 1982, Plate boundaries and extensional tectonics: Tectonophysics, v. 81, p. 239-256.

McKenzie, D., 1978a, Some remarks on the development of sedimentary basins: Earth and Planetary Science Letters, v. 40, p. 25-32.

———, 1978b, Active tectonics of the Alpine-Himalayan belt; the Aegean Sea and surrounding regions: Geophysical Journal of the Royal Astronomical Society, v. 55, p. 217-254.

Montadert, L., et al, 1979a, Rifting and subsidence of the northern continental margin of the Bay of Biscay, *in* L. Montadert and D. G. Roberts, eds., Initial reports of the deep sea drilling project: Washington, D.C., U.S. Government Printing Office, v. 48, p. 1025-1060.

———, et al, 1979b, North-east Atlantic passive margins: rifting and subsidence processes, *in* M. Talwani, et al, eds. Deep-drilling results in the Atlantic Ocean: Washington, American Geophysical Union, Continental Margins and Paleoenvironment, series 3, p. 164-186.

———, et al, 1981, Extension rates measurements on Galicia Portugal and North Biscay continental margin, consequences for continental margins evolution models: Galveston, Texas, 1980 Hedberg Research Conference on Continental Margin Processes (Abs.).

Morton, W. H. and R. Black 1975, Crustal attenuation in Afar, *in* A. Pilger and A. Rosler, eds., Afar depression of Ethiopia: Stuttgart, Schweizerbart'sche Verlagsbuchlandlung, v. 1, p. 55-65.

Parsons, B., and J. G. Sclater, 1977, Analysis of the variation of ocean floor bathymetry and heat flow with age: Journal of Geophysical Research, v. 82, p. 803-827.

Proffett, J. M., Jr., 1977, Cenozoic geology of the Yerington district, Nevada, and implications for the nature and origin of basin and range faulting: Geological Society of America Bulletin, v. 88, p. 247-266.

Royden, L., and C. E. Keen, 1980, Rifting process and thermal evolution of two continental margins of eastern Canada determined from subsidence curves: Earth and Planetary Science Letters, v. 51, p. 343-361.

———, J. G. Sclater, and R. P. von Herzen, 1980, Continental margin subsidence and heat flow: Important parameters in formation of petroleum hydrocarbon: American Association of Petroleum Geologists Bulletin, v. 64, p. 173-187.

Sittler, C., 1974, Le fossé rhénan ou la plaine d'Alsace, *in* J. Debelmas, ed., Géologie de la France: Paris, Doin, p. 78-104.

Turcotte, D. L., J. L. Ahern, and J. M. Bird, 1977, The state of stress at continental margins: Tectonophysics, v. 42, p. 1-28.

Werner, D., and H. G. Kahle, 1980, a geophysical study of the Rhine graben, parts I and II: Geophysical. Journal of the Royal Astronomical Society, v. 62, p. 617-647.

## Abstract

Models of formation and evolution of passive margins have been proposed, modified and tested over the starved passive continental margins of the Nord-East Atlantic Ocean where numerous detailed geological and geophysical data have been acquired, in particular by French and British institutions. The main conclusions are the following :

- During the rifting episode, the motions of North America, Europe and Iberia plates are the same as the opening directions of the adjacent oceanic areas.

- In order to quantify the total amount of extension during the rifting episode, the mechanisms of formation of continental margins have to be better understood. The amount of superficial extension measured from the tilted fault block geometry of the upper portion of the West-Iberian margin is in close agreement with the uniform stretching model as deep as 5.5 km. The S reflector lying at the base of the continental margin, below the tilted fault blocks, is explained as a mechanical discontinuity which appears for tensional values larger than 2.8 - 3.2 when the tilting of blocks reaches the asymptotic value of 20 to 30°. At that level, the measured extensions are lower than the ones predicted by the uniform stretching model. This could be due to the fact that synrift sediments deposited at the beginning of the rifting have been later on incorporated in the tilted fault blocks. West Iberian continental margin data are therefore as a whole compatible with the uniform stretching model. This type of margin can be considered as the final evolution of a symmetrical intra-continental basin formed by uniform stretching.

On the contrary, for the Northern Bay of Biscay margin, Le Pichon and Barbier (1987) have demonstrated that a decollement surface crossing the whole upper crust down to the brittle-ductile limit has been active since the beginning of rifting. Normal faults along which tilted blocks have been displaced would be antithetic faults. This type of margin can be considered as the final evolution of an asymmetrical basin in which a decollement surface is active since the beginning of extension.

As a conciliatory hypothesis we propose a model of formation of passive margins by uniform stretching in which any pre-existing crustal discontinuity could be used as a decollement surface at any stage of the formation of the margins.


***

## Résumé

Les modèles de formation et d'évolution des marges continentales passives n'ont pu être élaborés, modifiés et testés que parce que de nombreux levés géologiques et géophysiques de détail ont été acquis, notamment par les institutions françaises et anglaises, sur les marges peu sédimentées de l'Atlantique Nord -Est. L'intégration de l'ensemble de ces données nous amène aux conclusions suivantes :

- Au cours de l'épisode de rifting, les directions des mouvements des plaques Amérique du Nord, Europe et Ibérie sont identiques aux directions d'ouverture du domaine océanique adjacent.

- Quantifier l'extension totale résultant du rifting nécessite de mieux appréhender les processus de formation des marges. Les valeurs de l'extension superficielle, mesurées à partir de la géométrie des blocs basculés de la marge ouest-ibérique, sont compatibles avec le modèle d'étirement uniforme pour la partie supérieure de la marge, jusqu'à une profondeur de 5,5 km. En bas de marge, le réflecteur S est observé. Il est interprété comme une discontinuité mécanique qui apparaîtrait pour des valeurs de l'extension supérieures à 2,8 - 3,2, lorsque le basculement des blocs atteint la valeur limite de 20 à 30°. L'extension mesurée est inférieure à celle prédite par le modèle d'étirement uniforme car elle ne rend compte que d'une partie de l'extension, celle qui affecte les sédiments synrifts déposés au début du rifting. Les données de la marge ouest-ibérique sont cependant compatibles avec le modèle d'étirement uniforme. Ce type de marge pourrait être considéré comme l'évolution finale d'un bassin intra-continental symétrique créé par étirement uniforme.

Au contraire, en ce qui concerne la marge nord-Gascogne, Le Pichon et Barbier (1987) supposent qu'une surface de décollement, traversant toute la croûte supérieure jusqu'à l'interface fragile-ductile, aurait fonctionné dès le début de la phase de rifting. Les failles limitant les blocs basculés seraient alors des failles antithétiques. Ce type de marge pourrait être considéré comme l'évolution finale d'un bassin intra-continental asymétrique où une surface de décollement reprendrait un accident ancien et fonctionnerait dès le début de l'extension.

A titre d'hypothèse, nous proposons un modèle de formation des marges continentales par étirement uniforme dans lequel, après une phase d'extension, où localement l'extension peut atteindre 2,8 à 3,2, la surface cohérente située à la transition fragile-ductile évoluerait en surface incohérente. Lorsque des accidents structuraux majeurs existent dans la croûte continentale, un accident particulier pourrait être utilisé comme surface de décollement privilégiée. Cette surface de décollement pourrait fonctionner dès le début du rifting (modèle Le Pichon et Barbier) ou à partir d'un stade intermédiaire de formation du bassin.


***